INSTITUTUL DE GEOLOGIE ŞI GEOFIZICĂ

STUDII TEHNICE ŞI ECONOMICE

SERIA D *Prospecţiuni geofizice* Nr. 10

A XIII-a ADUNARE GENERALĂ A COMISIEI SEISMOLOGICE EUROPENE

(PARTEA A III-a)

Braşov, 28 august – 5 septembrie 1972

BUCUREŞTI
1975

Răspunderea asupra conţinutului acestor articole revine în exclusivitate autorilor.

INSTITUTUL DE GEOLOGIE ŞI GEOFIZICĂ

STUDII TEHNICE ŞI ECONOMICE

SERIA D *Prospectiuni geofizice* Nr. 10

A XIII-a ADUNARE GENERALĂ A COMISIEI SEISMOLOGICE EUROPENE

(PARTEA A III-a)

Braşov, 28 august — 5 septembrie 1972

BUCUREŞTI
1975

INSTITUTE OF GEOLOGY AND GEOPHYSICS

TECHNICAL AND ECONOMICAL STUDIES

D SERIES *Geophysical Prospecting* No. 10

THE XIIIth GENERAL ASSEMBLY OF THE EUROPEAN SEISMOLOGICAL COMMISSION

(PART III)

Braşov, 28th August — 5th September 1972

BUCHAREST
1975

TABLE OF CONTENTS

SYMPOSIUM 1. MICROSEISMS AND GROUND NOISE

POWER SPECTRA IN STORM MICROSEISM RESEARCH AT OULU

BY

HEIKKI KORHONEN[1]

This investigation develops my earlier spectral analysis of microseisms at Oulu (K o r h o n e n, 1971). In this study power spectra computed from selected samples of LP-Z recordings by the method of S o u t h w o r d (1960) are transformed into two different forms : sonograms and cumulative power spectra. The sample lenght is mostly 6 minutes, sampling interval one second and maximum lag number 40. This corresponds to ca 17 degrees of freedom (B l a c k m a n, T u k e y, 1958). The sonograms are constructed from succesive power spectra using selected power distribution ranges, which are presented in figure 1. The cumulative power curves are obtained by summing up the power density values for frequency band 40 —310 mHz. In each spectrum the sum of all these values is called cumulative power *Pc*. Correspondingly the half power point is notated (*Pc*/*fm*), where *fm* presents the median of the power distribution in question.

Figure 1 shows two sonograms from different types of microseism storms. The source area of the storm 1967, Jan. 22 —23 is assumed to be over the North Atlantic, where a 970 mb cyclone center is situated SW of Iceland. During this storm winds of up to 40 —50 knots are blowing on the ocean and wave heights of up to 10 meters are reported from the North Atlantic weather ships. The power maximum of microseisms occurs at relatively low level in frequency band 75 —130 mHz during this storm. Quite different is the situation during the storm 1965, Nov. 29 —30, when the source area probably lies over the North Sea. The maximum power level is remarkably higher occuring in frequency band 160 —200 mHz. As the storm grows the power shifts towards lower frequencies. Similarly, as the storm weakens an opposite shift can be observed.

[1] Department of Geophysics, University of Oulu. Oulu, Finland.

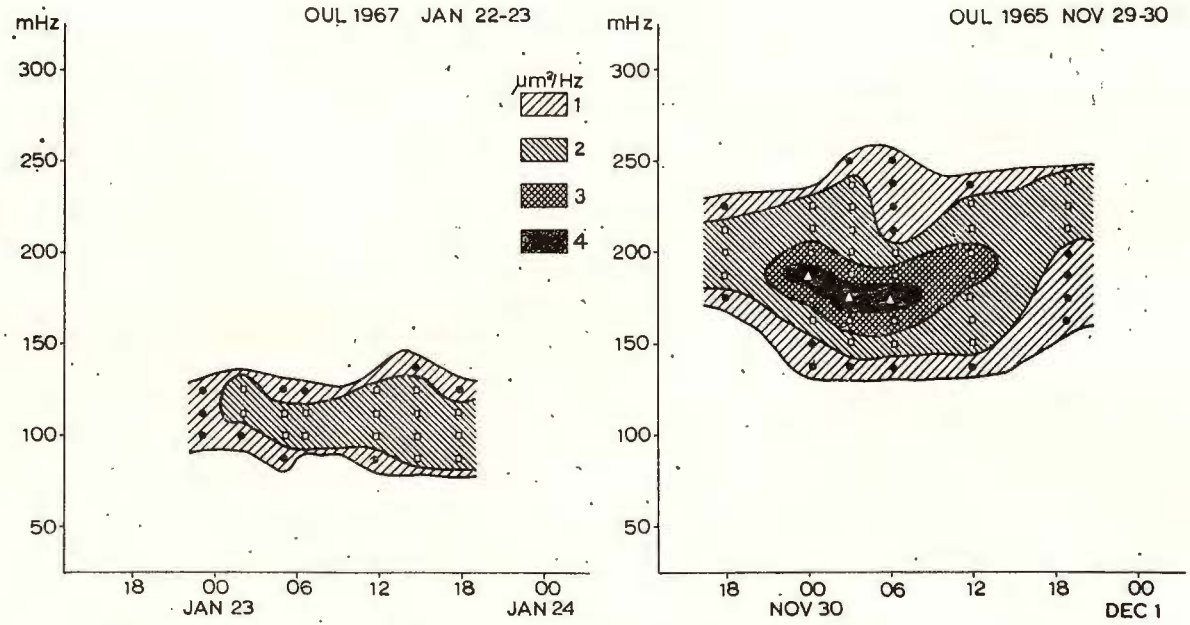

Fig. 1. — Sonograms obtained from successive microseism spectra during two different storms :
Power ranges : 1, 0,50 – 0,99 ; 2, 1,00 – 4,99 ; 3, 5,00 – 9,99 ; 4, 10,00 →

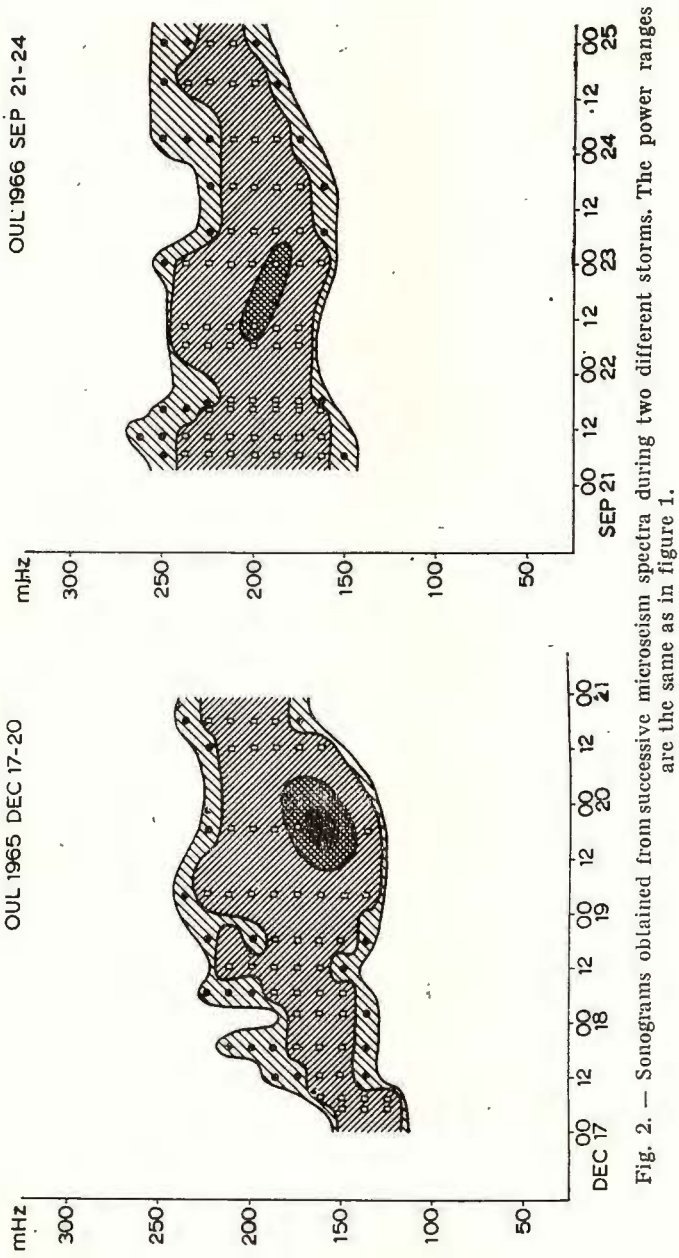

Fig. 2. — Sonograms oblained from successive microseism spectra during two different storms. The power ranges are the same as in figure 1.

Two more sonograms from different types of microseism storms are presented in figure 2. On 1965, Dec. 17 a cyclone is moving from SW of Iceland towards the Norwegian Sea, which it enters the next day. Correspondingly the microseism power increases and shifts towards higher frequencies. On Dec. 19 the center of this cyclone still lies over the Nor-

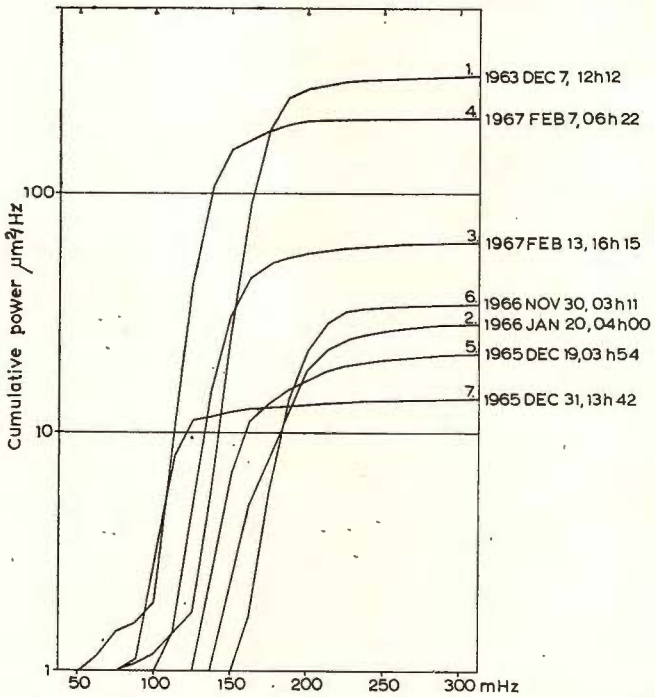

Fig. 3. — Cumulative power spectra of microseisms computed from selected storms.

TABLE 1

Case No.	Date	$Pc/2$ (μm^2/Hz)	fm (mHz)
1	1963 Dec. 7 12 h	158.0	183
2	1966 Jan. 20 04 h	14.2	205
3	1967 Feb. 7 06 h	104.6	150
4	1967 Feb. 13 16 h	31.4	162
5	1965 Dec. 19 04 h	10.7	173
6	1966 Nov. 30 03 h	17.2	205
7	1965 Dec. 31 14 h	7.0	122

wegian Sea (fig. 4, position 5) and the microseism storm reaches its maximum. On the next day when the center of the cyclone moves over the land the power decreases remarkably and shifts towards higher frequencies. During the storm 1966, Sep. 21 —24 a depression covers the whole Fenno-

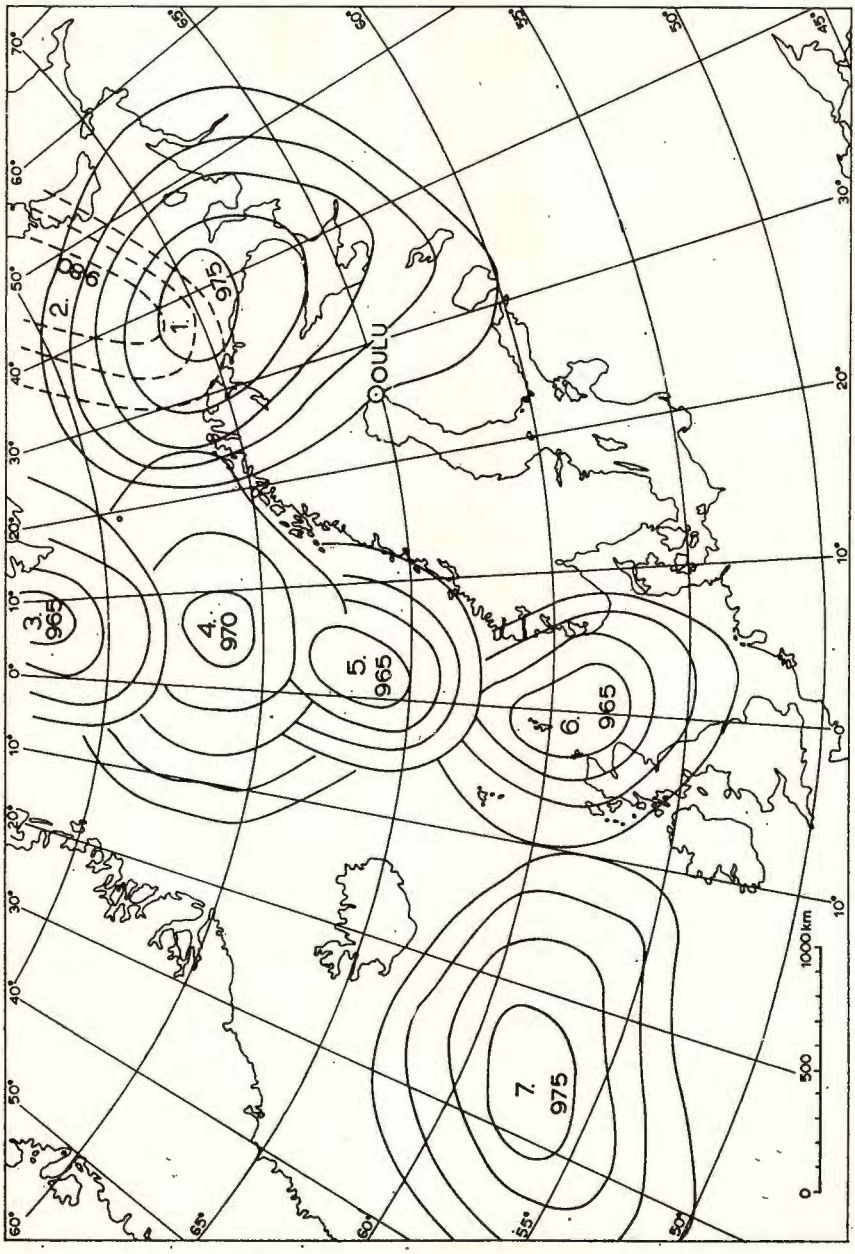

Fig. 4. — Cyclone centers in the cases of figure 3.

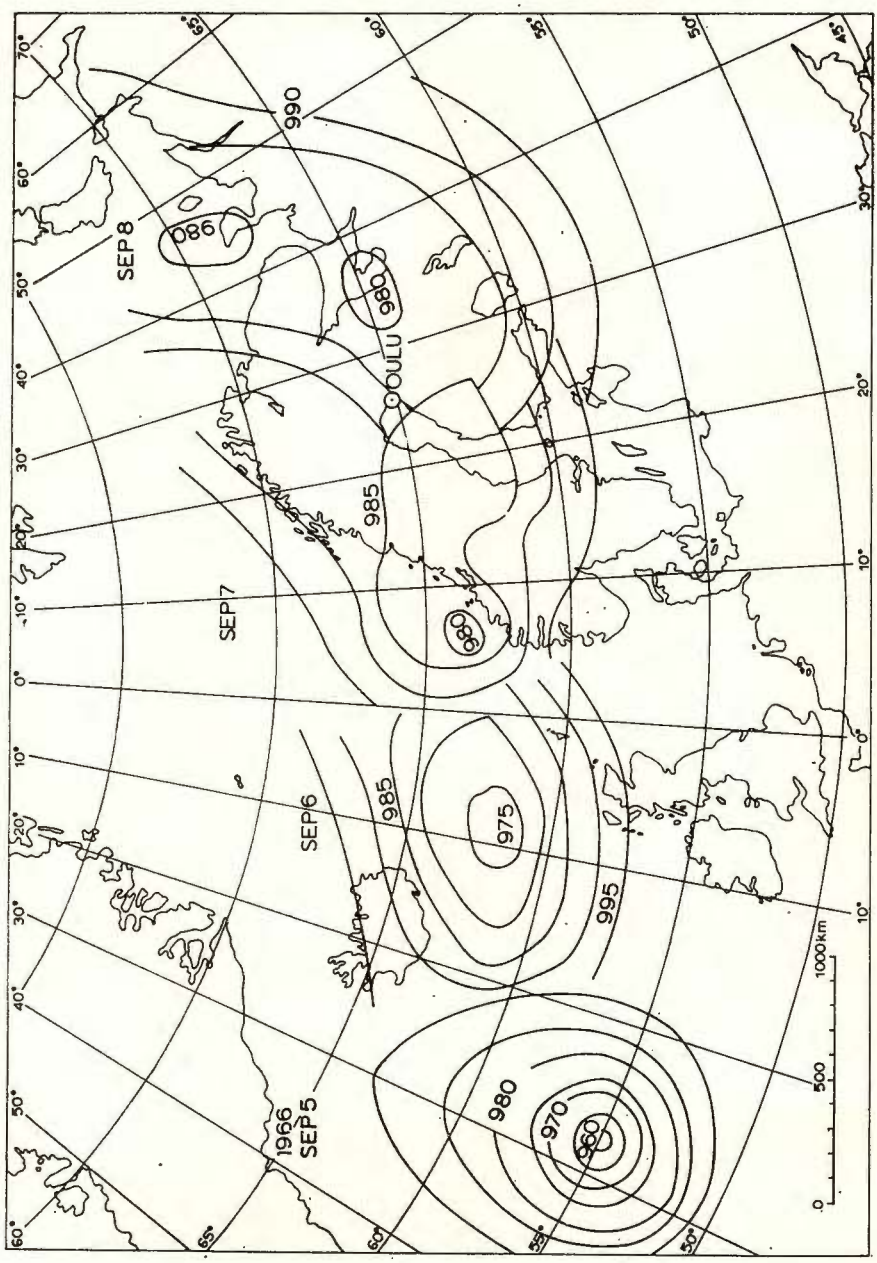

Fig. 5. — Position of the cyclone center during the storm 1966, Sep. 5 — 8.

scandia with its center over the Barents Sea. Winds of up to 30 knots are blowing nearly orthogonally towards the Norwegian west and NW coasts. During the storm maximum the power shifts towards lower frequencies and then back again.

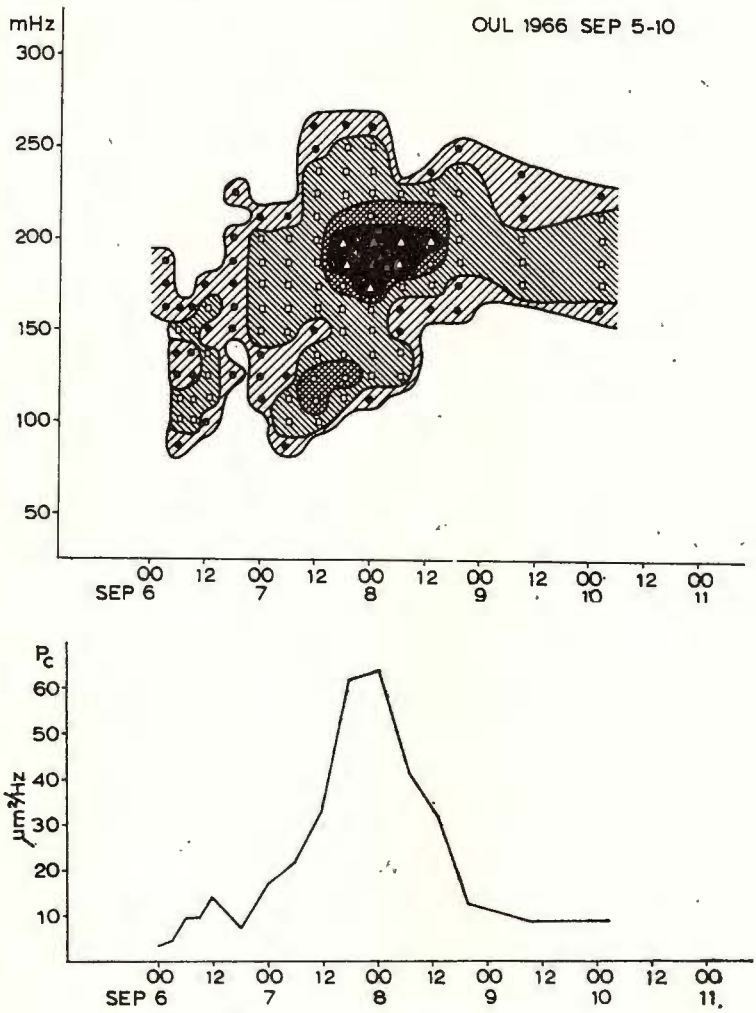

Fig. 6. — Sonogram and cumulative power curve obtained from successive microseism spectra during the storm 1966, Sep. 5 — 10.

In figure 3 some cumulative power spectra are presented from selected microseism storms. Corresponding weather conditions are characterized in figure 4. The half power points of these cumulative spectra are listed in table 1.

In cases 3, 4 and 5 the source areas lie on the Norwegian Sea. In these cases the half power points occur systematically at lower frequencies with increasing power. In cases 1, 2 and 6 the centers of the cyclones lie over the Barents Sea or over the North Sea. Half power points occur at relatively higher frequencies than in the cases when the cyclone centers lie over the Norwegian Sea. The most remarkable exception in figure 3 is case 7, when the storm center lies on the North Atlantic. In this case the power occurs at lower frequencies than in the cases of Fennoscandian microseisms. Thus the differences in the spectral composition of microseisms reflect different source conditions as well as various paths of wave propagation and they can be used in source identification.

Figure 5 shows the trace of a tropical cyclone moving with a speed of ca 15°/day across the North towards Scandinavia 1966, Sep. 5—8. Corresponding development of microseisms at Oulu is presented in figure 6. The sonogram in the upper part of this figure shows the shift of power towards higher frequencies until the storm maximum is reached in the afternoon Sep. 7. The cumulative power curve in the lower part of figure 6 shows clearly how the microseismic energy increases one power of ten, when the storm center enters the Norwegian Sea. Probably the geological discontinuities reaching from the British Isles to Iceland screen out the major part of microseismic energy propagating from North Atlantic to Fennoscandia. On Sep. 8 the center of the storm moves from the Norwegian Sea to land and weakens. Correspondingly the cumulative power decreases remarkably. The minimum of this cumulative power curve on Sep. 6 afternoon presumably associates to the source approach on the geologically disturbed areas between the British Isles and Iceland.

Acknowledgements

The author wishes to express his gratitude to the Emil Aaltonen Foundation (Emil Aaltosen Säätiö) and to the State Committee for Natural Sciences (Valtion Luonnontieteellinen Toimikunta) for financial support for this work.

REFERENCES

Blackman R. B., Tukey J. W. (1958) The measurements of power spectra Dover Publications Inc., New York.

Korhonen H. (1971) Types of storm microseism spectra at Oulu. *NORDIA* 3.

Southworth R. W. (1960) Autocorrelation and spectral analysis. Mathematical methods for digital computers. John Wiley & Sons Inc., New York.

A TWO-YEAR VARIATION OF MICROSEISM INTENSITY AT APATITY STATION AND ITS CORRELATION WITH SIMILAR FLUCTUATIONS IN TEMPERATURE REGIME

BY

G. D. PANASENKO[1]

Abstract

A two-year periodicity with about a four-month delay relative to the similar temperature variation is observed in the microseism intensity fluctuations recorded at Apatity seismic station for 1960—1970.

Numerical relation between the amplitudes of the two-year variations of microseism intensity and the lowest atmospheric layer temperature is approximately equal to

$$A_{ms} \approx 0.1\, A_t.$$

A two-year periodicity manifests itself in the course of numerous planetary and locally developing meteorological processes and a number of nature phenomena directly or indirectly dependent on meteorological factors. The alternation of cold and warm winters (Воейков,, 1891) and the two-year variation of Gulf Stream temperature (Лесгафт, 1899) have long been observed; the two-year rhythm in the W-E air flows of the lower stratosphere in tropical and sub-tropical latitudes (Ebdon, 1960; Ebdon, Varyard, 1961; Ebdon, 1963; Дубенцов, 1964; Зайцева, Усманов, 1964; Dartt, Belmont, 1964) and in typhoon activity (Фадичева, 1966) have been proved to exist. Botanists note the two-year periodicity of climatic changes by annual rings of perennials and geologists by interlayers in the varved clays.

The two-year cycle in also traced in certain geophysical phenomena, for example, in secular variations of geomagnetic field (Калинин, 1952; Мансуров, 1960). The two-year variation of velocity of development of secular tilts of Earth surface at Apatity station (the Kola Peninsula) is found ((Панасенко, 1972).

As is known, microseism intensity in Europe is mainly determined by meteorological processes and primarily by cyclonical activity in North

[1] Polar Geophysical Institute, Apatity, Murmansk district, USSR.

Atlantic. Since the above meteorological processes display the two-year cyclic recurrence, it is likely to be available in the microseism intensity fluctuations. To reveal the two-year recurrence standard observationa data on the microseisms obtained at Apatity station were properly analysed. Average fortnightly vertical component amplitudes were computed

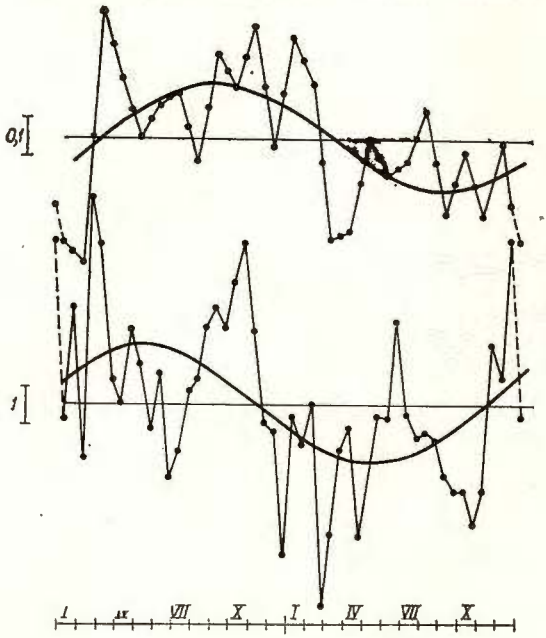

Fig. 1. — The two-year variations (average for 1960 — 1970) of microseism intensity are in micron/yr (top) and the lowest atmospheric layer temperature in deg. C/yr (bottom) at Apatity station (the Kola Peninsula) and sinusoids approximating them.

from the station bulletins. (When estimating microseism intensity it would be more correct to take the ratio of amplitudes to periods $-A/T$. Since the comparison of estimate results from the amplitudes and the ratios A/T showed their absolute qualitative identity, the amplitude alternative was chosen as less labour consuming in performing calculations).

Seasonal effect was eliminated by considering annual microseisms intensity increments, i.e. by subtracting the like (in a calendar sense) amplitude of the preceding year from each average fortnightly amplitude. The obtained succession of the annual microseism amplitude increment was broken down into 5 two-year intervals the averaging of which gave the values of annual increments for the average two-year interval illustrated in figure 1.

An empirical curve is adequately approximated by a sinusoid. The most probable values of its parameters determined by using ACM are as follows :

$$A_{ms} = 0.139 \text{ micron/yr};$$

$$\varphi_{ms} = -38.3°;$$

$$\varepsilon = \pm 0.133,$$

where A_{ms} and φ_{ms} — the amplitude and the phase of the two-year variation of annual increment value of microseism intensity (amplitude) respectively; ε — the square dispersion of empirical values relative to the approximating sinusoid.

Since the microseisms recorded at Apatity seismic station and the meteorological regime of the Kola Peninsula are mainly consequent to the same meteorological processes in North Atlantic, it can be expected that the two-year variations of the microseism intensity and the temperature regime in the area of the station will prove to be similar. To accomplish this the data of one-hour measurements of the lowest atmospheric layer temperature at Apatity station for the same period of time (1960 — 1970) were treated in a similar way.

Obtained empirical curve (fig.) of the two-year temperature variation is approximated by a sinusoid with parameters

$$A_t = 1.55 \text{ deg.C/yr};$$

$$\varphi_t = 18.7°;$$

$$\varepsilon = \pm 1.98.$$

The parameters of approximating sinusoids indicate their likeness: the ratios ε/A defining to some extent accuracy and reliability of approximation are close to 0.96 for the microseisms and 1.28 for the temperatures; the phase difference is comparatively small and makes up 57°, the temperatures being followed by the microseisms with a shift of about 4 months.

In both cases the ratios ε/A proved to be rather large and this bears witness to the deficient reliability of periodic approximation. Their large value can partly be accounted for by the presence of variations with periods differing from two years in controlling meteorological factors and by random fluctuations. This seems to a great extent to result from distorting affects of physico-geographical peculiarities: generation area and propagation line up to the recording station — for microseisms; relation between water plane and land and the latter's orography on the main ways of air mass transfer — for temperature of the lowest atmospheric layer.

The genetic unity and the likeness of the two-year microseism and temperature variations appear to serve as a sufficient basis for their direct numerical correlation. Then we have

$$A_{ms} \approx 0.1 \ A_t,$$

i.e. the annual air temperature increment per 1°C is followed by (whith a four-month delay) an adequate increase in microseism amplitudes approximately by 0.1 μ.

REFERENCES

Воейков А. И. (1891) Чередование теплых и холодных зим. *Метеорологич. вестник*, 9 .

Дубенцов В. Р. (1964) Некоторые особенности циркуляции в северной и центральной частях Тихого океана по материалам наблюдений на экспедиционных судах ,,А. И. Воейков'' и ,,Ю. М. Шокальский''. *Тр. ЦИП*, 137.

Зайцева Н. А., Усманов Р. Ф. (1964) Вертикальный разрез атмосферы в экваториальной зоне центральной части Тихого океана. *Тр. ЦИП*, 137.

Калинин Ю. Д. (1952) О некоторых вопросах изучения вековых вариаций земного магнетизма. *Тр. НИИЗМ*. 8(18).

Мансуров С. М. (1960) Вековые вариации геомагнитного поля Восточной Антарктиды. Сб. Геомагнитные возмущения, Изд. АН СССР, М., 4.

Панасенко Г. Д. (1972) Двухлетняя вариация скорости ,,векового'' хода наклонов земной поверхности на станции ,,Апатиты'' (Кольский полуостров). Сб. Современные движения земной коры на геодинамических полигонах, Изд. Фан УзССР, Ташкент.

Фадичева Е. Н. (1966) О двухлетней периодичности повторяемости тайфунов. *Тр. ЦИП*, 152.

Ebdon R. A. (1960) Notes of the wind flow at 50 mb in tropical and sub-tropical regions in January 1957—58. *Quart. J. R.M.S.*, 86, 370, London.

— (1963) Evidence of the permanency of the tropical stratospheric wind fluctuation. *Quart. J. R.M.S.*, 89, 379, London.

— R. G. Varyard (1971), Fluctuations in equatorial stratospheric winds. *Nature*, 189, 4767, London .

Dartt D. G., Belmont A. D. (1964) Periodic features of the 50 mb zonal winds in the tropics. J. *Geophys. Res.*, 69, 14, Richmond.

THE APPLICATION OF THE FSSS FOR THE MICROSEISMS INVESTIGATION

BY

O. V. PAVLOV, L. I. ALEKSEEVA [1]

The station FSSS (frequency-selected-seismic-station) as an equipment for getting of seismic oscillations spectra was considered in the papers of K. K. Zapolsky, M. A. Gostev, V. I. Khalturin. Nevertheless, the working conditions of the FSSS as a seismic canal were not considered, although to get the objective characteristics it was necessary to have the exact calculation of working conditions for the seismometric canal in this or that range of frequencies. It is more important for the FSSS canal which includes the amplifier, filters and in some cases the integrating and differentiating cells.

The possibility of such analysis and the exact calculation of working conditions is available if to take into consideration the followings :

A back coupling between seismometer and galvanometer is absent because of the presence of the amplifier in the FSSS canal. That is why the motion and working conditions of the seismometer in the FSSS canal will correspond to the motion equation and working conditions of pendulum without galvanometer. Solving the equation of forced motion of pendulum we shall get the decision in the adopted form but with the additional term in the damping coefficient. Depending upon the constants of galvanometer and ratio between the periods of galvanometer and seismic wave the displacements of seismometer coil are proportional to displacements velocity and acceleration of ground.

With the investigation of the FSSS canal containing additionally functional cells the galvanometer motion equation is reduced to the form in order to leave the term proportional to the forced current in the right part of equation. The forced current in case of differentiating, intergrating cells is proportional accordingly to the derivative and double integral from the displacement of oscillations centre of pendulum (with the recording conditions of ground displacement by seismometer).

[1] The Earth's crust Institute, Academy of Sciences of the USSR, Lermontova 128, Irkutsk, USSR.

The FSSS station canal consisting of seismometer, amplifier, and box of filters and galvanometers over filters outlets was considered. Besides, the cases of including in the FSSS canal of differentiating, integrating and double cells were considered. The different working conditions of the FSSS station were investigated. The exact calculation of the FSSS working conditions to record displacements, velocities, accelerations in motion of the ground for different frequencies was carried out. The constants of seismometers and galvanometers for the working condition of velocity of the ground motion were calculated. With these constants the operational frequency ranges have errors in amplitude and phase-amplitude characteristics which do not exceed 2—12 % according to amplitudes and 5—13 % according to phase.

For the velocity recording condition we may use the following systems for the station work: *a*) seismometer records displacements of the „ground", galvanometers record the velocity of oscillations centre of pendulum. It is necessary to include the differentiating cell into the canal provided that galvanometer is included in the recording condition of the displacement of the oscillations centre of pendulum; *b*) seismometer records acceleration in the ground motion, the double integrating cell is included into the canal after the preliminary amplifier, galvanometers records oscillations centre of pendulum velocity.

Thus, if each time with putting forward the seismological or engineering-seismological problem, which is solved with the help of the FSSS and if to calculate exactly the FSSS seismometer canal then it becomes possible according to cited above to get the spectra of velocities, displacements or acceleration in seismic oscillations.

The FSSS theory of the random functions is put forward to define the microseisms. The microseismic oscillations totality is identified with the random functions.

Briefly the FSSS theory of the random function analysis is reduced to define the analytical connection between the FSSS recordings (the canals of which produce over the outlets the weighted composing the realizations of the current spectrum) and the statistical spectra of random process, which more completely defines this process. To simplify the calculations we consider the random process as stationary and ergodic one, but as a final result we shall take in account non-steadness by additional averaging in time. We obtain the sought for connection if to equate the full instantaneous power of the stationary ergodic process (this process is determined according to Wiener—Chinchin formula as a autocorrelation function with $t=0$) and the full power of the random function realization accumulated during the realization (it is determined through the current spectrum of realization according to Raileygh formula). In this case the square of the random function realization is replaced by the square of rounding of fluctuating oscillations over the outlets of the narrow banded systems (the FSSS filters) since the process over the outlet of the FSSS filters may be regarded as the narrowbanded process.

In such a way the formulas for the instantaneous spectrum of this random process power for the energetic current spectrum and the statistical spectrum during the realization were got.

In field testing of the FSSS station collected in the engineering seismological laboratory in the Institute of the Earth-'s crust in the canal of station worked : the seismometer S5S in the recording condition of displacements, octave filters with pass bands in 0.16 —31 cps, 0.23 —0.46 cps, 0.47 —0.95 cps, 1 —2 cps, 2 —3 cps, 4 —8 cps, 7 —14.5 cps, 15 —32 cps, galvanometers GB —IV worked in the recording conditions of velocities. Wide-banded canals in 1 —40 and 0.16 —1 cps were included in the canal of station to facilitate identification of the wave pattern and to compare with the recordings of standard seismic stations. The wide-banded amplifier using for strengthening of seismic signals and deviding seismometer from galvanometers had strictly uniform frequency characteristics.

For the through electron-dynamic graduation the generators MGPA (in field conditions) and NGPK (in stationary conditions) were used. An increase in canals ranged from 5000 to 30000.

The principle characteristic spectra of microseism and Fourier machine spectra for the same places of recordings at the same observation point were calculated for comparison. For the statistical FSSS spectra a good agreement for different places of the recordings at their sufficient lenght and at the same observation point was obtained, this fact proves more complete characteristics of microseisms in comparison with the standard spectra.

The differences between the spectra of microseisms for different points of observations are due to the difference in ground conditions, the level of microseisms being the same; this corresponds to the seimic features of grounds of these places for the positive temperature conditions.

Thus, the FSSS stations enable us to get sufficiently complete characteristics of microseisms in the form of the statistical spectra. And these spectra may give the information which may be used for the seismic microzoning.

SOME DATA ON RESEARCH OF LONG-PERIOD MICROSEISMS

BY

T. A. PROSKURYAKOVA, VASILY ALKAS[1]

Over the last years the world seismic network gets more and more systems which are capable of recording the long-period signals. Therefore, the interest of studying of long-period Earth's shakes rises.

In this work the attempt to investigate the microseisms in the range from 10 to 130 s recorded by long-period instruments in Baldone (Riga) and Pulkovo was made.

The used data. The microseismic storm (September 28—30, 1969) was sorted. The parameters of instruments for Pulkovo (a) and Baldone (b) are shown in table 1.

TABLE 1

The parameters of instruments for Pulkovo (a) *and Baldone* (b).

(a)				(b)			
	Z	N—S	E—W		Z	N—S	E—W
Ts	30	30	30	Ts	25	25	25
Tg	26.1	23.2	25.3	Tg	79	82.4	82.3
Ds	0.6	0.6	0.6	Ds	1	1	1
Dg	0.7	0.7	0.7	Dg	0.479	0.468	0.487
σ^2	0.2	0.21	0.21	σ^2	0.236	0.218	0.250
$\overline{V}$	1980	1710	1730	$\overline{V}$	421	430	458

The 38 parts of records of microseisms and seismograms (19 parts for every station) were selected at the time when long-period signals may be sorted well. The example of records is shown in figure 1.

The frequency analysis. We have done the spectral analysis of microseisms storms referred to it. Calculations of spectra were made by electronic computer using the F o u r i e r method. The amplitude and phase

[1] Physical department, Moscow State University, Leninskie gory, Moscow V—234, USSR.

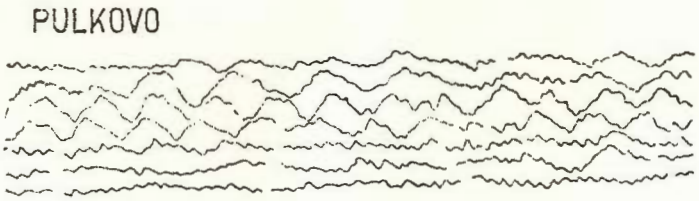

Fig. 1. — a, example of seismogram at Pulkovo station; b, example of seismogram at Baldone station.

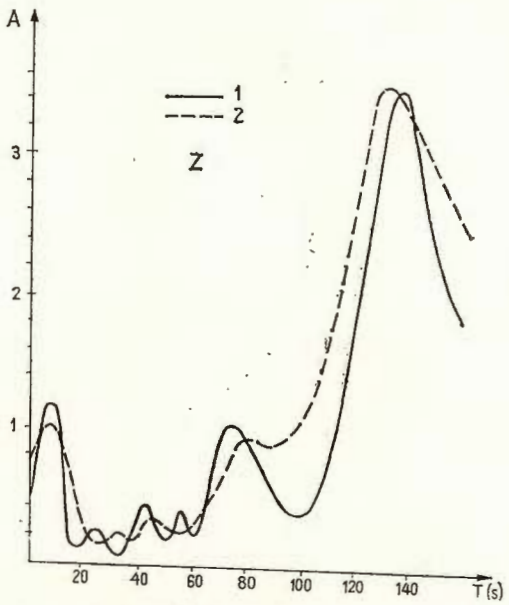

Fig. 2. — a, the amplitude spectrum of z-component of recording of Baldone and Pulkovo stations;

spectra in the range of period from 10 to 130 s were examined. The example of amplitude spectra obtained for 3 components is shown in figure 2 (a, b, c). From the figures one can see that maximums in spectra coincide for appointed values of source of microseisms of these periods and they

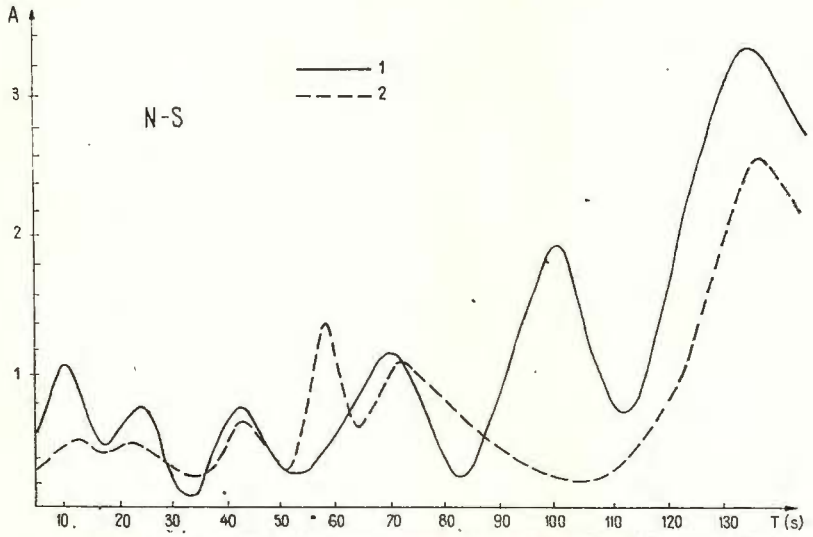

Fig. 2 — b, the amplitude of NS-component of recording of Baldone and Pulkovo stations;

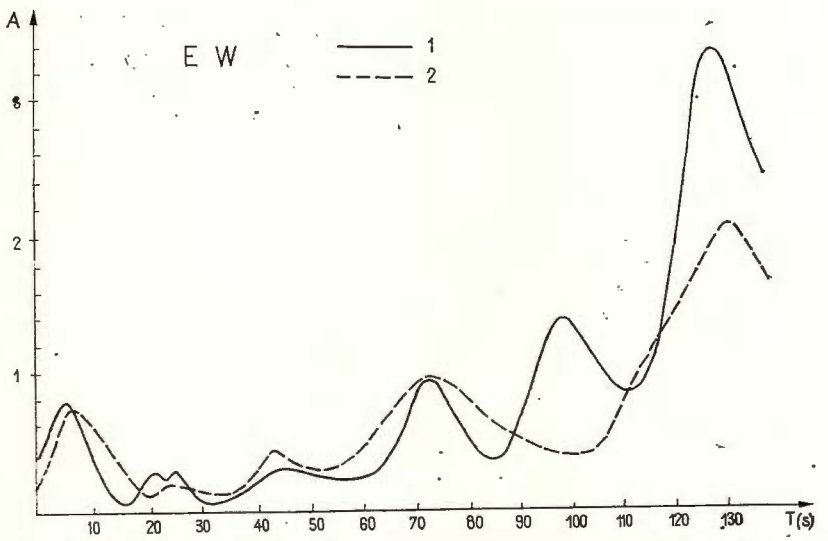

Fig. 2 — c, the amplitude spectrum of EW-component of recording of Baldone and Pulkovo stations.

1, Baldone; 2, Pulkovo.

distinctly expressed maxima for periods 8 —10 s, 24 —26 s, 45 —47 s, 120 — 130 s. All these periods may be seen on seismograms directly except the periods from 120 —130 s, which became visible only by using the spectral analysis.

The second class microseisms (2 and 3 maxima) have the amplitude 5 —8 times smaller than the first class microseisms (4 —10 s). The maxima of microseisms with periods 70 —75 s have the same order that microseisms of the first class, the maxima of periods of 120 —130 s reach the greatest value. Moreover, there are maxima only of local origin in spectra, particularly on Baldone station (55 —58 s and 100 s and so on).

Determination of the direction of microseism propagation. The analysis of amplitude-frequency spectra made it possible to draw conclusion about existence of the only source of studying microseism records in Baldone and Pulkovo. The method of determinating microseism origin offered by J e n s e n (1958) was used. The histograms obtained on

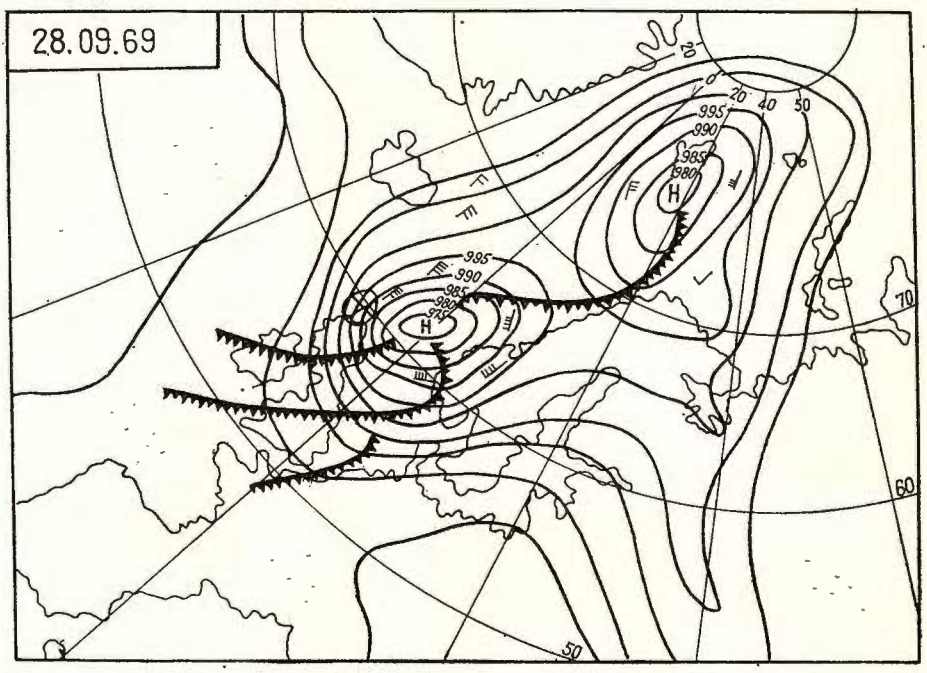

Fig. 3. — Sinoptic maps of the Northern hemisphere of 28. IX.69.18h.

the directions of the shakes origin of microseisms observed directly with periods of 10 —80 s shown that the source is situated in the Atlantic Ocean.

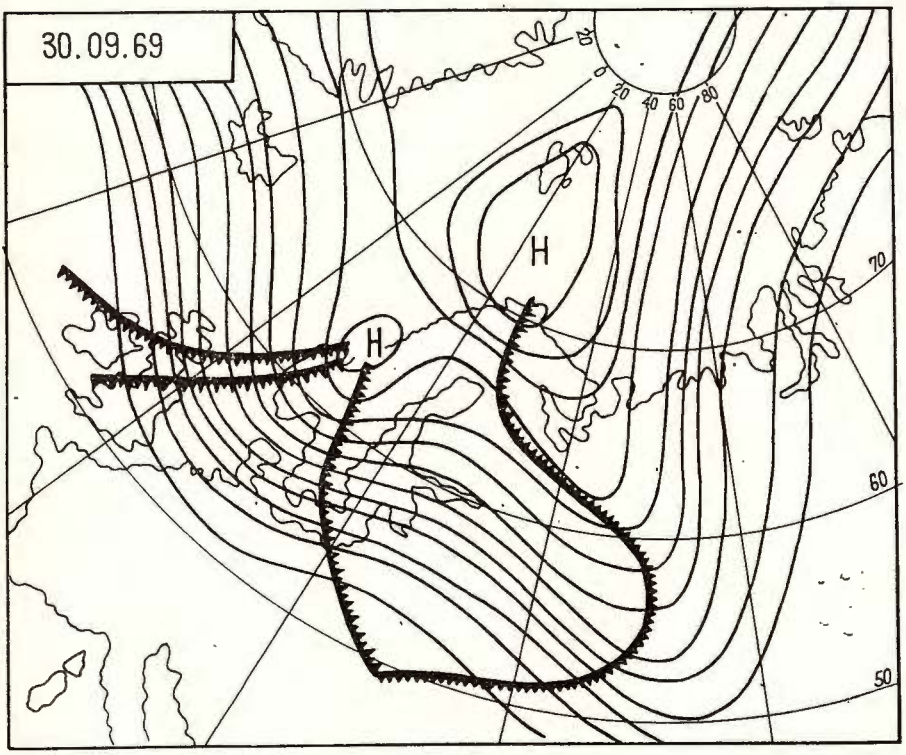

Fig. 4. — The atmospheric pressure map of the Northern hemisphere of 30. IX.69.

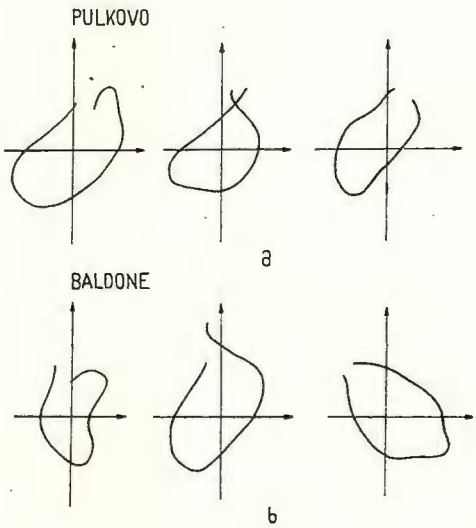

Fig. 5. — a, the trajectory of motion of soil particles in the vertical plane according to Pulkovo station recording.

b, the trajectory of motion of soil particles in the vertical plane according to Pulkovo station recording.

The 80 % of the received values of the azimuth directions cross in the rear part of the deep cyclon the coordinates of the centre of the cyclon being $\lambda = 0°20'E$, $\varphi = 61°07'N$ on the 28 of September, 1969.

The synoptic situation is shown in figure 3. The development of the cyclon could be observed in azimuthal direction during the three days of the storm. The microseisms with periods of 120 —130 s could not

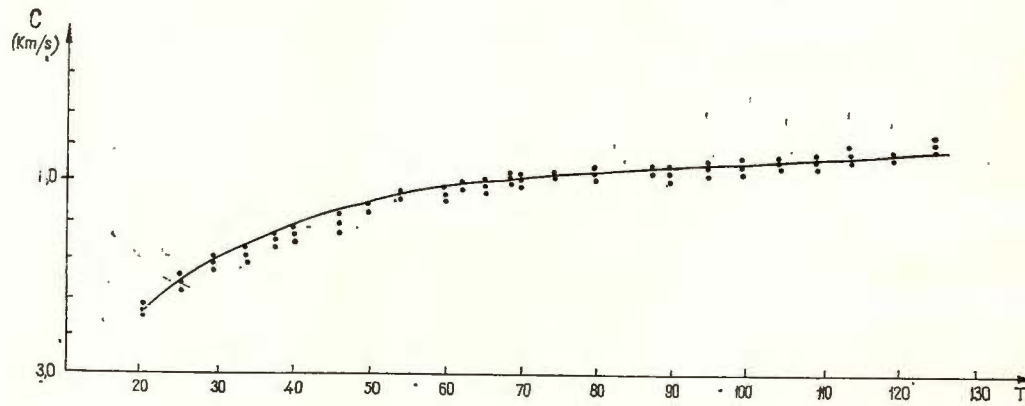

Fig. 6. — The experimental data (dots) of phase velocity (z-component) and theoretical dispersion curve (line) of phase velocity.

be observed visually and so the direction of the origin of these were not determined. Such microseisms may be supported to be due to the fluctuations of the atmospheric pressure in result of the passing of air fronts including great areas of space. Figure 4 shows the baric map of 30.09.69.

Polarization of long-period microseisms As is well known polarization is one of the most important characteristics of wave processes. The investigation of the short period microseisms in this aspect have shown that the microseisms consist of the surface Rayleigh and Love waves and body waves (R y k u n o v, 1967; V i n n i k, 1968), while there exist no data on the wave characteristics of the long-period microseisms.

This paper deals with the investigation of the wave characteristics of microseisms, without any analysis of quantitative relationship between the components of this oscillations.

Figure 5 (a, b) shows some examples of trajectory curves of the soil particles movement in Pulkovo and Baldone, which approaching ellipses.

The plane of oscillation in all cases proved to be deviating from vertical, which may be due to the fact that the wave is propagated in the inhomogeneous medium (B o a t h, 1962).

Thus, the long-period microseisms include both R and L waves.

Phase velocities. The velocity of wave propagation is also a very important feature. Using the data of phase spectra an attempt was

made to determine the phase velocities as microseisms according to the following well known formula :

$$C(T) = \frac{2\pi\,\Delta}{T[\varphi_2(T)-\varphi_1(T)^\circ] + [\gamma_2(T) - \gamma_1(T)] + 2\pi\, m}$$

where φ_2; φ_1 — phase spectra
γ_2; γ_1 — phase shifts, caused by the apparatus
Δ — distance between the stations
m — number of wavelenghts, that can be propagated between the stations.

The observed values of the microseisms phase velocities for z—component are represented by points (fig. 6). The numerical values of velocity prove the analysed long wave microseisms to include the surface R waves.

The relative error in the calculation of velocities is 4 %. On basis of the experimental curve of phase velocities of microseisms an attempt was made to find a theoretical model which would fit for corelating the experimental data with the theoretical curve. Table 2 shows the parameters of the model of the Earth structure up the depth of 400 km.

TABLE 2

The parameters of the Earth structure model up the depth of 400 km.

	h km	*a* km/s	*b* km/s	ρ g/cm³
1	1.8	3.1	1.2	2.35
2	17.5	5.65	3.35	2.65
3	18.5	7.0	4.1	2.93
4	76	8.1	4.6	3.15
5	100	8.2	4.55	3.49
6	100	8.3	4.5	3.53
7	80	8.7	4.76	3.6
		9.3	5.12	3.76

Note : *h* — thickness of the layer
a — velocity of longitudinal wave propagation in *i* layer
b — velocity of transverse wave in *i* layer
ρ — the density of *i* layer.

The theoretical dipersion curve, corresponding to the chosen model is given in figure 6 (solid line). The chosen model implies the thickness of the Earth's crust equal to 37.8 km and in the mantle at the depth of the order of 115 km a slight decrease of velocity of the transverse waves may be observed.

REFERENCES

Boath M. (1962) Direction of approach of microseisms. *Geoph. Journ. Res.*, 6, 4.

Jensen H. (1958), A procedure for the determination of direction of approach of microseismic waves. *Geodeat. Inst. Medd.* 36, Kobenhavn.

Rykunov L. N. (1967) Microseisms. Eksperimentalnye kharakteristiki estestvennykh mikrovibratsij grunta v diapazone periodov 0.007 — 8 s. Izd. AN SSSR, *sejsmologiya*, 7.

Vinnik L.P., Dolbilkina N. A. (1968) Zavisimost skorosti rasprostraneniya mikrosejsm ot perioda. *Izv. AN SSSR, ser. Fiz. Zemli*, 4, Moskva.

COMPARISON OF SOME THEORETICAL NOISE MODELS WITH THE NORSAR MICROSEISMIC NOISE FIELD

BY

EIVIND RYGG[1]

Abstract

The effectiveness of large arrays in mapping the noise field is well known. This paper describes an attempt to estimate the noise field by using a small number of sensors. The noise fields are defined by their power densities in the frequency-wavenumber space, and their validity will be judged by comparing coherence estimates of real data with coherence computations on the basis of the models. The real data base has been recordings from Oyer array — the first large installation in the NORSAR area.

INTRODUCTION

During the last few years methods for mapping the noise fields have been presented in literature and results from different sites have been presented in numerous reports.

A commonly used and excellent way of presenting the results is by displaying the power density as a function of the frequency and the wavenumber, thus giving the distribution in azimuth and velocity of the noise fields. However, to map the noise field this way, one must have access to data from large and properly spaced arrays, and of course the results are valid only at or near the array sites.

Now, the number of large aperture arrays is not very large, and usually the number of sample points in space is very limited. The normal case will be recordings from one or a few (2—3) sensors at each site. In this paper we have investigated the possibility of estimating the noise field in frequency-wavenumber space by using the experimental data from only a small number of sensors. The procedure has been to design noise models with specific power distributions and to check the models by coherence computations.

[1] Seismological Observatory. University of Bergen, Villavei 9. N—500 Bergen, Norway.

THE NOISE MODEL

Before defining the noise mode[1], let us point out a few requirements that must be met : First of all the model must be simple enough to be mathematically formulated and to allow the calculation of the parameter of interest. Secondly it should not deviate too much from the noise fields as mapped by using arrays in the same area, and thirdly it must explain certain

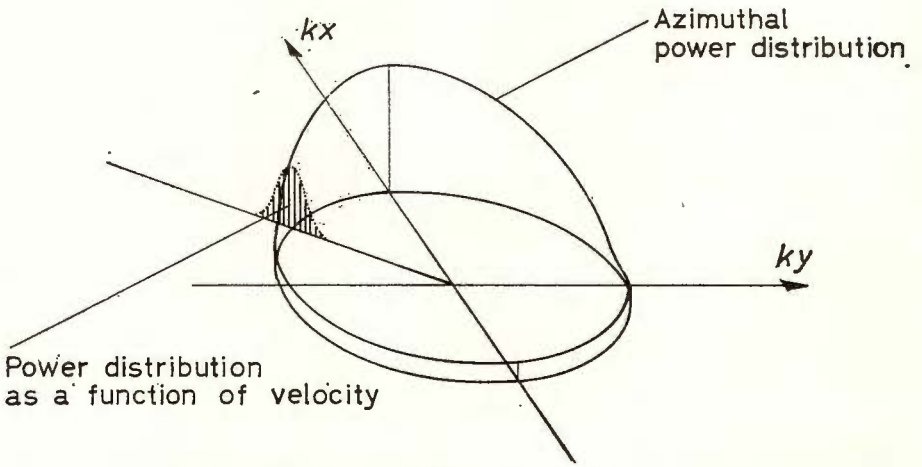

Fig. 1. — The theoretical Noise Model.

peculiar observations such as variation of coherence with direction (R y g g et al.)[2]. With these restrictions in mind we define the model as follows : The theoretical noise field consists of a number of plane, uncorrelated wavetrains approaching from all azimuths and distributed over a certain velocity range (fig. 1). Each wavetrain is assumed to have a flat spectrum inside the frequency band of interest for our computations (white noise), and the power density is distributed with varying strenght along the periphery.

The reason for chosing this model instead of disc noise sources or a combination of disc noise and fixed velocity arc noise is that we have experienced that this model is a good approximation to the experimentally estimated noise field (B u n g u m et al., 1971). In the model we have also allowed for some power variation associated with varying velocity, thus taking into account energy connected with different modes of propagation. On evaluating the theoretical coherence function for this model we follow the lines of M u r d o c k and P f l u k e (1970) : The periphery is divided into K discrete directions. From each direction we assume that L discrete wavetrains propagate with different velocities, carrying diffe-

[2] R y g g E., B u n g u m H., B r u l a n d L. Spectral Analysis and Statistical Properties of Microseisms at NORSAR. 1969. Sci. Rep., No.1, University of Bergen, Norway.

rent amounts of power. The total number of wavetrains reaching a sensor is then K, L. The output in the transform domain is :

$$S(f) = \sum_{k=1}^{K} \sum_{l=1}^{L} A_{k,l}(f) \cdot H_{k,l}(f)$$

Here $A_{k,l}$ is the Fourier transform at a spatial reference point of the wavetrain with direction index k and velocity index l. $H_{k,l}(f)$ is a transfer function expressing the effect of the medium from the reference point to the sensor. (We assume the instruments to be identical).

The cross-spectrum between two sensors (1 and 2) is then :

$$P_{12}(f) = \overline{S_1(f)} \cdot S_2(f) = \sum_{k=1}^{K} \sum_{l=1}^{L} \sum_{m=1}^{K} \sum_{n=1}^{L} \overline{A_{k,l}(f)} \cdot A_{m,n}(f) \cdot \overline{H_{1,k,l}(f)} \cdot H_{2,m,n}(f)$$

The bars represent complex conjugates. Now, since the wavetrains are mutually uncorrelated :

$$E\{\overline{A_{k,l}(f)} \cdot A_{m,n}(f)\} = PW_{k,l}(f), \text{ when } m = k \text{ and } n = l$$
$$= 0 \text{ otherwise.}$$

Here, $PW_{k,l}(f)$ is the (auto)-power spectrum of the wavetrain coming from the k'th direction and propagating with the velocity which is tied 1, to velocity index l.

If we neglect attenuation and dispersion across the site, the transfer functions $H_{k,l}(f)$ represent merely phase delays. Thus, if $t_{1,k,l}$ is the time required for a specific wavetrain to pass from the reference point to sensor the associated transfer function can be written :

$$H_{1,k,l}(f) = e^{-i\omega t_{1,k,l}} \quad (\omega = 2\pi f)$$

Then we have :

$$\overline{H_{1,k,l}(f)} \cdot H_{2,k,l}(f) = e^{i\omega t_{1,k,l}} \cdot e^{-i\omega t_{2,k,l}} = e^{-i\omega(t_{2,k,l} - t_{1,k,l})}$$

$$P_{12}(f) = \sum_{k=1}^{K} \sum_{l=1}^{L} PW_{k,l}(f)\ e^{-i\omega \Delta t_{k,l}}$$

$$P_{21}(f) = \sum_{k=1}^{K} \sum_{l=1}^{L} PW_{k,l}(f)\ e^{i\omega \Delta t_{k,l}}$$

Here $\Delta t_{k,l} = t_{2,k,l} - t_{1,k,l}$ is the time required for the wavefront with the direction index k and velocity index l to pass from sensor 1 to sensor 2 The expression for the coherence is

$\gamma = \left(\dfrac{P_{12}(f)\ P_{21}(f)}{P_{11}(f)\ P_{22}(f)} \right)^{1/2}$, and according to this formula and the foregoing

the coherence estimate will be

$$\left\{ \frac{\sum_{k=1}^{K} \sum_{l=1}^{L} \sum_{m=1}^{K} \sum_{n=1}^{L} PW_{k,l}(f)\ PW_{m,n}(f)\ \cos\omega\ (\Delta t_{k,l} - \Delta t_{m,n})}{\sum_{k=1}^{K} \sum_{l=1}^{L} \sum_{m=1}^{K} \sum_{n=1}^{L} PW_{k,l}(f)\ PW_{m,n}(f)} \right\}^{1/2}$$

DATA AND RESULTS

In the following we shall compare some of the theoretically computed coherence curves with coherence estimates of real data collected at Oyer subarray (fig. 2). The theoretical, continuous noise field has been approxi-

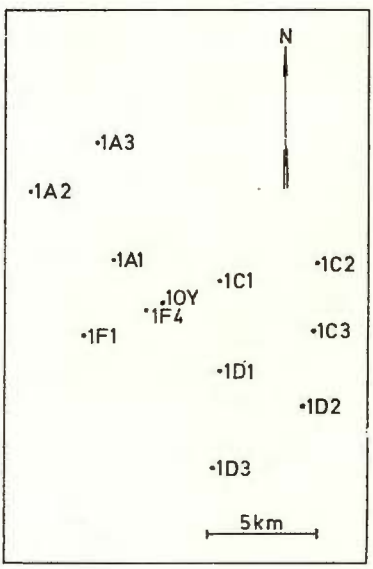

Fig. 2. — Oyer Subarray.

mated by 35 discrete azimuth directions and 7 individual wavetrains associated with each direction. The power densities of the wavetrains decrease exponentially from a maximum value at a velocity of 3.3. km/2s. The total velocity span is 3.0 —3.6 km/s (fig. 1). The cross and auto spectral power estimates of the real data have been obtained by averaging over 50 nonoverlapping blocks, each of 51.2 s. Thus each estimate covers 42 2/3 min of recording starting at the times given on the figures. The sampling interval was 0.05 s.

Figure 3 shows a weather map for May 18, 1968. Meteorologically this is a very quiet day, and by experience we do not expect a very anisotropic noise field due to Atlantic or coastal sources under such conditions. An assumed power distribution at Oyer is shown on top of figure 4. Even if we assume that the noise field has a maximum in one direction, there

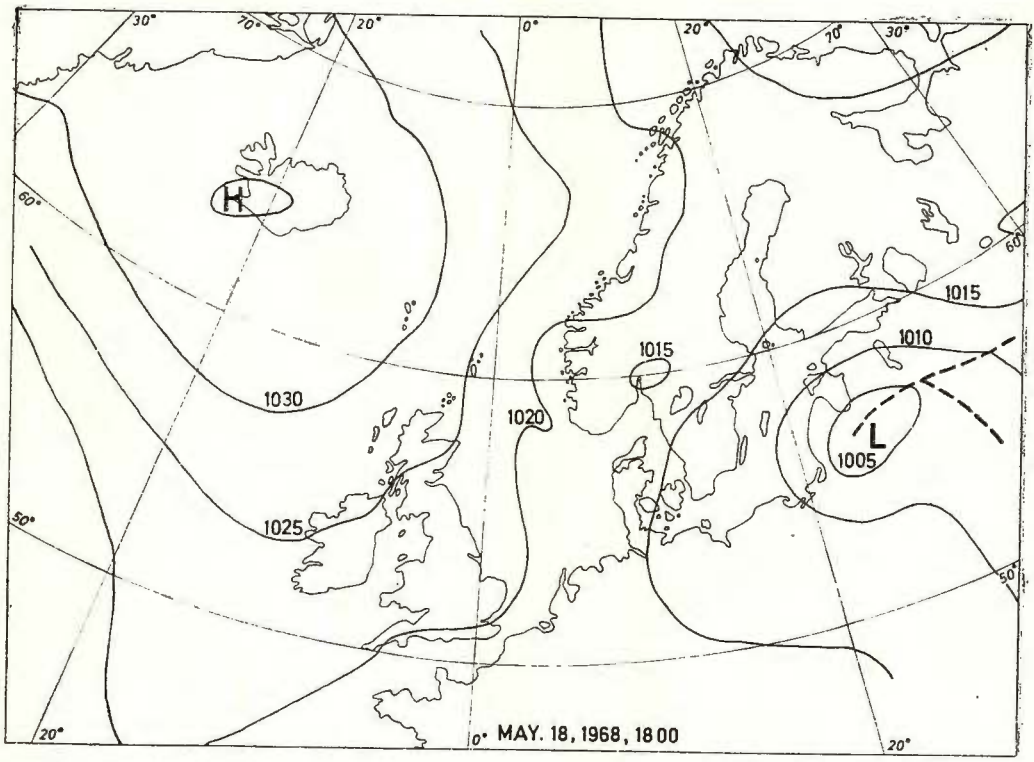

Fig. 3. — Weather Map May 18, 1968.

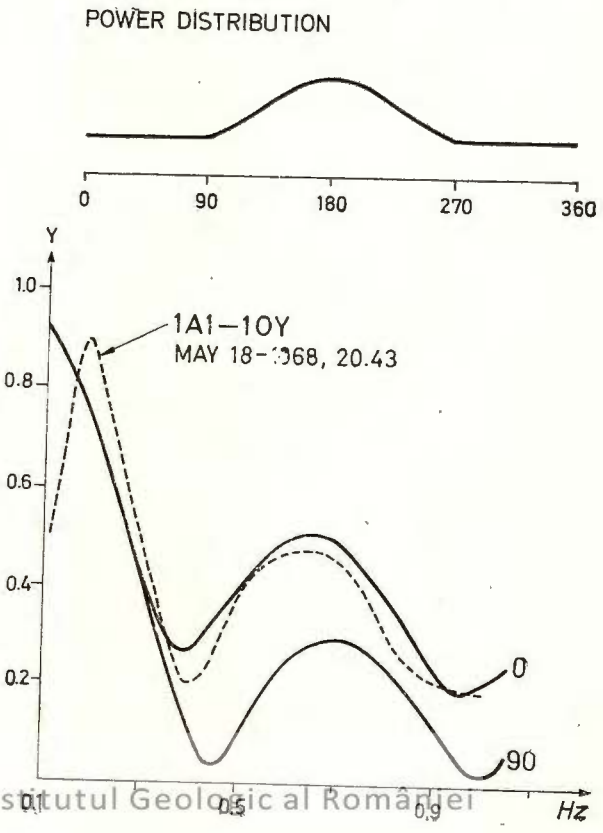

Fig. 4. — Comparison between theoretical coherence curves (solid lines) and a real coherence estimate (dotted line). The theoretical curves have been calculated using the azimuthal power distribution shown on top. 0 refers to the curve calculated for a sensor combination pointing towards the maximum noise power, while 90 refers to a sensor combination at 90 degrees to this direction. In both cases the sensor separations was 3 km.

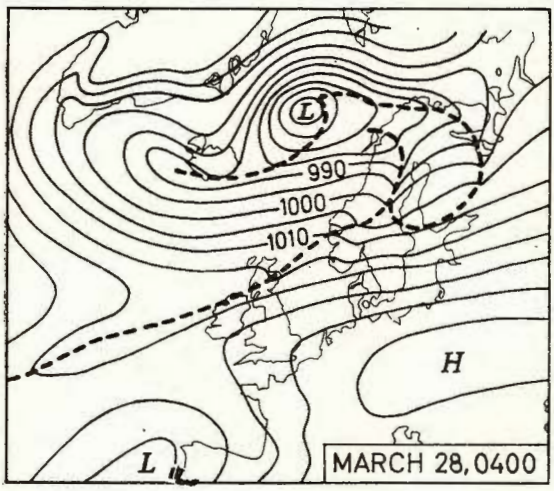

Fig. 5. — Weather Map March, 28, 1968.

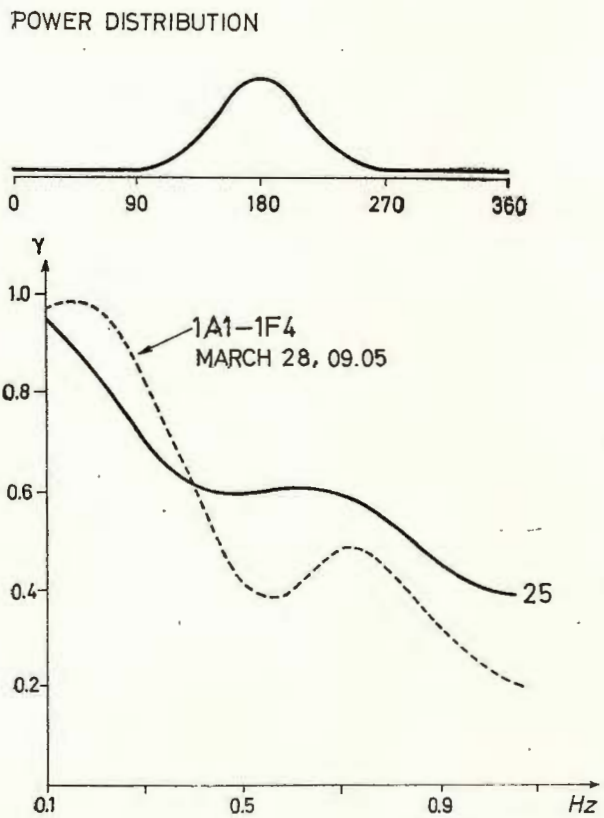

Fig. 6. — A real coherence estimate (1A1—1F4), and a theoretical curve (solid line). The theoretical curve gives the coherence between two sensors 2.8 km apart and whose connection line is inclined 25 degrees relative to the maximum noise power direction.

is no reason to believe that there is a minimum in the opposite direction. Therefore we propose isotropic condition around the opposite half periphery. As we see there is a very good fit between the experimental data for 1A1 — 10Y and the theoretical curve calculated for a sensor combination pointing towards the maximum noise power. The result is a support

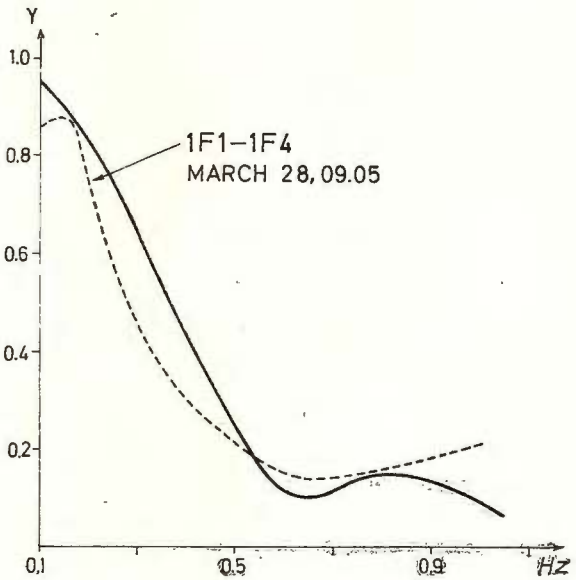

Fig. 7. — The coherence estimate between 1F1 an 1F4 compared with a theoretical curve for two sensors 2.8 km apart and making an angle of 80 degrees with the direction of maximum noise power. The power distribution is the same as in figure 6.

for the noise model proposed, and if we use this model it should be located with its maximum in a north-west direction.

In the following we present examples of a more anisotropic model, and for comparison we have selected coherence estimates made on a day with dominating Atlantic and coastal noise sources (fig. 5). In the upper part of figure 6 is given a proposed power distribution for the weather situation shown in figure 5. The coherence curves of figures 6 and 7 demonstrate the general increase in coherence compared to the more isotropic situation. This is particularly pronounced when the sensor pair is oriented towards the maximum noise power. If we look at a sensor combination abreast of the maximum noise concentration (fig. 7), the coherence drops rapidly from a high start value.

One may object that the fit between the real estimates and the theoretical curves in figure 6 and 7 is not very good. We feel therefore it should be pointed out that there has been made no attempt to get a better fit by for instance varying details in the parameters. This has several reasons : The noise fields are estimated the indirect way — through the coherence, and for computational reasons the power fields were defined using assumptions which are not valid in general (e.g. whiteness). Further-

more, finer details in the noise field structure can not be explored when one is using only two or three space sampling points.

CONCLUSION

In this paper we have used a most commonly measured parameter — the coherence — to estimate the noise power distribution. The procedure applied only allowed the corroboration of noise models which were crude approximations to the actual noise fields.

In the way suggested the noise field can be roughly estimated even if the number of space sampling points is small (2—3), and one gets a direct measure of the noise anisotropy.

REFERENCES

Bungum H., Rygg E., Bruland L. (1971) Short Period Seismic Noise Structure at the Norwegian Seismic Array. *Bull. Seism.Soc. Am.*, 61, 2, Berkeley.

Murdock J. N., Pfluke J. H. (1970) NORSAR Microseisms. *Essa Technical Report* ERL 176-ESL 9, Earth Sciences Laboratories, Boulder, Colorado.

GEOTHERMAL FIELD INFLUENCE ON MICROSEISMS PARAMETERS

BY

A.P. SINITSYN [1]

STATEMENT OF PROBLEM

Microseisms propagation conditions were studied in detail in scientific works by Savarensky (1959), Tabulevich (1960), Proskuriakova (1970), Bernard (1971), Tillotson (1971) and others. There was pointed out, that the mechanism of microseisms propagation is very sensitive to the change of physical conditions of the upper layers of the Earth crust including the change of geothermal field. Let us study the influence of temperature field of the parameters of longitudinal waves in conditions of one-dimensional problem. In this case the differential equations of motion for the displacements should be as following (Sinitsyn, 1971):

$$\frac{1}{C^2}\frac{\partial^2 u}{\partial t^2} = \frac{\partial^2 u}{\partial x^2} - \alpha \frac{\partial T}{\partial x} \tag{1}$$

$$\rho c_\varepsilon [1 + 2\varepsilon(1 - \nu)] \frac{\partial T}{\partial t} + \alpha T_0 E \frac{\partial^2 u}{\partial x \partial t} = \lambda \frac{\partial^2 T}{\partial x^2} \tag{2}$$

There are:
u — displacements of the particles in wave P; $T(x, t)$ — temperature function; α — coefficient of expansion; c — waves' velocity; ρ — density; c_ε —specific heat rate; E—elasticity modul; λ—heat transfer rate; ν—Poisson rate; T_0—initial temperature. In formula (2) there is parameter ε by which the coherency between equations (1) and (2) is establi shed. The value of parameter ε is calculated by formula:

$$\varepsilon = \frac{\alpha T_0}{\rho^2 C_\varepsilon K_T^2 v_p^2} \tag{3}$$

[1] Council for Seismology and Earthquake Engineering, B. Grouzinskaya 10, Moscow 123810, USSR.

$$K_T^2 = 3(1 - 2\nu)/E \tag{4}$$

$$v_p^2 = \frac{E}{\rho} \frac{(1 - \nu)}{(1 + \nu)(1 - 2\nu)} \tag{5}$$

To solve the equations (1) and (2) we shall make the following substitution :

$$u = u_d + u_s \tag{6}$$

u — total displacement ; u_d — displacement due to inertia forces ; U_s — displacement due to temperature. To determine u_s the equation (1) is used ; it should be simplified and then we have :

$$\frac{\partial^2 u_s}{\partial x^2} - \alpha \frac{\partial T}{\partial x} = 0 \tag{7}$$

Now we integrate the equation (7) by „x" and obtain :

$$\frac{\partial u_s}{\partial x} = \alpha T \tag{8}$$

Then we differentiate the equation (8) in respect with „t" and substitute the result in equation (2) :

$$\rho c_\varepsilon [1 + 2\varepsilon (1 - \nu)] \frac{\partial T}{\partial t} + \alpha T_0 E \alpha \frac{\partial T}{\partial t} = \lambda \frac{\partial^2 T}{\partial x^2} \tag{9}$$

The equations (1) and (2) are separated now for U_s we obtain the usual solution from the equation (7).

DEERMINATION OF LONGITUDINAL WAVES'VELOCITY

To determine the dynamic part of the displacement which corresponds to the waves propagation process we shall study the linear alteration of the temperature field in coordinate „x" domain, now the second derivative $\frac{\partial^2 T}{\partial x^2} = 0$ and the equation (2) should be homogeneous. The integration of this equation by „t" gives :

$$\rho c_\varepsilon [1 + 2\varepsilon (1 - \nu)] T + \alpha T_0 E \frac{\partial u}{\partial x} = 0$$

The differentiation of this equation by „x" gives :

$$\rho c_\varepsilon [1 + 2\varepsilon (1 - \nu)] \frac{\partial T}{\partial x} + \alpha T_0 E \frac{\partial^2 u}{\partial x^2} = 0 \tag{10}$$

From the equation (10) $\frac{\partial T}{\partial x}$ is obtained and substituting it in equation (1) after transformation we have :

$$\frac{1}{(c')^2} \frac{\partial^2 u_d}{\partial t^2} = \frac{\partial^2 u_d}{\partial x^2} \tag{11}$$

c' is the modificated velocity of longitudinal seismic wave in the presence of temperature field. This velocity is connected with the usual velocity „C" of longitudinal waves by the following formula :

$$(c')^2 = \left[1 + \frac{\varepsilon\ (1 - \nu)\ (1 - 2\nu)}{(1 + \nu)\ [1 + 2\varepsilon\ (1 - \nu)]} \right] C^2 = \eta\ C^2 \tag{12}$$

From formula (12) it is clear that in the presence of temperature field the velocity of longitudinal waves changes its value, and depends

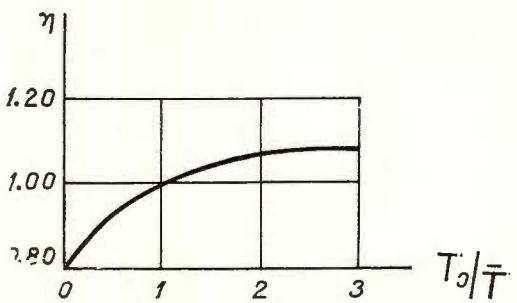

Fig. 1. — The diagram of velocity coefficient.

on the value ε which is proportional to the initial temperature according to the formula (4). The alteration of coefficient η as a function of T_0 is shown in figure 1.

AMPLITUDE DETERMINATION

The estimation of the influence of temperature field on the alteration of amplitudes of longitudinal waves let us study the case when :

$$T(x, t) = T_0\, te^{-bx} \tag{13}$$

Now the solution of equation (11) is :

$$u_d = Ae^{-b\,(x - c't)} + Be^{-b\,(x + c't)} \tag{14}$$

But providing $t = 0$; $u_d = 0$, $A = -B$ and

$$u_d = A\ [e^{-b(x - c't)} - e^{-b(x - c't)}\ ] \tag{15}$$

using the second initial condition : providing $t = 0$; $\frac{du}{dt} = 0$ we obtain the amplitude :

$$A = \frac{\alpha T_0}{2b^2 c'} \tag{16}$$

From this formula it is clear that the displacements' amplitude due to temperature field is inversely proportional to the waves' velocity. If the velocity increases the amplitude should decrease and the amplitude rate is equal to :

$$A/A_0 = \frac{c}{c'} = \sqrt{\frac{1}{\eta}} \tag{17}$$

To determine a total displacement of particles in a seismic wave it is necessary to evaluate the displacements due to the temperature. Using the equation (8) we shall substitute the value $T(x, t)$ from formula (13) and become :

$$\frac{\partial u_s}{\partial x} = \alpha T\ (x, t) = \alpha\ T_0 t\, e^{-bx} \tag{18}$$

After integration of this equation by "x" we obtain :

$$u_s = -\ \alpha\ T_0 t \frac{e^{-bx}}{b} \tag{19}$$

The value A from formula (16) is substituted in formula (15) and adding u_s from formula (19) we obtain when $x > c't$

$$u = \alpha\ \ T_0\, e^{-bx}\left[\frac{sh\,(b\,c't)}{b^2\,c'} - \frac{t}{b}\right] \tag{20}$$

The following conclusion may be made : in the presence of the temperature field there is a decrease of displacements. The stresses in the wave with consideration of the temperature field should be calculated by formula :

$$\sigma = E\left[\frac{\partial u}{\partial x} - \alpha\ T\ (x,\ t)\right] \tag{21}$$

Making necessary substitutions we obtain :

$$\sigma = -\frac{ET_0\alpha}{bc'}\left\{\begin{matrix} e^{-bc't}\ sh\,(b\,x) \\ e^{-bx}\ sh\,(b\,c't) \end{matrix}\right\}\begin{matrix} x < c't \\ x > c't \end{matrix} \tag{22}$$

The amplitude of stresses should be calculated when $x = c't$

$$\sigma_{max} = -\frac{E\,\alpha T_0}{2\,bc'}\left(1 - \frac{1}{e^{2bc't}}\right) \tag{23}$$

The stress waves have a characteristic configuration as it is clear from the equations (22) and (23), this is due to the influence of temperature field. The scheme of stress wave propagation from the free surface is shown in figure 2.

DISCUSSION OF RESULTS

The investigations carried out in recent years, as it is shown by professor Bernard (1971), pointed out that in microseisms there are *P*-waves too, and that the microseisms sometimes have small amplitudes when according to synoptic map these amplitudes should be high (Tillotson, 1971) and vice versa. These contradictions indicate that the study of those physical conditions under which the recording of microseisms are fulfilled must be done more accurate. The formulae obtained in this paper show that the geothermal state and the temperature of the environment may considerably effect the velocity of wave propagation and the amplitudes of microseisms. As it is known, the study of geothermal field influence on longitudinal waves propagation velocities in lower layer of the upper mantle attract the attention of the seismologists long ago. The results obtained in this domain (Jacob, 1971) show that it is necessary to evaluate the influence of the geothermal field. While the investigation of microseisms this problem must be studied more precisely, particularly, while determining the microseisms parameters the attention should be payed to the state of temperature field under condition of which the microseisms propagate. It is essential to point out that the temperature field may effect also the vertical component of the surface waves although this problem requires further investigations. It is noteworthy, the theoretical results should be checked by experimental data.

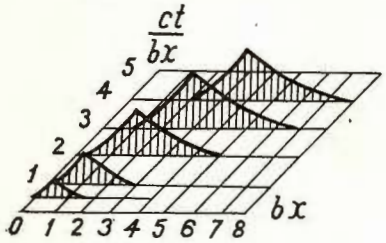

Fig. 2. — The diagram of stress wave propagation.

REFERENCES

Bernard P. (1971) Results du symposium International sur les Microseismes". *Proc. XII gen. Ass. CSE*, Luxemburg.

Jacob K.H. (1971) Residuals, the Thermal State of Lithosphere. *In*: Symposium on State of substance in the Earth Mantle, IASPEI, Moscow.

Proskuriakova T. A. et al. (1970) On side Refraction of surface seismic waves. *Proc. X gen. Ass. CSE*, Moscow.

Savarensky E. F. (1959) Elementary theory of layer influence on Earth Surface vibrations. *Ser. geophys.*, 10, Nauka, Moscow.

Sinitsyn A.P. (1971) Design of structures on Thermal Shock. Strojisdat, Moscow.

Tillotson E. (1971) Some Aspects of some Microseisms Affecting the U.K. *Proc. XII gen. Ass. CSE*, Luxemburg.

Tabulevich V.N. (1970) Propagation of global microseisms. *Proc. X gen. Ass. CSE*, Moscow.

ON THE POWER AND ENERGY OF SOURCES OF EXCITATION OF MICROSEISMS

BY

V.N. TABULEVICH[1]

Due to the experience of modern seismology the urgent need for a parameter has arosen, which would permit the comparison of the intensities of various seismic processes (earthquakes, explosions, microseisms) eliminating such variable quantities as, for instance, distance, dispersion and others. As an adequate parameter the energy of elastic vibrations in the source was proposed. Originally it was introduced 1911 (1960) by B. B. Golytsyn in an analysis of the Sarez earthquake.

A transfer of the procedures of determination of seismic energy into the field of microseismic vibration would be rather promising, as it would permit a comparison of the intensities of the sources of excitation of microseisms, atmospheric disturbances (cyclones, typhoons), wave patterns, infrasound, which would develop under conditions given on various aquatories (lakes, seas, oceans), on various latitudes, in various seasons etc. However, the basic differences between earthquakes, explosions and sources of microseismic excitation are to be kept in mind. Earthquakes are impulsive phenomena and the introduction of the term „energy" occurs for them quite naturally, whereas the term „power" is meaningless.

Microseisms are quasistationary or semiperiodic phenomena. Here the concept of "power" is easily applicable. As microseismic storms last sometimes for a several days, the conversion factor between power and energy may sometimes reach 10^6. For stationary periodic processes the therm "energy" can not characterize the intensity of the source of excitation of microseisms at a time instant given. A comparison of microseismic sources by their energies can provide one and the same values for quite different processes, for instance, for a weak long acting source, and a short one, but with great intensities.

Procedures of determination of absolute energy values developed during earthquakes at present encounter some difficulties, as for instance, the account of residual deformations, which are impossible or difficult to

[1] Politehniceskii Institut, Irkutsk, USSR.

eliminate. On the other hand, the energy of elastic body and surface waves of earthquakes can be principally determined separately.

In the case of microseisms we have a simpler process of energy transfer than the stress relaxation during earthquakes. It can be shown that microseismic vibrations in the source cause elastic waves only. The maximum values of bottom pressure may be estimated as $5 \cdot 10^5$ mkbar or 500 g/cm^3. These values are substantially below the thresholds of elasticity for all substances forming the sea bottom. On the other hand, in the case of microseisms the summary vibration is recorded, the conception of a radiation angle becomes meaningless. Therefore, the deduction of the correspondent relation has to be begun from basic principles.

The Umov-Poynting vector $\bar{p}$ characterizes the energy transmitted though a unit surface in a time unit (density of power). To obtain the whole energy developed inside a close volume during the time interval t we must summarize with respect to surface and time:

$$E = \int_t \oint_s \bar{p} \, d s \, d t.$$

As we shall assume the microseisms to be a stationary process, the time integration can be omitted and the power will be:

$$W = \frac{d E}{d t} = \int_s \bar{p} \, d s.$$

Generally $p = p(x, y, z)$. Vibrations measured at the surface are not representative for a certain wave front. For example, processes of refraction inside the surface from hidden obstacles can lead to the fact that it becomes impossible to draw a wave front i.e. a surface through which a similar vibration sequence should follow. This is accounted for by C a r d e r et al. (1962) by means of a factor Q, giving, as the authors believe, account of energy dissipation during refraction. It is known, however, that during refraction no energy dissipation takes place and Q, is to be regarded as an empyric factor, correcting computed values.

In our work (1964) is was shown, that microseisms, similar to elastic earthquake waves, are composed of body and surface waves. The law of the amplitude decrease is given by

$$A = a r^{-2} + b r^{-1/2}.$$

It was shown that $a/b = (1 \cdot 5 + 3 \cdot 0) \cdot 10^4$ provides an optimal fit to observe values.

The isoamplitude surface (wave front) for surface waves is a cylinder. If for body waves the dependence $1/r$ could be accepted, the wave front would be spherical. In the case of the amplitude decrease of the body waves proportional to $1/r^2$ (S a v a r e n s k y, 1955) the shape of the isoamplitude surface should vary in time, because there does not exist a simple geometric image, the surface of which varies as $1/r^4$. For an approximate

approach to the problem consider that if at the Earth surface (the boundary) the amplitude varies as $1/r^2$, then the rate of variation in the directions perpendicular to the horizontal plane should be lower. The shape of the isoamplitude surface is schematically shown on figure 1a. We represent this surface by means of an equivalent cylinder of equal surface

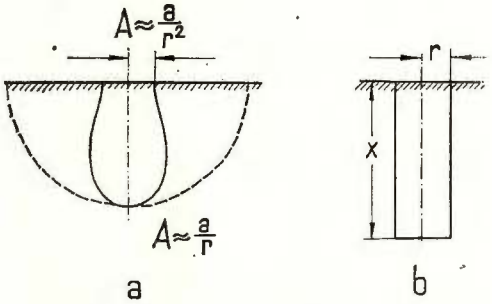

Fig. 1. — Isoamplitude surface of body waves.
a, schematic shape of the isoamplitudine surface; *b*, equivalent isoamplitudine surface.

(fig. 1b). Computing the sizes of the equivalent cylinder from considerations of the constance of the power flow of the body waves :

$$W = |\bar{p}|\, S = 2\pi^2 \rho_B C_B (\pi r^2 + 2\pi r x) \frac{A_B^2}{T_B^2}$$

Assuming $x \gg r$,

$$x \approx \frac{W_B T_B^2}{4\pi^3 \rho_B C_B A_B^2 r}$$

(we neglect the radiation through the bottom of the cylinder). At $r = 0$ the amplitude should become infinite. To eliminate this alogism we assume that the amplitude in the source of microseismic excitation is determined by a definite dimension of the source r_0. Then $\frac{W_B}{|\bar{p}|} = \frac{2\pi}{r_o^2} r^4$

It follows $x = \frac{r^3}{r_o^2}$

Generally

$$W_B = 2\pi^2 \frac{A_B^2}{T^2} \rho_B C_B \, 2\pi r x = \gamma' \frac{A_B^2}{T^2} r^4$$

Here

$$\gamma' = \frac{4\pi^3}{r_o^2} \rho_B C_B$$

On the other hand for the surface waves the relation is valid :

$$W_S = 4\pi^3 \frac{A_S^2}{T_S^2} \rho_S C_S \lambda r = \varepsilon' \frac{A_S^2}{T_S} r$$

Here

$$\varepsilon' = 4\pi^3 \rho_S C_S^2$$

The bulk power of the source will be equal to the sum of the powers of body and surface waves :

$$W = W_B + W_S = \gamma' \frac{A_B^2}{T^2} r^4 + \varepsilon' \frac{A_S^2}{T} r$$

or

$$W = A_S^2 \left[\varepsilon r + \left(\frac{A_B}{A_S} \right)^2 \gamma r^4 \right] = A_S^2 r \left[\varepsilon + \left(\frac{a}{b} \right)^2 \gamma \right]$$

Here a/b are taken from our initial relation

$$\varepsilon = \frac{\varepsilon'}{T} = \frac{4\pi^3 \rho_S C_S}{T} \quad \text{and} \quad \gamma = \frac{\gamma'}{T^2} = \frac{4\pi^3 \rho_B C_B}{r_o^2 T^2}$$

Hence the expression in the brackets depends on the period only and does not depend on distance.

The value of A_S is unknown from seismograms, since the summary amplitude of all kinds of seismic waves is recorded, which can not be subdivided without complementary theoretic constructions.

The bulk amplitude of microseisms equals to the sum of amplitudes of body and surface waves :

$$A = A_B + A_S = A_S \left(1 + \frac{A_B}{A_S} \right)$$

and

$$A_S = \frac{A}{1 + \frac{A_B}{A_S}} = \frac{A}{1 + \frac{a}{b} r^{-1,5}}$$

Substituting we obtain :

$$W = \left(\frac{A}{1 + \frac{a}{b} r^{-1,5}} \right)^2 \left[\varepsilon + \left(\frac{a}{b} \right)^2 \gamma \right].$$

In our developments we have not accounted for damping of microseismic vibrations (the waste of energy for irreversible processes). Our wave front is in a strict sense not exactly a locus of equidistant points from the source, nevertheless we shall ascribe the value e^{kr} conventionally to the parameter r to obtain finally :

$$W = \left(\frac{A}{1 + \frac{a}{b} r^{-1,5}} \right)^2 \left[\varepsilon + \left(\frac{a}{b} \right)^2 \gamma \right] e^{kr}$$

In estimates of energies of earthquakes it is convenient to use not absolute values, but rather to relate them to a reference value, arbitrally chosen. The dependence of the amplitude of the vibration of such a source from distance at a definite period is referred to as a calibration curve.

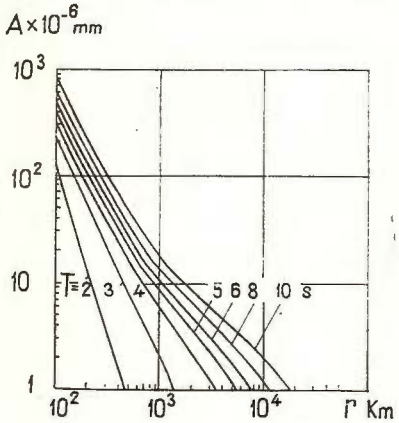

Fig. 2. — Calibration curves for a source of microseismic vibrations with a power 10^{12} erg.s^{-1} and periods of vibration from 2 to 10 s.

We introduce a similar conception. Taking a minimum reference power level 10^{12} erg/s^{-1} and the source radius $r_0 = 100$ km, we obtain the calibration curves given in figure 2. In introducing the calculation formulae we involve the same considerations as in the deduction of the relations for the energies and amplitudes of earthquakes, namely

$$\log W = \log W_o + 2\,(\log a - \log a_o)$$

$$\log W = 12 + 2(\log a - \log a_o),$$

here a is the amplitude of the microseisms, measured at a distance r and a_o is the amplitude of microseisms obtained from the calibration curve (fig. 2).

Analogous to earthquakes the conception of the magnitudes of microseisms can be introduced :

$$2\,M = \log\ W - 12.$$

Now consider some examples of microseismic storms. We have selected cases of microseismic storms stipulated by powerful oceanic cyclones, less powerful events on aquatories of limited dimensions (Okhotskoye and Caspian seas) and finally have considered microseisms on smaller aquatories, as the lake Baikal. In table 1 the results of the determination of the power on various stations.

It should be noted that the power of the vibrations in the source, as computed on hand of the records of various stations, located at different distance nearly does not vary. Hence the power is actually invariant from absolute values of amplitudes and distances, which is in full concordance to the physical meaning of the physical parameter introduced.

TABLE 1

Power of sources of excitation of microseisms

Station	Distance km	Amplitude A mmk	Period T s	Power erg/s^{-1}	
				individual station	average
			Atlantic ocean		
Plk	1 890	3 500	8.6	$10^{17.4}$	
Apt	1 940	2 800	8.0	$10^{17.3}$	
Kshn	2 800	1 400	9.0	$10^{16.9}$	$10^{17.2}$
Sv	3 550	2 000	9.0	$10^{17.3}$	
And	5 400	500	9.0	$10^{17.0}$	
			Caspian Sea		
Mk	100	9 000	3.5	10^{15}	
Bk	320	2 000	3.4	$10^{15.7}$	$10^{15.5}$
K—A	600	600	3.2	$10^{15.8}$	
			Okhotskoye Sea		
P—K	650	2 000	4.5	$10^{16.3}$	
Mgd	200	2 000	5.0	$10^{14.6}$	$10^{15.4}$
Tx	2 000	200	5.0	$10^{15.4}$	
			Indian ocean		
Perth	3 000	5 500	8	$10^{18.2}$	
Irk	11 000	700	8	$10^{17.9}$	10^{18}
			Baikal lake		
Kb	50	3 000	2.8	10^{13}	
Zak	200	40	2.8	$10^{11.9}$	$10^{12.5}$
Arsh	150	100	2.5	10^{12}	
Kyakhta	200	110	2.5	10^{13}	

The introduction of the magnitudes allows to draw a parallel between earthquakes characterized by energies and microseisms, characterized by power.

From comparison of our data it follows that oceanic microseisms phenomena are characterized by a power $10^{17} - 10^{18}$ erg/s and a magnitude 3. Sea microseisms — by a power 10^{15} and $M = 2$ and lake microseisms have $W = 10^{12.5}$ and $M = 0 - 0.5$. We determine the energy transmitted to the Earth during the duration of the microseismic storm. So the energy transmitted to the Earth by a cyclone in the Indian ocean from 12.00 h 20.IX till 00 h 23.IX equals $2 \cdot 10^{23}$ erg. In the Okhotskian sea from 00 h. 29.X till 00 h. 30.X $E = 10^{20}$ erg. On the Baikal lake $E = 10^{17}$ erg.

The introduced conception of power of microseisms closely correlates with alternative hydrometeorological and atmospheric estimates of the energy and destructive power of spontanous processes.

REFERENCES

Carder D. S., Cloud U. C. (1962) Ground vibrations during underground explosions *In*: Underground Nuclear Explosions (in Russian). Moscow.

Savarensky E. F., Kirnos D. P. (1955) Elements of seismology and seismometry (in Russian). Moscow.

Tabulevich V. N. (1964) On the composition of microseismic vibrations. *VII Tagung ESK*, Jena.

ON THE SIMILARITY OF GENERALIZED AMPLITUDES OF MICROSEISMS

BY

ALOIS ZÁTOPEK[1]

INTRODUCTION

It is well known that in many cases of microseismic storms the course of the amplitudes has a similar shape at many stations. The present contribution is not concerned with such individual similarities; it is devoted to the striking similarities found in the course of smoothed generalized amplitudes, derived by an adjustment described below, from the long-term observation of meteorological microseisms. in the period range 3—10 seconds. The observations are related to 18 selected European and 7 Japanese stations and have been made through the period of the International Geophysical Year (IGY) 1957—1958 (Zátopek, 1961; Nat. Comm. IGY, Japan, 1959; 1960). The similarity we are interested in, regards the general march of the smoothed amplitude curves, representing the general tendencies of variations of the microseismic "activity" with the time during the period considered. As the term "period" has a double meaning here, we will use expressions like "active period", "period of activity", "active interval" etc. in order to avoid the misinterpretation with regard to the period of vibrations of the ground. For the European microseisms the long-term similarities of smoothed amplitude curves, i.e. statistically simultaneous occurrence of increasing and decreasing amplitudes with equal variation tendencies in time, the in general similar shape of the smoothed amplitude curves with the relative extrema, appearing, in the limits of the accuracy of the method, at the same time, have been dealt with in several previous papers, and so the relationship between the smoothed amplitude curves and the smoothed curve of a meteorological index (Zátopek, Zikmunda, 1960), derived for the north-atlantic frontal zone and roughly proportional to the W—E component of the geostrophic wind in the 500-millibar level. A similar procedure was applied to the microseisms recorded during the IGY in

[1] Institute of Geophysics, Charles University, Ke Karlovu 3, Praha 2, Czechoslovakia.

7 selected stations situated in various parts throughout Japan (Z á t o p e k, 1970, fig. 1). Apart from the mutual similarity of the smoothed amplitude curves which has been found down to the latitudes less than 35°N, it was stated that the shape of these curves was fairly comparable with that of the curves derived earlier for the European IGY microseisms (Z á t o p e k, 1963). This seems to be a confirmation of the idea of

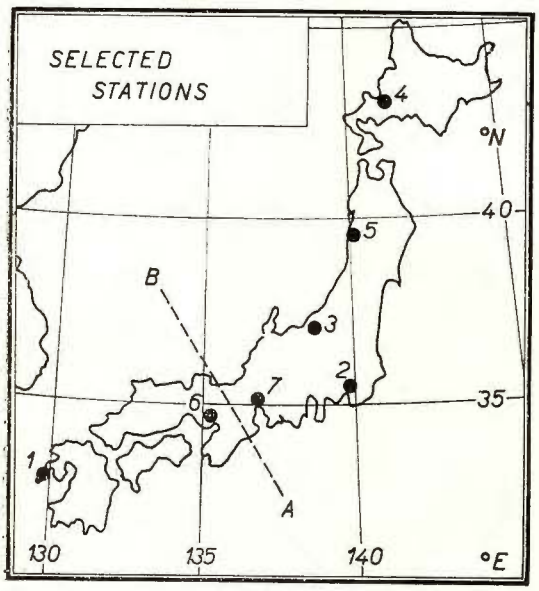

Fig. 1. — Map of selected stations in Japan. A-B line of deep-focus earthquakes crossing Japan.

the existence of a uniform large-scale mechanism, operating at the northern polar front; this mechanism is considered responsible for the large-scale phenomena of atmospheric circulation, including the microseisms.

GENERALIZED AMPLITUDES

To obtain the generalized amplitudes a suitable smoothing procedure or adjustment is necessary so that in the numerical or graphical representation the individual storms disappear, but characteristic variations of, say, one-month duration or longer are made recognizable within the whole time interval studied (Z á t o p e k, Z i k m u n d a, 1960), which, may be one year, several years, one cycle of solar activity etc. (Z á t o p e k, 1963). In our case it is the time interval of the IGY, i.e. from July 1st, 1957, until December 31, 1958.

The curves of generalized amplitudes may be obtained in several ways. The observed values of the microseismic amplitudes represent a set of numbers equidistant in time as they are associated with the main meteorological terms at 0h, 6h, 12h and 18h UT, respectively.

The most suitable methods giving comparably equivalent results are as follows :

a) Differentiation of idealized (= suitably smoothed) cumulative (= summation) curves of amplitudes throughout the whole time interval T in consideration (expressed in days the number of amplitude values involved $N = 4T$). A sequence of values

$$S_k = \sum_{n=1}^{k} A_n, \quad k = 1, 2, \ldots, N \tag{1}$$

defines a non-continuous function $S_k(t)$ of time t in the range $(0, T>$. The adjustment consists in replacing (numerically or graphically) the function $S_k(t)$ by a simple, continuous and smooth [2] function (curve).

$$S(t) = \int_0^t f(t')\, dt' \tag{2}$$

satisfying in $(0, T>$ the conditions

$$| S(t_k) - S_k | \leqq \varepsilon_k, \quad \varepsilon \to 0, \tag{3a}$$

and

$$S(t_N) = \sum_{n=1}^{N} A_n \tag{3b}$$

for a suitable choice of the small values ε_k.

This mathematically rather intricate problem may be practically replaced, as it is usually done by physicists, by an interpolation "by eye", i.e. in tracing a continuous and smooth curve through the set of discrete points $S_k(t)$.

Differentiating numerically or graphically the function $S(t)$ after t, one gets a curve of smoothed "generalized" amplitudes $A(t)$:

$$A(t) = \frac{\mathrm{d}S(t)}{\mathrm{d}t}. \tag{4}$$

This procedure depends, of course, on the choice of $S(t)$, which represents a kind of filtration of the primary set of A_n. This should be a subject of a special study, but is not necessary for our purpose. According to the experience, the arbitrariness is strongly reduced by the requirement of simplicity, concerning the shape of the curve $A(t)$; in fact, only small differences occur among $A(t)$ — curves if derived by trained specialists. The element of subjectivity could be also reduced by dividing the time interval $(0, T>$ into suitable sub-intervals, where e.g. a quadratic or cubic interpolarion would be introduced on a basis of the method

[2] In differential geometry a curve is called "smooth", if it has a tangent at all points, and the angle of inclination of the tangent is a continuous (and in our case also differentiable) function of the arc of the curve.

of least squares with the additional condition that the derivative at the end of each sub-interval be equal to the derivative at the beginning of the following one.

Several variants of the procedure just described have been used with comparatively equal results using the data of the European stations mentioned, as illustrated in figure 2 for five stations situated along a N—S profile through the European continent.

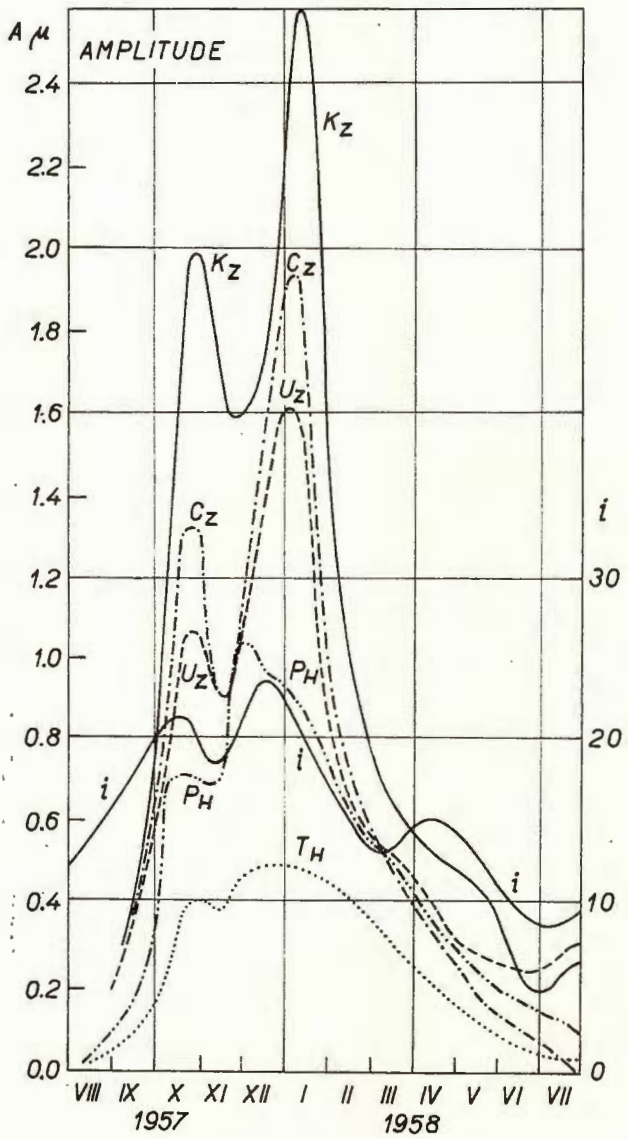

Fig. 2. — Generalized amplitudes of 5 European stations situated along a N—S profile through Europe :

K_Z, vertical component Kiruna; U_Z, vertical component Uppsala; C_Z, vertical component Copenhagen; P_H, horizontal component Prague; T_H, horizontal component Trieste; i, smoothed curve of a meteorological index, roughly proportional to W—E component of geostrophic wind in 500—mb—level for north-atlantic frontal zone (after Zátopek, 1963).

b) Gliding means of the amplitude values, calculated for a statistically suitable sub-interval τ, and gliding along the time axis from 0 to T. The average value $\bar{A}$ of the amplitudes A_k over τ is always attributed to the central point of the actual position of the interval τ. The most appropriate length of τ could be assessed on a theoretical way; in this study it was found empirically, and applied both to the European and Japanese sets of initial values. It is useful to have $T = n \cdot \tau$, where n is an integer, following from the choice of τ, which, itself, contains, say, s values of the amplitudes A_k.

Then, a displacement of the interval τ to the neighbouring point causes a variation $\delta\bar{A}$ of the mean values $\bar{A}_{r+1}$ and $\bar{A}_r$, respectively,

$$\delta\bar{A} = |\bar{A}_{r+1} - \bar{A}_r| = \frac{1}{s}\left|\sum_{k=r+2}^{r+s+1} A_k - \sum_{k=r+1}^{r+s} A_{k'}\right| =$$

$$= \frac{1}{s}|A_{r+s+1} - A_{r+1}| \leqq |\Delta A_{\max}|/s \leqq \frac{1}{s} A_{\max}, \tag{5}$$

where $\Delta A_{\max}$ denotes the maximum difference of amplitudes in $\langle 0, T\rangle$, and $A_{\max}$ the maximum amplitude. If we use, for comparison, the reduced amplitudes for each of the stations considered, i.e. $A_k/A_{\max}$, we get

$$\delta A_{\text{red}} \leqq 1/s \tag{5}$$

as a reduced amplitude variation. For a day this reduced variation is less than $4/s$. Empirically, we have found $\tau \doteq 20$ days. Thus, $\delta A_{\text{red}} \leqq 0.0125$, and, for a day, $\leqq 5\%$.

The basic data of Japan (Nat. Committee IGY, Japan, 1959; 1960) were given in a form of graphs the size of which made the determination of amplitudes at the main meteorological terms very difficult. Therefore, the average amplitudes $\bar{A}_k$ were digitized for all successive time intervals $\tau_0 = 2$ days, and, with $\tau = 20$ days, the method just described was somewhat simplified. Gradual sums $\bar{S}_s(t)$ of $\bar{A}_k^{(\tau)}$ were formed for every successive 20 days; the sums have been attributed to the respective times of 10, 20, ..., 10s, ..., i.e. $(s\tau)/2$ days. Consequently, a sequence of points $\bar{S}_s(t)$ was obtained

$$\bar{S}_s(t) = \sum_{k=1}^{s} \bar{A}_k^{(\tau)} \tag{6}$$

for $t = 10s$ days, $s = 1, 2, \ldots$

Then, an adjustment followed, taking the average

$$\bar{S}'_s(t) = [\bar{S}_{s-1}(t) + 2\,\bar{S}_s(t) + \bar{S}_{s+1}(t)]/4; \tag{7}$$

$$s = 2, 3, \ldots,$$

or, with nearly the same result,

$$\bar{S}'_s(t) = [\bar{S}_{s-1}(t) + \bar{S}_s(t) + S_{s+1}(t)]/3. \tag{7'}$$

The result for the seven selected stations in Japan as plotted in figure 1 is represented in figure 3 ; use is made of the amplitudes reduced to a unit maximum for all selected stations.

COMPARISON OF RESULTS FOR EUROPE AND JAPAN

In figure 2 the curves of generalized amplitudes are represented for five of 18 European stations considered. These five stations are situated along a N—S profile, passing in a length of about 2.500 kms through the European continent. The shape of all 18 generalized amplitude curves was similar: in figure 2 one sees that the curves for Kiruna, Uppsala, Copenhagen, Prague and Trieste exhibit two respective maxima, one in November and another one in December-January. The course of the smoothed curve of the meteorological index "*i*" mentioned above is similar to that of the amplitudes ; the absence of a marked maximum on the amplitude curves in April may be explained by a smaller turbulent interaction between the warmer atmosphere and the oceanic surface, especially in lower latitudes. The decay of amplitudes southwards indicates that the source region was situated in the North.

The summer season activity is negligible in comparison with that occuring during the active period from September to May. But the latter may have, as we have seen, a characteristic structure connected with the character of general circulation in the 500 -mb-level as indicated by the index "i" în figure 2. This structure is remarkable over an area of at least continental dimensions. For Europe all this is related to the circulation in the north-atlantic frontal zone. The effects of minor sources of microseisms are incomparably smaller.

The shape of generalized amplitudes obtained for seven selected Japanese stations the situation of which is plotted in figure 1 (1 = Nagasaki, 2 = Tokyo, 3 = Matsushiro, 4 = Sapporo, 5 = Akita, 6 = Abuyama, 7 = Nagoya) is more complicated than that of the European stations. We may divide them into two groups showing a different behaviour : the stations 2, 3, 4 and 5 are closely related to those of Europe, especially to the northern ones, while 1, 7 and 6 differ greatly from this form. The curves 1 and 7 with high amplitude values due to the typhoons in the late summer 1957, show the winter maximum in agreement with the other curves, but the summer minimum 1958 is relatively higher than that in Europe. The actual amplitudes of microseisms due to typhoons may reach 100 microns and more. That is a multiple of the amplitudes of microseisms of Europe, except Reykjavik in Iceland, where amplitudes of the order of hundreds of microns occur during the stormy winter period. The maxima of generalized amplitudes are much smaller than those actually observed ; they are surprisingly small at 3 (Matsushiro, 4 microns), 6 (Abuyama, 6 microns), 1 (Nagasaki, 7 microns), and 4 (Sapporo, 7 microns), respectively, but if compared with the amplitudes as given in figure 2 they still remain much higher than in Europe, in agreement with a higher intensity of the atmospheric circulation in the region of Japan. The coa-

stal stations are characterized by higher amplitudes than the inland ones. This effect seems to prove a considerable attenuation of microseismic energy when propagated through the geological structures. No relationship between the distribution of sources and the size of amplitudes was found. This may be a consequence of quite different conditions of gene-

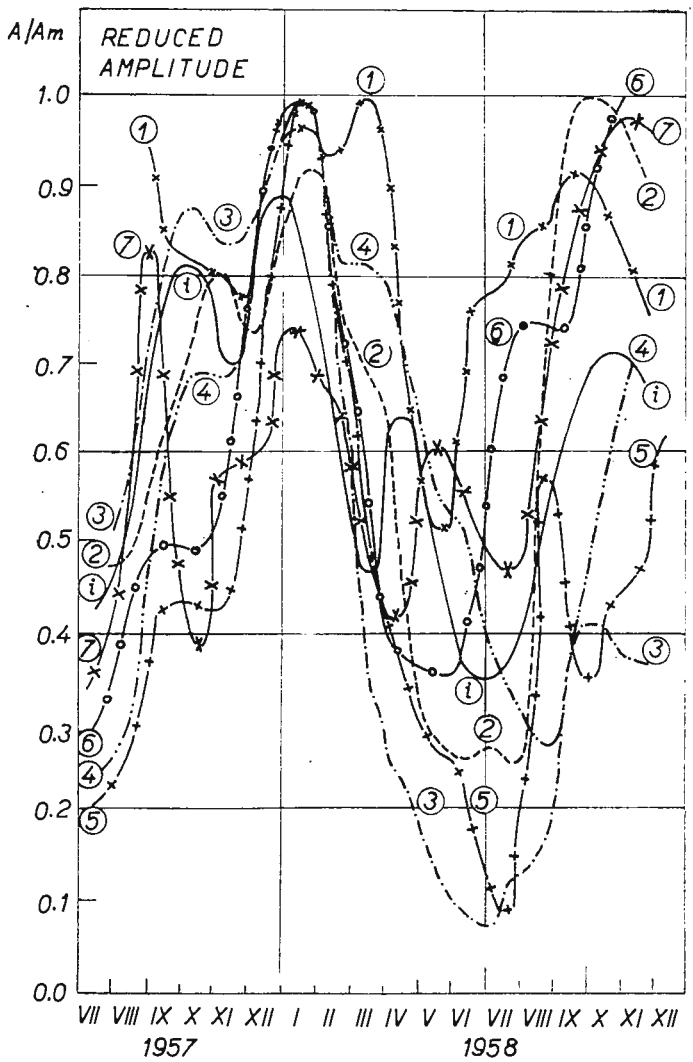

Fig. 3. — Generalized amplitude curves for 7 selected stations given in figure 1, N- component. Amplitudes reduced to a unit maximum, and so the index ,,i''

1, Nagasaki; 2, Tokio; 3, Matsushiro; 4, Sapporo; 5, Akita; 6, Abuyama 7, Nagoya; i, meteorological index in 500 mb for north-atlantic frontal zone.

ration of microseisms in the Japan region and due to a more complicated pattern of atmospheric circulation (S a n t ô, 1959; 1960).

On the whole, one can conclude that down to the latitudes of about 35°N the similarity in the course of generalized amplitudes exists in spite of different conditions of the atmospheric circulation. The agreement is better in higher latitudes and for the cold season of the year. In the lati-

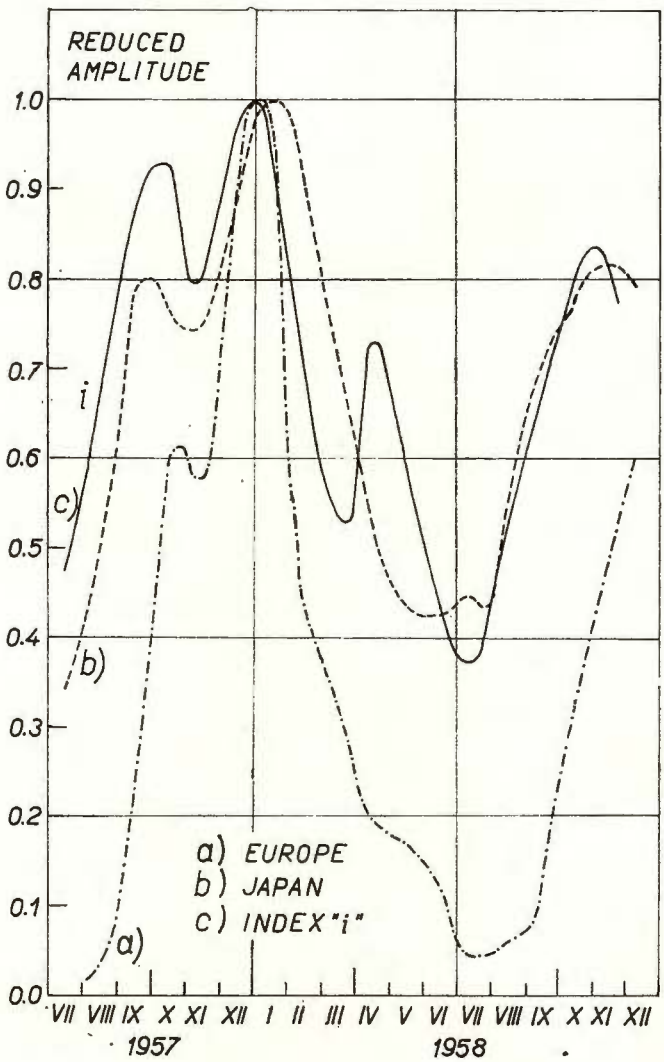

Fig. 4. — Reduced average generalized amplitude curves.

tudes less than 35°N the shape of the curves changes. In South Japan the relative changes of the amplitudes are considerably larger during the warm season than in winter. An important role in the generation of summer or early autumn microseisms belongs to the tropical cyclons coming as typhoons from the southern directions. Occasionally, a typhoon may cause a considerable increase in the generalized amplitudes even at a station situated as far in the North as 5 (Akita), if the centre passes near the station.

In figure 3 we have plotted also the smoothed curve of the meteorological index "*i*". One sees its shape fitting well into that of the set of the generalized amplitude curves in spite of the fact that it was derived for the north-atlantic frontal zone and the compared amplitude curves have been obtained from the data of Japanese stations. This suggests the idea that there must exist a common factor dominating the microseismic activity both in the region connected with the circulation in the north-atlantic frontal zone and in the region of Japan down to 35°N. Such a mechanism should then represent a determining factor of the global regime of the polar cell as a whole, working for a certain interval of time mostly in a range of a few weeks, and changing in a way that affects globally the activity of the pattern of troughs and ridges radiated toward lower latitudes.

In order to see the relationships more clearly we averaged the European curves of generalized amplitudes as plotted in figure 2, and so the Japanese curves as given in figure 3, and put them together with the curve of the index "*i*". As a result figure 4 was obtained showing a fairly good similarity of the three curves. This relation would have been even better if we had used only the curves 2—5 of figure 3, where the agreement with the European curves was so good, and had omitted the curves 1, 6 and 7. It is interesting to note that the curves last named are situated west or close to the axis of the belt of deep-focus earthquakes crossing Japan as indicated in figure 1 (line A—B). This may well be seen as a proof that apart from specific conditions of the atmospheric circulation, also the tectonic structure may be involved in the creation and propagation of microseisms in this region.

CONCLUSION

The fact that both the European and Japanese curves of generalized amplitudes of IGY microseisms exhibit a similar shape and a clear relationship to each other down to the latitude of 35°N, and to the generalized course of a meteorological index, which is roughly proportional to the W—E component of geostrophic wind at the 500-mb-level in the north-atlantic frontal zone, suggests the idea of the existence of a uniform large-scale mechanism operating at the northern polar front. This "great polar vortex" may be considered responsible, among other phenomena associated with the circumpolar atmospheric circulation, also for the similar course of the generalized long-term amplitude curves of microseisms in

polar, and partly also in moderate zones of microseismic activity in the northern hemisphere.

A similar study for other regions and epochs, and especially for the southern hemisphere would be of considerable interest also because of possible structural effects. It would provide a promising supplementary information as regards the general character of the atmospheric circulation and, indirectly, the solar activity.

REFERENCES

Santô T. A. (1959) Investigations into Microseisms Using the Observational Data of Many Stations in Japan (I, II) *Bull. Earthq. Res. Inst.*, 37, Tokyo.

— (1960) Investigations into Microseisms Using the Observational Data of Many Stations in Japan. (III), *Bull. Earthq. Res. Inst.* 38, Tokyo.

Zátopek A., Zikmunda O. (1960). Die harmonische Bodenunruhe in Mitteleuropa im Internationalen Geophysikalischen Jahr 1957/58. *Freiberger Forschungshefte*, H. C81, Freiberg.

— (1961) Sur la nature et l'origine des microséismes européens. *Stud. geophys. geod.* 5, Academia, Praha.

— (1963) Neue Ergebnisse der Mikroseismenforschung in Prag. *Freiberger Forschungshefte*, H. C101, Freiberg.

— (1970) Generalized Amplitudes of IGY Microseisms in Europe and in Japan, *Bull. Int. Inst. Seism. Earthq. Eng.*, 7, Tokyo.

* * * (1959) National Committee for the IGY. Report of Microseismic and Sea Wave Observations in Japan during the International Geophysical Year 1957/1958. 1, July 1957—July 1958, Science Council of Japan, Tokyo.

* * * (1960) National Committee for the IGY. Report of Microseismic and Sea Wave Observations in Japan during the International Geophysical Year 1957/1958. 2, August-December 1958, Science Council of Japan, Tokyo.

SYMPOSIUM 2. STRUCTURE OF THE LITHOSPHERE AND ASTHENOSPHERE

THEORY

THE ESTIMATES OF THE Q_p VALUES IN THE EARTH'S MANTLE

BY

I. S. BERZON, I. P. PASSECHNIK, A. M. POLIKARPOV[1]

The study of the waves absorption in the Earth's mantle is of a great interest as to determine its properties so to solve other geophysical problems, including the determination of the fine structure of the Earth's core. The literature data about the values of the absorption coefficient α_p and quality factor Q_p in the different parts of the mantle varies significantly (A n d e r s o n et al., 1964; K n o p o f f, 1964; K a n a m o r i, 1966). Probably, it is connected on one hand with variability of the absorption parameters in the upper mantle in different regions (T a k a n o, 1970) and on the another hand with the application for their evaluation the methods of the different accuracy. In the number of published papers the accuracy of the parameters evaluation is not mentioned at all.

Undoubtedly the use of the additional experimental data, their careful choice and analyses are necessary for further corrections of our knowledges about the waves absorption in the mantle.

In this report the results are presented dealing with the determination of the longitudinal waves absorption in the mantle on the basis of the large enough amount of data obtained in the wide range of the epicentral distancies $\Delta = 1100 - 11\,000$ km.

THE METHOD OF THE DETERMINATION AND THE USED DATA

The determination of the longitudinal waves absorption in the mantle was conducted by the change of the form of the amplitude spectra

[1] O. Yu. Schmidt Institute of Physics of the Earth, Academy of Sciences of the USSR, Moscow, USSR.

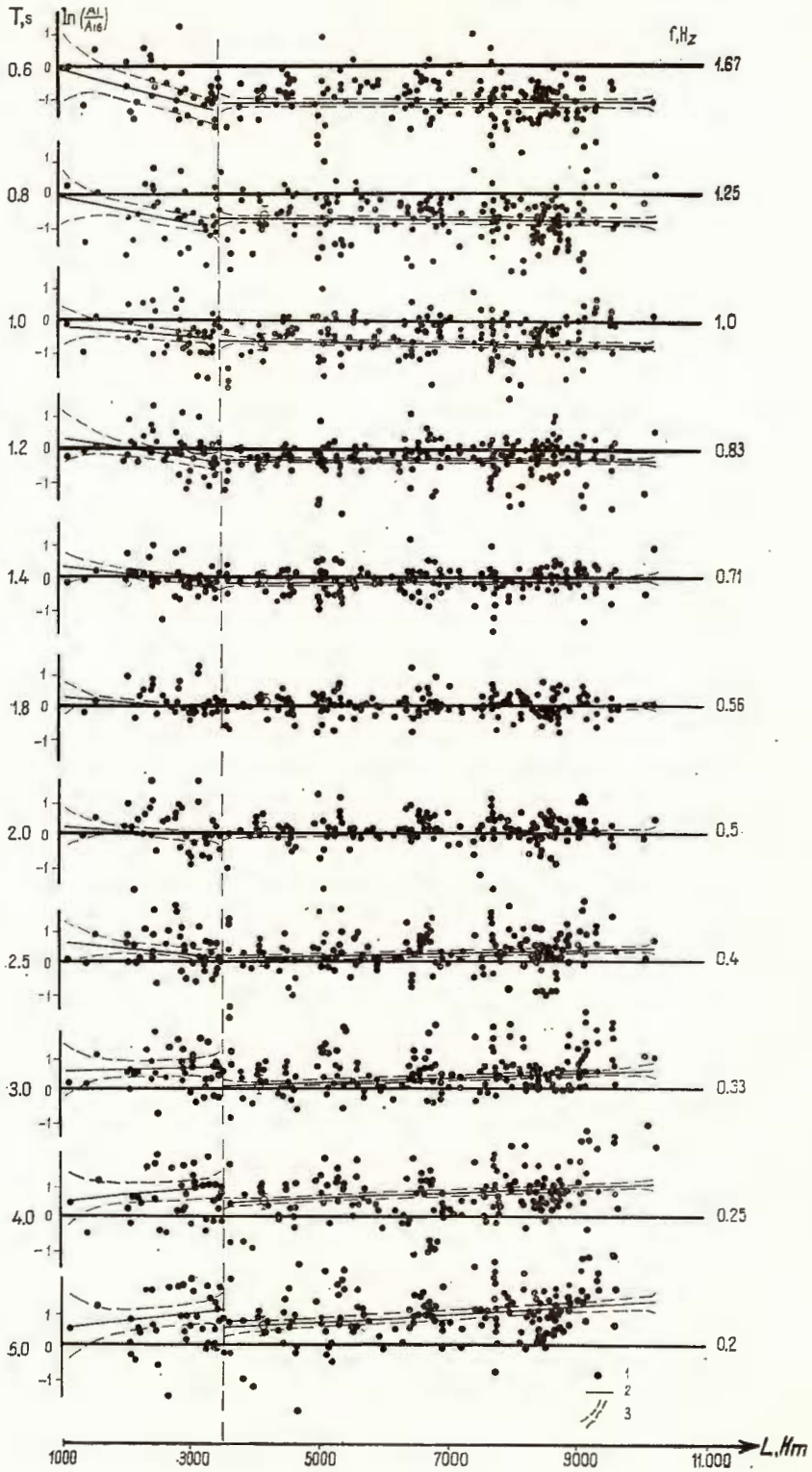

of P waves registered at the different epicentral distances. This method described in detail in different books and articles (B e r z o n et al., 1962; P a s s e c h n i k, 1970) permits determining the difference of the absorption coefficients $\Delta\alpha_p = \alpha_p(f_i) - \alpha_p(f_k)$ for different frequences f_i and a fixed frequency f_k. Then using the condition of the equality to zero of the absorption coefficient at the zero frequency, it is possible to find the absolute values of the absorption coefficients and their frequency dependence.

To exclude the influence of the source mechanism of P wave amplitude we used only the records of the waves, excited by the surface axisymmetrical sources. The records are obtained with the network stations of the USSR, situated in Asia and Europe by the seismometers of the SVKM type (P a s s e c h n i k, 1970) with the amplitude-frequency response curves having the maximal magnification at the frequency $f = 1$ c.p.s. The amplitude spectra were calculated with the computer, using the digitized P wave records. The spectra were corrected due to the apparatus amplitude-frequency response curve.

THE AMPLITUDE CURVES FOR THE DIFFERENT SPECTRAL COMPONENTS

In figure 1 there are plots of the logarithm of the ratio of the spectral components amplitudes for different periods T_i to those with the fixed period T_k=1.6 s versus the length L of the seismic ray, calculated for the different epicentral distances Δ. Plots are built in the range of periods $T_i = 0.6-5.0$ s (or frequency range $f_i = 0.2-1.67$ c.p.s.)

It is seen from the figure 1 that the large scattering of the experimental data is present due to some factors which are difficult to take into consideration —the influence of the different horizontal inhomogeneities on the path ray propagation, the different stations conditions and etc. Naturally in this case the determination of the averaged law of attenuation is possible without taking into consideration the regional peculiarities of the media structure. Despite of the data scattering one sees the marked tendency of the more strong absorption with the distance of the highfrequency components in compare to the lowfrequency ones. The slope of the regression line, averaging the experimental points characterized the difference $\Delta\alpha_p = \alpha_p(f_i) - \alpha_p(f_k)$ of the absorption coefficients at the frequencies f_i and f_k. To find $\Delta\alpha_p$ we tried average the complete amount of the data as a whole and the different variants of its dividing to the intervals ΔL with the different values of $\Delta\alpha_p$. The least scattering was obtained, when all data were divided into the following two intervals ΔL with the

Fig. 1. The dependence of the logarithms of the ratio $\frac{A_i}{A_{1.6}}$ of the spectral components amplitudes A_i for different periods T_i to those at the period 1.6 s versus the P wave ray length L
1, the experimental values of the ratios; 2, regression lines, the slopes of which are averaged values $\Delta\alpha p = \Delta\alpha p(L)$, for the interval of the P wave penetration depth from 100 to 760 km and from 760 to 2900 km; 3, confidence ranges at 90% level.

different values $\Delta\alpha_p=\Delta\alpha_p(f)$: *a*) $\Delta L=1140-3510$ km that corresponds to the depths of the rays penetration $H=100-760$ km (a number of the points $n=43$) and

b) $\Delta L=3510-10244$ km that corresponds to $H=760-2900$ km (the number of the points $n=245$). The value $H=760$ km is relatively close to depth of the boundary between the upper and the lower mantle. At the figure 1 these straight regression lines for both intervals are shown with the 90% confidence ranges.

The α_p frequency dependence Using obtained values of $\Delta\alpha_p$ for every of the above mentioned distances intervals we obtained the linear dependence of the α_p on the frequency f with the confidence ranges at 90% level (fig. 2,3). Approximately these dependencies can be attributed to the intervals of the rays penetration depths.

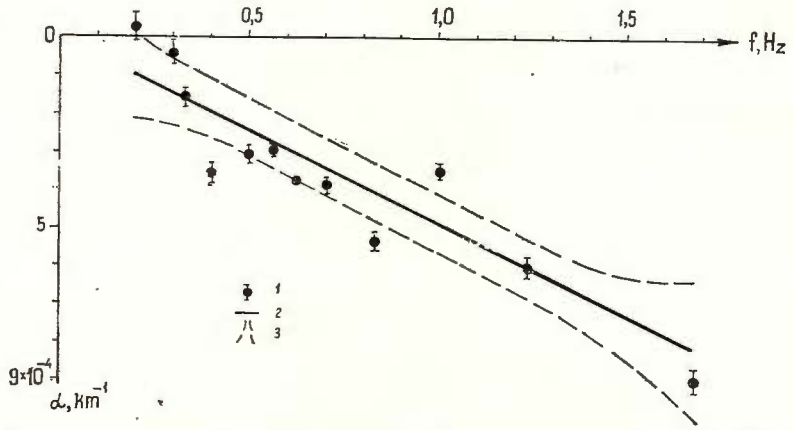

Fig. 2. The dependence on frequency f of the absorption coefficient α_p of the P wave in the upper mantle in the range of depths from 100 to 760 km :

1, the experimental values with the 90% confidence region; 2, averaging regression line $\alpha_p(f)$; 3, 90% confidence ranges for the regression line.

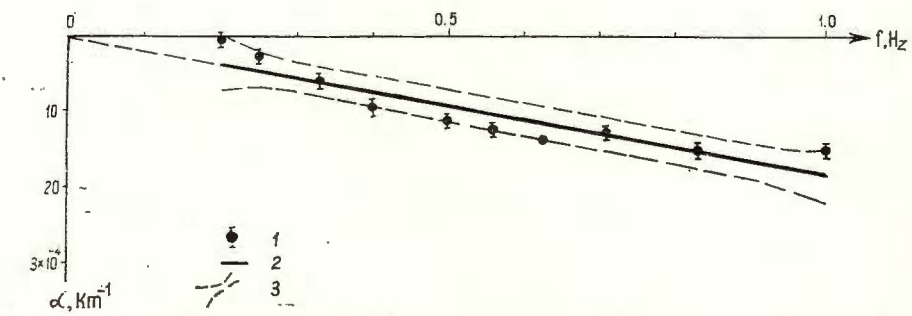

Fig. 3. The frequency dependence of the absorption coefficient α_p for the P wave in the lower mantle (solid line) in the interval of depth from 760 to 2900 km :

1, the experimental values with the 90% confidence region; 2, averaging regression line $\alpha_p(f)$; 3, 90% confidence ranges for the regression line.

The equations of the obtained regression lines are :

$$\text{for } H = 100 - 760 \text{ km}, \quad \alpha_p = (4.88 \pm 1.31).10^{-4} \text{ km}^{-1} \tag{1}$$

$$\text{for } H = 760 - 2900 \text{ km}, \quad \alpha_p = (1.82 \pm 0.63).10^{-4} \text{ km}^{-1} \tag{2}$$

The averaged dependence of α_p upon f for the whole investigated interval of the depths, calculated using (1) and (2) is :

$$\text{for } H = 100 - 2900 \text{ km}, \quad \alpha_p = (2.54 \pm 0.79) \cdot 10^{-4} \text{ km}^{-1} \tag{3}$$

The factor Q_p mean values. In the case of the linear dependence $\alpha = kf$ upon the frequency the mean value of the quality factor Q_p in the examined interval of the depths becomes

$$Q_p = \frac{\pi}{kV_p} \tag{4}$$

where V_p — the mean value of the velocity in the depth interval under consideration. To calculate the mean velocities along the vertical line in the range of the depth under consideration the standard dependence of the longitudinal waves velocities is admitted.

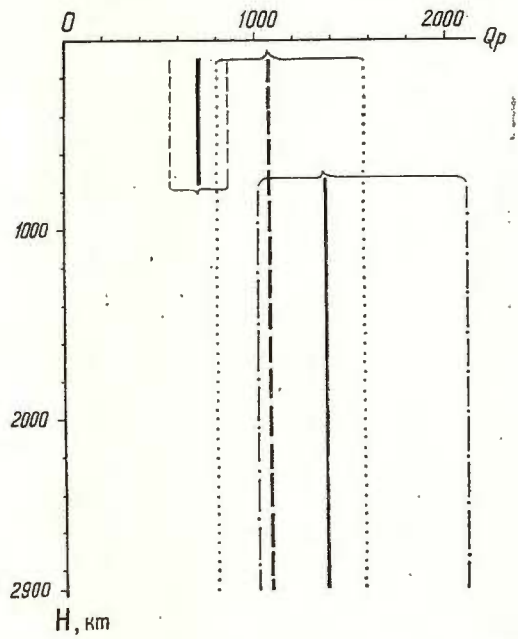

Fig. 4. The average Q_p values in the depth interval from 100 to 760 km and from 760 to 2900 km and the mean value in the depth interval 100—2900 km. The dotted thin line shows the boundaries of the 90% confidence ranges.

Using the obtained dependencies (1—3) α_p versus frequency f we get the Q_p values at the different depths with the corresponding confidence ranges at 90% level. Calculated Q_p values are shown at the figure 4. It is seen there that the absorption in the upper part of the mantle is more

than in the lower one. The confidence ranges for Q_p values in the upper and the lower parts of the mantle do not cross.

At the figure 4 it is shown also the mean value $Q_p = 1080$ in the whole range of the depth 100—2900 km calculated from the data obtained for the upper and lower mantle.

THE COMPARISON WITH THE DATA IN LITERATURE

In the table 1 the comparison is made between the obtained Q_p values and the data received by the different authors which had used the other methods.

There are tabulated the data by Mikumo and Kurita (1968), Kanamori (1966) and averaged Q_p values for the different depth intervals, calculated by us for the model MM8' by Anderson (1965) and from another paper by Kanamori (1967), put in the paper by Ibrahim (1971).

To calculate the absorption in the whole upper mantle including the Earth's crust it is necessary taking into account the absorption in the depth interval $H = 0-100$ km. We in correspondence with the experimental data of Passechnik (1969) approved the value of $Q_p = 220$ that is like one calculated for the Anderson's model.

TABLE 1

The comparison of the Q_p values in the upper and lower mantle

Depth interval km	Used Velocities values km/s	Q_p according to: Authors	Anderson (1965)	Kanamori (1967)	Kanamori (1966)	Mikumo and Kurita (1968) M—5	M—10	M—11	M—14
100— 760	9,04	710 ± 150	380	165					
760—2 900	12,48	$133 \pm \frac{730}{360}$	3 210	1 210		1 690	2 310	4 060	4 900
100—2 900	11,45	$1080 \pm \frac{420}{285}$	990	420					
0— 100	7,62	320	230	100					
0— 760	8,91	530 ± 150	345	150		120	166	195	274
0—2 900	11,29	$845 \pm \frac{420}{260}$	850	375	410— 630	292	417	508	702
0 — 900					180— 240				
900—2 900					1 600—6 000				

One can see from the table that the difference of the values in the upper and the lower mantle according our calculations being less than in the models of the other authors. The probable cause of difference is that the Q_p values in the mantle in the Anderson's and Kanamori's

models are obtained on the ground of Q_s values for shear waves using different chosen rations $\eta = \frac{Q_p}{Q_s}$ (Anderson — $\eta = 2-2.5$, Kanamori — $\eta = 1.0$).

According to our data the Q_p value in the upper mantle is more than in the other models and the Q_p value in the lower mantle is less than in Anderson's model and the part of the models of Mikumo and Kurita and is close to the minimal value in Kanamori's model. The Q_p value in the upper mantle, determined by us, is most like the Anderson's data and the value $Q_p = 480-800$ obtained by Vinnik et al. (1970) on the base of the amplitude ratio of the waves PP and P along the P ray penetrating up to a somewhat greater depth $H = 1100$ km.

In conclusion we'd like to point out that our data did not allow us to make more detailed Q_p dividing of the mantle because of their large scattering. However the used method can principally solve this task, It is necessary to make the further accumulation of the experimental data and also to increase the accuracy of the Q_p determination in the different parts of the mantle. It is rather important to extend the range of frequencies where the dependence $\alpha_p = \alpha_p(f)$ is determined. In order to make it one should use the P wave records, obtained with the broad-band seismometers.

REFERENCES

Anderson D. L., Kovach R. (1964). *Proc. Nat. Acad. Sci. U.S.A.* 51, 2, USA.
— Ben Menahem A., Archambeau C. B. (1965). *Geophys. Rev.*, 70, 6.
Berzon I. S., Epinatjeva A. M., Parijskaya G. N., Starodubrovskaya S. P. (1962). Dinamicheskie harakteristiki seismicheskih voln v. realnih sredah. Izd. Nauka, Moskva.
Ibrahim Abou-Bakr K. (1971). *Pure Appl. Geophys.* 91, Basel.
Kanamori H. (1966). *Bull. Earthq. Res. Inst.*, 45, 2, Tokyo.
— (1967). J. *Geophys. Res.* 72, 2, Richmond.
Knopoff L. G. (1964). *Rev. Geophys.* 2, 4.
Kovach R. L., Anderson D. L. (1964). *Bull. Seismol. Soc. Am.*, 54, 6 Berkeley.
Kurita, T. Y. (1966). J. *Phys. Earth*, 14, 1, Tokyo.
Mikumo T., Kurita T. (1968). J. *Phys. Earth.* 16, 1, Tokyo.
Passechnik I. P. (1960). *Izv. AN SSSR, ser. geofiz.*, 12. Moskva.
— (1969). Különlenyomat a Proceedings of the Earth Assembly of the European Seismological Commission Cimu Kiadványbol., Budapest.
— (1970). Harakteristiki seismicheskih voln pri jadernyh vzryvah i zemletrjasenijah. Izd. Nauka, Moskva.
Press F. (1956). *Science*, 124, 1204, Philadelphia.
Takano K. (1970). *J. Phys. Earth*, 18, 2, Tokyo.
Vinnik L. P., Dashkov G. G. (1960). *Doklady AB SSSR*, 190, 6, Moskva.

SEISMIC WAVES IN INHOMOGENEOUS MEDIA—A REVIEW

BY

VLASTISLAV ČERVENÝ, KAREL PŠENČÍK[1]

INTRODUCTION

The purpose of this paper is to give a short outline of theoretical methods used in the investigation of the propagation of seismic body and surface waves in inhomogeneous media. The main attention is devoted to the seismic wave propagation in the Earth's crust and the uppermost mantle. In restricting this survey the authors have focused on elastic waves in perfectly elastic media. The scattering problems and the theory of seismic sources are not included.

The four main theoretical approaches to the investigation of seismic wave propagation are as follows : *a*) The ray series method and its modifications, *b*) The exact ray theory, *c*) The wave method, *d*) Direct numerical methods, such as the finite-difference and finite-element methods. The ray theory and its modifications can be used for the investigation of seismic wave propagation in very general, laterally inhomogeneous media with curved interfaces. Unfortunately, the method is only approximate and has a number of serious restrictions. The other two methods — the exact ray method and the wave method — can be used only for relatively simple models of media, such as the medium composed of homogeneous parallel layers. The wave method has played a basic role in the investigation of surface waves. In the investigation of body waves, its great value consists in the possibility to give an exact solution to certain specific problems, such as the reflections from a strictly horizontal transition layer. The finite-difference method has been applied to seismological problems only lately. Since it is based on a direct numerical integration of partial differential equations of motion, it can be applied, in general to rather complicated media. The same applies to the finite-element method. However, it will take some time to develop them for the solution of more complex seismological problems.

In the following, the possibilities and limitations of mentioned methods in the solution of various problems of seismological interest will be

[1] Geophysical Institute, Charles University, Prague 2, Ke Karlovu 3, Czechoslovakia

discussed in some detail. The bibliography given at the end of the paper is far from being exhaustive. For more extensive bibliography on the theory of seismic body waves [2] see Červený (1972 *b*). Note that certain parts of this paper depend heavily on Červený (1972 b).

RAY METHOD

Most interpretation methods in seismology which use seismic body waves as a background have been based on the ray concepts. The basic principles of the ray theory have been known for a long time. While previously the ray theory was used particularly for the media with one-dimensional velocity distribution, at the present time methods have been elaborated for constructing rays, wavefronts and travel times and computing ray amplitudes of body waves propagating in media where the velocity depends on two or three coordinates and in which non-plane interfaces of first order may exist. Computational methods are based mostly on the numerical solution of systems of ordinary differential equations. These systems can be solved by standard numerical techniques. (Belonosova et al, 1967; Marcinkovskaia, Krasavin, 1968; Wesson, 1970; Červený, Ravindra, 1971; Pšenčík, 1972). The possibility to compute theoretical time-distance curves and ray amplitudes in laterally inhomogeneous media can help us to check preliminary interpretations of seismic measurements of the structure of the Earth's crust, which are usually based on the assumption of horizontal layering. It is clear that in simple media, where the layering is nearly horizontal, the discrepancies will be small. In regions, however, where the lateral changes of velocity are large, e.g. in regions of block structure, the differences can be rather expressive. These differences can help us to revise the model. In the following, some examples from the international profile VI of deep seismic sounding measurements in Czechoslovakia are presented. The preliminary interpretations based on standard methods gave different velocity-depth distributions in different parts of the seismic profile. Thus the Earth's crust was found to be laterally inhomogeneous (Bèranek et al, 1971). The ray diagrams and time-distance curves were computed to check the interpretations. Examples of computations for two regions of the profile VI are taken from Pšenčík (1972), where more details can be found.

a) Computations for the Moldanubicum (a part of the Bohemian Massif). The structure of the Earth's crust is not very complicated there. Figure 1 shows the results of preliminary interpretations, the isolines of velocity and the geometrical shape of Mohorovičić discontinuity. Computed ray diagrams of refracted waves propagating within the Earth's crust are

[2] Červený V. Theory of seismic body wave propagation. 1972. Upper Mantle Seismological Investigation, Progress Report II, ESC, Soviet Geophysical Committee, Moscow (in press).

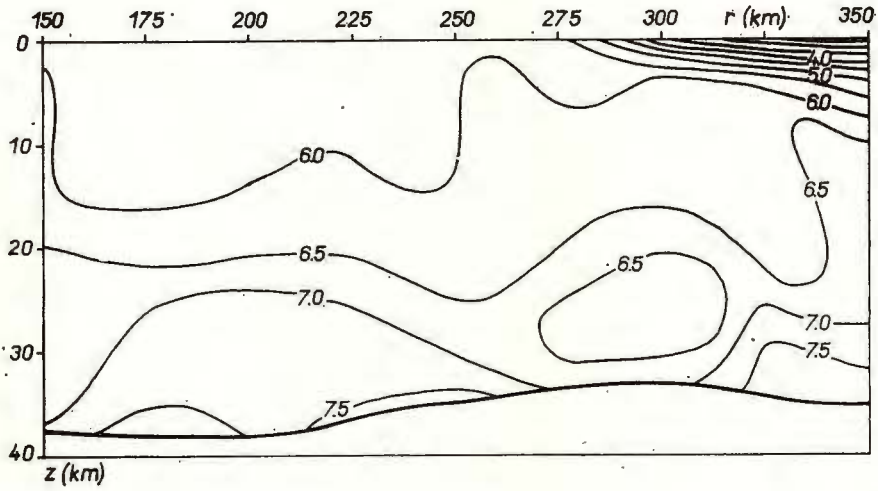

Fig. 1. — Preliminary interpretations, velocity-isolines and the geometrical shape of the Mohorovičić discontinuity in the Moldanubicum region.

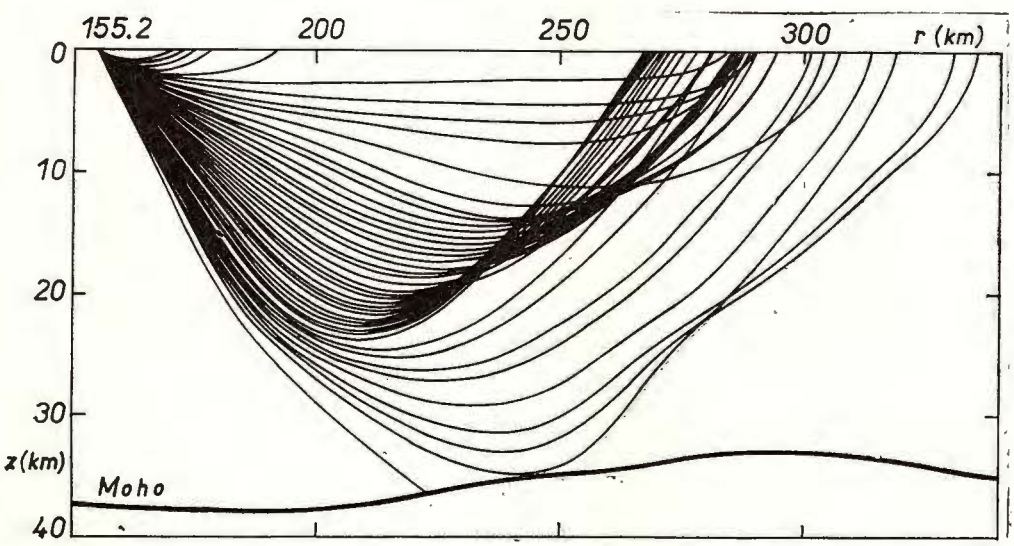

Fig. 2. — Computed ray diagrams of refracted waves, in the Moldanubicum region.

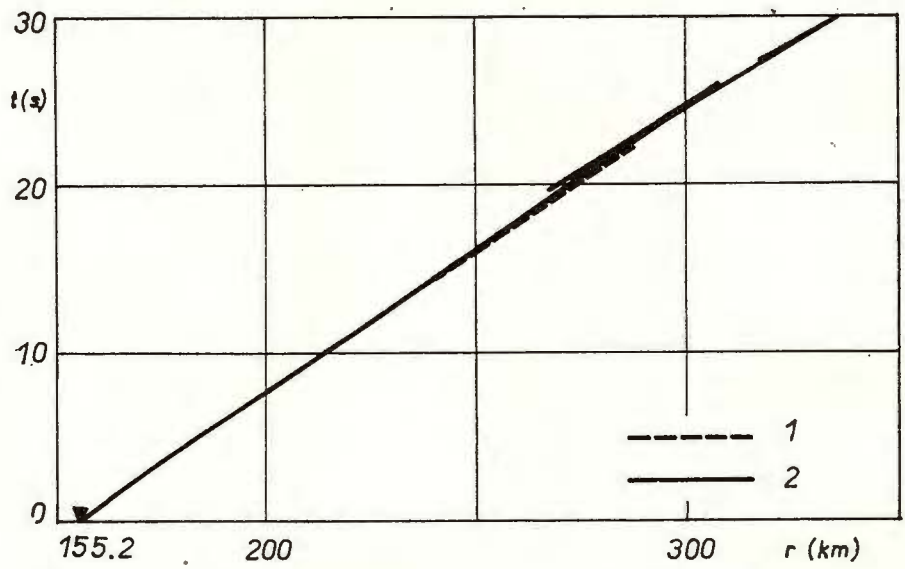

Fig. 3. — Time-distance curves of refracted waves, in the Moldanubicum region.
1, experimental curves; 2, theoretical curves.

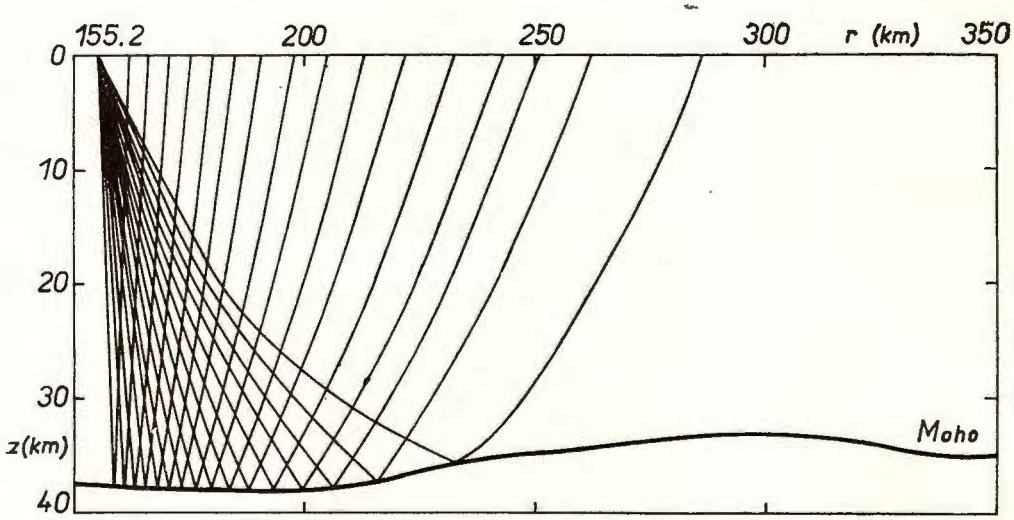

Fig. 4. — Ray diagram of reflected waves from the Mohorovičić discontinuity, in the Moldanubicum region.

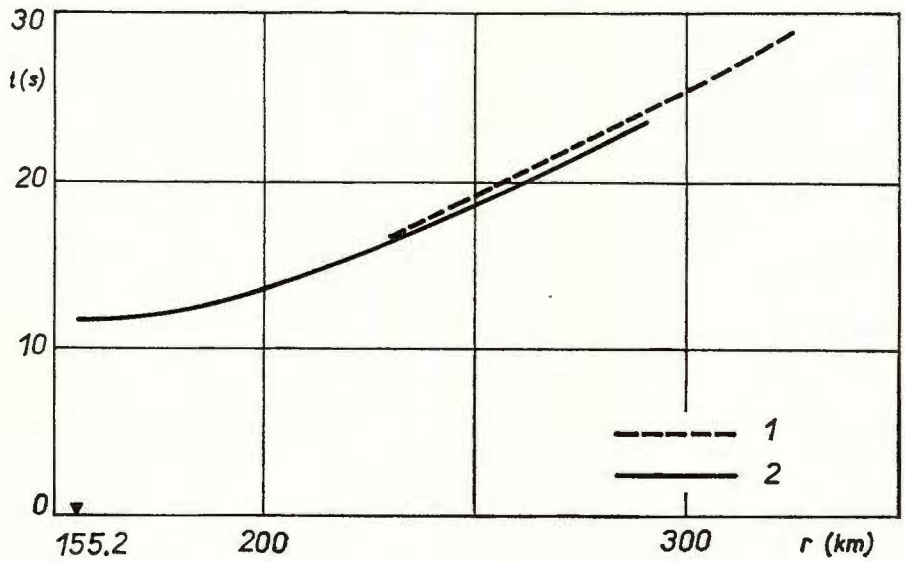

Fig. 5. — Time-distance curves of reflected waves from the Mohorovičić discontinuity, in the Moldanubicum Region.
1, experimental curves; 2, theoretical curves.

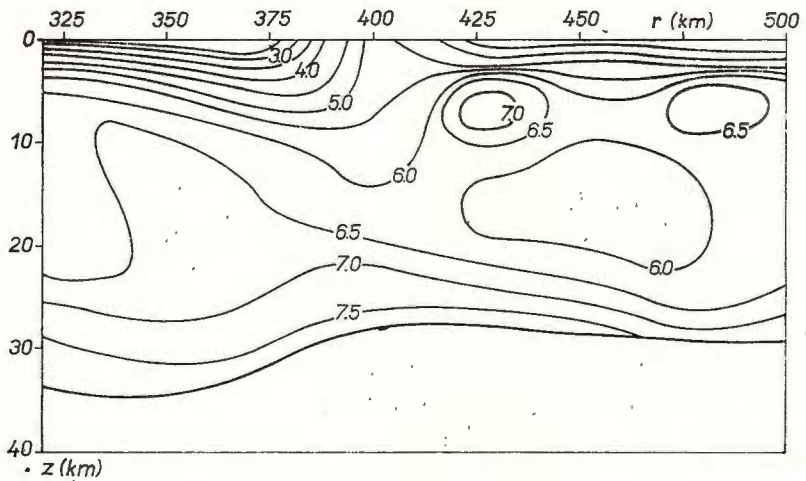

Fig. 6. — Velocity-isolines in the Earth's crust, in the Bohemian-Carpathian transition zone.

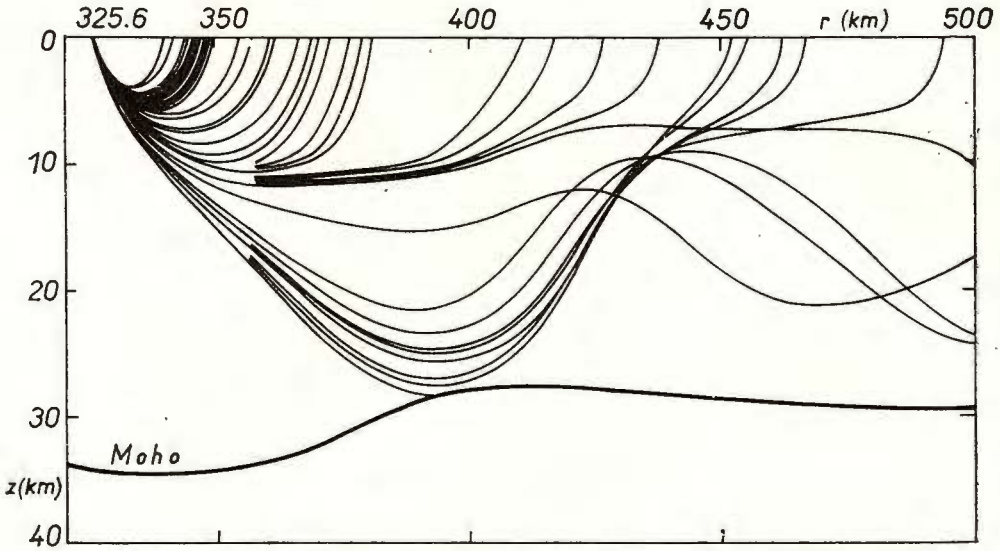

Fig. 7. — Ray diagram of refracted waves in the Bohemian-Carpathian transition zone.

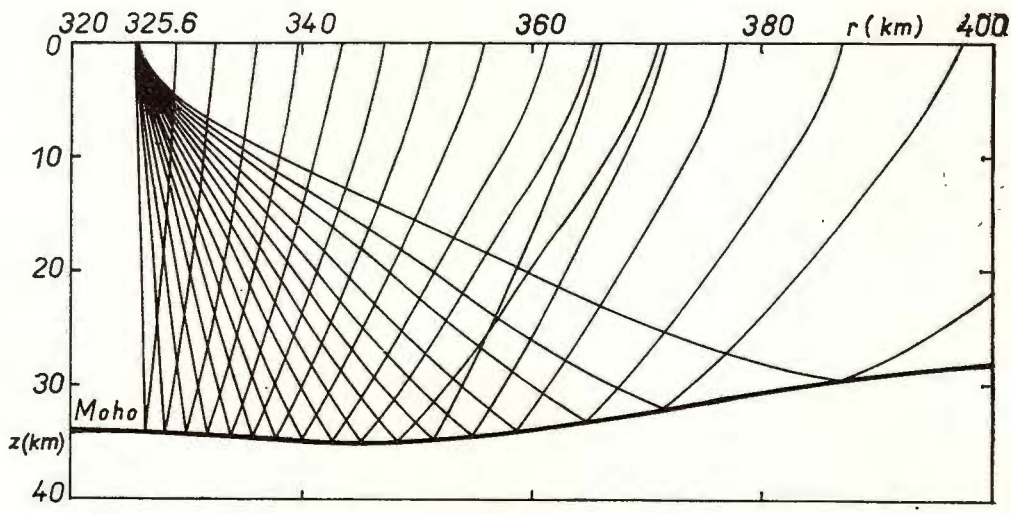

Fig. 8. — Ray diagram of the reflected waves from the Mohorovičić discontinuity, in the Bohemian-Carpathian transition zone.

given in figure 2. The formation of a caustic caused by a strong gradient of velocity at depths near 20 km can be clearly seen in the figure. Figure 3 shows time-distance curves of refracted waves. Dashed lines are experimental, the full ones theoretical. In the region, where the experimental time-distance curve exists, its aggreement with the theoretical one is satisfactory. Figure 4 presents the ray diagram of waves reflected from the Mohorovičić discontinuity. No complications. Figure 5 shows time distance curves of these reflected waves. The differences between the theoretical and experimental arrival times are about 1/2 s.

b) Computation for the transition region between Bohemian Massif and Carpathians. The structure of the Earth's crust is considerably more complicated there. The isolines of velocity are given in figure 6. Large velocity changes in horizontal direction cause that the ray diagram of refracted wave is rather chaotic (fig. 7). The ray diagram of the wave reflected from the Mohorovičić discontinuity in the same region is considerably simpler than that of the refracted wave (fig. 8). The time distance curves for this region are not presented here. The differences between theoretical and experimental arrival times in this region are, of course, larger than in Moldanubicum.

No attempt will be made here to explain the observed differences. This will be the object of further studies. However, it can be clearly seen from the presented figures that the new approach to the construction of time-distance curves in laterally inhomogeneous media can help to improve the interpretations based on simpler methods. The kinematic inverse problem is considerably more complicated than the direct one. It is well known that the broad range of seismic velocity depth models can be found that are consistent with any given set of travel-time points. Detailed investigation of the Wiechert-Herglotz method for the one dimensional velocity distribution with possible low velocity layers was performed by Gerver and Markushevich (1966 ; 1967), see also McMechan and Wiggins (1972). The investigation of inverse kinematical problem for laterally inhomogeneous media has just started. Certain methods for the velocity determination in laterally inhomogeneous media have been proposed by Alekseyev et al. (1970 ;1971), Fazylov (1971) and their colleagues in Novosibirsk. These methods have been verified both on theoretical and real models of media. Results have been obtained concerning the uniqueness and stability of these inversion problems (Lavrentyev, Mukhometov, 1969). Note that the Wiechert-Herglotz method was generalized for the case of two-dimensional velocity distribution by Belonosova and Alekseyev (1967). General procedures of the inversion of geophysical data were proposed by Backus and Gilbert. For a detailed description of the Backus-Gilbert method of inverting travel-time data see Johnson and Gilbert (1972).

Greater attention has recently been paid also to the anisotropy of seismic velocities and to its influence on time distance curves of seismic waves. Today, the computation of seismic rays, wave fronts and time-

distance curves of quasi-compressional and quasi-shear waves in inhomogeneous anisotropic media does not cause principal difficulties. Similarly as in isotropic medium, a seismic ray is described by a system of ordinary differential equations which can be solved by standard numerical methods (Červený, 1971 a). We have computed ray diagrams and travel-time curves, for certain simple models of the inhomogeneous anisotropic Earth's crust. The results indicate that even slight anisotropy can cause remarkable errors in the interpretation of the materials of deep seismic soundings of the Earth's crust, mainly in the determination of the depth of interfaces (Červený, Pšenčík, 1972 a).

Up to now, only the computation of kinematic properties of individual body waves, as rays, wave fronts and time-distance curves, has been discussed. It should be noted that the computation of ray amplitudes of body waves in laterally inhomogeneous, possibly anisotropic media, does not cause principal difficulties, either. (Wesson, 1970; Červený, 1972 a). Thus, we can conclude that the time-distance and amplitude-distance curves of individual elementary seismic waves can be computed, either for very general types of media.

Certain difficulties, however, can arise when we wish to construct the ray theoretical seismograms. The methods for the construction of theoretical (synthetic) seismograms in the case of normal incidence are well known. At larger epicentral distances, the problem becomes more complicated. In inhomogeneous media with curved interfaces an infinite number of elementary waves can arrive at the receiver within even a narrow time window. The problem of constructing ray theoretical seismograms in inhomogeneous media with curved interfaces has not yet been solved quite satisfactorily. The problem becomes considerably simpler in the medium composed of plane parallel homogeneous layers, when we do not take into account the *PS* and *SP* conversions. The number of waves which arrive at the receiver within a finite time window is always finite in this case. The situation is simplified by the fact that the individual elementary waves can be grouped into the families of kinematically and dynamically analogous waves. This considerably decreases the number of waves which must be taken into account (Petrashen, Vavilova, 1968, Vavilova, Volodko, 1968; Hron, 1972). However, even this case the number of groups remains very high, mainly when the epicentral distance is large and/or when thin layers are present in the medium and/or when we are interested in a long interval of the theoretical seismogram.

An example of theoretical ray seismograms is shown in figure 9. Theoretical seismograms were constructed for a simple model of a five layer Earth's crust (submitted kindly by dr. Kosminskaya), shown in figure 10. The theoretical seismograms are self-explanatory. (It should be only noticed that the phase denoted by arrows at epicentral distances of 40 and 50 km corresponds to the wave reflected from a sharp interface at a depth of 1.5 km. To simplify the picture, this phase is plotted 10 times weaker with respect to reality). All possible types of compressional

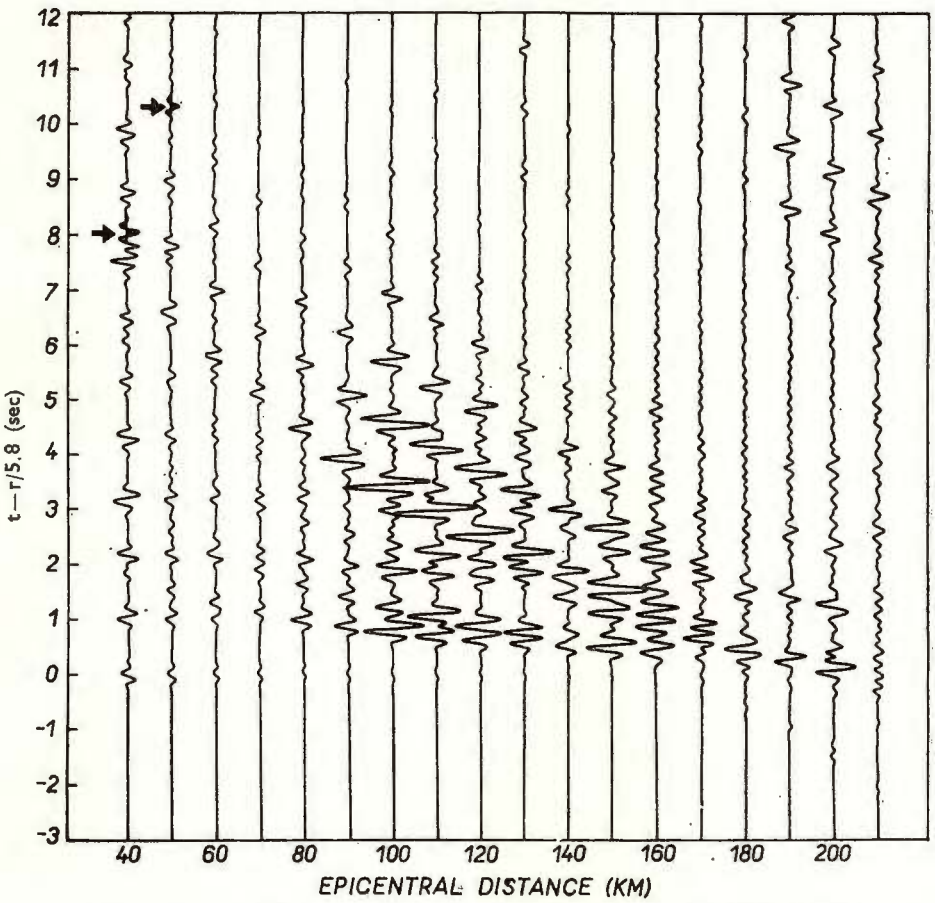

Fig. 9. — Theoretical ray seismograms for a simple five-layer crust model.

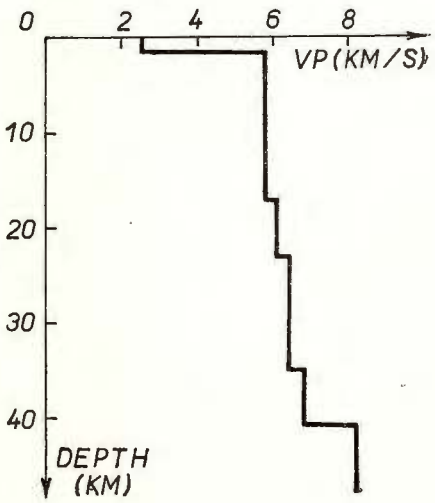

Fig. 10. — Earth's crust model with five layers

waves arriving within 15 s time interval are considered. Both the number of elementary waves and of kinematic groups increase quickly with increasing epicentral distance. For the epicentral distance of 40 km, the number of kinematic groups is 215 and the number of elementary waves 1522. For the epicentral distance of 200 km, however, the number of kinematic groups is 2495 and the number of elementary waves 353706.

In the case of more complicated models, even the number of kinematic groups can be very high and the computations become lengthy. Then we must use various amplitude criteria to exclude „a priori" certain types of waves the intensity of which is very small. In spite of these difficulties, we hope we shall be able to construct ray theoretical seismograms even for rather complicated models of media (including inhomogeneous media) in the near future.

The ray theory has certain serious restrictions. It is not applicable in the case of rapid changes of velocity within short distances. The most typical example is a transition zone. Further, it is not applicable when the radii of curvature of an interface of the first order are of the same order of magnitude or smaller than the wavelength. An example is the corrugated interface. The ray theory can neither be used for the investigation of waves in shadow zones, for the investigation of various types of inhomogeneous and diffracted waves and in the neighbourhood of singular points (such as caustics, critical region, grazing rays, a.s.o.). Very serious difficulties also arize in the case of low velocity layers.

In some of the mentioned situations, certain modifications of ray method can be used. The modified ray methods are again applicable to inhomogeneous media with slightly curved interfaces and remove certain difficulties of the ray theory. For example, the ray method can be modified to include certain types of diffracted waves propagating within shadow zones. The modification consists in introducing new rays, called diffracted rays, by extending the laws of ray theory. The numerical calculation of diffracted rays and corresponding time-distance curves in laterally inhomogeneous media with curved interfaces does not cause difficulties (Červený, Pšenčík ,1972 b). The modified ray methods can be also used in the neighbourhood of singular points, such as caustics and critical points. (See details in an excellent book of Babich, Buldyrev, 1972). Note that the singular points are of considerable importance in seismology, as they are usually connected with strong maxima of amplitude-distance curves. The position of these maxima is frequency dependent.

With frequency decreasing, the maximum of the amplitude curve shifts to larger epicentral distances. The exception is the maximum corresponding to a caustic which is connected with the right reversal of the time-distance curve. There the shift is opposite-to smaller epicentral distances. More details and other references can be found in Červený and Zahradník (1972). Generally, the approximate computations of amplitudes in the neighbourhood of singular points does not cause serious dificulties today.

Another, very powerful modification of the ray theory has been used for the computation of theoretical seismograms in a thick-layered medium, in which the layers are separated by transition zones. The transition zone is simulated by a stack of homogeneous parallel layers. The thick layers are attacked by the ray theory, the transition layers by wave methods, such as Thomson-Haskell matrices. See Berzon and Ratnikova (1971), where are given other references. It is obvious that the combination of the ray method with other methods is very perspective.

Various modifications of the ray theory have been also for the investigation of short-wavelength asymptotics of surface waves in complicated media. For details see Babich and Molotkov (1970), Babich and Buldyrev (1972). Molotkov and Ozerov (1968) have treated the problem of Love waves within a thin layer with a variable thickness. The formulae for phase and group velocities have been derived. Further, Babich and Molotkov (1966) have given asymptotic solution of the problem of Love waves in a halfspace inhomogeneous in two coordinates. Another important problems of surface waves propagating along curved interfaces in rather general laterally inhomogeneous media have been studied by Babich (1967), Krauklis (1969), Ozerov (1966) and others.

All the methods mentioned in the preceeding are only approximate. In the frequency domain, they give the better results the higher is the frequency. It is not simple to appreciate quantitatively the accuracy of these methods. One approach is to compare the ray results with the exact ones, obtained by different methods (for the situations where they are known). In a medium composed of homogeneous planparallel layers the exact ray theory can be used for this purpose. Also wave method and finite-difference method can be used. Of course, these methods do not serve only to checking the ray theory, but they are generally used to obtain an answer to problems which can be hardly attacked by the ray theory, mainly in situations where interference effects play a substantial role (transition zones, corrugated interfaces, surface waves, a.s.o.).

EXACT RAY THEORY

The exact ray theory is based on the decomposition of the wave field into contributions each of which can be attributed to a special ray from the source to the receiver. Various models have been used to obtain the exact expressions for individual contributions, suitable for numerical calculations. The problem, however, has been solved succesfully only for a medium composed of homogeneous plane parallel layers. Well known are the methods of Cagniard-de Hoop, Smirnov and Sobolev, Pekeris and other (Müller, 1968; 1969; Helmberger, 1968; Helmberger, Morris, 1969, 1970). Thus, we can compare the ray theory and the exact ray theory as follows : *a*) The ray theory is an approximate, the exact ray theory an exact method. *b)* The ray theory may be used in general inhomogeneous media with curved interfaces (except

of singular situations). The exact ray theory may be used only in a medium consisting of homogeneous layers bounded by parallel interfaces. It should be also added that the computations based on the ray theory are considerably faster than those based on the exact ray theory. Nevertheless, the computation of exact individual ray contributions — so called elementary seismograms — is also rather fast. The computations, however, become lengthy when a large number of elementary waves must be considered. Müller (1970) has studied the possibilities of the exact ray theory to the investigation of elastic wave propagation in vertically inhomogeneous media. The medium is simulated by a stack of homogeneous thin layers. Some approximations are necessary to save the computer time as the number of elementary waves would be very high. Computation of theoretical seismograms have been restricted only to certain low-order multiply reflected waves and the conversions have been deleted. In spite of these approximations, the Müller's method is very promissing for the solution of certain problems of seismological interest.

Note that the exact ray theory has been also succesfully used for the construction of theoretical seismograms in media with spherical symmetry. The expressions for individual waves, however, are not quite exact in this case (Müller, 1971).

WAVE METHOD

Another important method to investigate the seismic wave propagation is the wave method. It is based on a formal integral solution of equation of motion, satisfying desired initial and boundary conditions relevant to the model under study. The analytical wave solution describes compactly all the wave field, and automatically includes all *PS* and *SP* conversions and surface waves. Unfortunately, these solutions are known only for relatively simple models of media, such as the vertically inhomogeneous media. For the media separated by irregular interfaces and for laterally inhomogeneous media the wave solutions are known only exceptionaly. We shall consider here only the media in which the velocity is a function of depth only.

The wave method has been broadly used for the investigation of seismic surface waves. Therefore, a great deal of this section is devoted to the surface waves. Within the past period, surface wave studies have become an important supplement to the body wave methods. Methods of using surface waves depend mainly on the phenomenon of dispersion. The phase velocity of surface waves is conditioned by the weighted average of shear wave velocity, the depth of penetration depends on frequency. Then the shear wave velocity variation with depth implies the phase velocity variation with frequency. The meaning of surface wave methods increased so far by common use of wide band seismographs and by substantial progress in methods of computation of dispersion curves.

For the computation of dispersion curves in a vertically inhomogeneous medium simulated by a stack of homogeneous planparallel layers,

the well-known Thomson-Haskell formalism is in a common use today. The method is exact and very systematic. The total effect of the stack of homogeneous layers is expressed by a matrix multiplicaton, so that the method is very suitable for machine computation and has theoretically no limitations for any number of layers. Unfortunately, the original Haskell matrix contains exponential terms which become large at high frequencies and the accuracy of computation of the short-period branches of dispersion curves rapidly decreases. The fact that certain of these terms cancel one another during the process of computation offers an alternative approach which avoids the mentioned inconveniencies. This work has been done by Knopoff (1964), Dunkin (1965) and Thrower (1965). A detailed description of the application of Knopoff's formulations is given, e.g., in Randall (1967) and in Schwab and Knopoff (1972). Randall's treatment includes the factorization of the layer matrix into a matrix-vector product such that all frequency dependent terms are excluded from the matrix and the frequency is considered as a dependent variable. However this procedure involves additional matrix multiplication for each layer. Watson (1970) and Schwab (1970) modified the method to give faster machine computation. The accuracy at high frequencies is also included.

For the solution of the inverse problems it is very helpful to know not only the theoretical dispersion curve for an appropriate model but also the partial derivatives of the phase and/or group velocity with respect to the layer parameters. For calculation of these partial derivatives three approaches have been used. The initial work was carried out by Brune and Dorman (1963) who have computed them numerically by slightly varying layer parameters and making use of Thomson-Haskell method. The accuracy of the numerical method has been appreciated by Savarensky et al. (1967). However the numerical method is very slow and even with the help of high speed computers the trial and error method of modifying structure in order to fit the observed data is a tedious process. Consequently it is very desirable to get the computational process as fast as possible. In applying Rayleigh's principle, Anderson (1967) gives an exact method to determine the effect of changes of velocity or density structure. Harkrider and Anderson (1966) calculated by use of Rayleigh's principle partial derivatives for the fundamental mode Love wave velocities applying the correction to the sphericity of the Earth. They used the same principle to compute group velocity and amplitude partial derivatives. The results were given for the fundamental and for three higher modes of Love waves for one oceanic and one shield earth model in a form of tables. Another method, which is very fast and quite exact, and which is based on the application of the theorem on implicit functions, has been proposed by Novotny (1970), Schwab and Knopoff (1972).

It has been shown that partial derivatives may be succesfully used to investigate the properties of low velocity zones. The low velocity zones are very important regions of the Earth, but the investigation of their

detailed structure meets considerable difficulties since body wave methods are indirect in this case. Supplementary methods for exploring this region are needed. A good deal of the up to date knowledge of mantle low-velocity zone has been obtained using surface wave dispersion studies. Mainly the fundamental mode has been used of. Recent studies indicate

i	b_i	ϱ_i	d_i
1	3.47	2.7	6
2	3.64	2.8	10.5
3	3.85	2.85	18.7
4	4.72	3.3	80
5	4.54	3.44	100
6	4.51	3.53	100
7	4.76	3.6	80
8	5.12	3.76	∞

i number of the layer
b_i shear wave velocity
ϱ_i density
d_i thickness
h depth

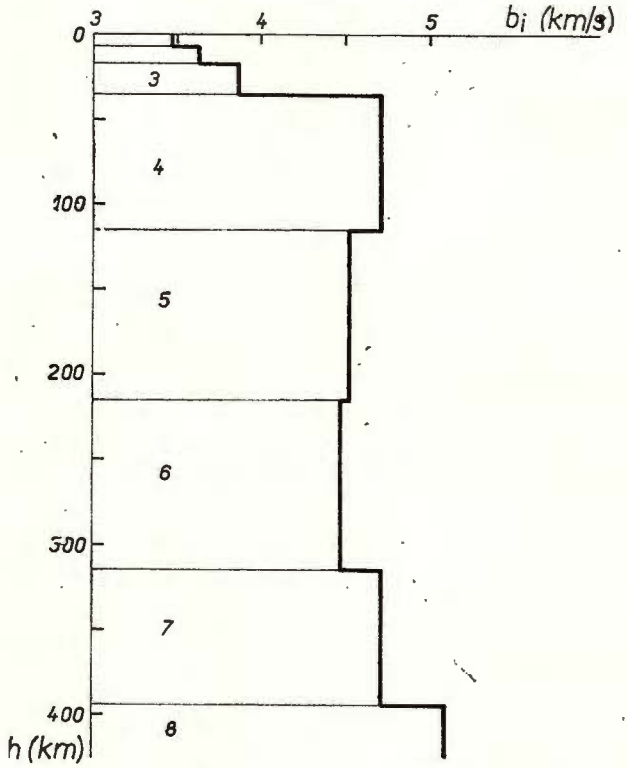

Fig. 11. — Shield model with one mantle low velocity zone

increasing interest in the use of higher modes of surface waves as a tool for obtaining information about the low-velocity zone in the crust and in the upper mantle, about focal depth and the source mechanismus. Several investigators—Kovach and Anderson (1964), Harkrider (1970), Alterman (1969), Pšč and Novotný (1971)—have shown the possibility of utilizing them for several reasons to the low velocity structure dererminations. First, a considerable amount of surface energy propagates in a certain period range within the low velocity zone and under suitable circumstances the share of higher modes energy on the whole surface wave energy is considerable. Further, for the fundamental mode, there is not a period range where the influence of the low velocity layer would be predominant. The sensitivity of the dispersion curves to the

variation of layer parameters and consequently the possibility to utilize them to the structure determination is expressed by partial derivatives of the dispersion curve with respect to the layer parameters. As an example, the partial derivatives of the fundamental mode of Love wave for a shield model with one mantle low velocity zone (fig. 11), with respect to the shear

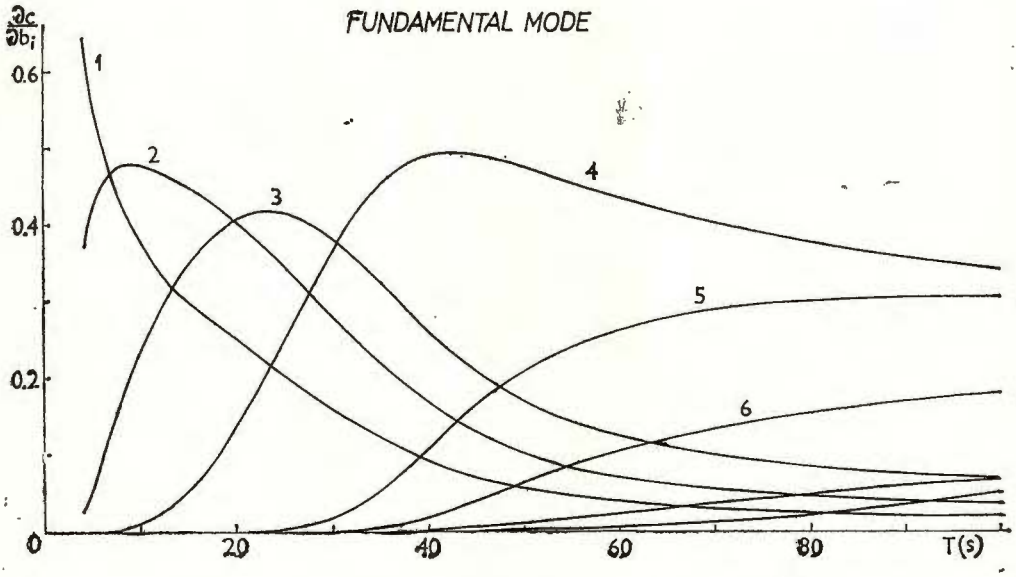

Fig. 12. — The partial derivatives of the fundamental mode of Love wave for a shield model with one mantle low velocity zone.

velocities of separate layers is shown in figure 12 (P ě č, N o v o t n ý, 1972). The numbers at the curves denote the layer numbers (1, 2, 3 are the crustal layers, 4 the high velocity layer and 5, 6 are low-velocity layers). It is seen that the overburden of the low velocity zone has a screening effect through the whole period range. Higher mode dispersion curves behave in a quite different way. Figure 13 shows the partial derivatives of the first higher mode of Love waves with respect to the shear wave velocities. The period of 9 s divides the pattern into two separate ranges in which the curves behave in a quite different way. Within the short period range the highest value of partial derivatives is reached by the curves associated with the crustal layers 1, 2 and 3. In the long period range two curves corresponding to the low velocity layers 5, 6 are predominant. It follows that higher modes discriminate fairly between low velocity zone and crustal layers. The fundamental mode has not that property. The importance of higher modes among the other phases have been shown by A l t e r m a n and A b r a m o v i c i (1967) who computed theoretical seismograms for spherical models and a *P*-wave point source.

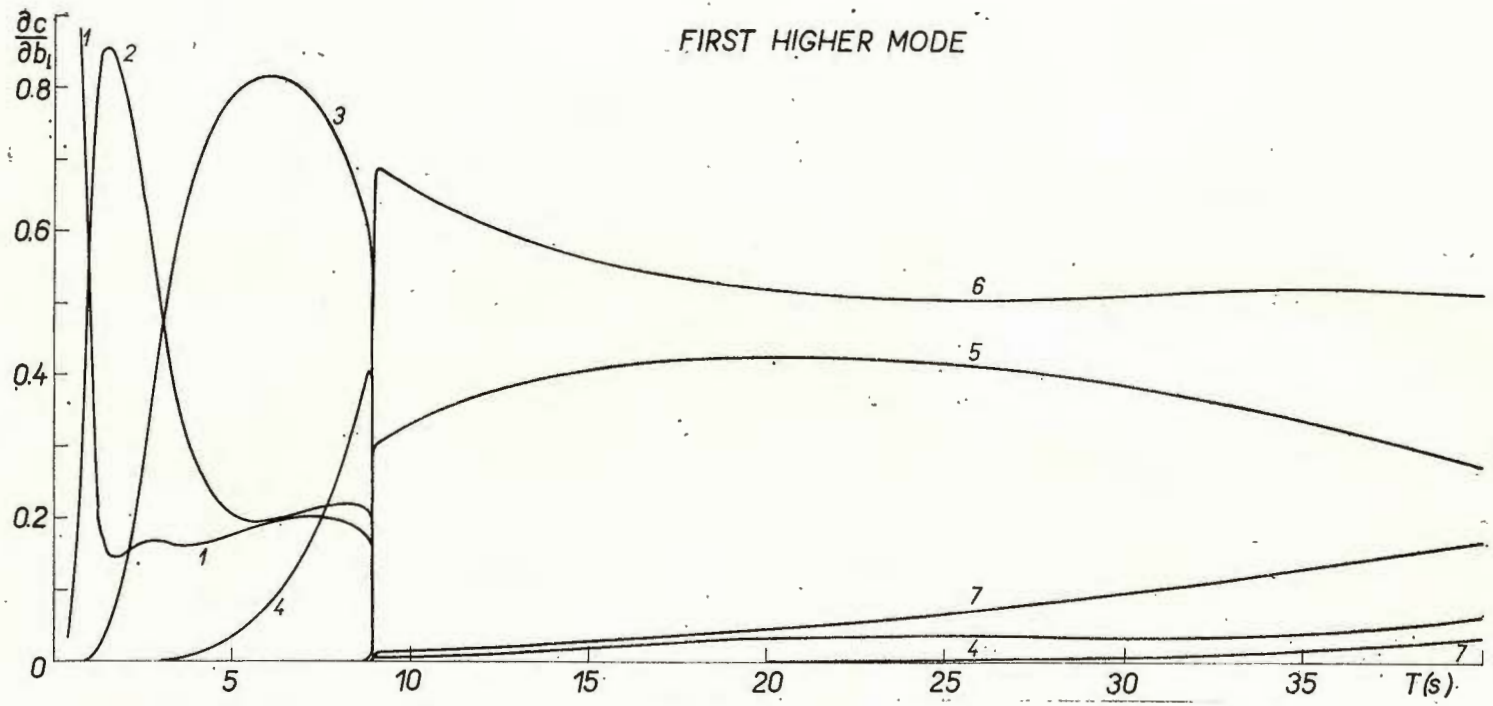

Fig. 13. — The partial derivatives of the first higher mode of Love waves.

In order to be able to explore succesfully the favourable properties of higher modes, it is essential to know the amplitude ratios of the higher modes to the fundamental one. In other words, to know the partition of energy among surface wave modes. Harkrider and Anderson (1966) studied the partition of energy among surface wave modes by means of their amplitude spectra. A similar way to get an image about the ratio of amplitudes of surface waves is the computation of theoretical seismograms. The computation of theoretical seismograms in a horizontally layered medium by wave method is not a simple problem, especially when we are interested in body wave phases. However, the part of theore-

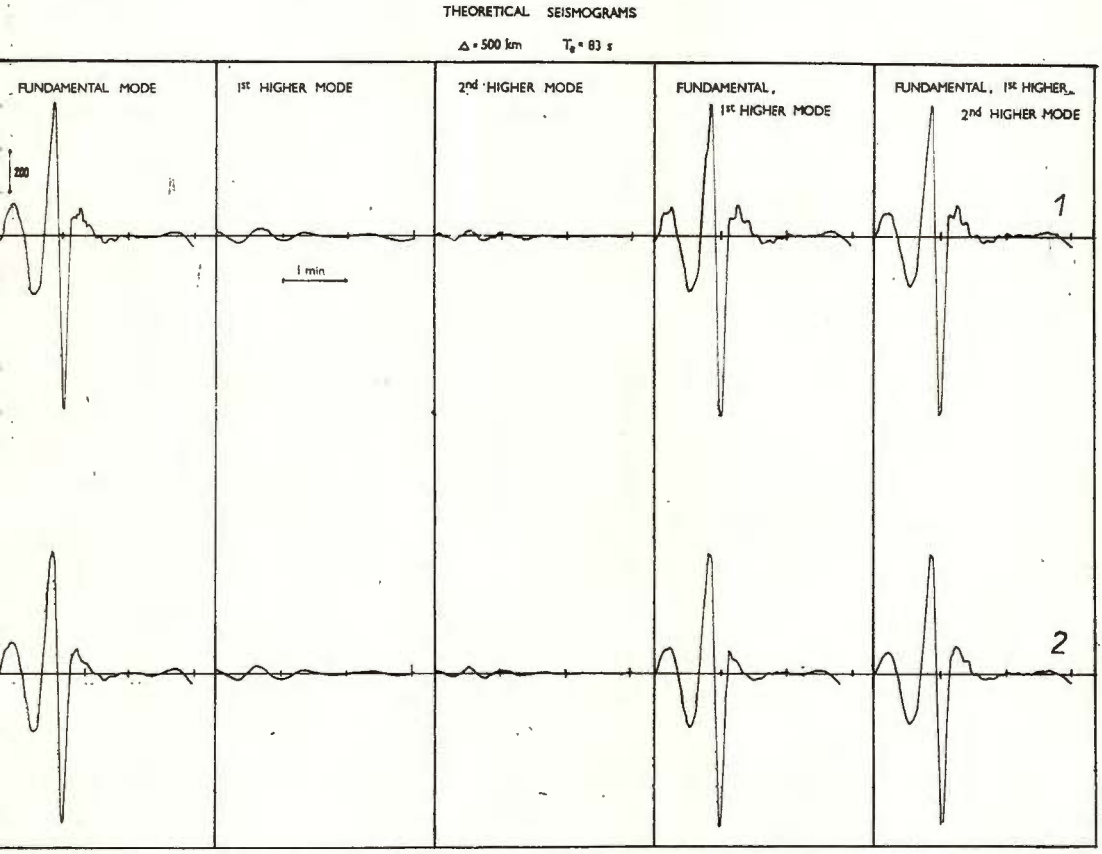

Tig. 14. — Theoretical seismograms of Love waves, computed for a shield model having a mantle low velocity zone.

tical seismogram which corresponds to surface waves can be computed without difficulties. Figures 14 and 15 show theoretical seismograms of Love waves computed for a shield model having mantle low velocity zone. It is the same model which is shown in figure 11. In the first row, the

seismograms for the source situated at the top of the first layer are given, the second row corresponds to the position of the source situated in the second layer a.s.o. It is seen that the seismograms corresponding to surface foci contain a negligible portion of higher mode energy, the mutual separation of individual modes is practically excluded. If the seismic

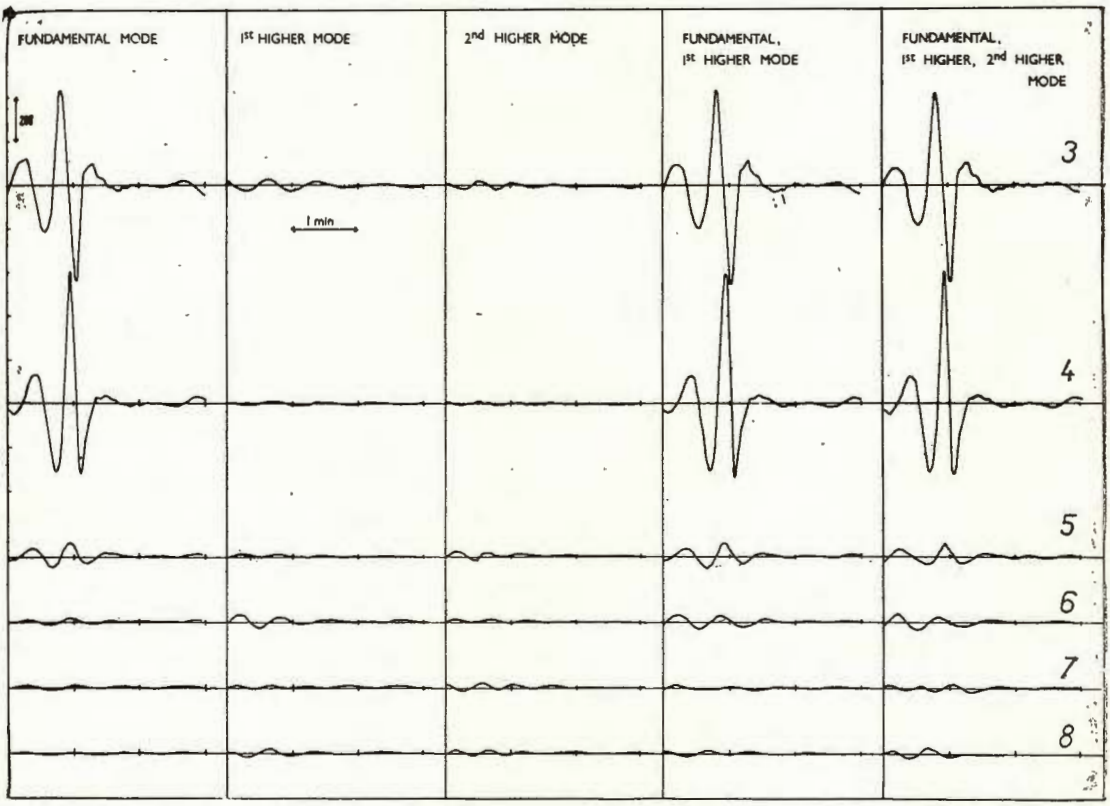

Fig. 15. — Theoretical seismograms of Love waves, computed for a shield model having a mantle low velocity zone.

source is situated in the low velocity zone or below it, the higher modes have the amplitudes comparable with the amplitudes of the fundamental mode.

The pecularities of higher modes of surface waves have been studied by Thatcher and Brune (1969) and by Boore (1969), who have also investigated the limitations in the application of higher modes to the structure studies.

The systematic discrepancies between the structure determinations made by use of Love and Rayleigh waves indicate that the theoretical models are oversimplified. The nature of some of these discrepancies

suggests that they may be due to the anisotropy of seismic velocities. One of the earliest investigators dealing with the seismological implications of anisotropy was Jeffreys (1934). Theoretical studies of anisotropy in a horizontally layered medium in relation to the surface waves and their dispersion curves have been carried out by a number of investigators, e.g. by Stoneley (1949), Crampin (1967), Anderson (1967), Johnson (1970). The problem of anisotropy is not so far solved in an exhaustive way and keeps on to be in the center of attention of many seismologists.

Considerable attention has been also devoted to surface waves in vertically inhomogeneous media. The continuous variation of elastic parameters and density with depth has been represented by various laws, namely by an exponential and power law.

The application of spectral theory to problems of surface waves has made possible taking into consideration more general media and types of source. Levshin and Yanson (1971) have solved the case of medium which is supposed to be subject to any law of variation of elastic constants and density with depth. The expression of the displacement in terms of eigenfunctions has been made use of.

The wave method has been used not only for the investigation of surface waves, but also for the investigation of various problems of seismic body waves in vertically inhomogeneous or in horizontally layered media (Gilbert, Backus, 1966). The classical problem in this field is the computation of reflection coefficients from transition layers. Various approaches can be used (Fuchs, 1968 a; Ratnikova, Levshin, 1967; Richards, 1971; Gupta, 1966). The reflection coefficient being found, an integration must be performed to evaluate the wave field from a transition layer due to a point source. The numerical integration meets a number of serious difficulties. Certain approaches to the computations of discussed integrals have been proposed by Fuchs (1968 b) and Phinney (1965). Fuchs has investigated in detail the reflections from transitions and laminated layers and obtained a number of results of considerable seismological interest. Also asymptotic methods can be used to evaluate the integrals (Fuchs, 1971; Nakamura, 1968; Merzer, 1971). Note that the first quite exact solution of the point source — linear transition layer problem has been obtained by Hirasawa and Berry (1971). Exact solutions are derived by numerical evaluation of the contour integral in the complex wave number plane.

The wave theory has been also used to solve the problem of reflections from irregular interface. The theory of reflection of seismic wave from an irregular interface is very complicated. The difficulty is caused mainly by the boundary conditions which must be applied on the irregular interface. When the curvature of the interface is small, the ray theory can be often applied (Gel'chinskiy et. al., 1968). The ray theory, however, is not applicable when the curvature is large. Various methods have been used to investigate the mentioned problems (Abubakar, 1962; 1963; Aki, Larner, 1970). Considerable progress has been acheived by the application of direct numerical methods, see the next section.

DIRECT NUMERICAL APPROACHES

During recent years substantial progress has been acheived in the direct numerical solutions of equations of motion of elasticity by means of finite difference method. A series of important papers has been published by Alterman. The method has been applied to study the pulse propagation in a heterogeneous sphere, in a layered halfspace, in a quarter and three-quarter plane, a.s.o. (Alterman, 1968; Alterman Aboudi, 1971; Alterman, Karal, 1968; Alterman, Loewenthal, 1970; 1972). A detailed review is given in Alterman and Loewenthal (1972). Results of computations carried out by means of the method of finite-difference for a point source in a layered halfspace were compared to results of earlier computations carried out by means of the exact ray theory by Alterman and Karal (1968). The agreement between the theoretical seismograms obtained by two different methods was very good. The finite-difference computations proved to be much faster than the calculations based on the exact ray theory. The use of finite differences turned out to be advantageous not only for problems for which analytic solutions have not been found but also for problems for which analytic solutions are lengthy. Very promissing is the combinations of finite-difference method with other methods, e.g., with the perturbation method. This combination has been used for the investigation of certain problems of wave propagation in laterally inhomogeneous media by Landers and Claerbout (1972) and in a medium with the corrugated surface by Alterman and Aboudi (1972).

The finite-difference method and the finite-element method are very convenient for the investigations of surface waves in inhomogeneous media with irregular boundaries. Detailed reviews are given in Boore (1972), Lysmer and Drake (1971; 1972).

REFERENCES

Abubakar I. (1962) Scattering of elastic plane waves at rough interfaces. I. *Proc. Cambridge Phil. Soc.*, 58, Cambridge.

— (1963) Scattering of plane elastic waves at rough interfaces. II. *Proc. Cambridge Phil. Soc.*, 59, Cambridge.

Aki K., Larner K. L. (1970) Surface motion of a layered medium having an irregular interface due to incident *SH* waves. *J. Geophys. Res.*, 75, Richmond.

Alekseyev A. S., Lavrentyev M. M., Mukhometov R. G., Romanov V. G. (1969) Numerical method for the solution of three-dimensional inverse kinematic problem of seismology. (in Russian) *Mathematical problems of geophysics*, 1, AN SSSR, Novosibirsk.

— Lavrentyev M. M., Mukhometov R. G., Nersesov I. L., Romanov V. G. (1970) Method for numerical investigation of lateral inhomogeneities in the Earth's mantle from seismological data. *X Gen. Ass. ESC*, Acad. Sci. USSR, Moskow.

— Lavrentyev M. M., Mukhometov R. G., Nersesov I. L., Romanov V. G. (1971) Numerical method for determination of the structure of the upper mantle of the Earth. (in Russian) *Mathematical problems of geophysics*, 2, AN SSSR, Novosibirsk.

Alterman Z. S. (1968) Finite difference solution to geophysical problems. *J. Phys. Earth*, 16.

— (1969) Higher mode surface waves. *Geophys. Monogr.*, 13, The Earth's crust and upper mantle, ed. P. J. Hart, Am. Geophys. Un., Washington.

— Aboudi J. (1971) Propagation of elastic waves caused by an impulsive source in a half space with a corrugated surface. *Geophys. J. R. Astr. Soc.*, 24, London.

— Abramovici F. (1967) The motion of the sphere caused by an impulsive force and by an explosive point source. *Geophys. J.R.Astr. Soc.*, 13, London.

— Karal F. C. (1968) Propagation of elastic waves in layered media by finite difference methods. *Bull. Seism. Soc. Am.*, 58, Berkeley.

— Loewenthal D. (1970) Seismic waves in a quarter and three-quarter plane. *Geophys. J.R.Astr. Soc.*, 20, London.

Anderson D.L. (1967) Latest information from seismic observations. *In*: The Earth's mantle, ed. T. F. Gaskell, Acad. Press, New York.

Babich V. M. (1967) Energy conservation for propagation of nonstationary waves. (in Russian) *Problems of the dynamic theory of propagation of seismic waves*, 7, Nauka, Leningrad.

— Babich G. N., Fomina N. A. (1968) On Love waves computations using asymptotic formulae of the WKB method. (in Russian) *In*: Some direct and inverse problems of seismology. *Computational seismology*, 4, Nauka, Moscow.

— Molotkov I. A. (1966) Propagation of Love waves in a half space inhomogeneous in two coordinates. (in Russian) *Bull. (Izv.) Acad. Sci. USSR, Geophys. Ser.*, 6, Moscow.

— Molotkov *I. A.* (1971) Application of asymptotic methods in the theory of surface waves. (in Russian) *Proc. V. Symp. on Diffraction and Wave Propagation*, Nauka, Leningrad.

— Buldyrev V. S. (1972) Asymptotic methods in the problems of diffraction of short waves. (in Russian) Nauka, Moscow.

Belonosova A. V., Alekseyev A. S. (1967) On one formulation of inverse kinematic problem of seismology for two-dimensional continuously inhomogeneous medium. (in Russian) *In*: Certain methods and algorithms in the interpretation of geophysical data. Nauka, Moscow.

— Tadzimukhamedova S. S., Alekseyev A. S. (1967) Computation of travel-time curves and geometrical ray spreading in inhomogeneous media (in Russian) *In*: Certain Methods and algorithms in the interpretation of geophysical data. Nauka, Moscow.

Beránek B., Zounková M., Holub K. (1971) Results of deep seismic sounding in Czechoslovakia. *In*: Upper Mantle Project Programme in Czechoslovakia 1962—1970, Geophysics, Final Report, Academia, Prague.

Berzon I. S., Ratnikova L. I. (1971) Approximate calculations of seismic reflected waves in multilayered thinlayered media. (in Russian) *Izv. AN SSSR, Fiz. Zemli*, 10, Moskva.

Biswas N. N., Knopoff L. (1970) Exact earth-flattening calculation for Love waves. *Bull. Seism. Soc. Am.*, 60, Berkeley.

Boore D.M. (1969) Effect of higher mode contamination on measured Love wave phase velocities. *J. Geophys. Res.*, 74, Richmond.

— Larner K. L., Aki K. (1971) Comparison of two independent methods for the solution of wave scattering problems: Response of a sedimentary basin to vertically incident *SH* waves. *J. Geophys. Res.*, 76, Richmond.

Bortfeld R. (1967) Elastic waves in layered media. *Geophys. Prosp.*, 15, Hague.

Brune J., Dorman J. (1963) Seismic waves and Earth structure in the Canadian Shield. *Bull. Seism. Soc. Am.*, 53, Berkeley.

Červený V., Ravindra R. (1971) Theory of seismic head waves. Univ. Toronto Press, Toronto.

— (1972 a) Seismic rays and ray intensities in inhomogeneous anisotropic media. *Geophys. J. R. Astr. Soc.*, 29, London.

— (1972 b) Theory of elastic wave propagation in inhomogeneous media. *Z. Geophys.*, 38, Würzburg.

— Pšenčík I. (1972 a) Rays and time-distance curves in inhomogeneous anisotropic media. *Z. Geophys.*, 38, Würzburg.

— Pšenčík I. (1972 b) Computation of diffracted rays in inhomogeneous media with curved interfaces. *Stud. Geophys. Geod.*, 16, Prague.
— Zahradník J. (1972) Amplitude distance curves of seismic body waves in the neighbourhood of critical points and caustics. A comparison. *Z. Geophys.*, 38, Würzburg.
Chatterjee S. N. (1971) Propagation of Rayleigh waves in a layer over a heterogeneous halfspace. *Pure Appl. Geophys.*, 86, III, Basel.
Crampin S. (1965) Higher modes of seismic surface waves. Second Rayleigh mode energy. *J. Geophys. Res.*, 70, Richmond.
— (1967) Coupled Rayleigh-Love second mode. *Geophys. J. R. Astr. Soc.*, 12, London.
Dunkin J. W. (1965) Computation of modal solution in layered elastic media at high frequencies. *Bull. Seism. Soc. Am.*, 55, Berkeley.
Fazylov F. N. (1971) Numerical solution of one inverse kinematic problem of seismology. (in Russian) *Mathematical problems of geophysics*, 2, Acad. Sci. USSR, Novosibirsk.
Fuchs K. (1968 a) Das Reflexions- und Transmissionsvermögen eines geschichteten Mediums mit beliebiger Tiefenverteilung der elastischen Moduln und der Dichte für schrägen Einfall ebener Wellen. *Z. Geophys.*, 34, Würzburg.
—, (1968 b) The reflection of spherical waves from transition zones with arbitrary depth-dependent elastic moduli and density. *J. Phys. Earth*, 16.
— (1970) On the determination of velocity-depth distributions of elastic waves from the dynamic characteristics of the reflected wave field. *Z. Geophys.*, 36, Würzburg.
— (1971) The method of stationary phase applied to the reflection of spherical waves from transition zones with arbitrary depth-dependent elastic moduli and density. *Z. Geophys.*, 37, Würzburg.
— Müller K. (1971) Computation of synthetic seismograms with the reflectivity method comparison with observations. *Geophys. J. R. Astr. Soc.*, 23, London.
Fukao Y., Ate K. (1971) Multimode Love waves excited by shallow and deep earthquakes. *Bull. Earthq. Res. Inst.*, 49, Tokyo.
Garvin W. W. (1956) Exact solution of the buried line source. *Proc. R. Soc. London*, A 234, London.
Gel'chinskiy B. Y., Smirnova N. S., Ozerov D. K. (1968) On one way of Rayleigh surface wave computation. (in Russian) *Problems of the dynamic theory of propagation of seismic waves*, 9, Nauka, Leningrad.
— Karayev N. A., Kogan L. D., Prokator O. M. (1968) Theoretical and model investigation of wave fields, reflected from corrugated curved interfaces. (in Russian) *Problems of the dynamic theory of propagation of seismic waves*, 9, Nauka, Leningrad.
Gerver M., Markushevich V. (1966) Determination of a seismic wave velocity from the travel-time curve. *Geophys. J. R. Astr. Soc.*, 11, London.
— Markushevich V. (1967) On the characteristic properties of travel-time curves. *Geophys. J. R. Astr. Soc.*, 13, London.
Gilbert F., Backus G. E. (1966) Propagator matrices in elastic wave and vibration problems. *Geophysics*, 31, Tulsa.
Grudeva N. R., Levshin A. L., Francuzova V. I. (1971) On the nature of channel seismic waves. *In*: Algorithms for interpretation of seismic data, *Computational seismology*, 5, Nauka, Leningrad.
Gupta R. N. (1968) Reflection of plane elastic waves from transition layer with arbitrary variation of velocity and density. *Bull. Seism. Soc. Am.*, 56, Berkeley.
Haskell N. A. (1953) The dispersion of surface waves on multilayered media. *Bull. Seism. Soc. Am.*, 43, Berkeley.
Harkrider D. G. (1968) The perturbation of Love wave spectra. *Bull. Seism. Soc. Am.*, 58, Berkeley.
— (1964) Surface waves in multilayered elastic media 1. Rayleigh and Love waves from buried sources in a multilayered elastic halfspace. *Bull. Seism. Soc. Am.*, 54, Berkeley.
— (1970) Surface waves in multilayered elastic media 2. Higher mode spectra and spectral ratios from point sources in plane layered earth models. *Bull. Seism. Soc. Am.*, 60, Berkeley.
— Anderson D. L. (1966) Surface wave energy from point sources in plane layered earth models. *J. Geophys. Res.*, 76, Richmond.
Helmberger D. V. (1968) The crust-mantle transition in the Bering Sea. *Bull. Seism. Soc. Am.*, 58, Berkeley.

— Morris G. B. (1969) A travel-time and amplitude interpretation of a marine refraction profile : primary waves. *J. Geophys. Res.*, 74, Richmond.
— Morris G. B. (1970) A travel-time and amplitude interpretation of a marine refraction profile : transformed shear waves. *Bull. Seism. Soc. Am.*, 60, Berkeley.
Hirasawa T., Berry M J. (1971) Reflected and head waves from a linear transition layer in a fluid medium. *Bull. Seism. Soc. Am.*, 61, Berkeley.
Hron F., Kanasewich E. R. (1971) Synthetic seismograms for deep seismic sounding studies using asymptotic ray theory. *Bull. Seism. Soc. Am.*, 61, Berkeley.
— (1971) Criteria for selection of phases in synthetic seismograms for layered media. *Bull. Seism. Soc. Am.*, 61, Berkeley.
— (1973) Numerical methods of ray generation in multilayered media. *In* : Methods of Computational Physics, *Seismology*, 12, New York.
James D. E. (1971) Anomalous Love wave velocities. *J. Geophys. Res.*, 76, Richmond.
Jeffreys H. (1934) The surface waves of earthquakes. *Mon. Not. R. Astr. Soc., Geophys. Suppl.*, 3, London.
Johnson W. W. (1970) The propagation of Stoneley and Rayleigh waves in anisotropic elastic media. *Bull. Seism. Soc. Am.*, 60, Berkeley.
Johnson L E., Gilbert F. (1972) Inversion and inference for teleseismic ray data. *In* : Methods of Computational Physics, *Seismology*, 12, New York.
Kovach R. L. (1965) Seismic surface waves. Some observations and recent developments. *Phys. Chem. Earth*, 6.
— Anderson D. L. (1964) Higher mode surface waves and their bearing on the structure of the Earth's mantle. *Bull. Seism. Soc. Am.*, 54, Berkeley.
Knopoff L. (1964) A matrix method for elastic wave problems. *Bull. Seism. Soc. Am.*, 54, Berkeley.
— (1969) Phase and group slowness in inhomogeneous media. *J. Geophys. Res.*, 74, Richmond.
— Schwab F. A. (1968) Apparent initial phase of a source of Rayleigh waves. *J. Geophys. Res.*, 73, Richmond.
Knauklis P. V. (1969) Nonstationary Stoneley waves. (in Russian) *Problems of the dynamic theory of seismic wave propagation*, 9. Nauka, Leningrad.
Lal T. (1970) Love waves in an inhomogeneous interstratum. *Pure Appl. Geophys.*, 79, II, Basel.
Landers T., Claerbout J. F. (1972) Numerical calculations of elastic waves in laterally inhomogeneous media. *J. Geophys. Res.*, 77, Richmond.
Landisman M., Dziewonski A., Sato Y. (1969) Recent improvement in the analysis of surface wave observations. *Geophys. J. R. Astr. Soc.*, 17, London.
Lavrentyev M. M., Mukhometov R. G (1969) Investigation of stability of inverse kinematic problem of seismology. (in Russian) *Mathematical problems of geophysics*, 1, Acad. Sci. USSR, Novosibirsk.
Levshin A. L., Francuzova V. I., Shkadinskaya G. V. (1968) Amplitude spectra of surface waves. *In* : Some direct and inverse problems of seismology. *Computational seismology*, 4, Nauka, Moscow.
— Yanson Z. A. (1971) Surface waves in vertically and radially inhomogeneous media. (in Russian) *In* : Algorithms for interpretation of seismic data. *Computation seismology*, 5, Nauka, Mosow.
Lysmer J., Drake L. A. (1971) The propagation of Love waves across nonhorizontally layered structures. *Bull. Seism. Soc. Am.*, 61, Berkeley.
— Drake L. A. (1972) A finite element method for seismology *Methods of Computational Physics*, 11, Acad. Press, New York.
Marcinkovskaya N. G. Krasavin V. G. (1968) Algorithm for calculation of the reflected wave field in media with curved interfaces (in Russian) *Problems of the dynamic theory of propagation of seismic waves*, 9, Nauka, Leningrad.
Merzer A. M. (1971) Head waves from different transition layers. *Geophys. J.R.Astr. Soc.*, 24, London.
Mc. Mehan G. A., Wiggins R. A., (1972) Depth limitations in body wave inversions. *Geophys. J. R. Astr. Soc.*, 28, London.

Molotkov I. A., Ozerov D K. (1968) Love wave propagation in a halfspace inhomogeneous in two coordinates and in a layer with variable thickness. (in Russian) *Problems of the dynamic theory of propagation of seismic waves*, 9. Nauka, Moscow.

Müller G. (1968) Theoretical seismograms for some types of point sources in layered media. Part 1 : Theory. Part 2 : Numerical calulations. *Z. Geophys.*, 34, Würzburg.

— (1969) Theoretical seismograms for some types of point sources in layered media. Part 3 : Single force and dipol sources of arbitrary orientation. *Z. Geophys.*, 35, Würzburg.

— (1970) Exact theory and its application to the reflection of elastic waves from vertically inhomogeneous media. *Geophys. J. R. Astr. Soc.*, 21, London.

(1971) Approximate treatment of elastic body waves in media with spherical symmetry. *Geophys. J. R. Astr. Soc.*, 23, London.

Nakamura Y. (1968) Head waves from a transition layer. *Bull. Seism. Soc. Am.*, 58, Berkeley.

Novotný O. (1970). Partial derivatives of dispersion curves of Love waves in a layered medium. *Stud. Geophys. Geod.*, 14, Prague.

Ozerov D. K. (1966) On dispersion equation for interfered *SH* waves, propagating in media with spherical boundaries, obtained by a ray method. *Problems of the dynamic theory of seismic waves*, 8, Nauka, Leningrad.

Pěč K., Novotný O. (1972). The influence of the low-velocity zone on phase velocities and amplitudes of Love waves. *Z. Geophys.*, 38, Würzburg.

Pekeris C. L., Alterman Z., Abramovici F., Jarosch H. (1965)Propagation of a compressional pulse in a layered solid. *Rev. Geophys.*, 3. Washington.

Petrashen G. I., Vavilova T. I. (1968) On the calculation of the intensity of summary multiple waves in multilayered media for arbitrary position of source and receiver. (in Russian) *Problems of the dynamic theory of propagation of seismic waves*, 9, Nauka, Leningrad.

Phinney R. A. (1965) Theoretical calculations of the spectrum of first arrivals in layered elastic mediums. *J. Geophys. Res.*, 70, Richmond.

— (1970) Reflection of acoustic waves in a continuously varying interfacial region. *Rev. Geophys.*, 8, Washington.

Pilant W. L., Knopoff L. (1970) Inversion of phase and group slowness dispersion. *J. Geophys. Res.*, 75, Richmond.

Podyapolskiy G. S. (1959) The propagation of elastic waves in a layered medium, I, II. *Bull. (Izv.) Acad. Sci. USSR, Geophys. Ser.*, Moscow.

Pšenčík I. (1972) Kinematics of refracted and reflected waves in inhomogeneous media with non-planar interfaces. *Stud. Geophys. Geod.*, 16, Prague.

Randall M. J. (1967) Fast pograms for layered half-space problems. *Bull. Seism. Soc. Am.*, 57, Berkeley.

Ratnikova L. I., Levshin A. L. (1967) Computation of spectral characteristics of thin layered media. *Izv. AN SSSR, Fiz. Zemli*, 2, Moskva.

Richards P. G. (1971) Elastic wave solutions in stratified media. *Geophysics*, 36, Tulsa.

Savarensky E. F., Glasko V. B., Trapit Y. M. (1967) Dependence of phase and group velocities of Rayleigh and Love waves on two-layer crust parameters. (in Russian) *Izv. AN SSSR, Fiz. Zemli*, 3, Moskva.

— Glasko V. B., Peshkov A. B. (1971) On determination of the thickness of two-layer crust using regulating algorithms. (in Russian) *Izv. AN SSSR, Fiz. Zemli*, 6, Moskva.

— Fedorov S. A., Starovoit O. E. (1970) On surface seismic waves formation. *Pure Appl. Geophys.*, 82, V, Basel.

Schwab F. A. (1970) Surface wave dispersion computations: Knopoff's method. *Bull. Seism. Soc. Am.*, 60, Berkeley.

— Knopoff L. (1971) Surface waves on multilayered anelastic media. *Bull. Seism. Soc. Am.*, 61, Berkeley.

— Knopoff L. (1972) Fast surface wave and free mode computations. *Methods in Computational Physics*, 11, Acad. Press, New York.

Stoneley R. (1949) The seismological implications of aelotropy. in continental crust. *Mon. Not. R. Astr. Soc., Geophys. Suppl.*, 5, London.

Thatcher W., Brune J. N. (1969) Higher mode interference and observed anomalous apparent Love wave phase velocities. *J. Geophys. Res.*, 74, Richmond.

Thomson W. T. (1950) Transmission of elastic waves through stratified solid medium. *J. Appl. Phys.*, 21, Lancaster.

Throver E. N. (1965) the computation of the dispersion of elastic waves in layered media. *J. Sound Vib.*, 2, London.

Thapliyal V. (1971) Love waves in inhomogeneous and anisotropic earth. *Pure Appl. Geophys.*, 91, VIII, Basel.

Upadhyay S. K. (1971) Separation of equation of motion of Love waves in curvilinearly anisotropic inhomogeneous medium. *Pure Appl. Geophys.*, 86, VIII, Basel.

— (1970) Love wave propagation in multilayered anisotropic inhomogeneous media. *Pure Appl. Geophys.*, 81, IV, Basel.

Vavilova T. I., Volodko L. V. (1968) Algorithm and programme for the calculation of the intensity of summary multiple reflections propagating without conversions in axially symmetric inhomogeneous layered media. (in Russian) *Problems of the dynamic theory of propagation of seismic waves*, 9, Nauka, Leningrad.

Vlaar N. J. (1968) Ray theory for an anisotropic inhomogeneous elastic medium. *Bull. Seism. Soc. Am.*, 58, Berkeley.

Watson T. H. (1970) Fast computation of Rayleigh wave dispersion in a layered half-space. *Bull. Seism. Soc. Am.*, 60, Berkeley.

Wesson R. L. (1970) A time integration method for computation of the intensities of seismic rays. *Bull. Seism. Soc. Am.*, 60, Berkeley.

SYNTHÈSE D'ONDES *PL* ET *PL (S)* À PARTIR DE MODES NORMAUX[1]

PAR

NELLY JOBERT[2]

Résumé

On construit à l'aide des premiers harmoniques sphéroïdaux d'un modèle de Terre sphérique a croûte continentale une onde *PL* à courte distance, et une onde *S* aux distances où peut apparaître un couplage avec l'onde *PL*. Les caractères de l'onde *PL* (son amortissement en particulier) peuvent être retrouvés sur une somme de modes normaux. L'aspect de l'onde *S* au voisinage de la distance de couplage résulte de l'interférence entre différents harmoniques, des groupes à dispersion anormale caractéristiques de la présence de la croûte.

Les ondes *PL*, imparfaitement guidées dans la croûte, sont associées à des racines complexes de l'équation de dispersion d'un modèle plan. Si on considère un modèle sphérique, toute phase d'un sismogramme pouvant alors être obtenue par synthèse de modes normaux, correspondant à des racines réelles, on peut espérer faire apparaître des ondes *PL* par un choix convenable du domaine spectral.

Poupinet (1970) a montré que la dispersion des premiers harmoniques spéroïdaux d'un modèle sphérique à croûte continentale (modèle de Gilbert, 1964) présentait des anomalies caractéristiques de la présence de la croûte : on voit sur la figure 1b une famille de maxima et minima de la vitesse du groupe, tendant vers un point d'inflexion avant de disparaître ; pour une sphère homogène, la famille analogue tend rapidement vers une vitesse de groupe plus grande (fig. 1a) et correspond (Alterman, 1969) à des réflexions multiples en surface de type $P_\mu S_\nu$; les périodes et vitesses de phase des groupes de la famille de la figure 1b se placent (fig. 2) sur la courbe de dispersion de l'onde *PL* dans la „zone d'observations" à plus faible amortissement, les vitesses de phase sont alors voisines de V_2. Georges Poupinet a montré l'existence d'autres familles, correspondant à des harmoniques de modes à perte.

En ce qui concerne la première famille, les calculs de Georges Poupinet ont été effectués pour les quarante premiers harmoniques jusqu'à un ordre n voisin de 300. Les sismogrammes théoriques sont bâtis à partir des valeurs propres lp_n correspondantes, en cherchant à faire apparaître des accords de phase entre harmoniques. On considère la composante lon-

[1] Contribution I.P.G. N 60.

[2] Institut de Physique du Globe. Université Paris VI. E.R.C.N.R.S. N 115. Paris, France.

gitudinale du déplacement provoqué par une source brusque située à l'origine en un point de la surface à la distance angulaire Δ. Pour chaque harmonique de rang l, on calcule :

$$\sum_{1}^{N} A_n P_n^1(\cos \Delta) \cos l p_n t$$

où P_n^1 est la dérivée par rapport à Δ du polynôme de Legendre $P_n(\cos \Delta)$. L'amplitude A_n, arbitraire, est lentement variable avec l'indice n, comme

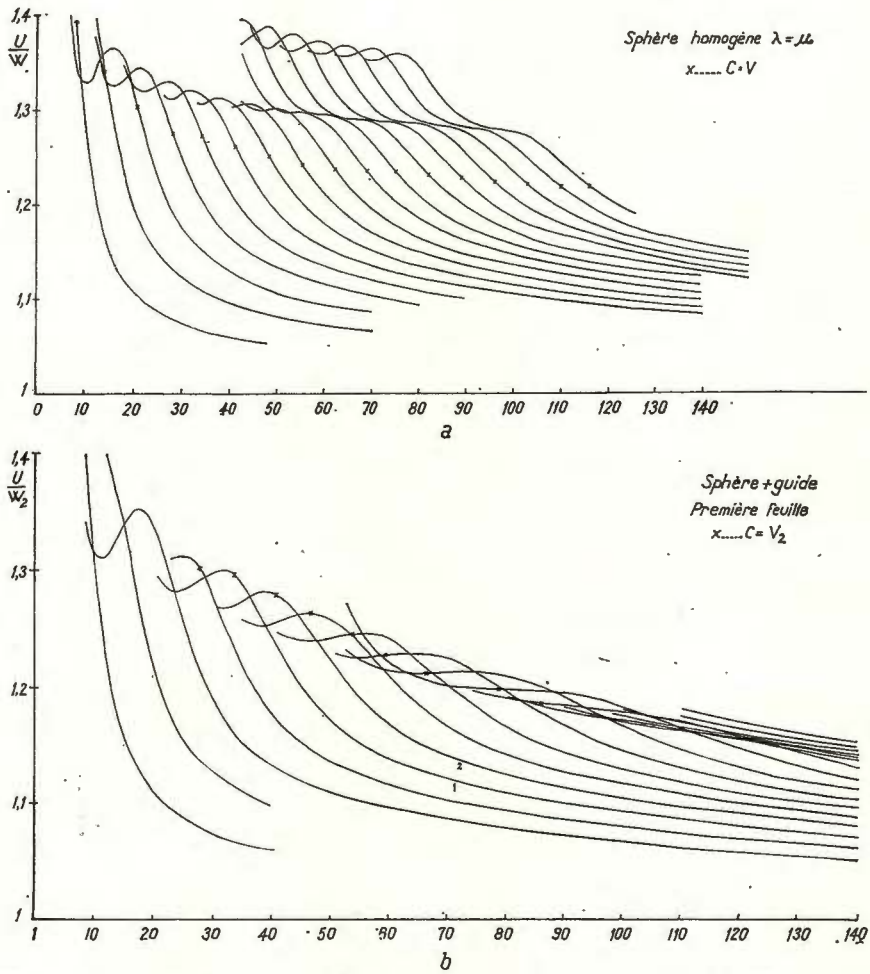

Fig. 1. — a) Dispersion (vitesse de groupe en fonction de l'indice n de l'harmonique sphérique) des premiers harmoniques sphéroïdaux de la sphère homogène ;

b) Dispersion des premiers harmoniques d'un modèle sphérique stratifié ayant les propriétés du modèle continental de Gilbert (1964) :

$H = 35$ km ; $V_1 = 5{,}9$ km/s ; $W_1 = 3{,}41$ km/s ; $\rho_1 = 2{,}67$g /cm^3. demi-espace ; $V_2 = 8{,}1$ km/s ; $W_2 = 4{,}68$ km/s ; $\rho_2 = 3{,}27$ g/cm^3.

c'est le cas pour une source voisine de la surface. Ensuite on somme la contribution des différents harmoniques ; le résultat, dans ces conditions, est influencé seulement par les déphasages entre harmoniques.

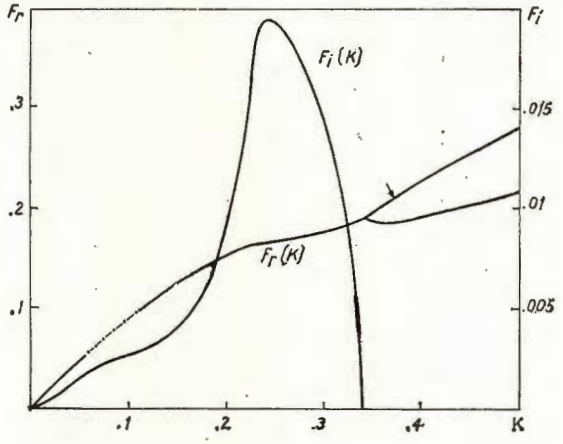

Fig. 2. — Comparaison des anomalies de dispersion des harmoniques sphéroïdaux avec le mode de $P+-$ de Gilbert (1964) : $F = H/V_2T$; $K = H$; Λ/Λ = longueur d'onde.

ONDE PL

Aux courtes distances, la vitesse apparente de l'onde P este voisine de V_2. La limite N des sommes partielles a donc été prise de façon à assurer la synthèse des groupes ayant cette vitesse de phase, qui sont justement les groupes à anomalie de dispersion. Sur la figure 3, pour $\Delta = 5°$, on voit que les harmoniques sont d'autant plus en phase que leur rang augmente ; leur somme contribue à une onde P dont la période apparente est de l'ordre de 50 secondes. Quand la distance augmente, le déphasage entre les trains augmente et ils interfèrent de moins en moins. Dans la somme, leur contribution, sous forme d'une petite ondelette de 40 secondes de période environ, se détache de l'onde à grande période située au voisinage du temps d'arrivée des P (la reconstitution de la phase P nécessiterait la somme d'un très grand nombre d'harmoniques). L'ondelette devient de plus en plus faible, à $\Delta = 25°$ les harmoniques ont des phases trop différentes pour que l'interférence soit constructive.

On voit ainsi que l'amortissement de l'onde PL au cours de sa propagation résulte de l'augmentation avec la distance du déphasage entre les trains d'harmoniques.

La période apparente de l'ondelette résultant de l'interférence des groupes à anomalie de dispersion est de l'ordre de 36 secondes, ce qui correspond suivant les notations de Gilbert à des parties réelle et imaginaire de la fréquence réduite : $Fr = 0{,}12$; $F_i = 0{,}003$ (fig. 1) d'où une vitesse de groupe U_g de l'ordre de 5 km/s et un facteur de qualité théorique $Q = 15$; d'après les amplitudes des sismogrammes calculés, on trouve Q de l'ordre de 25, et une vitesse de groupe de 5,3 km/s.

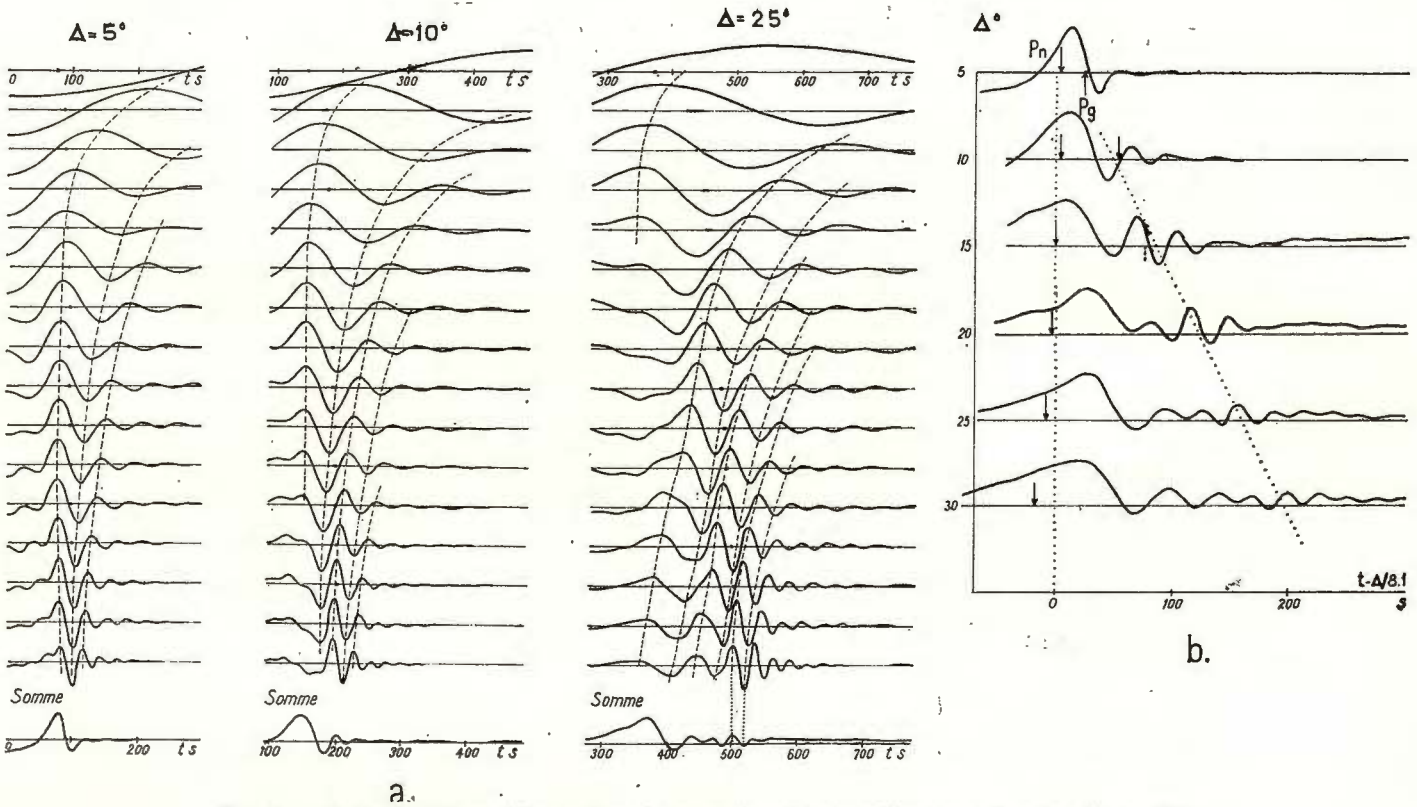

Fig. 3. — a) Contributions des premiers harmoniques et leur somme pour $\Delta = 5°$, 10° et 25°; b) Sismogrammes théoriques en fonction de la distance. Les amplitudes ont été normalisées.

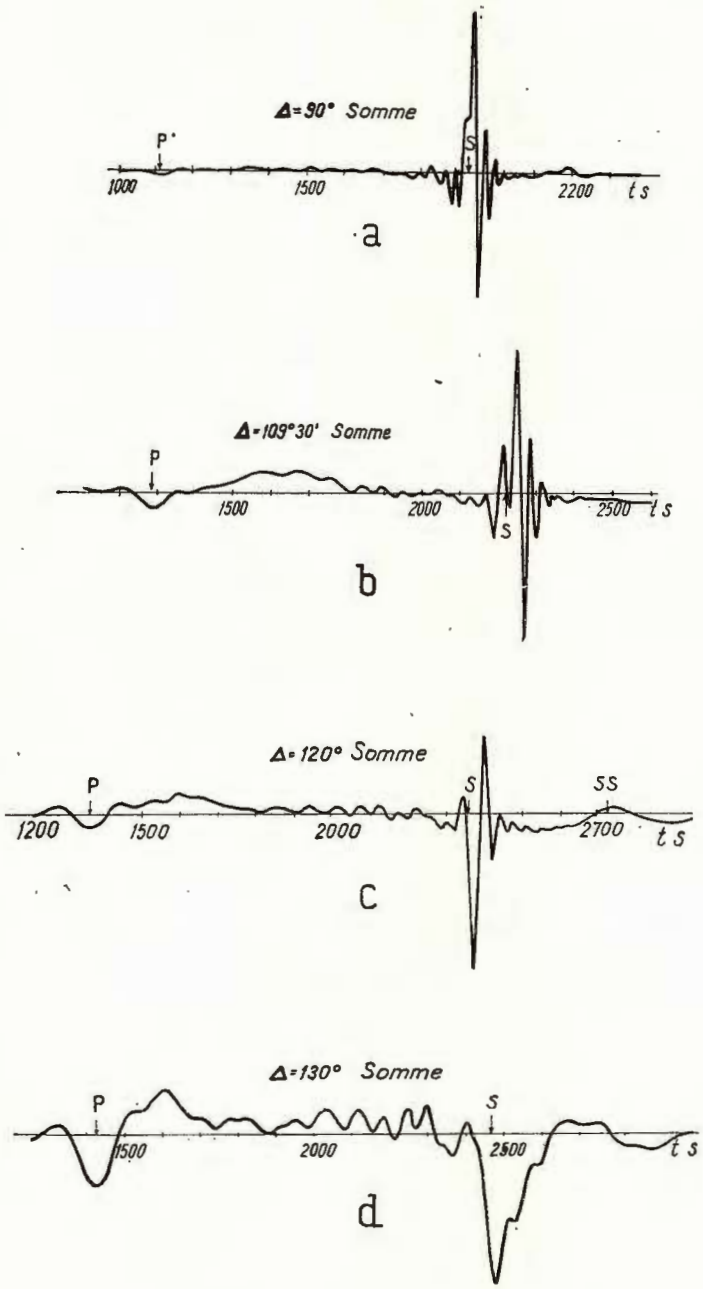

Fig. 4. — Somme des premiers harmoniques.

ONDE S

La théorie asymptotique des modes normaux permet de considérer l'onde *SH* comme formée lors d'interférences entre harmoniques, pour les groupes dont les vitesses de phase sont égales à la vitesse apparente de l'onde de volume (Ben Menahem, 1964; Pekeris, 1965); ces considérations sont applicables à d'autres phases (Brune, 1964). Pour le modèle considéré, la courbe de propagation des *S* est telle que la vitesse apparente $a\,\mathrm{d}\Delta/\mathrm{d}T \frac{\pi}{n} W_2 (\cos\Delta/2)^{-1}$ si le trajet dans la croûte est négligeable, devient voisine de V_2 pour $\Delta = \Delta_c = 109°30'$. On peut donc s'attendre ici à une contribution dans la phase *S* des groupes à dispersion anormale au voisinage de la distance Δ_c.

La figure 4 montre les résultats obtenus pour $\Delta = 90°$, 109°30', 120°, 130°; pour chaque harmonique, la somme a été limitée de façon à assurer la synthèse du groupe dont la vitesse de phase est égale à celle de l'onde *S*, de façon à favoriser les interférences entre harmoniques. Du fait du nombre limité d'harmoniques utilisé, l'onde *S* obtenue est incomplète à toutes distances; aussi sa période augmente-t-elle apparemment avec la distance. Les groupes à anomalie de dispersion sont bien synthétisés pour $\Delta \leqslant \Delta_c$; mais à distances inferieures, ils sont en avant de la zone d'interférence (fig. 4a) et, par suite de l'aplatissement à haute fréquence des courbes de vitesse de groupe, ce sont les groupes en fin de chaque train d'harmoniques qui sont prépondérants. Pour des distances supérieures à Δ_c, les groupes à anomalie de dispersion n'interfèrent plus, étant en arrière de la zone d'interférence (fig. 4d); sur la figure 4b, pour $\Delta = \Delta_c$ on voit l'interférence des groupes anormaux des derniers harmoniques. Les sommes ont été normalisées sur la figure 4, en réalité, l'amplitude maximum de la somme est obtenue pour $\Delta = 120°$.

On se propose d'améliorer la méthode en utilisant les amplitudes spectrales associées au modèle, en augmentant le nombre d'harmoniques et en cherchant l'effet de discontinuités plus profondes dans le manteau.

BIBLIOGRAPHIE

Alterman Z. (1969) Higher mode surface waves. *The Earth's Crust and Upper Mantle* Ed. American Geophys. Union.

Ben Menahem A. (1964) Mode-ray duality. *Bull. Seism. Soc. Am.*, 54, Berkeley.

Brune J. N. (1964) Travel times, body waves and normal modes of the Earth. *Bull. Seism. Soc. Am.*, 54, Berkeley.

Gilbert F. (1964) Propagation of transient leaking modes in a stratified elastic wave guide. *Rev. of Geoph.*, 2, 113, Washington.

Pekeris C. L. (1965) Asymptotic theory of the free torsional oscillations of the Earth. *Proc. N.A.S.*, 53.

Poupinet G. (1971) Relations entre les ondes PL dans un milieu borné et les modes normaux de vibration. *Ann. Geophys.*, 27, 105, Paris.

FUNDAMENTAL AND HIGHER MODES OF LOVE WAVES FOR DIFFERENT CRUST-MANTLE MODELS

BY

OLDŘICH NOVOTNÝ, KAREL PĚČ[1]

Abstract

The occurence of short period phases on theoretical seismograms and the properties of partial derivatives of dispersion curves for four crust-mantle models are studied. The individual models differ in a number of low velocity channels. The attention is also paid to the amplitudes and spectra of Love waves.

INTRODUCTION

The problem of the detailed structure of low velocity zones in the Earth's mantle and even the existence of these zones in the Earth's crust has become the object of numerous studies during the last period. Since the body wave methods carry only indirect information about the structure of low velocity zones, another independent features, highly dependent on low-velocity zone parameters, have been looked for.

In 1952 Press and Ewing discovered slow surface waves known as *Lg* phases, later Caloi (1954) described the so-called *Sa* wave and Båth (1957) the *Li* waves. These kinds of waves ware interpreted as channel waves propagating within low velocity zones of the Earth's crust (Gutenberg, 1955), propagating in the asthenosphere (Caloi, 1954), and as *S* rays multiply reflected beneath the Moho (Press, Ewing, 1955). That interpretation explains well the kinematic properties but is not getting well with the dynamics of the feature and puts the existence of these waves together with the existence of low velocity layers.

A different explanation based on the theory of normal modes was given by Oliver and Ewing (1958). They have associated the channel waves with local extremes of the group velocity dispersion curves. This approach explains the appearance of these waves on the sur-

[1] Geophysical Institute, The Charles University, Ke Karlovu 3, Praha 2, Czechoslovakia.

face as a basic property of normal modes without going to second order effects, as diffraction, etc. But the local extremes of group velocity dispersion curves do exist even for Earth's models without low velocity zones. The nature of this kind of waves is not so far clear and a question occurs whether the low velocity zone is or is not necessary for their existence. Recently Grudeva et al. (1971) have shown that pronounced short period phases, having properties very similar to observed *Lg* phases, exist regardless of the presence or absence of the low velocity zones. In this respect very important information has been received in numerous studies concerning the energy distribution among individual surface wave modes.

Many investigators (Alterman, 1969; Harkrider, 1970; Harkrider, Anderson, 1966; Pěč, Novotný, 1972) dealing with the properties of the fundamental and higher mode dispersion curves of surface waves have shown increasing importance of higher modes for the total energy budget at short periods and for channel depth sources. They found that, in general, with increasing depth, the amount of energy in the fundamental mode decreases. A source situated in the low velocity channel may, under convenient circumstances, be a very efficient generator of higher mode waves which have a sufficient energy to be observed on the Earth's surface and carry valuable information on shear wave velocities in the low velocity zone.

DESCRIPTION OF MODELS

In order to get a better knowledge of the physical properties of Love waves which depend on the structure of the low velocity zone, four Earth crust-mantle models were studied (fig. 1). The first model M-CANSD has no velocity zone, the second model has one asthenospherical channel and the third and fourth models have both one asthenosperical and one crustal channel. The model CANSD is the model of the Canadian shield found by Brune and Dorman (1963). The fourth model MBC-CMC is the crust-mantle model along the profile Mould Bay — Coppermine in Canada found by Wickens and Pěč (1968). The models M-CANSD and M2CANSD have been derived from the CANSD model by interchanging the velocities in some layers. The model CANSD has given rise to the model M-CANSD by interchanging mutually shear wave velocities of the layers 4 and 6 in order to eliminate the low velocity channel. All other parameters have remained without a change. The model M2CANSD originated by mutual interchanging the shear wave velocities between crustal layers 2 and 3 of CANSD, the remaining parameters being unchanged. This interchange created an additional crustal low velocity layer. The model MBC-CMC is another model having two low velocity channels but derived directly from observations. The reason for choosing these models is the fact that they are considerably simple and furthermore represent roughly a real structure. Let us mention that the layers 1, 2, 3 are crustal layers in all cases, the low velocity layers for CANSD are layers 5 and, 6, for M2CANSD the layers 2 (crust) 5 and 6 (asthenosphere) and

for MBC-CMC the layers 3 (crust) and 6 (asthenosphere). Table 1 gives the parameters which have an influence on dispersion curves of Love waves for the considered four models.

The behaviour of the following quantities has been investigated: dispersion curves, partial derivatives of phase velocity with respect to

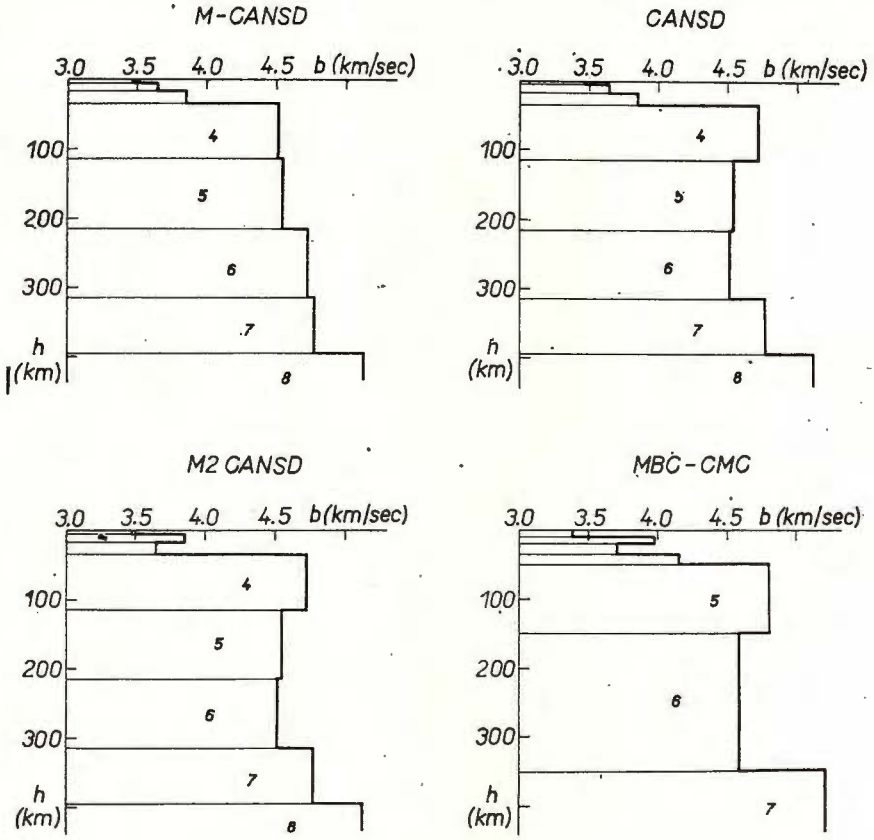

Fig. 1. — Shear wave velocity cross-sections.

shear wave velocities, amplitudes, spectra and theoretical seismograms. Particularly, the quantities which distinguish between M-CANSD and other models and which can be used for indication of low velocity layers, will be followed.

DISPERSION CURVES AND THEIR PARTIAL DERIVATIVES

The essential features associated with the existence of a low velocity channel or channels is the existence of very narrow period bands where the slopes of dispersion curves of higher modes change very quickly

(fig. 2). This feature is especially pronounced on the group velocity curves. For CANSD, the dispersion curves of the 1st higher mode vary quickly in the region of 9 s, for the 2nd higher mode in the regions of 9 and of 5 s. Dispersion curves corresponding to M-CANSD which has no channels are drawn in the same figure above. In this case the regions of rapid variations disappear. It is seen that the dispersion curves of the funda-

TABLE *1*

Parameters of the models M-CANSD, CANSD, M2CANSD and MBC-CMC.

M-CANSD

i	b_i	ρ_i	d_i
1	3.47	2.70	6
2	3.64	2.80	10.5
3	3.85	2.85	18.7
4	4.51	3.30	80
5	4.54	3.44	100
6	4.72	3.53	100
7	4.76	3.60	80
8	5.12	3.76	∞

CANSD

i	b_i	ρ_i	d_i
1	3.47	2.70	6
2	3.64	2.80	10.5
3	3.85	2.85	18.7
4	4.72	3.30	80
5	4.54	3.44	100
6	4.51	3.53	100
7	4.76	3.60	80
8	5.12	3.76	∞

M2CANSD

i	b_i	ρ_i	d_i
1	3.47	2.70	6
2	3.85	2.80	10.5
3	3.64	2.85	18.7
4	4.72	3.30	80
5	4.54	3.44	100
6	4.51	3.53	100
7	4.76	3.60	80
8	5.12	3.76	∞

MBC—CMC

i	b_i	ρ_i	d_i
1	3.38	2.65	10
2	3.98	2.70	10
3	3.70	2.70	15
4	4.15	2.90	15
5	4.80	3.30	100
6	4.58	3.40	200
7	5.20	4.00	∞

Note: Letter i is layer number, b_i— shear wave velocity in km/s, ρ_i— density in G/cm³, and d_i — thickness of the layer in km.

mental mode are smooth for both models, lacking regions of steep variation. The described feature is better pronounced on the curves of partial derivatives of phase velocity with respect to shear wave velocities (fig. 3). In this figure the derivatives of the 1st higher mode for models M-CANSD and CANSD are shown. The difference is obvious especially in the region of 9 s where the derivatives change very fast for CANSD and they are smooth for M-CANSD. It is very well to see in the figure for CANSD that the period of 9 s divides partial derivative curves into two quite

different patterns. On the left hand side, for periods less than 9 s, the highest values are reached by curves for crustal layers 1, 2, 3 and considerably less values for the layer 4 which is the top mantle layer of higher velocity. Velocities of the asthenospherical channel (layers 5 and 6) have no appreciable effect on phase velocity in this period range. For periods

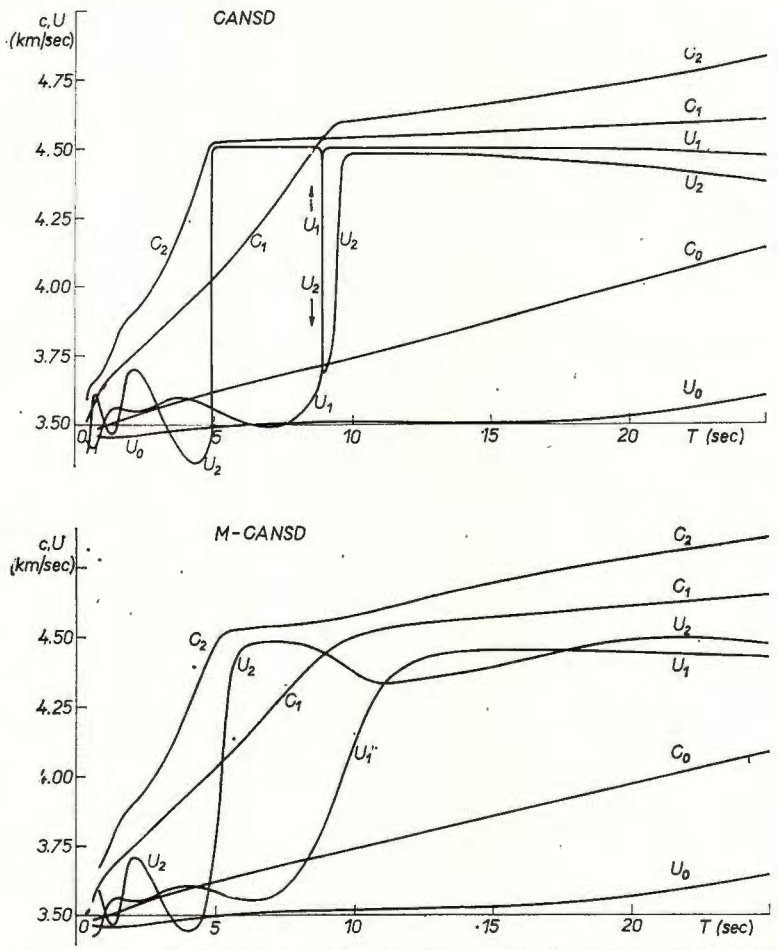

Fig. 2. — Love wave dispersion curves for the models M-CANSD and CANSD.

c_0, U_0, phase and group velocities for the fundamental mode;
c_1, U_1, phase anf group velocities for the first higher mode;
c_2, U_2, phase and group velocities for the second higher mode;.

greater than 9 s partial derivatives behave in quite an opposite manner. The highest effect is caused by low velocity layers 5 and 6, the effect of other layers is considerably less. It follows that the dispersion curve of the 1st higher mode is sensitive to shear wave velocities in the asthe-

nospherical channel for periods greater than 9 s. This property suggests that we can study the shear wave velocities of the low velocity zone with a considerable accuracy by means of observed higher mode dispersion curves for periods greater than approximately 9 s, supposing that the structure is close to CANSD. On the contrary, partial derivatives

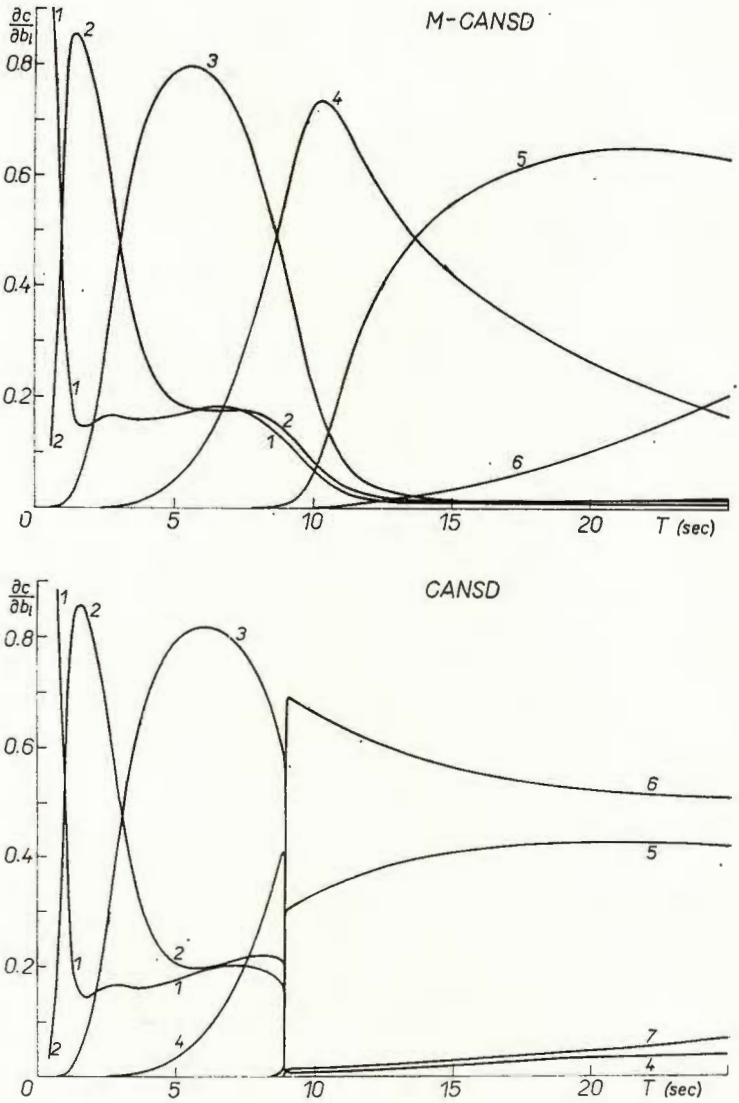

Fig. 3. — Partial derivatives of the phase velocity of the first higher mode with respect to layer shear wave velocities. The numbers with the curves represent the numbers of the layers in Table 1.

of the fundamental mode are smooth, and very similar for both models M-CANSD and CANSD (fig. 4). Let us mention that there is a lack of the period range for the fundamental mode where the influence of low velocity layers would prevail.

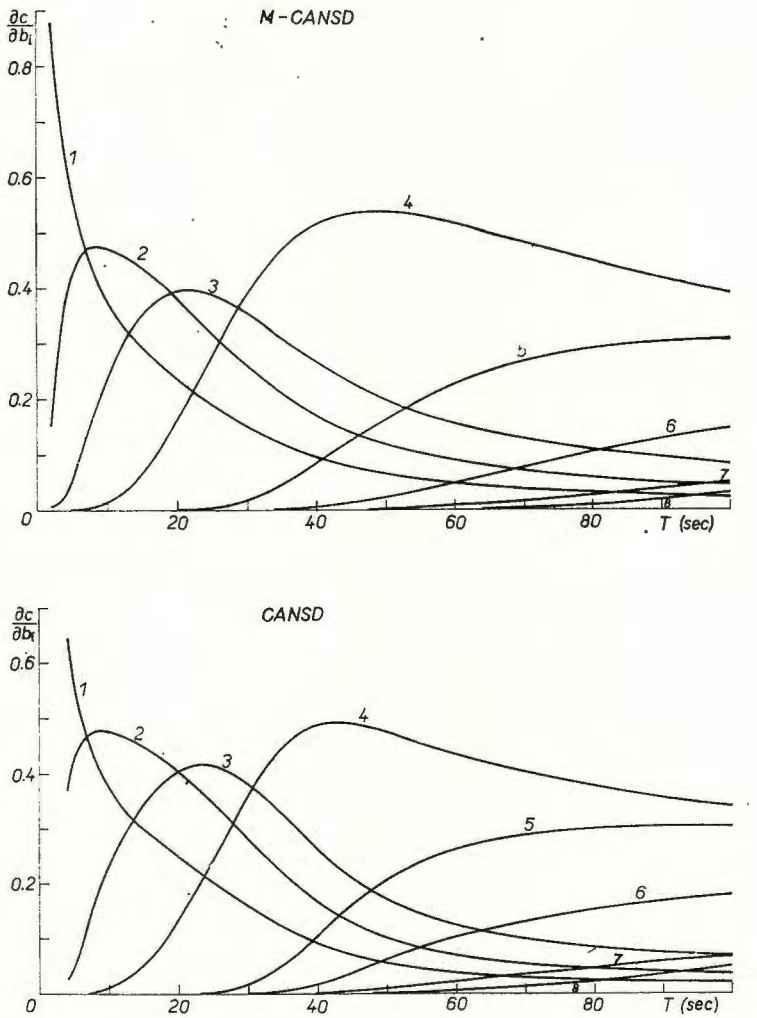

Fig. 4. — Partial derivatives of the phase velocity of the fundamental mode with respect to shear wave velocities.

Now we shall deal with the models possessing two low velocity channels, the crustal and the asthenospherical channel, i.e. models M2CANSD and MBC-CMC. Figure 5 shows the dispersion curves of the

fundamental and of the first higher mode for these models. The curves of the fundamental mode again are smooth. The curves of the 1st higher mode have similar features as those of CANSD. They change very quickly in the neighbourhood of 9 s for the model M2CANSD and in the neigh-

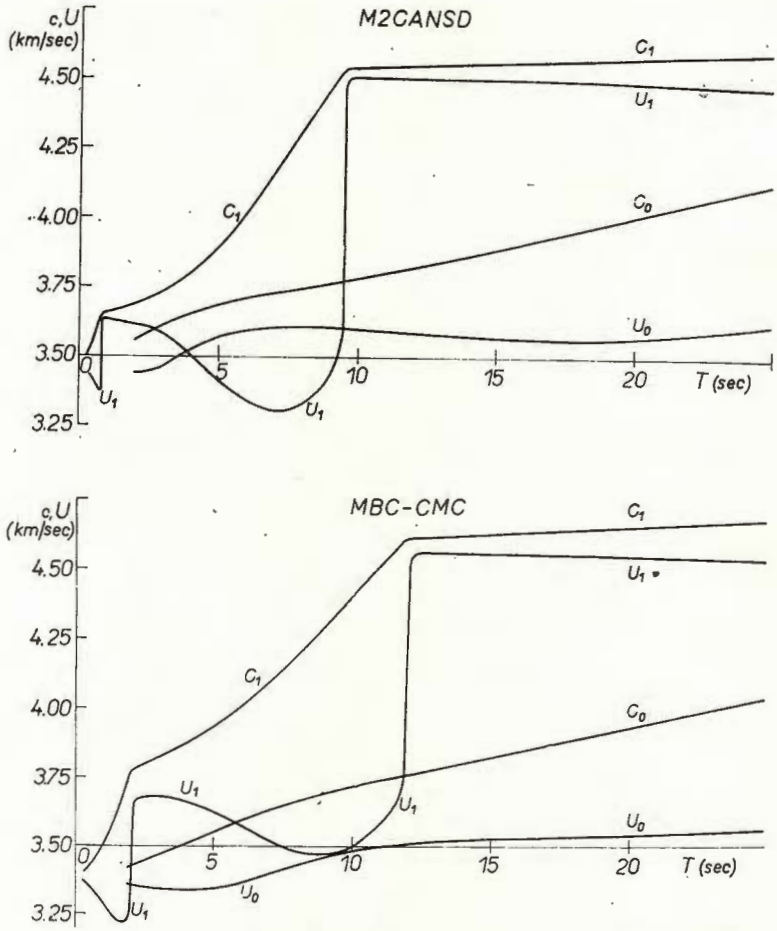

Fig. 5. — Love wave dispersion curves for the models M2CANSD and MBC-CMC.
c_0, U_0, phase and group velocities for the fundamental mode;
c_1, U_1, phase and group velocities for the first higher mode;
c_2, U_2, phase and group velocities for the second higher mode.

bourhood of 12 s for the model MBC-CMC. Fast changes of dispersion curves in these period ranges are caused by the presence of the asthenospherical low velocity channel. The crustal low velocity channel on both models produces an additional region of quick changes of dispersion curves at shorter periods. For M2CANSD these changes occur at about 1 s

and for MBC-CMC at about 2 s. Second, third, and higher modes, which are not drawn in our figures, yield a similar picture of quick changes and the number of such regions increases and the mentioned changes are even more pronounced. Figure 6 shows partial derivatives of the first

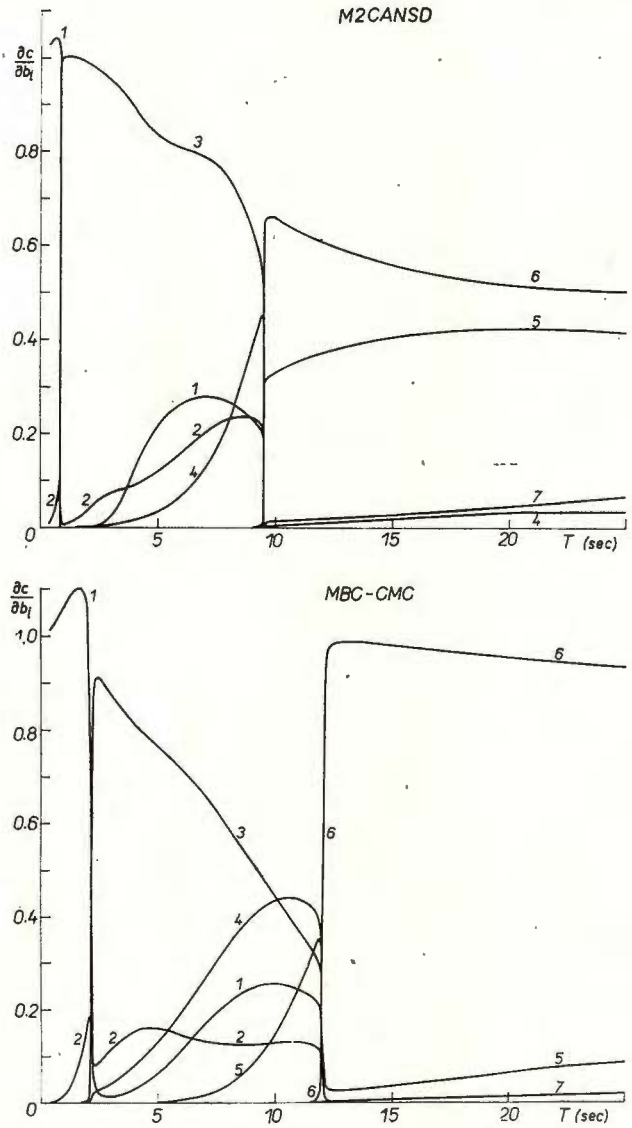

Fig. 6. — Partial derivatives of the phase velocity of the first higher mode with respect to shear wave velocities.

higher mode again with respect to shear wave velocity. The whole figure again is divided into separate regions by the intervals of fast changes. The part on the right hand side for M2CANSD is very similar to that for CANSD, the effect of the asthenospherical layers again prevails.

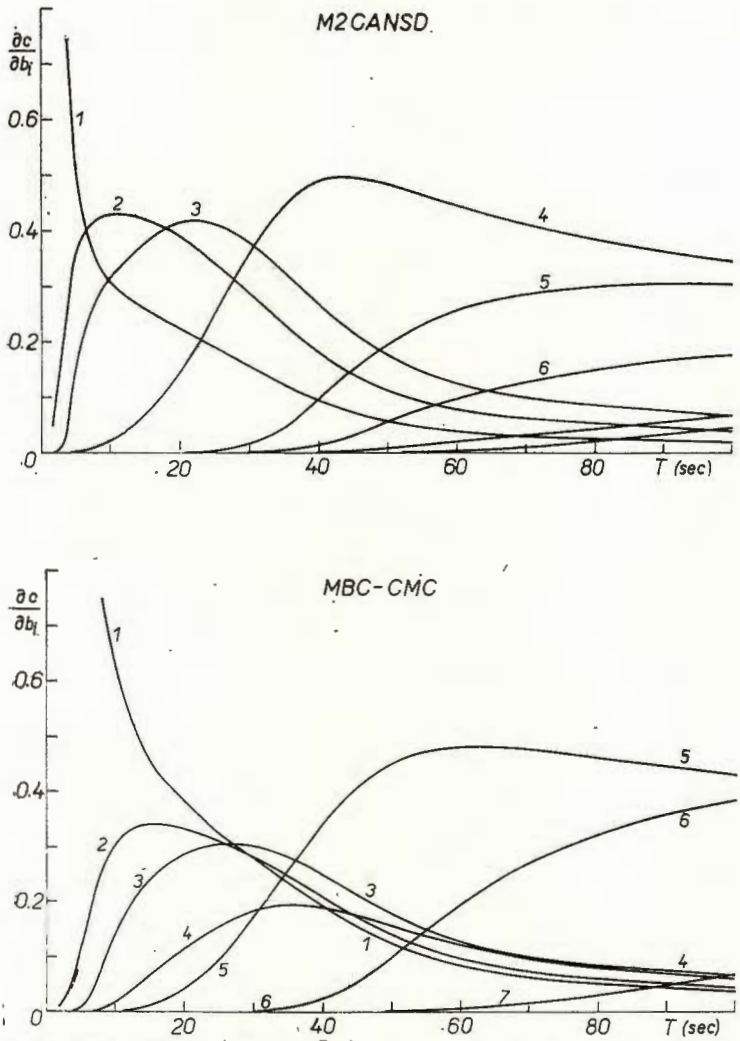

Fig. 7. — Partial derivatives of the phase velocity of the fundamental mode with respect to shear wave velocities.

The part on the left is more different from that for CANSD. In the period interval 1—9 s the greatest values of partial derivatives correspond to the low velocity crustal layer. It can be seen, for the second

double-channel model MBC-CMC, that the pattern is quite similar. Just the intervals of fast variations are a little shifted; within the interval 2—12 s the dispersion curve is mainly governed by the shear wave velocity in the crustal channel, for longer periods by the shear wave velo-

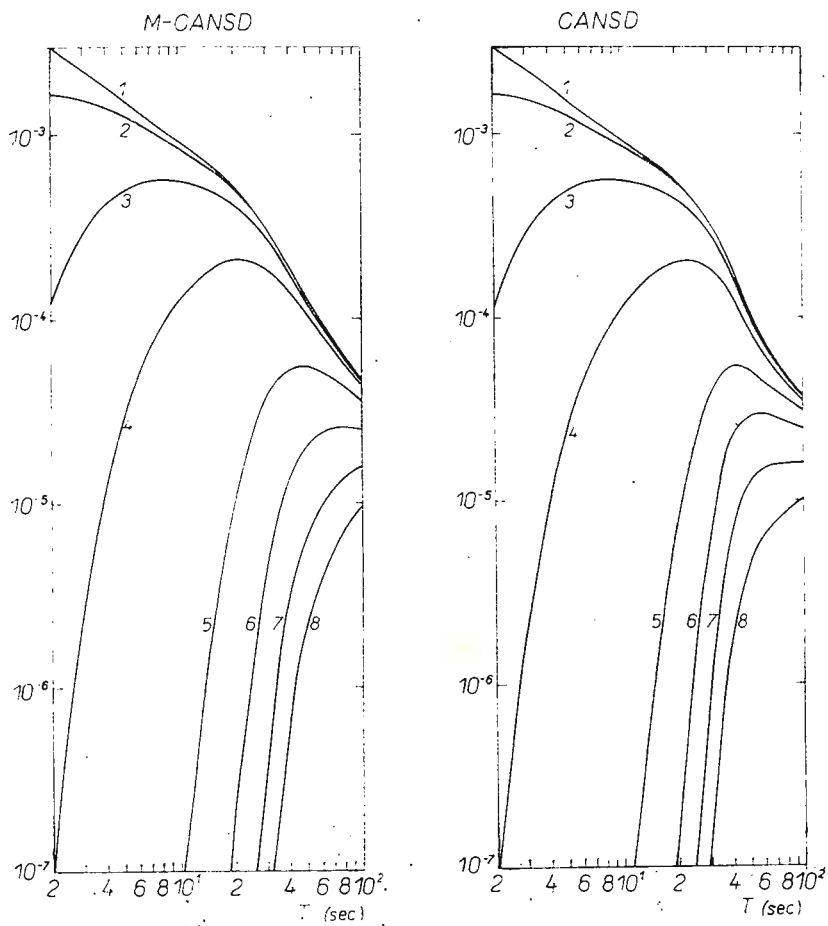

Fig. 8. — Amplitude response multiplied by depth dependent displacement for the fundamental mode. The number with the curve is the number of the source layer.

cities of the asthenospherical channel. The dispersion curves of the fundamental mode for both models are very similar to those shown for models CANSD and M-CANSD (fig. 7). It follows that the fundamental mode carries considerably less information about low velocity zones than do higher modes.

AMPLITUDE SPECTRA AND THEORETICAL SEISMOGRAMS

We have shown that within certain period ranges, the dispersion curves of the first higher mode are affected by the shear wave velocities of the low velocity zones. To be able to use higher modes for the studies

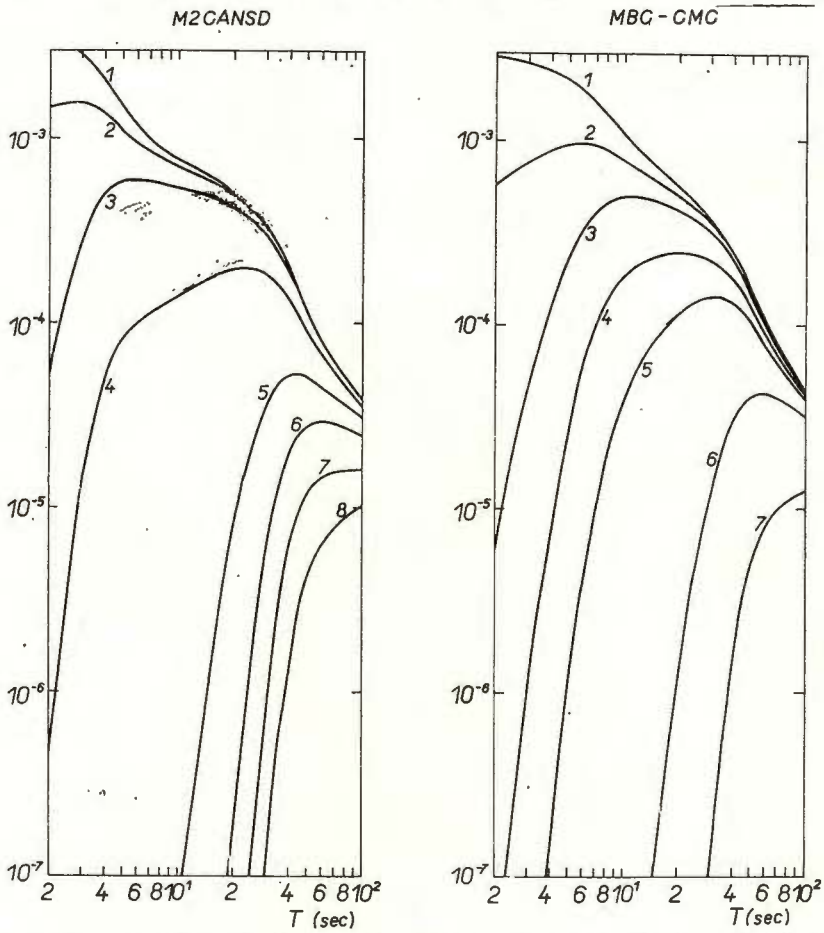

Fig. 9. — Amplitude response multiplied by depth dependent displacement for the fundamental mode.

of low velocity channels, we have to answer the question whether, in the mentioned period ranges, the higher modes are intensive enough to be observed on the surface. For this reason we have studied the amplitude spectra and theoretical seismograms separately for individual modes. The products of the amplitude response and the depth dependent displacement of the fundamental mode for models M-CANSD and CANSD are plotted against period in figure 8. The number of the curve is the number of the layer on the top of which the source is situated. As the depth dependent displacement has value one for the surface source,

the curve with the number 1 is the amplitude response. It is well to seen that the course of curves in both figures is nearly the same and consequently it is not affected by the presence of the low velocity layer. The increasing depth of the source affects the width of the period inter-

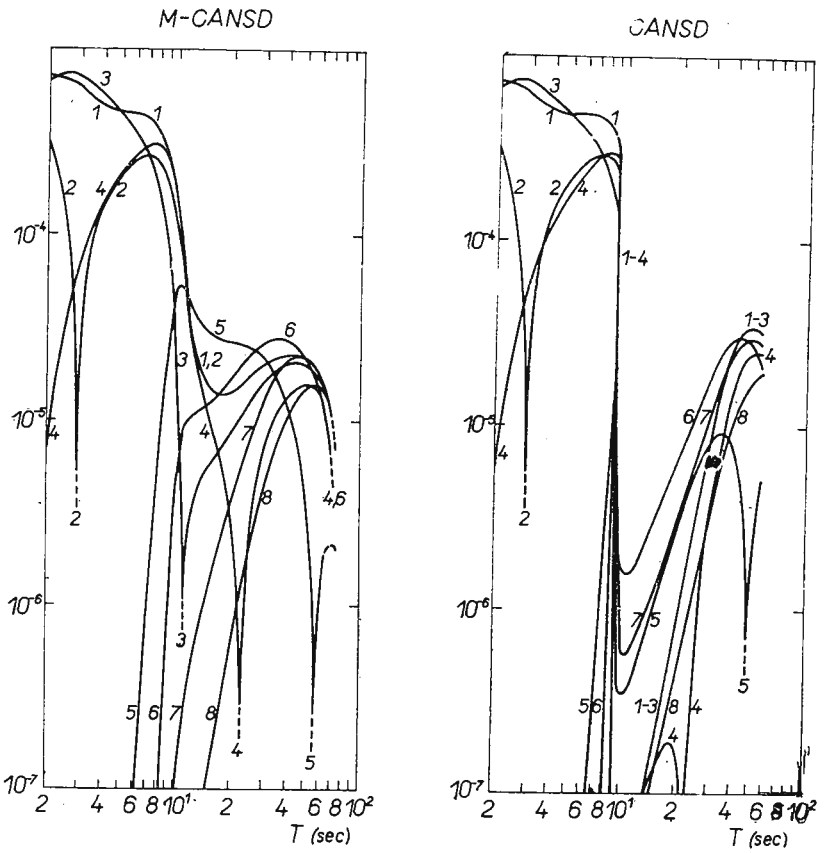

Fig. 10. — Amplitude response multiplied by depth dependent displacement for the first higher mode.

val, the periods of radiated waves are getting longer. Figure 9 shows the corresponding curves for both double low velocity channel models.

The amplitude spectra of the 1st higher mode behave in a different way (fig. 10). A considerable, but not essential, difference appears between M-CANSD and CANSD. For the model without channel M-CANSD the amplitude response keeps up to the period of 9 s, where the slope of the amplitude response becomes steeper. A shallow local minimum appears around 18 sec. All curves start dying away at the period of 50 s. There is no radiation, for deep sources in the short period

range. For CANSD, the low velocity layer affects the course of curves mainly at period of 9 s, where all the curves fall down quickly. The drop is of several orders of magnitude. Later the curves again increase. Consequently a very deep minimum in the amplitude spectra appears

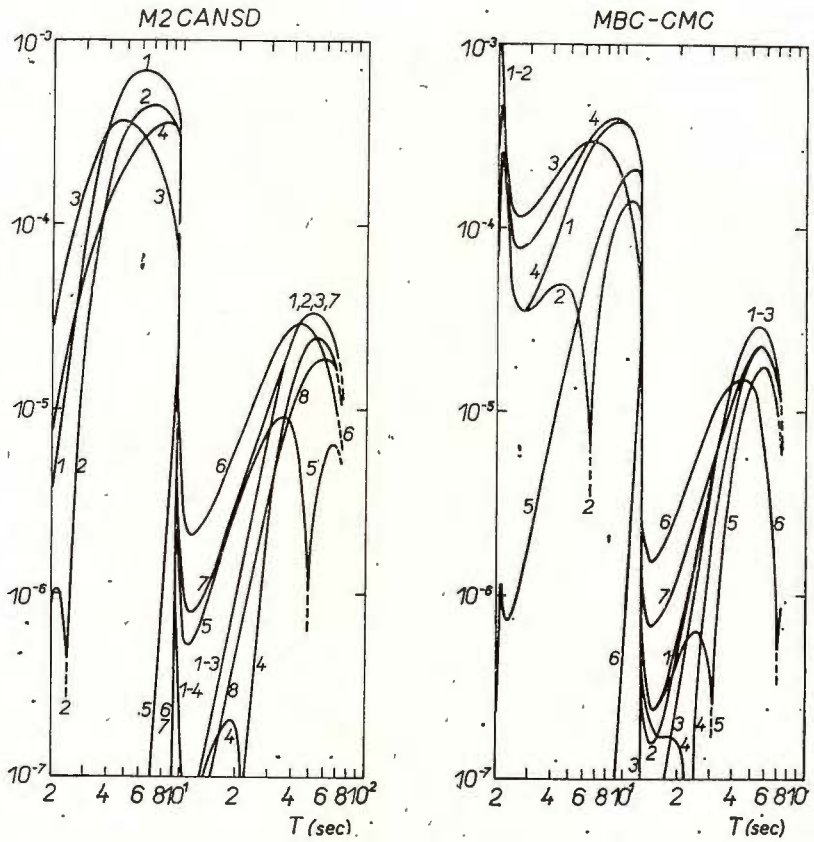

Fig. 11. — Amplitude response multiplied by depth dependent displacement for the first higher mode.

which practically means that a gap for intermediate periods will occur. Then, only short periods waves, on the one hand, and long period waves, on the other hand, will appear. It goes without saying that this holds only for shallow source depths. The same is valid for the spectra of M-CANSD but the mentioned gap is not well pronounced. It seems, that each low velocity channel causes, at a certain period which is identical with the critical period where the partial derivatives vary quickly, a very fast drop of spectral curves and originates a gap, where the amplitudes considerably decrease. Figure 11 demonstrates it for the double

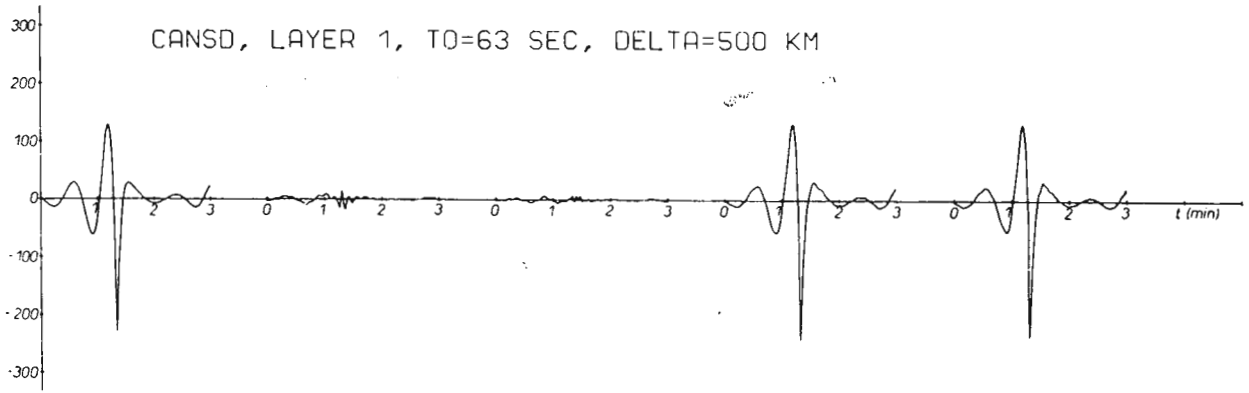

Fig. 12. — Theoretical seismograms of Love wave modes arranged in the following order: fundamental 1st higher, 2nd higher, fundamental + 1st higher, fundamental+ 1 st higher + 2nd higher. (Surface source, epicentral distance 500 km).

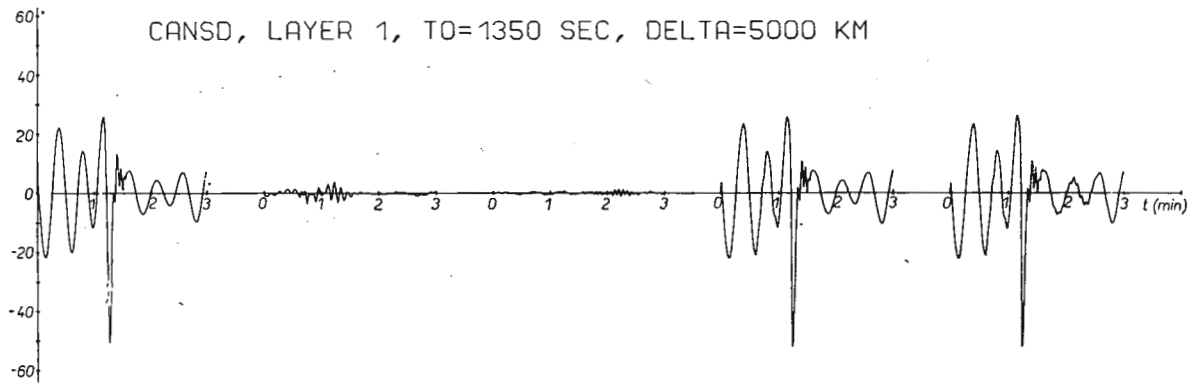

Fig. 13. — Theoretical seismograms of Love wave modes (Surface source, epicentral distance 5000 km).

channel model MBC-CMC. The additional gap caused by the crustal channel occurs in around 3 s.

The behaviour of the spectral curves suggests the idea that the observed short period phases *Lg* called originally by Gutenberg „channel

TABLE 2

Velocities of short period phases taken from the theoretical seismograms and velocities of the phases Li, Lg1, Lg 2′, and Lg2″ as measured from real seismograms (P ě č, 1961).

Model	Δ	Position of the source	Velocities (km/s)		
			Fundamental mode	1st higher mode	2nd higher mode
CANSD	500 km	1	—	3.70	3.54
		2	—	3.70	—
		3	—	3.60	—
		4	—	3.67	3.57
CANSD	5 000 km	1	3.50	3.61	3.45
				3.53	3.39
		2	3.50	3.62	3.40
		3	3.48	3.53	—
		4	—	3.61	3.41
				3.53	—
M-CANSD	500 km	1	—	3.68	3.78
		2	—	3.68	—
		3	—	3.73	3.57
		4	—	3.62	3.61
MBC-CMC	500 km	1	3.36	—	3.70
		2	3.34	—	—
		3	—	3.65	3.65
		4	—	3.71	—

Note: Li . . . . . 3.78 km/s Lg2′ . . . . . 3.43 km/s
Lg1 . . . . . 3.56 km/s Lg2″ . . . . . 3.35 km/s

waves“ correspond to the local maxima of the spectral curve. It follows that these waves do not need the low velocity zone for their existence. The presence of the low velocity channel merely makes the phenomenon more expressive.

In figures 10 and 11 there does not exist an interval where the amplitudes vary slowly, on the contrary, there is one or two regions where the amplitudes change very fast. Consequently, in applying the method of the stationary phase to the propagation of Love waves in a medium close to the considered models, the assumption of a slow variation of amplitudes, which is the basic assumption of the method, is not fulfilled and the method of the stationary phase may yield incorrect

results. The hypothesis that the *Lg* phases correspond to the local extremes of the dispersion curves is also based on the stationary phase estimate.

The quantities shown in figures 8 — 11 form the basis of theoretical seismogram computations. The theoretical seismogram contains moreover effects, of the source and epicentral distance (Harkrider, 1964). Two samples of theoretical seismograms are given in Figures 12 and 13. The spectrum of the initial pulse was supposed to be constant from 2 to 80 s, equal to zero otherwise. The seismograms given in figures 12 and 13 were calculated for the surface source. The ratio of higher modes to the fundamental one increases for deeper sources. The short period oscillations in seismograms are well seen. For great epicentral distances a special kind of short period oscillations also occurs in the fundamental mode (fig. 13).

The onsets of short period oscillations were measured on theoretical seismograms and the corresponding velocities were arranged in table 2. The table also gives the velocities of *Lg* phases as determined by observation. It is seen that the velocities of theoretical short period phases are close enough to the velocities of *Lg* phases determined by observation.

CONCLUSIONS

a) The properties of studied quantities seem to support the opinion that a rough information as the only presence of "channel" waves on seismograms can hardly be used for indication of low velocity layers.

b) In the theoretical seismograms for models with low velocity layers there have not been found any appreciable waves that would not exist on theoretical seismograms for close structures without channels. We can say that low velocity layers have only moderate effects on measurable quantities, like dispersion curves, amplitudes, and theoretical seismograms of Love waves.

c) It has been shown that especially the dispersion curves and amplitudes of higher modes contain valuable information concerning low velocity layers.

d) Partial derivatives of dispersion curves help to determine period intervals which, with respect to the low velocity channels, are important to study.

e) Theoretical calculations have shown that we must expect the amplitude spectra of Love waves in real structures, especially the amplitude spectra of higher modes, to be highly frequency dependent. This means that simplified calculations of theoretical seismograms based on the asymptotic method of stationary phase may often be very far from reality.

REFERENCES

Alterman Z. (1969). Higher mode surface waves. *Geophys. Monogr.* 13, The Earth's Crust and Upper Mantle, Ed. P. J. Hart, Am. Geophys. Union, Washington.

Båth M. (1957). A continental channel wave guided by the intermediate layer in the crust. *Geofis. Pura e Appl.* 38, Milano.

Brune J., Dorman J. (1963). Seismic waves and Earth structure in the Canadian shield. *Bull. Seim. Soc. Am.*, 53, Berkeley.

Caloi P. (1954). L'astenosfera come canale-guida dell'energia sismica. *Ann. Geofis.* 7, Roma.

Grudeva, N. P., Levshin A. L., Francuzova V. I. (1971) O prirode kanalovykh seysmicheskikh voln. *Computational Seismology*, 5, Nauka, Moscow.

Gutenberg B. (1955). Channel waves in the Earth's crust. *Geophysics* 20, Tulsa.

Harkrider D. G. (1964). Surface waves in multilayered elastic media. I. Rayleigh and Love waves from buried sources in a multilayered elastic half-space. *Bull. Seism. Soc. Am.* 54, Berkeley.

— (1970). Surface waves in multilayered elastic media. II. Higher mode spectra and spectral ratios from point sources in plane layered earth models. *Bull. Seism. Soc. Am.* 60, Berkeley.

— Anderson D. L. (1966). Surface wave energy from point sources in plane layered Earth models. J. *Geophys. Res.* 71, Richmond.

Oliver J. Ewing M. (1958). Normal modes of continental surface waves. *Bull. Seism. Soc. Am.* 48, Berkeley.

Pěč K. (1961). Continental waves in Central Europe. *Trav. Inst. Géophys. Acad. Tchécosl. Sci., Geofysikální sbornik* 152, Praha.

— Novotný O. (1972). The influence of the low evocity zone on phase velocities and amplitudes of Love waves. *Z. Geophys.* 38, Würzburg.

Press F., Ewing M. (1952). Two slow surface waves across North America. *Bull. Seism. Soc. Am.* 43, Berkeley.

— Ewing M. (1955). Waves with *Pn* and *Sn* velocity at great distances. *Proc. Nat. Acad. Sci.* 41, Washington.

Wickens A. J., Pěč K. (1968). A crust-mantle profile from Mould Bay, Canada to Tucson, Arizona. *Bull. Seism. Soc. Am.*, 58, Berkeley.

MODELLING

SEISMIC BOUNDARIES AND THEIR MODELS

BY

JÖRN BEHRENS[1], LUDVÍK WANIEK[2]

INTRODUCTION

During the past years the question as to the structure of the investigated seismic discontinuities has become more and more important.

As you know, the question concerning the structure of discontinuities has arisen, since — on account of field observations — the assumption of complicated boundary structures in the Earth has proved more and more urgent. The former assumption of discontinuities of first order was repressed in favour of the assumption of transition-zones between more or less homogeneous layers.

At present the form of these transition-zones is the subject of numerous investigations. Field work, theory, and model seismology study the influence of the properties of these transition-zones on the kinematic and dynamic parameters of seismic signals, respectively they examine the inverse question if and in which way these boundary structures respectively the structures of these transition-zones can be characterized by the seismogram.

The aim of this report is to try to give a summary of the most important results, obtained during the past years by model seismic measurements, concerning the questions of a characterization of seismic discontinuities, especially of transition-zones.

When treating the results, the systematics of the interrelation between boundary-type and the parameters of the seismic signals is intensionally brought into prominence, whereas the analoguous modelling of seismologically obtained or assumed velocity-depth distributions will not be discussed here.

On this line, this report is divided into two parts : The first part deals with the investigations on transition-zone structures, especially of

[1] Institut für Geophysik der Technischen Universität Clausthal, 3392 Clausthal-Zellerfeld, Adolf-Römer-Strasse 2A, BRD.

[2] Geofyzikální ústav CSAV, Praha 4 — Sporilov, Bocni II, Czechoslovakia.

the possible structure of the Mohorovičić-discontinuity, the second part deals with the evidence and the special feature of low velocity layers.

MODELS OF THE MOHOROVIČIĆ-DISCONTINUITY BY FIELD RESULTS

At the beginning of this survey we will have a look at the ideas on the possible structures of seismic discontinuities respectively transition-zones, developed by the field work up to now.

In 1970 Davidova, Kosminskaya and Michota give the shown picture (fig. 1) of three possible types of the specially thorough investigated Mohorovičić discontinuity. The sequence of the three types represents a certain valuation with respect to the plausibility of the shown structures in nature. The authors show in a more or less chronological sequence, which ideas on the structure of the Mohorovičić — discontinuity were considered to be possible and which structure-models have been superseded by others in the course of time, as they seemed to be more plausible.

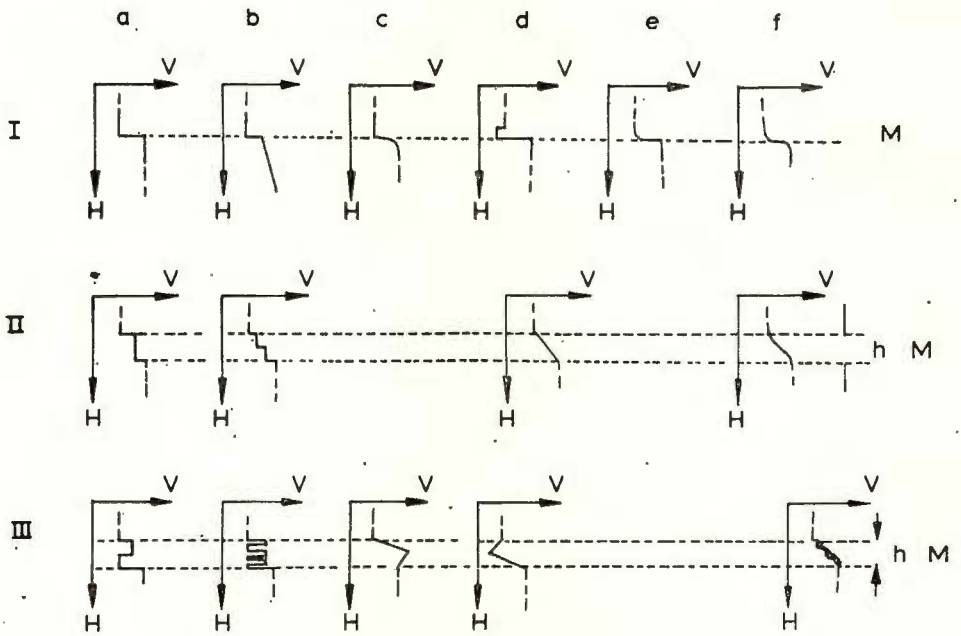

Fig. 1. — Possible structures of the Mohorovičić discontinuity (Davidova, Kosminskaya, Michota, 1970).

The shown structures reach from (fig. 1., first row) the discontinuity of first order with sharp and weak boundaries, with a gradient layer below the discontinuity of first order or a velocity inversion above the discontinuity of first order over (fig. 1, second row) the assumption

of a transition-zone with a step-shaped or a constant velocity increase with depth with sharp and weak boundaries, (which explain the experimentally observed properties of the dynamic parameters of the registered waves much better than the structures shown in row 1) to (fig. 1, third row) the forms of a laminated transition-zone or a zone with a complicated positive resp. negative velocity gradient, which are at present being considered as very plausibile.

All the here mentioned structures assume a linear horizontal geometry. However, as we know, in nature a complicated geometric structure of the boundaries has to be expected, which will have to be pointed out later in this report.

SEISMIC BOUNDARIES AND THEIR MODELS

Most of these models of discontinuities — assumed on the basis of field observations — have been investigated up to now by model seismic methods.

Figure 2 shows the structures of transition-zones which model seismology has especially investigated in the past time and their modelling with the aid of the 1-, 2-, and 3-dimensional model technique.

Easy to understand that only the simplest types of structures are mentioned here, from which however, a correspondingly complicated velocity-depth distribution can be composed.

First the "classical" transition layers are mentioned with a linear and a non-linear velocity-depth distribution (fig. 2, first and second row).

The one -dimensional model of such a transition layer can be fabricated from a stick of epoxy resin by realising the required velocity-depth distribution by a controlled sedimentation of filler (quartz sand, metal grains).

In 1967 Datta has described such a model.

In the 2-dimensional model technique the transition-zones are made by a removable perforation (Ivakin, 1956) or a wedge-shaped montage of the plates with different velocities (so called : "bimorphic models"), (Healy, Press, 1960; Riznichenko, Shamina, Khanutina, 1961).

The 3-dimensional as well as the 1-dimensional technique use a mixture of epoxy resin and quartz sand (Shamina, 1965) or the application of 3-component gels of the system water-glycerol-gelatine in a series of thin layers with different composition of the three components (Waniek, 1966 a, b).

The transition-zone with geometrical structure — to which the velocity-depth function shown in figure 2, row 3 can be co-ordinated — — are represented in the 2-dimensional technique by the first two models in row 3.

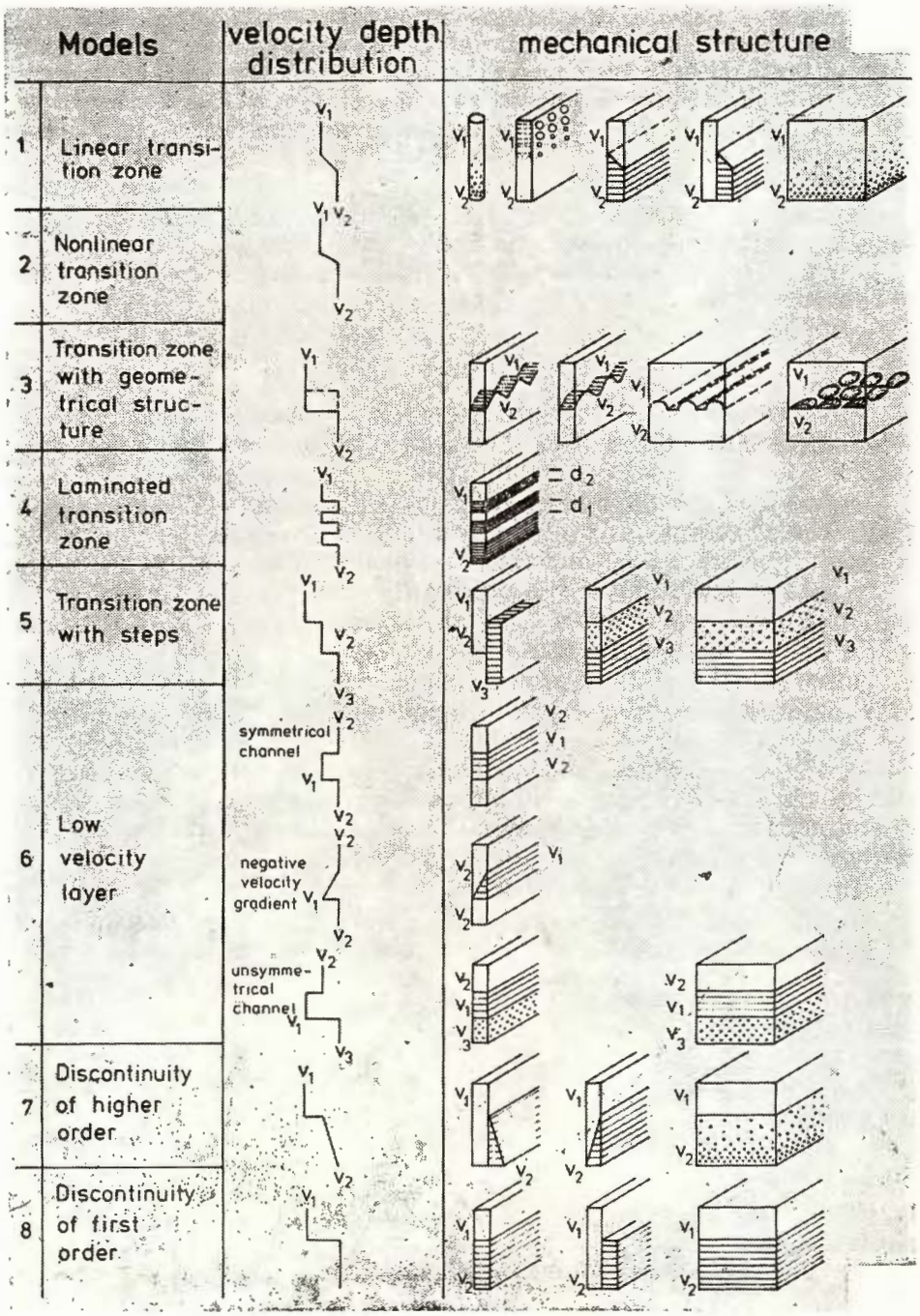

Fig. 2. — Boundary structures and their models.

In 1964 they have been thoroughly investigated and described by Nakamura and others, in 1969/1971 by Behrens[3] and 1971 by Behrens, Kozák, Waniek.

The 3-dimensional technique (fig. 2, the last two models in row 3) makes such structures with semicylindrical and hemispherical convexities of the boundaries. However, up to now they served more for representing rough reflecting horizons than for modelling transition-zones. The investigations on these rough boundaries are combined with the names of Rapoport (1961) and Voskresensky (1962).

The transition-zones with a laminated layering (proposed by Meissner (1967) Fuchs (1969) and others as a possible structure of the Mohorovičić-discontinuity) are constructed by a combination of thin laminea of the media with the velocity v_1 and v_2 (fig. 2, row 4).

The relation between the thicknesses d_1 and d_2 of the laminea is equal to the relation between the velocities v_1 and v_2. In the past time laminated transition zones have been investigated on 2-dimensional models by Behrens and Gommlich (1972). The model studies on thin layers (Ivakin, 1956; Shamina, 1960; Poley, Nooteboom, 1966) and on a series of parallel thin layers (Parchomenko, 1959) and dipped thin layers respectively (Ivakin, 1969) have been the forerunners of these just mentioned investigations by Behrens and Gommlich.

The transition-zone with steps (fig. 2, row 5) is realized in the 2- and 3-dimensional technique by joining together material of different velocity. Such a stepped transition-zone with intermediate layer is mentioned here, as it has been investigated with special regard to its being distinguishable from other structures of the transition-zones — the linear resp. non-linear transition-zones and those with geometrical structure.

Low velocity layers, wave-guides or channels belong to the construction elements which are important with respect to the structure of the Earth's interior and which have recently become of primary interest.

The channels with a symmetrical and an unsymmetrical velocity-depth distribution and with a negativ evelocity gradient belong to the main types of the low velocity layers (fig. 2, row 6). The 2- and 3-dimensional models are constructed as shown by joining together plates or layers with the corresponding elastic parameters.

The channels to be seen on figure 2 have sharp boundaries. In the case of channels with weak boundaries wedge-shaped interfaces are chosen or in the case of 3-dimensions there will be chosen a variation of the filler dependent on the depth.

During the past years investigations on low velocity layers have especially been carried out by Khorosheva (1962); Chowdhury Dehlinger (1963); Shamina (1966); Kapcan, Kislov-

[3] Behrens J. Die Charakterisierung seismischer Grenzflächen mit Hilfe modellseismischer Verfahren im Hinblick auf Deutungsmöglichkeiten des Krustenaufbaues. 1969. Habilitationschrift, Techn. Univ. Clausthal.

skaya (1966); Behrens, Dresen, Waniek (1971); Kozàk, Waniek (1970); Waniek (1972); Behrens, Siebels (1972).

The first order discontinuity in connection with a gradient layer and the mode of modelling them are indicated in figure 2, row 7 in principle. They also represent construction elements, from which a complicated velocity-depth function assumed in nature can be combined. At present, there exist only a few systematic investigations on the kinematics and dynamics of the wave propagation on such discontinuities. Partial results on perforated models have been presented by Ivakin in 1969, resp. by Behrens, Dresen, Waniek on bimorphic 2- and 3-dimensional models in 1971; the latter within the scope of the investigations carried out on the 'test models' proposed in 1966 at the ESC-meeting by Berckhemer and Waniek.

The discontinuity of first order generally served as a reference model for most of the enumerated investigations (fig. 2, row 8).

RESULTS OF MODEL INVESTIGATIONS

What do the results obtained on these structures look like? It has to be mentioned preliminarily that many investigations have been carried out with often very different aims and that it would be important to continue systematically the investigations on the mentioned 'test models' proposed by Berckhemer and Waniek in 1966. Therefore we have limited on pointing out especially the results of those investigations, whose special aim was to elaborate the criteria for a characterization of the discontinuities, that is to determine the kinematic and dynamic parameters of the elastic waves propagating on the considered models.

TRANSITION-ZONES WITH SIMPLE VELOCITY-DEPTH DISTRIBUTIONS

The investigations which Datta described in 1967 belong to one of the first model experiments on a transition layer. They have been carried out on a 1-dimensional model with vertical incidence (fig. 3). The velocities varied between 3 300 m/s and 2 000 m/s. The source was placed on the left or right front, the receiver was fixed on the surface of the model. The result showed that the amplitude spectrum of a wave reflected in such a layer is considerably shifted to the lower frequencies in relation to the transmitted wave.

The investigations with normal incidence and the observations of the reflected and transmitted wave have been carried out in 1967 by Schick and Schneider on a 2-dimensional model of paraffin, whereby the transition layer was obtained by a variable field of temperature in consequence of heating (fig. 4).

The lower part *d* of the figure shows the velocity-depth distribution and the arrangement of source (T) and receiver (R).

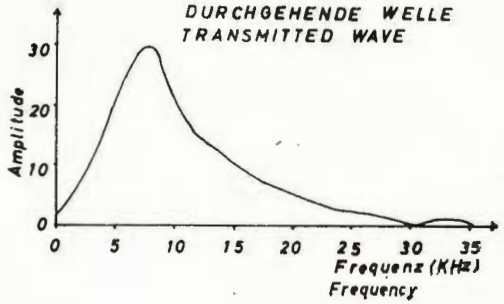

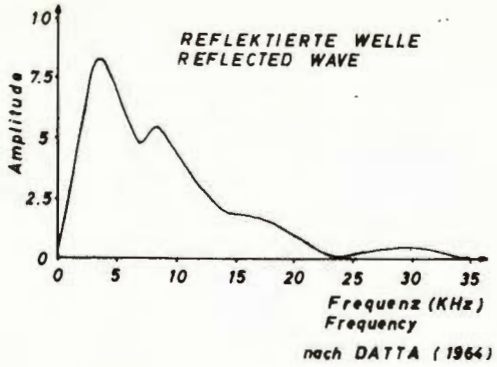

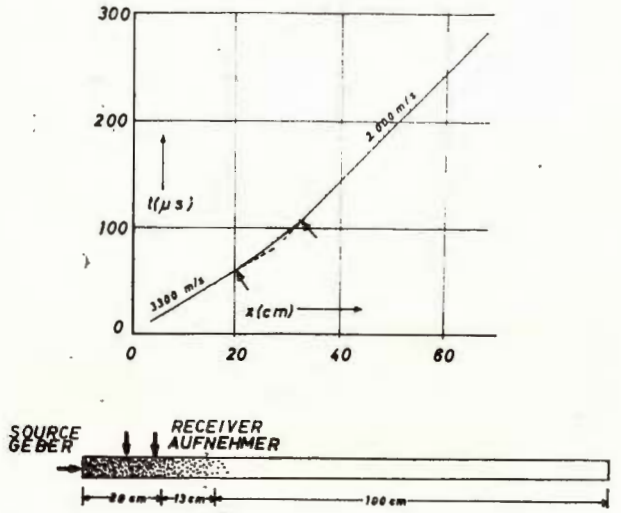

Fig. 3. — One-dimensional model of a transition layer (D a t t a , 1967)

Upper part: Model and travel-time graph

Left part: Frequency spectra of the transmitted and reflected wave.

Part *a* of the figure shows the relation between the values of reflection (R) and transmission (T) coefficient as a function of wave number (k) times layer thickness (H).

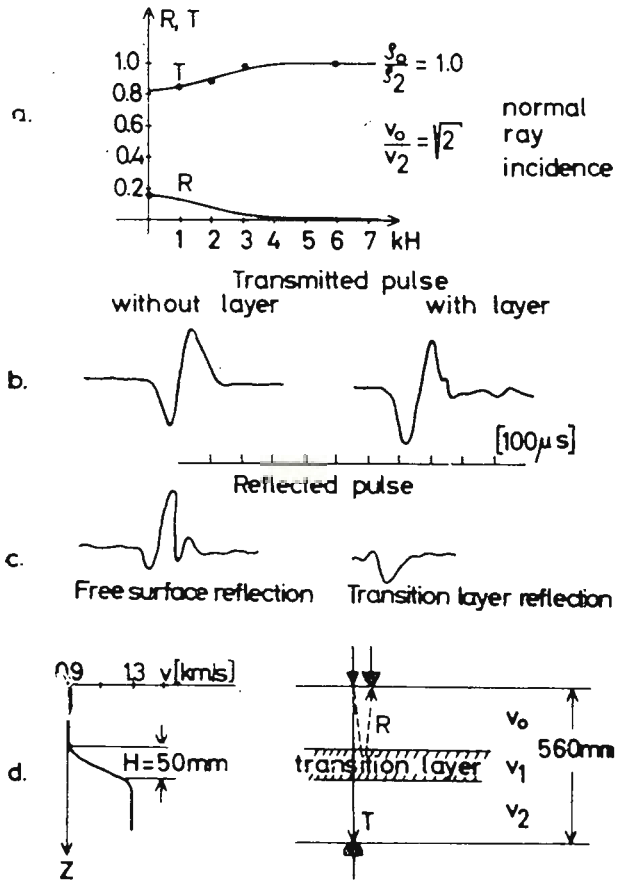

Fig. 4. — Two-dimensional thermic paraffin model of a transition layer (Schick, Schneider, 1967)

a) Reflection and transmission coefficients as a function of wave-number k times layer thickness H

b) and *c*) Transmitted and reflected pulse

d) Model, arrangement of source T and receiver R, velocity-depth distribution.

For very short wave lengths the reflection coefficient becomes zero and the transmission coefficient approaches one. For very long wave lengths, both the reflection and transmission coefficient take on the value which can be expected for a sharp boundary.

Modell: Plexiglas - Aluminium
Model :

Untersuchte Grenzflächen - Strukturen
Investigated types of interface structures

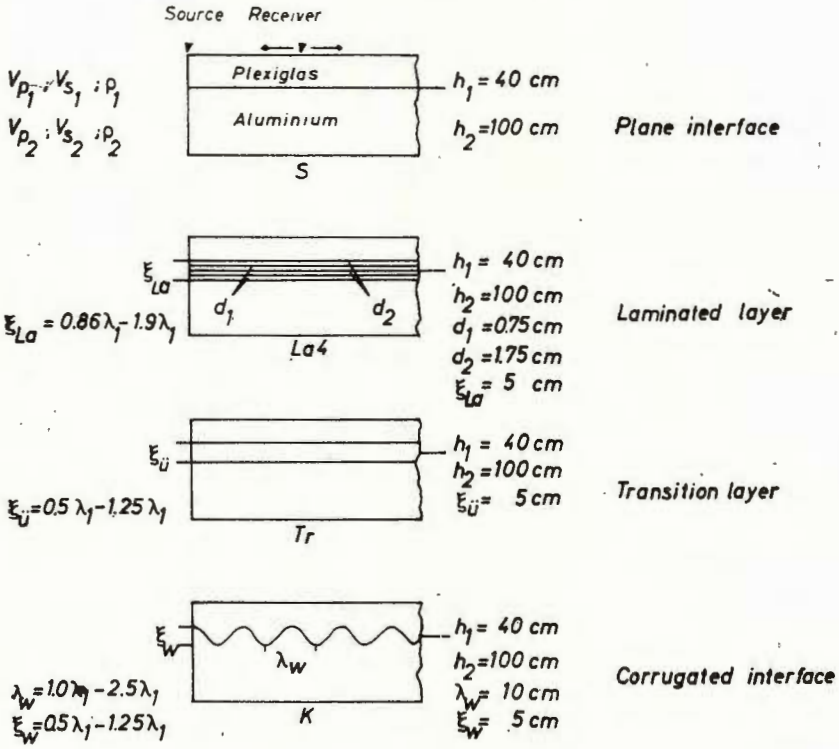

λ_1 = Wellenlänge der einfallenden Welle	λ_1 = Wavelength of the incident wave
λ_w = Wellenlänge der Grenzflächen-Welligkeit	λ_w = Wavelength of the interface-corrugation
ξ_w = Amplitude der Grenzflächen-Welligkeit	ξ_w = Amplitude of the interface-corrugation
$\xi_ü$ = Mächtigkeit der Übergangsschicht	$\xi_ü$ = Thickness of the transition layer
ξ_{La} = Mächtigkeit der Lamellenschicht	ξ_{La} = Thickness of the laminated layer
d = Mächtigkeit der Lamelle	d = Thickness of the lamella

V_{p_1} = 2.32 (mm/µs) ; V_{s_1} = 1.35 (mm/µs) ; ρ_1 = 1.2 ($g \cdot cm^{-3}$)

V_{p_2} = 5.4 (mm/µs) ; V_{s_2} = 3.12 (mm/µs) ; ρ_2 = 2.8 ($g \cdot cm^{-3}$)

Fig. 5. — Transition-zone structures with complicated velocity-depth distribution (Behrens, Gommlich, 1972).

From part *b* of figure 4 it can be seen that the difference in the shape of pulses transmitted through a homogeneous halfspace and through a two-layered medium with the given transition-zone is only small.

On the other hand, in the case of a pulse reflected from a transition zone (part *c* of the figure) there is a prominent relation increase of low-frequency amplitudes.

TRANSITION ZONES WITH COMPLICATED VELOCITY-DEPTH DISTRIBUTION

In 1969 Behrens [4], resp. 1971 Behrens, Dresen, Waniek resp. 1972 Behrens, Gommlich have thoroughly investigated two-layered models with transition layers by means of the 2-dimensional model technique (fig. 5). These investigations covered the subcritical and overcritical area as well as the region of observation of the head wave. The kinematic and dynamic parameters of the reflection and of the head wave have been determined dependent on the distance. These measurements have been carried out together with the investigations on laminated and corrugated transition-zones and discontinuities of first order aiming at finding different properties of the kinematic and dynamic parameters of the seismic signals observed on the different structures.

The models consisted of a layer of Plexiglass overlaying a halfspace of aluminium. (The values of the *P*-and *S*-wave velocities and the densities are shown in figure 5 below the models.) Source and receiver were placed analogeous to field measurements on the free surface of the models.

The common feature of all the models — with the exception of the discontinuity of first order — is the thickness of the covering layer (40 cm), of the halfspace (100 cm) and of the transition-zone (5 cm).

The laminated transition — zone is constructed in this case by a combination of four laminea, two laminea of Plexiglas with the thickness d_1 and two of aluminium with the thickness d_2. The relation between d_1 and d_2 is equal to the relation between the velocities in the two media. The thickness d_1 and d_2 are about a quarter of the predominant wavelength λ_1 of the incident wave. Those models with the ratio d to λ_1 equal 0.25 and the shown velocity reversals were investigated theoretically by Fuchs (1969, 1970) and as mentioned before and shown in figure 1 presumed as the structure of the Mohorovičić-discontinuity by Meissner (1967), Davidova, Kosminskaya, Michota (1970) and others.

The investigated transition layer is characterized by a nonlinear velocity-depth distribution. It has been constructed according the method of bimorphic models.

The next model of a transition-zone has a sinusoidal corrugated structure. λ_w is the wavelength of corrugation, ξ_w the amplitude of corrugation. This type of boundary structure has been investigated theoretically by Asano (1966) at first.

[4] *Op. cit.*, p. 3.

Travel-time investigation

The measurements of the travel-time gave, in brief, the following picture (fig. 6) :

With a laminated transition-zone (left side, upper part of figure 6) besides the usual P_1P_1-reflections and the onsets of the ordinary head wave $P_1P_2P_1$ (vanishing very early at 90 cm) a second and a third head wave with strong onsets can be observed with a very complicated path of propagation.

Onsets of a head wave travelling in the halfspace are not clearly recognizable. The P-wave velocity within the laminea is slower than the expected P-wave velocity within the halfspace.

The travel-time measurements on the transition layer (right side, upper part of figure 6) show reflections from the most upper part of the layer because of the chosen nonlinear velocity-depth distribution. From that reason the travel-time curve of the refracted wave is not curved as aspected in the case of a transition-zone and gives the picture of a discontinuity of first order. The velocity of the refracted wave in the layer is smaller than the P-wave velocity within the halfspace. The dashed lines belong to the straight interface of first order, the solid lines are the computed travel-time curves of the transition-zone model. The curves (1) or (2) represent the travel-time curves of the reflections from the upper and lower boundary of the transition layer.

The travel-time graph of the model with the sinusoidal geometrical structure differs much from those of the other models (fig. 6, lower part).

The diagram contains only the curves wich can be observed neglecting the reflection from the interface beyond the left side of the source.

The solid lines are the computed travel-time curves for the P_1P_1-reflections, the dashed lines belong again to the model of the plane first order discontinuity.

The subcritical area is characterized by a series of second onsets with travel-time curves of different apparent velocities. In this area the branches of the reflection travel-time curves are separated sufficiently, so that single onsets can be identified — we have the picture of a multilayered transition-zone particularly with differing dipped reflecting elements. The impression of a laminated zone is given for this model much more than for the laminated model itself. This can be derived from the seismogram, too, as we will see later.

The special feature of the overcritical area is characterized by the convergency of the travel-time branches. Here strong interferences will form the seismograms. It is remarkable, that on this zone with geometrical structure a clear head wave with large amplitudes can be observed. The velocity of this refracted wave is lower than in the halfspace.

The possibility to differentiate the transition layer and the first order discontinuity is very small in this case. Between these models and the models of the laminated and corrugated transition-zone more distinctive marks can be noticed.

The laminated zone is characterized by the second head wave and by the disappearence of the ordinary head wave at relatively short distances.

The corrugated zone is specified by the plurality of travel-time curves in the subcritical region and the relative broad band of travel-time branches in the overcritical area.

Seismograms

More than the kinematic parameters the dynamic parameters of the observed seismic signals are able to characterize the different properties of the concerned structures.

Figure 7 shows the influence of the different structures on the seismograms. In this figure, the single seismogram traces of the four models

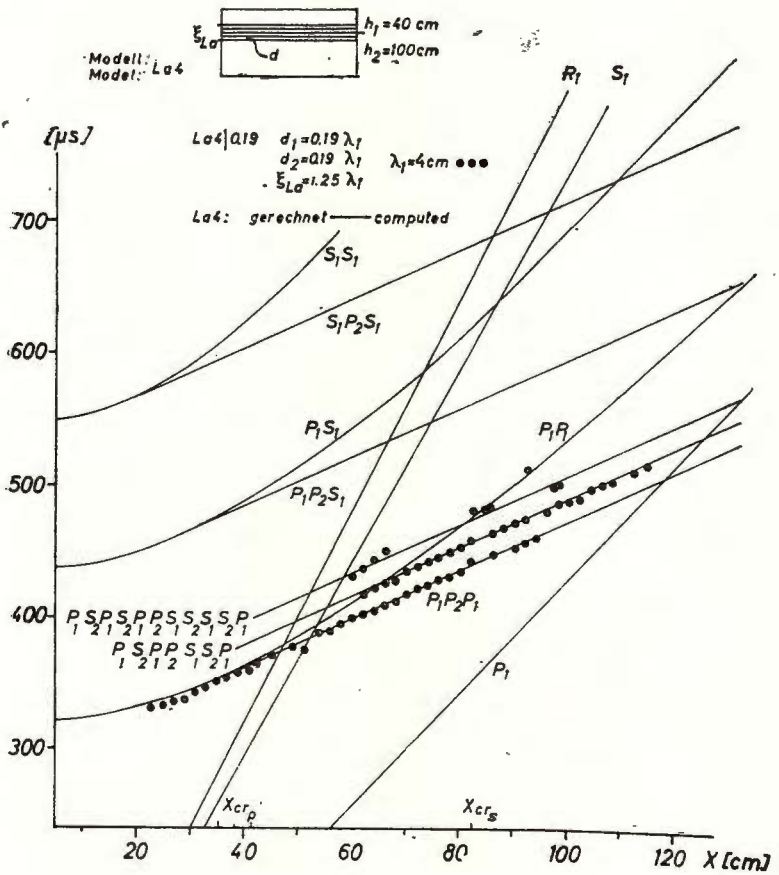

Fig. 6 a

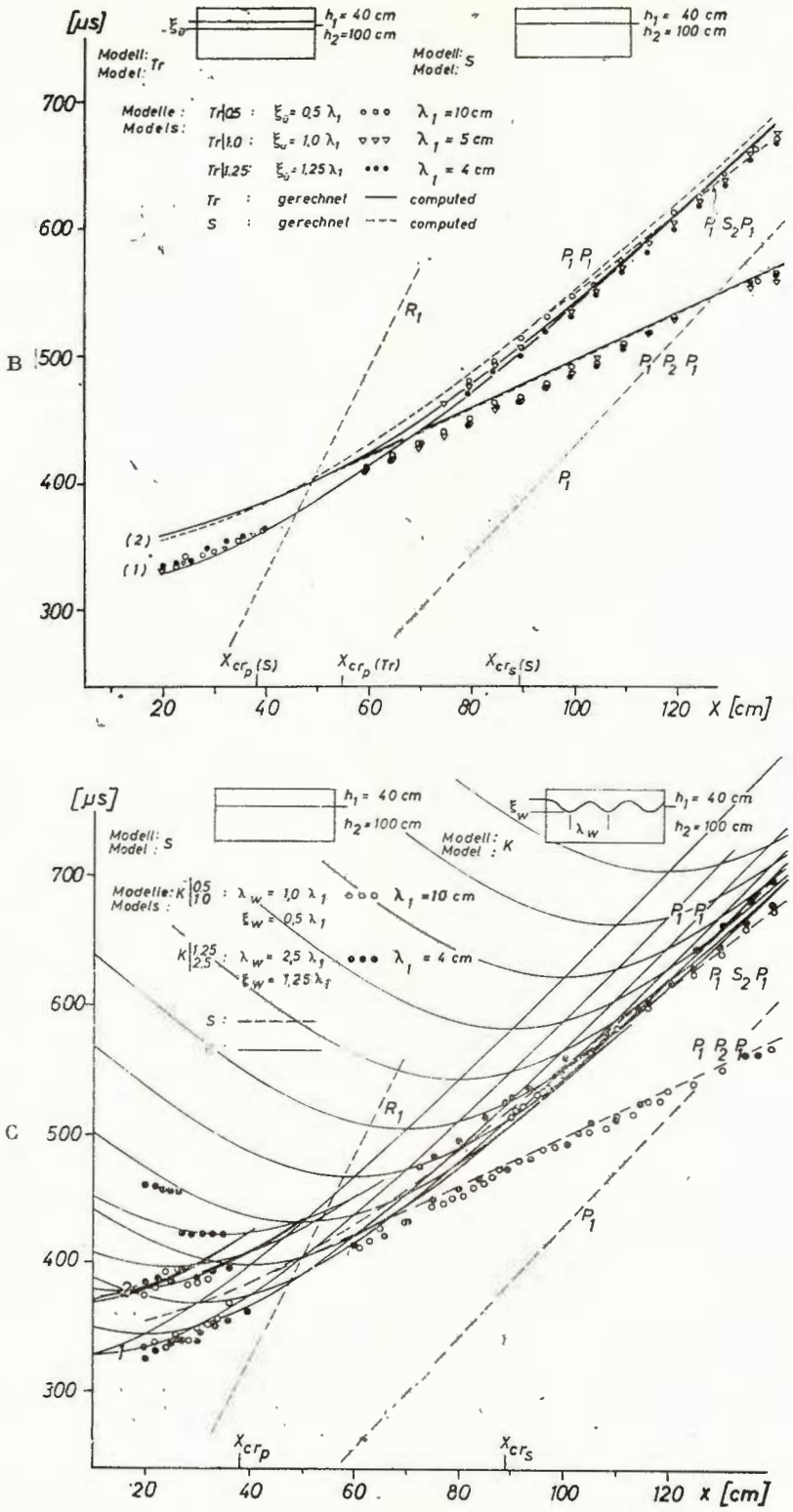

Fig. 6. — Travel-time graphs for the models shown in figure 5.

(plane first order discontinuity, laminated transition zone, transition layer with non-linear velocity-depth distribution and corrugated transition-zone) are compared at certain distances in the subcritical area (20, 30, 40 cm) and in the overcritical area (90, 100, 110 cm).

We will have a look at first at the area of subcritical reflections (fig. 7, left side).

Considering the sensitivity of the amplification in this montage, the different shape, that means the different amplitudes and frequencies of the recorded signals, becomes obvious.

In comparison with the first order discontinuity the P_1P_1 — reflection from a transition layer shows smaller amplitudes and — confirmed

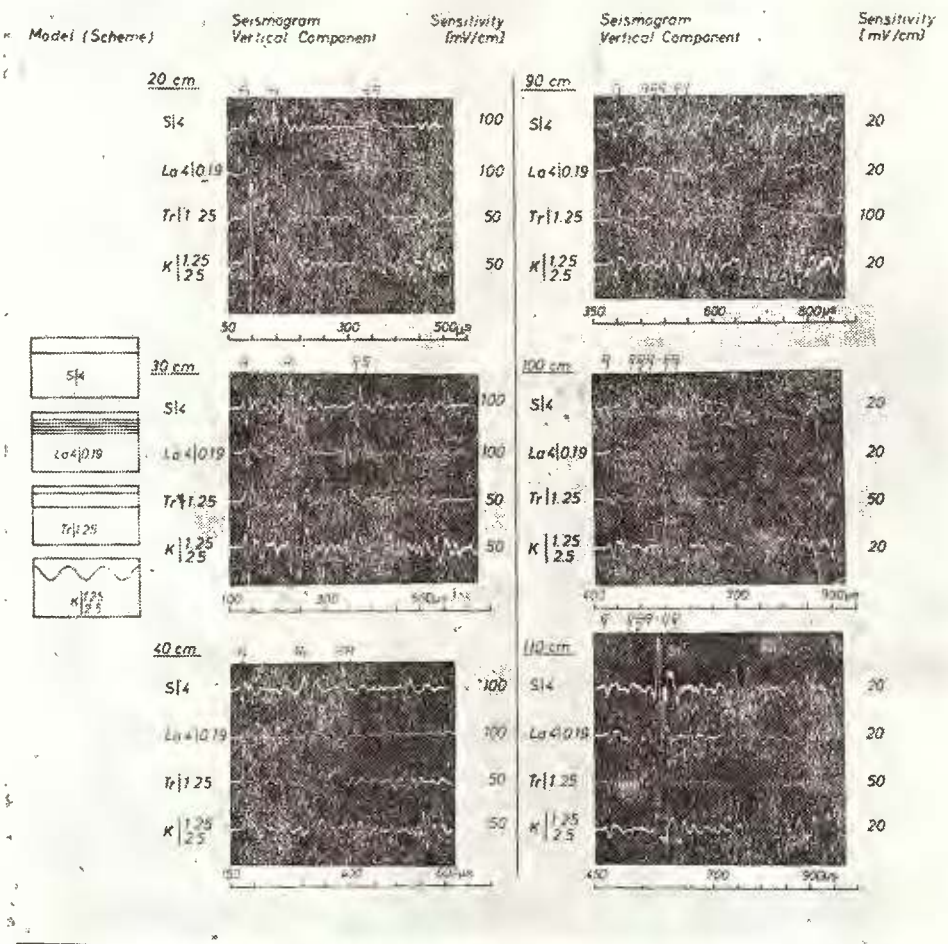

Fig. 7. — Seismogram sections of the subcritical region (left side) and overcritical region (right side) for the models shown in figure 5.

by the Fourier-analysis — a higher content of low frequencies confirming the results of Datta (1967) and Schick, Schneider (1967). The reflections from the laminated zone has a more complicated form, nearly in correspondence with the computed seismograms by Fuchs (1969). But the number of the subsequent onsets is relatively small in comparison with the series of onsets and reverberation in the seismogram of the corrugated transition-zone.

This effect could be confirmed by model investigations by means of the schlieren-method (Behrens, Kozák, Waniek, 1971).

Figure 8 shows a series of two-layered models (a layer of water over a halfspace of Plexiglas) with corrugated boundary structures in comparison with a plane interface. The P-wave field generated by this type of boundary is very complicated. On the schlieren frames the direct wave (P_1) the refracted wave (P_1P_2), the head wave ($P_1P_2P_1$) and the plurality of the reflected waves (P_1P_1) are clearly to be seen.

From the complicated form of the wavefield the series of onsets in the seismograms (fig. 7) are explainable.

The model seismograms from corrugated structures show a good agreement with the seismograms obtained from deep seismic sounding, especially of the P^M-reflections (fig. 9).

In the upper part of the figure deep crustal reflections from the depth ranges of the Mohorovičić-discontinuity are shown (after Liebscher, 1964). in the lower lower part seismograms from models with a plane interface of first order (left side) and with a corrugated interface (right side).

Because of the similarity of the model seismograms from the corrugated structure and the field seismograms, a corrugated transition zone could be assumed as a possible structure of the Mohorovičić-discontinuity (Behrens, Kozák, Waniek, 1971; Behrens, 1971). This assumption has been established by model experiments under the condition of deep seismic sounding.

Figure 10 shows the investigated model with the arrangement of the shotpoints SP 1-SP4 (lower part) and the model seismograms with the 43 geophon-traces belonging to the respective shotpoints (upper part).

It could be shown by Behrens, Gommlich, Bortfeld, Köhler, (1972), that the evaluation of the model-deep-seismic-sounding-seismograms by the commonly used method of "mirror image" produces only the from field measurements wellknown series of single reflecting elements and not the true (corrugated) structure of the zone (fig. 10).

The true structure can be estimated very well by the new developed method of "seismic imaging"[56] — however in the case of the Mohoro-

[5] Bortfeld R. Seismic and optical imaging. 1971. Paper presented at the 33rd Meeting of the EAEG, Hannover.

[6] Bortfeld R. Seismische Abbildungen. 1971. Paper presented at the 16th Geophysical Symposium, Siófók, Hungary.

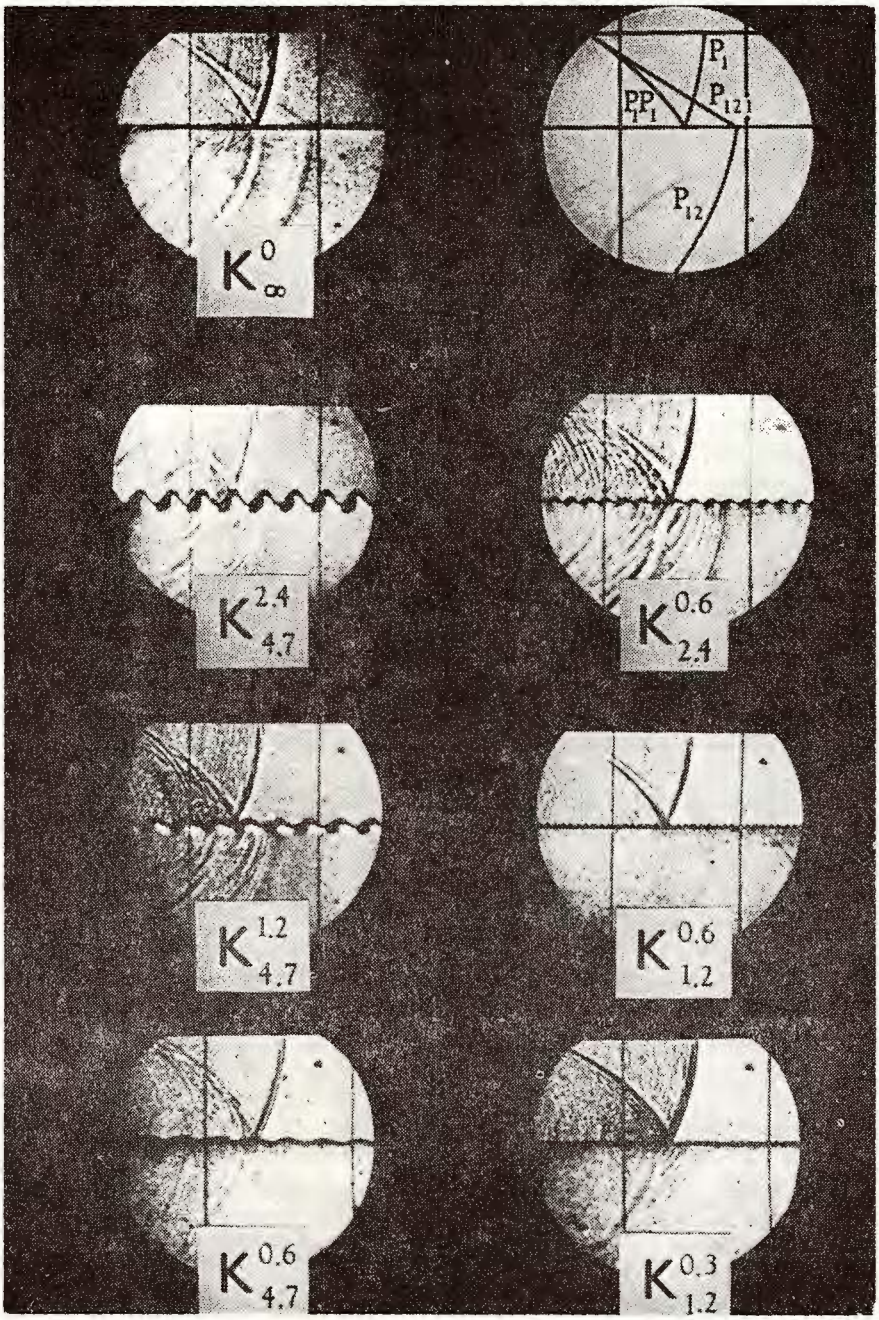

Fig. 8. — Studies of wave pattern in dependence on corrugation parameters by means of schlieren-measurements. (Behrens, Kozák, Waniek, 1971)

K^i_j — symbol denoting the corrugated boundary;

i, — amplitude; j, wavelength of corrugation expressed by the wavelength λ of the incident wave.

vičić-discontinuity only by means of a 80 km profil with geophon distances of 200 — 300 m.

Nevertheless here quite new starting points of common efforts of theory and model seismology appear with respect on the interpretation of boundary structures. They should be worthy of note in the near future.

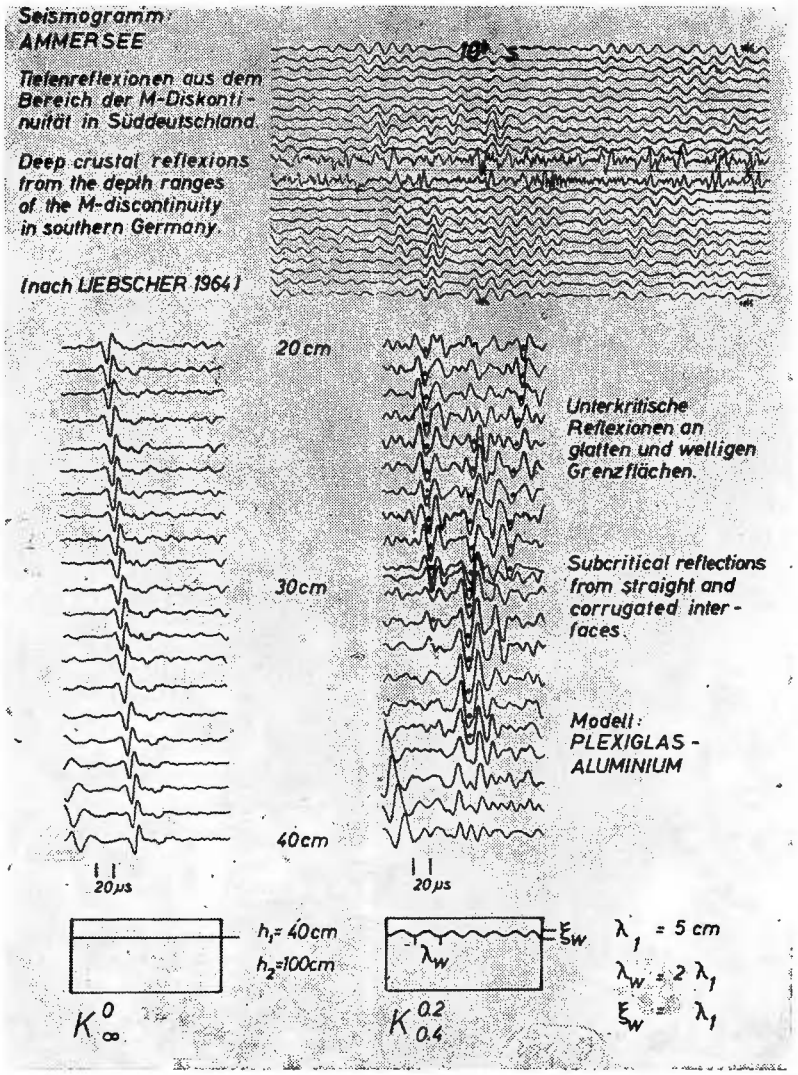

Fig. 9. — Comparison of deep crustal reflections and model-seismograms of reflections from plane and corrugated boundaries (B e h r e n s, 1971).

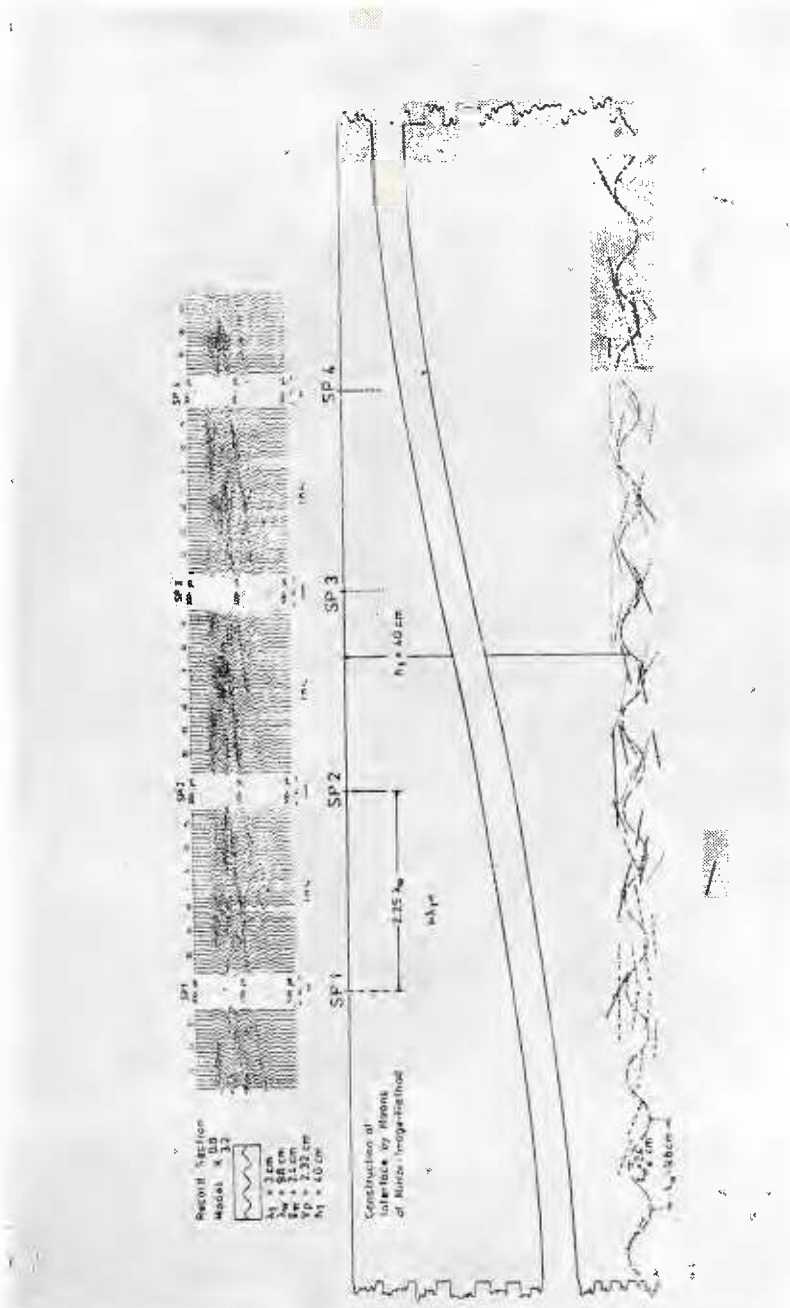

Fig. 10. — Model-deep-seismic-sounding-seismograms and construction of the corrugated transition-zone by means of „mirror-image-method"
(Behrens, Bortfeld, Gommlich, Köhler, 1972).

Amplitude investigations

The comparison of the amplitude-distance curves of the discussed transition-zones gives an additional material of characterizing the differing zone structures.

In figure 11 the amplitude-distance curves of the vertical component of acceleration are shown. On the abscissa the pick-up distances are

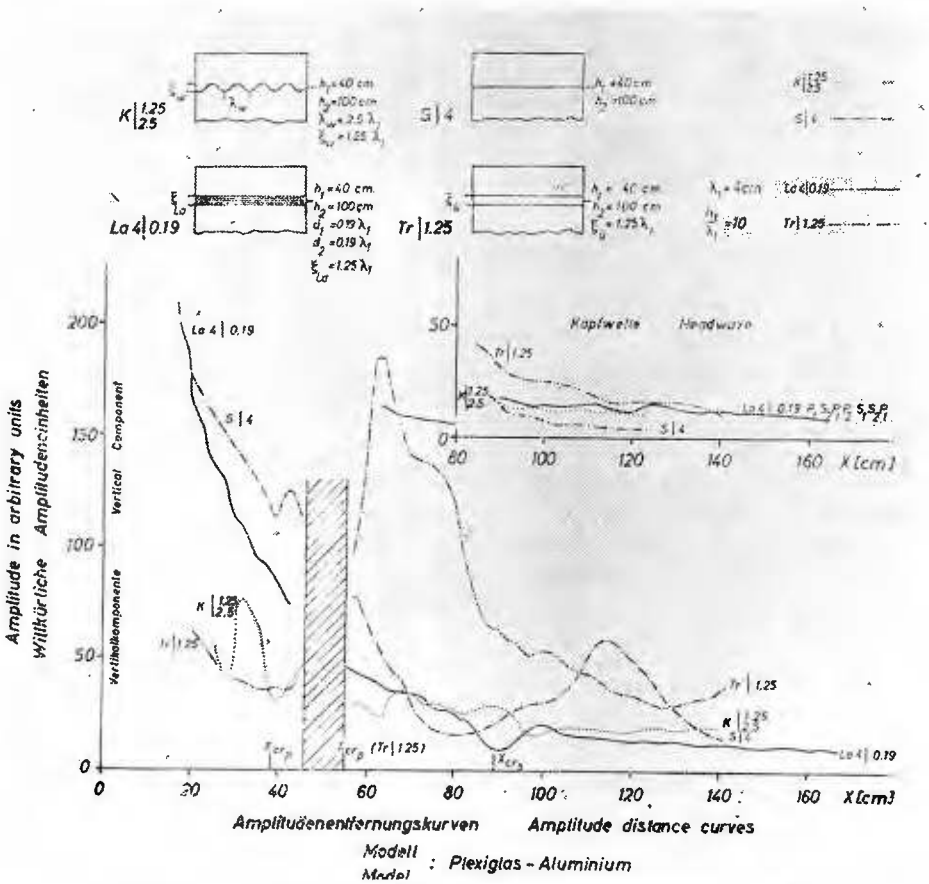

Fig. 11. — Amplitude-distance curves for the models shown in figure 5.

plotted with the respective critical distances, on the ordinate the amplitudes of the reflected signals in arbitrary units.

The head wave amplitudes are shown in a separate coordinate system with the same scale. The radiation pattern of the source was eliminated.

The amplitude distance-curves of the different transition-zones show a quite different behaviour.

The reflectivity of the laminated transition-zone in the vicinity of the shotpoint is higher than of a first order discontinuity, the amplitude-distance curve of this model has no first and second critical maximum as the first order discontinuity.

The transition layer with the nonlinear velocity-depth distribution has the same reflectivity as the corrugated transition-zone — the amplitude undulation in the sub-and overcritical region and the absence of the second critical maximum can be taken as a distinctive mark of the corrugated structure.

The strong maximum in the amplitude-distance curve of the transition layer is caused by a caustic as a result of the chosen nonlinear velocity-depth distribution. The form of the maximum depends on the velocity gradient (B e h r e n s, D r e s e n, W a n i e k, 1971; Č e r v e n ý, Z a h r a d n i k, 1972).

Head wave investigations

The relation between the head wave amplitude and the structure of the transition-zone is of a special interest.

From the results of the investigations of the head wave shown in figure 11 it can be pointed out generally, that the head wave amplitude from a transition-zone is always larger than from a first order discontinuity[7]. For the laminated zone however this is valid only for the second observed head wave with the complicated travel path. The ordinary head wave can be observed only up to 80—90 cm and becomes very small. This can be seen already from the seismograms (fig. 7, right side). The small onset before the large amplitudes at 90 cm is that of the ordinary head wave whereas the large amplitudes belong to the second head wave. This fact seemed to be important for the evaluation of field results and for the discussion and the decision about the most plausible structure form of the Mohorovičić-discontinuity.

As it is to be seen already from the seismograms in figure 7, a great difference of the head wave amplitudes dependent on the structure of the transition-zone or boundary can be noticed. On this subject or problem of the interrelation between the head wave amplitude and the velocity gradient in a transition layer and the frequency of the elastic wave propagating in this layer N a k a m u r a (1968), S i s k i n d, H o w e l l (1967) and H o w e l l, B a y b r o o k (1967) carried out comprehensive model experiments during the last years.

At first they pointed out (fig. 12), that — for a given velocity gradient within the transition layer — the head wave amplitude shows a rapid decrease with increasing frequency if the refracting boundary is a transition layer with a velocity gradient comparable with the frequency of wave motion. The cutoff frequency, where the amplitude starts decrea-

[7] *Op. cit.*, p. 3.

sing is determined by the velocity gradient in the layer (fig. 12, upper part).

Further they showed, that at low frequencies, where the wavelength is much longer than the thickness of the transition-zone, little difference is observed between head waves from a transition-zone and those from a sharp discontinuity (fig. 12, lower part). At certain frequency range where the wavelength is close to the thickness of the transition-

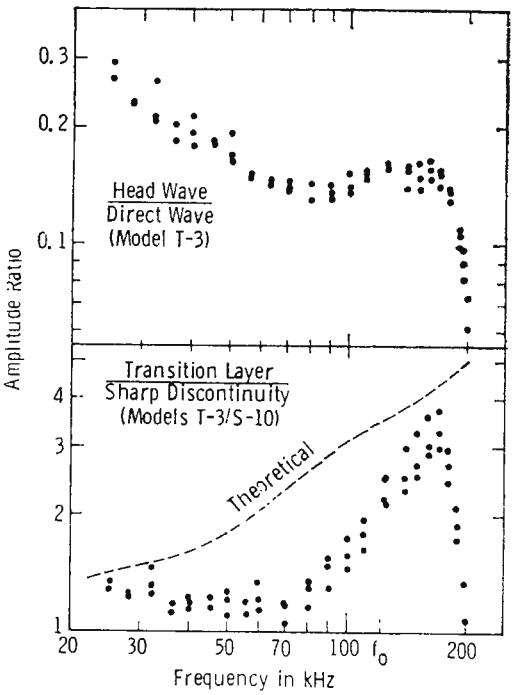

Fig. 12. — Frequency dependence of the head wave amplitudes observed on a model with a transition layer (N a k a m u r a 1968).

zone, the measured head wave amplitude from the transition layer becomes a few times larger than that from a sharp discontinuity.

At last they indicated, that these effects can be observed in the same way from a transition-zone with a linear velocity-depth distribution (fig. 2, row 1), with steps (fig. 2, row 5) and from a transition-zone with an irregular geometric structure (fig. 2, row 3).

These results of N a k a m u r a and others in comparison with the foregoing described model experiments indicate very clearly that the head wave amplitude increases if — with respect to the predominant wavelength of the incident signal — the boundary between two layers becomes more complicated, less and less sharp, with other words poorly defined.

Even the acoustic contact for a first order discontinuity between two homogeneous layers has its important influence on the dynamic parameters of the head wave.

S h a m i n a (1965) has published amplitude-distance curves for the head wave on discontinuities with rigid and sliding contact (fig. 13).

The relatively large amplitudes at greater distances and the small attenuation for sliding contact is clearly to be seen.

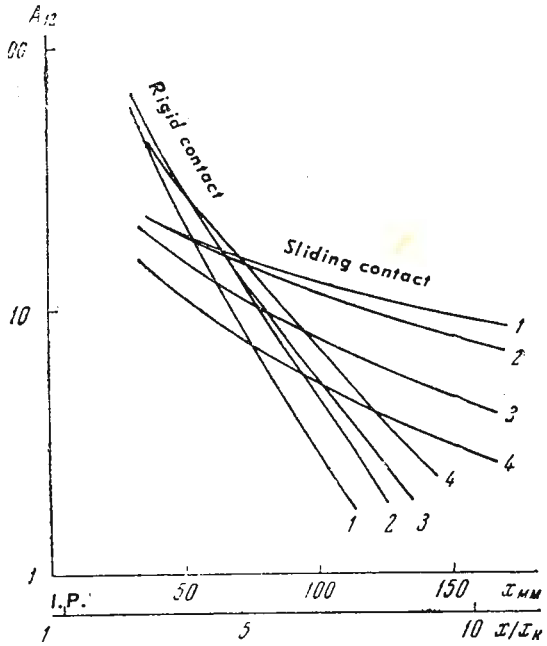

Fig. 13. — Amplitude-distance curves of head waves for rigid and silding contact observed on iron beds.
(S h a m i n a , 1965).
I.P. = intial point of the head wave. The beds are numerated in order of increasing thickness.

Additionally in figure 13 the dependence of the head wave amplitudes on the thickness of the beds wherein the wave is travelling is shown. For sliding contact, the amplitude of the head wave decreases if the thickness of the layer increases, for rigid contact S h a m i n a observed the reverse.

These results from the described model experiments seemed to be important for the understanding of the results of field measurements in so far, as they may explain the possibility of observing large amplitudes of refracting waves even when the amplitudes of reflections are small and the reflections disappear relative suddenly as observed for the P^M-reflections (B e h r e n s, 1971).

However, the comparison of the results of N a k a m u r a with recent results of B e h r e n s and S i e b e l s indicates, that the increase of head wave amplitude in dependence of the sharpness of the boundary becomes smaller if the index of refraction and the velocity gradient decreases (B e h r e n s, S h a m i n a, W a n i e k, 1972).

HIGHER ORDER DISCONTINUITIES

The higher order discontinuities might be considered as an important construction element of transition zones in the Earth. In general only scarce results are published. It is the aim of the before mentioned project of the 'test-models' recommended by the ESC in Copenhagen 1966 to support these investigations.

As an example of the first results of these 2- and 3-dimensional investigations on testmodels in figure 14 the travel-time — and amplitude measurements on a first order discontinuity with differing velocity gradients in the lower halfspace are shown.

The travel-time curves do not demonstrate in a doubtless way that there is a velocity gradient underneath the first order discontinuity. The characteristic features of the travel-time curves could be produced for example by a normal first order discontinuity.

However the evident difference between the course of the amplitude-distance curves indicates the influence of the different velocity gradients on the dynamic parameters of the observed signals. The velocity gradient in the 2- dimensional case is 10 times larger than in the 3-dimensional case.

LOW VELOCITY LAYERS

In contrast to the investigations of higher order discontinuities a great number of different models of low velocity layers, channels or wave guides has been examined. The investigations were carried out mainly along two directions : research of the first arrivals on the surface of the models (simulating the Earth's surface) and research of the wave pattern for channel waves P_a and S_a.

Some general characteristics of the behaviour of the studied waves can be selected and in spite of the difference in methods of model fabrication and the character of the considered low velocity zone some general conclusions can be drawn (Behrens, Shamina, Waniek, 1972) :

a) The first arrivals recorded on the surface of models with homogeneous, non-sharp, horizontal wave guides have following typical features : For the P-waves on the amplitude-distance curve a minimum can be observed, well known as „shadow zone". This minimum shifts towards the epicenter and disappears when the source is submerged (fig. 15*a*).
The minimum on the amplitude-depth curve for the P-wave, observed in the region of the shadow-zone has the same depth as the waveguide axis (fig. 15*b*).
Both minimum on amplitude-distance curve and minimum on amplitude-depth curve disappear, if the period of the recorded waves increases (fig. 15*c*).
If the wave guide is submerging (or rising) the just mentioned peculiarities cannot be observed.

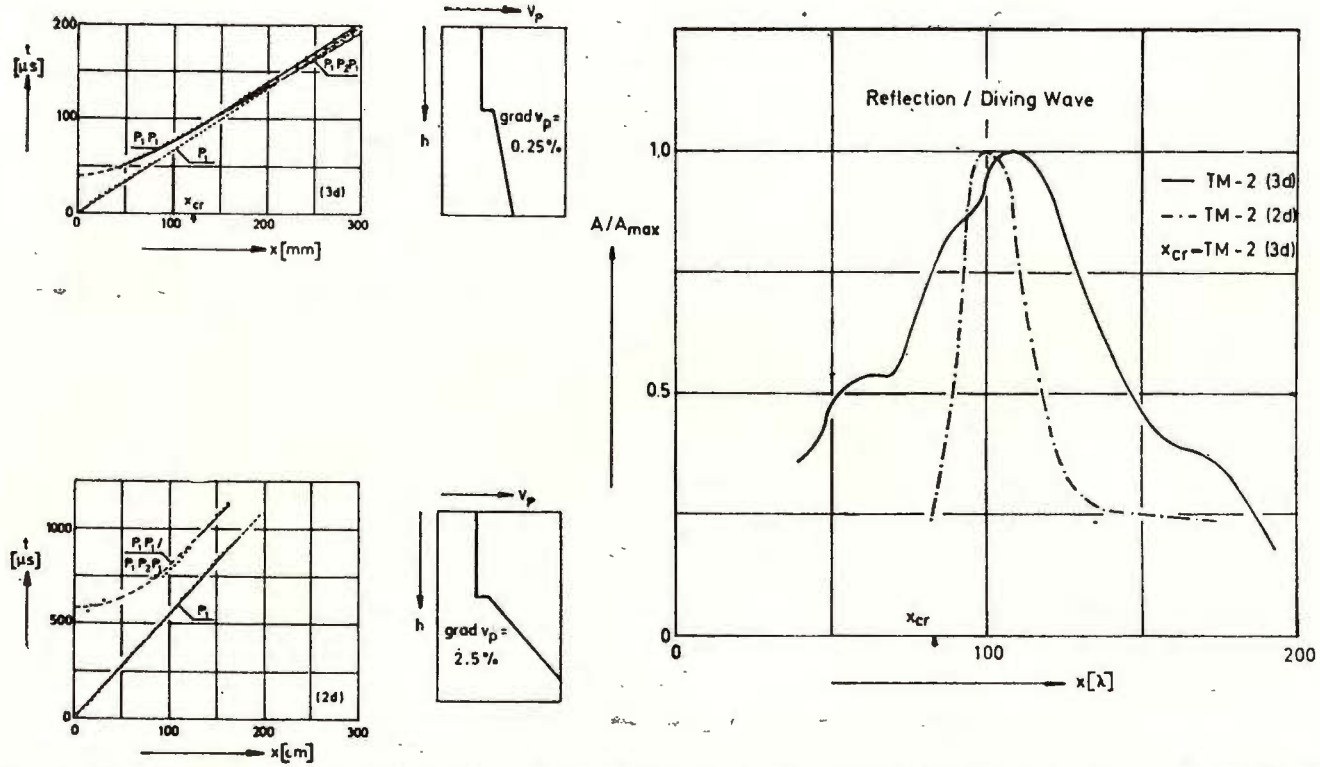

Fig. 14. — Influence of different velocity gradients in the lower layer on the observed travel-time curves and on the amplitude-distance curves of reflected *P*-waves.

(Behrens, Dresen, Waniek, 1971).

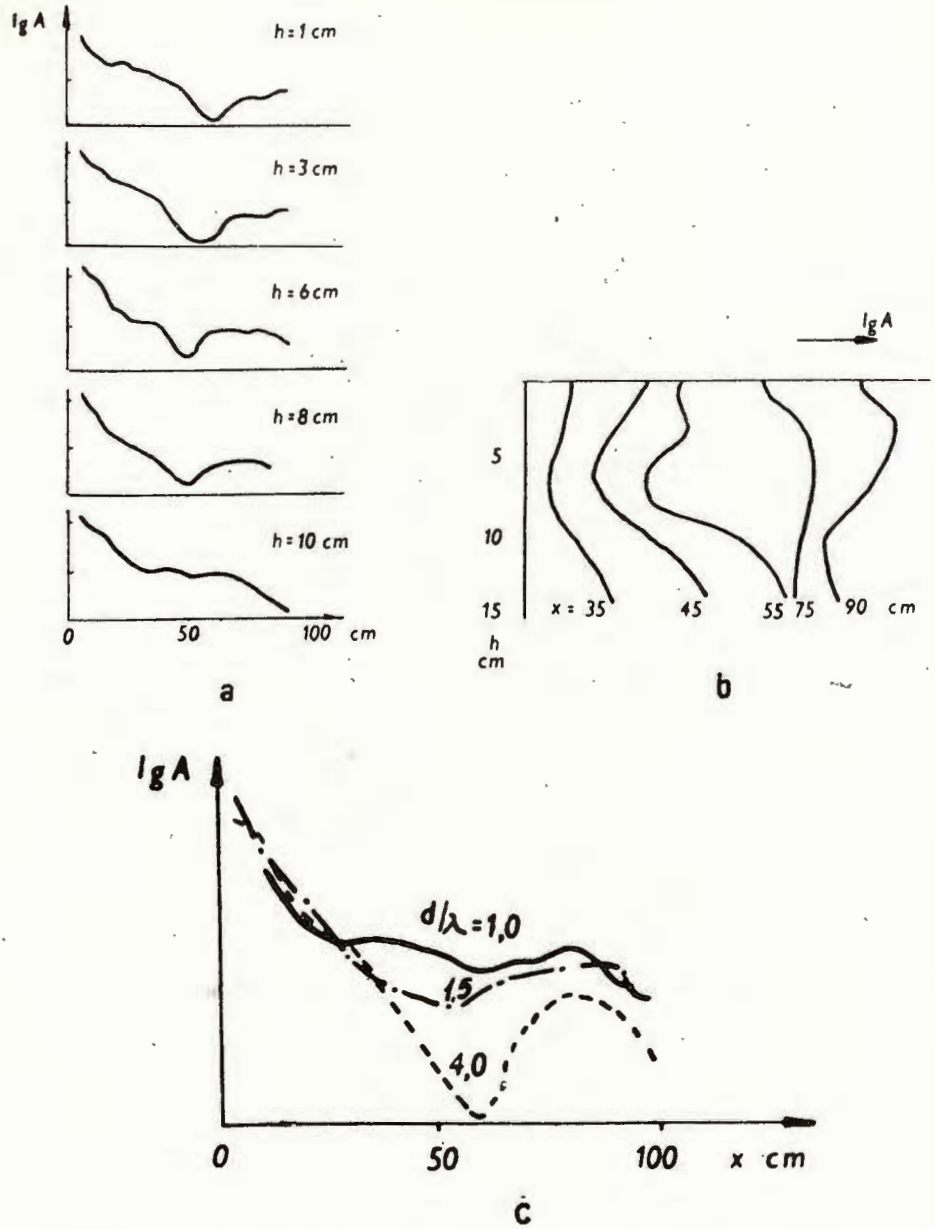

Fig. 15. — *a*) Amplitude-distance curves for *P*-waves in a wave guide model:
h, source depth (depth of the wave guide axis 7,5 cm).
b) Amplitude-depth curves for *P*-waves in a wave guide model:
x, epicentral distance.
c) Amplitude-distance curves for *P*-waves in a wave guide model:
d, thickness of the wave guide;
λ, wave-length of the incident wave.
(Riznichenko, Shamina, 1964).

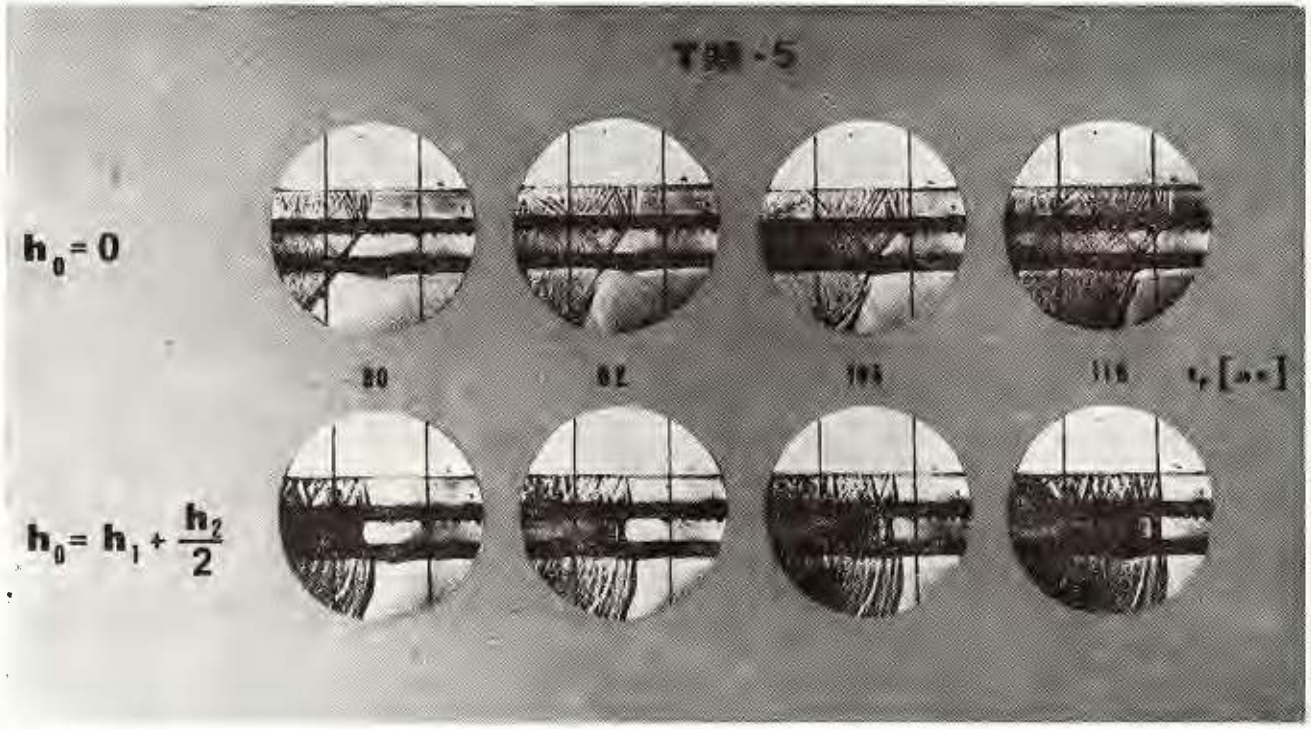

Fig. 16. — Studies of wave propagation of *P*-waves in a low velocity layer (testmodel 5).

The upper part corresponds to the position of the source on the surface of the model, the lower part to the position of the source in the middle of the low velocity layer.

t_P is the time scale derived from the direct *P*-wave travel-time.

(W a n i e k , 1972).

b) The first arrivals recorded at internal points of the model have following specific characteristics :
The velocity of wave propagation in wave guides with sharp boundaries decreases when the period of the recorded waves decreases.

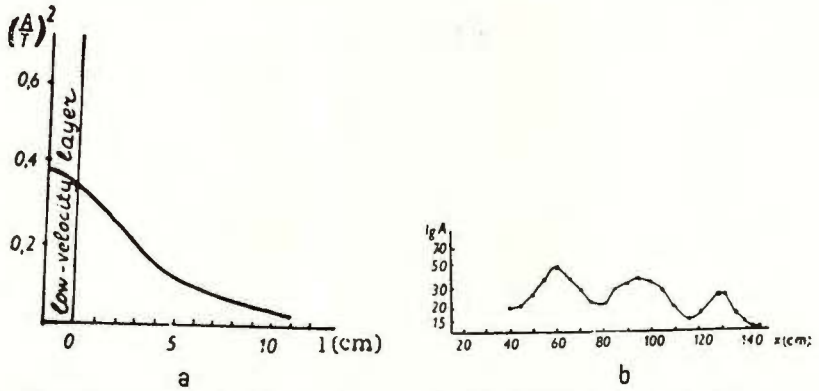

Fig. 17. — a) Dependence of the channel wave *Pa* on distance from the boundary of the low velocity layer
(K h o r o s h e v a, 1962).
b) Amplitude-distance curves of *P*-waves along the wave guide axis (K a p c a n, K i s l o v s k a y a, 1966).

If the source is situated within the wave guide (fig. 16) a phenomenon of energy concentration is observed regardless of the sharpness of the boundaries. The maximum of the amplitude can be observed in the inner part of the wave guide.
On this figure the results of model investigations on symmetrical low velocity layers by means of the schlieren-method are shown (W a n i e k, 1972). The energy concentration within the channel is clearly to be seen (fig. 16, lower part). In the schlieren frames also the forming process of head waves generated by the refracted waves are visible. In the beginning they are coupled with the front of the channel wave, in greater distances the waves are ahead of the channel wave and form a separate wave group.
The wave field generated by the source acting on the surface of the model (upper part of the figure 16) is without any significant changes with increasing distance (t_p is the time scale derived from the *P*-wave travel time).

c) The channel wave has the following features when the source is located within a low velocity zone :
The channel wave is observed inside and outside of the wave guide at a distance of about one wave lenght (fig. 17a) (K h o r o s h e v a, 1962).
The channel wave shows normal dispersion, the group velocity increases when the period of wave increases. When the source (or the receiver) moves along the axis of a wave guide (fig. 17), an inter-

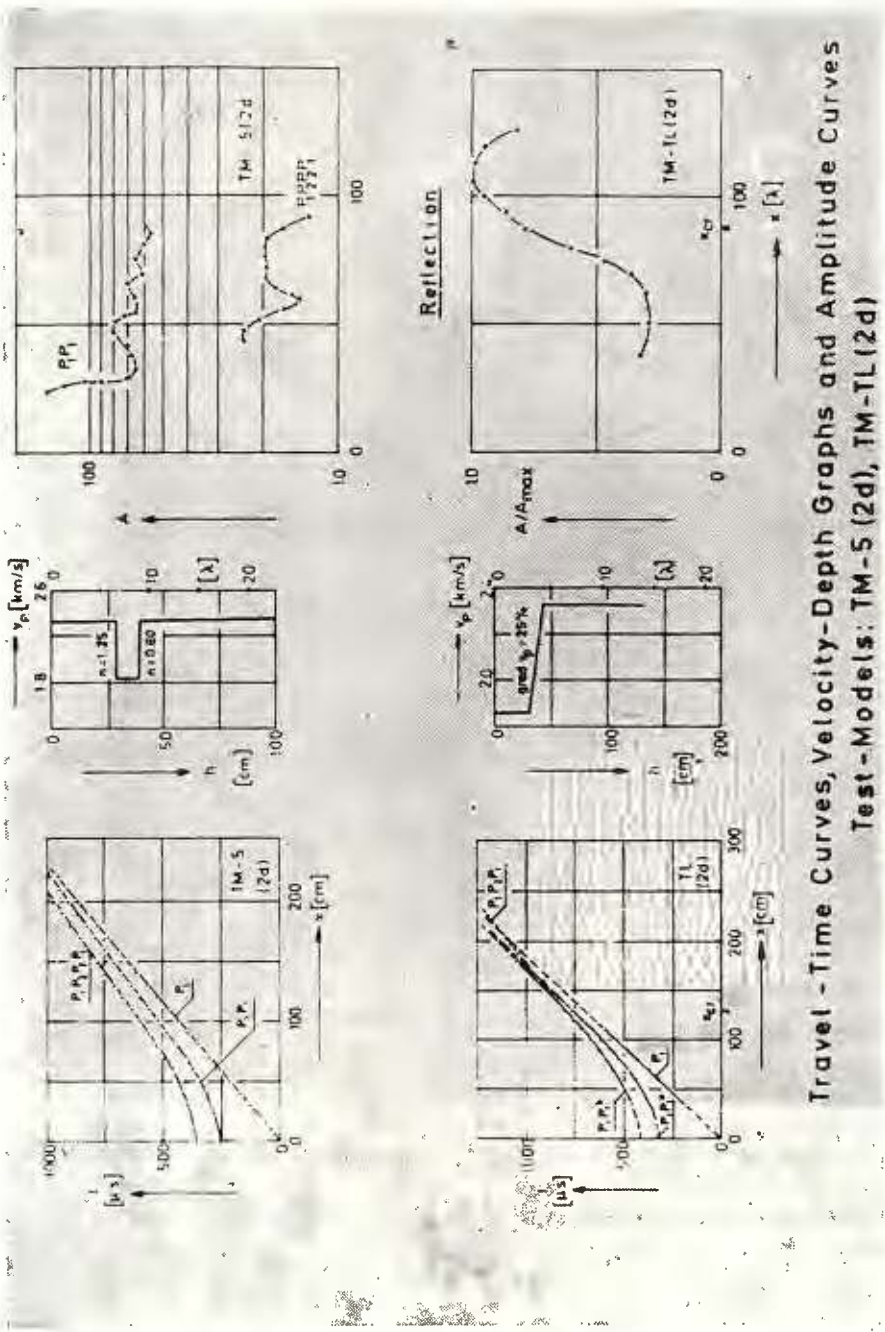

Fig. 18. — Comparison of the travel-time curves and the amplitude-distance curves of a model with a low velocity layer (upper part) and a model with a transition layer (lower part).

change of maxima and minima can be observed (K a p c a n, K i s l o v s k a y a, 1966).

d) An interesting result of the investigations on low velocity zones (B e h r e n s, D r e s e n, W a n i e k, 1971) seems to be the fact, that the amplitude-distance curves of the P_1P_1-reflection from the surface of a low velocity zone with sharp boundaries observed at the surface of the model show also a series of undulations (fig. 18). This could be observed independently on 3- and 2-dimensional models, where the source was not located within the low velocity layer. A satisfying interpretation of this phenomenon could not be given until now.

However from the amplitude-distance curves observed on the model of a symmetrical low velocity layer with sharp boundaries we are able to distinguish between a channel and a transition-zone, whereas the possibility of a misinterpretation on the basis of travel-time measurements might be very great.

CONCLUSIONS

The results on the diagram in figure 18 seems to be typical for the situation of the interpretation of boundary structures and transition-zone structures.

The kinematic parameters do not contain th necessary and sufficient information to characterize or to identify the structure. Studying the dynamic parameters of the observed signals it is possible to get more information about the actual boundary structure.

As we have seen, there are promising perspectives along this line.

We have seen the reaction of the traveltime, of the amplitudes and of the amplitude spectrum to the respective structure of the boundary or transition-zones in the subcritical and overcritical area.

We have seen the interrelation between the head wave amplitude and the sharpness of the boundary, the interaction between the amplitude and the velocity gradient of transition-zones and we have seen the special features of the wave propagation on low velocity channels.

As we hope, this report has shown, that the model seismology has made great efforts — in co-operation with theory and field experiment — in order to enlarge the possibilities for characterizing all kinds of seismic discontinuity structures.

As it has already often been mentioned here and at the symposium on „Interpretation of Seismic Discontinuities" in Liblice/Prague, 1971, many further systematic model seismic and theoretical investigations will be necessary, to explain sufficiently sure the results of seismological observations.

In our opinion, it depends now on gathering more intensely the present facts, on classifying them accordingly to the kind of signal parameters dependent on the form of structure parameter and on comparing them with the field dates.

REFERENCES

Asano S. (1966) Reflection and refraction of elastic waves at a corrugated interface. *Bull. Seism. Soc. Am.*, 56, Berkeley.

Behrens J. (1971) Model investigations on the boundary structure Earth's crust/mantle. *Proc. 12th Assembly ESC*, Luxembourg.

— Kozák, J., Waniek L. (1971 a) Investigation of wave phenomena on corrugated interfaces by means of the schlieren-method. *Proc. 12th Assembly ESC* Luxembourg.

— Dresen L., Waniek L. (1971 b) Investigation on two-and three-dimensional test-models. *Proc. 12th Assembly ESC*, Luxembourg.

Shamina O. G., Waniek L. (1972) Interpretation of discontinuities by seismie modelling methods. *Z. Geophys.*, 38, Würzburg.

—. Bortfeld R., Gommlich G., Köhler K. (1972) Interpretation of discontinuities by seismic imaging. *Z. Geophys.*, 38, Würzburg.

— Gommlich H. (1972) Model investigations with respect to the interpretation of complicated seismic discontinuities. *Z. Geophys.*, 38, Würzburg.

—. Siebels J. (1972) Model investigations on low velocity layers. *Z. Geophys.*, 38, Würzburg.

— Waniek L. (1972) Modellseismik. *Z. Geophys.*, 38, Würzburg.

Červený V., Zahradnik J. (1972) Amplitude-distance curves of seismic body waves in the neighbourhood of critical points and caustics — A comparison. *Z. Geophys.*, 38, Würzburg.

Chowdhury D. K., Dehlinger P. (1963) Elastic wave propagation along layers in two-dimensional models. *Bull. seism. Soc. Am.* 53, 3, Berkeley.

Datta B. (1967). Das Spektrum seismischer Wellen bei der Reflexion an einer Übergangsschicht. *Z. Geophys.*, 33, Würzburg.

Davidova N. I., Kosminskaya I. P., Michota G. G. (1970) The thickness and nature of seismic discontinuities based on deep seismic sounding data. *Tectonophysics*, 10, Amsterdam .

Dresen L. (1971) Amplitudenuntersuchungen and seismischen Wellen zur Charakterisierung von Verwitterungsschichten mit vertikalem Geschwindigkeitsanstieg. *Z. Geophys.*, 37, Würzburg.

Fuchs, K., Müller G. (1971) Computation of synthetic seismograms with the reflectivity method and comparison with observations. *Geophys. J. R. Astr. Soc.*, 23, London.

—. (1969) On the properties of deep crustal reflectors. *Z. Geophys.*, 35, Würzburg.

Healy J. H., Press F. (1960) Two-dimensional seismic models with continuously variab e velocity-depth and density functions. *Geophysics*, 25, Tulsa.

Howell Jr., B. F. Baybrook T. G. (1967) Scale-model study of refraction along an irregular interface. *Bull. Seism. Soc. Am.*, 57, Berkeley.

Iyakin B. N. (1956) Golovye, prochodjaschie i drugie volny v sluchae tonkogo sloja v zhidkosti (Head, passing and other waves for a thin solid layer in a liquid). *Trudy Geofiz. Instituta AN SSSR*, 35, Moskva.

—. (1966)Methods of seismic modelling. *Stud. geophys. geod.*, 10, 3, Praha.

— (1969) Metody modelirovanija seismicheskich javlenij (Modelling of seismic wave processes). Izd. Nauka, Moskva.

Kapcan A. D., Kislovskaya V. V. (1966) Investigation of a waveguide with weak boundaries in two-dimensional perforated models. *Stud. geophys. geod.*, 10, Praha.

Khorosheva, V. V. (1962) The study of a wave guide on a solid two-dimensional model with sharp boundaries. *Bull. (Izv). Acad. Sci. USSR, Geophys. Ser.*, 8, Moscow.

Kozák, J., Waniek L. (1970) Schlierenoptische Untersuchungen an seismischen Gelmodellen mit photometrischer Auswertung des Wellenfeldes. *Z. Geophys.*, 36, Würzburg.

Meissner R. (1967) Zum Aufbau der Erdkruste. Ergebnisse der Weitwinkelmessungen im bayrischen Molassebecken. *Gerl. Beitr. Geophys.*, 76, 3, 4, Leipzig.

Nakamura Y. (1968) Head waves from a transition layer. *Bull. Seism. Soc. Am.*, 58, Berkeley.

Parchomenko I. S. (1959). On the intensity of a wave which has passed through a series of layers with higher velocity. *Bull. (Izv.) Acad. Sci. USSR, Geophys. Ser.*, 5, Moscow.

Poley J. P., Nooteboom J. J. (1966) Seismic refraction and screening by thin high-velocity layers (a scale-model study). *Geophys. Prosp.*, 14, Hague.

Rapoport M. B. (1961). On the reflection of seismic waves at non-specular boundaries. *Bull. (Izv.) Acad. Sci. USSR*, 2, Moscow.

Riznichenko Ju. V., Shamina O. G., Chanutina R. V. (1961) Elastic waves with generalized velocity in twodimensional bimorphic models. *Bull. (Izv.) Acad. Sci. USSR, Geophys. Ser.*, 4. Moscow.

— Shamina O. G. (1964) A comparison of amplitude curves obtained on a wave guide model of the mantle with seismic data. *Bull. (Izv.) Acad. Sci. USSR, Geophys. Ser.*, 8, Moscow.

Schick R., Schneider G. (1967) The propagation of seismic pulses in media with variable velocity. *Proc. 9th Assembly ESC*, Copenhagen.

Shamina O. G. (1960). An investigation of the dynamic features of longitudinal waves in layers of different thickness. *Bull. (Izv.) Acad. Sci. USSR, Geophys., Ser.*, 8, Moscow.

— (1965a) A method of three-dimensional modelling of a wave-guide layer with solid media. *Bull. (Izv). Acad. Sci. USSR, Earth Physics*, 7, Moscow.

— (1965 b) Attenuation of head waves from thin beds for rigid and sliding contact. *Bull. (Izv.) Acad. Sci. USSR, Earth Physics*, 3, Moscow.

— (1966). Experimental investigation of necessary and sufficient characteristics of a waveguide. *Stud. geophys. geod.*, 10, Praha.

Siskind D. E., Howell jr., B. F. (1967) Scale-model study of refraction arrivals in a three-layered structure. *Bull. Seism. Soc. Am.*, 57, Berkeley.

Voskresenskij Ju. V. (1962) The study of seismic reflections from nonspecular boundaries in three-dimensional models. *Bull. (Izv.) Acad. Sci., Geophys. Ser.*, 5, Moscow.

Waniek L. (1966 a) The system water-glycerol-gelatine as a medium for three-dimensional seismic models. *Stud. geophys. geod.*, 10, Praha.

— (1966 b) Fabrication and properties of three-dimensional seismic models of the upper mantle. *Stud. geophys. geod.*, 10, Praha.

— (1972) Model studies of wave propagation in low velocity layers with sharp boundaries. *Z. Geophys.*, 38, Würzburg.

METHODS

COMPUTATION OF EARTH'S CRUST STRUCTURE AND THE DEPTH OF LVL IN CARPATHIAN BASIN

BY

EDE BISZTRICSÁNY[1]

Two years ago, in Luxembourg, the resonance properties of the coda waves was representated. On basic of this imagination, in course of two years the Earth's crust structure was computed for three seismological stations in Hungary. These stations can be found on the area as follows (fig. 1).

The frequency peaks of periods was nearly same at all stations (fig. 2), therefore the structure roughly similar at every station. The thickness of layers of the Earth's crust computed by coda waves can be seen on the table 1 in km.

At stations of Sopron and Piszkéstető the Moho-level is deeper than at Budapest because of neighbourhood of mountains. It has to be emphasised because the Earth's crust thickness in Hungary is general thinner as compared to average.

To the determination of LVL, a method was worked out, because the difficulty lies in the fact, that the travel times of first motions of earthquakes show rather great scattering against to epicentral distance even if they are iP character.

This difficulty, however can be overcome by a simple procedure making the determination of the inflection point independent from the origin time.

Let us suppose that the travel time curve of P waves because of the influence of the LVL can be approximated, within a short range, by a curve of the third order, that is

$$t = a\Delta^3 + b\Delta^2 + C\Delta + d \qquad (1)$$

[1] MTA GGKI Bp, XI. Meredek u. 18, Hungary.

If we have several station then for the i-th station it is true

$$t_i = a\,\Delta_i^3 + b\,\Delta_i^2 + c\,\Delta_i + d \tag{2}$$

and for the k-th station likewise :

$$t_k = a\,\Delta_k^3 + b\,\Delta_k^2 + c\,\Delta_k + d \tag{3}$$

Fig. 1. — The Hungarian seismological stations for which the Earth's crust structure was computed.

TABLE 1

Budapest	Piszkéstetö	Sopron
	14.2	13.2
20.4	20.2	18.4
27.5	30.6	29.7

Subtracting 3 from 2

$$t_i - t_k = (\Delta_i^3 - \Delta_k^3)\,a + (\Delta_i^2 - \Delta_k^2)\,b + (\Delta_i - \Delta_k)\,c \tag{4}$$

dividing equation 4 by $\Delta_i - \Delta_k$ one obtains

$$\frac{t_i - t_k}{\Delta_i - \Delta_k} = a\,(\Delta_i^2 + \Delta_i\Delta_k + \Delta_k^2) + b\,(\Delta_i + \Delta_k) + c \tag{5}$$

The data of shallow focus earthquakes as recorded by the five Hungarian stations yield an adequate number 205 of the couples Δ_i, Δ_k respectively t_i, t_k thus the constants a, b, c can be determined by least squares method.

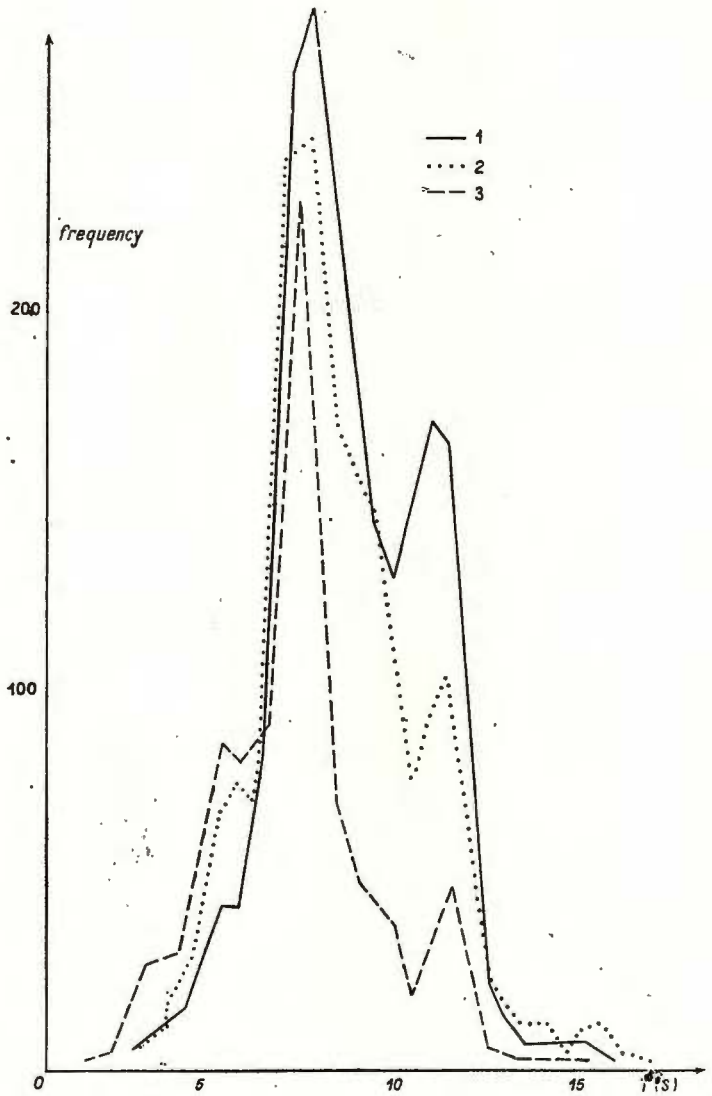

Fig. 2. — The frequency curves of the coda waves recorded in the Hungarian seismological stations:
1, Budapest; 2, Sopron; 3, Piszkèstetö

In order to obtaining the inflection point, t should be differentiated two times, with respect to Δ

$$\frac{dt}{d\Delta} = 3a\Delta^2 + 2b\Delta + c$$

$$\frac{d^2t}{d\Delta^2} = 6a\Delta + 2b = 0$$

$$\Delta = -\frac{b}{3a}$$

Now, if one knows the radius to vertex, belonging to the distance $\Delta = \frac{b}{3a}$ of the region in question the depth of the LVL can be calculated.

From the iP recordings of the Hungarian stations it is possible to determine the function $\Delta = f(r_v)$ with the traditional Wiechert-Herglotz method as follows:

TABLE 2

Δ[degree]	1	2	3	4
r_v[km]	6341,65	6336,38	6330,26	6322,88
Δ [degree]	5	6	7	8
r_v[km]	6317,21	6308,10	6295,64	6282,99
Δ[degree]	9	10	11	12
r_v[km]	6267,16	6258,38	6244,03	6230,17

where Δ is the epicentral distance in degree with the restriction $1° < \Delta < 13°$ and r_v is the radius to the vertex (fig. 3).

Using the restriction for $\Delta_i - \Delta_k$, that

$$0{,}5° \leqslant \Delta_i - \Delta_k \leqslant 3°$$

for the constants of third degree equation we obtained

$$a = 0{,}09226$$

$$b = -2{,}2095$$

Hence the Δ value at the inflection point

$$\Delta = -\frac{b}{3a} = 7{,}98°$$

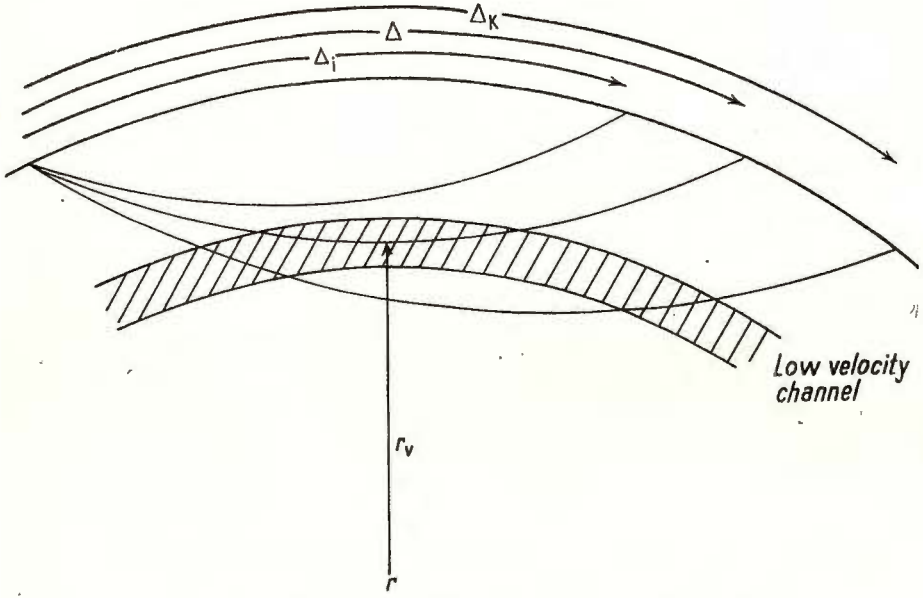

Fig. 3. — Determination of the function $\Delta = f(r_v)$ by the Wiechert-Herglotz method, from the iP records of the Hungarian stations.

Fig. 4. — The Δ values for the Carpathian Basin (using Polish data).

According to table before mentioned, to an epicentral distance of 8°, 6283 km radius to the vertex belongs. Thus the depth is 6371—6283 = 88 km.

This data refers to a distance of $\frac{\Delta}{2}$ that is somewhat to the south in vicinity of Belgrade.

Later we wanted to compute the LVL depth for Hungarian Basin therefore we had to use Polish data. (fig. 4). From 193 couples of Δ_i, Δ_k, t_i, t_k the result was given as follows

$$\Delta = 6{,}93°$$

From this epicentral distance the depth of vertex is 74,5 km for Carpathian Basin. This depth is less as it was obtained for Belgrade. Therefore we can draw perhaps daring conclusing, that : the LVL depth similarly to Moho-level is nearer to the surface in Carpathian Basin than in its neighbourhood.

MÉTHODES D'ENREGISTREMENT DES GRANDS PROFILS EN FRANCE

PAR

ALFRED HIRN J. C. RUEGG[1]

A partir de 1968—1969 s'est posé en France le problème de réaliser systématiquement des sondages sismiques profonds afin de déterminer la structure profonde de la croûte terrestre, et de coordonner dans le cadre d'une opération inscrite au plan, les recherches de sismologie expérimentale qui avaient été faites jusqu'alors par des groupes isolés avec du matériel inhomogène et des moyens limités.

A partir de cette date s'est donc constitué le groupe Grands Profils Sismiques (G.P.S.) dans le cadre d'une opération de l'Institut Géographique National. On a donc eu à décider du *choix de l'appareillage du type de profil á réaliser* et de la *technique de tir á employer*.

L'appareillage (Souriau et al.)[2]. L'appareillage est constitué par un géophone à trois composantes perpendiculaires de 2Hz de fréquence propre et que l'enregistrement est effectué sur bande magnétique analogique en modulation de fréquence (système Lennartz) ce qui procure une dynamique importante (55 à 60 db) et une large bande passante (2 à 100Hz).

Les signaux sismiques enregistrés lors des Grands Profils ont un spectre entièrement compris dans la bande passante du système d'enregistrement; quelques exemples de spectres des principales phases à diverses distances sont montrés dans la figure 1.

Les dispositifs d'enregistrement ont été choisi en fonction du problème à étudier.

En 1970, il s'agissait d'étudier la structure fine de quatre régions géologiquement distinctes dans le Massif Central Français: la région

[1] Institut de Physique du Globe-Tour 14. Laboratoire de Sismologie. Université Paris 6 — 11, quai Saint-Bernard. 75230 Paris, France.

[2] Souriau M., Steinmetz L. Acquisition et traitement des données numériques pour les Grands Profils Sismiques. 1972 Communication à la sous-commission des instruments et traitements des données de la Commission Sismologique Européenne, Braşov.

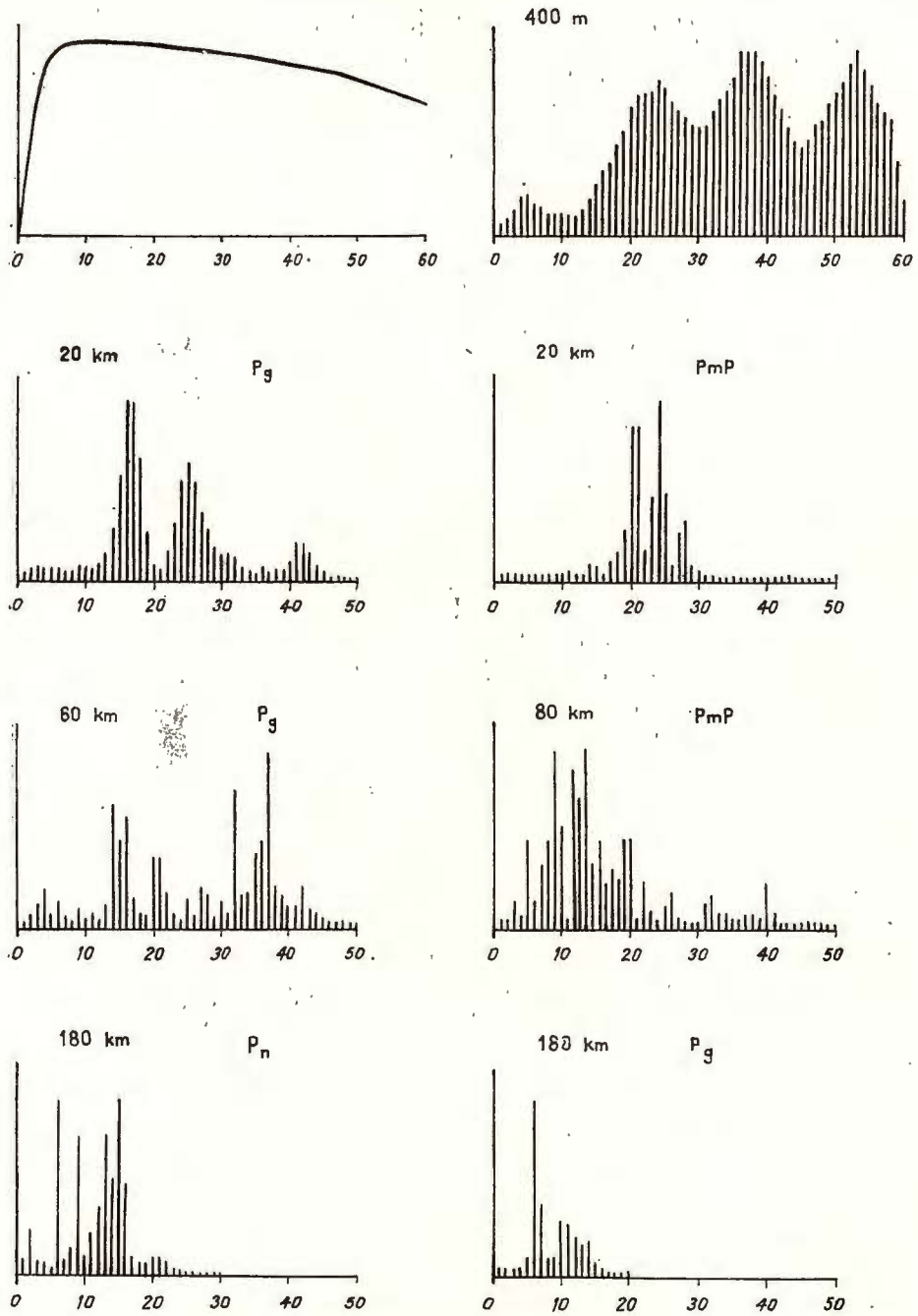

Fig. 1. — Courbe de réponse de l'appareillage et spectre d'énergie des principales phases pour différentes distances d'enregistrement.

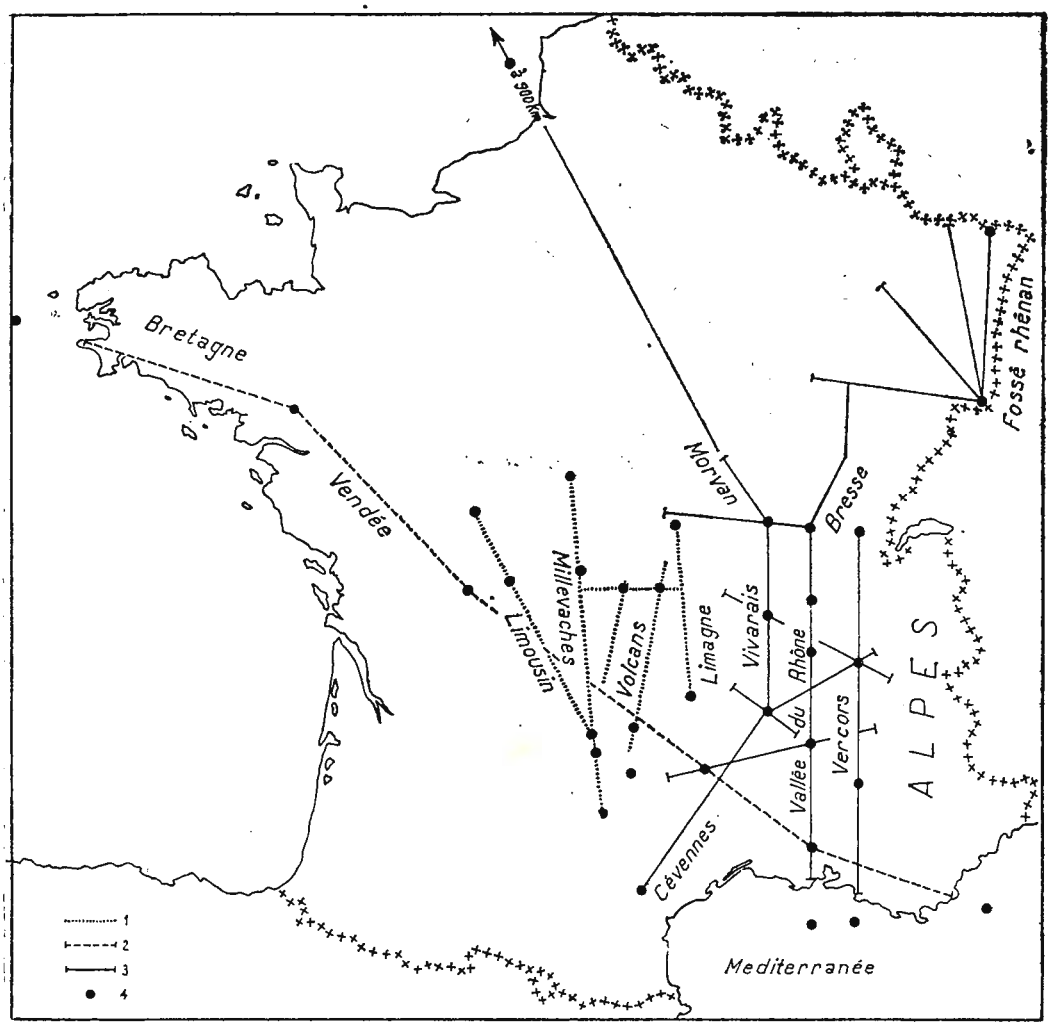

Fig. 2. — Profils réalisés en France dans le cadre de l'opération Grands Profils Sismiques en 1970, 1971, 1972 :
1, 1970 ; 2, 1971 ; 3, 1972 ; 4, Points de tir.

métamorphique du Limousin, le massif granitique de Millevaches, l'axe volcanique d'Auvergne et le fossé sédimentaire de Limagne (fig. 2).

Le dispositif d'enregistrement était composé de 30 stations identiques espacées de 2 à 3 km et occupait la moitié d'un profil.

Dans chacun des compartiments étudiés, ce dispositif a été implanté deux fois symétriquement de façon à obtenir dans le même compartiment des profils inversés en ondes réfléchies et réfractées (fig. 3).

En 1971, en collaboration avec les Instituts de Géophysique allemands et portugais, a été réalisé un Grand Profil à travers la France (fig. 2) dont le but principal était d'obtenir des renseignements sur la structure du manteau supérieur. Des tirs en mer de 2 tonnes ont été effectués à chaque extrémité et des tirs intermédiaires inversés ont permis,

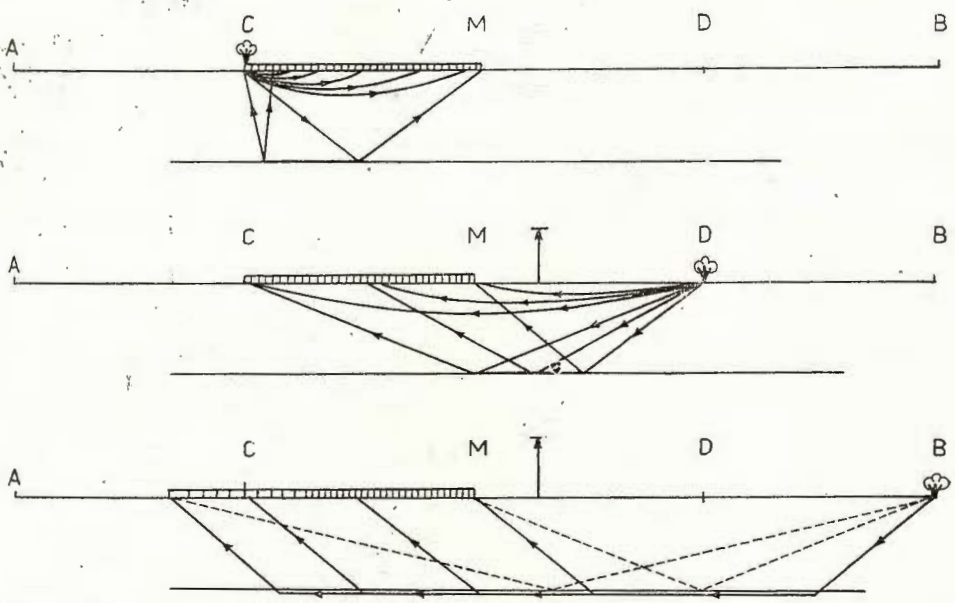

Fig. 3. — Dispositif d'enregistrement utilisé pour les profils éxécutés en 1970 dans le Massif Central. Schema de principe l'implantation :

Stations inplantées sur CM ; Tir en C(400 kg)
D(800 kg) CD = 150 km ;
B(2000 kg)

Stations inplantées sur MD ; Tir en D (400 kg)
C (800 kg) AB = 300 km.
A (2000 kg)

avec un dispositif simplifié par rapport à celui de 1970, d'obtenir la structure de la croûte tout le long de ce profil et ainsi éventuellement corriger le grand profil des variations de structure de croûte.

En 1972, il s'agissait d'étudier la structure du fossé Rhodanien et de ses abords et d'assurer le raccord entre les résultats obtenus en 1970—1971 dans le Massif Central et ceux plus anciens des Alpes.

Trois profils principaux ont donc été effectués longitudinalement de façon à obtenir des dispositifs inversés sur une grande longueur en réfraction et d'autre part on a effectué des tirs intermédiaires de telle façon que les zones déterminées en refléxion soient inversées. Par ailleurs, comme les variations latérales de structure pouvaient être importantes on a effectué des profils transversaux recoupant les premiers (fig. 2).

Techniques de tirs. On a cherché à se libérer de la contrainte des tirs de carrières et des tirs en lac qui ne permettent pas de choisir librement l'endroit, le jour et l'heure de tir et l'implantation des profils, et l'on a développé une technique de tirs en forage en pays habité (lignes de forages espacés de 20 à 40 mètres contenant chacun 200 à 500 kg d'explosif). Les forages et les tirs étant effectués sous notre direction par des entreprises privées.

Les *emplacements de tir* ont été choisis, en fonction des profils à réaliser, dans des endroits isolés situés en général à plus de 500 à 1000 mètres des habitations (suivant les charges) et avec chaque fois qu'un tir était effectué le contrôle des vibrations provoquées par un enregistrement au voisinnage de ces habitations.

Le rendement de ces tirs a en général été satisfaisant. Dans de bonnes conditions de bruit de fond (Millevaches 0,05 μ/s) on a pu enregistrer un tir de 50 kg jusqu'à 90 km (0,5 μ/s) et un tir de 800 kg jusqu'à 300 km.

Mais par sécurité nous avons choisi de tirer 500 à 800 kg pour les profils devant être enregistrés jusqu'à 150 km et 2 tonnes à 2,5 tonnes pour les profils de réfraction jusqu'à 300 km.

Depuis 1971, nous avons utilisés des tirs en mer là où les profils le permettaient, et les avons effectués avec la méthode préconisée par le Professeur M u e l l e r en tirant des charges à une profondeur calculée pour qu'il y ait résonnance entre la pulsation de la bulle de gaz et de la colonne d'eau.

L'organisation sur le terrain. L'organisation sur le terrain a été conduite de façon à réduire au minimum les temps d'expérience et d'obtenir par une répartition judicieuse des tirs et des stations le maximum de données.

Les observateurs sur le terrain étaient groupés en équipes légères et mobiles (4 personnes) chaque observateur disposant d'un véhicule et de deux ou trois stations semi-automatique à fenêtres d'enregistrement programmées. Un P.C. assurait chaque fois le contrôle des jours et heures de tir et du déplacement des observateurs.

Les enregistrements obtenus par les observateurs étaient regroupés par ramassage chaque jour et visualisés afin de contrôler l'avancement du travail et intervenir pour réparer les pannes éventuelles et contrôler les charges.

ON THE RELATION OF EARTHQUAKE RECORD VISUAL CHARACTERISTICS WITH FOCAL DEPTH AND ENVIRONMENTAL STRUCTURE

BY

A. A. POPLAVSKY[1]

The relation of the functions of empiric density distribution probability of the Kurile-Kamchatka earthquake visual characteristics with a focal depth is discussed. Simultaneously those empiric function dependence in the presence of boundaries within the upper mantle is revealed. The lying depth of source of these are managed to determine.

In the paper the methods of such the information processing are discussed as well as the certain results of their practical application.

If there is a certain relation between the pair of random variables x, y then their frequency distribution functions should be interrelated as well.

In a simple case (G u m b e l, 1965), when there is a reciprocally-single-valued dependence

$$y = f(x) \qquad X = \varphi(y) \tag{1}$$

between the corresponding frequency distribution function $P(x)$ and $Q(y)$ rationed to one, the ratio being the following :

$$Q(y) = P\ [\varphi(y)] \left| \frac{\mathrm{d}\,\varphi(y)}{\mathrm{d}y} \right| \tag{2}$$

x and y dependence may not be single-valued and it exists as a set of reciprocally-single-valued functions, where

$$y = f_i(x), \quad X = \varphi_i(y) \tag{3}$$

$i = 1, 2, \ldots, n$ and each of f_i, φ_i is randomly realized in observations with cyclicity $\rho_i \left(\sum_{i=1}^{i=n} \rho_i = 1 \right)$. Then

$$Q(y) = \sum_{i=1}^{i=n} \rho_i\ P\ [\varphi_i(y)] \left| \frac{\mathrm{d}\varphi_i}{\mathrm{d}y} \right| \tag{4}$$

[1] Sakhalin Complex Scientific Research Institute, Novoaleksandrovsk, Sakhalin 694050, USSR.

In some more general case

$$y = f_i(x) + \delta y, \quad X = \varphi_i(y) + \delta(x) \tag{5}$$

where $f_i(x)$, $\varphi_i(y)$ are still single-valued functions and δy and δx are random delays of variables discussed.

Up to now one cannot reveal some function relation between $P(x)$ and $Q(y)$ frequencies. Hence, mentioned frequencies in a definite sense „behaviour" differently than in the case of complete independence of x and y.

Let there be two pairs of such sampling distributions $P_1(x)$, $Q_1(y)$ and $P_2(x)$, $Q_2(y)$ that $P_1(x) \neq P_2(x)$, $Q_1(y) = Q_2(y)$.

We introduce the measure of distinction between sampling distributions:

$$F_x = \int_{-\infty}^{+\infty} |P_1(x) - P_2(x)| \, dx$$

$$F_y = \int_{-\infty}^{+\infty} |Q_1(y) - Q_2(y)| \, dy \tag{6}$$

The limits of possible variation are obvious from (6):

$$0 \leqslant F \leqslant 2 \tag{7}$$

It can be shown that if there is the relation between x and y, in the order of (1) and (3) with some additional limits then

$$F_y = F_x \tag{8}$$

The equality (8) is not true for the relation of (5). Hence, if $\overline{\delta x} = \overline{\delta y} = 0$, then F_x and F_y values should be near to each other. Such a pair of samplings can be worked out from observation data of x and y that $F_x = 2$. Specifically those samplings are found for $x_0 - \Delta x \leqslant x < x_0$ and $x_0 \leqslant x < x_0 + \Delta x$, where x_0 is an arbitrary fixed value and Δx is a certain fixed difference of the variable. For x variation intervals mentioned above, it is easy to plot the corresponding frequencies $Q_1(y/x_0 - \Delta x \leqslant x < x_0)$ and $Q_2(y/x_0 \leqslant x < x_0 + \Delta x)$ and to calculate F_y for them.

When $F_y(x_0)$ is small the conformable frequencies $Q_1(y)$ and $Q_2(y)$ differ slightly and the relation between x and y is absent. When $F_y(x_0)$ is near to 2, $Q_1(y)$ and $Q_2(y)$ are greatly different and the relation between x and y may be suggested.

The mentioned above properties of frequency distribution functions of interrelated random variables have been found useful to reveal the relation between visual characteristics of earthquake record and its focal depth.

The sampling of secondary wave delays τ relative to P-wave and focal depth h of corresponding earthquake were tabulated from the Far East Seismological Bulletin data for 1955—1964. It was suggested that

the observed secondary waves should be related to a small number of wave types, being generated at the foot and on the roof of the Earth's Crust and on the boundaries in the mantle, so their delays were dependent upon the earthquake focal depth only. By the concept the dependence $\tau(h)$ for the whole set of observations is not the same and it should be in the form of (3):

$$\tau = f_i(h)$$

where different numbers of i are related to different secondary wave types.

The probable specific form of each $f_i(h)$ was defined due to physical considerations and then empiric frequency distribution function $Q(\tau)$ was approximated by (4). In detail the approach is described in (P o p l a v s k y, 1971). One of the main results is that the occurence of secondary waves, generated in the boundaries of the Upper Mantle is to be assumed specifically to explain the whole complex of τ observed. Those boundaries suggestively observed at depth of 40, 60, 90, 120 and 200 km the fact being in rather good agreement with the published data (T a r a k a n o v, L e v y, 1969).

The value of $F_y(H)$ of earthquake of $H - 30 \leqslant h < H$ km and $H \leqslant h < (H + 30)$ km were calculated for each of 46 visual characteristics of earthquake record considered in (P o p l a v s k y, P i s a r e n k o, 1971). Those describe the frequency content A/T ratios, the form of record curve and a number of its other elements in the sections of P-waves, secondary waves and in interval between them. The values of H varied within $30 \leqslant H < 120$ km with the step of $\Delta H = 10$ km. In figure 1 the plot of function $F_y(H)$ built for a predominant period in P-wave is given as an example.

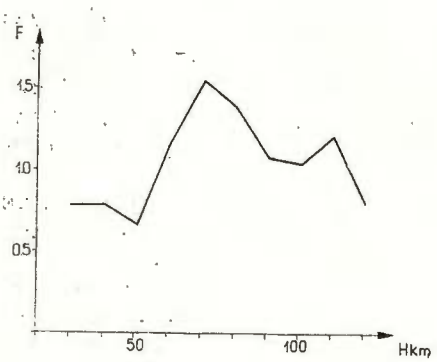

Fig. 1. — Functions $F_y(H)$ for P-wave predominant period.

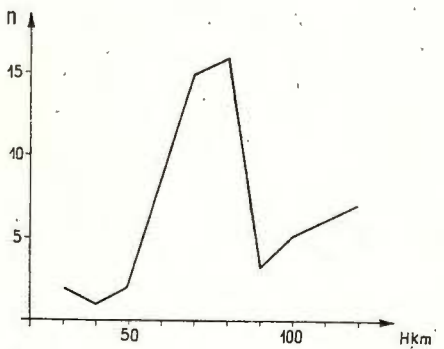

Fig. 2. — Functions $F_y(H)$ for the 46 visual caracteristics of earthquake record: H, depth; n, number of visual characteristics.

The discussing of similar plots for all 46 visual earthquakes record characteristics showed that the maximum value of $F_y(H)$ is more frequently reached for $H = 70-80$ km. This is rather clear from figure 2, where

H value is laid on the axis of abscissa and n number of visual characteristics—on that of ordinates — where $F_y(H) \geqslant 1$.

It has been found that the most „sensitive" to the depth of $H = 70-80$ km are the characteristics describing the frequency content of oscillations on the record. Thus, for instance, $F_y(H) = 1.53$, 1.49, 1.46,

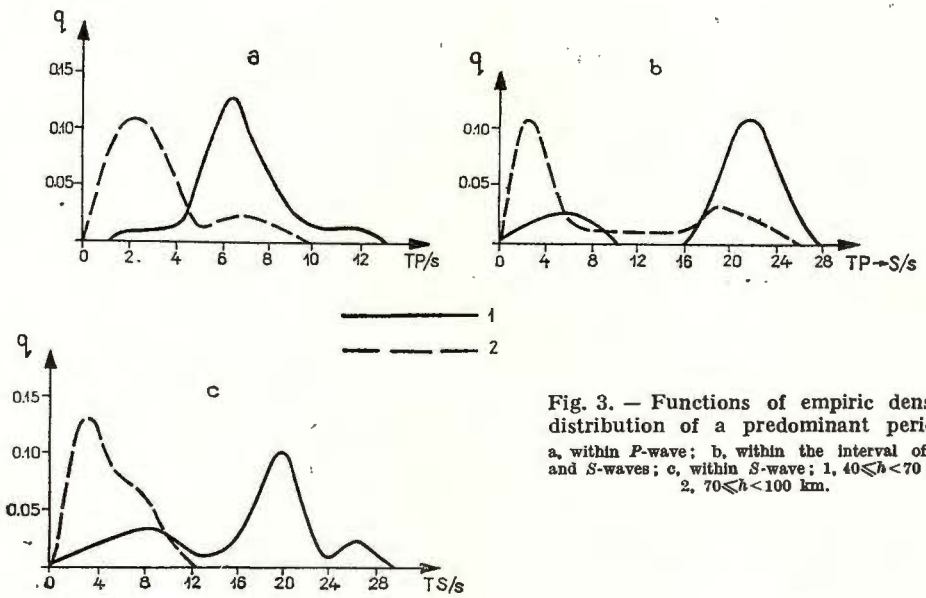

Fig. 3. — Functions of empiric density distribution of a predominant period; a, within P-wave; b, within the interval of P- and S-waves; c, within S-wave; 1, $40 \leqslant h < 70$ km; 2, $70 \leqslant h < 100$ km.

respectively for predominant periods in P, between P and S-waves and in S-waves, when $H = 70$ km. The functions of empiric density distributions of these values for earthquakes of $40 \leqslant h < 70$ km and $70 \leqslant h < 100$km are given in figure 3 a, b, c. It is shown that predominant periods over the whole record are obviously decreasing beneath 70 km (fig. 3).

The fact specifically well seen in figure 3 is worthy to be noted as well. Frequency distribution functions of predominant periods have more than one maximum or, at any rate, are rather asymmetric.

Consequently, it is impossible to reveal any variations on the period beneath the depth of $H = 70$ km, while analysing immediately the correlation of the predominant period with focal depth. This can be done by comparison of frequency distribution functions only.

Majority of other record characteristics has $F_y(H) < 1$ for every value of H.

The revealed decreasing of predominant periods in seismic waves due to depth transition of $H = 70 - 80$ km should be explained by obvious difference of physical properties of structure of layers, occurring above and beneath the depth mentioned.

While analysing the data observed sometimes it is very useful to discuss frequency distribution functions of values under question. It should be done when usual approach of statistical data treatment could not provide proper results.

The analysis of functions of empiric density distribution of secondary wave delays relative to *P*-wave allowed to reveal certain boundaries in the mantle. Those data are not completely reliable since a great number of suggestions a priori are called for obtain these, in particularly, some data on the nature of secondary waves observed.

The analysis of frequency distribution functions of some visual earthquake record characteristics allowed to reveal the physical boundary at the depth of 70—80 km.

The author acknowledge the translation of the report made by A. P. Vasilieva.

REFERENCES

Gumbel E. (1965) Statistics of the external meanings. M., Mir, Moscow.

Poplavsky A. A. (1971) Statistical investigation of secondary wave arrival times of Far East earthquakes. *Izv. AN SSSR, ser. Fiz. Zemli*, 9, Moscow.

— Pisarenko V. F. (1971) Statistical method of earthquake focal depth recognition from a single station record. *In*: Sb. Algorithms of seismic data interpretations, Nauka, Moscow.

Tarakanov R. Z., Levy N. V. (1969) A new model of the layered Upper Mantle structure of the Earth of the Kurile-Japanese region in the transition zone from the Asiatic continent to the Pacific from seismic data. *In*: Sb. Structure and development of the Earth's Crust in the Soviet Far East, Nauka, Moscow.

APERÇU SUR QUELQUES PROBLÈMES D'INTERPRÉTATION

PAR

J. C. RUEGG, ALFRED HIRN, GEORGES PERRIER[1]

Les profils sismiques réalisés en France ces dernières années posent un certain nombre de problèmes de corrélation et de méthode d'interprétation.

Les profils réalisés dans le Massif Central en 1970 ont été effectués avec un écartement entre stations très réduit (2 à 3 km) et pour un profil réalisé dans la région granitique du Millevaches (1 à 2km).

Ondes Pg

Sur ce profil Millevaches, les ondes Pg ont été observées en première arrivée jusqu'à une distance de 130 km. Les hodochrones montrent une courbure progressive et on a déterminé par la *méthode d'Herglotz-Wiechert*, la loi de vitesse des ondes *P* et *S* dans les premiers kilomètres de profondeur de la croûte (fig. 1).

Réflexions proches. L'observation de phases tardives sur de nombreux enregistrements proches des points de tir (R u e g g, H i r n, 1970) a permis de mettre en évidence un ou plusieurs réflecteurs profonds dont le plus net est le Moho (fig. 2).

De telles réflexions sont obtenues pour les ondes longitudinales *PmP* ou *P1P*, transversales (*SmS*) ou quelquefois de trajet mixte *PmS* ou *SmP*.

Réflexions au voisinage de la distance critique. Pour des distances comprises entre 60 et 100 km on observe des phases réfléchies sur le Moho (*PmP*) et des phases intermédiaires qui sont interprétées comme des réflexions intra crustales. Dans de nombreux cas on ne retrouve pas les branches réfractées correspondantes, l'énergie étant trop faible ou par manque de continuité des horizons.

[1] Institut de Physique de Globe — Tour 14. Laboratoire de Sismologie. Université de Paris 6 — 11, quai Saint-Bernard. 75230 Paris, France.

Cependant la netteté de ces phases est variable d'un profil à l'autre ou même d'un enregistrement à l'autre sur un même profil et il est quelquefois difficile de les corréler entre elles.

Cependant ces corrélations ont été améliorées par l'utilisation d'assemblages d'enregistrements filtrés passe-bande et la discrimination des arrivées sur les trois composantes par leur polarisation.

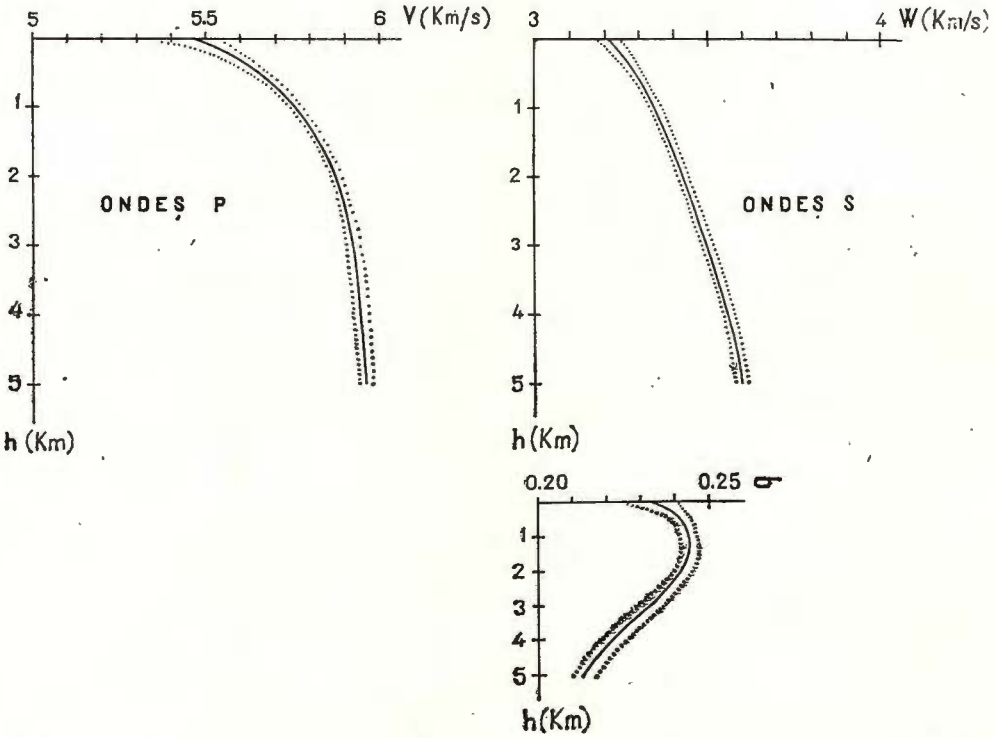

Fig. 1. — Loi de vitesse des ondes *Pg* et *Sg* dans la partie superficielle de la croûte pour la région granitique du Millevaches (Massif Central Français).

L'interprétation de ces phases intermédiaires en réflexion est obtenue par la méthode des T^2, Δ^2 qui permet de déterminer la vitesse et la profondeur moyenne du milieu surmontant la surface réfléchissante puis par restitution des points de réflexion à partir de la vitesse moyenne ainsi obtenue.

L'estimation de la vitesse sous ces discontinuités est obtenue par deux méthodes :

1) En considérant la vitesse apparente de ces phases au voisinage de leur distance critique. Cette méthode est souvent imprécise car il est quelque-fois difficile de déterminer avec certitude la distance critique. Les amplitudes observées ne correspondant pas à la distance critique théorique (C e r v e n y, 1966) cela fournit cependant une limite supérieure.

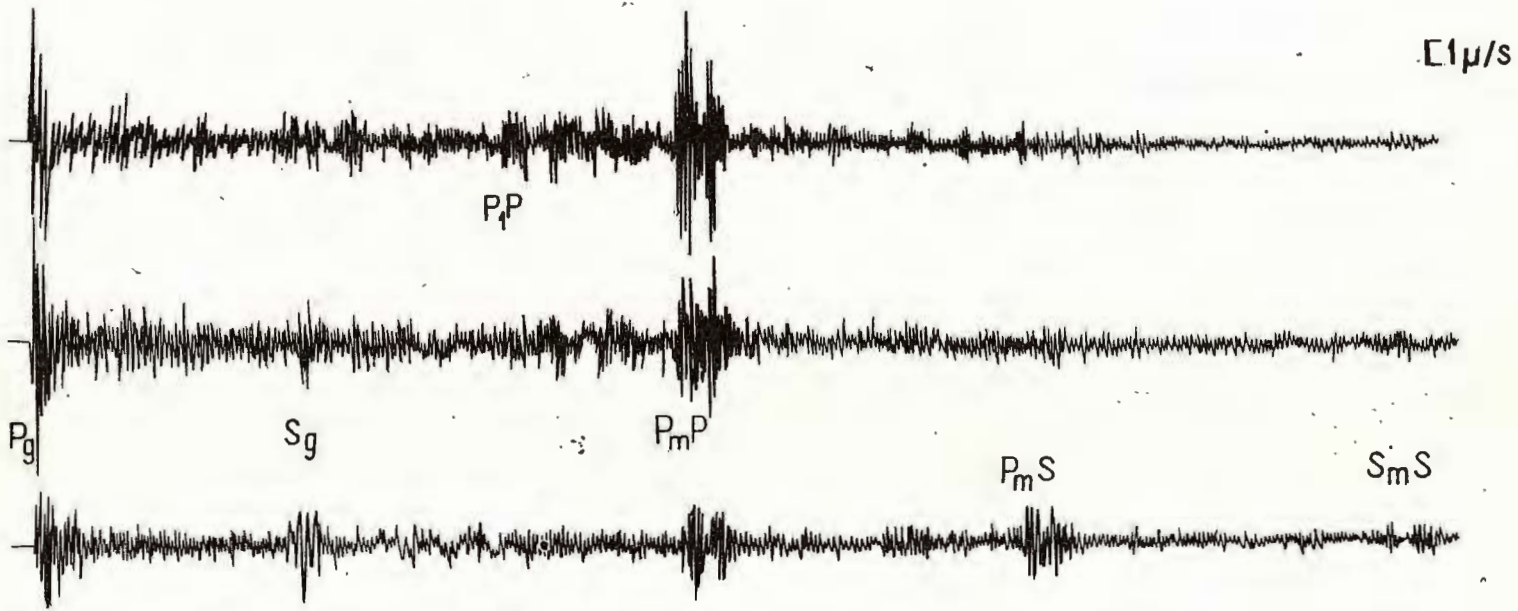

Fig. 2. — Exemple d'enregistrement à courte distance ($\Delta = 19{,}5$km) d'ondes réfléchies sur le Moho (*Pmp*) et sur une discontinuité intermédiaire (P1P) Profil Millevaches. Tir de Bagnac (400 kg).

2) Epluchage des couches supérieures. A partir des hodochrones (Δ, T) des ondes réfléchies à la base du milieu dans lequel on veut déterminer la vitesse moyenne, ou retrancher les temps et distances correspondant aux trajets du rai sismique dans les couches qui le surmontent.

On obtient ainsi un nouvel ensemble de valeur (Δ', T') auquel on applique la méthode des T^2, Δ^2.

A partir de 100 à 120 km les hodochrones des différentes phases intermédiaires et des réflexions sur le Moho interfèrent et il est difficile de préciser avec certitude la nature de ces phases et de corréler entre elles les différentes arrivées d'énergie.

Au-delà de 150 km on observe des phases énergiques de vitesse apparente voisine de 6 km/s qui sont quelquefois interprétées comme des ondes *PmP* réfléchies sur le Moho. Ceci est en contradiction avec l'existence de milieux intermédiaires de vitesse supérieure à 6 km/s, car la vitesse apparente d'une telle phase réfléchie sur le Moho devrait être celle du milieu surmontant immédiatement le Moho. Il s'agit plus vraisemblablement d'une onde réfléchie à grande incidence ou d'une onde guidée dans la partie supérieure de la croûte (H o l d e r, B o t t, 1971).

A partir des données de la réflexion au voisinage du critique et de la réfraction on a néanmoins essayé de construire un modèle de croûte rendant compte des hodochrones observés.

Un premier modèle MO3 a été construit avec des accroissements de vitesse correspondants aux différentes couches trouvées (fig. 3).

Un tel modèle rend bien compte des hodochrones observés, cependant les distances critiques calculées ne correspondent pas aux grandes amplitudes observées, mais sont repoussées à trop grande distance par rapport à celle-ci.

Pour diminuer les distances critiques correspondant aux différentes phases il a fallu augmenter le contraste de vitesse aux différentes discontinuités, ce qui impose, si l'on veut respecter les valeurs observées de vitesse d'introduire un modèle de type MO7 (fig. 4).

Un tel modèle respecte assez bien les rapports d'énergie des différentes phases. Cependant les branches lointaines réfractées sous les discontinuités intermédiaires ne sont pas observées et l'énergie de la grande phase au-delà de 150 km est un peu faible par rapport aux valeurs observées.

On doit remarquer qu'un tel modèle comprenant des couches à plus grande vitesse n'est pas du tout improbable du point de vue géologique, car il existe en bien des endroits dans le monde des intrusions de gabbro ou de roche de plus grande densité à l'intérieur de massifs granitiques dont les dimensions atteignent plusieurs dizaines de kilomètres.

Cependant le calcul d'un modèle par la théorie des rais ne donne qu'un système d'hodochrone et ne permet pas un choix entre les différents modèles possibles. Un tel choix peut être fait par le calcul d'assemblages de sismogrammes synthètiques et la comparaison entre les amplitudes théoriques et celles réellement enregistrées.

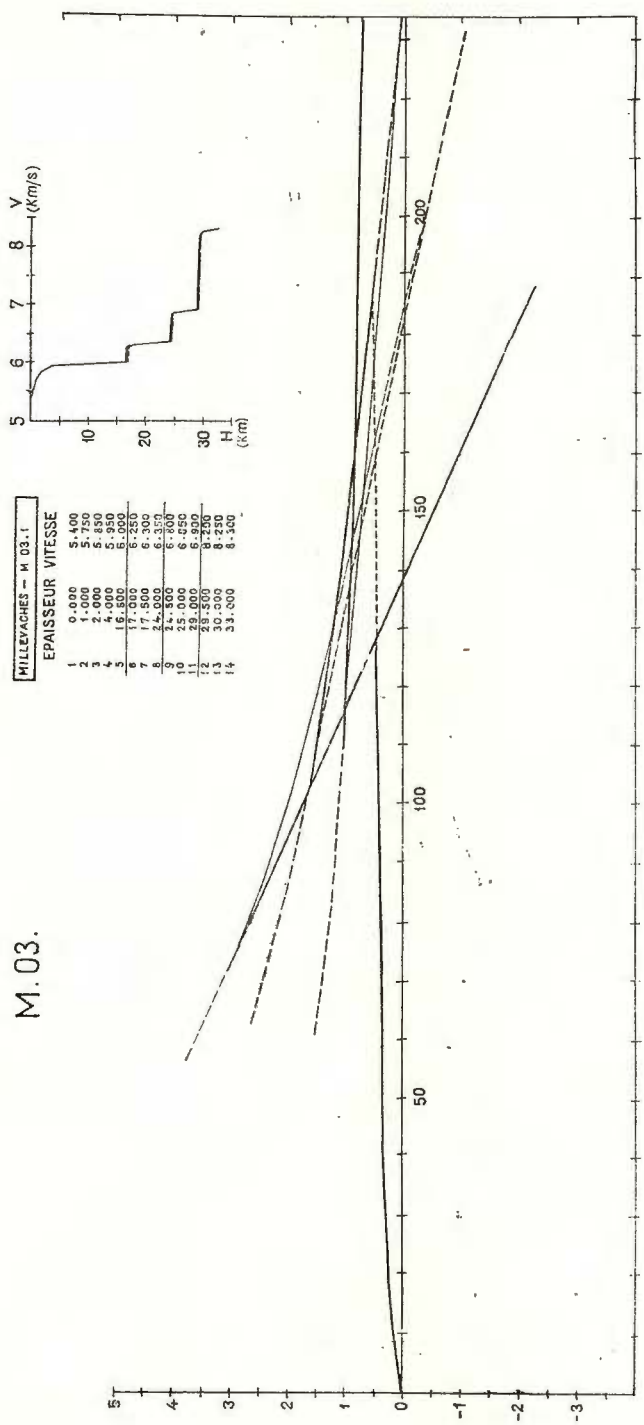

Fig. 3. — Modèle M03 de loi de vitesse en fonction de la profondeur. Profil Millevaches.

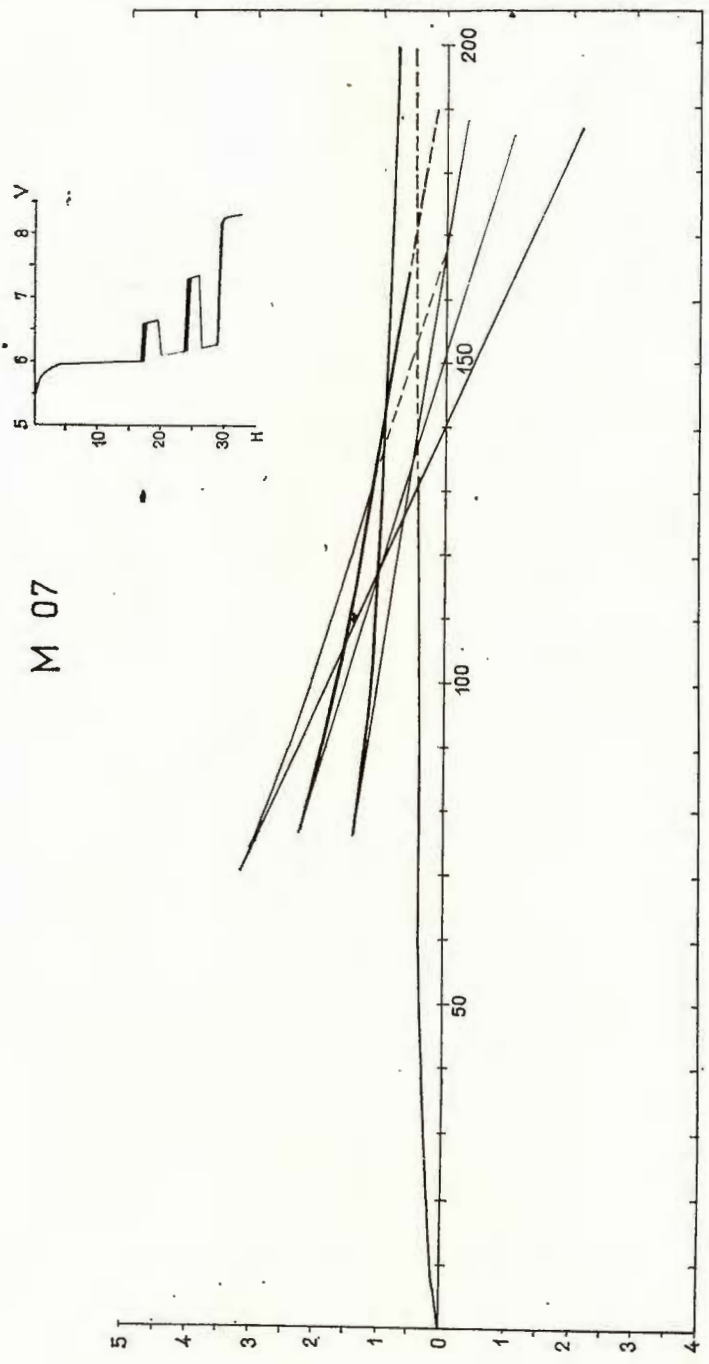

Fig. 4. — Modèle MO7 de loi de vitesse en fonction de la profondeur. Comparaison avec les hodochrrones observées.

D'autre part, des modèles tels que MO3 ou MO7 ne peuvent représenter qu'une approximation grossière de la loi de vitesse en fonction de la profondeur car il paraît probable d'après les coupes obtenues par réflexion que les discontinuités intermédiaires sont soumises à des variations latérales importantes et ne présentent pas une continuité suffisante pour que l'on puisse considérer que la croûte présente la même structure tout le long d'un même profil et qu'un modèle stratifié horizontalement puisse représenter correctement la structure fine de la croûte.

Remarque concernant l'existence ou la non existence de couches à faible vitesse dans la partie supérieure de la croûte :

Dans les profils effectués en France et plus particulièrement dans le Massif Central, on ne peut trouver que peu d'arguments pour prouver l'existence d'une couche à faible vitesse.

En effet, la vitesse moyenne dans la partie supérieure de la croûte est de l'ordre de 6 km/s et d'autre part on peut remarquer que sur la plupart des profils la tranche réfléchie à grande distance n'est pas décalée par rapport au prolongement des ondes *Pg*.

BIBLIOGRAPHIE

Cerveny V. (1966) On dynamic properties of Reflected and Head waves in the *n*-layered earth's crust. *Geophys. J. R. Astr., Soc.*, 11, London.

Holder A. P., Bott M. H. P. (1971) Crustal structure in the Vicinity of South West England. *Geophys. J. R. Astr. Soc.*, 23, 5, London.

Ruegg J. C., Hirn A. (1971) Reflexions sismiques profondes observées à courte distance dans le Sud du Massif Central. *C.R.A.S.*, 272, Paris.

SOUNDING OF THE MANTLE AND THE CORE BY THE CONJUGATE POINTS METHOD

BY

L. P. VINNIK, A. A. GODZIKOVSKAYA [1]

In this communication we present a new method and discuss some results of measurement of the specific quality factor Q for short-period P wave in the Mantle and in the Core. We are interested in the absolute values of Q, dependence of Q on frequency, its lateral variations.

The idea of the method is following. Let us imagine 3 points along the great circle at the Globe. Point B is located at the halfway between A and C. There are seismic sources around A and seismograph stations around B and C. Seismic wave P is recorded at the point B, reflected from the surface of the Earth in the vicinity of this point, retransmitted into the mantle and recorded at the point C as PP. Points B and C are located at the ends of one and the same seismic ray. We call them seismic conjugate points. The term is borrowed from the theory of geomagnetic field where it means almost the same. Our method consists in direct measurement of the amplitude decay of the various frequency components of the wave between the conjugate points.

Advantages of the method are following.

a) Measurements are made along one and the same ray. Ignorance of source radiation patterns does not affect results of measurement.

b) It can be shown that the ratio of spectra in conjugate points is described by the formulae:

$$\ln \frac{S_c(f)}{S_B(f)} = \ln \frac{K}{2\sqrt{\cos \Delta}} - \pi f \int_B^C \frac{dt}{Q}.$$

$S_c(f)$is spectrum in the second conjugate point, $S_B(f)$ — spectrum in the first conjugate point, f — frequency in cps, k —Earth's surface reflection coefficient, Δ — distance between conjugate points, t — travel time along the ray. It is evident that amplitude attenuation due to geo-

[1] O. Yu. Schmitt Institute of Physics of the Earth, Academy of Sciences of the USSR, B. Grouzinskaya 10, Moscow 123810, USSR.

metrical spreading of wave front does not depend on the velocity distribution in the Earth.

c) Without absorption amplitude of PP in the point C is only two times less than the amplitude of P in the point B. It is important advantage since the dynamic range of a photopaper seismogram is limited.

d) Next advantage of our method lies in the fact that it works without any assumption about dependence (or independence) of Q on f. Attenuation of each harmonic can be measured separately from all others.

e) Measurements in our method correspond to the definite path in the mantle, and the study of lateral variations of Q is possible. Effects of small scale inhomogeneities in the crust and upper mantle can be diminished if a number of stations and a number of events are used.

For obvious reasons the data for one and the same pair of conjugate points are scattered. Smoothing of data is essential step in our method. As a rule PP is among the late arrivals on a seismogram and its record may be disturbed to some extent by the preceding noise. Various frequency components of the signal may be weaker or stronger than the noise. Many experimenters in this situation just omit observations with the low signal to noise ratio. Such practice may result in wrong conclusions. In our method all data are treated independently of signal to noise ratio. Mean value of the logarithm of the amplitude ($\ln\beta$) corresponds to the maximum of the modified function of likelihood:

$$L(\mu,\sigma) = -\sum_{i=1}^{N} \frac{(\ln\beta_i - \mu)^2}{2\sigma^2} - N\ln\sigma + \sum_{j=1}^{M} \ln\left[1 + \Phi\left(\frac{\ln\alpha_j - \mu}{\sqrt{2}\sigma}\right)\right] + C$$

μ is mean value of the $\ln\beta$, σ^2 — variance of the $\ln\beta$, β_i — values of β exceeding ambient noise, α_j — upper limits of β masked by the noise, $\Phi(X) = \frac{2}{\sqrt{\pi}}\int_0^x e^{-t^2}\,dt$, C — constant quantity. Relevant theory is published recently (Vinnik, Dashkov 1970).

Figure 1 shows the position of conjugate points in our experiment. The distance between conjugate points in each pair is about 55 degrees. Seismic ray corresponding to this distance penetrates into the mantle to the depth of 1400 km. PP is observed at the distance around 110 degrees in the shadow zone of P. In each pair we make use of a few events recorded at a few seismograph stations. Records of shortperiod vertical component seismograph are used as a rule.

Figure 2 shows examples of spectral ratios in conjugate points corrected for geometrical spreading and for coefficient of reflection from the surface of the Earth. Equal values of the parameter $H = \frac{dt}{Q}$ are shown by dotted lines. The least value of H which is close to 0,5 is observed for the path between the South Kazakhstan and the Iberian peninsula. Almost the same estimate of H is obtained for the path from North Canada to Siberia. Some deviations from this value in Siberia will

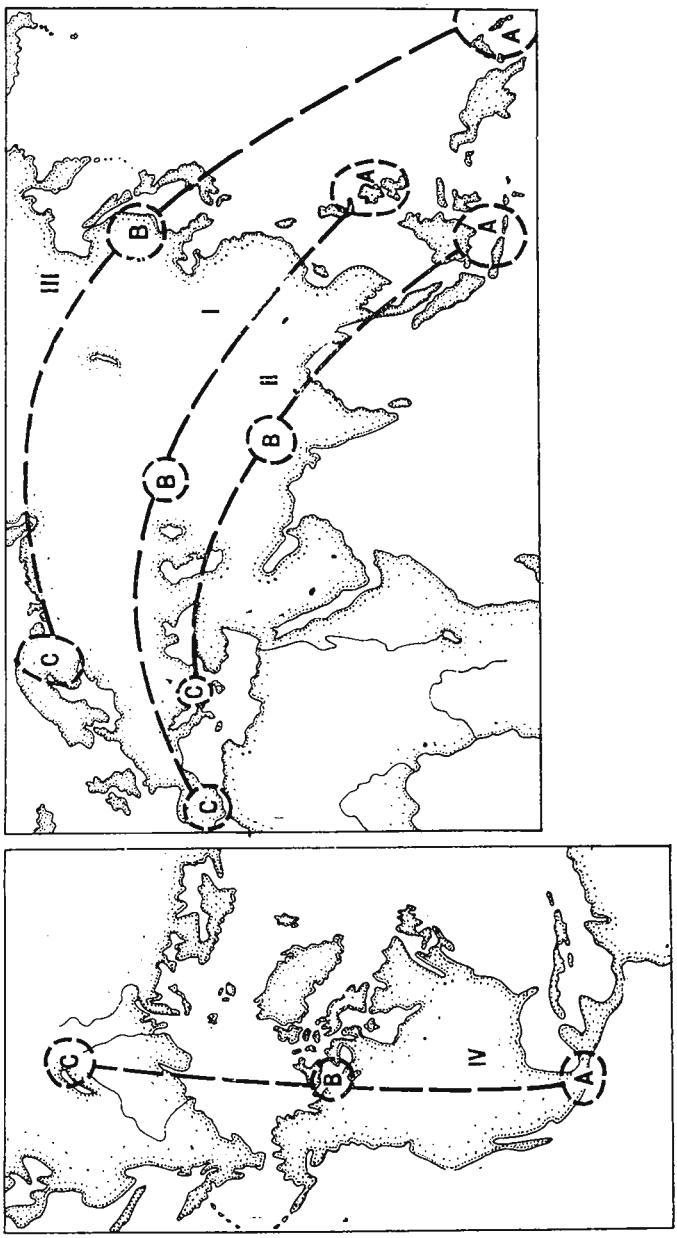

Fig. 1. — Position of conjugate points :
A, source region ; B and C, conjugate points.

be discussed separately. The strongest absorption and the highest value of H is observed for the path between the Far East and Baltic Shield. In this case almost certainly anomaly lies in the upper mantle of the Far East.

Now we may consider the most obscure problem of dependence of Q on frequency. We assume that the values of H between 0,4 — 0,7 are

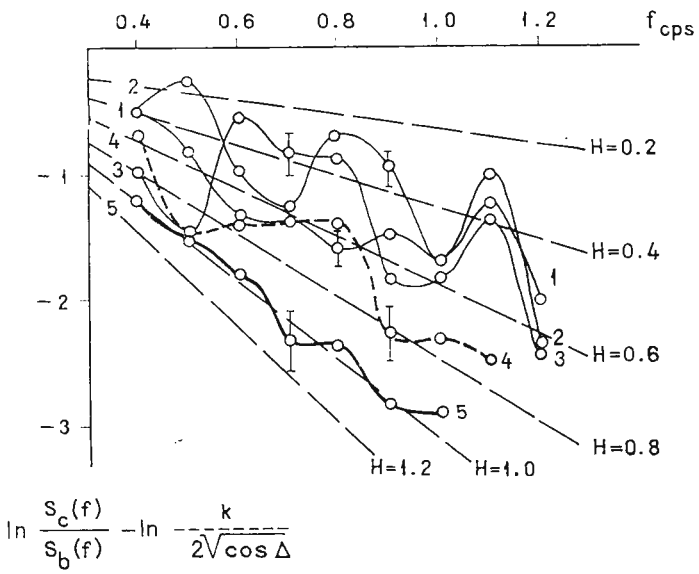

Fig. 2. — Examples of spectral ratio in conjugate points corrected for the geometrical spreading and for Earth's surface reflection coefficient:

1—3, spectral ratios for the path I; 4, averaged spectral ratio for the path II; 5, averaged spectral ratio for the path III.

representative for the stable tectonic regions in the frequency range around 1 cps. At the same time one may suggest that the most part of the Earth's surface is covered by the stable regions. One may answer the question about dependence of Q on frequency by means of comparison between our data for short-period P waves in the stable tectonic regions and world-average data for long-period surface waves. Such comparison reveals that mean value of Q in the mantle of stable tectonic regions practically does not depend on frequency in the period range from 1 s to 200 — 300 s. Mean value of Q for the upper 300 km of the mantle of stable tectonic regions is close to 400.

An interesting anomaly of absorption is found in South Siberia under the lake Baikal. Figure 3 shows the system of geophysical observations in this region. Records of PP approaching from North-East to 3 western stations are almost identical. Records of station 4 is completely different. Figure 4 shows spectra of PP at the station 4, average spectrum of 3 other stations and the spectrum of station 3, neighbouring to 4. Spec-

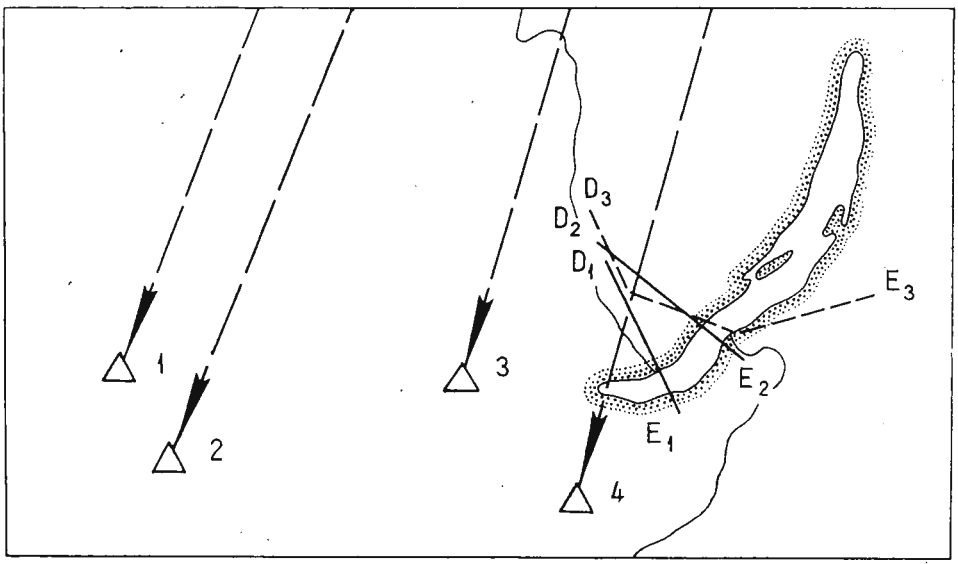

Fig. 3. — Geophysical observations in the Baikal rift area :

Δ, seismograph stations; D_1E_1, heat flow profile (Lubimova et al.); D_2E_2, magneto-telluric profile (Kosygin et al.); D_3E_3, DSS profile (Krylov et al.).

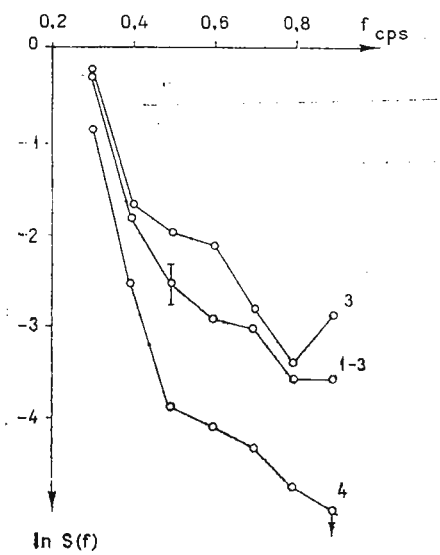

Fig. 4. — *PP* spectra :

3, spectrum at the station 3; 1–3, averaged spectrum at the stations 1, 2, 3; 4, spectrum at the station 4.

trum of station 4 is strongly devoid of high frequencies due to high absorption. Mean value of Q in the upper 300 km of the mantle under the Baikal is close to 80 or 5 times less than in the normal mantle.

Figure 5 shows various geophysical fields along the profiles crossing the Baikal. All of them suddenly change over the lake. Another pronoun-

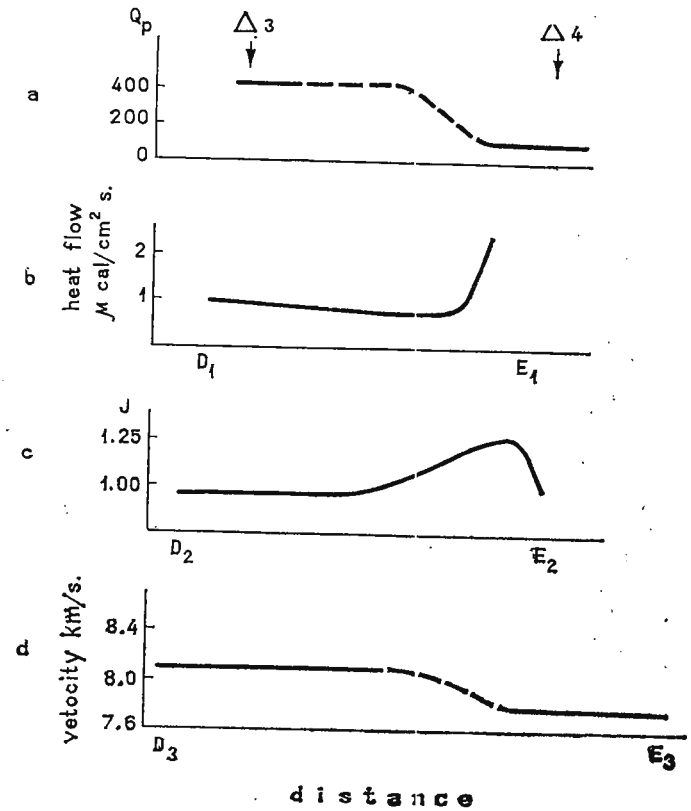

Fig. 5. — A comparison between geophysical fields: a, average Q for the upper300 km of the mantle; b, heat flow; c, magneto-telluric curve; boundary velocity at Moho.

ced anomaly is found at the Far East in the tranzition zone between Asia and the Pacific. Value of Q in the upper mantle of this region is equal to that under the Baikal. Other geophysical fields behave differently. Boundary velocity at Moho is normal, heat flow on the continent is close to its normal value. Apparently anomalous piece of the mantle is located deeper and related to the tectonic process responsible for the deep earthquakes.

Recently we applied our method of analysis to the waves PKP and $PKPPKP$. Principal result of this study is surprisingly low Q (about

300) in the inner core. No dependence of Q on frequency is found. It is decisive evidence for the solid state of the inner core.

Recently american seismologists claimed detection of short-period wave crossing inner core as shear wave, V_s being close to 3 km/s (J u l i a n et al., 1972). It follows from our data that if the mechanism of attenuation in the inner core is like that in the upper mantle, Q_s in the inner core should be 30 — 60. Such small value of Q leaves no hope for the detection of short-period shear waves in the inner core.

Another interesting result of our study is the detection of strong and unexplained arrivals preceding *PKPPKP* by 25 — 50 s in the distance range 30^0 — 50^0.

It is our pleasant duty to express the most sincere gratitude to the persons who greatly assisted to our research providing their seismograms. We would like to mention Drs. V. G a i s k y, G. B u g a e v s k y, K. P l e s k a c h of Soviet Union, Dr. K h a d z i e v s k y of Jugoslavia, Dr. L u o s t o of Finland, Mr. R. J. H a l l i d a y, of Canada, Prof. N. V l a a r of Holland.

REFERENCES

J u l i a n B. R., D a v i e s D., S h e p p a r d R. M. (1972) Evidence for 2,95 km^{-1} shear velocity in inner core. *Nature*, 235, 5337, London.

V i n n i k L. P., D a s h k o v G. G. (1970) Volna *PcP* pri atomnich vzrivach i charakter granizi jadro-mantija. *Fiz. Zemli*, 1, Moskva.

REGIONAL RESULTS

ON THE CRUSTAL STRUCTURE IN CZECHOSLOVAKIA AND THE EAST-ALPINE REGION

BY

BŘETISLAV BERÁNEK[1], ALOIS ZÁTOPEK [2]

INTRODUCTION

The present communication is intended as a review of results obtained by deep seismic soundings (DSS), carried out on the territory of Czechoslovakia and neighbouring countries in the framework of the international DSS project in East and South Europe. These results have been combined with the results obtained by the study of quarry blasts and other independent geophysical evidence based on gravimetrical, geomagnetical, seismological and other studies, including some geological analysis.

The said project of the DSS has been performed in close cooperation of three international bodies, interested in geophysical investigations in this part of Europe, i. e. the Geophysical Commission of the Carpatho-Balkanic Geological Association, the Commission of Academies for Planetary Geophysics, and the European Seismological Commission. The measurements have been conducted, apart from national profiles, in a network of international profiles I — XII as reported several times at the previous meetings of the ESC and other bodies. This network is shown in figure 1.

In our report we present only a few relevant data on the position of the Mohorovičić discontinuity (Moho) in the whole region for a general orientation; the main subject to be referred to is related to the measurements which have been performed on international profiles VI, V and VII, partly in cooperation with colleagues in the German Democratic Republic (profile VI), Hungary (VI and V), Poland (V and VII) and the German Federal Republic (VII and VIIa).

[1] Institute of Applied Geophysics, Ječná 29, Brno-Řečkovice, Czechoslovakia.
[2] Institute of Geophysics, Charles University, Ke Karlovu 3, Praha 2, Czechoslovakia.

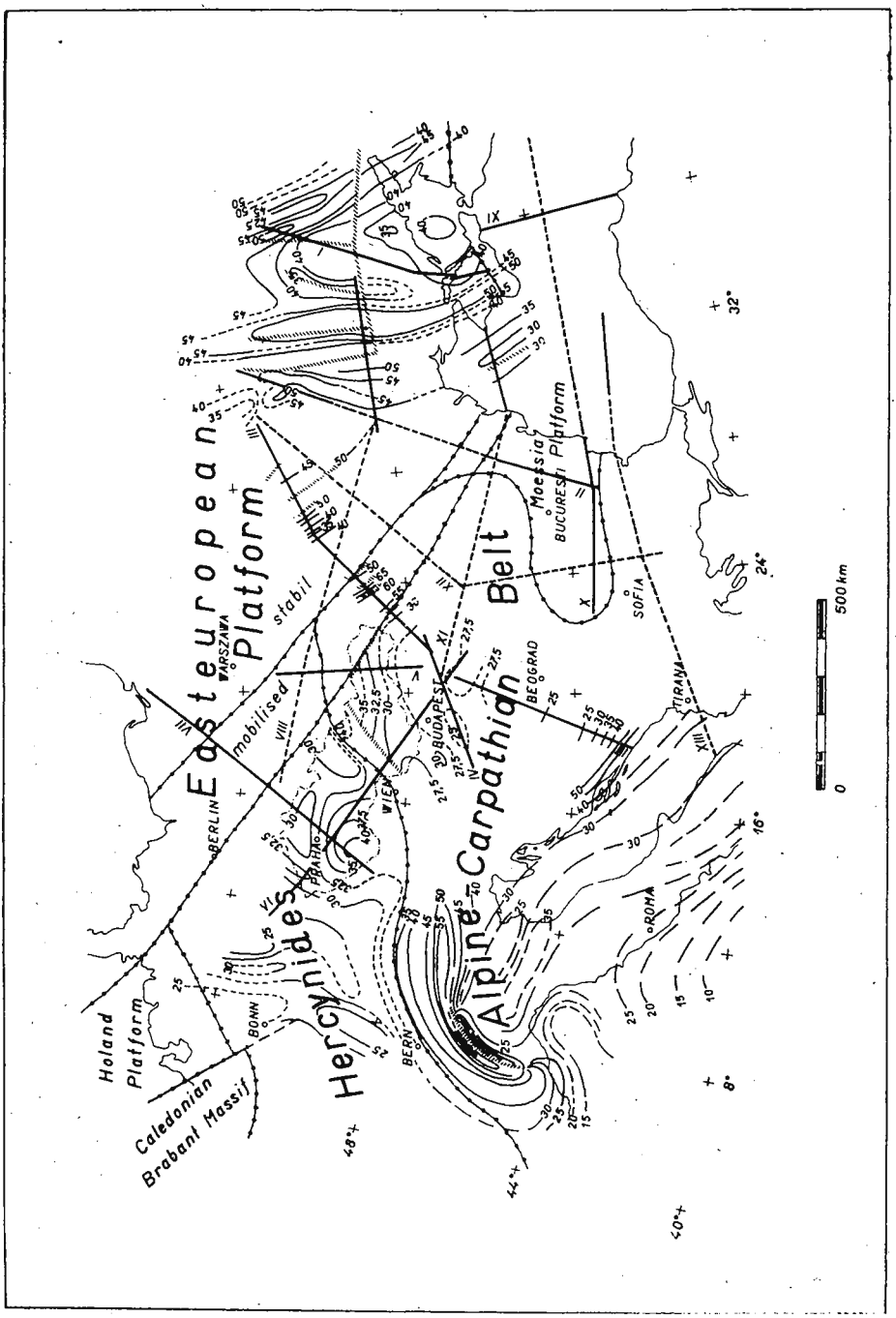

Fig. 1. — International profiles I—XII in the region of the Carpathians and Balkans, and the course of the Moho.

The geophysical synthesis that we are giving here should not represent a final stage of the research, but rather a door-opening attempt to find the way to a progress in the solution of the intricate structure of the Earth's crust in this part of Central Europe, which is, in our opinion, one of the key problems of the European tectonics. It involves the border zones of the Bohemian Massif with the adjacent units of Saxony-Thüringen, the West Carpathians, the Eastern Alps, and the Pannonian Basin with its extremities. We want also to try to amalgamate the results gained for the broader region of the Carpathians, the Pannonian Basin, the Balkans and the eastern Variscian features with our findings.

DESCRIPTION OF THE METHOD AND RESULTS OBTAINED

GENERAL

A method of continuous profiling has been applied on the 12 profiles as plotted in figure 1. The position of the Moho could be followed by the aid of the P^M waves, reflected at the Moho near and behind the critical point. A suitable density of shot-points with a corresponding choice of epicentral distances have enabled us to find the depths of various strata of the crust, including the Moho, and, moreover, to assess the position and properties of deep fault zones. The distance range for the registration of the first onsets of head waved *Pn* connected with the Moho was, according to its depth, about 130 up to 200 km; that for P^M waves 60 to 80 km. Waves reflected or refracted from the Conrad discontinuity could be found only in some sections of the profiles. A number of other reflected and/or refracted waves may be used for detailed investigations. On the whole, the method yields the velocity-depth pattern for individual waves, the location of the discontinuities in the crust, including the Moho, and the determination of the position and some properties of deep fault zones. The respective data have been published in a monograph which was presented at the XVth IUGG General Assembly, Moscow, 1971 (B e r á n e k et al., 1971).

Just for orientation we remark that the maximum thickness of the crust was found to be about 65 km in the elbow of the Carpathians, and in the flysch zone of the Outer Carpathians on profille III (S o l l o g u b et al., 1971). Thicknesses over or round 40 km have been found in the zone of the Precambrian metamorphic features in the Ukrainian Shield and also in the Moldanubicum of the Bohemian Massif. As the deep fault zones are concerned the most important appears the geologically known line of the peri-Pieninian lineament separating in its western part the Outer and Central Carpathians; it may be observed in a length of about 600 km and is distinguished by its higher seismic activity.

PROFILES VI, V, VII AND VIIa. CHARACTERISTICS AND RESULTS

The profiles VI, V and VII have been preliminarily suggested at the ESC General Assembly in Alicante, 1959; in the southern part of profile VII a supplementary profile was added (fig. 2). Their brief characteristics are as follows:

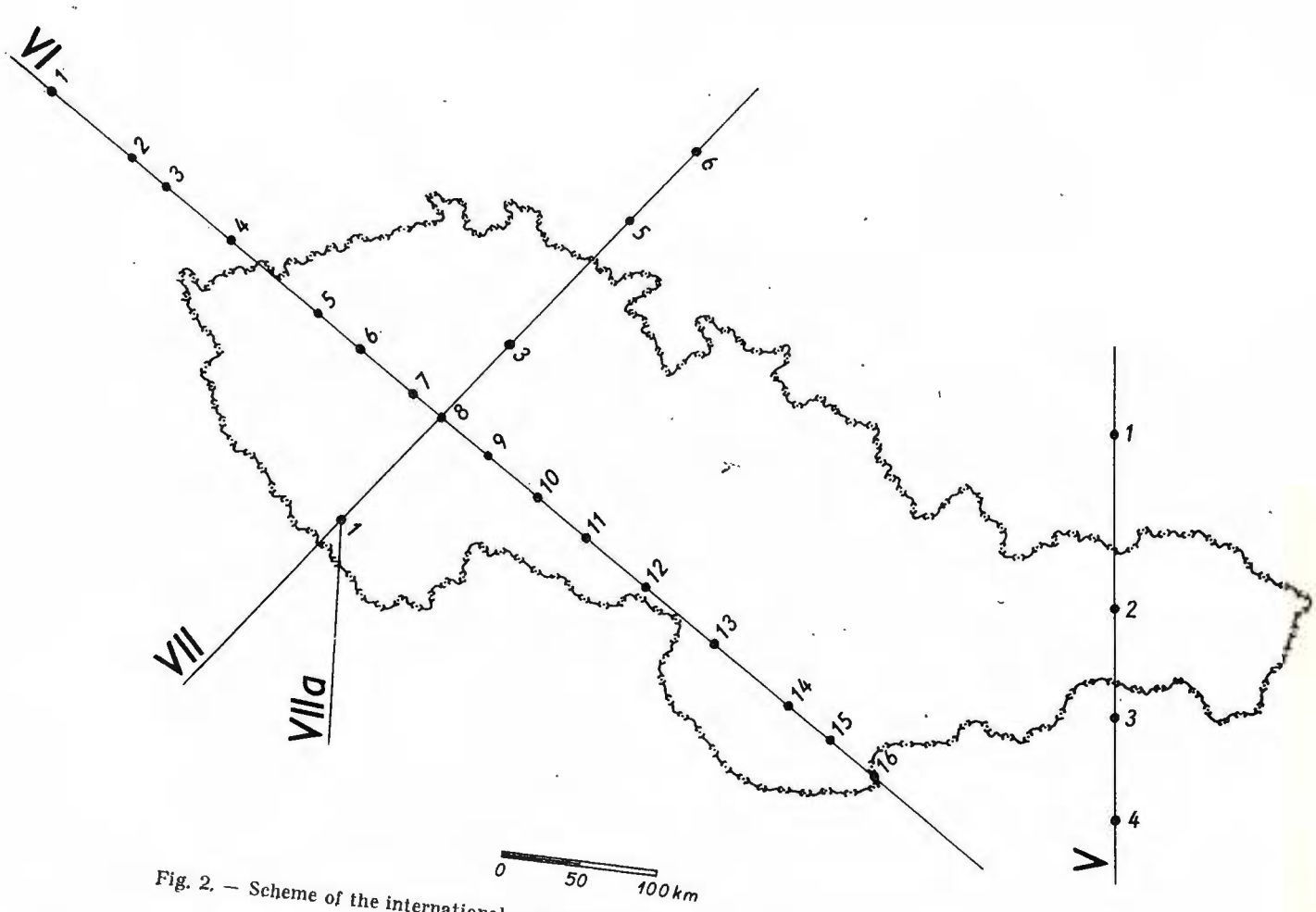

Fig. 2. — Scheme of the international profiles V, VI, VII and VIIa with shot-points indicated.

Profile VI :

It begins near Gera (GDR) and runs throughout Czechoslovakia in a length of about 500 km in the direction NW-SE (line Jáchymov-Stúrovo) and continues in Hungary in the direction toward Szolnok. It crosses the fault system of the Erzgebirge, passes through the Teplà-Barrandian region and enters the Moldanubicum, the most extensive unit of the Bohemian Massif ; then it proceeds over the Carpathian foredeep into the Carpathian system, and, finally, the Pannonian Basin. From both geological and geophysical points of view it is the most important of our profiles.

Profile V:

Running N-S from Poland over Czechoslovakia to Hungary, it starts south of Warsaw on the Russian platform, crosses the region of Caledonides and Hercynides, enters the Outer Carpathians, traverses the inner zone of cliffs into the Central Carpathian features, and, having passed the volcanic belt in North Hungary it ends in the Pannonian Basin at the cross-section of the Hungarian profiles. Its length on the Czechoslovak territory is about 90 km.

Profile VII (and VIIa) :

It starts in the western part of the Russian platform near Gdansk, passes the Polish Palaeozoic platform, crosses the Sudetes at the frontier of Czechoslovakia, then it runs through the Cretaceous Table of NE-Bohemia and proceeds through the Bohemian pluton and the Moldanubicum into the Bavarian Molasse zone and ends in the North Calcareous Alps. From the shot-point Vimperk in South Bohemia, an additional profile called VIIa was attached running southwards through the Austrian Molasse into the Austrian North Calcareous Alps. The length of profile VII in Bohemia is about 250 km.

The seismic sections along the profiles VI, V, VII, respectively, are given in figure 3.

The position of deep fault zones has been determined from the kinematic and dynamic anomalies in the pattern of the waves used (especially, anomalous variations of mean velocities proved very efficient) and the geometry of seismic discontinuities. The most important fault zone already mentioned, the peri-Pieninian lineament (PL) was well assessed on profiles VI and V. Its northern branch separates the Carpathians from the East European Palaeozoic platform ; its western branch seems to play a similar role at the contact of the Bohemian Massif with the Carpathians. A further marked deep fault zone at the contact of the named two units is the so called Lednice-zone, running almost parallelly west of the former. Inside the Bohemian Massif six distinguished fault zones may be stated very clearly. Among them the Labe (Elbe)-line, the Erzgebirge-zone, Lusatian-zone, further two zones in Central Bohemia, and the so-called Přibyslav-zone are known from surface geology, but their deep character has been experimentally proved. Many of them are in a fairly good correspondence with the Z á t o p e k's zones of increased mobility (Z á-

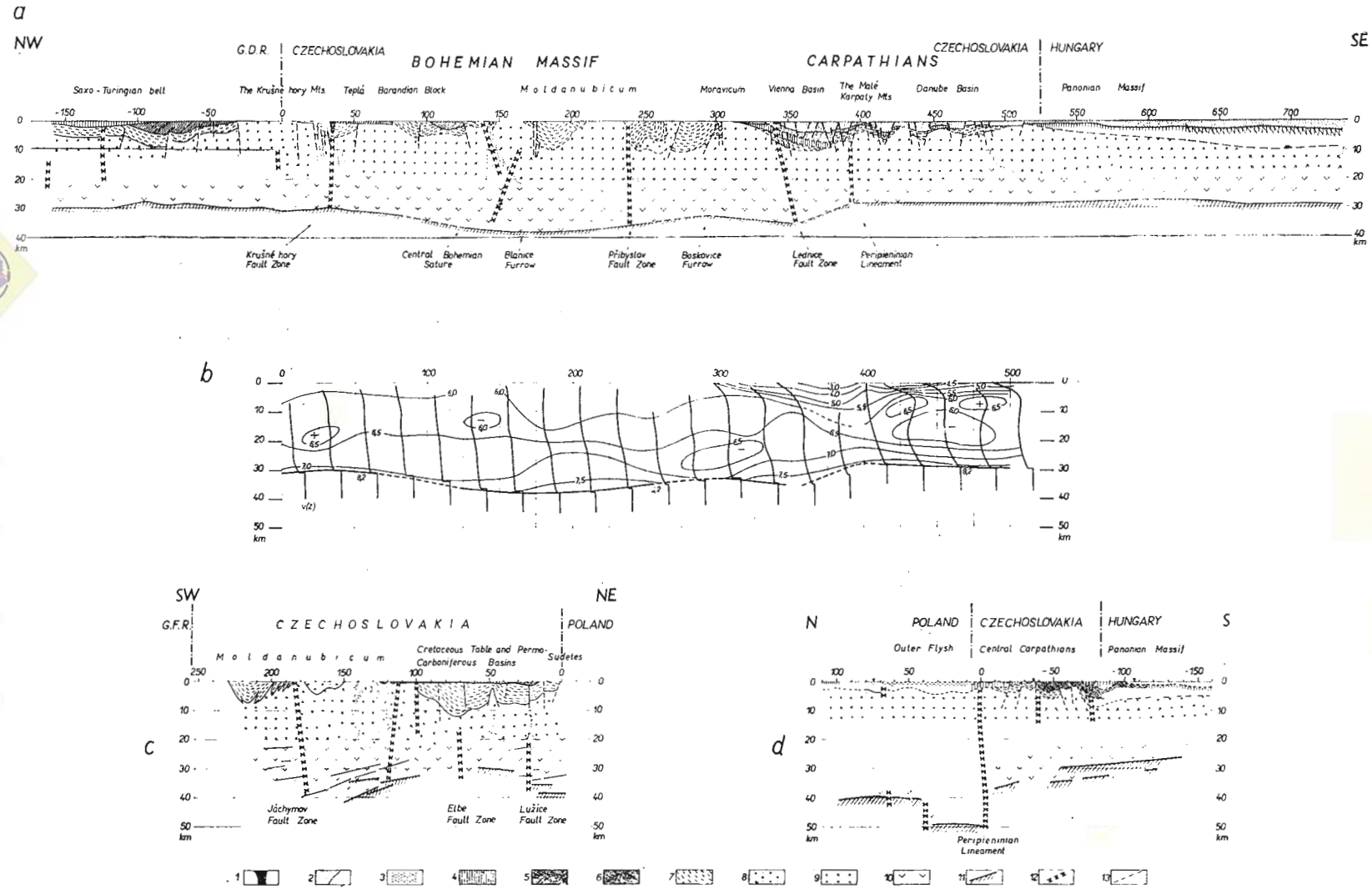

Fig. 3. — Cross-sections along the profiles V, VI, VII: *a*) Profile VI; *b*) Course of layer velocities on profile VI; *c*) Profile VII; *d*) Profile V.

1, neovolcanics; 2, Neogene sediments; 3, flysch belt; 4, Mesozoic; 5, Palaeozoic (Bohemian Massif; 6), Palaeozoic; (Carpathians); 7, crystalline schists; 8, durbachites; 9, granite zone; 10, basalt zone; 11, M-discontinuity (Moho); 12, deep faults, principal regional faults, Geological interpretation by B. Beránek, A. Dudek, J. Chaloupsky, E. Kadlec, M. Suk, J. Weiss, 1970.

t o p e k , 1948), derived from the propagation of the East-Alpine earthquakes, originated at the Vienna thermal line, northwards through the Bohemian Massif and in the westernmost part of the West Carpathians. Z á t o p e k interpreted the mobile zones as an indication of the deep boundaries in the fundamental block structure of the Bohemian Massif.

On the basis of measurements on the named three profiles and with respect to the map of regional Bouguer anomalies a structural scheme of the Moho was compiled as given in figure 4.

In comparison with its adjacent structural units like the Saxony-Thüringen system in NW and the Pannonian block in SE, the Bohemian Massif appears as a deeply plunged unit of the Earth's crust [3] (B e r á n e k, D u d e k , 1972). Near the crossing point of the profiles VI and VII, respectively, the crustal thickness in the Moldanubian increases up to 42 km ; it decreases toward NE to some 30 km below the Cretaceous Table of NE-Bohemia. There are no marked indications of mountain roots below the Erzgebirge ; however, well developed roots seem to exist in the basement of the Sudetes, mainly in the area of the Krkonoše (Giant Mountains).

At the eastern boundary of the Moldanubicum there is a striking elevation or crest of the Moho extending northwards to the Sudetes where we meet a relatively livid seismic activity (fig. 5).

The transition zone between the Bohemian Massif and the Carpathians characterized by the peri-Pieninian lineament and the Lednice zone possesses, apart from being a deep fault zone, a further particularity. It is an elevation of the Moho at the eastern boundary of the Moldanubicum. One observes gravimetric and magnetic anomalies in this region as plotted in figure 6, the regional Bouguer anomaly being denoted by Δg, and that of the geomagnetic total intensity T by ΔT. The Lednice zone exhibits a marked positive SW-NE magnetic anomaly, caused obviously by the elevation of basic eruptive rocks, lying west of the axis of an elongated gravimetric minimum, situated just in the zone of the maximum horizontal gravity gradient. The Lednice zone must be closely related to three systems of shallower dislocations discovered by oil prospectors. A similar observation was made in the Vienna basin, too. The elevation just mentioned is characterized by the presence of high velocities at smaller depths, caused obviously by basic rocks of the Bohemian Massif, which have been shifted towards the Carpathians. The phenomenon resembles the Ivrea anomaly in the West Alps, but occurs at a depth of 10 — 15km. A strip of positive gravity anomalies, parallel to the Carpathian mountain range together with the magnetic anomalies is typical for this part of the peri-Pieninian zone.

With respect to the tectonic development of the Carpathians the cross-section of profile VI, passing at the northern edge of the Vienna basin, with the Carpathians is not very representative. The Vienna basin

[3] B e r á n e k B., D u d e k, A. The contribution of deep seismic sounding to the study of deep fault tectonics. 1972. Presented at the International Geological Congress, Montreal, Canada.

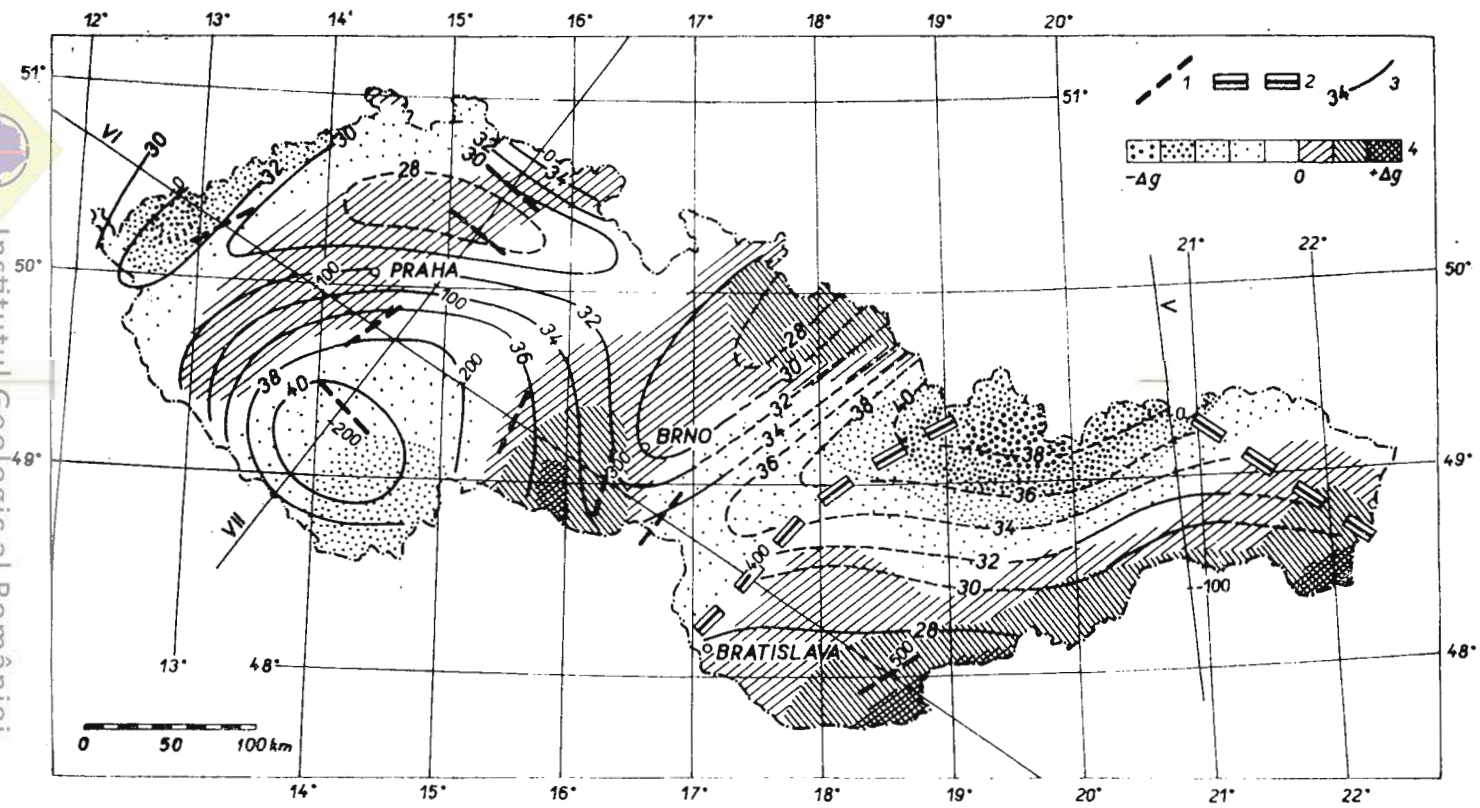

Fig. 4. — Scheme of the M-discontinuity on the Czechoslovak territory (after B e r á n e k, D u d e k, 1971) and regional Bouguer anomalies (M. B l i z k o v s k ý et al.).

1, deep faults on the international profiles; 2, peri-Pieninian lineament; 3, isohypses of the Moho; 4, regional Bouguer anomalies.

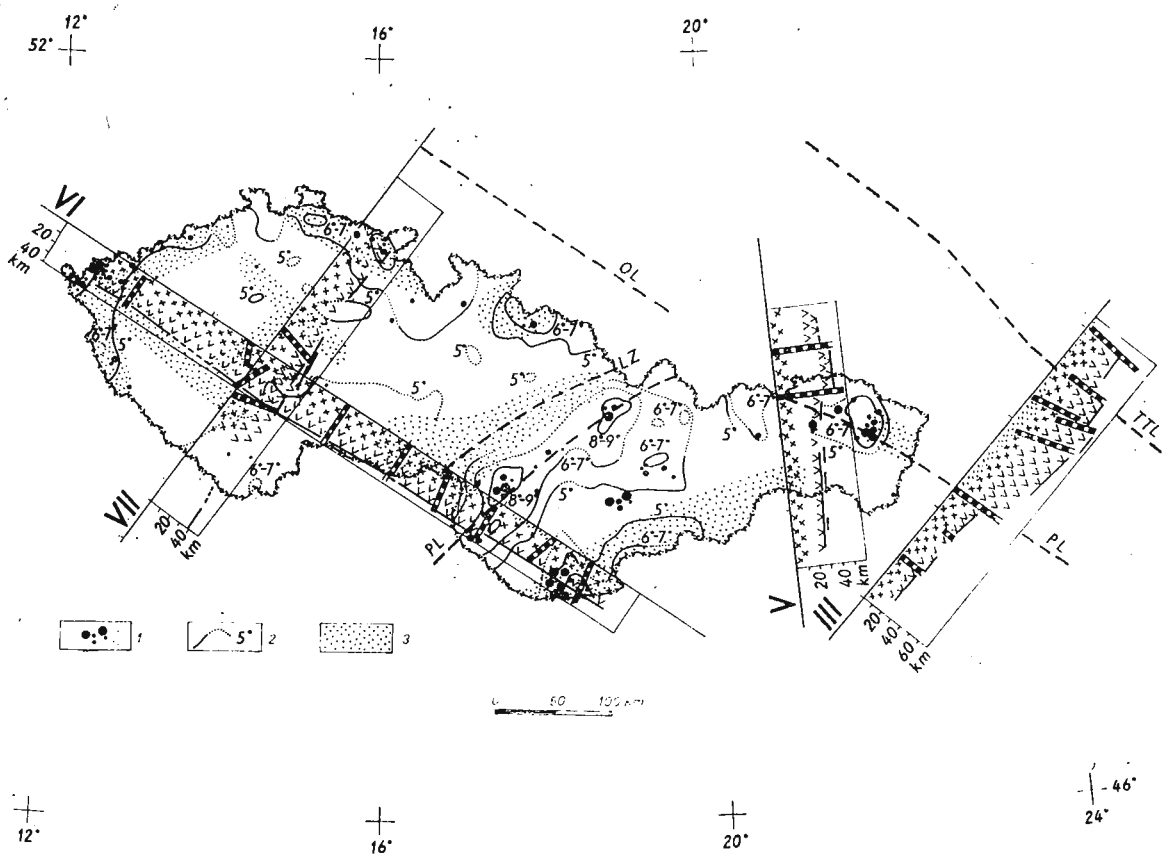

Fig. 5. — Seismic faults on profiles III, V, VI and VII compared with zones of increased seismic activity (after K á r n í k, 1959) and aeromagnetic anomalies (after M a n, 1966):

1, earthquake foci; 2, maximum isoseismals; 3, magnetic anomalies; OL, Odra line; PL, peri-Pieninian lineament; LZ, Lužice zone; TTL, Tornquist-Teisseyre lineament.

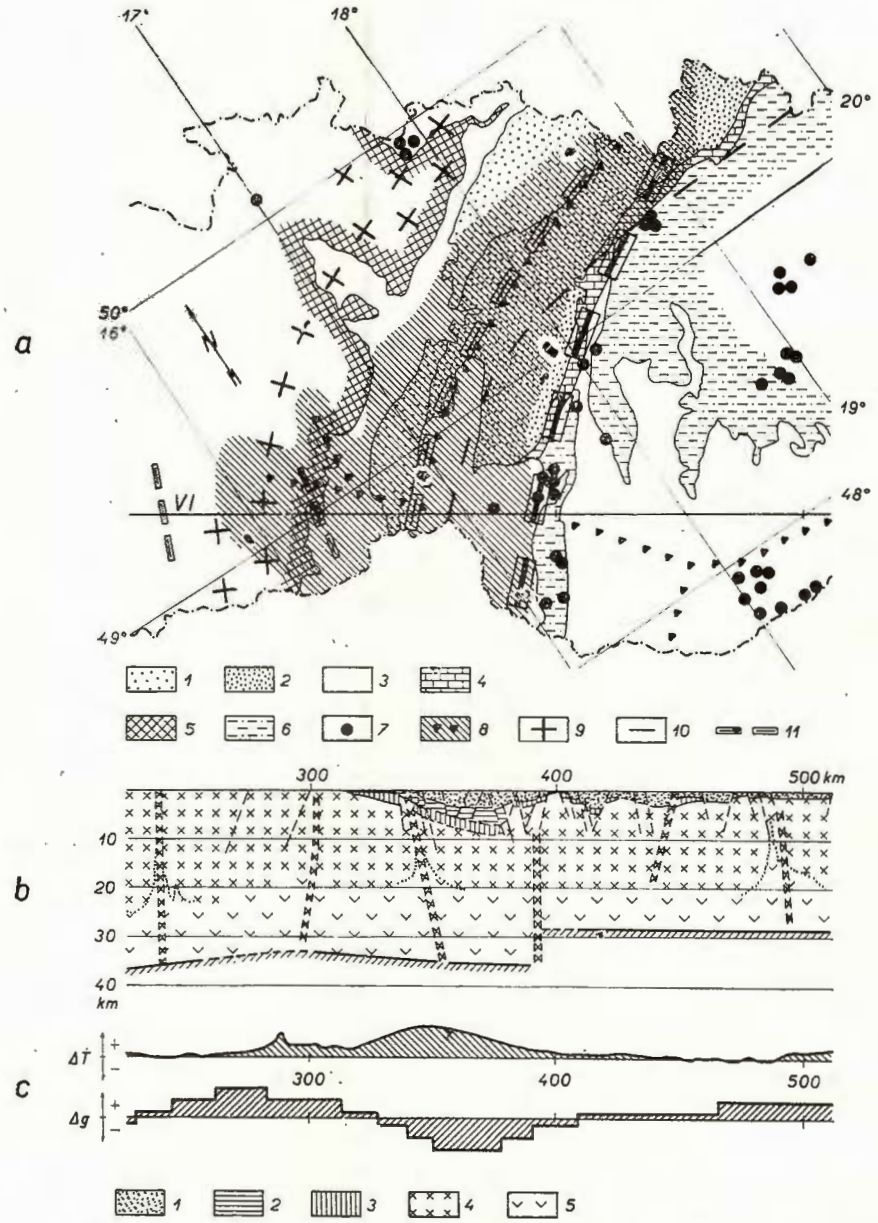

Fig. 6. — Contact between the Bohemian Massif and the Carpathians.

a) geological scheme :

1, inner flysch belt; 2, outer flysch belt; 3, Neogene; 4, cliff belt; 5, Bohemian Massif; 6, Central Carpathians; 7, macroseismic epicentres; 8, regional magnetic anomalies with their axes; 9, axes of positive gravity anomalies; 10, axes of negative gravity anomalies; 11, fault zones.

b) seismic cross-section :

1, Neogene sediments; 2, flysch belt; 3, Mesozoic; 4, granite zone; 5, basalt zone.

c) ΔT anomalies of total geomagnetic intensity T and Bouguer gravity anomalies Δg.

represents a transition from the Alps to the Carpathians, where the crystalline basement was covered by Neogene sediments the thickness of which amounts up to 5 km. Zátopek assumes, in view of a rapid attenuation of the energy of East-Alpine earthquakes toward NE in this area, the existence of a fault system, roughly parallel to profile VI, reflecting the seismic energy downwards.

As already stated, the maximum thickness of the crust was found in the East Carpathians. On the intersection of profile III with the Carpathians the Moho finds itself at a depth of 50 km. The peri-Pieninian lineament is marked very clearly on profile V. In the Central Carpathians the crustal thickness decreases gradually to the South. No evidence of mountain roots has been found in the Central Carpathians in spite of the mightly developed surface relief; the roots find themselves in the flysch zone of the Outer Carpathians. A double Moho found in this region is the most interesting result obtained in this region.

THE ALPINE REGION

The measurements in this region have been conducted in discrete points distant some kilometres of each other. Therefore, the phase correlation is not possible, and, sometimes, even the group correlation is rather difficult. The location of seismic discontinuities is possible only under simplifying assumptions. The maximum thickness of the crust was found in the West Alps; the Central Alps possess a characteristic thickness of the crust more than 50 km. Northwards and southwards from the Central Alps the thickness of the crust decreases. In the South the gradient of the rise of the Moho is much higher. In West Germany the dominant feature is the Rhine-graben which exhibits an elevation of the Moho in the North of the West Alps (Angenheister et al. 1972).

In the so-called German triangle the thickness of the crust is 28 — — 30 km. In the Molasse-zone it increases gradually towards the Alpine trough, and towards the Bohemian Massif as well (Giese, Stein, 1971).

THE SCHEME OF THE MOHO IN THE REGION OF THE EAST ALPS, THE BOHEMIAN MASSIF AND THE WEST CARPATHIANS

The results as obtained in Czechoslovakia, Hungary, in the area of the Alps and the Bavarian Molasse-zone combined with the data related to profile VII give a satisfactory basis for compiling a preliminary scheme of Moho for the region of Central Europe. This is represented in figure 7, and figure 9, respectively.

In the structural scheme some great units may be observed. The most significant is the Alpine-Carpathian trough. The alpine depression passes into the Carpathian trough in the Vienna-basin region. While the deepest root of the Alps finds itself in their central crystalline Massif, the thickness of the crust in the Carpathians reaches its maximum in the

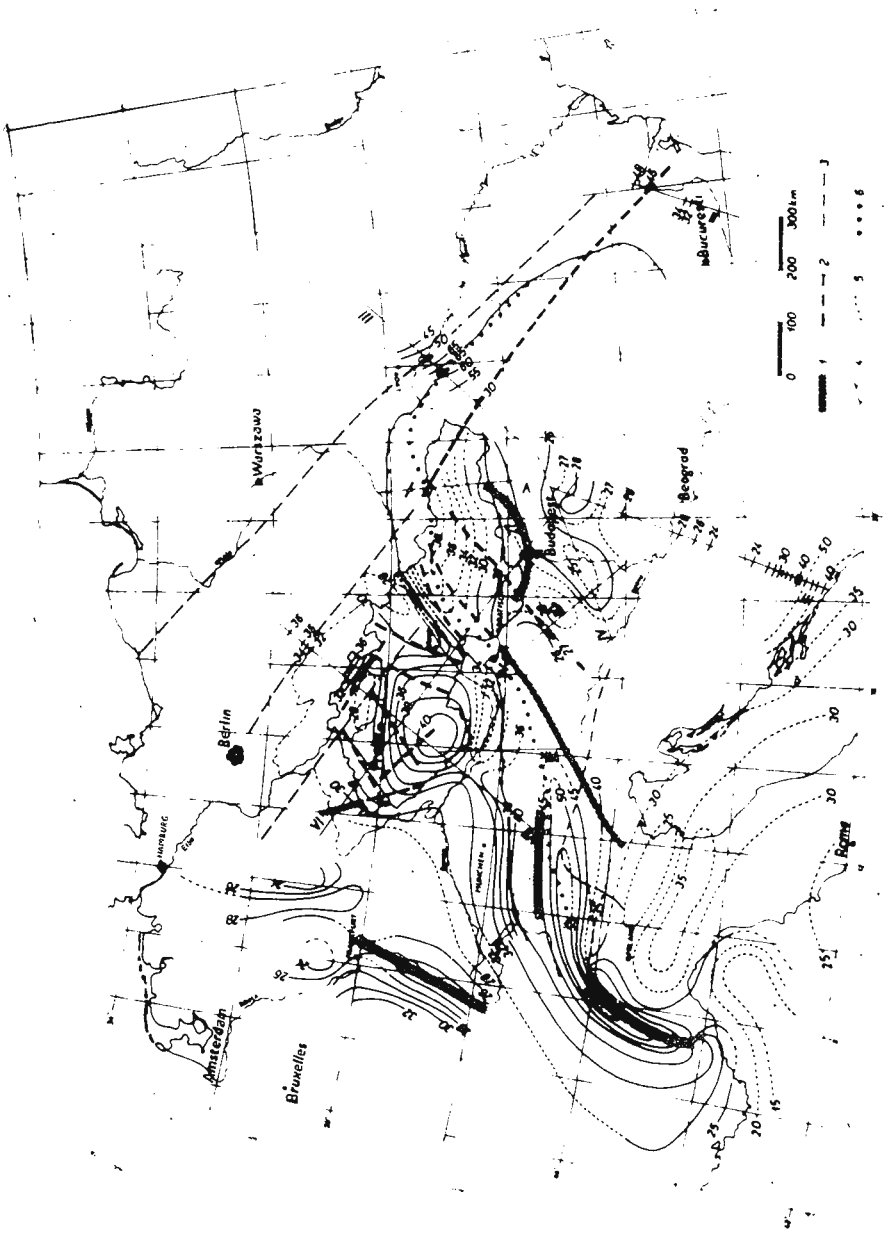

Fig. 7. — Structural scheme of the M-discontinuity in Central Europe:

1, seismic zones; 2, deep faults found in the Czechoslovak territory; 3, other deep faults; 4, overthrust of the Alps; 5, boundary of the Bohemian Massif; 6, axes of the negative gravity anomalies.

outer flysch zone. The correlation of the course of the Moho in the respective parts of the Alps and the Carpathians allows to mark off the Moho depression in the southern part of the Moldanubicum in Bohemia. The elevation of the Moho at the eastern margin of the Moldanubicum and the western one of the Carpathian trough reappears at the contact of the Moldanubicum with the Austrian Molasse. However, the problem of the transition still remains to be solved in detail.

Towards the North and Northwest of the Moldanubian geosyncline, and similarly in the area of the Teplice-Barrandian block, one observes a crest of the Moho. The Sudetes region, on the contrary, is characterized by a well marked depression. From the Moldanubicum the Moho is rising up to the NW; this rise is slightly interrupted by a not very marked depression in the Erzgebirge region.

The DSS-results have not detected any border between the Central Carpathians and the Pannonian block, but the line of separation of the two units may be seen in the mao of seismicity by K á r n í k (1971, fig. 9). The region of Central Carpathians is characterized by a monotoneous rise of the Moho southwards to the Pannonian Basin, which is a very interesting part of the Carpathian region, where the crustal thickness reaches a minimum in the depth range 23 — 28 km. The results of Hungarian geophysicists point to a multiple structure of the Moho and its slight undulations with a not very marked depression in the area of the Bakony Forest, and a small elevation in a SW-NE belt south of Budapest.

There is a very interesting question regarding the character of the transition zone between the East Alps and the Pannonian block. This must be solved in the course of the future research to be organized in this area.

REGIONAL GEOPHYSICAL RESULTS

Gravimetry and geomagnetism:

A basic information of gravimetric anomalies on the territory of Czechoslovakia may be derived from the gravimetric map of Czechoslovakia compiled by I b r m a j e r in 1966. Figure 8 shows their distribution over Central Europe.

In the map of regional Bouguer anomalies the belt of high negative anomalies passing through the region of the central range of the Alps and the Outer Carpathians is the most striking phenomenon. The axis of these megaanomalies on te territory of Austria is oriented in a W — E direction. This changes to SW—NE in the West Carpathians, and turns to a NW — SE direction in the Polish Carpathians. The gravity minimum in the Alps which lies in the highest central part of the mountain range, is shifted in the Carpathians into the outer flysch zone. The only exception is to be seen in the area of the High Tatras, where the situation resembles that in the Alps. Both in the Alps and in the Carpathians the higher thickness of the crust coincides with the negative gravity belt. The same principle is valid in general also in the region of Variscides.

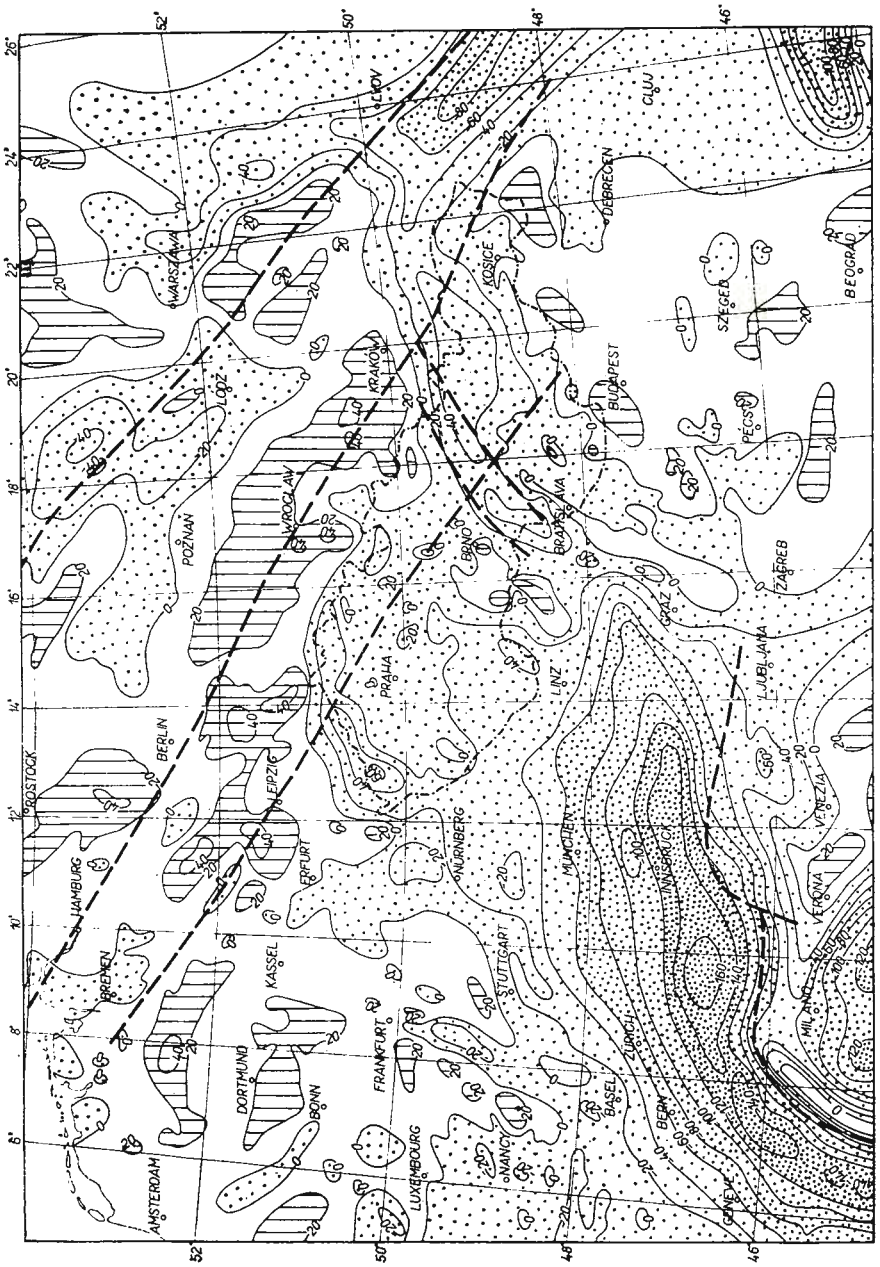

Fig. 8. — Map of Bouguer gravity anomalies in Central Europe (after I b r m a j e r).

For example, the respective regions of the Moldanubicum (with the increased thickness of the crust) and of the Sudetes are indicated by negative gravimetric anomalies. On the contrary, the thinner crust below the Cretaceous Table of NE-Bohemia, and the Moho elevation west of the Carpathian trough in the SE zone of the Moldanubicum, are distinguished by a positive anomaly of gravity.

The Pannonian Basin, in correspondence with the small crustal thickness, typical for this region, appears positive, too. All examples introduced demonstrate that the isostasy principle is respected only in general in the region considered as a whole. However, in detail, we find deviations at a number of places. For instance, the absence of marked mountain roots in the Erzgebirge could indicate a non-isostatic state of the local crustal blocks. Nevertheless, if we consider a higher thickness of the granitic layer, we can explain the negative anomaly found by observation fairly well, assuming that the Airy model is not appropriate enough for the explanation of the type of the isostatic equilibrium in this region, characterized also by earthquake swarms.

It is interesting to note that a map of the deflections of the vertical on the territory of Czechoslovakia (B u r š a , 1969), where reductions on the relief effects have been applied, yields a picture of geoid undulations which, qualitatively, is closely connected with the map of Bouguer gravity anomalies as given in figure 4, and, moreover, indicates the position of many of Z á t o p e k 's zones of higher seismic mobility, mentioned above (Z á t o p e k, 1948), as well as the situation of the pattern of great tectonically disturbed zones. In the space, it gives, qualitatively, a reversed shape of the Moho.

An interesting comparison is that of the map of regional geomagnetic vertical anomalies or, better, of the aeromagnetic map of Czechoslovakia (M a n , 1966), where total-intensity anomalies are represented, with the topographic distribution of the DSS and other data we were speaking of. We find that in the transition zone between the Bohemian Massif and the Carpathians there is a marked regional positive anomaly, (fig. 6), which, against expectation, does not continue either in the Austrian and Bavarian zone of the Molasse in the SW, or in the Polish platform in the NE. The presence of positive magnetic anomalies is conspicuous for contacts of big structural units also in other cases, as e.g. that of the Russian platform (i.e. its western margin) with the Polish Palaeozoic platform.

It should be introduced with respect to the zones of increased mobility found by Z á t o p e k that many of them coincide with the zones of positive aeromagnetic anomalies. That demonstrates a close connection with the regional magmatism and indicates a new approach to the study of all processes involved.

Seismology:

The mobile zones mentioned, found by Z á t o p e k (1. c.), and their obvious connection with deep faults, gravimetric anomalies and deviations of the vertical as well, and their coincidence with geomagnetic

Fig. 9. — Map of maximum macroseismic intensity in Central Europe (after K á r n í k, 1971) in relation to the main fault lines:

1, seismicity scale; 2, fault lines (TTL, T o r n q u i s t - T e i s s e y r e lineament; PL, peri-Pleninian lineament; RL, Raab line; OL, 'Odra line; EL, Elbe lineament; PAL, Periadriatic lineament); 3, neovolcanics belt; 4, overthrust of the Alps; 5, boundary of the Bohemian Massif.

anomalies, were integrally interpreted already in 1948 as a natural consequence of seismic energy guided through a block structure. This seems to be a good evidence for a multilateral geophysical synthesis.

Important information is given also from the maps of seismicity (K á r n í k , 1959 ; 1971). For the region in question K á r n í k compiled the maps of seismic zones and maximum intensities, which are, in spite of the relatively low seismicity in the region of the Bohemian Massif and the Polish and Russian platforms, very useful for the structural studies in the orogenic zones of the Alps and the Carpathians, where we find a number of seismically active areas (fig. 9). Among them a very marked zone is situated along the peri-Pieninian lineament, a zone which proceeds towards SW from the Carpathians as far as into the South Alps. In the Alps themselves, one sees several zones of livid seismic activity in the West Alps, and a marked one, oriented N — S, lying near the meridian 10°E. Let us add that both the northern and southern boundaries of the Carpathians are seismically active, too.

SYNTHESIS AND CONCLUSIONS

A synthesis of the results of DSS and other geophysical data available for the region of Czechoslovakia and the East Alps give the opportunity to compile a three-dimensional model of the Morhorovičić discontinuity in this part of Central Europe and to bring it into correlation with gravimetrical, geomagnetical, seismical and other geophysical information. From this evidence we may conclude that the Alpine trough passes from the Vienna basin into the Carpathian trough, which is running in the zone of the Outer Carpathians. The peri-Pieninian lineament, which is a deep fault zone, represents a border line of the West Carpathian trough against the Central Carpathians. The line of separation between the Carpathian trough and the Bohemian Massif, i. e. the zone of Variscides, is formed by the zone of Lednice, characterized by expressed magnetic anomalies. Geomagnetic, and especially aeromagnetic anomalies coincide in many cases with the axes of seismically mobile zones in the Bohemian Massif. This can be seen as an indication for the transcurrent character of these zones and promises a better understanding of geomagnetic (especially palaeomagnetic) phenomena and their relation to the tectonic processes in deeper parts of the Earth's crust.

The results available so far indicate a connection of the seismic activity, related to the peri-Pieninian lineament, with that which originates at the seismic lines of the East Alps, i. e. lines running towards SW, in the prolongation of the peri-Pieninian lineament, into the Alpine region. Most probably, just there it is the deep fault boundary between the Alps and the Pannonian block. In the South this zone joins the so-called peri-Adriatic (or insubric) line, which separates the Central Alps from the Southern Calcareous Alps. The transition zone between the Alps, which are a unit with increased thickness of the crust, and the Pannonian block with a crust substantially thinner, will require a joint

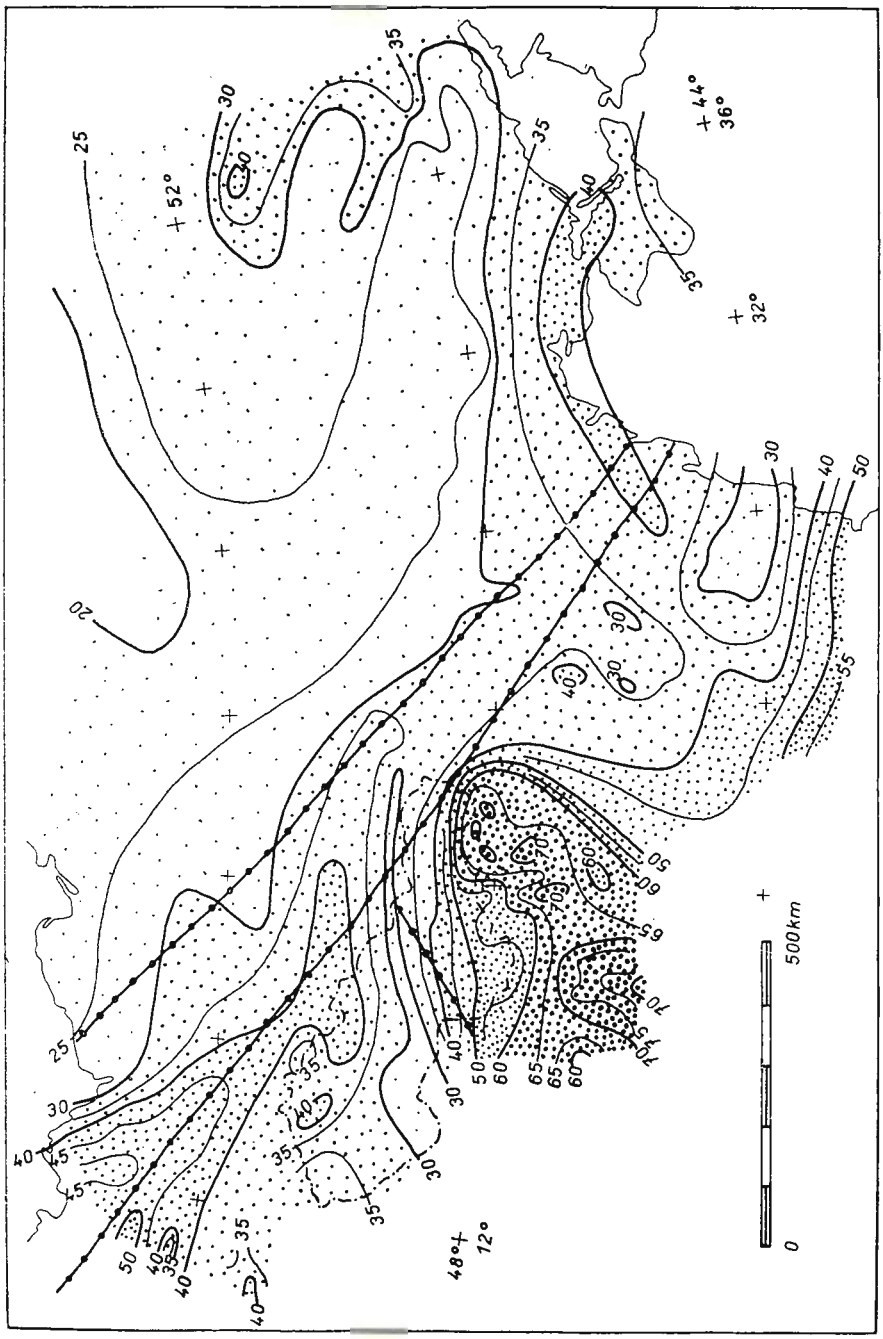

Fig. 10. — Map of geoisotherms in the depth of 1 km after L. Stegena, 1971.

study by Czechoslovak, Austrian and Hungarian specialists, and the same the transition area between the Alps and the Carpathians. A deeper knowledge concerning the dynamics and the geological role of the zone of negative gravimetric anomalies nearly parallel to the peri-Pieninian lineament and the insubric line is necessary, too. The northern branch of the former continues in the NW as a zone geologically known as the Odra (Oder)-line, assessed as a deep fault zone an profile VII. In the SE direction, the northern branch of the peri-Pieninian lineament goes on, forming finally, at the coast of the Black Sea, the western boundary of the Russian platform. In the region of the Bohemian Massif the Labe (Elbe)-lineament may be geophysically followed from the German Democratic Republic over Bohemia and Moravia far into Slovakia. Many problems arise from the new knowledge; among them one is to establish a satisfactory geophysical evidence for the continuation of the deep fault zone into the neighbouring units. The seismicity maps enable us to assess the eparation line between the Central Carpathians and the Pannonian Basin, what was not possible from the DSS-data. On the map plotted in figure 9 we see this line following the arc of young-Tertiary volcanism at the north frontier of Hungary and then bending towards the peri-Pieninian lineament.

In such a connection the comparison with the position of the belt of higher geoisotherms found by Stegena (fig. 10) seems to be of interest.

In view of the unsolved problems regarding the structure of this very important region of the European continent, our contribution aims at a recommendation in favour of stimulating the international cooperation of the countries involved of the East and West Europe [4]. Supplementary measurements on new international and national profiles are very desirable. These and other geophysical investigations are also of a high practica interest. The European Seismological Commission appears the very best international body to sponsor the respective research.

REFERENCES

Angenheister G. et al. (1972) Recent investigations of surficial structure of the Eastern and Southern Alps. *Geol Rundsch.*, Stuttgart.

Beránek B., Dudek A. (1972) The Results of Deep Seismic Sounding in Czechoslovakia *Z. Geophys.*, 38, Physica Verlag, Würzburg.

— Zounková M., Holub K. (1971) Results of deep seismic sounding in Czechoslovakia UMP Czechoslovakia 1962—1970, Final Report, Praha.

[4] Giese P., Morelli C., Steinmetz L. Crustal structure of Western and Southern Europe. 1971. Report of XVth IUGG General Assembly, Moscow.

Buršа M. (1969) Effect of removed topography and condensation on deflections of the vertical on the territory of Czechoslovakia, *Trav. Inst. Géophys. Ac. Sci.*, XVII, Academia, Praha.

Giese P., Stein A. (1971) Versuch einer einheitlichen Auswertung tiefenseismicher Messungen aus dem Bereich zwischen der Nordsee und den Alpen. *Z. Geophys.*, 37, Physica Verlag, Würzburg.

Ibrmajer J. (1966) Gravimetrická mapa ČSSR 1 :1000000. Praha.

Kárník V. (1959) Neue seismische Karten der Tschechoslowakei. *Trav. Inst. Geophys. Ac. Sci.*, VII, 88, Academia, Praha.

— (1971) Seismicity of the European Area, Academia, Praha.

Man O. (1966) Aeromagnetic map of Czechoslovakia. Praha.

Sollogub V. B., Prosen D., Militzer H. (1971) Strojenije zemnoj kory centralnoj i jugovostočnoj Evropy, Naukova Dumka, Kijev.

Zátopek A. (1948) On the Propagation of East Alpine Earthquakes through the Bohemian Mass. *Inst. Géophys. Nat., Tr. Spéc.* 3, Praha.

THE STRUCTURE OF THE UPPER MANTLE DERIVED FROM A 1000 km LONG SEISMIC REFRACTION PROFILE IN FRANCE[1]

BY

ALFRED HIRN [2] RAINER KIND [3], KARL FUCHS [3]

Waves propagating from two 1-ton and one 3-ton shots fired in the Atlantic Ocean 150 km from the coast were recorded alorg a 1000 km profile across France. The location of this profile is shown in the figure 1 of Sapin and Prodehl[4] who discuss the crustal structure along the same line. Sixty magnetic tape recording stations were set up for each shot; station spacing was 5 km out to a distance of 660 km and 10 km thereafter.

The data shows clear first arrivals from the upper mantle at distance up to 900 .m (fig. 1), and second arrivals, with the same apparent velocity as the first arrivals and having intercept times of 14 and 21 seconds, are interpreted as reflected and refracted events. Late arrivals with an apparent velocity of about 6 km/s, and observed up to a distance of 600 km, are interpreted as wide-angle Moho reflections.

A closer inspection of the first arrivals (fig. 2) reveals a large variation of amplitude with distance, and this was interpreted as being caused by several discontinuities underneath the Moho.

Several models, consistent with the observed travel-times, were calculated, with and without velocity inversions and gradients. However, simple models with homogeneous layers and first-order discontinuities do not fit the observed variation of amplitude with distance. Synthetic seismograms after Fuchs, Müller (1971) for a model which was used in a first attempt to fit the amplitude-distance data are shown in figure 3.

Although final results have not yet been obtained, there is evidence for the existence of a velocity inversion at about 50km depth and for a

---

[1] Contribution No. 89 Geophysical Institute, University Karlsruhe

[2] Institut de Physique du Globe. 11 Quai St. Bernard. Paris, France.

[3] Geophysikalisches Institut. Hertzstrasse 16 Karlsruhe, Germany.

[4] Sapin M., Prodehl C. Long-range profiles in western Europe : I. Crustal structure between the Bretagne and the Central Massif of France. 1972 (in press).

rapid increase of velocity at about 80 km depth. More detailed studies of the range of possible variation of the model, and an extension to greater depth, are now being undertaken.

REFERENCES

Fuchs K., Müller G. (1971) Computation of synthetic seismograms with the reflectivity method and comparison with observations. *Geophys. J.R.Astr. Soc.*, 23, London.

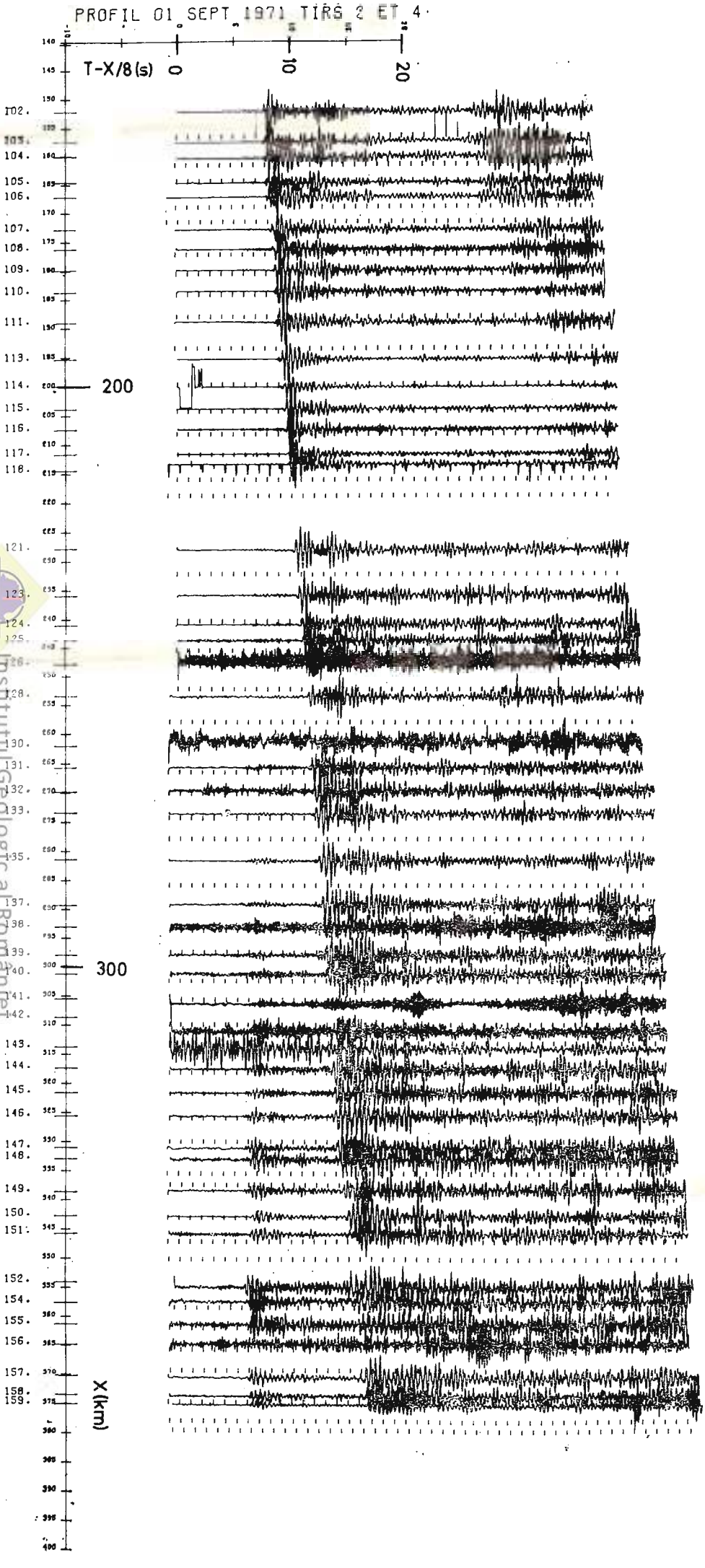

Fig. 1a — a) Seismogram section between 150 and 400 km;

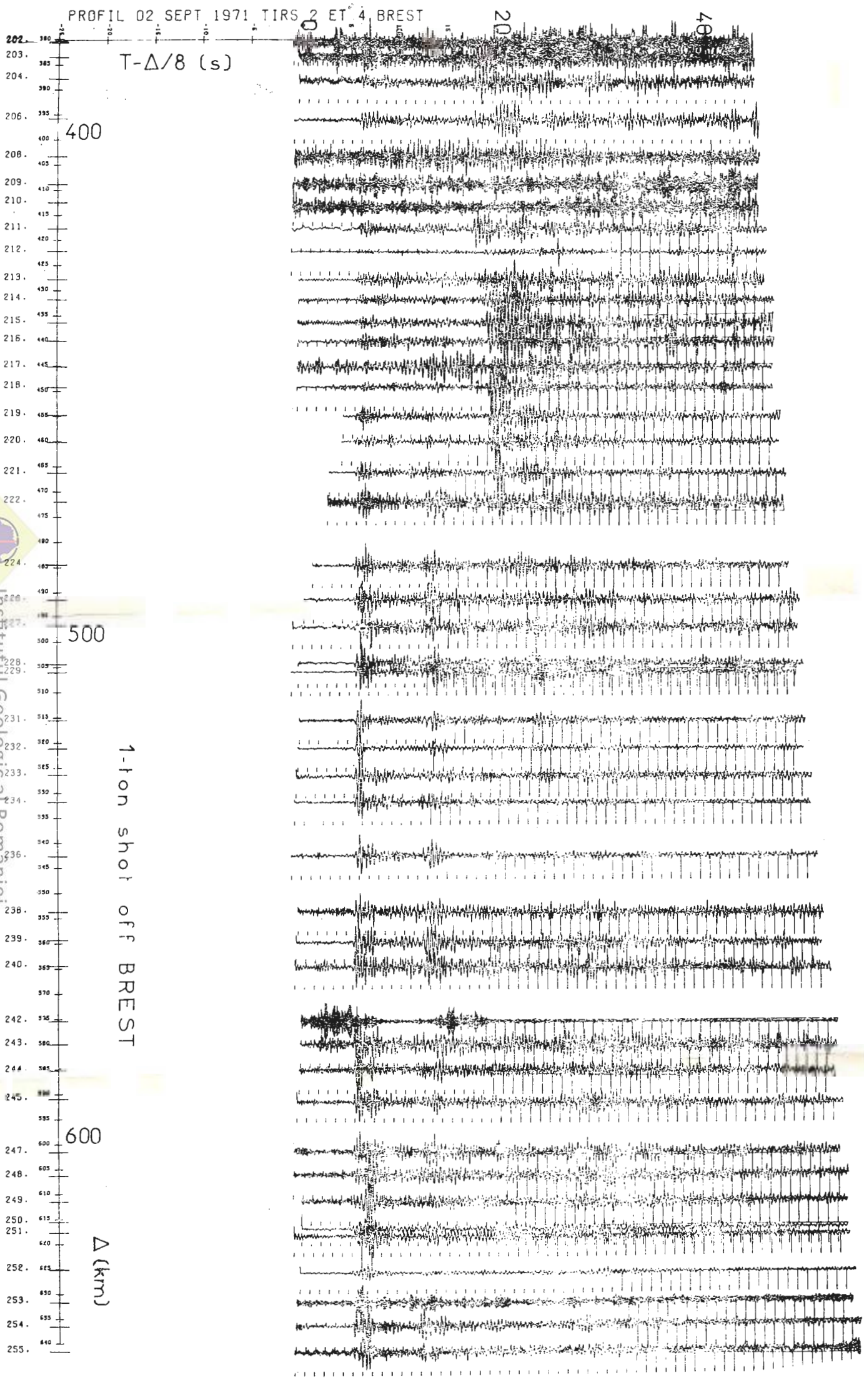

FIGURE 1. — b) Seismogram section between 400 and 600 km.

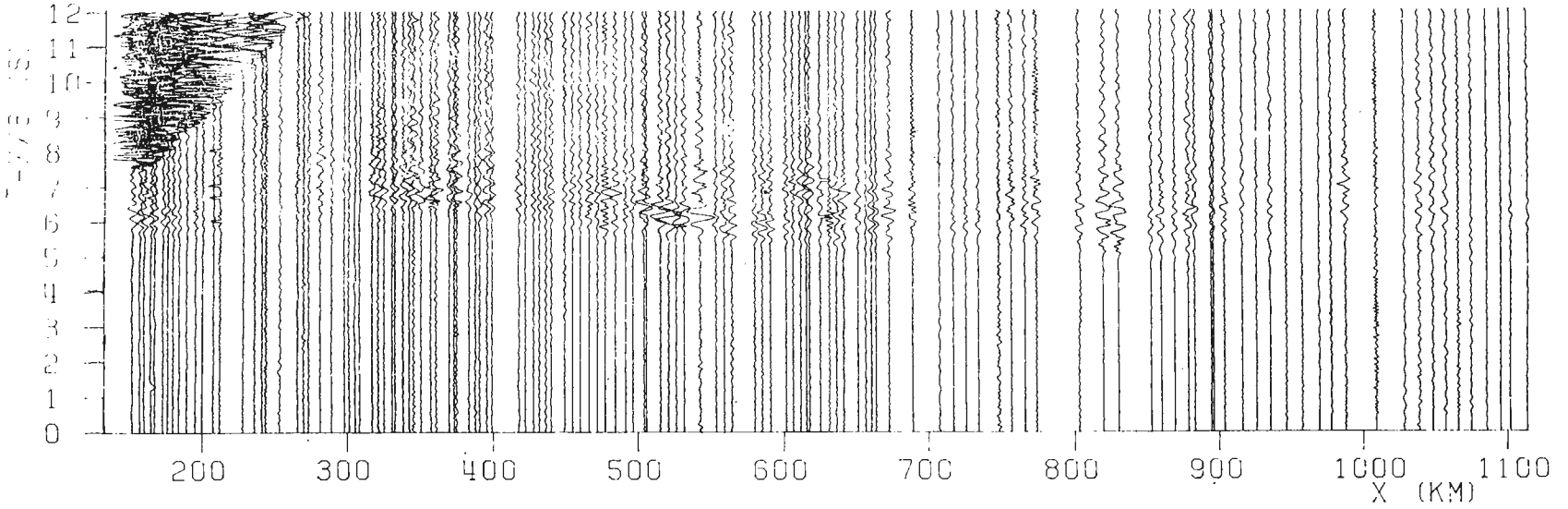

Fig. 2. — Enlarged first arrivals of figure 1.

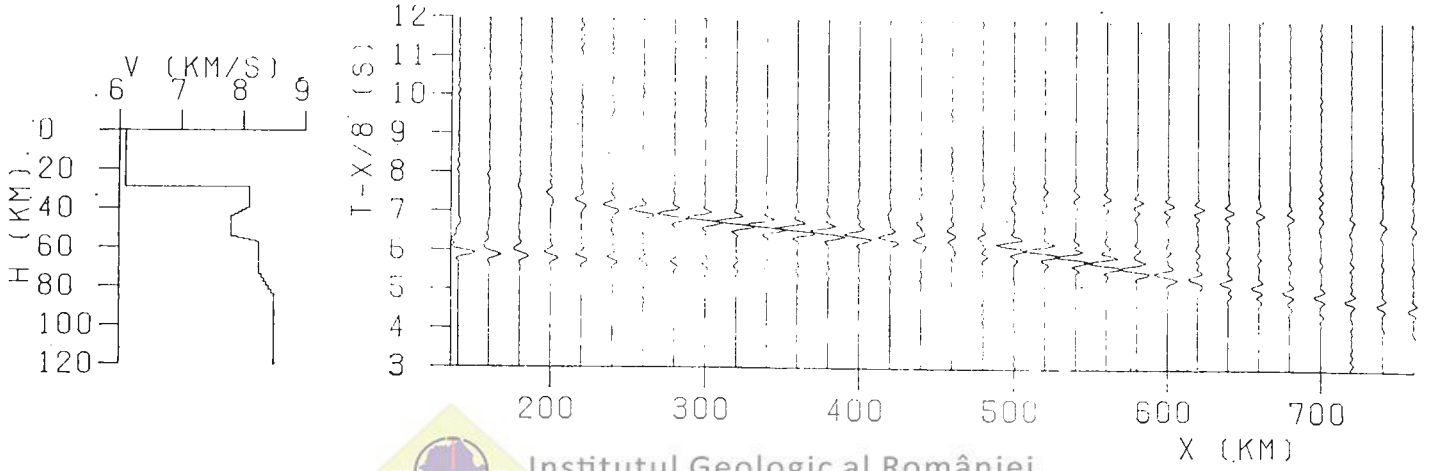

Fig. 3. — Synthetic seismograms of a model, consistent with amplitude-distance data.

THE SEISMOACTIVE ZONES OF AZERBAIJAN CONNECTED WITH STRUCTURE AND EVOLUTION OF THE EARTH'S CRUST

BY

V. I. KULIKOV [1], F. T. KULIYEV[2], V. A. KASPAROV [2]

Azerbaijan region and an adjoining water area of the Caspian Sea, which are concerned to Alpine fold of the south part of the USSR (fig. 1), are characterized by a high seismic activity, that as ($A_{10} = 0.26$; $\gamma = -0.56$). It is confirmed by seismostatic (the maps of isoseismal lines maximum earthquakes, which are observed, of seismic activity, of maximum possible earthquakes) and by neotectonic data (K u l i y e v, K a s p a r o v, 1972).

As concerning to the seismic data there are distinguished ten seismoactive zones of the studied region ($0.3 \leqslant A_{10} \leqslant 1.0$), which are mainly found (figs. 1, 2) in transitional areas from the large-scale geotectonic uplift (Great and Minor Caucasus) to intermountain and submontane troughs (the Kura depression and others).

During of its development the Alpine geosyncline inheritted the Gersin and more ancient the Baikalo-Kaledon fold (S o r s k y, 1967). The south-east part of the Great Caucasus, which involves Shemakha, Vartashen, Belokan and Apsheron seismoactive zones, was shaped in the course of a long geologic cycle — from Mesozoic to Anthropogen. The structures are of a linear character here. Zones are distributed along the Caucasian trend fold.

However the deviation of submeridional direction, which reflects the influence of the more ancient Baikalo-Kaledon fold, is observed here. Especially it is better seen for seismoactive zones of Kura intermontane trough. Saatly-Geokchai medial uplift of the Jurassic basement, which is situated in this area, is a relic of the Baikalo-Kaledon fold and is characterized by a submeridional strike.

On the whole according to geophysical data for the East Caucasus there are directions to reworking of submeridional before-Cambrian folding into all-Caucasian, which is correspondingly represented by deep

[1] The Azerbaijan Section of the All-Union Scientific-Research Institute of Geophysics, Baku, USSR.

[2] The Institute of the Geology, Baku, USSR.

fault on geologic maps, by structure of crystalline basement, by distribution of zones of active vertical neotectonic movements and also by seismicity. At the present time the strike of faults in asimuths from the NNW-SSE to WNW-ESE (Akhmedov, Kulikov, 1970; Shikhalibeily, 1967) are predominant.

The south-west part of the given zone is characterized by mosaicity of structures and structures of different directions, by young lavas, which are connected with a relatively young tectonics and by in block structure meganticline of the Minor Caucasus (Shikhalibeily, 967).

During the historical time there were observed earthquakes of nine balls on the scale MSK-64. Correlation of observed maximum earthquakes with a medium seismic activity A_{10} in the area, responsible for this earthquake and surrounded his epicentre by method (Riznichen-

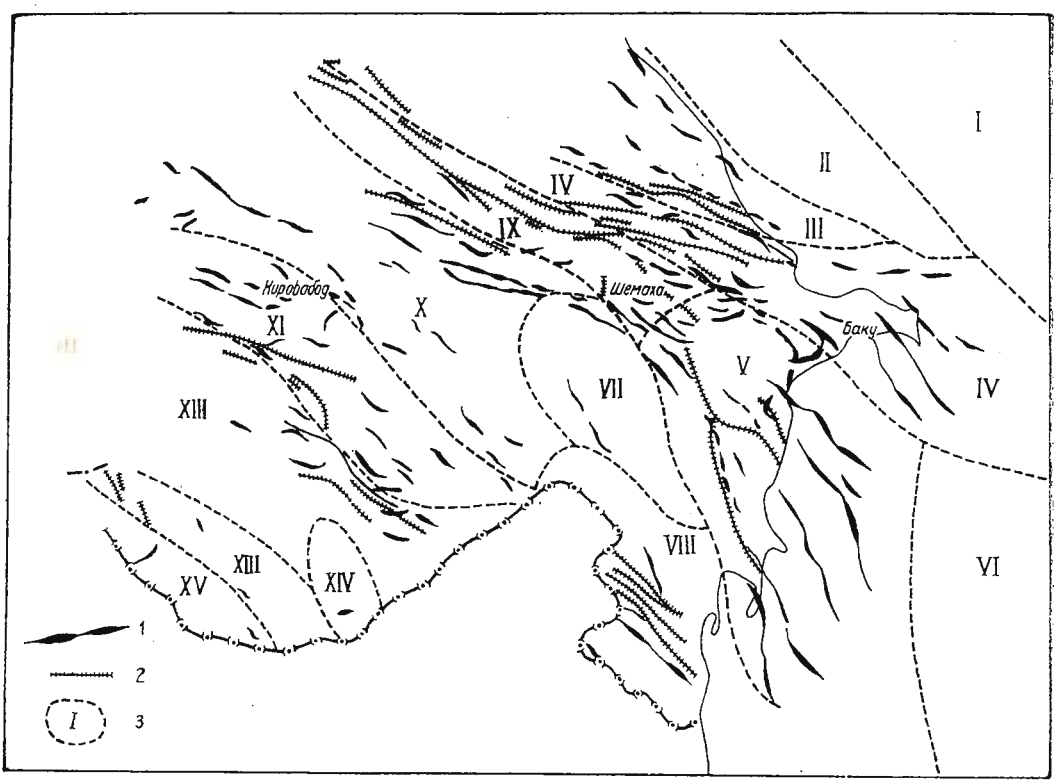

Fig. 1. — The tectonic map of the Azerbaijan SSR:

I, Monocline of Epigerzing platform; II, Zone of the Tersko-Caspian trough; III, NE wing of meganticlinorium of the Great Caucasus; IV, SE periclinal submersion of meganticlinorium of the Great Caucasus; V, South branch from meganticlinorium of the Great Caucasus; VI, South Caspian Lowland; VII, Saatly-Kyurdamir middle uplift; VIII, Subtalysh submontane anticlinorium; IX, Zakataly-Vandam submontane anticlinorium; X, Middle Kura intermontane trough; XI, Idzhevano-Aghdam submontane anticlinorium; XII, Central part of meganticlinorium of the Minor Caucasus; XIII, Velidag-Ordubad anticlinorium; XIV, The Kafan anticlinorium; XV, The Nakhichevan mould; 1, anticlinal folds; 2, faults; 3, geotectonic zones.

k o, 1967) was carried out for the purpose to determine the upper bound of a possible seismic danger. The regresssion equation for Azerbaijan is presented in the fo1 m of :

$$\log A_{10} = \bar{1}20 + 0.21\ (K_{\max.} - 15).$$

Using this equation, we have wo1 ked out the map $K_{\max.}$ (fig.3). The largest energy $K_{\max} = 16$ takes place in Shemakha seismoactive zone, where most powerful earthquakes took place in the past (in 1902 with $K = 17$).

On the whole the values A_{10} and $K_{\max.}$ in the studying area are decreasing along both sides from a trend of the more active ($0.5 \leqslant A_{10} \leqslant 1.0$, $K_{\max}$ 15 ÷ 16) transitional zone — from the South foothills of the Great Caucasus uplift to the North edge of the Kura depi ession.

For characteristic of field velocity tension of vertical neotectonic motions the neotectonic activity map is wo1 ked out with using formula (N i k o l a y e v, 1969) :

$$A_T = \frac{100 \cdot h}{S \cdot T}\ M^{-1} \cdot \text{year}^{-1},$$

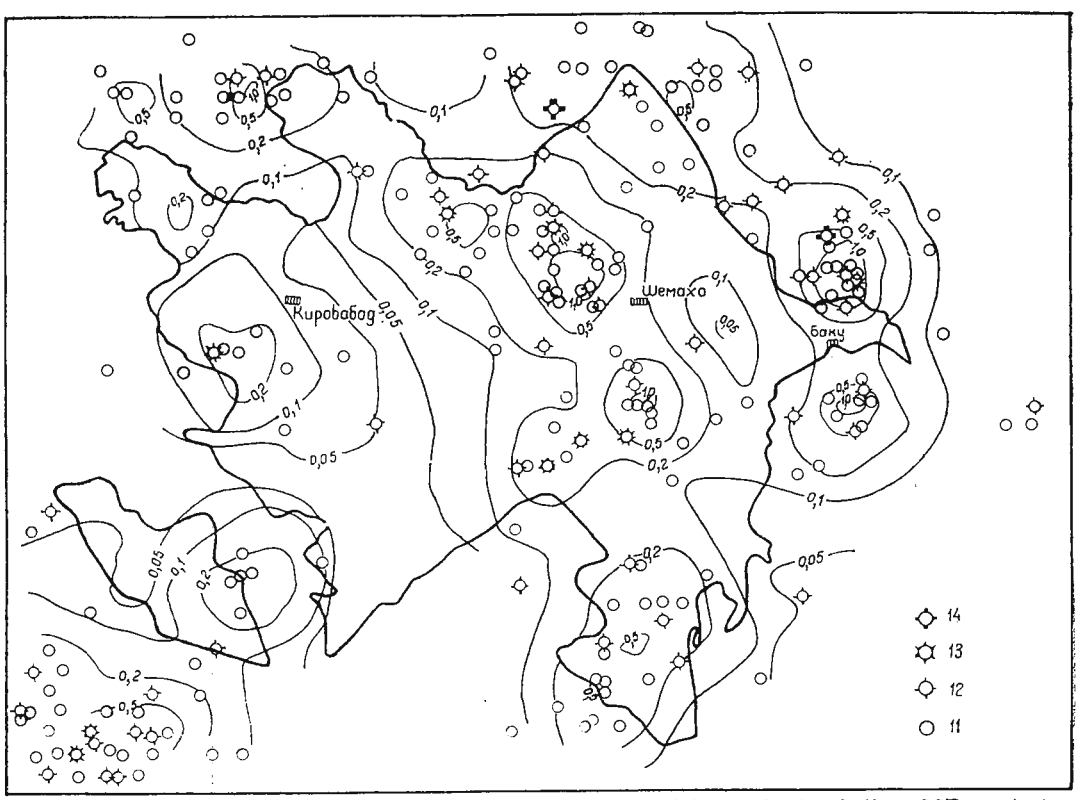

Fig. 2. — The map of epicentres of earthquakes and of seismic activity of the Azerbaijan SSR on instrumental data by 1951—1970.

where A_T — is vertical neotectonic motion activity in the area S in the period $T = 3.4.10^6$ years — an absolute Akchagyl story age (G r o m o v et al., 1969); h — an amplitude of vertical neotectonic motions (A k h m e d b e i l y, N i k o l a y e v, K h a i n, 1968). While transforming this formula for the studying area conditions we have $\log A_T = q - 10.8$. Relative isoactives q showing how many orders the vertical neotectonic

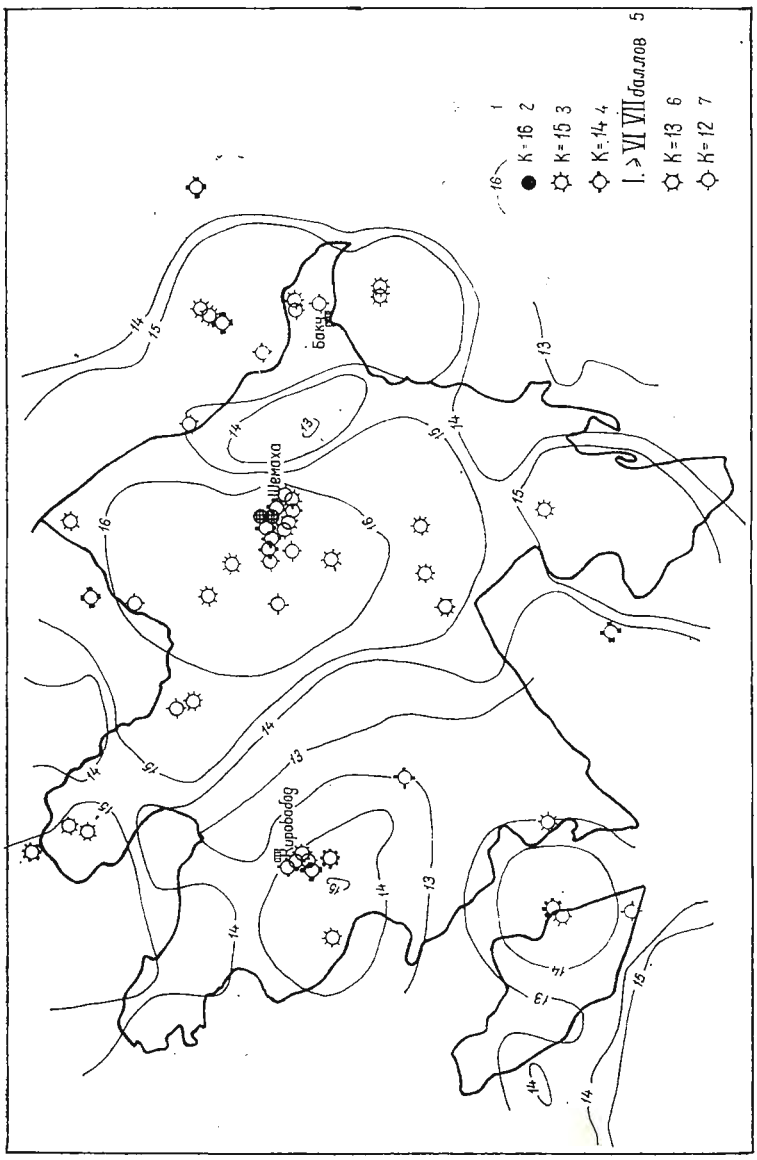

Fig. 3. — The map of maximum possibility earthquakes ($K_{max.}$) of the Azerbaijan SSR: — 16 —, isolines of $K_{max.}$

motions activity exceeds its minimum meaning in the studying area are shown in the neotectonic activity (fig. 4) map. On the whole the largest meanings $q = 3.5$ are observed in central part of area. This zone is complicated with the deep faults and the most active thrusts at the latest time.

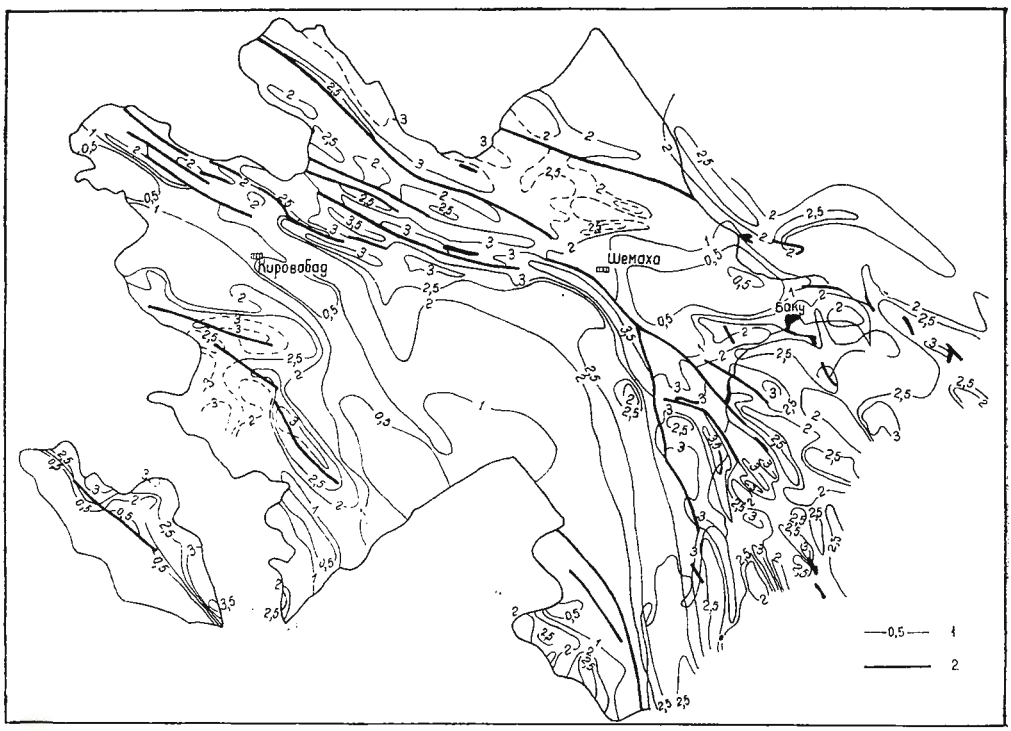

Fig. 4. — The map of neotectonic activity of the Azerbaijan SSR :
1, isolines of relative geotectonic activity ; 2, tectonic faults.

At the ends of this tectonic zone there are Shemakha ($0.5 \leqslant A_{10} \leqslant 1.0$; $K_{max} = 16$) and Sabirabad ($0.5 \leqslant A_{10} \leqslant 1.0$; $K_{max} = 15 \div 16$) ones.

The level of seismic activity of distinguished zones is in the definite dependence from the depth range of the crystalline basement (fig. 5) within these zones limits. As is shown in case of transition from seismoactive zones of the Minor Caucasus (Zangezur, Kirovabad) to he Great Caucasus zones is the increase of seismic activity level and depth range basement from 0.2 till 1.0 and from 4 —5 km till 7 —11 km correspondingly is observed. While this transition takes place also the common subsidence of the crystalline basement surface (from + 2 km in the area of the Minor Caucasus till 22 km in the Caspian water area) and an increasing crush of the basement with deep faults and upper structural stories with regional tectonic ruptures. The vertical dislocation within the limits of seimoac-

tive zones along faults is average 2.5 km (from 1 to 5 km) (H a d j i y e v, 1965).

The focuses of an overwhelming majority of earthquakes with $K \leqslant 12$ are in the interval of changing deeps of basement within the limits of 0 —20 km but the majority of destructive ones — with $K \geqslant 13$ are found considerably deeper (30 —50 km) in consolidated crust.

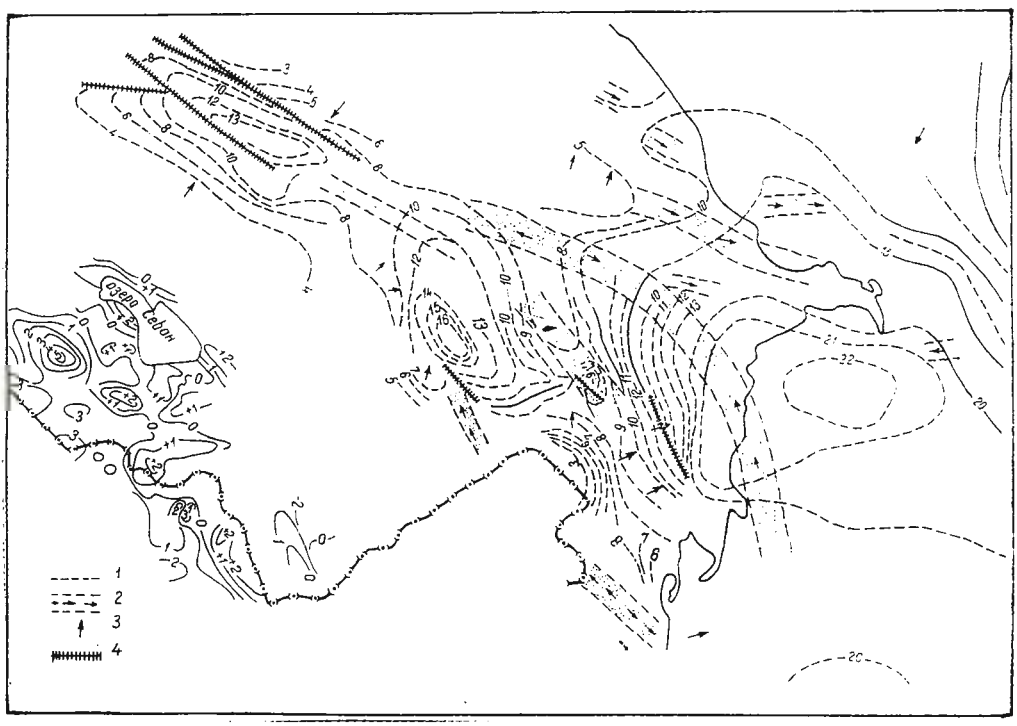

Fig. 5. — The map of hypogene structure of the Azerbaijan SSR by geophysic dates :
1, isodepth of surface of consolidating crust ; 2, zones positive structures or faults (on dates of gravimetry) ; 3, gravitational steps (great gradients of AFG) ; 4, tectonic faults.

Seismoactive zones are usually characterized by gravitational steps and also by transitions of the more increased meanings of the Bouguer effect to more low.

In the limits of Azerbaijan the magnetic anomalies do not show correlation with seismic and neotectonic activity of the zones, which are singled out.

There is an area of the falling seismic activity ($0.05 \leqslant A_{10} \leqslant 0.1$; $K_{max} = 13 \div 14$) between Apsheron and Shemakha zones, where calm occurrence of crystalline basement, absence of deep faults, low degree of seismic activity ($q = 1.0$) and development of mud volcano are observed.

Between Talysh and Zangezur zones of the Minor Caucasus there is situated the zone with the minimum meanings of seismic ($A_{10} \leqslant 0.05$)

and neotectonic ($q \leqslant 0.5$) activity with a calm occurrence of basement. However, there is the zone (Ust-Kura) with an increased neotectonic activity ($q = 2.5 \div 3.0$), with a great range and an increasing crush of the basement but with the low level of seismic activity ($0.05 \leqslant A_{10} \leqslant 0.1$).

The level of seismic activity and peculiarities of distribution of Azerbaijan seismoactive zones and adjacent Caspian water area on the whole is better characterized by local special features of the crystalline basement structure — i.e. by a great range of external meanings abyssal of the basement and by differential motions of large-scale blocks along deep faults, which display great activity of neotectonic motions of the Earth's crust.

REFERENCES

Akhmedbeily F. S., Nikolayev N. I., Khain V. I., (1968) Neotectonic map of the Azerbaijan SSR. Baku.

Akhmedov G. A., Kulikov V. I. (1970) The Azerbaijan Abyssal structure on geological and geophysical data. In : The main results of geophysical investigations, Baku.

Gromov V. I. et al. (1969) Anthropogen subdivision scheme. *The Commission Report on Quaternary period investigations*, Acad. Sci. USSR, 36.

Hadjiyev R. M. (1965) Azerbaijan abyssal geological structure. Baku.

Kuliyev F. T., Kasparov V. A. (1972) Maps of seismic and neotectonic activity and $K_{max.}$ of the Azerbaijan SSR. *The Sci. Works of the All-Union Conf. on seismic behaviour* (Kishinev, 1971), Moscow.

Nikolayev P. N. (1969) Conception of a middle activity of vertical tectonic motions as a quantitative characteristic of kinematics of vertical tectonic motions of the Earth's crust. *In* : The latest tectonics, the latest deposits and the man, Ed. State Moscow Univ., Moscow.

Riznichenko Yu. V. (1967) Seismic activity and energy of maximum earthquakes. *In* : Geophysical problems of the Middle Asia and Kasakhstan, Nauka, Moscow.

Shikhalibeily A. Sh. (1967) Geological structure and history of development of the east part of the Minor Caucasus. Baku.

Sorsky A. A. (1967) Special features of Caucasus structure and development in connection with its abyssal structure. *In* : Caucasus abyssal structure, Nauka, Moskow.

STRUCTURE DE LA DISCONTINUITÉ DE VITESSE VERS 600 KM. EXEMPLE SOUS LA FRANCE

PAR

PIERRE MECHLER[1]

Les anomalies de temps de propagation des ondes sismiques, différence entre le temps de propagation observé et le temps calculé, ont été notées dès les premières tables de propagation. Leur étude a été facilitée par la création de stations sismiques complexes (Array) qui permettent de mesurer non seulement le temps de propagation en fonction de la distance, mais aussi sa dérivée. L'étude que nous allons décrire dans cette communication essaye d'expliquer l'origine de ces anomalies.

Les réseau sismologique français, dont la maintenance est assurée par l'Ecole Normale Supérieure et le Laboratoire de Détection et de Géophysique, comprend une trentaine de stations reliées entre elles par télémesure et réparties sur l'ensemble du territoire français. Nous avons étudié pour plusieurs centaines de séismes, les anomalies de temps de propagation : celles-ci sont assez dispersées d'un séisme a l'autre et d'une station a l'autre. Pour un séisme donné, il n'est en général pas possible de les interpréter simplement par un choix convenable du paramètre p.

Si l'origine des anomalies se trouvait au voisinage de l'épicentre, ou en tout cas à une grande distance du réseau, il devrait pourtant être possible de trouver une valeur de $dT/d\Delta$ compatible avec les données du réseau. Il résulte donc de nos observations qu'il y a une origine locale a ces anomalies. Précisons bien que nous ne pensons pas que toutes les anomalies se produisent au voisinage des stations, mais qu'une partie au moins est locale ; il est bien évident qu'il doit aussi y avoir des anomalies se produisant près de l'épicentre.

Si nous étudions une anomalie différentielle :

(temps observé — temps calculé) — (temps observé — temps calculé)

Station 1 Station 2

cette valeur doit mettre en évidence les causes locales de perturbation de propagation sismique, les origines lointaines devant être les mêmes pour les deux stations et donc, sinon se détruire totalement, au moins diminuer

[1] École Normale Supérieure. 24, rue Lhomond. 75230 Paris, France.

fortement par la différence prise. L'expérience montre effectivement que ces anomalies différentielles sont bien définies pour chacune des régions sismiques principales de la terre. Il est d'ailleurs normal que la dispersion soit réduite puisque nous supprimons, en tout état de cause, l'erreur sur le temps origine du séisme.

Notre hypothèse de travail consiste a admettre que l'origine principale de ces anomalies se trouve dans une variation de profondeur de la discontinuité de vitesse sismique qui existe vers 600 km de profondeur et qu'en première approximation il est possible de négliger les autres causes possibles.

Nous avons utilisé le modèle de vitesse publié par Ansorge et Mayer-Rosa (1968) pour l'Europe occidentale. Dans ce modèle, on constate une discontinuité de vitesse sismique vers 550 km de profondeur, la vitesse passant à peu près de 9 à 10 km/s. Nous avons étendu ce modèle en extrapolant les vitesses au-dessus et au-dessous de la discontinuité, et en laissant variable sa profondeur.

Un travail assez fastidieux permet alors de tracer la carte de la discontinuité sous la France. En admettant une profondeur a l'endroit où un rai sismique traverse la discontinuité avant d'arriver à une station, nous pouvons calculer les profondeurs et les lieux où les autres rais enregistrés dans l'ensemble du réseau la traverse. Un deuxième séisme, provenant d'une région différente et coupant la discontinuité en un point déjà connu permet d'étendre la carte. En choisissant convenablement l'ordre dans lequel on utilise les différentes régions sismiques, il est possible de construire la carte. Cette première approximation suppose que la discontinuité est horizontale aux intersections avec les rais ; les résultats contredisent cette approximation, les pendages obtenus sont importants. Nous introduisons alors ces pendages pour réaliser une deuxième approximation de la carte. Il ne semble pas utile de pousser plus loin les approximations vu les erreurs fatales inhérentes à la méthode.

La première figure représente la carte ainsi obtenue. La discontinuité que nous trouvons a une profondeur de 550 km dans le Nord-Est de la France mais descend jusqu'à 750 km dans le Sud et le Sud-Ouest.

Nous ne discuterons pas dans cette publication les conséquences géologiques et tectoniques de cette discontinuité, conséquences pourtant importantes. Il me semble plus utile d'asseoir notre hypothèse géophysique et de la justifier par d'autres mesures indépendantes.

L'idée première de l'importance de cette discontinuité pour la propagation des ondes a été obtenue par des considérations d'amplitude des signaux enregistrés. Une de nos stations — T.C.F. dans le centre de la France — reçoit faiblement les explosions russes de la région de Semipalatinsk, mais fortement les explosions nucléaires du Lop Nor. Les variations d'amplitude que nous considérons ne dépendent pas du séisme, nous faisons en effet le rapport de l'amplitude à la station considérée par l'amplitude moyenne enregistrée en France. Cet effet est forcément local puisqu'il n'est observé que dans cette station. Si nous l'attribuons à une focalisation des ondes par un dioptre, ce dioptre doit être suffisamment

profond pour que les zones de Fresnel des deux dioptres correspondant aux deux rais soient disjointes. Semipalatinsk et le Lop Nor étant vus de la station sous, à peu près, le même azimut, il est facile de calculer que le dioptre doit se trouver á, au moins, 500 km de profondeur.

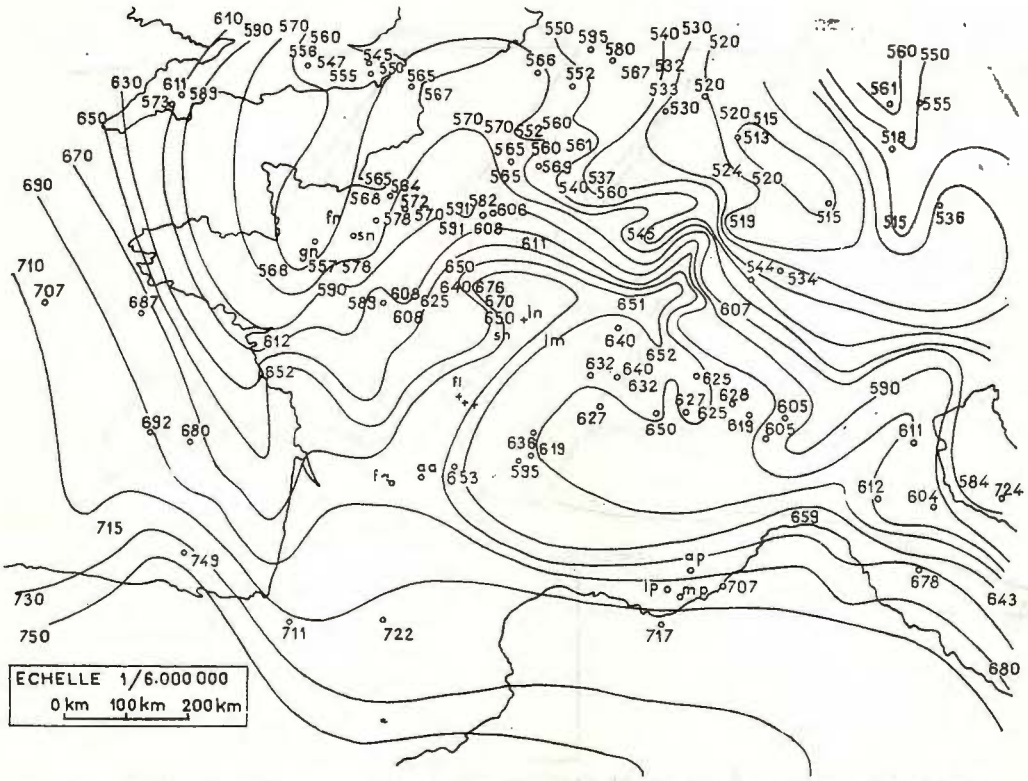

Fig. 1. — Profondeur de l'asthénosphère sous la France d'après les données sismiques ENS-LDG

Inversement, la carte précédente permet de recalculer le rapport d'amplitude précédent. Voici trois valeurs obtenues à partir d'explosions nucléaires :

	Observé	Calculé
TCF Lop Nor	4,2	3,2
TCF Semipalatinsk		
Provence Semipalatinsk	1,1	1,3
Provence Lop Nor		
Aquitaine Lop Nor	3,2	3,4
Morvan Lop Nor		

On observe donc une concordance remarquable entre les valeurs expérimentales et les valeurs calculées à partir de notre carte.

La deuxième figure montre une coupe de la discontinuité pour un azimut de 60°, azimut de réception des explosions nucléaires du Lop Nor et de Semipalatinsk. Nous avons tracé les rais sismiques de ces deux régions arrivant, dans quatre de nos stations, ainsi que les variations des

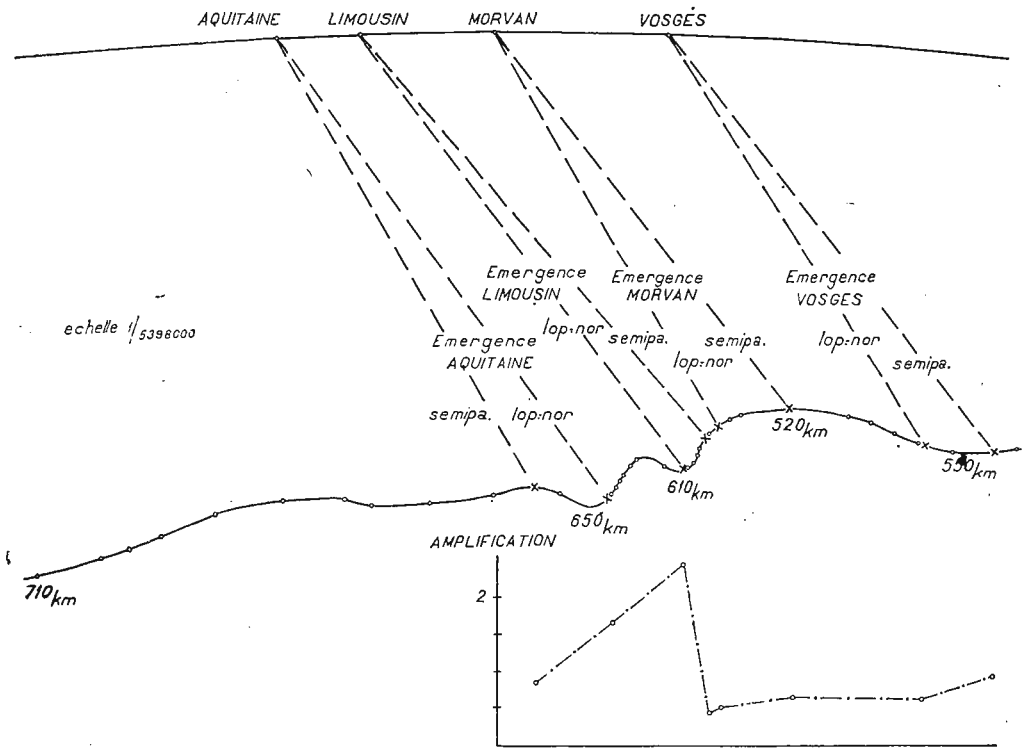

Fig. 2. — Profil Vosges-Morvan-Limousin (et Aquitaine). Explosions nucléaires de Semipalatinsk et de Lop Nor. Azimut 60°.

amplifications, c'est-à-dire des rapports d'amplitudes. Nous constatons de façon qualitative que les amplifications fortes correspondent toujours à des dioptres convergents, et inversement.

Nous obtenons donc une justification indépendente de notre hypothèse en même temps qu'un moyen d'expliquer les variations d'amplitudes des ondes sismiques, ce qui est un résultat remarquable.

Nous avons aussi pu confirmer notre carte par l'étude de séismes plus proches (Δ voisin de 20°). Les rais de ces séismes ont leur point le plus bas vers 600 km, nous les avons donc exclus de l'étude précédente puisqu'ils ne coupent pas la discontinuité. Par contre, nous avons pu inverser les temps d'arrivée par la méthode d'Herglotz Wiechert et obtenir directement une valeur de la profondeur de la discontinuité. Cette étude a été faite sur des séismes de Turquie et des séismes de Méditerranée occi-

dentale. Les profondeurs trouvées, respectivement 607 et 628 km, sont en concordance parfaite avec les valeurs déduites de la carte, 610 et 630 km.

Cet exposé a été volontairement limité à une présentation de nos résultats plus qu'à une explication complète de la méthode qu'il est possible de trouver dans Mechler[2], Msseddi[3], et Plantet[4]. Nous nous permettons cependant d'insister sur l'importance de telles études qui, non seulement expliquent les temps d'arrivée, mais aussi les amplitudes des ondes sismiques, sujet habituellement peu abordé par les sismologues en raison de sa difficulté.

BIBLIOGRAPHIE

Ansorge J., Mayer-Rosa D. (1968) Evidence of velocity reversals within the Upper Mantle in Europe. *C.S.E.*, Leningrad.

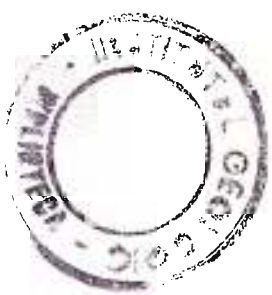

[2] Mechler P. Structure of a seismic velocity discontinuity at a depth of the order of 600 km. 1972. Bulletin du NORSAR (à paraître).

[3] Msseddi R. Structure du bas de l'asthénosphère sous la France. Implications sismotectoniques. 1972. Thèse. Université de Paris VI.

[4] Plantet J. L. Cartographie du bas de l'asthénosphère sous l'Europe occidentale. Vérifications sismologique. 1972. Thèse. Université de Paris VI.

DISPERSION OF RAYLEIGH WAVES IN MIDDLE EUROPE AND PHASE VELOCITY SPLITTING[1]

BY

HORST NEUNHÖFER, DOROTHEA GÜTH[2]

Abstract

The phase velocity of Rayleigh waves was investigated by a network of some seismic stations. It follows a mean phase velocity curve and a mean model of the Earth crust and the uppermost part of the upper mantle. The result is valid for the whole area of the network. With regard to the real discontinuities in the region under investigation the mean phase velocity curve is splitted by the use of a suitable mathematical algorithm into partial dispersion curves valid for suggestive parts of the investigation area.

For some years a network of seismic stations has been established in the region of the GDR having the special purpose to investigate the dispersion of seismic surface waves. The network described by Genschel, Neunhöfer, Teupser (1969) consists of eight stations, including the permanent seismic stations Moxa and Collm, the former second order stations Halle and Potsdam, and the especially added ones Berggießhübel, Pritzwalk, Oderberg, and Arkona.

It was planned to investigate mainly Rayleigh waves. As especially relatively short period waves are interesting for informations about the deeper Earth's crust and the upper mantle the middle period VSJ-I was chosen with the parameters $T_s = 20$ s, $T_g = 1.25$ s, $\alpha_s = 0.5$, and $\alpha_g = 8.0$. Using a suitable data processing it is possible to interprete surface waves principally up to a period of approximately 50 s.

The interpretation of the seismograms is basing on the principle of multiple bandpass filtering. After sampling the seismogram in steps of one second at first possibly existing sampling errors are eliminated. Then the filtering with digital Butterworth band pass filters is made. The band width of the filters is approximately one quarter of the middle period. Each of the filtered seismograms obtained so is treated by the Fourier

[1] Communication Nr. 291, Central Earth Physics Institute.

[2] Central Earth Physics Institute AdW der DDR, part Jena, 69 Jena, Burgweg 11, GDR.

technique for determining the Fourier amplitude and phase in a sliding window (N e u n h ö f e r, G e n s c h e l, 1970). The lenght of the window is equal to once or twice the middle period. The result is the time function of the Fourier amplitude and phase, which must be separated from disturbing oscillations caused by processing. The further interpretation yields

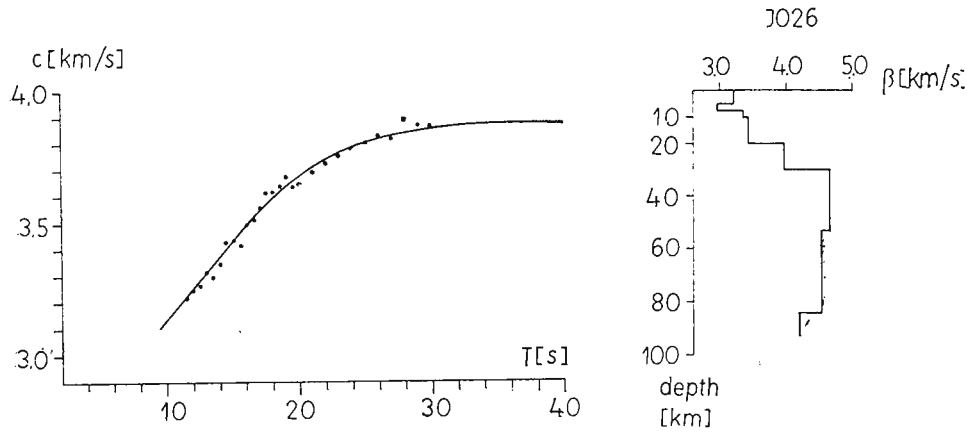

Fig. 1. — Phase velocity of Rayleigh waves.

the group velocity between focus and station and the phase velocity in a triangle. In all cases the azimuth to the focus coincides nearly with one side of the triangle. But for these relatively short periods the third station may not be neglected because the theoretical and the real azimuth often differ.

An advantage of this method is the possibility to recognize surface waves having propagated along multiple paths. Therefore it is possible to derive dispersion curves from different Rayleigh wave groups, that means some dispersion curves for one earthquake.

Altogether 15 dispersion curves are derived for different triangles, some of them for two or three different wave paths.

The mean dispersion curve found for the whole network is shown in figure 1. Only periods are used for which velocity values have been determined five times or more. The curve corresponds approximately to the curve known for the network around Stuttgart, in the south-western part of the FRG given by K n o p o f f, M ü l l e r, P i l a n t (1966). But there are some differences and it has been derived a model fitting our observed mean dispersion curve. It is the model JO26. The characteristic property of it is a depth of the Moho of about 30 km. Below the Moho-discontinuity the shear velocities are somewhat smaller than in the paper of K n o p o f f, M ü l l e r, P i l a n t (1966). In the crust the model has a low velocity channel in the depth of 10 km.

Now we leave out the assumption of an uniform structure under the whole network which fits the mean phase velocity results from all trian-

gles. We try to apply the crossing path technique for getting more details. For that reason the region under investigation must be subdivided into suitable sections and the phase velocity curve for each one must be recalculated. The most important tectonic line is the Elbe lineament which separates the North German Depression from the Mittelgebirge. Approxi-

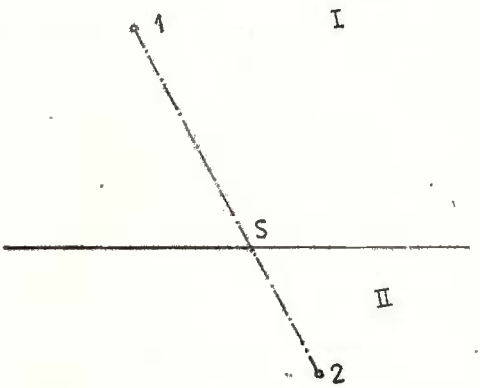

Fig. 2. — Drawing of the investigation area.

mating this tectonic element by a vertical plane it subdivides the whole area under investigation into two parts. A raw drawing is given in figure 2. The northern section is indicated by I, the southern one by II. A straight line connects the stations 1 and 2 which bound a side of a triangle. It crosses the dividing plane in S. For a given period the phase velocity is composed of two summands, which are proportional to the reciprocal velocities $v^{(1)}$ and $v^{(2)}$ in the sections I and II, respectively. The factor of proportionality p is equal to the normalized distance between the northern station and the crossing point S. If both stations are situated inside I p becomes 1 and $v = v^{(1)}$, but in the case that both stations are inside II p becomes 0 and $v = v^{(2)}$. For all other cases $0 < p < 1$.

If n earthquakes are observed we get for each period n equations

$$\begin{aligned} v_1 &= p_1 v^{(1)} + (1-p_1) v^{(2)}, \\ v_2 &= p_2 v^{(1)} + (1-p_2) v^{(2)}, \\ &\vdots \\ v_n &= p_n v^{(1)} + (1-p_n) v^{(2)}. \end{aligned} \tag{1}$$

From this system $v^{(1)}$ and $v^{(2)}$ follow by the method of least squares as

$$v^{(2)} = \frac{(\Sigma_i (1-p_i)\, v_i) / \Sigma_i p_i (1-p_i) - (\Sigma_i p_i v_i) / \Sigma_i p_i^2}{(\Sigma_i (1-p_i)^2) / \Sigma_i p_i (1-p_i) - (\Sigma_i p_i (1-p_i)) / \Sigma_i p_i^2} \tag{2}$$

$$v^{(1)} = (\Sigma_i p_i v_i - v^{(2)} \Sigma_i p_i (1-p_i)) / \Sigma_i p_i^2$$

The formulas are applied to the mean dispersion curve of the whole area. The result is shown in figure 3. For making clear, the starting observation is once more indicated by the theoretical dispersion curve JO26. The phase velocities obtained for both subregions for different periods have been drawn by different symbols. In the investigated period range

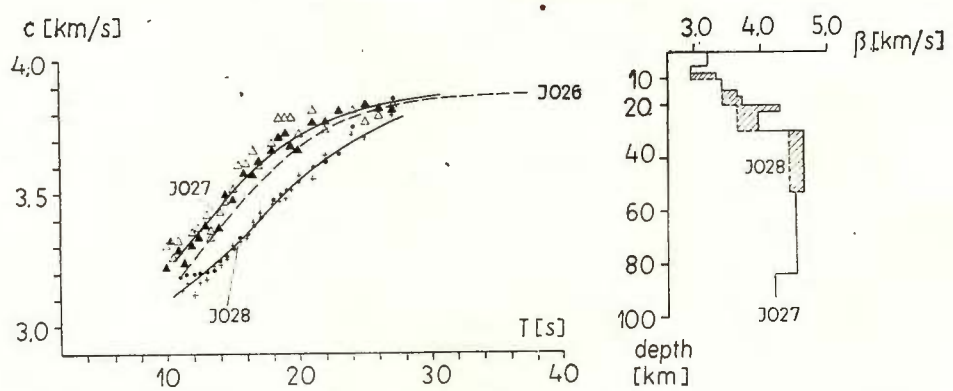

Fig. 3. — Splitted phase velocity curves.

the phase velocities of the southern area are all above the curve JO26, while the velocities of the northern one are clearly below it. For checking the reliability of these results the splitting has been made twice : first by using all phase velocity values (the results are the black triangles and the crosses) and secondly only with such phase velocities obtained purely in the adequate section (open triangles, dots). Though both calculations are not completely independent it follows from the good coincidence that the results are reliable enough.

The splitted phase velocity values are fitted by the models JO27 and JO28, respectively, shown also in the figure 3. The right contour of the velocity-depth function belongs to the model JO27 valid for the Mittelgebirge. It gives informations on possibly two low velocity zones of the shear velocity in a depth of approximately 10 and 25 km, respectively. The model JO28 valid for the North German Depression belongs to the left contour of the velocity-depth function. The upper low velocity channel seems to be more distinctly than in the southern case, the second one is absent. Up to the depth of around 60 km the shear velocity is somewhat lower than in the southern area. The shear velocity immediately under the Moho is in the northern part somewhat lower than in the southern one where it is already lower than in the Stuttgart region. This seems to be a general regional trend for that part of Middle Europe.

Finally we will give an outlook of a possible methodical improvement. One can increase the information of the phase velocity splitting if the discontinuity between the different sections is not fixed at the beginning. Supposing that each section has an uniform structure and that G_0 is a discontinuity there is valid $v^{(1)}(G) - v^{(2)}(G) = \max$ for $G = G_0$.

If G_0 is unknown an arbitrary discontinuity has to vary as long as this condition is true. The plane which fulfils this condition is the wanted G_0. It is a function of T. From it, there can follow possibly informations on the depth extension of the boundary.

REFERENCES

Genschel G., Neunhöfer H., Teupser Chr. (1969) Das Netz standardisierter seismologischer Stationen in der DDR. *Veröff. Inst. Geodynamik Jena, Ser. A*, 14, Jena.

Knopoff L., Müller St., Pilant W. L. (1966) Structure of the crust and upper mantle in the Alps from the phase velocity of Rayleigh waves. *Bull. Seism. Soc. Amer.*, 56, Berkeley.

Neunhöfer H., Genschel G. (1970) Beitrag zur Bearbeitung digital gefilterter Seismogramme im Bereich der kurzperiodischen Oberflächenwellen, *Gerl. Beitr. Geophys.*, 79, Leipzig.

CRUST-MANTLE VELOCITIES IN THE IBERIAN PENINSULA AND TECTONIC IMPLICATIONS OF THE SEISMICITY IN THIS AREA

BY

GONZALO PAYO [1]

Abstract

Twenty-five clear aftershocks of the earthquake of 1969 March 28 at the Azores-Gibraltar fracture are used to determine the crustal velocities between the epicentral zone and the standard stations TOL, MAL and PTO. These values, added to those previously obtained, make it possible now to provide a summary of crust-mantle velocities for the Iberian region; and a regional model for the crust and first layers of the mantle is tentatively presented.

The residuals of the deep earthquake on 1954 March 29 strengthens the idea of the existence of a low velocity channel for *P* waves in the asthenosphere, which seems to be of irregular thickness.

The recent seismicity of this region, mainly distributed along the Azores-Gibraltar-Algerie line and southeastern Spain, leads to the postulation of the existence of a small subplate (the Alboran subplate), which is considered to have formed part, in past times, of the large African plate.

INTRODUCTION

This paper presents, together with several new results, a summary of the last values obtained for the seismic wave velocities in the crust and in the first mantle layers for the Iberian peninsular area. All the work on velocity determinations discussed in this paper has been done in the last 10 years and most of it is based on the near earthquake or explosion phases, as well as on surface wave dispersion methods. The studies on group and phase velocity of surface waves give information about the thicknesses of the crust-mantle layers, the corresponding shear velocities and the characteristics of the low velocity channel in the asthenosphere, while the studies on *P* wave amplitudes and residuals have contributed to determine the deep structure under some Iberian seismological stations.

[1] Instituto Geográfico y Catastrál. Observatorio Central Geofísico. Toledo, Spain.

The interpretation of the present seismicity of this region, according to the new ideas on global tectonics, explains many of the features observed.

VELOCITIES FROM THE AFTERSHOCKS OF THE 1969 FEBRUARY 28 EARTHQUAKE

The strong earthquake of 1969 February 28, to the southwest of the Iberian Peninsula, produced a large number of aftershocks, which were clearly recorded on the short period instruments of the three standard stations Toledo, Málaga and Porto. Twenty-five of such aftershocks, with magnitudes between 4 and 5, have been selected.

The epicentres of these 25 aftershocks were computed independently, with the help of a computer program that selects the origin time and location producing the smallest P wave residuals at the nearby stations, for a discrete number of depths. All the clear onsets on the seismograms of the three components at Toledo, Málaga and Porto were read and the corresponding velocities computed. These velocities are plotted in a form of histograms in figure 1; thus, the identification of each phase, corresponding to each maximum, is made as a function of its velocity.

The velocities of the different phases, obtained directly from the histogram, are shown in figure 1. Almost all Pn phases at Toledo (and sometimes the Sn) are preceded by an onset of smaller amplitude than the main pulse. This could be interpreted in terms of a discontinuity close to and below the Mohorovičić discontinuity. These phases have been designated Pn_1 and Sn_1, though the difference in velocity between Pn and Sn is very small. There are only few onsets with velocity of Pg or Sg. Most of them correspond to Pn or Sn velocities.

The average velocities of all Pn and Sn observations at the three observatories are, respectively,

$$v\,(Pn) = 7.54 \pm 0.08 \text{ Km s}^{-1}$$

$$v(Sn) = 4.41 \pm 0.06 \text{ Km s}^{-1}$$

Similarly the histograms for Toledo and Porto give, as average velocities for P^* and S^*,

$$v(P^*) = 6.72 \pm 0.08 \text{ Km s}^{-1}$$

$$v(S^*) = 3.71 \pm 0.14 \text{ Km s}^{-1}$$

We consider that these values are not affected by the velocities assumed in the program for the crust and upper mantle, since the program operates with a different velocity ($v(Pn) = 8.0$ Kms^{-1}). In addition, the parameters have been calculated independently for each after-shock; consequently the well-defined maxima in the histograms are really significant.

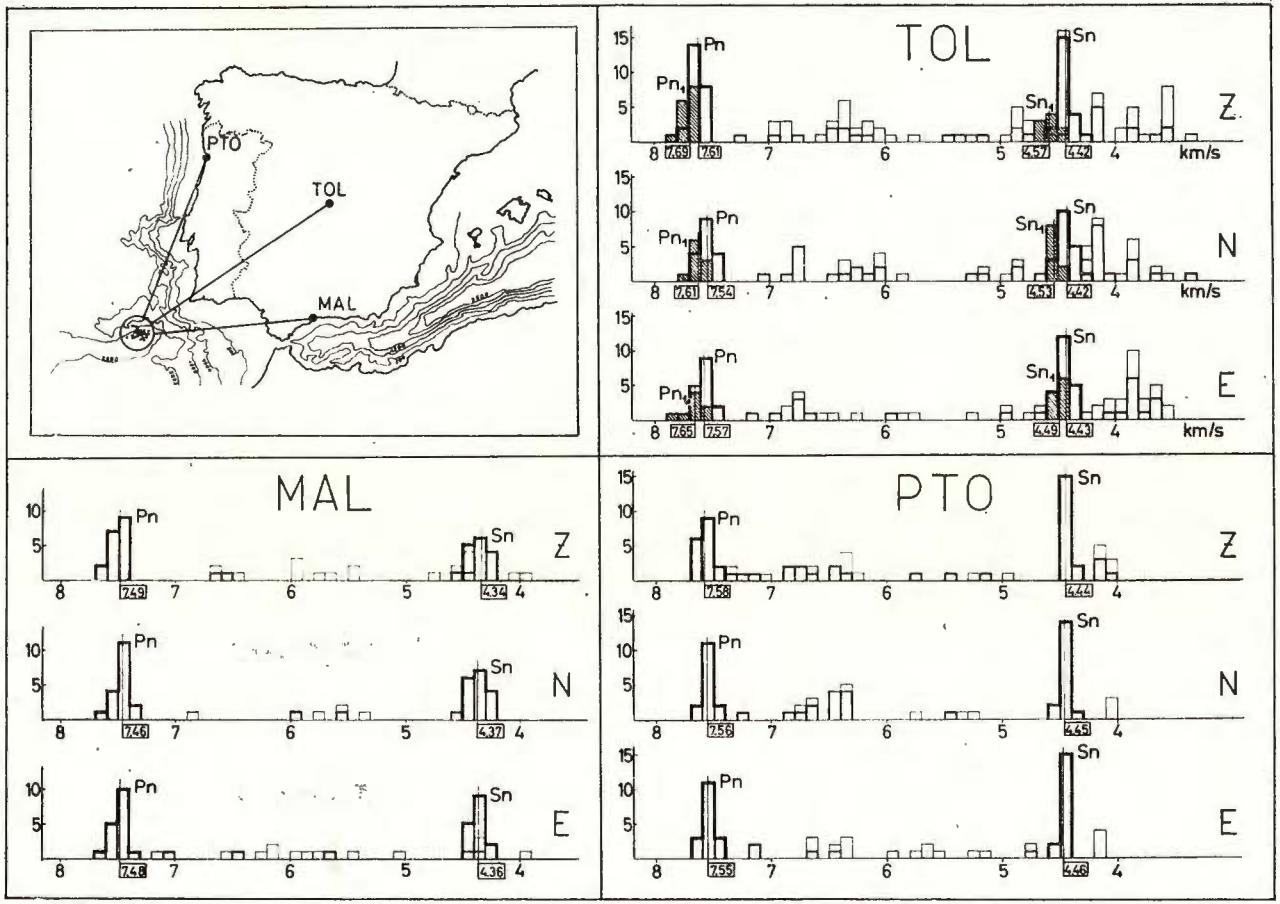

Fig. 1. — Velocity histograms of the crustal phases for the aftershocks of the earthquake of 1969 February 28.

VELOCITY DATA IN THE PENINSULAR AREA

Figure 2 summarizes the results about thicknesses and velocities of the first 100 km of crust and upper mantle, obtained during the last few years.

The models with thicknesses and velocities are, in the main, those determined by surface wave dispersion methods (P a y o, 1970) which

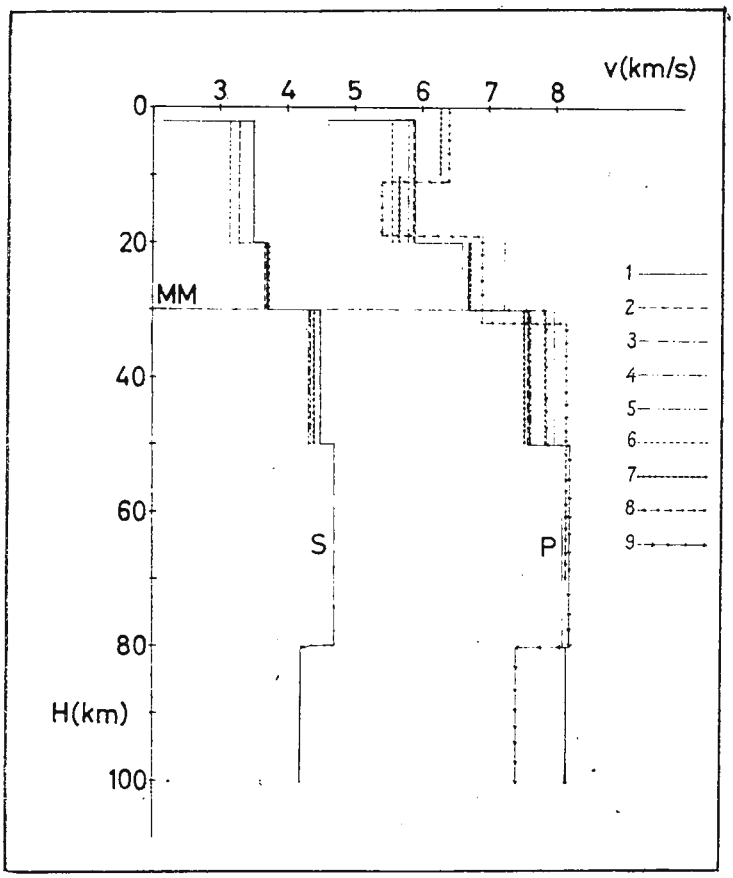

Fig. 2. — Summary of crust and upper mantle velocities so far obtained in the Iberian Peninsula area :

1, P a y o, 1970; 2, P a y o, 1964; 3, P a y o, 1964; 4, P a y o, 1962; L ó p e z - A r r o y o, P a y o, 1966; 6, C a l d e r ó n, 1969; 7, P a y o, 1972; 8, M e n d e s, S o u s a - M o r e i r a, M u e l l e r, 1971; 9, P a y o, 1971.

are generally valid for shear waves. The thicknesses based on P wave velocities are those obtained in the study of P wave residuals (P a y o, 1971); they concern only the structure beneath the stations. M u e l l e r et al. (1971) have obtained a crustal model, with a low velocity channel

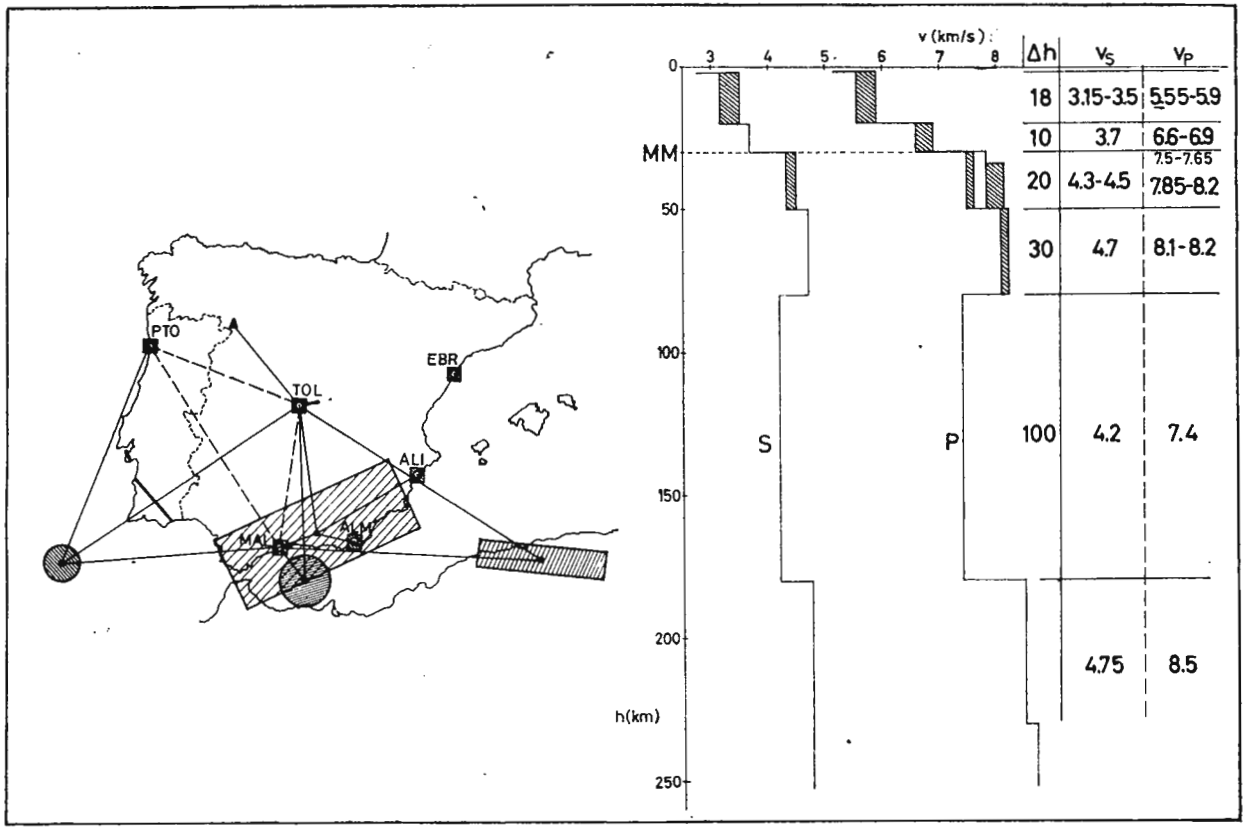

Fig. 3. — The map indicates approximate profiles and zones concerning which some velocity data are available. A crust-mantle model summarizing the P and S velocity structure, is also shown.

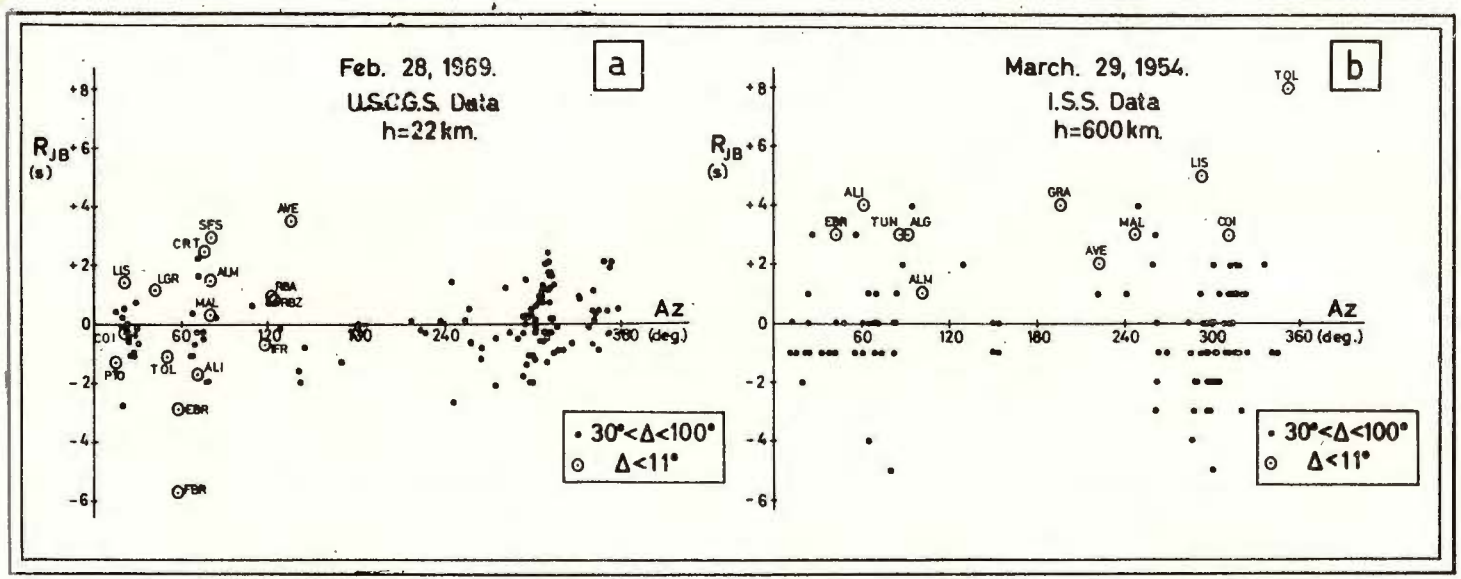

Fig. 4. — Residuals from the shallow earthquake on 1969 February 28, (a), and from the deep earthquake on 1954 March 29 (b).

in the base of the granitic layer, by means of a refraction profile between Fuzeta and Sines to the south-west of Portugal. These data also appear in the figure. The rest of the lines refer to the above thicknesses, so they only represent average values of velocity in the crust-mantle layers. Most of these velocities are based on the travel time slopes of the main crustal phases (P a y o, 1962, 1964; F l o r e s, 1969). Figure 2 also shows the *Pg* and *Sg* velocities obtained for one small segment between Toledo Observatory and the Yepes quarry, where explosions were controlled to determine the velocity in the first crustal layers (L ó p e z A r r o y o, P a y o, 1966). N u t t l i (1954) made a *P* velocity determination (v = 10.37 km s^{-1}) at 655 km depth beneath the hypocentre of the Spanish deep earthquake of 1954 March 29 but the relative data do not appear on figure 2. Finally, the velocities here studied from aftershocks of the earthquake of 1969 February 28, have been included in the summary of figure 2. Figure 3 shows the stations and approximate profiles below which we have some information on thicknesses or velocities. As will be seen, the data concerning the northern half of the Peninsula are very scanty. This is mainly due to the absence of stations and earthquakes in this region. Therefore, an average model based on all these data only should represent the structure for the southern half of the Iberian Peninsula.

At the right side of figure 3, a crust-mantle model for the Iberian Peninsula area is shown; this is based on all the results here considered. The hatched part represents the variation of the velocity results that we have analysed. The layer thicknesses seem to be well defined and the crustal velocities vary between narrow limits. In the mantle, below the Moho, the slight disagreement between the data can be interpreted in terms of the effect of a first layer of 20 km thickness, with a velocity about 7.60 km s^{-1}, overlapping another of larger velocity (about 8.10 km s^{-1}), below which the low velocity channel of the asthenosphere begins.

FURTHER VELOCITY OBSERVATIONS

The notable deep earthquake of 1954 March 29 provides data also for some conclusions relative to the upper mantle velocities beneath the Iberian Peninsula.

If we plot the *P* residuals of this earthquake (obtained from the ISS Bulletin and using the J e f f r e y s-B u l l e n travel times), it is apparent [fig. 4(b)] that the residuals for stations at epicentral distances larger than 30°, are distributed symmetrically around the zero line, as it is to be expected ted. However, all the residuals for the stations close to the epicentre ($\Delta < 11°$) are positive. A systematic difference between the real travel times and those from J-B tables is generally compensated for in the origine-time computations, but the distribution of residuals remains almost unaffected. Therefore this difference between the local residuals and the others is clear evidence that, in this first 600 km of the mantle, a low velocity channel exists in the region. A different result is obtained with the residuals of another strong, but shallow, earthquake in this area: that of 1969 February 28, where the residuals for the near stations behave exac-

tly the same as those for distant stations [fig. 4(a)]. Thus the asthenosphere shows clear signs of a low-velocity channel for P waves as is observed for shear waves. Our previous study of P wave residuals supports this fact and the form and dimensions of this channel were there pointed out. We consider that the low velocity and the thickness of this channel

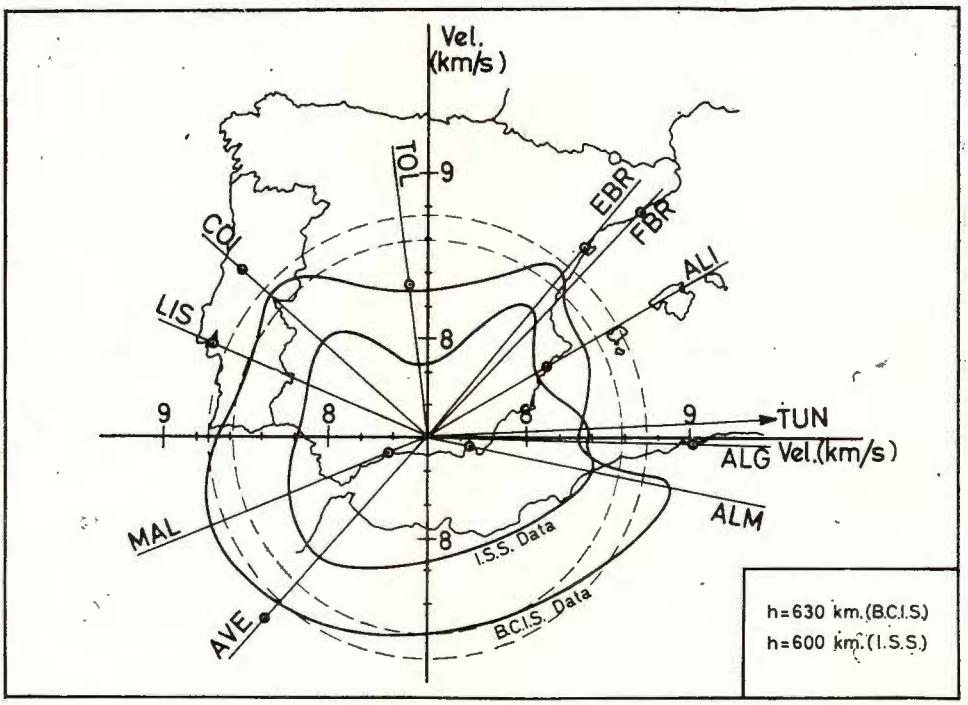

Fig. 5. — Average P wave velocity from the hypocentre to station for some stations near the epicentre of the deep earthquake on 1954 March 29. Velocities reduced to the distance from Ep. to TOL.

must be fairly important to produce these residual differences, rising up to about three seconds [Fig. 4 (b)].

On the other hand, it has also been pointed out (P a y o, 1971) that this low velocity zone does not seem to be bounded by horizontal planes. This asymmetry is also manifested in the data of the deep earthquake. In figure 5, the average velocity hypocentre to station for the stations near the epicentre is shown. Two different epicentral determinations (BCIS and ISS), giving slightly different parameters, have been used. To make the velocities comparable they have been normalized to a unique distance, the one corresponding to Toledo, and the values have been joined with a continuous line. As the figure shows, the velocity for the observatories in the N-N.E. region is, in the two determinations, about 0.3—0.4 km s^{-1} smaller than the remaining velocities. An explanation of

this fact may be that the seismic rays from the hypocentre to those stations has a larger path through the low velocity channel. In the other directions the thickness of the channel might be modified by the effect of a lithospheric slab introduced into the upper mantle and then dropped up to the low asthenosphere.

SEISMICITY AND TECTONICS OF THE REGION

The seismic activity of this region is small by comparison with the large seismic zones of the world. In the Iberian Peninsula area, about 250 earthquakes a year are being recorded, most of them with a magnitude less than 5, though exceptionally large earthquakes have been produced in the Azores-Gibraltar fracture. In figure 6, a sample of the recent seismicity has been drawn; this includes all the epicentres located by the Seismological Service I.G.C. (Madrid) from 1950 up to date and contains data from the Spanish, Portuguese and North African stations. All epicentres have been located by geometrical procedures, but the computation was repeated numerically by a least squares program when the number of recording stations were sufficient. As can be seen in the figure, the seismicity of this zone mainly corresponds to the line Azores-Gibraltar-Algerie but its extension through the Alboran Sea up to the Nap Cape, covering all the south-eastern part of Spain is very significant.

To try to explain this seismicity it is useful to note the influence that the displacements of the large plates have had on this small region. As a matter of fact any interaction of the Euroasiatic and African plates is a consequence of the relative motion between the two plates, therefore we can disregard the northwards motion that they had together as forming an unique block (D i e t z, H o l d e n, 1970).

In figure 7 we represent schematically the different phases of the relative motion of the two plates, at both Atlantic sides, from the beginning of its opening some 200 My ago. In these drawings it is intended to co-ordinate the evolution of the Mediterranean tectonic (M c K e n z i e, 1970; H s ü, 1971) with the global movements of the large plates (D i e t z, H o l d e n, 1970).

In the initial situation of Pangea (fig. 7 (a)) we can admit with H s ü the Italy-Greece-Sicily ensemble formed a salient of the African plate, strongly compressed, together with Corsica and Sardinia, against the east side of the Iberian Peninsula. On the other hand, in the least squares fitting of the continents to form the Pangea (B u l l a r d, 1969), an overlap appears between the present Iberian peninsula limits and the North Africa lands. This points to the possibility that another small salient of the African plate was joined in the beginning to the old Iberian

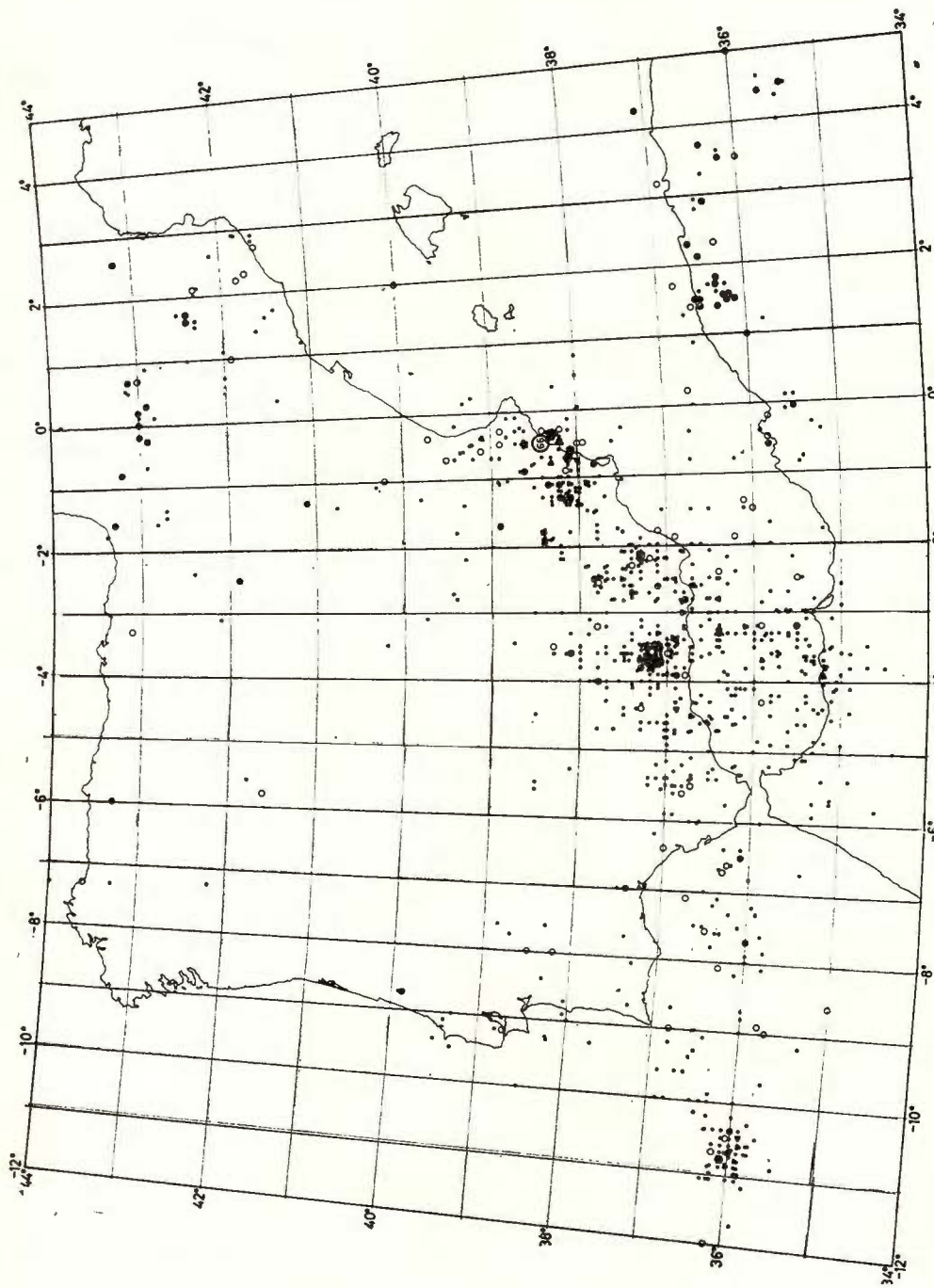

Fig. 6.— Located epicentres in the Iberic region from 1950 up to 1972. The number within the small circle represents the number of shocks located on this point.

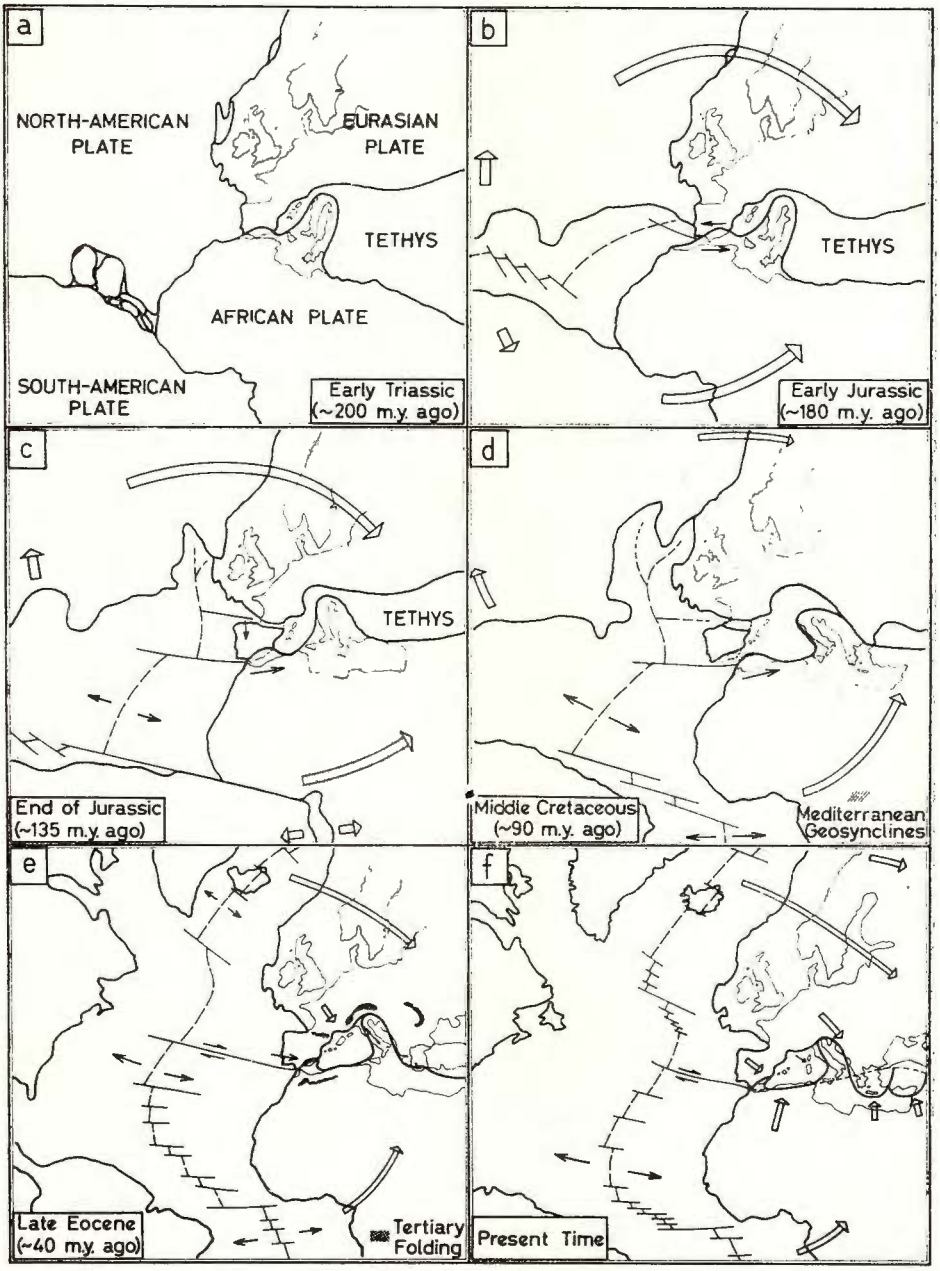

Fig. 7. Tectonic evolution of the Mediterranean zone, as a consequence of the Atlantic opening and the corresponding interaction of the Euroasiatic and African plates.

shield [fig. 7 (a)]. Then, the Tethys was a wide sea placed between the two plates.

With the Middle Atlantic opening along all the Triassic period [fig. 7(b)], North America and Eurasia rotate clockwise as a unique plate, while South America and Africa rotate in the contrary sense. This made the Iberian Peninsula begin to move towards the West relative to Africa ; the Italo-Greek ensemble initiated its separation and the Tethys began to be closed. At the end of the Jurassic [fig. 7(c)], the Middle Atlantic opening continued, and Africa followed its eastward motion. The interaction of this motion with the Iberian Peninsula caused its counterclockwise rotation (some 35°) and, consequently, the opening of the Bay of Biscay. During the next 40 My, that is up to the middle Cretaceous approximately, the rupture and separation of the South American and African plates, with the rapid formation of the South Atlantic Ocean, produced a wide displacement of the African plate towards the east and a simultaneous counterclockwise rotation. As a consequence of this motion, the Iberian Peninsula reached its most westward position, its separation from the Italian-Greek block increased notably and the large geosynclines, Betic and Pyrenees on one side and Alpine and Apennine on the other, were formed. At this time Corsica and Sardinia still remained joined to the western side of the Iberian Peninsula (H s ü, 1971). About this period the western Tethys side was almost closed and the opening of the North Atlantic Sea, in the direction of Greenland, began.

From middle Cretaceous to late Eocene, the opening of the North Atlantic with the separation of Greenland from America and Europe, and the counterclockwise rotation of Africa caused by the widening of the South Atlantic, produced a strong compression of the Euroasiatic and African plates. This thrust gave rise, in the Mediterranean region, to the folding of the accumulated sediments in the geosynclines, thus creating the Betic-Rif, Pyrenees, Alpine and Apennine mountains [fig. 7(e)]. As the eastward motion of Eurasia was faster than that of Africa, the Iberian Peninsula then moved rapidly eastward along the Azores-Gibraltar fracture, approaching its present position. This movement could produce an underthrusting of lithospheric material, possibly dropped later up to the low asthenosphere, which could be the reason for the scarcity of deep seismicity which has been represented, up to the moment, only by the notable Spanish earthquake of 1954 March 29. On the other hand, this eastward motion strongly compressed the assumed salient of the African plate, accreting its north side with the Betic foldings and deforming it towards the east as is shown schematically in figures 7(e) and (7f).

Finally, this motion has continued from the Eocene up to the present, and it has been during this period when Corsica and Sardinia seem to have rotated counterclockwise approaching Italy. The genesis of the

western Mediterranean as an opening of a large geosyncline between the African and Euroasiatic plates, as well as this late rotation of the Corsica-Sardinia block, leaving in the rear a deep oceanic basin without signs of any ridge, are features still not clearly understood. In any event, the hypothesis presented here to account for the present seismicity of the south-east of the Iberian Peninsula, which is similar to that of H s ü to explain the Greco-Italian rotation, premises that the interaction of two plates, strongly compressed and having a tangential relative motion can deform the contact border, which seems fairly logical. Extending these ideas a little further, it could be allowed that the large eastward displacement of Eurasia relative to Africa in the last 40 My might have produced the rupture, along the base, of the salients of the African and Euroasiatic plates. The resultant fracture line might be considered as the prolongation of the Azores-Gibraltar fault through North Africa, north of Greece and Turkey, as is shown in figure 7 (f). In this way, four small plates with active borders are formed : the Alboran and Italy subplates, belonging formerly to the African plate and the Aegean and Turkey subplates (M c K e n z i e, 1970) that were included in the Euroasiatic plate. At present, the focal mechanism of the earthquakes of the Azores-Gibraltar fracture (U d i a s, L ó p e z-A r r o y o, 1972) clearly indicates an eastward motion of Eurasia relative to Africa that, at the south of the Iberian Peninsula, tends to be changed in underthrusting of the Iberian block below the African plate.

This more irregular limit of the Euroasiatic and American plates, which includes the existence of small intermediate subplates, can explain some of the observed features. For instance, the deep earthquakes at the Lipari are suppose an intrusion of the African plate below Sicily and the South of Italy, which cannot be explained if we do not consider the old Italian-Greek salient as separated from the African plate and forming now a small subplate. Similarly, the Aegean earthquakes suppose an underthrusting of the African plate below the Aegean and Turkey subplates.

Concerning the Alboran subplate, already suggested from the geological study of the Betic and Rif Cordilleras (A n d r i e u x, F o n t b o t e, M a t t a u e r, 1971) this genesis of considering the subplate as the excision of a salient of the large African plate, previously deformed by the eastward thrusting of the Iberian Peninsula, explains fairly well the weakest part of the geological model, i.e. the present seismicity and its sudden interruption at the Nao Cape and at the western side of the Alboran Sea. Figure 8 shows what can be the present situation of the Alboran subplate in relation to the seismicity and the fracture line Azores-Gibraltar-Sicily.

By this train of ideas, we could also explain the present seismic zones of the Pyrenees and some others, less significant, below them (hat-

ched areas in the figure)) as tensional zones produced by the dificulty of the Iberian block to follow the eastward motion of Eurasia, due to the continuous collision of the Spanish southeastern against the African plate. Dietz, Holden, (1970) in their vision of the future global tectonic

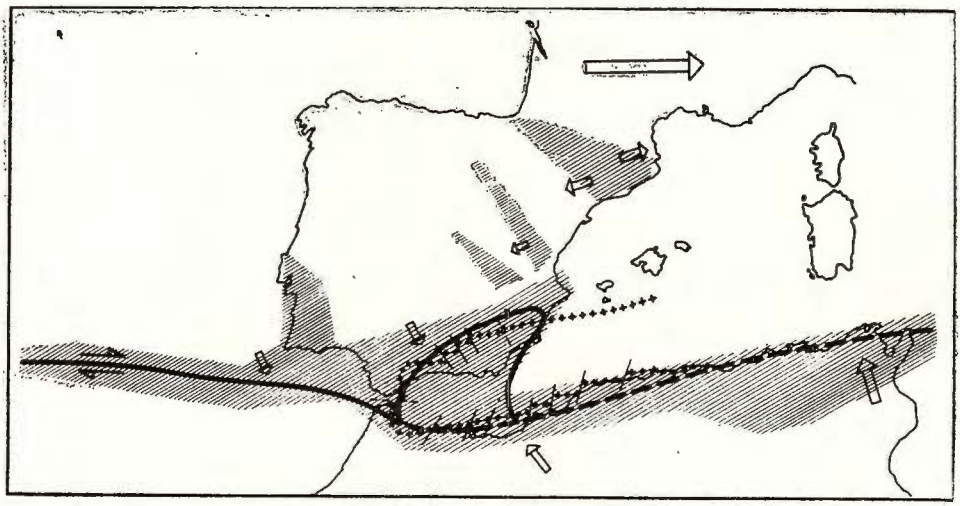

Fig. 8. — Explanation of the active seismic zones in the Iberic region in terms of a small sub-plate (thick contour), that is considered to have once formed part of the large African plate (see the text). The crossed line represents this Alboran sub-plate as pointed out by Andrieux et al. (1971).

seems to support the idea of a possible excision of the Iberic block from the rest of Europe by a mechanism similar to that pointed out here.

To confirm these hypotheses, which are based mainly on the form of the seismicity, it would be interesting to know the focal mechanism of the small earthquakes in the Pyrenees and in the Spanish south-eastern, which are at present unknown, partly because of their small magnitude. Future geological and geophysical studies will undoubtedly bring new data to improve our knowledge of the complicated Mediterranean tectonic.

REFERENCES

Andrieux, J., Fontbote, J. M., Mattauer, M. (1971) Sur un modèle l'Arc de Gibraltar, *Earth Planet. Sci. Lett.*, 12, Amsterdam.

Bullard, E. C. (1969) The origin of the oceans, *Scient. Am.*, 221, New York.

Dietz R. S., Holden, J. C. (1970), The breakup of Pangean. *Scient. Am.*, 223, New York.

Flores Calderón J. L., (1969) Dromocrónicas medias para el área de la Peninsula Ibérica. *Rev. Geofis.*, 28, — Madrid.

Hsü, K. J. (1971) Origin of the Alps and Western Mediterranean, *Nature*, 233, London.
López-Arroyo A., Payo, G. (1966) Crustal Structure of the Spanish Central Plateau. *IX Eur. Seism. Con.*, Copenhagen.
McKenzie, D. P. (1970) Plate tectonics of the Mediterranean region, *Nature*, 226, London.
Mueller S., Mendes A., Prodehl. C., Moreira, V. S. (1972), Deep-seismic sounding experiments in the Iberian Peninsula. *Geophys. J. R. astr. Soc.* 29, London.
Nuttli, O. W. (1954) The velocity of *P* and *S* waves at approximately 650 km depth as determined from the Spanish earthquake of March 29, 1954. *Earthq. Notes*, XXV.
Payo. G., (1962) El notable sismo de Zamora del 10 de Febrero de 1961. *Publ. Inst. Geográfico y Castastral*, Madrid.
— , (1964) Crustal phases across the Iberian Peninsula Region, *Ann. Geofis.*, 17, Roma.
— ,(1970) Structure of the crust and upper mantle in the Iberian shield by means of a long period triangular array. *Geophys. J. R. astr. Soc.*, 20, London.
— ,(1971) Estudios de los residuos y de las amplitudes de la onda *P* en algunas Estaciones Sismológicas Ibéricas. *Rev. Geofis.* 31, Madrid.
Udias, A., López, A. (1972) Plate tectonics and the Azores-Gibraltar region. *Nature*, 237r London.

STRUCTURE DU MASSIF CENTRAL FRANÇAIS

PAR

GEORGES PERRIER, J. C. RUEGG[1]

En 1970, pour sa première campagne, l'opération „Grands Profils Sismiques"[2] réalisait des sondages sismiques profonds dans quatre régions, géologiquement distinctes, du Massif Central français. En effet, au moment où s'achevaient les expériences internationales de Sismologie expérimentale dans les Alpes occidentales, un certain nombre de profils sismiques étaient réalisés, dans la partie Est du Massif (1962—1967). Il importait donc d'étendre l'étude structurale aux parties centrale et occidentale avec un appareillage homogène et une densité de tirs et de stations d'enregistrement plus importante.

Schématiquement, comment se présente le Massif Central? C'est un fragment de la chaîne hercynienne dont le plissement se situe vers la fin du Paléozoïque. Actuellement, il se présente comme une vieille pénéplaine antétriasique qui a été déformée, d'une part au Jurassique où une transgression marine a recouvert une large partie du Massif, d'autre part à l'Oligocène où sont apparus de grands fossés de subsidence tels que les Limagnes. Simultanément, une activité volcanique se développait en Limagne pour prendre une grande extension au Miocène, au Pliocène et surtout au Villafranchien avec l'édification de grands massifs volcaniques (Cantal, Monts-Dore, etc.). A la fin du Villafranchien, le Massif subissait une surélévation générale avec inclinaison vers l'ouest. Enfin, au quaternaire récent, s'édifiait la chaîne volcanique des Puys.

D'un point de vue gravimétrique [3], la carte des anomalies de Bouguer nous montre que, si le principe de l'isostasie s'applique bien au Massif Central, l'anomalie isostatique moyenne calculée pour la région centrale est de + 25 mgal. Si on tient compte de l'age du socle, il est difficile de

[1] Institut de Physique du Globe-Tour 14. Laboratoire de Sismologie. Université de Paris 6—11, quai Saint-Bernard. 75230-Paris ,France.

[2] Hirn A., Ruegg J. C. Méthodes d'enregistrement des grands profils en France, 1972. CSE, XIII e Assemblée générale. Braşov. (Sous presse)

[3] Aubert M., Perrier G. Structure profonde du Massif Central. 1971. Symposium J. Yung : Géologie, Morphologie et Structure profonde du Massif Central Français. Ed. Scientifiques, Clermont-Ferrand. (sous presse)

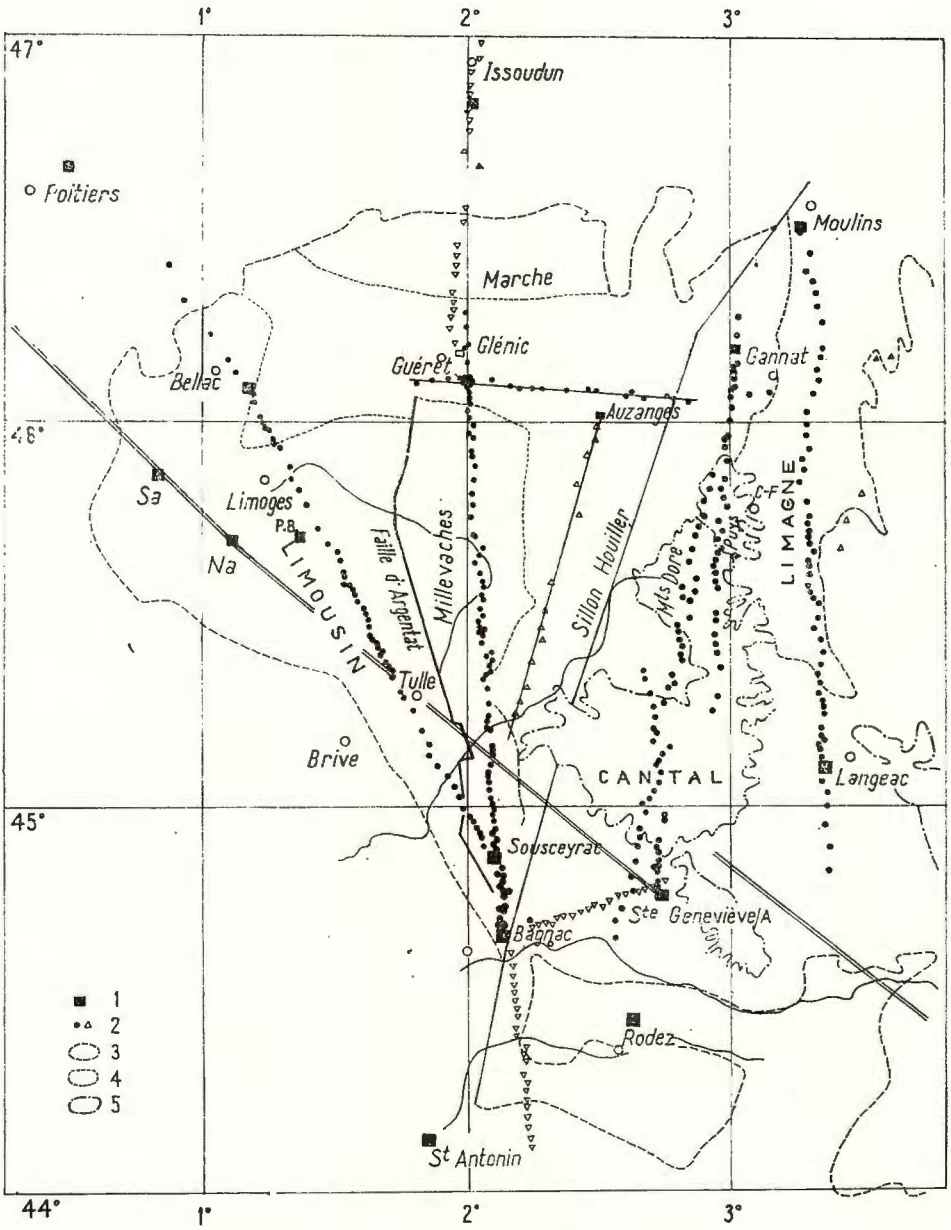

Fig. 1. — Grands profils sismiques réalisés en 1970 dans le Massif Central Français :
1. Point de tir ; 2. Station d'enregistrement ; 3. Limite du socle cristallin ; 4. Limite de régions granitiques ; 5. Limite de terrains volcaniques.

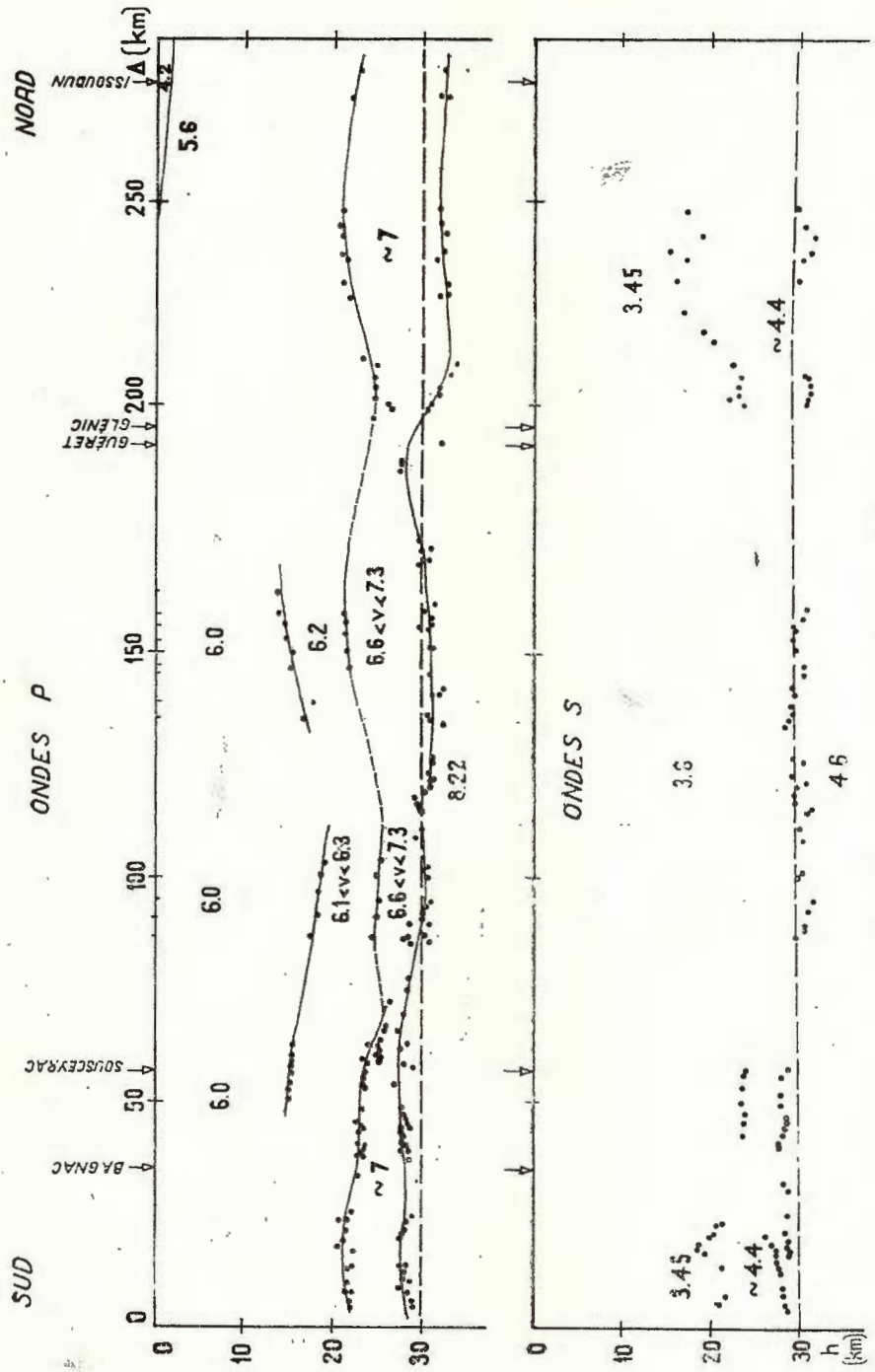

Fig. 2. — Coupe structurale du plateau de Millevaches.

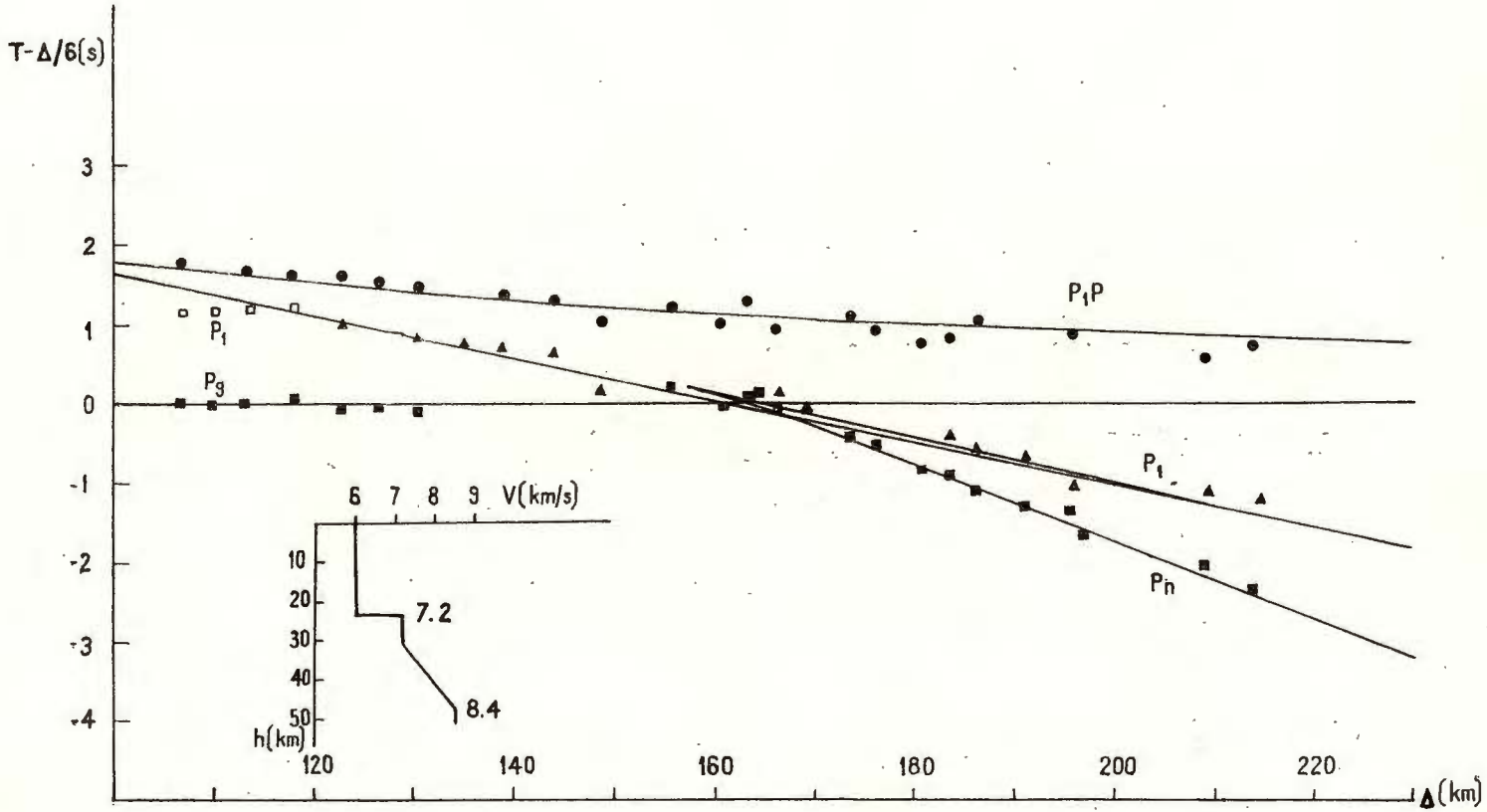

Fig. 3. — Loi de vitesse V(z) et hodochrone sous les Volcans d'Auvergne ;
1, phase observée ; 2, hodochrone calculée

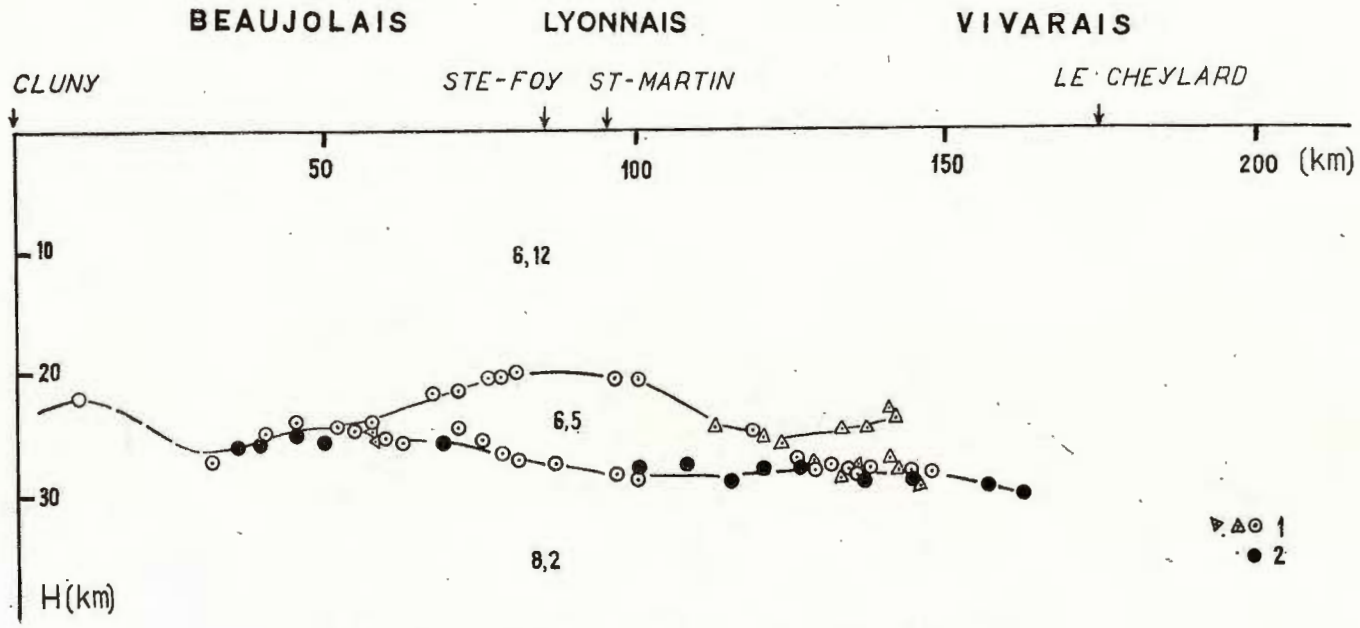

Fig. 4. — Coupe structurale sous la partie Est du Massif Central :
1, Réflexion; 2, Réfraction

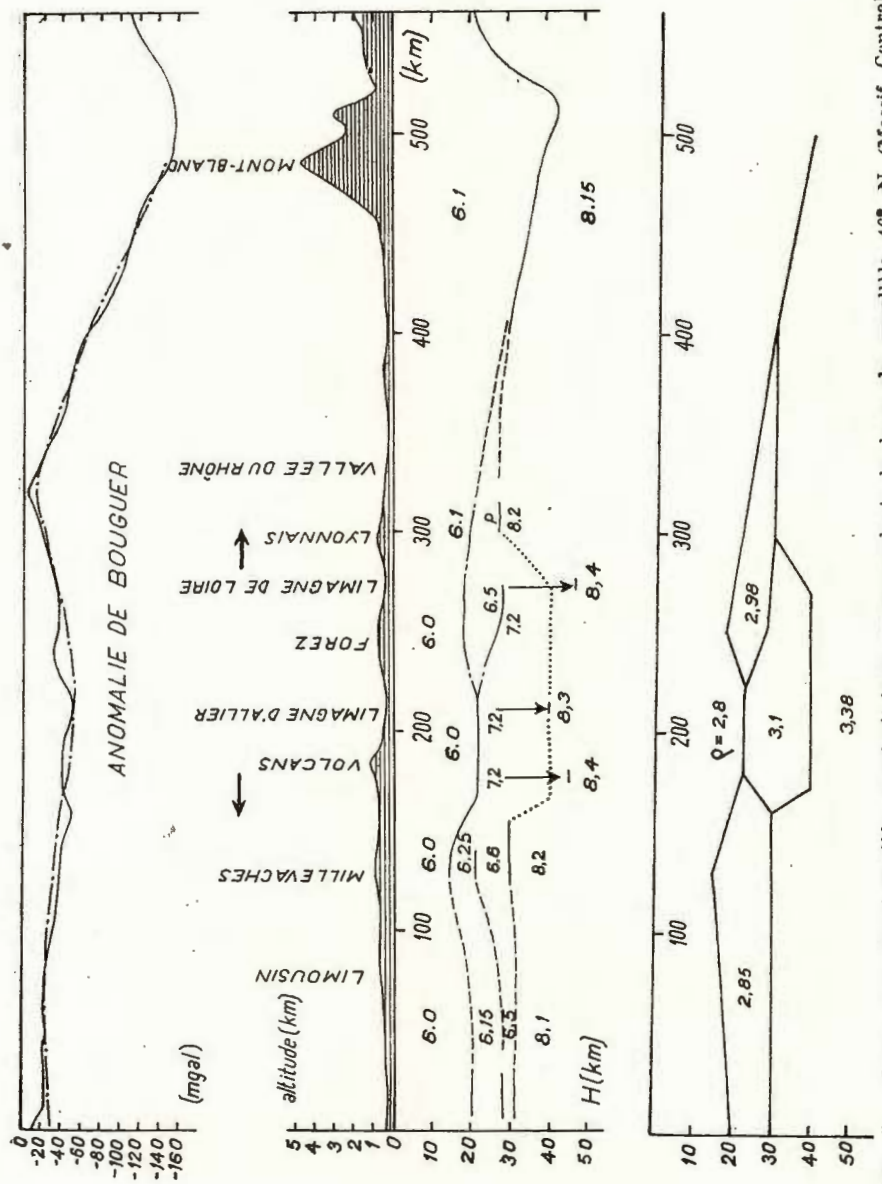

Fig. 5. — Coupe sismique et modèle gravimétrique correspondant, le long du parallèle 46° N (Massif Central et Alpes).

lui attribuer un état de déséquilibre isostatique. Cet excès de pesanteur peut donc provenir d'un relèvement général du substratum plus lourd de l'ouest vers l'est. Signalons aussi qu'une continuité de structure apparaît sur la bordure Est alors qu'elle n'existe pas à l'Ouest

En 1970, les profils furent situés dans les quatre régions suivantes (d'Est en Ouest) (fig. 1) : le socle métamorphique (micaschistes et gneiss) du Limousin, le socle granitique du plateau de Millevaches, la zone volcanique du Cantal, des Monts Dore et de la chaîne des Puys, le fossé d'effondrement de la Limagne. Les méthodes d'enregistrement et d'interprétation sont définies par Ruegg, Hirn, Perrier[4,5]. Deux types principaux de structure furent mis en évidence : l'un, dans le Limousin et le Millevaches (fig. 2) où la croûte apparaît constituée de couches successives de vitesses moyennes 6,0—6,2 et 7,0 km/s, la discontinuité de Mohorovičić surmontant un manteau de vitesse 8,2 km/s étant située vers 30 km de profondeur en moyenne ; l'autre, sous les Volcans (fig. 3) et la Limagne [6], où la discontinuité de Mohorovičić est remplacée par une zone de transition, épaisse de 15 à 23 km, où la vitesse des ondes P passe de 7,2 (25 à 22 km) à 8,4 km/s (40 à 45 km). Dans le premier cas, les ondes de grande amplitude sont les ondes réfléchies sur le Moho ; dans le second cas, elles correspondent à des ondes réfléchies sur une discontinuité intermédiaire, séparant des milieux de vitesses 6—6,3 et 7,2 km/s.

A l'Est du Massif, des profils réalisés en 1972 sous le Beaujolais, le Lyonnais et le Vivarais ont montré que la croûte était moins épaisse qu'à l'Ouest (27 km) et qu'une couche intermédiaire de vitesse 6,5 km/s existait vers 20 km de profondeur (fig. 4). Cette couche semble prolonger vers l'Est celle mise en évidence sous le Forez (Perrier, 1963), horst situé entre les deux grabens des Limagnes d'Allier (appelée plus simplement Limagne) et de Loire (bassins de Roanne et du Forez). Mais, en profondeur, alors que la structure déterminée au Nord de la Limagne de Loire [7] présente de grandes analogies avec celle qui est trouvée sous la Limagne d'Allier, sous le bordure Est, on retrouve un manteau supérieur normal de vitesse 8,2 km/s.

Une synthèse de tous ces résultats résumés très brièvement, est schématisée dans une coupe Est — Ouest du Massif Central à la latitude de 46°N (fig. 5) : au centre de la figure, la coupe structurale met en évidence principalement une zone de manteau anormal, large de 150 km, centrée sous les deux fossés d'effondrement des Limagnes. De part et d'autre, on retrouve une structure de croûte et de manteau supérieur plus classique, avec cependant une discontinuité de Mohorovičić moins profonde à l'Est (27 km) qu'à l'Ouest (30 km) ; dans la partie inférieure de la figure, nous proposons un modèle gravimétrique, correspondant à la structure

[4] *Op. cit.*, p. 2.

[5] Ruegg J. C., A. Hirn, G. Perrier. Aperçu sur quelques problèmes d'interprétation. 1972. CSE, XIII-e Assemblée générale. Braşov.

[6] Hirn A., Perrier G. Deep seismic sounding in Limagne graben, in Approaches to Taphrogenesis, Karlsruhe. 1972 (sous presse)

[7] *Op. cit.*, p. 3.

sismique trouvée. La correspondance empirique entre les vitesses et les densités est celle de Nafe et Drake. Dans la partie supérieure, l'anomalie calculée (points-tirets) est comparée avec l'anomalie de Bouguer observée (trait plein). On remarque que la compensation isostatique s'explique au seul niveau de la croûte. Cela rejoint les résultats obtenus récemment pour les Alpes par Mueller et Talwani (1971).

Ainsi, est mise en évidence, sous le Massif Central Français, une structure profonde caractéristique d'une zone en extension, en équilibre isostatique, qui a débuté à l'Oligocène avec un bombement général du Massif, accompagné de la formation des rifts de Limagne. On retrouve également, au niveau du Moho, l'inclinaison du Massif vers l'Ouest, à la fin du Villafranchien, confirmant ainsi l'excès de pesanteur de + 25 mgal observé.

BIBLIOGRAPHIE

Perrier G. (1963) Ondes séismiques enregistrées dans les monts du Forez. *C.R.A.S.*, 257, Paris.

Mueller S., Talwani M. (1971) A crustal section across the Eastern Alps based on gravity and seismic refraction data. *Pure Appl. Geophys.*, 85, Basel.

STRUCTURE DE LA CROÛTE DE LA BRETAGNE AU MASSIF CENTRAL

PAR

MARTINE SAPIN, CLAUS PRODEHL [1]

En septembre 1971, dans le cadre des expériences en France de l'Opération "Grands Profils Sismiques", un profil qui s'étend de la Bretagne à la Provence a été réalisé en collaboration avec des géophysiciens allemands, suisses et protugais.

Le premier but de l'expérience était d'étudier la structure du manteau supérieur en enregistrant des ondes propagées jusqu'à 1100 km à partir de tirs en mer au large de Brest et de Toulon.

La ligne Brest-Toulon (fig. 1) a été choisie car elle est située en majeure partie sur des affleurements de terrains du socle: régions granitiques et métamorphiques de Bretagne. Vendée, Massif Central et Maures. Un recouvrement sédimentaire n'influence les observations que dans la vallée du Rhône.

Des tirs en forage de 0,8 et 2,4 tonnes à Blain, Limoges et Florac divisant la ligne en profils de 220 à 300 km de long, ont été exécutés pour permettre l'étude de la croûte terrestre par des profils inversés. Soixante stations homogènes espacées de 3 à 5 km étaient placées sur le terrain pour chaque tir.

Ce rapport donne des résultats sur la structure de la croûte le long de la ligne entre la Bretagne et le Sud du Massif Central.

En ce qui concerne les premières arrivées jusqu'à 100—130 km qu'on appelle ondes *Pg*, il est important de disposer sur le profil des stations d'enregistrement peu espacées avec un rapport signal/bruit suffisant pour déterminer avec précision les temps de propagation pour deux raisons :

a) Les hodochrones des ondes *Pg* se propageant dans la partie superficielle de la croûte permettent la mesure de la vitesse sismique des roches dont l'interprétation peut être reliée dans certains cas à la géologie locale.

[1] Institut de Physique du Globe-Tour 14. Université de Paris 6—11, quai St. Bernard. 75230. Paris, France.

b) Pour le calcul des modèles de la croûte intermédiaire et profonde, la valeur de la vitesse des ondes en surface détermine indirectement la loi de vitesse au-dessus du premier réflecteur.

Il est important de bien connaître cette valeur pour discuter la présence d'une inversion de vitesse dans la croûte supérieure.

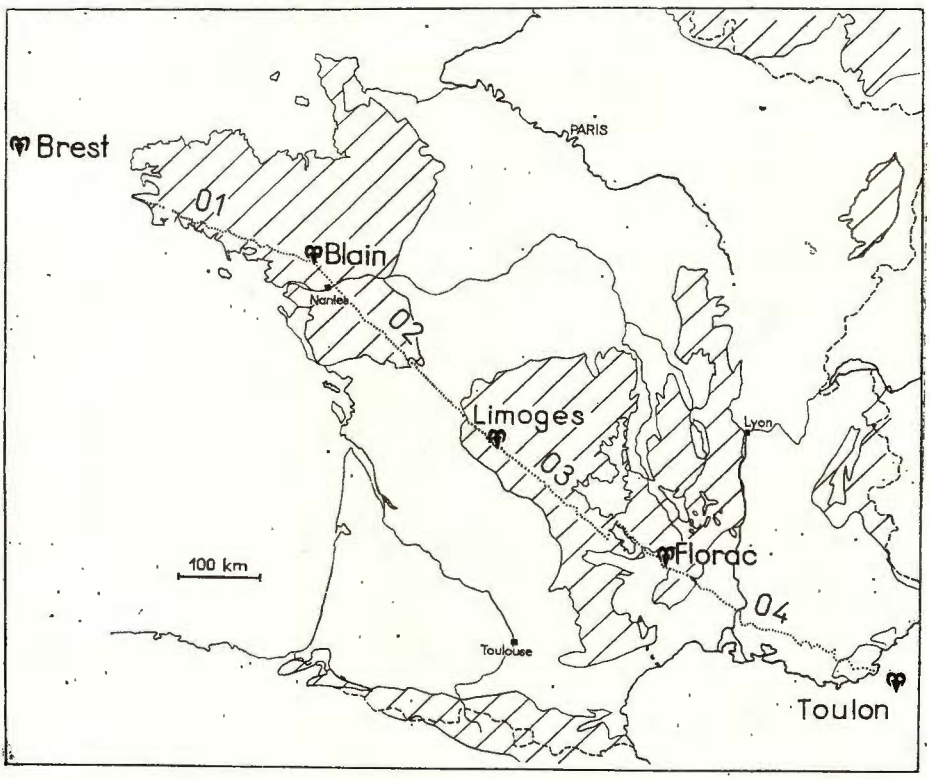

Fig. 1. — Le profil sismique Brest-Toulon.

Les hodochrones des ondes *Pg* sont de trois types différents : sur le profil 2 à partir de Blain et sur le profil 3 à partir de Florac, aucune vitesse supérieure à 6 km/s n'apparaît en première arrivée ; sur les profils 2 et 3 à partir de Limoges apparaîssent plusieurs branches de *Pg* ; sur le profil 1 ces courtes branches de *Pg* ont de grandes vitesses.

Sur le profil 2 depuis Blain, les stations sont situees en majeure partie pour l'intervalle de distance considéré sur les affleurements granitiques de la Vendée. L'homogénéité de ce massif explique le fait que la vitesse des premières arrivées soit peu élevée avec un gradient faible (vitesse apparente de 5,96 entre 35 et 100 km). Le profil 03 enregistré à partir de Florac présente la même hodochrone pour les ondes *Pg*.

Le profil 03 enregistré à partir de Limoges à travers diverses régions métamorphiques du Limousin montre des hodochrones très différentes. Les vitesses suivantes sont observées : 5,90 entre 10 et 35 km, 6,39 entre 35 et 60 km, les stations étant placées respectivement sur des embrechites leptyniques et des gneiss contenant des amphibolites. La valeur élevée de 6,39 km/s n'est pas observée à de plus grandes distances et peut être expliquée par la présence d'amphibolites dans le gneiss. Aux distances plus lointaines la vitesse des premières arrivées diminue (6,06 entre 60 et 130 km, 6,15 entre 60 et 85 km) lorsque les ondes se propagent dans des roches granitiques après le gneiss et les amphibolites (fig. 2).

Dans le cas où les vitesses des branches successives de *Pg* sont très différentes, il faut remarquer que ces vitesses ne sont définies que sur de courts intervalles de distance. Ces vitesses apparentes, aussi basses que 5,9 ou aussi élevées que 6,39, ne doivent pas être tenues comme valables pour les premiers kilometres de la croûte, ce qui condurait à une estimation erronée de la vitesse sous la couche superficielle, mais peuvent être corrélées avec les différents types de roches en surface.

LA CROÛTE

Pour l'étude de la structure de la croûte, les inhomogénéités locales superficielles ne sont pas prises en considération mais plutôt une valeur moyenne de la vitesse des *Pg* basée sur les données observées aux distances intermédiaires, de 50 à 100 km. Lorsqu'on examine les assemblages en temps réduit de chaque profil, derrière les premières arrivées, il apparaît possible de suivre d'un sismogramme à l'autre des arrivées d'énergie interprétées comme dues à des ondes réfléchies sur des discontinuités dans la croûte ou à la limite croûte-manteau.

Ces phases sont notées de 1 à 4 sur la figure 3. La phase 1 la plus importante est visible sur tous les profils. Elle a été observée aux stations proches des points de tir ainsi qu'aux plus éloignées, elle est interprétée comme réfléchie sur la discontinuité de Mohorovičić.

Les phases 2 à 4 qui n'existent pas sur tous les profils sont réfléchies sur des discontinuités à l'intérieur de la croûte.

Les profondeurs moyennes des réflecteurs et les vitesses moyennes dans les milieux supérieurs sont déterminées à partir des droites T^2 fonction de Δ^2 (T temps de propagation, Δ distance). La précision est de ± 1 km pour les profondeurs et $\pm$ 0,06 km/s pour les vitesses moyennes.

La discontinuité de Mohorovičić est ainsi trouvée à une profondeur de 31 km. Les réflecteurs correspondant aux phases 2 à 4 sont situés à des profondeurs comprises entre 15 et 30 km.

Les premières arrivées observées à des distances supérieures à 140 km (*Pn*) présentant une vitesse apparente supérieure à 8 km/s et une ordonnée à l'origine comprise entre 6 et 7 s sont interprétées comme réfractées sous la discontinuité croûte-manteau et sont pratiquement tangentes à l'hodochrone de la phase 1 vers la distance de 80 km.

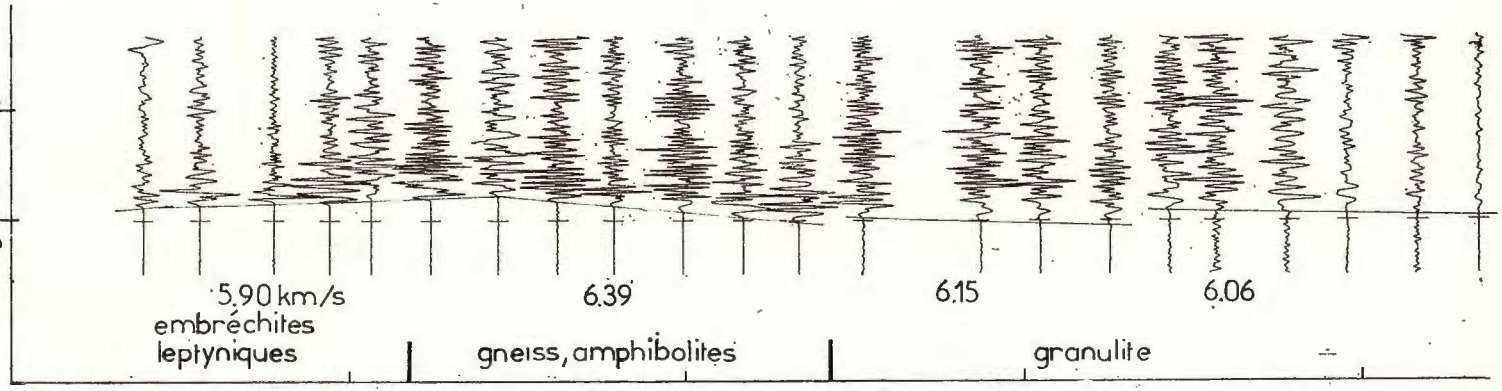

Fig. 2. — Le profil sismique 03 Limoges (Limousin) :
La propagation des ondes dans des roches granitiques après le gneiss et les amphibolites.

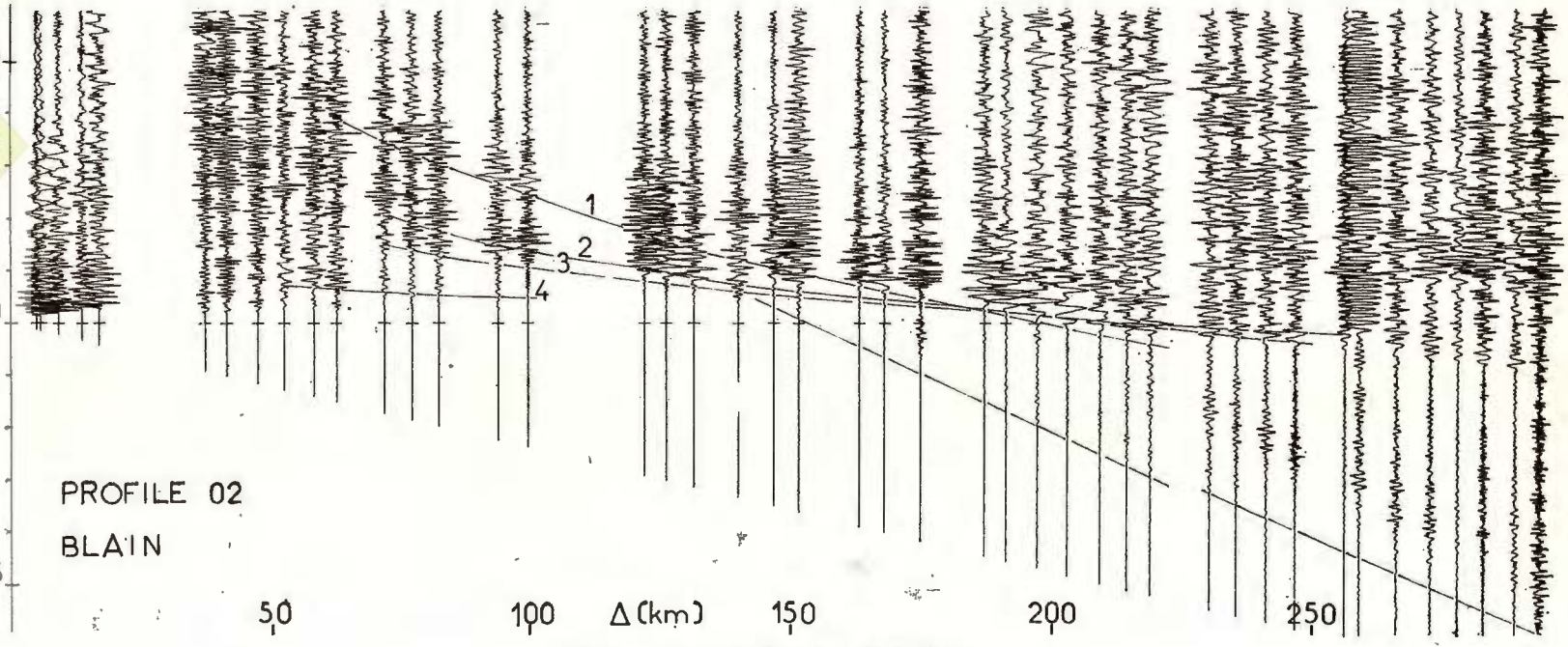

Fig. 3. — Le profil sismique 02 Blain :

1, onde réfléchie sur la discontinuité de Mohorovičić ; 2, 3, 4, ondes réfléchies sur des discontinuités à l'intérieur de la croûte ou à limite croûte-manteau.

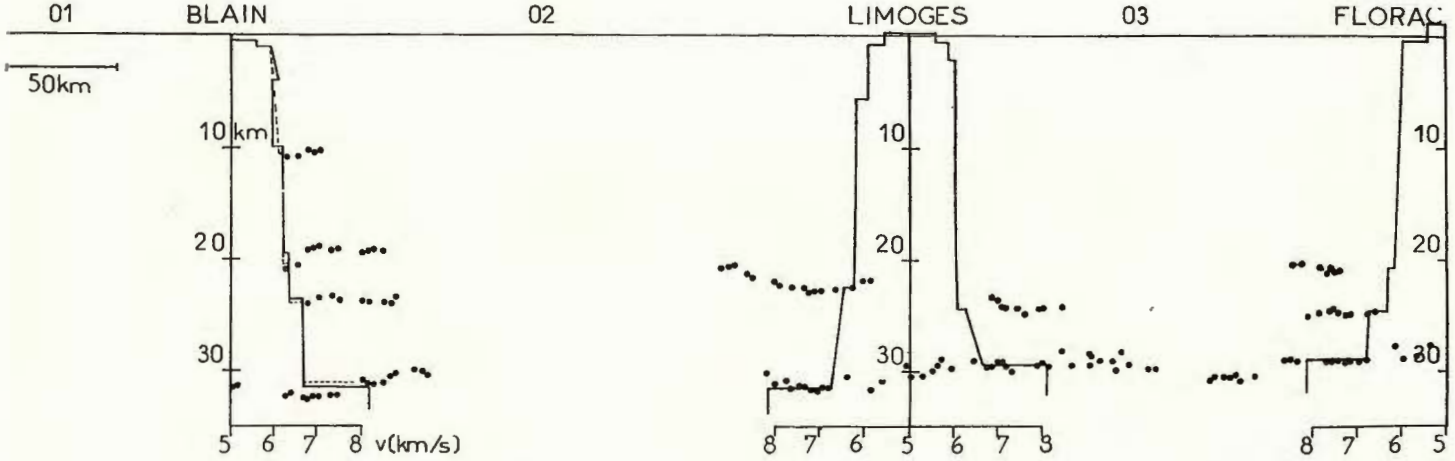

Fig. 4. — Les forages de Blain, Limoges et Florac :
Lois de vitesse en fonction de la profondeur.

Pour la détermination des vitesses entre réflecteurs on ajuste itérativement un modèle à couches horizontales de vitesses constantes séparées par des discontinuités jusqu'à ce que les hodochrones calculées soient en accord avec celles observées. Pour que l'accord soit conservé, les vitesses et profondeurs des couches ne peuvent varier de plus de quelques pour cent.

D'autres familles de modèles satisfaisant les données des temps de propagation peuvent être imaginées : modèles comprenant des zones avec gradient de vitesse ou des zones d'inversion de vitesse.

L'information contenue dans l'amplitude des ondes permet dans certains cas de choisir entre ces familles de modèles par la comparaison des points de rebroussement des hodochrones sur les données observées et des sismogrammes synthétiques.

La figure 4 montre des lois de vitesse en fonction de la profondeur pour chaque profil.

La vitesse moyenne pour toute la croûte est comprise entre 6,18 et 6,23 km/s. Il apparaît que la croûte n'est stratifiée que dans sa partie inférieure et que plus la discontinuité de vitesse est profonde plus elle est observée avec une certaine continuité le long du profil Brest-Florac.

La phase réfléchie vers 10 km de profondeur n'a été corrélée que sur le profil de Nantes vers Limoges. Dans le Massif Central il n'y a pas d'arrivée correspondant à cette profondeur.

Sur les profils 02 à partir de Blain et 03 à partir de Florac des arrivées observées sur des intervalles de distance de 70 à 100 km montrent l'existence d'un réflecteur vers 20 km de profondeur.

Seul le réflecteur se situant entre 23 et 25 km dans la croûte inférieure existe sur tous les profils. La discontinuité de Mohorovičić qui reste voisine de 31 km de profondeur, remonte de Blain jusqu'à Florac.

Entre ces 2 discontinuités, la vitesse au bas de la croûte a sensiblement la même valeur (6,65 en moyenne). La vitesse des ondes *Pn* passe de 8,15 km/s au NW du profil à 8,10 km/s dans la Massif Central.

Bien que la structure interne de la croûte varie le long du profil, les paramètres tels que : épaisseur et vitesse moyenne dans la croûte et vitesse des ondes réfractées à la base de la croûte montrent une grande continuité. Il n'est donc pas indispensable dans une première étude d'apporter des corrections dues à la croûte aux ondes se propageant dans le manteau supérieur.

TYPES OF CRUSTAL MODELS ON AN EXAMPLE FROM THE UKRAINE AND ADJACENT SEAS

BY

VSEVOLOD SOLLOGUB, ANATOLIY CHEKUNOV[1]

Deep seismic soundings in the Ukraine and adjacent regions have been carried out on a thick network of profiles with dense observational systems providing a continuous tracing of waves from the main boundaries within the crust. These detail observation have revealed not only the main, gross, structural features of the crust, but very fine ones as well. This seems to be of importance for studying geological regions of different tectonic nature, for identification of their common and discriminating features. A great amount of DSS data available and the fact that the area under study covers a remarkably wide range of structures, have encouraged an attempt of classification of the latter according to deep structures of the crust.

Analysis has shown that, with some exceptions, the crustal structures of geotectonic units of the same type have very much in common, while on regions of different types considerable distinctions are found. This is, undoubtedly, an important evidence of a close relationship between subsurface and deep structures and of similarity of the causes that have originated the structures. The investigations of distinctions of deep crustal structures of units that belong to different types but follow each other in the course of evolution have made it possible to examine the alterations that take place during a geotectonic process at a great depth and thus to approach a better understanding of the nature of the process. Distinctions and similarities of crustal cross-sections in different regions have been determined by wave field characteristics, crustal thickness, character and thickness of a set of layers composing the crust, character of transition from one layer to another, degree of seismic differentiation, character of velocity distribution, degree of seismic "turbidity" of the section, etc.

According to a combination of the above features the Earth's crust of the regions in question is divided into two major types : continental and suboceanic. These are widely distributed in other regions of the globe

[1] Institute of Geophysics, Academy of Sciences, Uk SSR 32 Novo-Belichanskaya st, Kiev, USSR.

as well. The main distinctions between the types are in total thickness of the crust and in presence or absence of "granitic" layer. The continental crust in the whole is much thicker than suboceanic (30—60 km versus 20—30 km), the latter having no "granitic" layer. Besides the two major types, a transitional crust is distinguished, but generally it does not play any independent role and corresponds to the periphery of suboceanic regions.

A great variety of features characteristic of the continental type allows to distinguish the following subtypes : *a*) the crust of geosyncline regions with orogens and median massifs developed here and : *b*) the crust of platform regions.

For the orogens of all the possible age, young as well as old, denudated at present (the Carpathians, Crimea, Caucasus, Great Krivoy Rog, etc) a thick crust is a prominent feature (45—65 km). Records of overcritical reflections from the bottom of the crust show a complicated transition to the mantle with rather thick transitional zones. Head waves from the M discontinuity are very poor and difficult to trace. A specific feature of a number of the structures of this type is a presence of two or even more seismically equivalent M boundaries at the crustal bottom. It is not improbable that these boundaries correspond to different positions that the Moho and "fore-Moho" occupied in different spans of time, sliding up and down the crust section due to a successive transformation of a part of the crust into mantle and vice-versa. This transformation, if any, may evidently, be explained as an elementary phase transition of an eclogite basalt type; the transformation went by jumps keeping the intial and all the subsequent positions of the M discontinuity fixed in the lithosphere. An important feature of some orogens (the Carpathians, Dinarides and, possibly, Krivoy Rog) is also the asymmetry of the structure of their "roots", displaced to the marginal parts of the orogens in the direction of an intensive tangential displacement of the mountain masses in the course of the sediment folding.

The Earth's crust of median massifs and intrageosyncline superimposed depressions (the Great and Minor Hungarian depressions, etc.) is of a small thickness (20—30 km). Here, at the bottom of the crust transitional zones to mantle are sometimes outlined, but their thicknesses are much smaller than those of the previously mentioned areas. Head waves from the M discontinuity become stronger and in some places (the Transcarpathian trough) their amplitudes are comparable with those of overcritical reflections from the same boundary. In this region low velocity layers are found, the deepest of them, with elastic properties of a granitic series, being located directly above the M discontinuity. Here, thus, a continuous basaltic layer composing the lower crust is absent. The existence of the low velocity layers within the crust of the Transcarpathians is, evidently, related genetically to the recent volcanic activity of the region. It should be kept in mind that the rework of the median massifs' crust during formation of intrageosyncline superimposed depressions may

well result in origination of areas with suboceanic type of crust — the Black Sea depression is, evidently, the case.

Platforms are characterized by an intermediate thickness of the crust (35—45 km); this subtype is collective, it includes a number of particular models, such as shields, plates, aulacogens, etc. Shields, in general, have greater crustal thicknesses than plates, to say nothing of great depressions, such as the Near-Caspian, North-German, etc. It is a curious fact, that needs an explanation too, that in some ancient shields (the Ukrainian, Canadian), where an active tectogenesis was completed as far back as in Prepaleozoic time, the M relief is sharply differentiated, in Early Proterozoic folding areas of the Ukraine the M discontinuity being located at a depth to 60 km. It has been noted that in zones of the Ukrainian shield with strong manifestation of basic magmatism, the Conred discontinuity has lost the features of a sharp seismic horizon; here, in the upper crust, higher velocity horizons occur that alternate with acid rocks and form peculiar "granite-basaltic" "mixtures". Aulacogens are characterized by a thinner crust in comparison with shields. Plates are in intermediate position between aulacogens and shields.

It is rather characteristic, that with sinking of consolidated substratum and, correspondingly, with an increase of sedimentary thickness, a continental character of the crust fades gradually and an oceanic character is emphasized. In the Black Sea depression, which is a limit case of the regions in question and has a typical suboceanic crust with a total thickness of 18—25 km and the "granitic" layer absent, the upper 10—15 km of the section are mainly composed (besides water) by low velocity unconsolidated sediments of young age. In contrast to the continental regions of the Black Sea depression, the DSS wave field here is formed not by reflections, but by refracted-dipping waves that dominate on the records obtained and characterize all the main boundaries within the crust including the M discontinuity.

Further investigations and comparative analysis of crustal structure of geologic units of different genesis is, undoubtedly, the way we should go to approach a thorough understanding of the general structure of the Earth' solid cover and the nature of the processes operating there.

LEGEND OF THE FIGURES

Fig. 1. — Typification of crustal models for the Ukraine and adjacent regions:

1, consolidated Earth's crust surface; 2, Conrad discontinuity; 3, M discontinuity; 4, individual reflectors; 5, refracting horizons with boundary velocities; 6, water layer; 7, sedimentary layer; 8, lower structural stage within sedimentary layer of Great Hungarian Depression; 9, „granitic" layer; 10, Precambrian synclinore structures of Ukrainian Shield; 11, Baikalo-Paleozoic metamorphosed complex within basement of Scythian Plate; 12, „basaltic" layer; 13, deep seated faults; 14, faults by seismic data; 15, faults by geologic evidence; 16, points of diffraction.

Fig. 2. — Seismological cross-section along the generalized geotraverse Adriatic Sea — Voronegh Massif (international profile III). Compiled on the basis of data reported by E. Mituch K. Posgay, D. Prosen, T. Dragaševič, K. Morelli, et al.:

1, consolidated Earth's crust surface (basement); 2, Conrad discontinuity; 3, M discontinuity; 4, M discontinuity; 5, faults by geologic evidence; 6, faults by seismic data; 7, deep seated faults; 8, water layer; 9, sedimentary layer; 10, lower structural stage of sedimentary layer in Great Hungarian Depression; 11, „granitic" layer; 12, gabbro-labradorites of Korosten Pluton, Ukrainian Shield; 13, „basaltic" layer; 14, points of diffraction; 15, typification of crustal section according to figure 1.

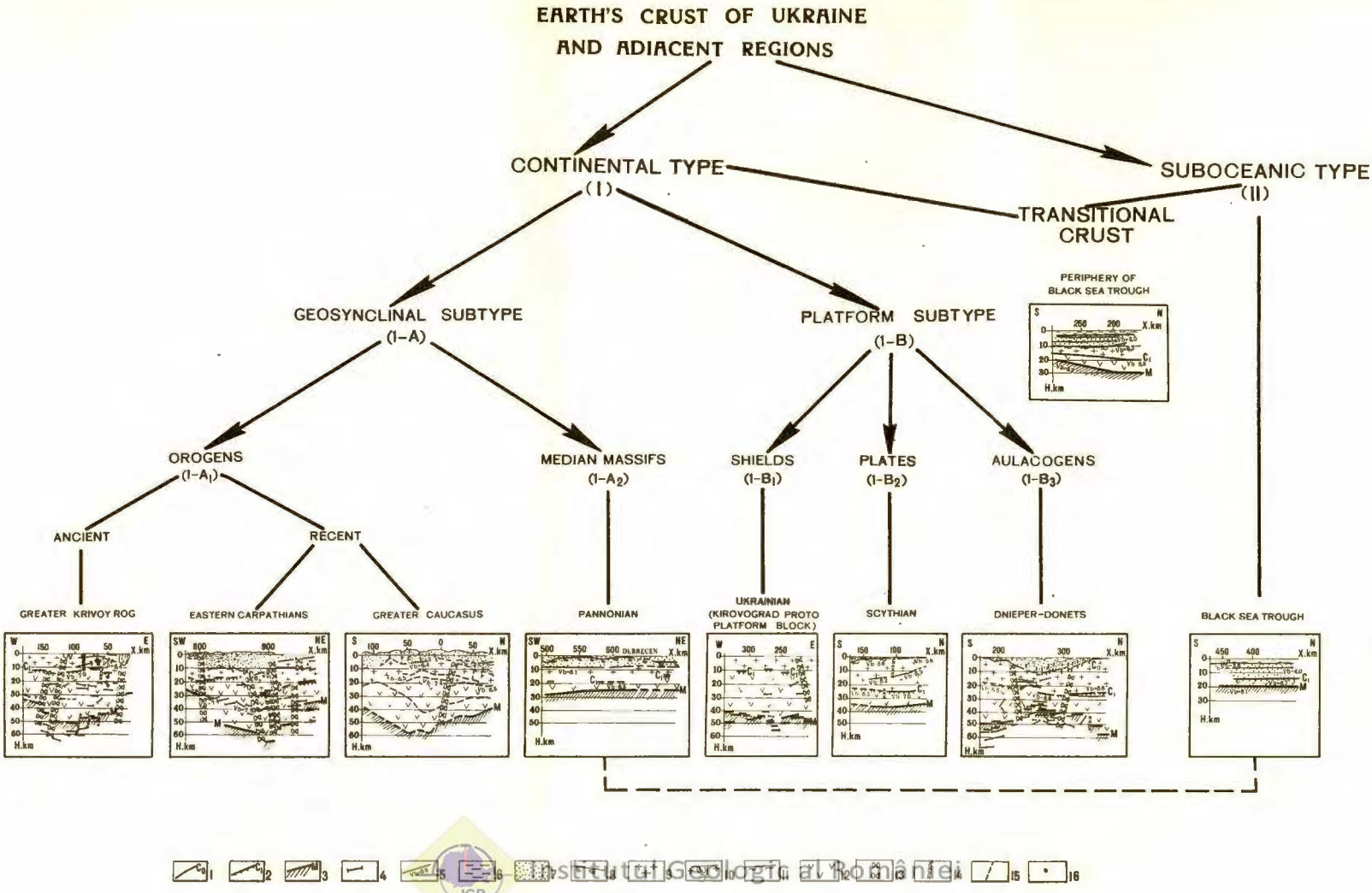
EARTH'S CRUST OF UKRAINE
AND ADJACENT REGIONS
CONTINENTAL TYPE
(I)
SUBOCEANIC TYPE
(II)
TRANSITIONAL
CRUST
GEOSYNCLINAL SUBTYPE
(I-A)
PLATFORM SUBTYPE
(I-B)
PERIPHERY OF
BLACK SEA TROUGH
OROGENS
(I-A1)
MEDIAN MASSIFS
(I-A2)
SHIELDS
(I-B1)
PLATES
(I-B2)
AULACOGENS
(I-B3)
ANCIENT
RECENT
GREATER KRIVOY ROG
EASTERN CARPATHIANS
GREATER CAUCASUS
PANNONIAN
UKRAINIAN
(KIROVOGRAD PROTO
PLATFORM BLOCK)
SCYTHIAN
DNIEPER-DONETS
BLACK SEA TROUGH

Fig. 1

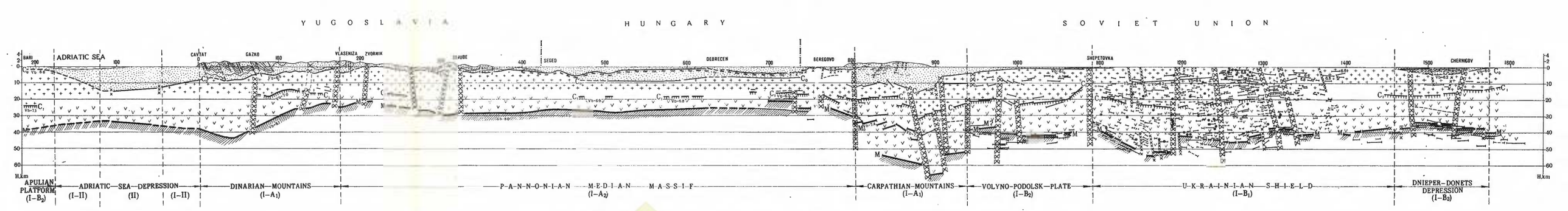

Fig. 2

SYNTHESIS OF OBSERVATIONAL RESULTS AND DATA GENERALIZATION

BY

VSEVOLOD SOLLOGUB [1], CARL PRODEHL [2]

During the past ten to twenty years extensive seismic crustal studies were carried out in western Europe. Today, there exists a large amount of seismic crustal data, and there have been several attempts to compile all this information.

Assuming a two-layered crustal model with first-order boundaries compilations have been made for several parts of Europe to get to a synthesis of all the data observed. So, e.g., for western Germany contour maps of the Conrad and Mohorovičić-discontinuity have been presented (German Research Group, 1964, figures 9 and 10) Morelli, Bellemo, Finetti, and de Visintini (1967, figures 1 and 2) have compiled all available data and presented a synthesis for Europe showing contour maps of the Conrad- and the Mohorovičić-discontinuity. However, the results used for the construction of these contour maps had been published by many different authors, using different conceptions and correlations of first and later arrivals and different methods of interpretation to determine the crustal structure of the respective area under investigation. The discrepancy of results thus obtained got especially clear in the Alps. For the western Alps two models had been established. Fuchs et al. (1963) interpreted later arrivals as *SPP* phases originating from the Mohorovičić-discontinuity, while Labrouste et al. (1963) used only first arrivals interpreting them as P_n phases whenever the velocity exceeded 7 km/s. On the profiles in the eastern Alps, however, the first and later arrivals were interpreted as *PPP* phases only.

It is clear that a synthesis based on a compilation of such heterogeneous material offers a great variety of errors. Rather it is necessary first to apply homogeneous interpretation before compiling them to a synthesis, that means a generalization of data. One attempt in this direction was a map showing lines of equal traveltimes based on profiles

[1] Institute of Geophysics, Academy of Sciences, UkSSR, Kiev, USSR.

[2] Geophysikalisches Institut, Universität Friedericiana, Karlsruhe, BRD.

originating radially in one shot-point. Here only first arrivals were used (Prodehl, 1964).

A first attempt to compile seismic results covering a larger area was performed by Choudhury, Giese, and de Visintini for the Alps in 1971. In order to avoid the complexity of correlation, these authors used only the most important phases in the records: the P_g, P^M, and P_n waves. These phases could be detected more or less distinctly on all record sections (Choudhury et al., 1971, figures 3—10). Knowing on the problems of depth calculation these authors tried to present some basic data which are taken from the traveltime diagram and give already some qualitative informations about the structure of the crust and upper mantle before calculation of velocities and depth: e.g., the contour map of the critical distance x_c for the P^M wave and the contour map of the distance x_d at which the P_n wave crosses the line representing the velocity 6 km/s (Choudhury et al., 1971, figures 11—14).

Including the possible existence of transition zones as well as low velocity zones the velocity distribution was displayed in cross-sections showing lines of equal velocity. The M-discontinuity was defined as characterized by the depth of strongest velocity gradient in the velocity range 7.5—8.2 km/s (Choudhury et al., 1971, figures 24 and 25).

A similar presentation for the area of western Germany based on the same principles was published by Giese and Stein in 1971. In addition, some other quantities were mapped, especially the velocity in the zone of the strongest gradient. Here values between 7.0 and 8.25 km/s are shown (Giese, Stein, 1971, figures 4—8, and 12—14).

Velocity columns and velocity cross-sections give very valuable information on the behaviour of the physical parameters of the crust. But it must be pointed out that single velocity isolines ($V = 6.0$ or $V = 8.0$, e.g.) cannot be identified with stratigraphic horizons by identifying these isolines with the crystalline basement or the M-surface e.g. (Garkalenko, 1972, figures 27 and 28). Rather the velocity isolines must be drawn in a dense interval in order to detect abrupt changes of the velocity with depth that means discontinuities respectively transition zones where the velocity changes rapidly with depht. The most complete information we obtain when a cross-section contains not only velocity isolines, but when also reflecting and refracting horizons are included (as Garkalenko (1972) has demonstrated).

In general DSS data information is based on some classic formulas derived with the assumptions that seismic boundaries are horizontal and that lateral velocity inhomogeneities can be neglected. As the results of detailed investigations show the structure of the Earth's crust, however, is very complicated and the assumptions mentioned above are not correct. So it becomes evident that the interpretation of single profiles can only reveal first approximations of the structure. Rather, a more detailed system of observations is necessary in order to detect not only the general features but to locate local inhomogeneities, as there are

deep-seated faults or individual crustal blocks, and to map a seismic boundary in detail (Sollogub, Chekunov, 1971, figures 19—24).

A detailed system of observations especially gives additional information on the possible existence of low velocity zones. One main indication of the existence of a low velocity zone is a break and a displacement of the first arrivals. However, this phenomenon is characteristic for faults as well. Consequently, a single time-distance curve may not always provide a unique determination of a low velocity zone, if not other parameters can be taken into account. A detailed system of reversed traveltime curves, however, gives the possibility to distinguish if a delay of arrivals is mainly due to the existence of a low velocity zone or of a fault zone.

It is clear that because of the different observation schemes which are used in different countries many difficulties result in interpretation and generalization of the DSS data. Nevertheless, the problem of data generalization should not be removed, but evidently should be performed at the level of seismic and velocity cross-sections. For individual regions such as Hungaria, Ukraine, etc. a compilation of all data has been performed (Sollogub, Prosen, Militzer, 1972) and the question rises how to combine these data with the data of other countries.

These problems were discussed at several meetings and recommendations, which were prepared by a working group in Moscow in 1969 and discussed by Giese, Pavlenkova and Volvovski[3], have been tested.

For most areas the definition of the M-discontinuity is clear and it can be defined also as depth of the strongest velocity gradient. However, it may become difficult and arbitrary when the velocity range has to be defined. For instance, Steinhart (1967) defines the Mohorovičić-discontinuity as that level in the Earth where the compressional wave velocity increases rapidly or discontinuously to a value between 7.6 and 8.6 km/s. In the absence of an identifiable rapid increase in velocity the Mohorovičić- discontinuity is taken to be the level at which the compressional wave velocity first exceeds 7.6 km/s. Giese, Morelli and Steinmetz (1972), however, define the velocity range between 7.2 and 8.4 km/s.

This discrepancy is clear if one regards the velocity distribution under the Rhinegraben area. Ansorge et al. (1970) define the corresponding velocity range of 7.6—7.7 km/s as rift cushion which overlies the upper mantle whereas Giese and Stein, according to the definition of Giese et al. (1972) given above, have mapped this depth range as Mohorovičić-discontinuity.

A similar fact has been found in central France. Under the Central Massif of France the thickness of the crust was presented by Aubert

[3] Giese P., Pavlenkova N. I., Volvovski I. S. Possibilities on a generalized interpretation in deep seismic sounding. 1970. ESC, XII. Ass., CS XVII, 1, Luxembourg.

and Perrier[4]. If one uses the typical reflections (Choudhury et al., 1971, figure 4) and defines them as P^M reflections the velocity of the upper mantle decreases from 8.0 to 7.2 km/s (Giese et al., 1972, figure 5), when moving from west to east from the Limousin to the Limagne. Here the M-discontinuity is identified with the zone of the greatest velocity gradient. But, as Perrier and Ruegg[5] have shown the M-discontinuity can also be defined by the velocity range around 8.0—8.4 km/s which is derived from refracted P_n arrivals without observing corresponding reflections.

Also under the northern Apennines the zone of greatest gradient is found for the velocity range around 7.2 km/s (Giese, Günther, Reutter, 1970).

As mentioned above the same question arises for the zone of Ivrea. Labrouste, Baltenberger, Perrier, and Recq (1968) have defined a map of the M-discontinuity from first arrivals whenever the corresponding velocity exceeds 7 km/s. This map comprises velocities in the range from 7.3 to more than 8km/s. The reinterpretation of Choudhury et al. (1971, figures 25, 29) shows: Moving from east to west it is a question of definition what is to be called Moho and what not.

By these examples it becomes evident that a compilation of data is not possible without clear and unique definition of the quantities which are displayed in cross-sections or contour-maps. It is evident that a simple definition of the Conrad-discontinuity is still mor questionable. In some regions the M-discontinuity as well as the Conrad-discontinuity can be defined well, but in other regions a second boundary zone evidently does not exist. Any attempt of a synthesis of all data available must also comprise the anomalous regions some of which have been shown above and which comprise large areas of western Europe.

REFERENCES

Ansorge J., Emter D., Fuchs K., Lauer I. P., Müller St., Peterschmitt E. (1970) Structure of the crust and upper mantle in the rift system around the Rhinegraben, *In*: Graben Problems, Schweizerbart, Stuttgart.

Choudhury M., Giese P., de Visintini G. (1971) Crustal structure of the Alps: Some general features from explosion seismology. *Boll. Geofis. teor. appl.*, 13, Trieste.

Fuchs K., Müller St., Peterschmitt E., Rothé J.P., Stein A., Strobach K., (1963) Krustenstruktur der Westalpen nach refraktionsseismischen Messungen. *Gerl. Beitr. Geophys.* 72, Leipzig.

Garkalenko I. A. (1972) The Black Sea offshore and deep water region. *In*: The crustal structure of central and southeastern Europe based on the results of explosion seismology

[4] Aubert M., Perrier G. Structure profonde du Massif Central. 1971. *In*: Symposium, Géologie, morphologie et structure profonde du Massif Central français. Ed. Clérmont-Ferrand (in press).

[5] Perrier G., Ruegg J. C. Structure du Massif Central français XIII Gen. Ass. ESC, Braşov (in press).

Geophys. Trans. Hung. Geophys. Inst. „Roland Eötvös", Spec. ed., Müszaki Könyvkiadó, Budapest.

German Research Group for Explosion Seismology (1964) Crustal structure in western Germany. *Z. Geophys.* 30, Würzburg.

Giese P., Günther K., Reutter K. J. (1970) Vergleichende geologische und geophysikalische Betrachtungen der Westalpen und des Nordapennins. *Z. deutsch. geol. Ges.*, Jahrg. 1968, 120.

— Morelli C., Steinmetz L. (1972) Main features of crustal structure in western and southern Europe based on data of explosion seismology. *Tectonophysics* 14, Amsterdam.

— Stein A. (1971) Versuch einer einheitlichen Auswertung tiefenseismischer Messungen aus dem Bereich zwischen der Nordsee und den Alpen. *Z. Geophys.* 37, Würzburg.

Labrouste Y., Choudhury M., Perrier G. (1963) Recherches séismologiques dans les Alpes Occidentales au moyen de grandes explosions en 1956, 1958 et 1960, VI. B : Essai d'interprétation N° 2. *Séismologie*, Mémoire Collectif, Année Geophysique International. C.N.R.S., Sé. XII, 2, Paris.

— Baltenberger P., Perrier G., Recq M., (1968) Courbes d'égale profondeur de la discontinuité de Mohorovičić dans le Sud-Est de la France. *C. R. Acad. Sc. Paris, Ser. D*, 266, Paris.

Morelli C., Bellemo S., Finetti I., de Visintini G., (1967) Preliminary depth contour maps of the Conrad- and Mohorovičić-discontinuities in Europe. *Boll. Geofis. teor. appl.* 9, Trieste.

Prodehl C. (1964) Vorläufiger Tiefenlinienplan der Mohorovičić-Diskontinuität im bayerischen Alpenvorland und in den Ostalpen zwischen München und Padua. *DFG-Kolloquium*, Bad Kreuznach, 9, 7.

Sollogub V. B., Chekunov A. V. (1972) The Ukrainian Soviet Socialist Republic. *In* : The crustal structure of southeastern Europe based on the results of explosion seismology. *Geophys. Trans. Hung. Geophys. Inst. „Roland Eötvös"*, spec. ed. Müszaki Könyvkiado, Budapest.

— Prosen D., Militzer H. (1972) The crustal structure of southeastern Europe based on the results of explosion seismology. *Geophys. Trans. Hung. Geophys. Inst. „Roland Eötvös"*, spec. ed. Müszaki Könyvkiado, Budapest.

Steinhart J. S. (1967) Mohorovičić-discontinuity. *In* : International dictionary of Geophysics, Pergamon Press, Oxford.

SYMPOSIUM 3. TIME AND SPACE VARIATIONS OF SEISMIC ACTIVITY

SISMICITÉ DU BASSIN MÉDITERRANÉEN ET DES RÉGIONS ENVIRONNANTES [1]

PAR

PAUL BEUZART [2]

Dans l'hypothèse de la tectonique des plaques, les ceintures sismiques sont des zones linéaires où se produisent des mouvements différentiels entre plaques rigides. La sismicité est le guide le plus sûr pour définir les limites actuelles des plaques en déplacement [3]. Le but de cette communication est de montrer sur des cartes de sismicité du bassin méditerranéen et des régions environnantes les limites des plaques Europe et Afrique et les frontières des plaques intermédiaires que sont les plaques Egée et Turque... Les séismes reportés sur les différentes cartes présentées ici sont ceux survenus pendant les années 1900 à 1971 dans la région limitée par les méridiens 45 W et 45 E et les parallèles 50 N et 25 N. La période de cette étude est trop courte pour avoir une image exacte de la sismicité de cette région. Davies et Brune (1972) ont montré que la fréquence des gros séismes qui se produisent à la frontière de deux plaques est fonction de la vitesse du mouvement différentiel existant entre ces deux plaques, soit d'après eux, pour la Méditerranée occidentale où la vitesse est de l'ordre de 1 à 2 cm/an, une période d'observation de deux siècles permettrait d'avoir une image fidèle de la sismicité. Néanmoins, l'étude des cartes de sismicité de ces 70 dernières années permet de délimiter les plaques Europe et Afrique dans cette région.

Les paramètres des séismes utilisés pour dresser ces cartes proviennent de nombreuses sources. Les données des séismes précédant l'année 1960 ont été tirées principalement de trois ouvrages portant sur la sismicité du monde et de l'Europe de Gutenberg, Richter (1954),

---

[1] Contribution n° 147 du Département Scientifique, Centre Océanologique de Bretagne.

[2] Centre Océanologique de Bretagne. B. P. 337—29273 Brest, France.

[3] Le Pichon X., Francheteau J., Bonnin J. Plate Tectonics. 1972. in press.

de Rothe (1969) et de Karnik (1969). Pour la période de 1960 à 1971, les publications du "Bureau Central International de Sismologie" de l'"U.S. Coast and Geodetic Survey" et de l'"International Seismological Centre" ont été surtout utilisées.

Les magnitudes reportées sont celles définies par les ondes de volume "m". Pour les séismes dont on ne connait que la magnitude "M" calculée d'après les ondes de surface, celle-ci a été ramenée à celle des ondes de volume d'après la formule de passage établie par Båth (1966) : $m = 2.9 + 0.56\ M$. Les séismes superficiels (0—70 km) sont représentés par des carrés, les séismes intermédiaires (70—300 km) par des triangles pointe en haut et les séismes profonds (300—700 km) par des triangles pointe en bas. La taille des différents symboles, qui correspond au côté des carrés et à la hauteur des triangles, varie comme la puissance quatrième de la magnitude. La précision sur la détermination des épicentres est aussi reportée sur la figure, les symboles carrés ou triangles restent vides quand la précision est inférieure à 0,5°, les symboles contiennent une barre quand la précision est comprise entre 0,5° et 0,1°, les symboles contiennent une croix quand la précision est supérieure ou égale à 0,1°.

LES CARTES DE SISMICITÉ

Les cartes générales (fig. 1, 2) englobent une partie de l'Océan Atlantique, la mer Méditerranée et la mer Noire, ainsi que les pays bordant ces deux mers. Sur la carte de séismes du bassin méditerranéen (fig. 1) sont reportés tous les séismes qui ont été enregistrés par cinq stations au minimum, alors que sur la carte des grands séismes (fig. 2), seuls les séismes de magnitude égale ou supérieure à 5 sont représentés. La comparaison de ces deux cartes montre sur les continents une dispersion importante des épicentres de faible magnitude particulièrement au sud de l'Espagne et dans les Alpes, alors que sur les rifts les épicentres se trouvent bien alignés. Il est donc possible de distinguer deux types de domaines dont les caractéristiques sismologiques sont différentes :

a) Un domaine de rift océanique, limité à l'est par le méridien 22 ouest, est composé de trois branches qui se coupent vers 39 nord et 29 ouest pour former le point triple des Açores. Les traits principaux sont une dispersion très faible des épicentres de part et d'autre d'une ligne. La magnitude des séismes est rarement supérieure à 6. La densité des épicentres est constante aussi bien pour les gros séismes que pour les petits.

La branche nord orientée N—S correspond à la partie de la dorsale médio-atlantique qui forme la frontière des plaques Amérique et Europe, La branche sud orientée SW—NE est la partie de la dorsale médio-atlantique qui marque la frontière des plaques Amérique et Afrique. La branche ouest, appelée rift de Terceira par Udias et Arroyo (1972), forme une partie de la frontière des plaques Europe et Afrique. Le point triple des Açores est le point de contact des plaques Amérique, Europe et Afrique.

b) Un domaine continental montre une dispersion notable des épicentres, surtout pour les séismes de faible magnitude. Néanmoins, sur la

carte des grands séismes (fig. 2), il apparaît des alignements qui marquent les zones frontières des différentes plaques. Depuis le méridien 10 ouest, une zone sismique linéaire se suit (fig. 3) jusqu'en Tunisie. Elle correspond à la continuation du rift de Terceira et de la ligne sismique venant des Açores qui se continue à travers l'Atlas Tellien au sud de la Petite et de la Grande Kabylie jusqu'au cap Bon. La frontière commune des plaques Afrique et Europe est marquée par une ligne sismique continue des Açores jusqu'en Tunisie. Plus à l'est, ces deux plaques sont séparées par deux plaques intermédiaires individualisées, qui sont la plaque Egée et la plaque Turque. La plaque Adriatique (fig. 5) se situe entre les deux axes sismiques parallèles qui soulignent les chaînes des Apennins à travers l'Italie et les Dinarides du côté yougoslave. Au nord, l'arc alpin limite cette plaque qui n'a pas de frontières clairement définies au sud. Elle peut être considérée comme une partie intégrante de la plaque Afrique.

La plaque Egée (fig. 4) regroupe à ses frontières plus de la moitié des épicentres déterminés dans le bassin méditerranéen. Au sud, un arc sismique en demi-cercle allant des îles Ionniennes à l'île de Rhodes en passant au sud de la Crête, est caractérisé par des séismes superficiels très nombreux. Au nord de cet arc, une série de séismes intermédiaires de magnitude élevée indiquent l'existence d'un plongement d'une plaque lithosphérique sous un arc insulaire semblable à celui des petites Antilles (Dorel et al., 1971) ou des Kouriles (Fedetov, 1965) dont une caractéristique est que la profondeur de ces séismes ne dépasse pas 200 km. Ce plan de Benioff est souligné par une série de volcans actifs (Papazachos, Comninakis, 1971). A l'est, la frontière de cette plaque est située le long de la côte turque et au nord une série de séismes importants marque la limite à travers la chaîne des Balkans. La bordure méridionale du fossé situé au nord de la mer Egée correspond à un alignement de séismes qui fait penser à une structure de rift océanique. Cette ligne compte en effet pour les dix dernières années trois séismes importants et toute une série de secousses de faible magnitude qui présentent une faible dispersion comme cela apparaît sur la carte de la mer Egée (fig. 4).

La plaque turque, enfin, limitée au nord par la zone de fracture nord-anatolienne, par la mer Egée à l'ouest et au sud par la grande zone de chevauchement du Taurus qui est souligné par un alignement de séismes du lac Van à l'île de Chypre (fig. 5). La partie occidentale de cette plaque est compartimentée par des failles actives de direction E—W qui ont été réactivées par les séismes de Burdur, de Guedig et d'Adapazar.

Les cartes de sismicité de ces soixante-dix dernières années délimitent ainsi les frontières des plaques Europe et Afrique, ainsi que les plaques intermédiaires Egée et Turque à travers le bassin méditerranéen.

Ces cartes doivent être considérées comme un document de travail qui peut suggérer l'existence d'autres plaques intermédiaires comme la plaque Sinaï limitée à l'est par la vallée du Jourdain et le golfe d'Aqaba et à l'ouest par une ligne qui relierait le golfe de Suez à l'île de Chypre ; une plaque mer Noire—Roumanie qui serait limitée au sud par les Dinarides, les Balkans, et la zone de fracture nord-anatolienne. Au nord, la

frontière suivrait une ligne longeant les Alpes, les Carpates, la Crimée et le Caucase (fig. 5).

Cette étude suggère qu'il faut tenir compte de la magnitude et de de l'énergie élastique dissipée par les séismes pour définir les frontières de plaque et pour caractériser différents types de limites. Pour le domaine des rifts océaniques, la densité des épicentres est presque constante et le logarithme de l'énergie dissipée, exprimée en ergs, n'excède pas 21. Dans le domaine continental et le long des grandes zones de fractures, le logarithme de l'énergie peut atteindre 24 mais la répartition des séismes est beaucoup moins régulière que le long des rifts. Il reste encore le cas des séismes isolés ou des lignes de séismes ne se rattachant à aucune frontière de plaque. Dans le bassin méditerranée, de tels groupes de séismes se trouvent dans la zone pyrénéenne, la flexure sud-atlasique et la Libye. Ces zones sismiques intra-plaques (S y k e s, 1972) ne trouvent pas encore d'explication dans la théorie de la tectonique des plaques telle qu'elle est exprimée actuellement. Les solutions apportées par des études de mécanisme au foyer peuvent conduire à la confirmation de l'existence de déformations à l'intérieur des plaques. Ces déformations restent inférieures à celles que l'on peut mesurer le long des frontières des plaques. La sismicité permet de définir les frontières des plaques, les directions des mouvements entre les différentes plaques doivent être, d'un point de vue sismologique,déterminés par l'étude des mécanismes au foyer.

Je remercie Monsieur *Guy Perrier*, de l'Institut de Physique du Globe de Paris, d'avoir bien voulu présenter cette communication en mon nom et place.

BIBLIOGRAPHIE

B å t h M. (1966) Earthquake energy and magnitude. *Physics and Chemistry of the Earth.*, 7, Pergamon Press, New York.

D a v i e s G. F., B r u n e J. M. (1971) Regional and global fault slip rates from seismicity. *Nature*, 229, London.

D o r e l J., E s c h e n b r e n n e r S., F e u i l l a r d M. (1971) Contribution a l'étude sismique de l'arc des Petites Antilles. *Annales de Géophysique*, 27, Paris.

F e d e t o v S. A. (1965) Upper mantle properties of the southern part of Kuril Island arc according to detailed seismological investigations. *Tectonophysics*, 2, Amsterdam.

G u t e n b e r g B., R i c h t e r C. F. (1954) Seismicity of the Earth. 2nd ed., Princeton University Press, U.S.A.

K a r n i k V. (1969) Seismicity of the European area (part 1). D. Reidel Publishing Company, Dordrecht.

R o t h é J. P. (1969) La seismicité du globe 1953—1965. *Earth Sciences*, Unesco 1.

S y k e s L. R. (1972) Seismicity as a guide to global tectonics and earthquake prediction. The upper mantle. *Tectonophysics*, 13, 1—4, Amsterdam.

U d i a s A., L o p e z A r r o y o A. (1972) Plate tectonics and the Açores-Gibraltar region. *Nature*, 237, London.

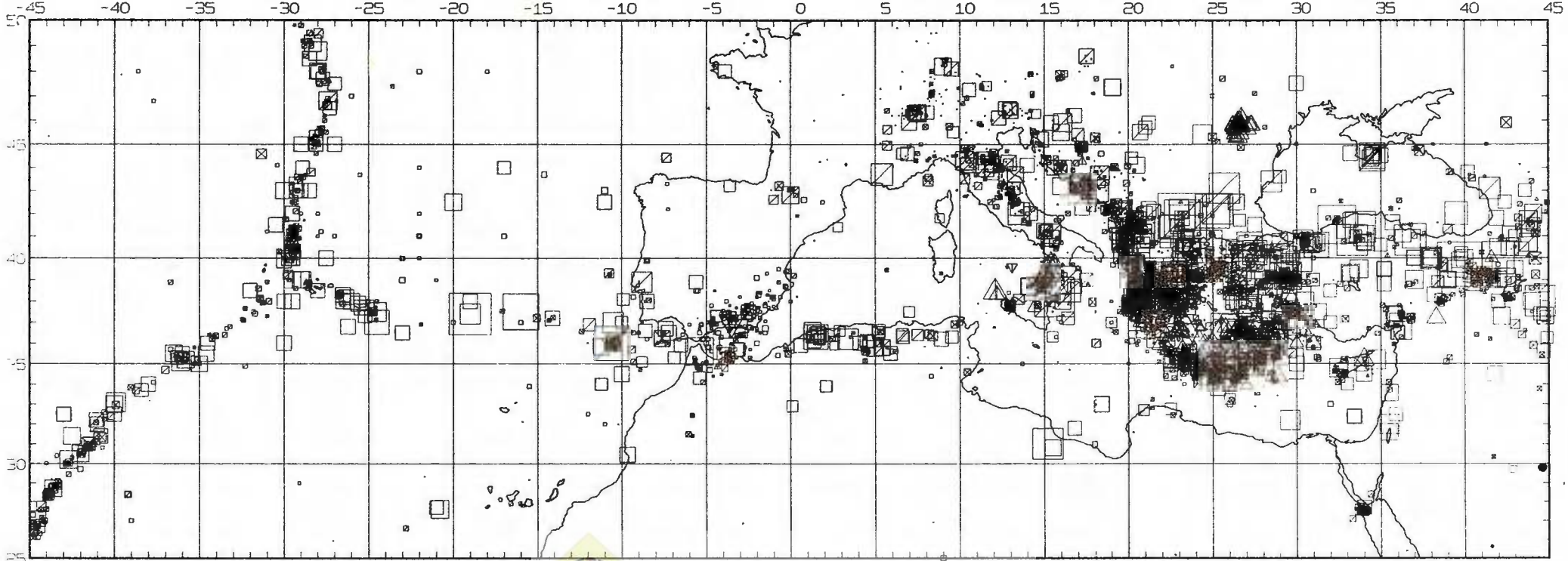

Fig. 1 - Séismes du bassin méditerranéen 1900 - 1971

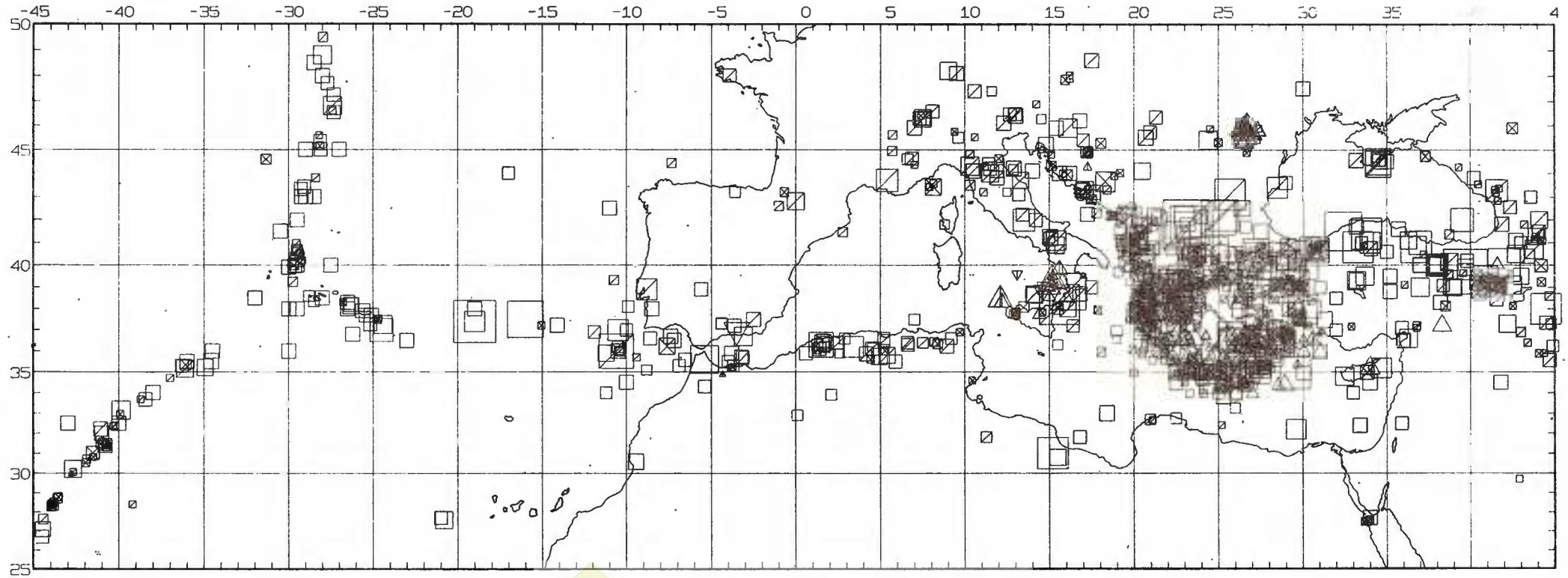

Fig. 2- Séismes du bassin méditerranéen 1900-1971 dont la magnitude est supérieure ou égale à 5

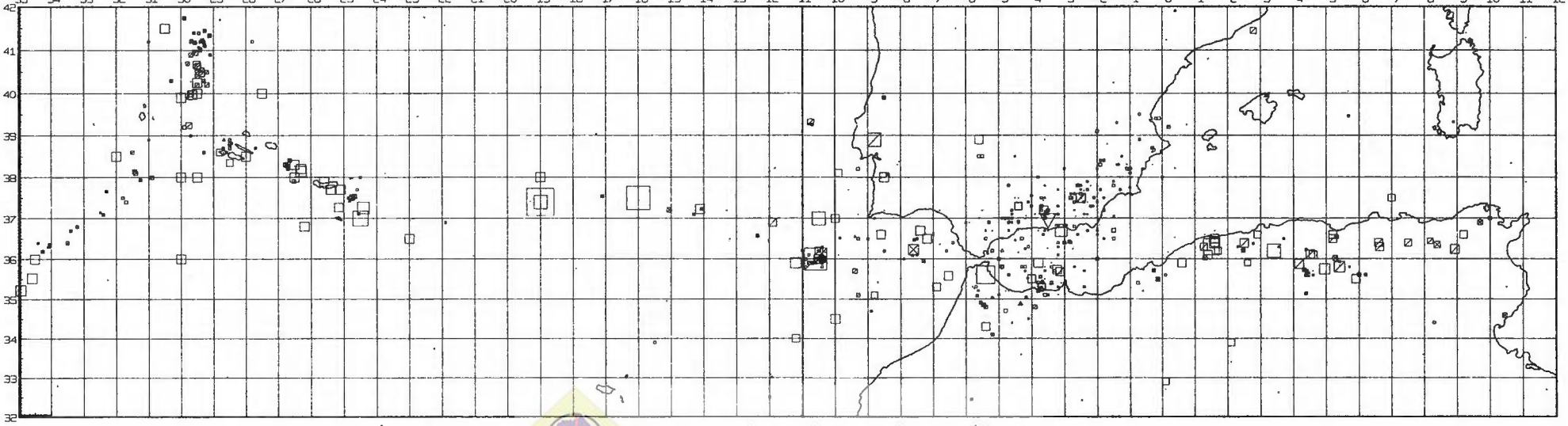

Fig. 3 - Séismes de la ligne Açores - Gibraltar - Tunisie 1900 - 1971

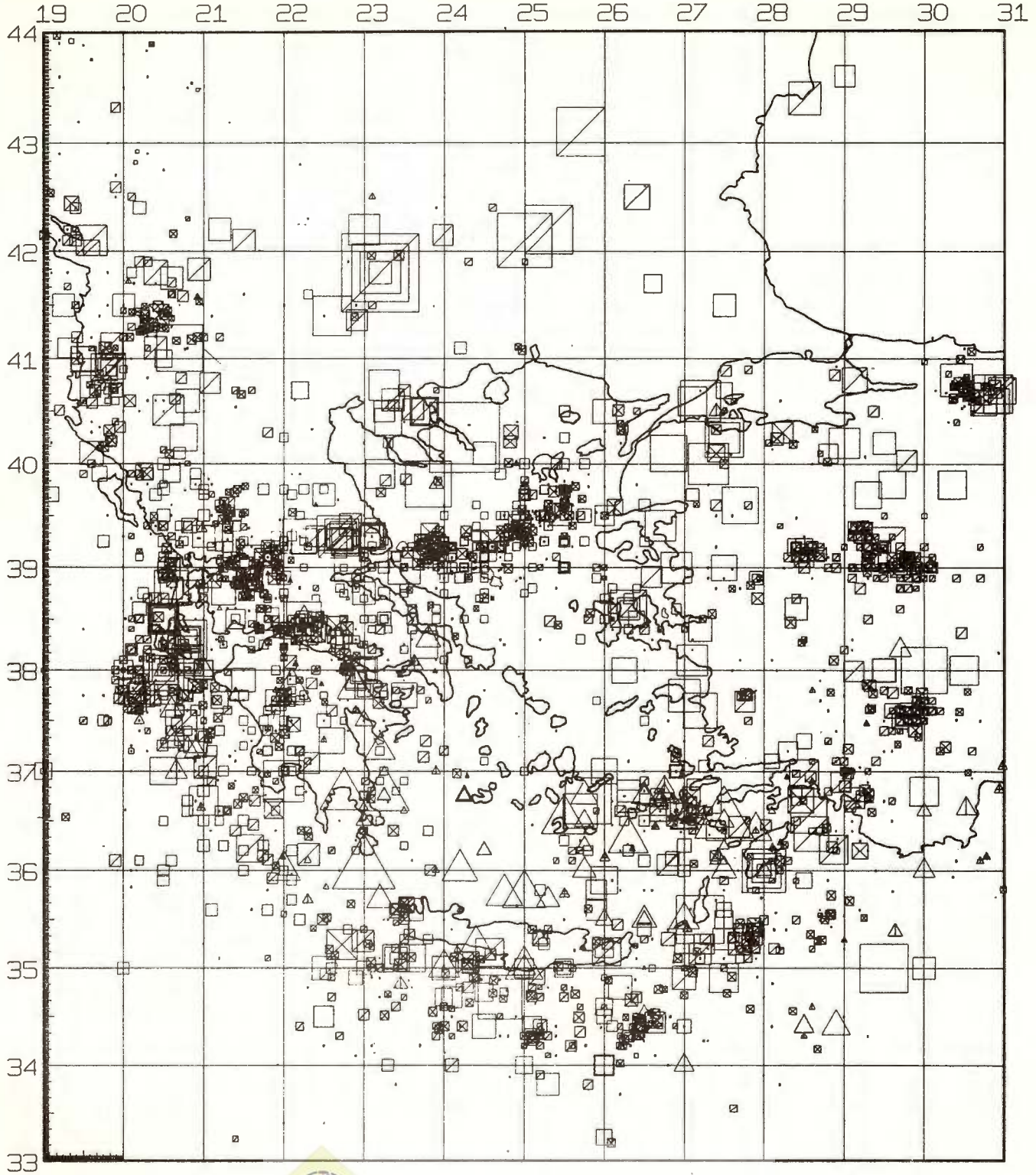

Fig. 4 - Séismes de la mer Egée 1900 - 1971

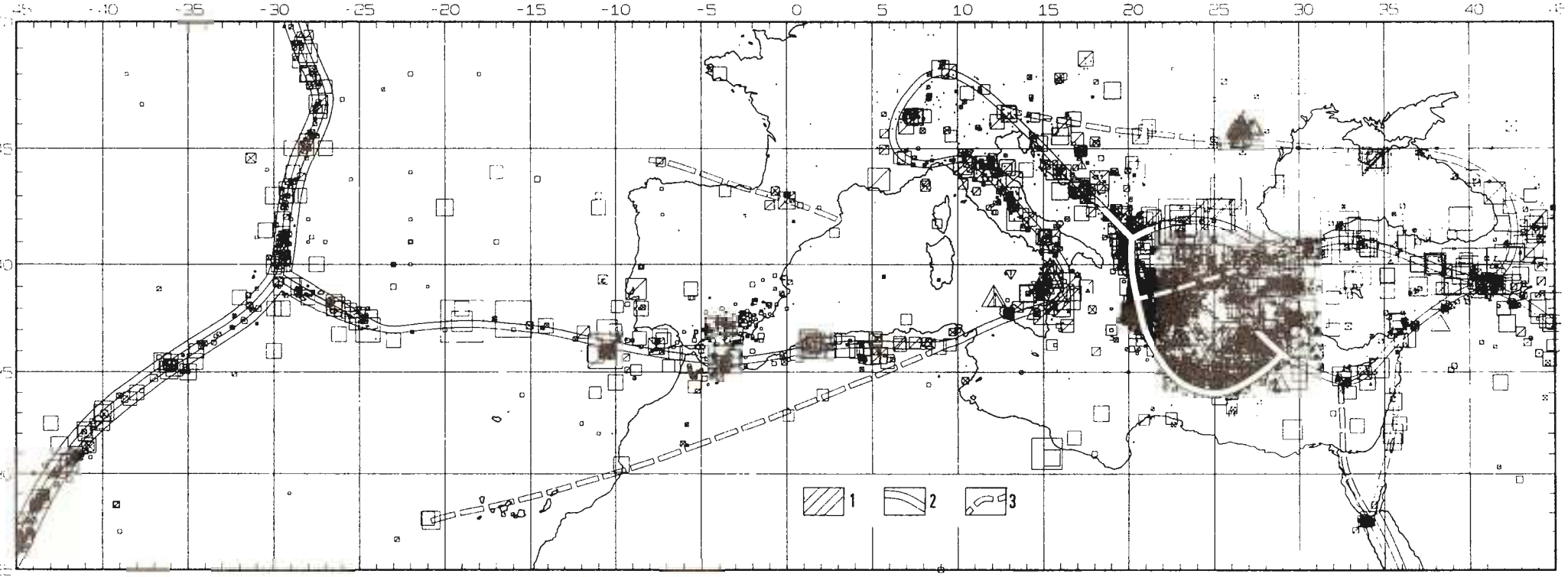

Fig. 5 - Frontières de plaques définies par la sismicité dans le bassin méditerranéen:
1, Rift médio-océanique; 2, frontière de ploque; 3, frontières supposées et zones sismiques intra-plaques

STATISTICAL ANALYSIS AND PREDICTION OF EARTHQUAKES IN THE REGION VAL PADANA, ITALY

BY

JIŘÍ BUBEN[1]

INTRODUCTION

The catalogue of earthquakes which had been felt in the area between the Prealps (including) and the foreland of Appennines during the period 150—1969 has been published in the paper of Caloi (1970). In this basic paper the seismicity of the region has been discussed in great detail including both seismological and geological aspects.

In this paper but only simple methods of analysis and prediction of random series are applied both to the values of magnitude and to earthquake recurrence intervals. This paper introduces also other random series, the autocovariance function of which having greater values than that of magnitude or time intervals. Simplified formulae for easy numerical calculation of optimal, final length prediction operators for such series are developed and verified in this paper.

THE SERIES OF VALUES OF MAGNITUDE

The time series of above-mentioned values of magnitude M_i of earthquakes, where $i = 1, 2 \ldots N$ is to be considered as a sample of a discret random ergodic process. To describe such a sample following statistical moments are used:

i) the mean value $$\overline{M} = 1/N \cdot \sum_{1}^{N} M_i \tag{1}$$

ii) the statistical dispersion

$$D_M = 1/N \sum_{i=1}^{N} (M_i - \overline{M})^2 = \overline{(M_i - \overline{M})^2}$$

iii) the autocovariance function $C_M(k) = \overline{(M_i - \overline{M})(M_{i+k} - \overline{M})}$ (2)

where $i = 1, 2 \ldots\ldots N - k$

$k = 0, 1, \ldots\ldots N/20$

$C_M(0) = D_M$

[1] Geophysical Institute, Faculty of math. and phys., Ke Karlovu 3, Praha 2, Czechoslovakia.

and the autocorrelation function

$$R_M(k) = C_M(k)/C_M(0)$$

A random sample would be extrapolated rather easy, if it is stationary, that means if the values of the autocovariance function $C(k)$, $k = 0, 1, 2 \ldots N/20$) do not vary with the time of observation. If this

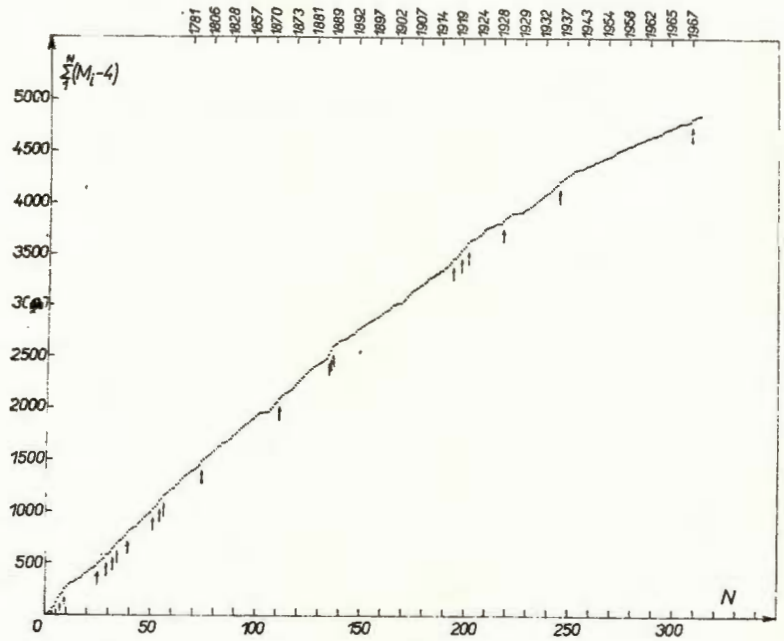

Fig. 1. — Cumulative graph of magnitude values $M_i - 4$.

condition is fulfilled only for the mean value $\overline{M} = C_M(\infty)$, we denote the sample M_i as weak stationary.

A graphical test of the weak stationarity of our series has been made using a cumulative plot (fig. 1). On the horizontal axis is the cummulative number N of earthquakes taken from the catalogue and on the vertical axis is the corresponding cumulative magnitude $\sum(M_i - 4)$. The slope of the curve is constant beginning with a relativly strong earthquake with $M = 7{,}3$, which appeared near Consiglio in October 1936. Another break of the slope can be distinguished after three strong earthquakes with $M = 7{,}9$ near San Remo in February 1887.

The catalogue as a whole may be not homogenous for all earthquakes with $M > 4$. Therefore we take into account only the series M_i beginning in the year 1936 and having the length $N = 66$. Within the period 1936—1969 our curve (fig. 1) has a nearly constant slope. It fol-

lows, that the mean value $\overline{(M_i - 4)}$ is constant and that the centred series $(M_i - 4)$ is weakly stationary. This series however is too short and no test of fluctuations of $C_M(0)$, $C_M(1)$ ... with time can be applied.

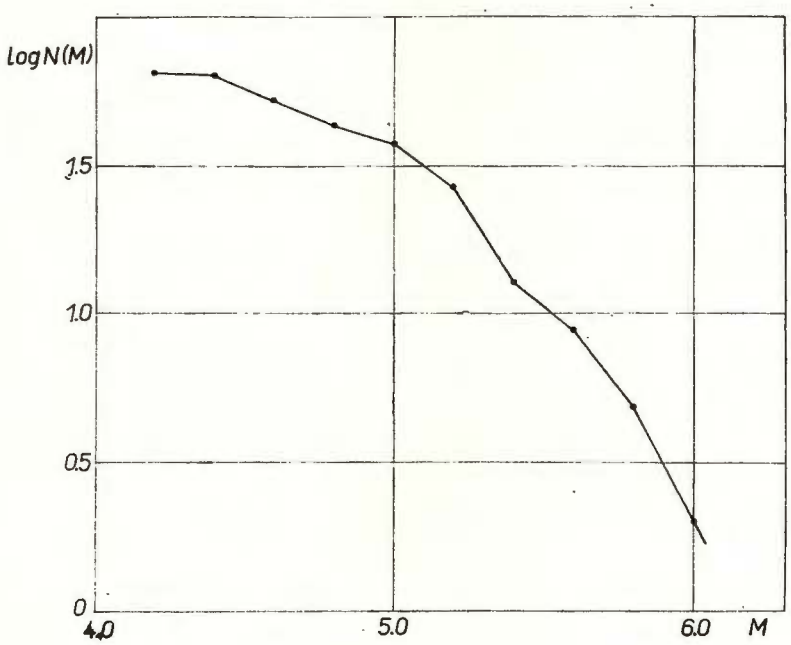

Fig. 2. — Cumulative magnitude-frequency relation.

So we do not know if M_i is strong stationary, but we must suppose this serious feature of our sample as a necessary condition of applicability of the following theory.

The magnitude-frequency relation $\log N = f(M)$ with the length of elementary intervals of magnitude $\Delta M = 0{,}2$ shows (fig. 2) that there are too little earthquakes with magnitude $4 < M < 5$. The well known relation

$$N(M) = 10^{a-bM} \tag{3}$$

with constant values a, b is clearly not satisfied by earthquakes within this region and time period, included into the above-mentioned catalogue. May be that this catalogue is not homogenous regarding to earthquakes with $M > 4$ even in the period 1937—1969. The mean value of magnitude in our series is $\overline{M} = 1/N \cdot \sum_{i=1}^{N} (M_i - M_0) = 0{,}95$, $M_0 = 4$ Substituting this into the formula (P u r c a r u, Z o r i l e s c u, 1971)

$$b = \frac{0{,}43}{\overline{M} - M_0} \tag{4}$$

we obtain $b = 0{,}45$ with the standard deviation of $\bar{M}$ $\delta_{\bar{M}} = 0{,}007$ which contrasts very with uncertain value of b obtained from figure 2. A random process (sample) is called the Gaussian process, if the distribution of its values may be represented by the Gaussian (normal) distribution. This

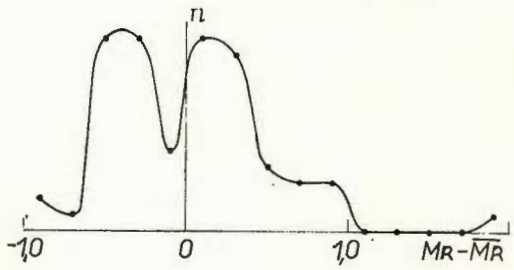

Fig. 3. — Frequency distribution function of reduced magnitude values $(MR - \overline{MR})$, $\overline{MR} = 5$.

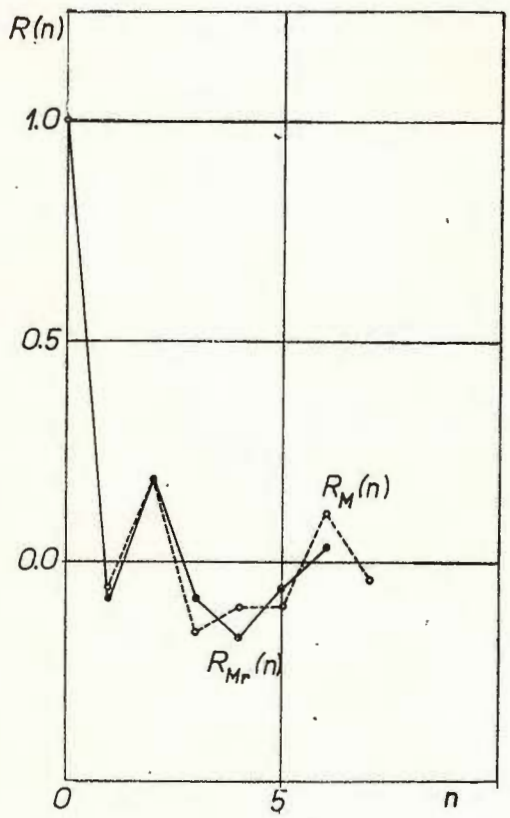

Fig. 4. — Autocorrelation functions of the series of magnitude values $R_M(n)$ (dashed line) and of the series of reduced magnitude values $R_{MR}(n)$ (full line)

is the fundamental condition of successfull application of simple statistical method of prediction, which will be used in this paper. The distribution of the values $(M_i - \bar{M})$ of our series shows, that this condition is satisfied only very approximately (fig. 3).

The autocorrelation function of the series $(M_i - \bar{M})$ $i = 1, 2 \ldots 66$ is denoted $R_M(n)$ and plotted by a dashed line in figure 4, the value of dispersion being $D_M = C_M(o) = 0{,}23$. The series analysed is drawn in figure 5 by the curve 1. It contains a weak harmonic component with the period 28 i, see curve 3, figure 5. By removing of this harmonical

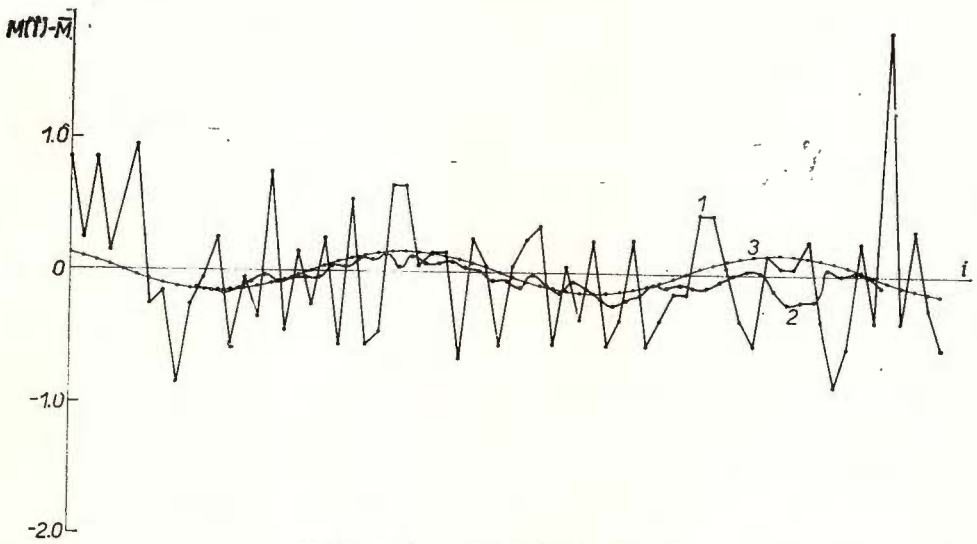

Fig. 5. — Series of magnitude values:
1. original values $\overline{M}_i - \overline{M}$. $\overline{M} = 5$. $\overline{M}_i$ taken from the catalogue of C a l o l; 2. values smoothed by mooving averaging with $m = 10$; 3. harmonical component of the series.

component a reduced series MR_i has been constructed, the autocorrelation function of which being drawn by a full line in figure 4. The value of dispersion D_{MR} of this reduced series is $D_{MR} = 0{,}8\, D_M$, what means that this extraction of the harmonical component is usefull. We do not know, if this component is the optimal one, but the small length of our series does not allow us to use any other more objective method e.g. the cosine transform of the autocovariance function (J e n k i n s, W a t t s, 1972).

Now, if all above mentioned conditions are satisfied, we may use a simple linear finite length prediction operator $(a_1\ a_2 \ldots a_n)$, $n \ll N$ with constant coefficients $a_1, a_2 \ldots a_n$, the optimal values of which are to be calculated from the condition of least squared prediction errors. The statistical prediction of the future i.e. not yet known value of our time series, say $\check{M}(t)$, let us express in terms of some known past values of magnitude $M(t-1)$, $M(t-2)$ ... according to the formula

$$\check{M}(t) = a_1 M(t-1) + a_2 M(t-2) + \ldots + a_n M(t-n) \qquad (5)$$

In order to calculate the optimal prediction operator, we write the condition

$$\sum_{i=1}^{s} [M(i) - \breve{M}(i)]^2 = \text{minimum} \tag{6}$$

and substituting for $M(i)$ according to (5)

$$M(i) - a_1 M(i-1) - a_2 M(i-2) - \ldots - a_n M(i-n) = \text{minimum} = f(a_1, a_2 \ldots a_n)$$

Evaluating the partial derivatives of this function and introducing conditions

$$\begin{aligned} &\frac{\partial}{\partial a_1} [f(a_1, a_2 \ldots a_n)] = 0 \\ &\frac{\partial}{\partial a_2} [f(a_1, a_2 \ldots a_m)] = 0 \\ &\vdots \\ &\frac{\partial}{\partial a_n} [f(a_1, a_2 \ldots a_n)] = 0 \end{aligned} \tag{7}$$

we obtain expressions containing products of the form

$$\sum_i M(i) \; M(i-k) \qquad k = 1,2 \ldots r$$

which are the values of the autocorrelation function $R_M(k)$. Introducing these values into the set of conditions (6) we obtain the so-called normal equations

$$\begin{aligned} R(1) &= a_1 R(0) + a_2 R(1) + \ldots . a_n R(n-1) \\ R(2) &= a_1 R(1) + a_2 R(0) + \ldots , a_n R(n-2) \\ &\vdots \\ R(n) &= a_1 R(n-1) + a_2 R(n-2) + \ldots a_n R(0) \end{aligned} \tag{8}$$

where $R(0)$, $R(1) \ldots R(n)$ are known values of the autocorrelation function of our series M_i. Unknown coefficients $a_1 \ldots a_n$ may be now calculated solving the system of normal equations. This solution is not too complicated to-day (R o b i n s o n, 1966). The value of mean squared prediction error should decrease with the increasing length of the prediction operator. As a rule, the optimal length of this operator corresponds to the number of non-zero values of the autocovariance function.

Let us now return to the prediction of the values of our series M_i. As well as the dispersion of this series is very low, $D_{MR} = 0{,}2$ it is not necessary to solve the system (8) exactly. To demonstrate it, let us use a very simple prediction operator of the length $n = 10$ with equal values of all coefficients $a_1 = a_2 = \ldots = a_{10} = 0{,}1$. In this case, predicted values

are identical with those obtained by moving averaging of last ten values of the series. Predicted values form the curve 2 in figure 5. The empirical mean squared prediction error in this case is $D_M^{\vee} = 0{,}25$. It follows that the standard deviation of one prediction of the next future value of this

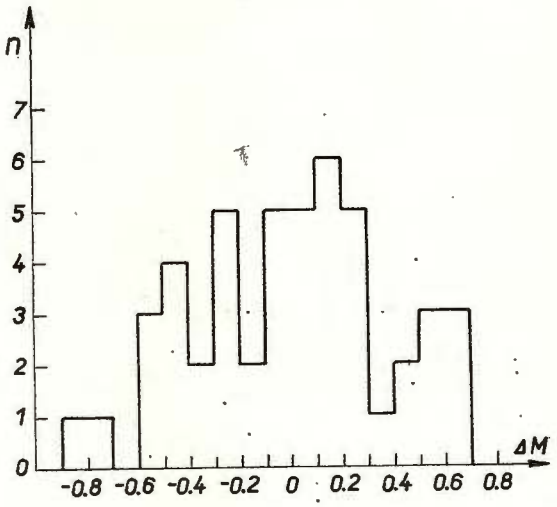

Fig. 6. — Frequency distribution of prediction errors ΔM.

series is $d = 0{,}5$. The frequency distribution function of prediction errors $n = f(M - M) = f(\Delta M)$ is given in figure 6.

We have seen (fig. 4) that the series of MR does not represent a fully uncorrelated random process, the so called white noise. Therefore the statistical prediction and autocorrelation analysis of the series of magnitude may have certain practical meaning. The fundamental condition for the application of the above-mentioned method is Gaussian distribution function of M_i. In some regions a lognormal distribution function has been reported (N e u n h ö f e r, 1969; S a c u i u, Z o r i l e s c u 1970). In these cases it will be more convenient to analyse the series of values (log M_i).

THE SERIES OF RECURRENCE INTERVALS

Let us now deal with the series of recurrence intervals $T_i = (t_i - t_{i-1})$ of all the earthquakes with focal times t_i and magnitude $M > M_0 = 4$ included into our basic catalogue (fig. 7). The mean value of T_i is $\bar{T} = 4$ months, the dispersion $D_T = C_T(0) = 20$. The values of the covariance function $C_T(k)$ of this series are zero for practically all $k = 0$. Our series of recurrence intervals does so represent the so-called white noise. The statistical prediction of such process has no practical meaning. All predictions are in this case equal to $\bar{T}$ and therefore the value of the mean squared prediction error is equal to the dispersion of the series D_T.

In many circumstances, however, the prediction of seismic activity is of great practical importance. As the value of the (cummulative) seismic

activity A is proportional to $1/\overline{T}$ let us mention here a method of prediction of smoothed values $S(T_i)$ of the individual recurrence intervals T_i.

The method most frequently used for smoothing is that of moving averaging. We mention here the series

$$S(i) = 0{,}1\,(T_i + T_{i-1} + \ldots + T_{i-9})$$

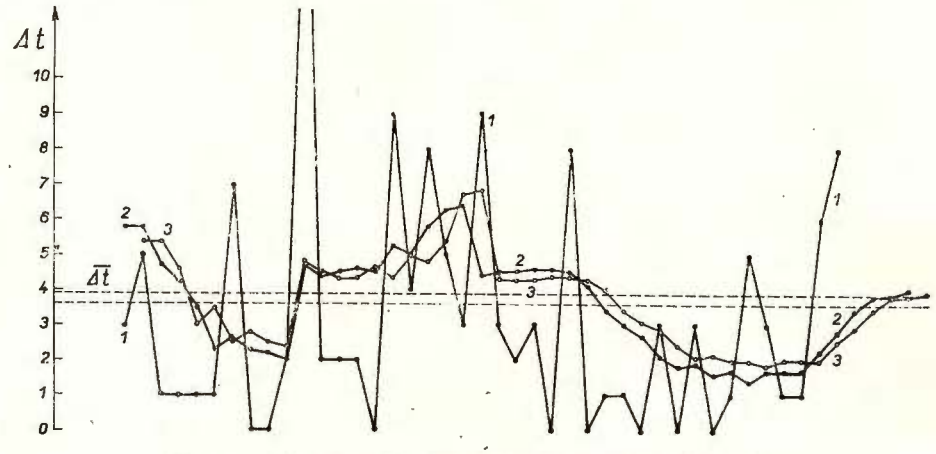

Fig. 7. — The series of earthquake recurrence intervals:
1, original values taken from the catalogue of C a l o i, $t_i = T_i = t_i - t_{i-1}$ in months, $\overline{T} = 4$ months; 2, smoothed recurrence intervals by mooving averaging with $m = 10$; 3, predicted values of smoothed intervals (curve 2).

$i = 10, 11, \ldots N$ see curve 2 in figure 7.

Such smoothing transforms the covariance function of the original series into the form

$$\begin{aligned} (C_{S,m}(k) &= D_T/m \cdot (1 - k/m) \quad \text{for } k \leqslant m \\ C_{S,m}(k) &= 0 \qquad\qquad\quad \text{for } k > m \end{aligned} \tag{9}$$

where m is the number of values taken into the moving averaging. In our case $m = 10$.

In the case of linear covariance function (9) is the prediction operator [2]

$$\begin{aligned} a_1 &= m/(m+1),\ a_2 = a_3 = \ldots = a_{m-1} = 0 \\ a_m &= a_1 - 1,\ a_{m+1} = a_{m+2} = \ldots = 0 \end{aligned} \tag{10}$$

The length of the operator does not depend on m having in all cases only two non-zero coefficients. Predicted values of smoothed series may be so calculated by means of the formula

$$\check{S}(i) = a_1\ S(i-1) + a_m\ S(i-m) \tag{11}$$

The theoretical value of the mean squared prediction error

$$D_{S(theor)} = 2\,D_T/(m^2 + m)$$

[2] R u d a j e v V., B u b e n J. Statistical prediction of rockburst activity. 19 72 *Mater. i pracy Inst. Geofys. Pol. Acad. Sci.* (in press).

In our case is the empirical dispersion $D_T = 20$ and $m = 10$ so that it shall be $D_{S\,(\text{theor})} = 0{,}4$.

The cumulative seismic activity series defined by moving averaging of recurrence intervals T_i has evidently no serious physical meaning. More adequate is the exponential smoothing according to the formula

$$Y_i = p\,T_{i-1} + p^2\,T_{i-2} + p^3\,T_{i-3} + \cdots \tag{12}$$

where the smoothing constant $|p| < 1$.
In this case, the smoothed series has the covariance function of the form

$$C_Y(k) = C_Y(0)\,p^k \tag{13}$$

The series Y_i belongs to the class of Markovian processes. If the value Y_i of such process is given than the value Y_{i+1} does not depend on the values Y_{i-2}, Y_{i-3} ...
In the case of Markovian process it is not necessary to calculate the prediction operator by solving the system of normal equations (8) and simple formula holds

$$\check{Y}(i+1) = p\,Y(i) \tag{14}$$

Moreover, the coefficients of the prediction operator may be easy calculated even in more complicated cases, where the values of series predicted, say X_i are measured not exactly. but only with definite errors dx_i. If the values dx_i are not dependent on X_i and if the distribution function of dx_i is Gaussian, the optimal prediction operator is as follows (B r o w n, 1971).

$$a_j = p\left(1 - \frac{B}{pA}\right)\left(\frac{B}{A}\right)^j \tag{15}$$

where

$$A = 0{,}5\,(b + 2pD_d)^{1/2} + 0{,}5\,(b - 2pD_x)^{1/2}$$

$$B = 0{,}5\,(b + 2pD_d)^{1/2} - 0{,}5\,(b - 2pD_x)^{1/2}$$

$$b = D_x\,(1 - p^2) + D_d(1 + p^2)$$

D_x is the dispersion of the series X_i
D_d is the dispersion of the errors dx_i
If errors dx_i are small enough, we put $D_d = 0$ and the prediction operator (15) is in agreement with (14).

Let us now return to our series of recurrence intervals (fig. 7) S_i which is the series of averaged values of T_i with $m = 10$. The covariance function of this series calculated empiricaly is expressed by the formula

$$C_S(k) = 2\,(1 - 0{,}13k) \tag{16}$$

which approximately corresponds to the theoretical one (9), see figure 8 curve 2. In figure 8 there is also the function

$$C\,(k) = 0{,}82^k$$

which corresponds to the relation (13). If this approximation is good enough, we have to use the simplest prediction formula (14) with $p = 0{,}82$. The predicted values of the curve 2 in figure 7 are given by the curve 3. The dispersion of prediction errors calculated empiricaly $D_{S\,(emp)} = 0{,}43$, which agrees well with its theoretical value 0,4.

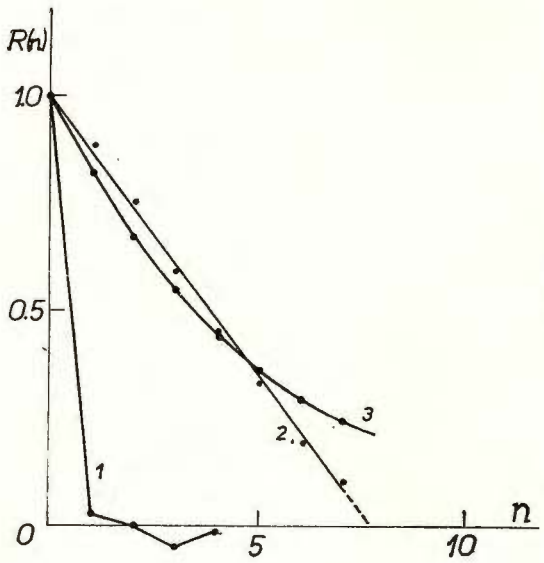

Fig. 8. — Autocorrelation functions of the series of recurrence intervals:
1, The original series T_i; 2, series of smoothed intervals by mooving averaging with $m = 10$; 3, the function $R(n) = 0{,}82^n$.

As a result of this chapter we may conclude, that the statistical prediction of seismic activity series A_i, which itself is not an individual but a statistical parameter, is of interest for special practical purposes.

THE SERIES OF SEISMIC POWER

Let us compare the cummulative curve $M(t)$ with the number of earthquakes $N(t)$ as functions of the time t with $t = 0$ in January, 1st, 1959. Both curves are very similar one to another (fig. 9) so that an empirical relation holds

$$M(t) = \overline{M}\, N(t)$$

If the function $N(M)$ has the simple (3) where a, b are constants, it holds according to (4)

$$\overline{M} = \sum_i M(t)/N(t) = 0{,}4343/b + M_0 \qquad (17)$$

We see that the similar shape of curves $M(t)$ and $N(t)$ is equivalent to $\partial b/\partial t = 0$ and $\partial M_0/\partial t = 0$. It follows that drawing the relation (16), time variations of b may be detected very easy.

In this paper all recurrence intervals have been calculated without respect to the magnitude of earthquakes. Under this condition the recurrence intervals form an uncorrelated series. Moreover the crosscovariance function of series M_i and T_i.

$$C_{M.T}(k) = \overline{(T_{i-k} - 2{,}6)(M_i - 5)}$$

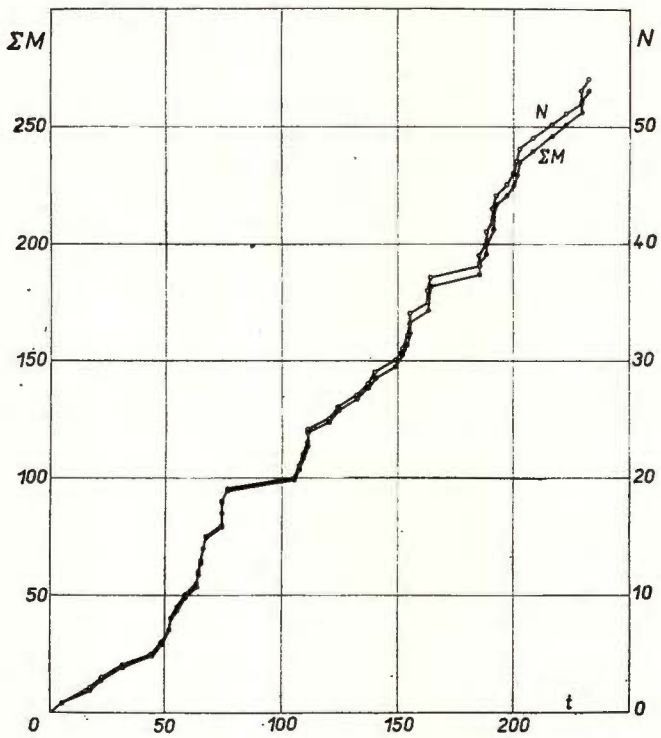

Fig. 9. — The function $\Sigma M(t)$ (full circles) and $N(t)$ (upper curve), the time t in months.

$i = 1, 2 \ldots (N - k)$ equals practicaly to zero for all $k \neq 0$. Similar result has been reported for earthquakes in the region Vrancea (S a c u i u, Z o r i l e s c u, 1970).

Let us now compare the variability of the series $M(t)$ and $N(t)$. On the horizontal axis in figure 10 there are the values ΣM. The curve $i(\Sigma M)$ represents the number of earthquakes, which is necessary to reach given values of ΣM. Analogicaly the curve $t(\Sigma M)$ represents the time t (in months calculated from 1950) which is necessary to reach the value ΣM. The variability of the series $M(t)$ is much more pronounced than that caused by various values of magnitude.

The basic catalogue of earthquakes contains values M_i as well as corresponding values of seismic energy E_i. Evaluating this material statisticaly we receive an approximation $\log E_i = K_i = 9{,}7 + 2M_i$ and it follows

$$\sum_i M_i = 0{,}5 \sum_i K_i - 4{,}9\, i$$

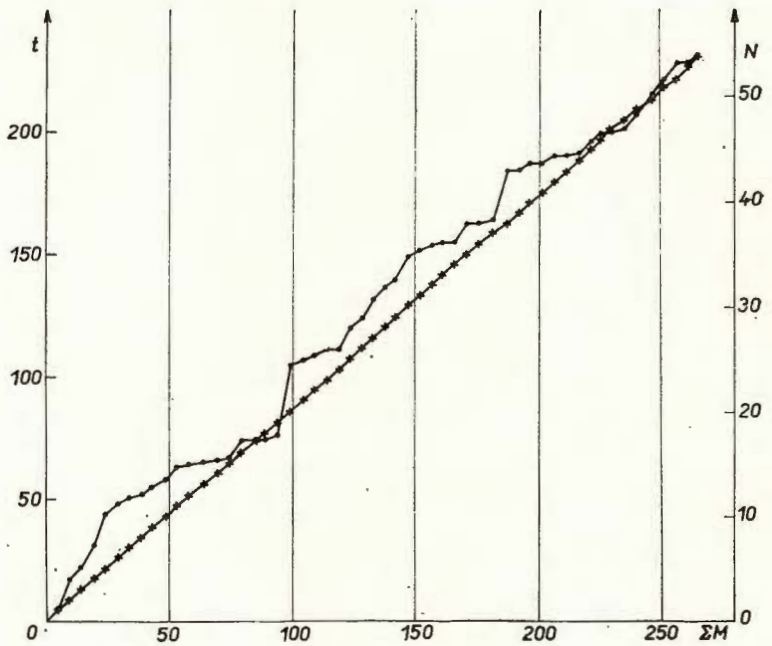

Fig. 10. — The function t (Σ M) (upper curve) and the function N (Σ M) (lower curve).

We have then a series of discrete values of seismic power W_i of the whole area

$$W_i = 1{,}15 \cdot 10^{-12} E_i/(t_{i+1} - t_i) \quad \text{(erg, day, watt)}$$

The covariance function of this series $C_w(k)$ has zero values for all $k \neq 0$ and moreover the distribution function $n(W)$ is not Gaussian. Statistical prediction of individual values W_i is therefore of no practical importance. The mean value $\overline{W}$ of seismic power in the period 1951—1967 is approximately of the value of 0,7 megawatt.

THE SERIES OF STRAIN RELEASE VALUES

In this chapter we shall make use of some results of measurements of the number $N(Q)$ of seismoacoustic impulses occuring in rock samples subjected to slowly growing axial stresses $Q(t)$ (B u b e n, 1971). The

irreversible part of the volume deformation of rock samples, called the dilatancy $dV(Q)$ had been measured parallel with the values $N(Q)$ (Scholz 1968). Evaluating a great number of experiments following empirical relation was found.

$$N(Q) = \text{const. } dV(Q) \tag{18}$$

The well known cumulative curve introduced by Benioff is very frequently used in seismicity research, the relation between $\sum\sqrt{E_t}$ and the mechanical deformation of the focal area being accepted with criticism. We shall here demonstrate a relation between series $N(t)$ and $\sum\sqrt{E(t)}$. First of all, using known formulae, e.g.

$$E = 10^{(9.15+2.15M)}$$

$$M_{H20} = \log(A/T) + 1{,}66 \log D + 3{,}3$$

we have the proportionality of series $\Sigma\sqrt{E(t)}$ and $\Sigma A(t)$. Now we shall demonstrate the proportionality of series $\Sigma A(t)$ and $N(t)$. In order to verify this proportionality, seismoacoustic impulses were registrated on rock samples as well as in rock-massiv under stress concentrations caused by mining excavations.

The proportionality of series $\Delta M(t)$ and $N(t)$ may also be derived from the distribution function (3), where a, b, M_0 are constants

$$\overline{M}(t) = \sum_i M(t)/N(t) = 0{,}43.b + M_0 = \text{const.} \tag{19}$$

We must now suppose the stationarity of the sample $M(t)$, i.e. that the value $\overline{M}(t)$ does not depend on the time t.
In this case it follows from (19)

$$M(t) = \text{const. } N(t)$$

and substituting this into (18) we become finally that the cumulative square root of seismic energies should be proportional to the irreversible (brittle) volume deformation of the active area.

We must suppose, that the mean rate of brittle deformations $\frac{\partial}{\partial t}$ ($\sum\sqrt{E(t)}$)of the Earths crust in active seismic zones varies only very slowly with the time, i.e.

$$\Sigma\sqrt{E(t)} = c \cdot t$$

where c does represent a steady trend.

According to this a random variable is introduced

$$Y(t) = \Sigma\sqrt{E(t)} - c \cdot t \tag{20}$$

as it had been done by Aki (1961). This process seems to be approximately Gaussian.

Similar random series has been introduced for the statistical prediction of rock bursts in coal-mines near Kladno, Czechoslowakia. It is the series $\sum A(t) - \bar{A} \cdot t$, where $A(t)$ is the maximal trace amplitude in the group of maximal waves registrated by a vertical component of a local seismic station and corrected according to various hypocentral distances.

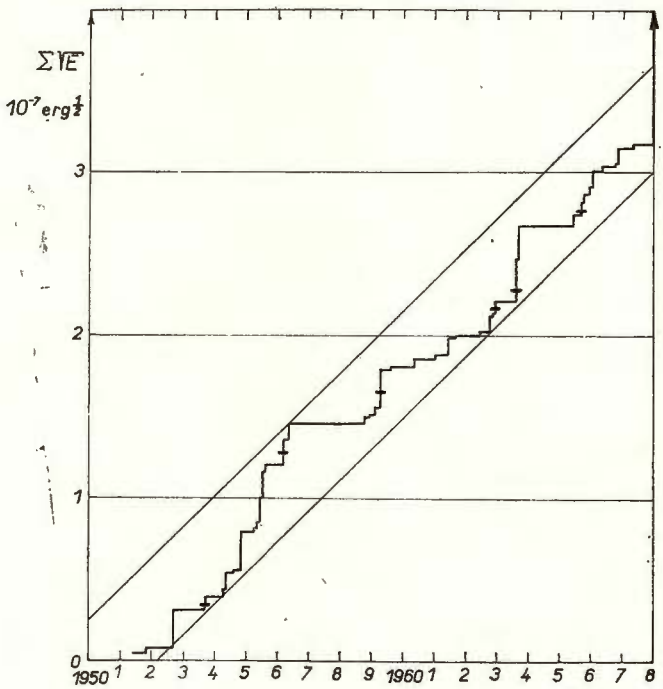

Fig. 11. — The strain-release curve of earthquakes in the period 1951—1968.

The cumulative plot $\sum \sqrt{E}$ of earthquakes studied in this paper does vary within a definite strip. Strong earthquakes however occur, which causes sometimes considerable deviations of the mean slope of the cumulative diagram. As an example we see the strong earthquake in 1968 (fig. 11). Such earthquakes are fully unpredictable events if there is no additional series of values parameters of tectonophysical processes in this area.

CONCLUSION

The values of magnitude M_i of earthquakes in the region Val Padana form a random time series, which appears weak stationary within certain periods of time. The autocovariance function of the series M_i has rather low values, but statistical prediction of future values of this series may have some practical meaning.

The interoccurence intervals of earthquakes are not correlated. Smoothed series of these intervals has been introduced, the autocovariance function of which has considerable values due to methods used for smoothing. This paper deals with a simple method of prediction of series of seismic activity constructed by moving averaging as as well as by exponential smoothing of individual interoccurence intervals.

Cumulative functions $\sum \overline{E(t)}$ and $N(t)$ may be proportional to the dilatancy of the focal area. The series of random variables $\Sigma E(t) - \bar{E}.t$ and $N(t) - \bar{N} \cdot t$ may be statisticaly predicted only within periods of the stationarity of $\bar{E}$ and $\bar{N}$. Some breaks of the values $\bar{E}$ coincide with strong earthquakes in this region.

REFERENCES

Aki K. (1961) Količestvennoje predskazanije častoty zemletrjasenij kak slučajnoj veličiny. *In*: Slabyje zemletrjasenija. Moskva.

Brown R. (1971) Smoothing, Forecasting and Prediction of Discret Time Series. London.

Buben J. (1971) O pewnych wlasnosciach sekwencji wstrasowych. *Mater. i pracy Inst. Geofiz. Pol. Acad. Sci.*, 47, Warszawa.

Caloi P., Romualdi G., Spadea M. G. (1970) Carratteristiche sismiche e geodinamiche della Val Padana qualli risultano dell' attivitá sismica ivi verificatesi dall'inizio dell'Era Volgare a tutto il 1969. *Ann. Geofis.*, XXIII, 2—3, Roma.

Jenkins G., Watts D. (1971) Spektralnyj analiz i jego priloženija. Moskva.

Neunhöfer H. (1969) Vergleichende Betrachtung de Energie-Häufigkeits-Verteilung von Erdbeben und Gebirgsschlägen. *Seism. Arbeiten Inst. Geodynamik*, 13, Jena.

Purcaru G., Zorilescu D. (1971) A Magnitude-Frequency Relation for the Lognormal Distribution of Earthquake Magnitude. *PAGEOPH*, 87, Basel.

Robinson R. (1966) *Geophys. Prosp.*, 14, 1, Hague.

Sacuiu I., Zorilescu D. (1970) Statistical analysis of seismic data on earthquakes in the Area of the Vrancea Focus. *Bull. Seism. Soc. Am.*, 60, 4, Berkeley.

Scholz C. H. (1968) Microfracturing and the inelastic Deformation of Rock in compression. *J. Geophys. Res.* 73, Richmond.

SEISMOTECTONIC MAP OF THE ROMANIAN TERRITORY

BY

LIVIU CONSTANTINESCU [1], ION CORNEA [2], VASILE LĂZĂRESCU [3]

INTRODUCTION

The Romanian territory overlaps the Northern Branch of the Alpine-orogenic belt and its East-European foreland in an area of spectacular trend change of the Carpathian folded chain. Here, the crown-shaped geological structure of the Eastern and Southern Carpathians and of the Apuseni Mountains discloses a central depression (Basin of Transilvania) and a continuous foredeep (Subcarpathian zone and the Getic depression), in front of a platform region of two conspicuously different ages : the older Epikarelian or Epialgomian East-European craton and the younger Epihercynian Moesian platform.

Although related to a volcanism extincted since the dawn of Quaternary time, these orogenic and platform areas are still seismotectonically active. Nevertheless, despite wide research carried out both seismological and geological-tectonical fields, a systematic study concerning the relationships between seismicity and tectonics is still lacking.

With a view to preparing the way for filling out this gap, an attempt has been made by the present authors to synthesize the information now available for compiling the seismotectonic map of the Romanian territory, at least as a preliminary stage of what should be such a complex picture of the territory taken into consideration. It is the presentation of the results obtained in this direction, as brought together in their cartographic plotting, and of their seismological as well as of their geological-tectonical substratum which constitutes the object of the present paper.

CONDITIONS OF COMPILING THE SEISMOTECTONIC MAP OF ROMANIA

For many years, the relationships between earthquakes occuring within the Romanian territory and the geological structure of this territory have remained a problem of mere conjecture. In spite of the great interest

[1] Department of Geophysics, IPGG, 6, Traian Vuia street. Bucharest 22, Romania.
[2] Institute for Applied Geophysics, 78, Izvor street. Bucharest 5, Romania.
[3] Department of Geology, IPGC, 6, Traian Vuia street. Bucharest 22, Romania.

presented by an integrated seismotectonic study of a territory with a wide variety of seismic events — even if not very frequent — , on the one hand, and a complex geologic structure together with peculiar tectonic features, on the other, the frontier domain between seismology and tectonics has not yet been explored for Romania in accordance with its potential scientific and practical productivity. Sporadic remarks concerning some seismotectonic implications may be found in seismological papers — especially in those having as object the study of the focal mechanism for the Vrancea earthquakes — , as well as references to seismic events are occasionally made in geological and tectonical contributions. Nevertheless, one cannot yet speak of a genuine seismotectonic research concerning the Romanian territory.

This fact is due, perhaps, to the character of integrated study of such a research in a complex frontier field, which is not easily accesible as long as the observational data do not satisfy some special conditions of completeness, geographical distribution and intrinsic reliability or as long as a close co-operation is not yet established between specialists in the various fields of interest for seismotectonics, having at the same time a comprehensive understanding for problems outside their own domain of research but connected to it.

During the last decade, or so, the conditions necessary for embarking on seismotectonic research work concerning the Romanian territory have remarkably improved. The high-fidelity reception and recording equipment of conventional seismological information as well as that of explosion seismology data, associated with the use of modern mathematical processing and analysis of observational results have led to a new approach of the seismotectonic problems of the Romanian territory. To the same purpose have contributed the obvious progresses made towards a better knowledge and clearer understanding of the structural features within the Carpathian range area and its foreland, thanks to deep drilling information and to seismic, gravity and magnetic regional surveys. On the other hand, geological research carried out on the neotectonics and geodynamics of the Carpathian regions in connection with their seismic activity provided new and wider qualitative information relevant for seismotectonic studies, equally supported by additional quantitative data coming from geodetical measurements of recent crustal movements.

A last but not least impetus for this kind of research work has been given by the UNDP/UNESCO Project for the survey of the seismicity of the Balkan region, whose implementing was involving, as an intermediate stage toward the achievement of the final aim, the compilation of the seismotectonic maps of the participating countries.

Thus, the present authors have been encouraged to undertake the study which has subsequently led to the results reported in a previous work, quoted here as „Paper I" [4], concerning the seismotectonics of the

[4] Constantinescu L., Cornea I., Lăzărescu V. An Approach to the Seismotectonics of the Romanian Eastern Carpathians. 1973. *Rév. Roum. Géol. Géogr. Geophys., Sér. Geophys.*, 17, 2 (in press).

Romanian Eastern Carpathians. Continuing and widening their research, under the favourable conditions mentioned above, have allowed to obtain the seismotectonically relevant information which plotted cartographically provided a first picture of the seismotectonics for the whole of the Romanian territory.

SEISMOTECTONIC RELATIONSHIPS WITHIN THE ROMANIAN TERRITORY

The Vrancea seismic region

From the seismotectonic point of view, by far the most important epicentral area in Romania is the Vrancea region, situated at the Carpathian Arc Bend. This region is well-known as ,,a remarkable source of intermediate shocks'' (Gutenberg, Richter, 1965), designated as Moldavian or Carpathian earthquakes (Atanasiu, 1961), sometimes also called ,,Romanian earthquakes'' in the foreign seismological literature (Lehmann, 1961; Bolt, 1965). Its seismic regime is determinative for the seismicity of the whole Romanian territory (Constantinescu, Enescu, 1964 b) and may be characterized, within the present context, by the following features :

a) Relatively frequent monokinetic shocks, casually of high energy ($M > 7$), as was, e.g., the case for the earthquakes of 10th November 1940 ($M = 7.4$), with large macroseismal area — even for tremors of low magnitude — and quasi-elliptical isoseismal lines, elongated in the NE—SW direction, while abnormally tightly spaced towards the mountains.

b) Limited epicentral area (less than 10 000 km^2) and unusual persistance of the earthquake foci located at intermediate depths (90—160 km), prevailingly grouped towards the deeper limit and with an obvious though slight trend (given the small size of the epicentral area) of having greater depths towards the mountain range; these characteristics are to be compared, at the planetary scale, only to those of the famous foci in the Hindu Kush Mountains (Gutenberg, Richter, 1965).

c) As far as the focal mechanism is concerned, the fault-plane solutions (Constantinescu, Enescu, 1964; Ritsema, 1969) indicate as prevailing the compressional type of shock, corresponding to a dip-slip reversed fault, with a horizontal component of the greatest compressive stress in a roughly WNW—ESE direction, consistent with the orientation of the tectonic forces responsible for the overthrusting ,,nappes'' produced in the Eastern Carpathians. Another possible ,,fault-plane'' indicated by focal-mechanism research is striking NW—SE with a dip towards SW, being generally parallel to the orientation trend of some important fault-lines in the foreland of the orogenic belt, as e.g. the Peceneaga-Camena and Capidava-Ovidiu fractures and parallel to the Podolian border of the Russian Platform too.

Considered as ,,reliable'', these results of wide research concerning the focal mecanism of Vrancea earthquakes have already been used for

seismotectonic purposes not only locally[5] (Constantinescu, Enescu, 1964a) but also at the continental scale (Ritsema, 1969) and even within a global survey (Isacks, Molnar, 1971).

d) Close association, at the same time, of the foci spatial distribution with the Carpathian Arc Bend, in strong neotectonic uplift (Constantinescu, 1966) and with the deep Sarmatian-Pliocene Focşani-Odobeşti Depression — Pliocene deposits being here almost 12 km thick and the thickness of the whole sedimentary cover amounting to about 18 km in front of the mountains — A close relation is also to be mentioned to a crossing zone of continental tectonic lineaments (the Podolian and the Tethys borders of the East-European Platform), as well as to the crossing of regional faults within the basement.

The information provided by earthquake seismology on some important tectonic features is supported and completed by additional data coming from explosion seismology. Thus, some of the faults mentioned above — as the prolongations of the Peceneaga-Camena and Capidava-Ovidiu fault lines — were proved by the latter technique to have considerable throws (5—6 km) down to the Conrad and Mohorovičić discontinuities (Constantinescu et al., 1972). There are also local faults which were recorded by seismic surveys within the Mesozoic basement. They disclose a mosaic-like pattern, tightly spaced around the Focşani-Odobeşti Depression, without having been made conspicuous beneath it, which cannot mean that the corresponding faults are lacking there but rather suggests that the excessively thick layer of young sediments prevented their detection.

As it was already advanced in Paper I, it seems reasonable to infer — but we emphasize that this is still a mere hypothesis — the possibility of existence of a subduction zone, generated by the Black Sea floor-spreading, which gave rise in the upper mantle to an inverted shear-zone with feather-like faults (sensu Maryland Billings) arriving up into the crust. Such fractures could be relayed into the crust by older faults, reactivated by subsequent tectonic forces.

Though not so important in the case of the collision-type mountains as in that of the cordilleran-type ones (Dewey, Bird, 1970), geothermic phenomena may also have influenced the process of generation of such deep-seated inverted fault-zones in the upper mantle, together with the more superficial influence of the old East-European Platform drifting. It is by such a complex process, in which subcrustal masses are both thermally and mechanically driven, that could be also explained the formation of a sialic root of the mountains, within the considered area, with an amplitude of about 15 km under the average depth of the M discontinuity.

Without going too far into details in adopting the plate-tectonics views for the case we are discussing — as it has already been done either on a prevailingly seismological basis (Roman, 1970) or by using exclusively geological information (Rădulescu, Săndulescu, 1973)

[5] *Op. cit.*, p. 4.

—we feel entitled by the above mentioned seismotectonical evidence, as resulting from both seismological and tectonic reliable data, to assume for the Vrancea region subduction active forces, outside the mountain zone, which induced by friction dragging forces for the orogenic root. Another subduction force, probably of less intensity, is inferred as coming from the subcrustal zone of the Transylvanian Basin. This view is also supported by the existence of a large regional magnetic anomaly contoured in the centre of this depression and by the thinning of the Earth's crust, within the same central zone, to about 32—34 km, while under the mountains — at the Carpathian Arc Bend — its thickness reaches 48—50 km. Such a regional structural pattern could reasonably reflect the presence, under the central part of Transylvania, of a zone of divergent subcrustal currents of secondary importance. The same suggestion is given by the discovery of a deep normal fault within the basement of this intermountainous depression and of a lateral thickening of the basaltic layer of the crust.

Of primary seismotectonic significance is, therefore, the fact that in this region there are complex correlations between the seismic phenomena, on the one hand, and tectonical peculiarities in the Earth's crust and upper mantle, on the other : the site of the seismic focal zone has been determined by certain tectonic features of the crust and upper mantle — of a continental size — and, in its turn, the seismic activity has produced geological tectonic effects of less regional scope (replay of old faults relayed by subcrustal fractures, generation of new faults, formation of locally important depressions).

Taking into account the persistence of the subsidence trend at the Eastern Carpathians Arc Bend since Cretaceous time, it seems also reasonable to conclude that the palaeoseismicity of this region has migrated in parallel with the tectonic and sedimentation processes from the inner to the outer orogenic zones. The seismic activity is likely to have not been at the same energy level during this entire geologic time, the earthquakes having begun to be stronger since the Sarmatian time. As to the present level of the seismic energy released yearly, it has been estimated as having, for the Vrancea intermediate eartquakes, an average value of about $6 . 4 \times 10^{19}$ erg. year^{-1}.

A last peculiar feature of the seismic zone of Vrancea to be made conspicuous in this seismotectonic context is the obviously lower intensity with which its earthquakes are felt at sites in Transylvania, as compared with that of their effects in other equally distant places. This fact could be explained by the energy absorption within the more plastic root of the mountains and along the planes of young fractures of gravitational type bordering the intramountainous depressions (as the Bîrsa and Sfîntu Gheorghe sinking areas), as well as at the limits of the Transylvanian Basin itself. In this respect it is interesting to be noted that similar information is provided by the deep seismic soundings : explosions fired outside the Carpathian Arc and clearly recorded at great distances in the foreland were not to be detected at locations in the inner zone of its bending.

Other seismic zones

To all the other epicentral zones in Romania correspond shallow earthquakes (i.e. normal ones, sensu Gutenberg and Richter) generally polykinetical and of relatively low magnitude, in direct relationship with crustal, almost allways young faults. As such are to be mentioned several areas of moderate seismicity. In the Rădăuţi and Bacău regions, the earthquake foci are related to crossing zones between step-faults produced along the sinking border of the platform under the foredeep and transverse faults with respect to the orogenic chain. Shallow earthquakes are also produced along the Eastern and Southern limits of the Focşani—Odobeşti Depression, in connection with the same kind of step-faults of normal type.

A similar explanation is to be given to the existence of seismic foci in the Southern Carpathians (in the Vinga—Moldova Nouă region) and along the periphery of the Pannonian Basin (Oradea region) or in the middle of the Transylvanian Basin (region of Tîrnava). The very shallow and consequently sometimes of great local intensity earthquakes in Banat (Curea et al., 1967) are also to be mentioned in this context.

An important exception seeems to be made by the Făgăraş—Loviştea region (Southern Carpathians), where several earthquakes of locally large intensities and accompanied by many aftershocks have occurred, constituting the object of earlier research (Atanasiu, 1961) but being only recently studied in some detail (Constantinescu et al., 1971). Another kind of exception is represented by the Urziceni—Pogoanele region (Eastern Valachia, in the Moesian Platform) where several deeper (probably subcrustal) shocks have been recorded.

A special case, which needs further investigation, is that of the epicentre area of Mangalia, sited near the shore of the Black Sea, in a zone where the continental shelf is getting narrower and narrower towards South. The earthquakes occurring in this area, probably of the same type as those with the foci in the Shabla and Varna regions in Bulgaria, are related to a fault system extending on land as well as at sea, up to the faults contouring the shelf and the continental slope.

CARTOGRAPHIC PLOTTING OF THE SEISMOTECTONIC INFORMATION

The most important data relevant for the seismotectonics of the Romanian territory have been represented cartographically, leading to the map which constitutes the main contribution of this paper. At the scale of this map (1 : 1000000) many details had to be disregarded but the really significant seismotectonic information now available is contained in the map. The preceding comments and the indications given by the key of the map secure the accessibility of this complex information, making conspicuous the relationships between the seismic events and the main tectonic features of the Romanian territory. As for the seismotectonics of the Eastern Carpathians (Paper I), the data of the seismotectonic map of the whole Romanian territory are aiming at providing the elements

necessary for both knowledge and understanding of the dynamic aspects of the geologic structure, whether considered intrinsically or with a view to using the corresponding information for further purposes, such as seismic zoning or assessment of the seismic risk.

CONCLUDING REMARKS

The main results of this paper, as plotted on the seismotectonic map of Romania and emphasized by the comments accompanying it, represent first of all a synthesis of the most significant data furnished up to now by earthquake and explosion seismology, on the one hand, and by geology and tectonics, on the other, in connection with the complex relationships between seismicity and geologic structure of the Romanian territory. From this point of view the present contribution has the character of a condensed review paper with an assessment of the state in which the problems constituting its object find themselves now.

On the other hand, from the point of view of future investigations, the whole of the results reported here may constitute an adequate framework apt to indicate the right place of a contingent detailed contribution and to ascribe to it a proper weight within the entire research field taken into consideration. As such, this paper may serve as a general guide for further research concerning Romania's seismotectonics.

Finally, despite its preliminary character — due to the relative scarcity and limited reliability of the primary observational data —, the seismotectonic information contained in the present contribution can already be used as a basis for approaching such practical problems as seismic zoning in connection with designing earthquake-resistant public works. As a matter of fact, it is to the latter purpose that the work having led to this paper was carried out.

REFERENCES

Atanasiu I. (1961) Earthquakes in Romania (in Romanian). Ed. Acad. R.P.R., Bucharest.

Bolt B. A. (1965) Gradients of Travel—Time Curves from Deep-Focus Earthquakes, *Rev. Geophys.*, 3, Richmond.

Constantinescu L. (1966) Evidence of Recent Crustal Movements in Roumania and Problems Facing Their Research. *Ann. Acad. Sci. Fennicae, Ser. A*, III, 90.

— Enescu D. (1964 a) Fault-Plane Solutions for Some Roumanian Earthquakes and Their Seismotectonic Implications. *J. Geophys. Res.*, 69, Richmond.

— Enescu D. (1964 b) Energy-Magnitude-Intensity Relations for the Carpathian Earthquakes. Parameters of the Seismic Regime of the Vrancea Region. *Rev. Roum. Géol. Géophys. Géogr., Sér. Géophys.*, 8, Bucarest.

— Georgescu Anca, Radu C. (1971) About a Shallow Earthquake in Romania and Its Aftershocks. *Rev. Roum. Géol. Géophys. Géogr., Sér. Géophys.*, 15, Bucarest.

— Cornea I., Enescu D. (1972) Structure de la croûte terrestre en Roumanie d'après les données géophysiques. *Rev. Roum. Géol. Géophys. Géogr., Sér. Géophys.*, 16, Bucarest.

Curea I., Marienuț U., Slimac E., Toro D., Nedin D. (1967) An Earthquake of Unusual Violence in Banat (in Romanian). Tip. Univ. Timișoara.

Dewey J. F., Bird J. M. (1970) Mountain and the New Global Tectonics. *J. Geophys. Res.*, 75, Richmond.

Gutenberg B., Richter C. F (1965) Seismicity of the Earth and Associated Phenomena. Hafner Publ. Co., New York.

Isacks B., Molnar P. (1971) Distribution of Stresses in the Descending Lithosphere from a Global Survey of Focal Mechanism Solutions of Mantle Earthquakes. *Rev. Geophys.*, 9, Richmond.

Lehmannn I. (1961) *S* and the Structure of the Upper Mantle. *Geophys. J.*, 4, London.

Rădulescu D. P., Săndulescu M. (1973) The Plate-Tectonics Concept and the Geological Structure of the Carpathians. *Tectonophysics*, 16, Amsterdam.

Ritsema A. R. (1969) Seismo-Tectonic Implications of a Review of European Earthquake Mechanisms. *Geol. Rundschau*, 59, Stuttgart.

Roman C. (1970) Seismicity in Romania — Evidence for the Sinking Litosphere. *Nature*, 228, London.

I. CONSTANTINESCU, I. CORNEA, V. LĂZĂRESCU

SEISMOTECTONIC MAP OF ROMANIA

SCALE 60 km

KEY OF THE MAP

STRUCTURAL INFORMATION

ALPINE CARPATHIAN OROGENIC BELT
- MOUNTAIN FOLDING REGION
- DEPRESSIONS

FORE-LAND OF CARPATHIANS
- PLATFORM REGIONS
- GEOLOGICAL DEFICED REGIONAL & CRUSTAL FAULTS
- SEISMICAL DEFICED: a. CRUSTAL AND REGIONAL FAULTS
- b. DEEP LOCAL FAULTS
- AGE OF FAULTS & TECTONIC CONTACTS: CRETACEOUS (K), MIOCENE (M), PLIOCENE (Pl), QUATERNARY (Q)

NEOTECTONIC MOVEMENTS
- STRONG SUBSIDENCE
- ZONES OF HIGH HORIZONTAL GRADIENT OF VERTICAL MOVEMENTS
- LINES OF STRONG CONTRASTED VERTICAL MOVEMENTS
- LESS ACTIVE REGIONS

RECENT VERTICAL MOVEMENTS
- STRONG UPLIFT (> 2 mm/year)
- STRONG SINKING (OVER -2 mm/year)
- LESS ACTIVE REGIONS
- LINES OF CONTRASTED VERTICAL MOVEMENTS

SEISMOLOGICAL INFORMATION
- SEISMICALLY SENSITIVE LINES
- AVERAGE ISOSEISMAL LINES
- LINES OF EQUAL DEPTH (in Km) OF INTERMEDIATE EARTHQUAKES

KEY OF EPICENTRES

h_{Km} / M	< 5	5,1 - 6,0	6,1 - 7,0	7,1 - 8,0
0 - 10		○	○	○
11 - 30		⊖	⊖	⊖
31 - 60		⊕	⊕	⊕
Shallow	•	⊙	⊙	⊙
> 60		▽	▽	▽

UNION OF SOVIETIC SOCIALIST REPUBLICS

HUNGARIAN PEOPLE'S REPUBLIC

FEDERATIVE SOCIALIST REPUBLIC OF YUGOSLAVIA

P. R. OF BULGARIA

BLACK SEA

BUCHAREST

SEISMIC REGIME AND SEISMOTECTONIC ANALYSIS OF EARTHQUAKES IN THE EASTERN ALPS

BY

GEORG GANGL[1]

For obtaining a general view of the earthquake activity in the Eastern Alps you can see in figure 1 isolines of equal *number of epicentres* of the macroseismic intensity $I_0 \geqslant 4$ of the Medvedev-Sponheuer Karnik Scale (1964) referring to an area of about 500 km². Epicentres with smaller intensities were dropped. Although the activity is a sporadic one — were catastrophic earthquakes are rare — the number of epicentres varies with regard to their location with a ratio of 1 : 10. For example in the area of the Semmering Pass — southwest of Vienna (Wien) — and the Bohemian Massif in the North of Austria.

In the time domain there are 10 epicentres in an average year in Austria, variating from 1 to 22 without considering the aftershocks in a time interval of one day. The variation of the time domain looks to be a random one neglecting the clustering effect of aftershocks, in space the activity is much more stationary.

The number of earthquakes in this chart is nearly complete for this century, as you can see from the logarithmic frequency graph — which is linear for this range (Gangl, 1969b).

If you pay attention to the symbols, which mark the epicentres of destructive earthquakes, you will find, that the strongest historical earthquakes (the asterisk marks epicentres with intensities 9 or more) do not coincide exactly with the highest frequencies of epicentres in this century, but they are more or less within the *east-alpine earthquake zone* (Gangl, 1969 b); this zone comes from Slovakia, striking ENE to WSW and is continued in Northern Italy. The different geologic units are the Little Carpaths, the Inneralpine Vienna Basin, the end of the Northern Calcareous Alps, the different units of the Central Zone and South of the Alpine Dinaric Fault the Southern Alps. In this connection I would like to underline that there is no change in the increased present earthquake activity with regard to the direction of striking of the East-

[1] Institut fur Meteorologie und Geophysik der Universität Wien. Hohe Warte 38, A 1190 Wien, Österreich.

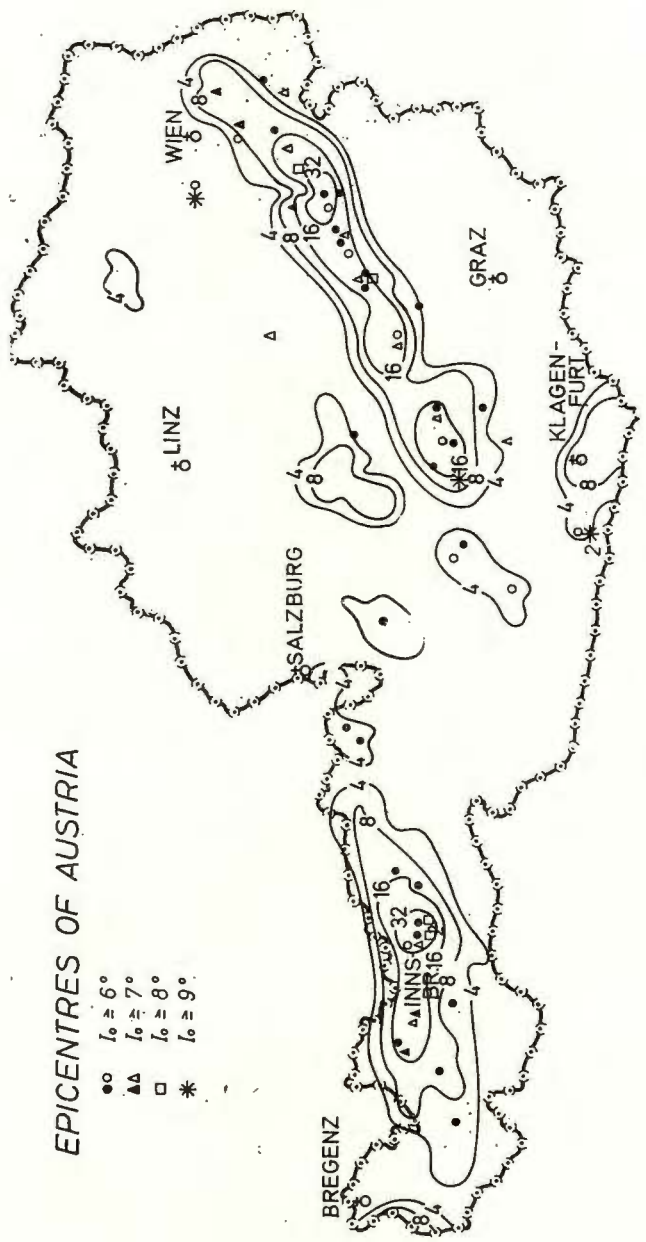

Fig. 1.— Epicentres of Austria :
1, $I_0 \geqslant 6°$; 2, $I_0 \geqslant 7°$; 3, $I_0 \geqslant 8°$; 4, $I_0 \geqslant 9°$.

Alpine Earthquake Zone in the Eastern Alps and the Southern Alps in Northern Italy. This might be interesting because the importance of the Alpine Dinaric Fault or Peradriatic Lineament within the tectonics of the alpine range is still under discussion.

For a map of maximum observed intensities a draft had been drawn including historical earthquakes. The difficulty is that there do not exist any isoseismal maps for earthquakes e.g. of Murau (1201). of Villach (1348, 1960), and of Neulengbach (1590). For obtaining the intensity values the *intensity distance relationship* was taken from strong earthquakes of this century whose epicentres were not further than twenty kilometers of the historical epicentre. At this attempt the observed intensity differences from the maximum value at the epicentre were shifted for the different directions separately taking into account the different extension of a certain isoseism from the epicentre.

On the 16th April 1972 at 11 a.m. there was an earthquake of the intensity 7,5 southsouthwest of Wiener Neustadt, which was felt 500 km NNW, but less than 200 km in the opposite direction of the Hungarian Plain where the energy is damped considerbly by thick cenozoic sediments. The perceptibility in the direction NNW may be caused by the presence of a wave guide realized by *a low velocity channel in the crust.* This interference made from isoseismal maps (G a n g l, 1969 a) has been verified recently by the results of explosion seismology (A n g e n h e i s t e r, 1972) and is certainly also the case for Tyrolian earthquakes. A low velocity channel with maximum thickness under the central parts of the Eastern Alps has been recorded ascending to the north.

For earthquakes in the extremaly south of the investigated area there is a marked difference in the direction of high perceptibility, for they are felt much more in the south : We observe a rapid decrease of the intensity on Austrian territory. This fact has been used for the construction of the map of maximum observed intensities for the famous Villach earthquake in 1348, whose maximum intensity is reported to have been even 10, by which the medeaval town of Villach has been destroyed (T o p e r c z e r, 1950). The intensity distance relationship was applied from an earthquake near Tolmezzo in 1959. The second earthquake of intensity 9 is reported from the same epicentre in 1690 although there is nearly no activity in the century.

The assumption for the calculation of the intensities is that the epicentres and the maximum intensities are known or may be checked easier for the historical earthquakes from chronicles than the intensity decrease by distance. For a more detailed comparison of the historical data with the described approximation see the extended version of this report [2].

The second question in this connection is that the strongest reported earthquakes have an intensity $I_0=7-8$ in this century. The maximum

[2] G a n g l G. Seismotektonische Untersuchungen und Erdbebengefährdung in den Ostalpen. 1973. Wien.

Fig. 2. — Maximum observed intensities :
1, I ⩾ 6° MS ; 2, I ⩾ 7° MS ; 3, I ⩾ 8° MS.

intensities of historical earthquakes are 9 or in the above mentioned case even 10. There is no doubt that these figures and the location of epicentres are less reliable than the information about the last century. For the construction of the shown draft of maximum observed intensities no reduction of intensities of historical earthquakes had been performed, so that the resulting intensities are even one degree higher than those obtained when this chart is constructed for the last century only (D r i m m e l, 1971).

Of special importance is the *earthquake mechanism* of this region. The analysis of the direction of first onsets shows that there is a different mechanism from that which is generally adopted for Central Europe and the alpine range. Figure 3 shows the northeastern part of the East Alpine Earthquake Zone. The chart shows the geologic units : starting in the

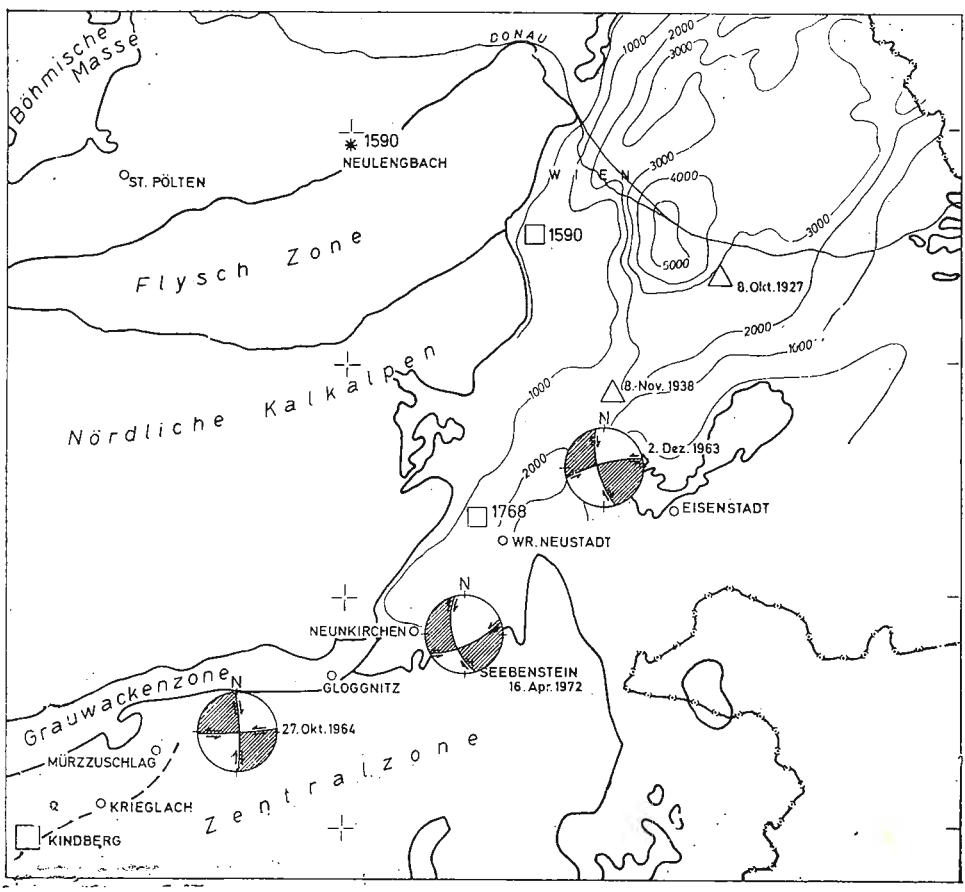

Fig. 3.— Earthquake activity and fault plane solutions at the eastern part of the East Alpine Earthquake Zone, Depth of the inneralpine Neogen basin of Vienna.

northwest with the Bohemian Massif, the Molasse Zone, and south of the border of the alpine range the zone of the Flysch and Helvetic Sediments, then the different nappes of the Northern Calcareous Alps, and the Central Zone of the Alps. The inneralpine Vienna Basin is limited by faults which cut obliquely across the Alpine-Carpathian structures. The basin is filled by sediments of Miocene and Pliocene age. A graben filled with quaternary sediments with a thickness of more than 100 m striking from Wiener Neustadt to NE (Mitterndorfer Senke) shows that there is a *tectonic activity* in the young geologic past. The isolines show the depth of the Tertiary base which is up to 5500 m (Kapounek, 1965).

An analysis of the first onsets of *P*-waves of the *Semmering* earthquakes shows that the condition of orthogonality of nodal planes is fullfilled (Earthquake of June 30th, and October 27th, 1964). The axis of maximum tension (*T*-axis) is approximately NW-SE showing that there is a relief normal to the general striking of the alpine range. A similar result is obtained for earthquakes in the NE. (Earthquake of April 16th, 1972 and of December 12th, 1963) Additional epicenters are marked by symbols as in figure 1.

The focal depth determined by means of macroseismic methods vary in the range of 5 (depth of basement rocks) and 20 km in the region of figure 3. The pleistocene graben structure corrresponds with the recent seismic activity in the upper crust and the analysis of first onsets of earthquake motion shows that there are tectonic movements interpreted as relief normal to the striking in the east of the Alps.

REFERENCES

Angenheister G., Bögel H., Gebrande H., Giese P., Schmidt-Thomée P., Zeil W. (1972) Recent investigations of surficial and deeper crustal structures of the Eastern and Southern Alps. *Geologische Rundschau*, 61, Stuttgart.

Drimmel J., Gangl G., Trapp E. (1971) Kartenmäßige Darstellung der Seismizität Österreichs. *Mitteilungen der Erdbebenkommission* N.F. 70, Wien.

Gangl G. (1969 a) Ein Beitrag zur Seismizität des Alpenostrandes. *Mitteilungen der Erdbebenkommission* N.F. 68, Wien.

— (1969b) Die Erdbebentätigkeit in Österreich. *Arbeiten aus der Zentralanstalt für Meteorologie und Geodynamik*, 7, Wien.

Kapounek J., Kröll A., Papp A., Turnovsky K. (1965) Die Verbreitung des Oligozäns, Unter-und Mittelmiozäns in Niederösterreich. *Erdöl-Erdgas Z.*, 81, Wien.

Toperczer M., Trapp E. (1950) Ein Beitrag zur Erdbebengeographie Österreichs. *Mitteilungen der Erdbebenkommission* N.F. 65, Wien.

SOME CHARACTERISTICS OF THE SEISMIC PROCESS OF BANJA LUKA EPICENTRAL AREA

BY

D. HADŽIJEVSKI [1], M. JANKOVIĆ [2]

INTRODUCTION

As a result of studying the largest earthquakes occuring in Banja Luka epicentral area form 1888 — 1969 it was established that these earthquakes form an identical zone which involves larger region of Banja Luka town. It is located in the central part of Yugoslavia and covers more than 1,000 sq.km of area. Figure 1 shows location of this zone and relation to the territory of Yugoslavia as well as the location of the largest earthquake (that of 1969) ever occured here up to present.

During the examined period there were three series of earthquakes characterized by strong foreshocks and a series of shorter or longer aftershocks. These earthquakes data back from 1888, 1935 and 1969.

The principal aim of this paper is to study some aspects showing some similar properties of the process occuring in their foci.

RESULTS OF MACROSEISMIC STUDIES

In the course of the examination undertaken by the author he used original macroseismic data referring to earthquakes occuring in 1969, compiled on the field.

Furthermore, for earlier series of earthquakes the data were taken from the Catalogue of Belgrade Seismological Institute as well as various seismological bulletins.

Thus, the investigation was made on the basis of overall data and by means of a uniform method. The initial data collected for the purpose of this paper refer to the earthquake dating from 1888. On the basis of macroseismic data from 1888 a isoseismal map was made, thus providing the background for calculation of main parameters of the focus.

[1] Seismological Observatory, 91000 Skopje, Yugoslavia.

[2] Seismological Institute, 71000 Sarajevo, P.b. 620, Yugoslavia.

Figure 2 shows the map 3 on which we can see, in addition to distribution of intensity shape of the intensity which is identical with isoseismic map from 1935 and 1969. It should be emphasized that decreasing of the intensity in function of distance in all 3 cases as above is equal. The lack of the instrumental data for earlier period makes more detailed study of the earthquake impossible but the earthquake from 1935 and especially the one in 1969 is well backed up with detailed instrumental data.

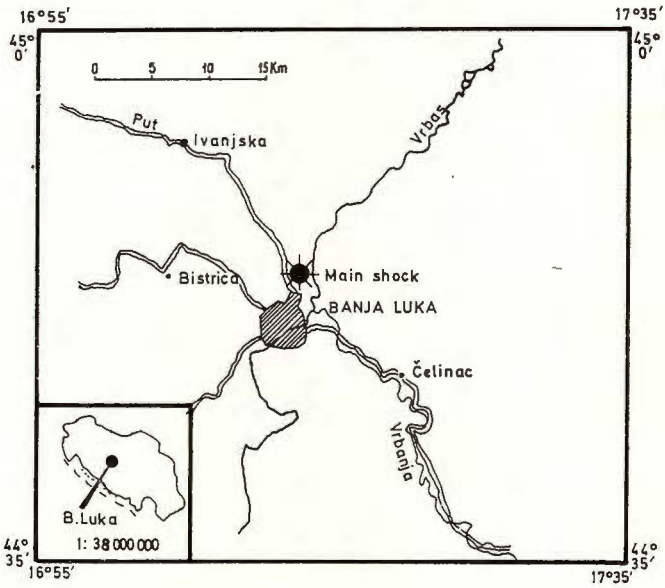

Fig. 1.— Geographic map of study area.

However, the results of examining this earthquake show us that it originated from the same focus which characteristics can be determined indetail on the basis of the shocks in 1969.

For the comparison we shall see the isoseismal map from 1935 and 1969. Figure 3 shows distribution of intensity of shock on October 11, 1935 (at 00 h 46) and figure 4 and 5 show isoseismal map of the shocks in 1969.

In October 26, 1969 first a foreshock occured and in October 27, 1969 the main shock developed. These maps clearly show the distribution of intensity as well as location and shape of that zone, it being the common characteristic of all the mentioned shocks.

---

[3] Janković M. Analysis of earthquake activity in Banya Luka region. 1972. Paper presented on the Third Ordinary Meeting of the Co-ordinating Committee of the UNDP/UNESCO Survey of the Seismicity of the Balkan region, 22—26 May, Athens.

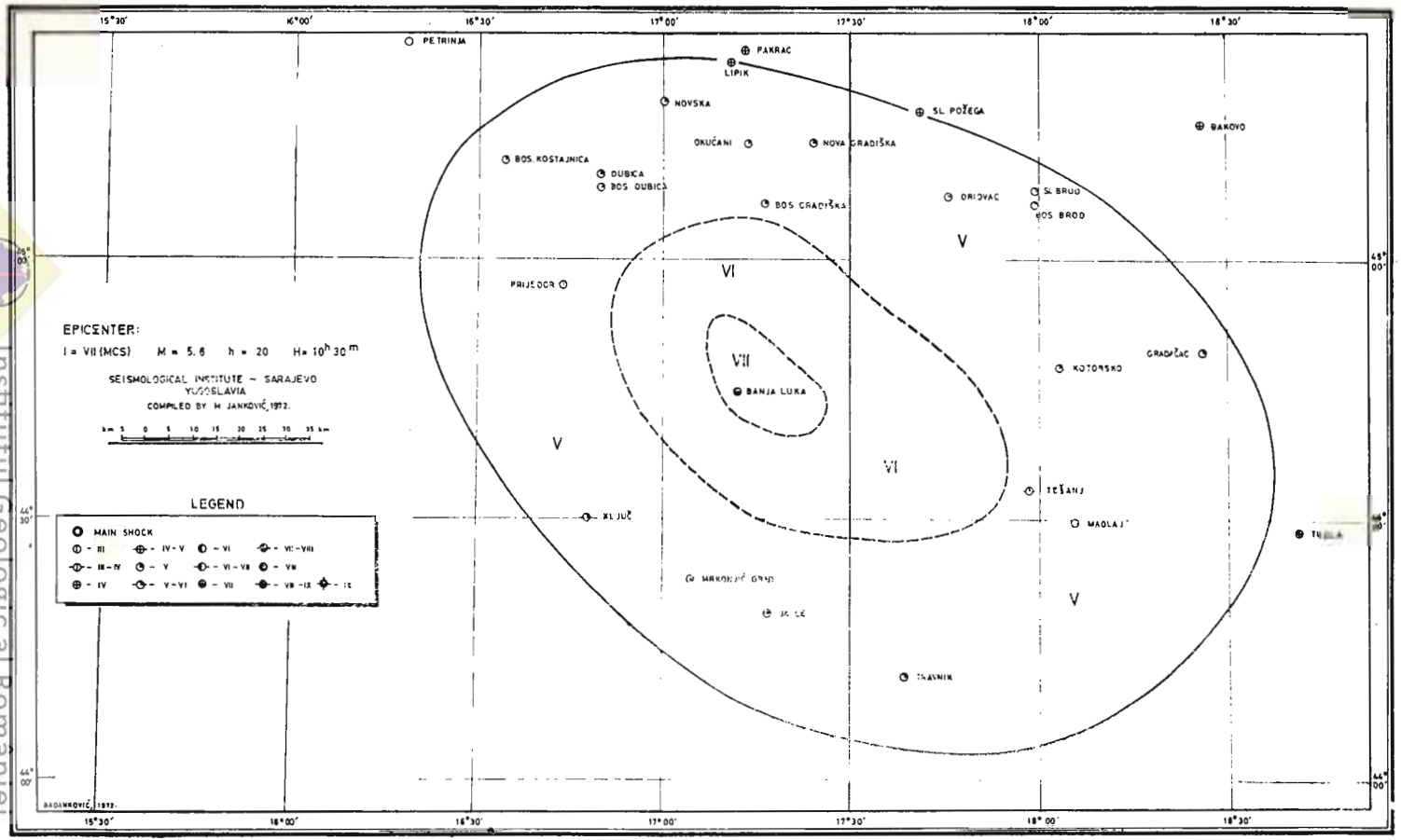

Fig. 2.— Isoseismal map of the earthquake of Banja Luka, 20-V-1888 (compiled by Jankovic 1972).

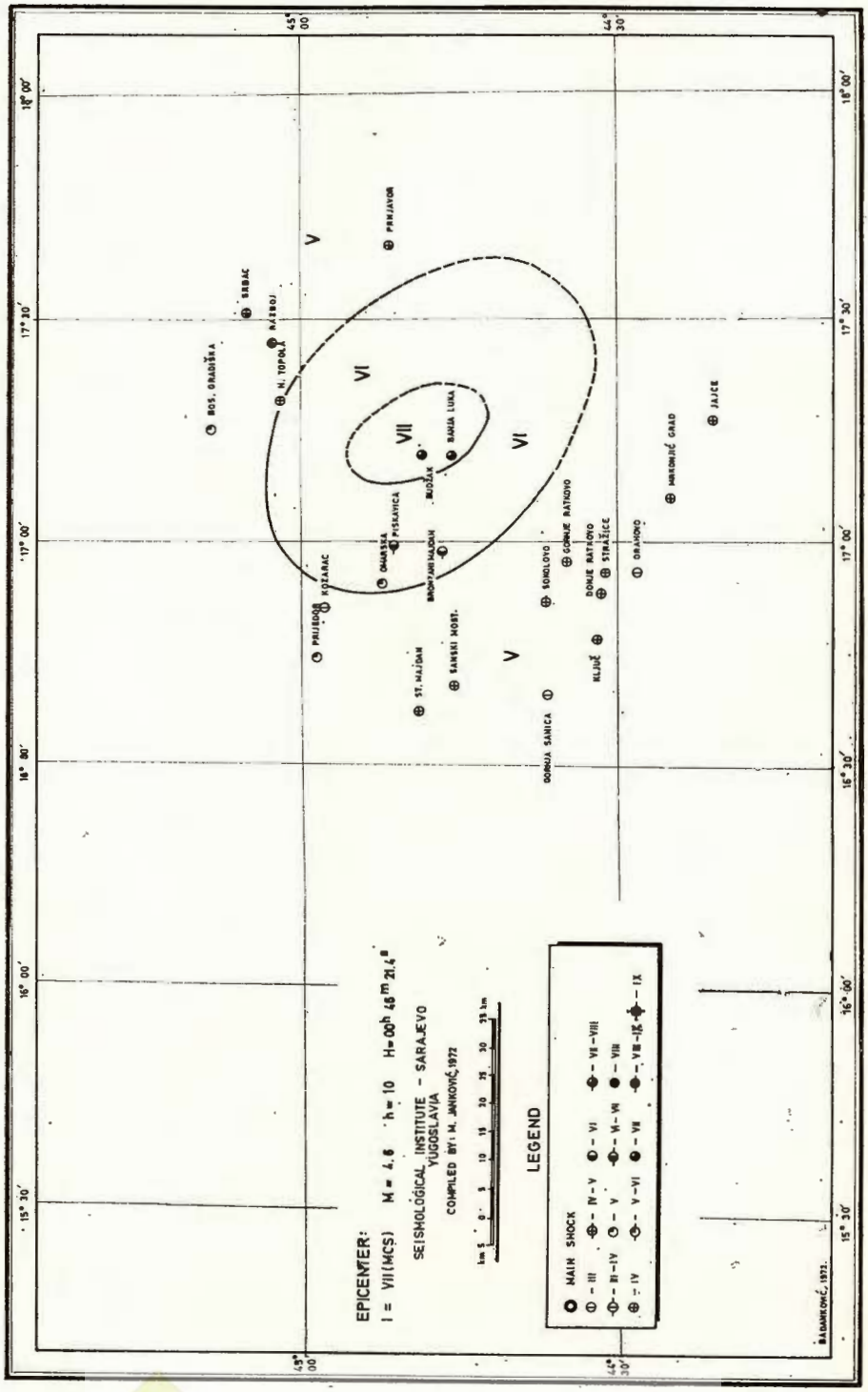

Fig. 3.— Isoseismal map of the earthquake of Banja Luka, 11-X-1935 (compiled by J a n k o v i ć, 1972).

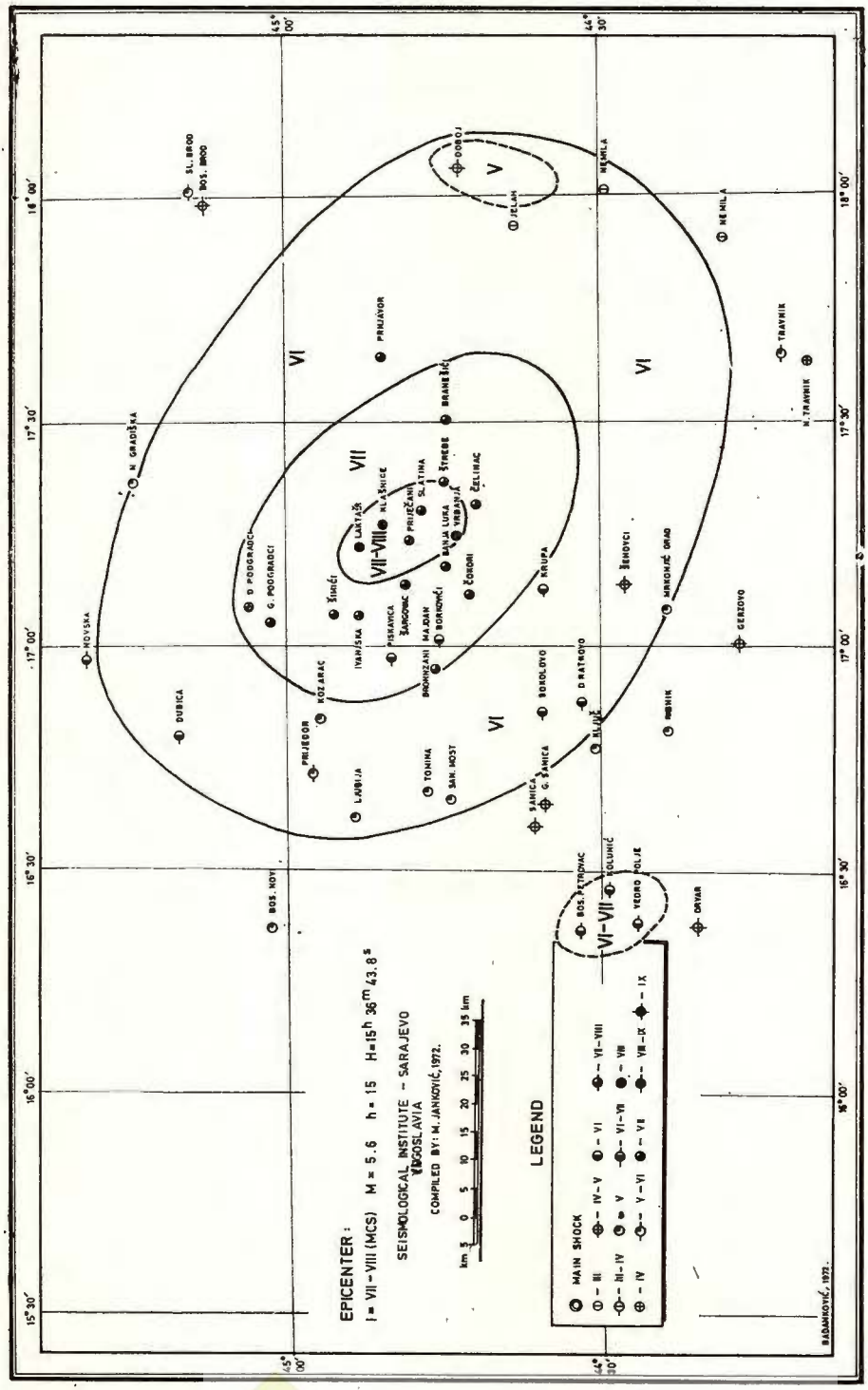

Fig. 4.— Isoseismal map of the earthquake of Banja Luka, 26-X-1969 (compiled by Jankoviċ, 1972).

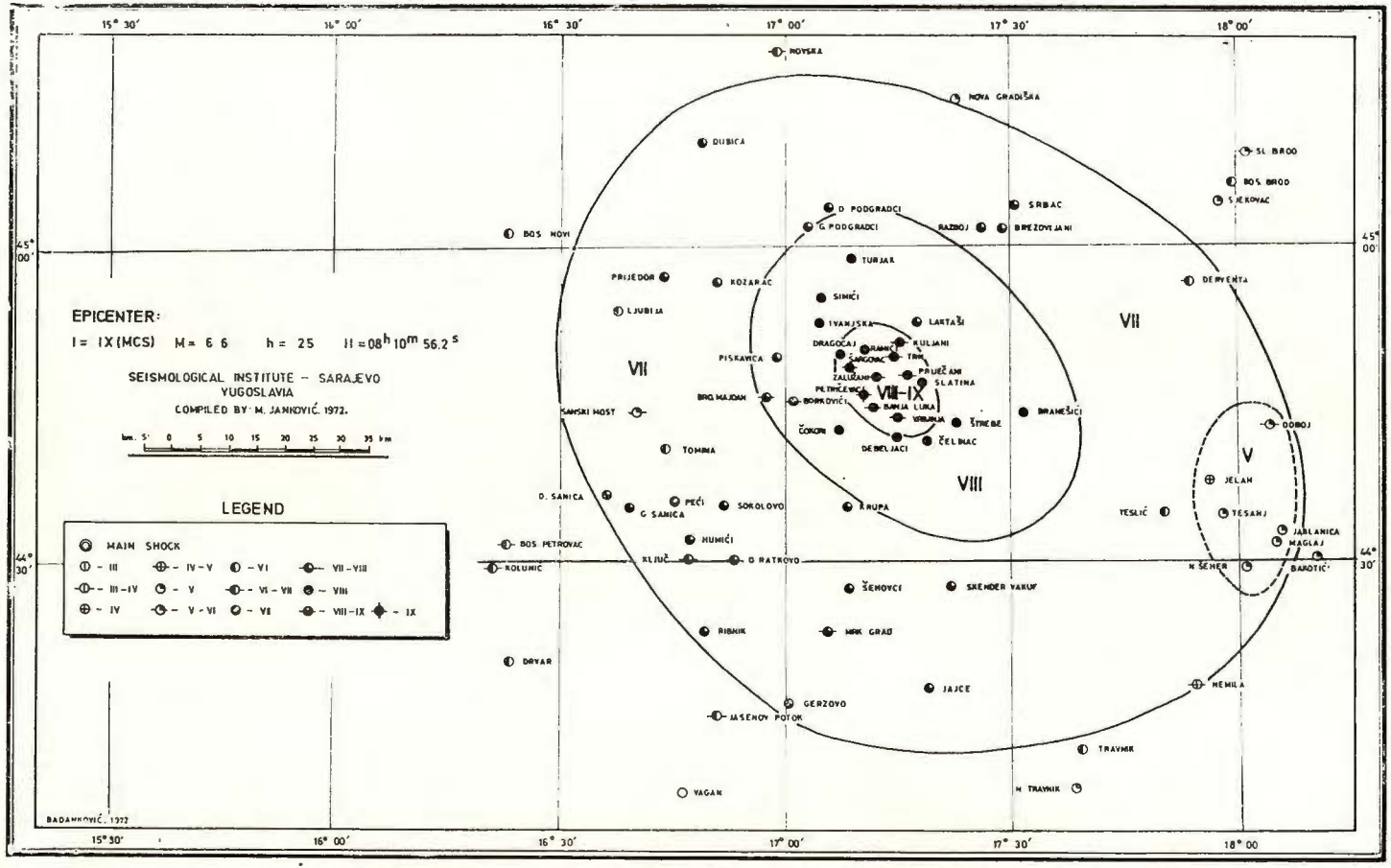

Fig. 5.— Isoseismal map of the earthquake of Banja Luka, 27-X-1969 (compiled by J a n k o v i ć, 1972).

RESULTS OF STUDY OF INSTRUMENTAL DATA

We shall start from thoroughly investigated shocks in 1969. Figure 6 shows a map of the epicentres of aftershocks for the period of 1 year in scale 1 :100,000. The same map presents the location of the foreshock, main shock and the aftershocks as well as location of mobile short-period seismological stations.

It is important to emphasize that the methodology of the investigation during the period was identical.

The location of those 5 mobile short-period seismic stations with seismographs galvanometric registration (seismometers Wilmor — England or Vegig—USSR 3 components, Z, NS and EW on each station period of seismometers 0.75 — 1.0 s, period of galvanometer is approximately 0.2 s) enabled the registration of weak shocks $K = 5 - 6$ ($K = \log E$; E in joule). The accuracy of the location of the epicentres was $\pm$ 4 km. The local mobile seismic stations were located about 3 months after the main shock.

In the same time the nt of most European stations registered shocks having magnitude of 3.5 and accuracy of location of focus was about $\pm$ 5 km. On this map the difference in some characteristics on the left and right side of the epicentral zone with regard to the concentration of biggest and weakest shocks and their energy and the depth are shown. The line of differentiation begins somewhere in the valley of the river Vrbas and continues up to Banja Luka. In addition to clearly estimating the longitudinal zone of the epicentres it also sets out one transversal zone which occupies the area in vicinity and along the river Vrbas bed. This was the main reason why we tried to enter the focus by means of vertical cross section along A — B. That cross-section is showed in the lower part of figure 6a. Here, the boundary zone which we shall conditionally call the dislocation and by which the focus area is devided into two different parts can be seen much better. The left side I is characterized by appearance of relatively small number of strong shocks with deepest focus (up to 25 km) while the right side is distinguished by numerous shocks which are weaker and shallow. In order to confirm this characteristic of the focus we carried out diagrams of strain release for every part separately. Assuming that deformations are proportional to released energy by measuring the amplitudes and the periods of maximum phases we calculated the magnitudes and classes of energy directly from seismograms. On the basis of sufficient number of data we made a relation between K, M, I and h concerning the examined zone.

The results are presented as graphs on figure 6 in cross-section for every part of the focus. From these graphs it is possible to see different character of energy release. In the first part of the focus releasing in inacted by stresses and in another by creeping of media rocks. This fact confirms double character of the earthquakes origin in the same focal region.

In this respect we would like to summarize the discovery of this occurence. In 1951, B e n i o f f who had been examining the earthquakes

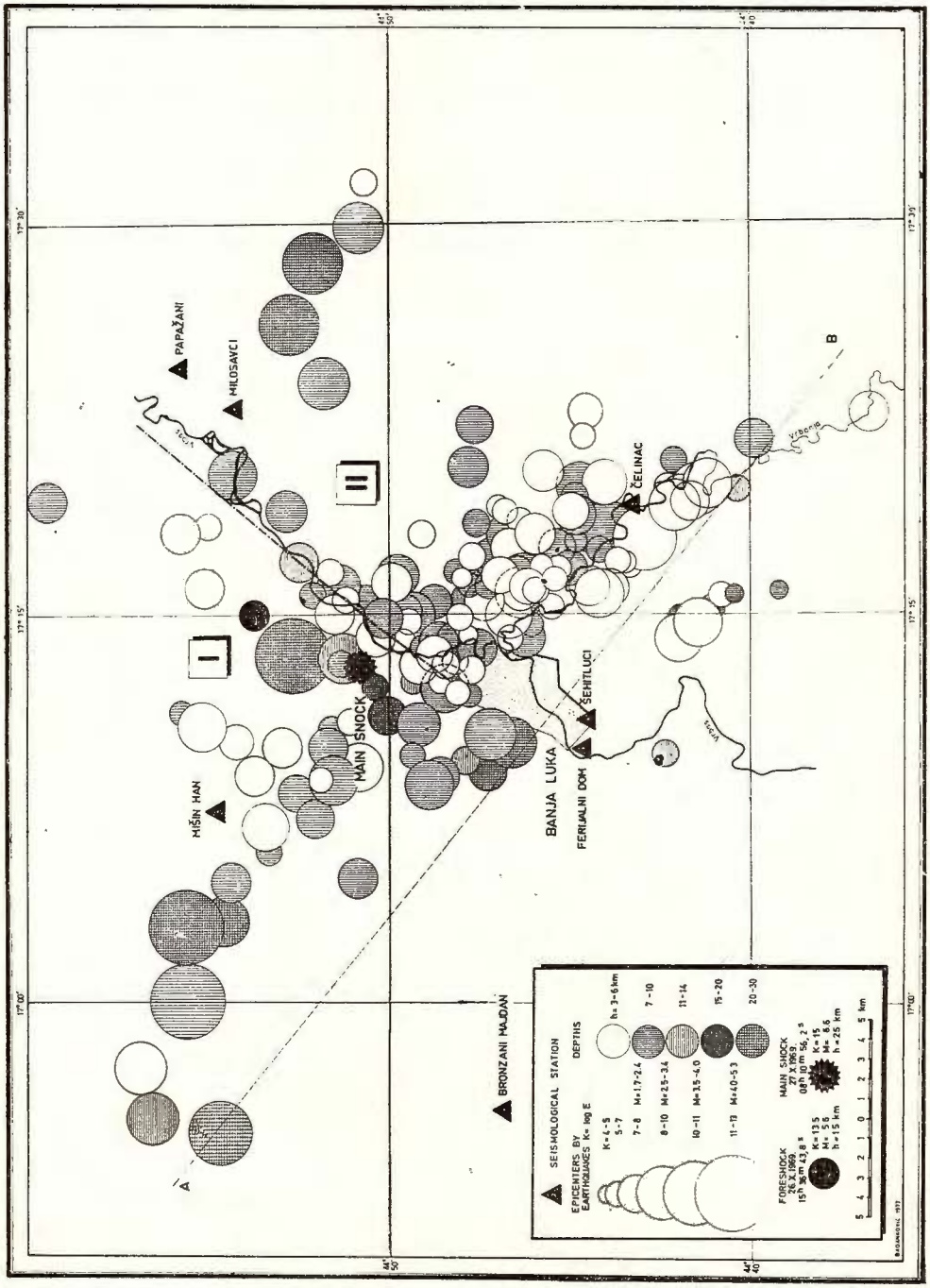

Fig. 6. — Map of aftershocks of thee arthquakes of Banja Luka, 1969—1970 (Oct. 26. 1969 — Oct. 15. 1970).

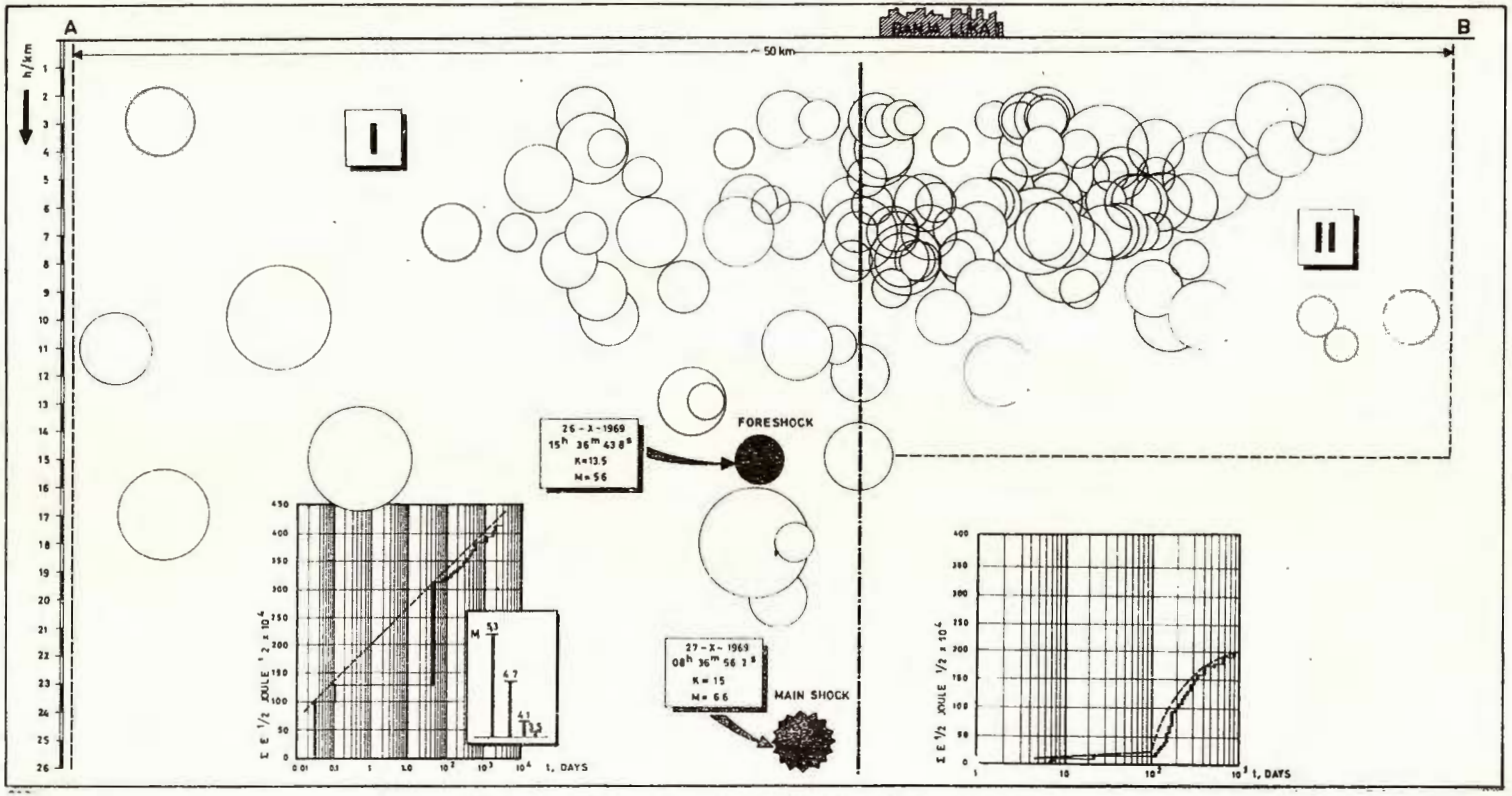

Fig. 6a, — Vertical cross-section in the Banja Luka zone,

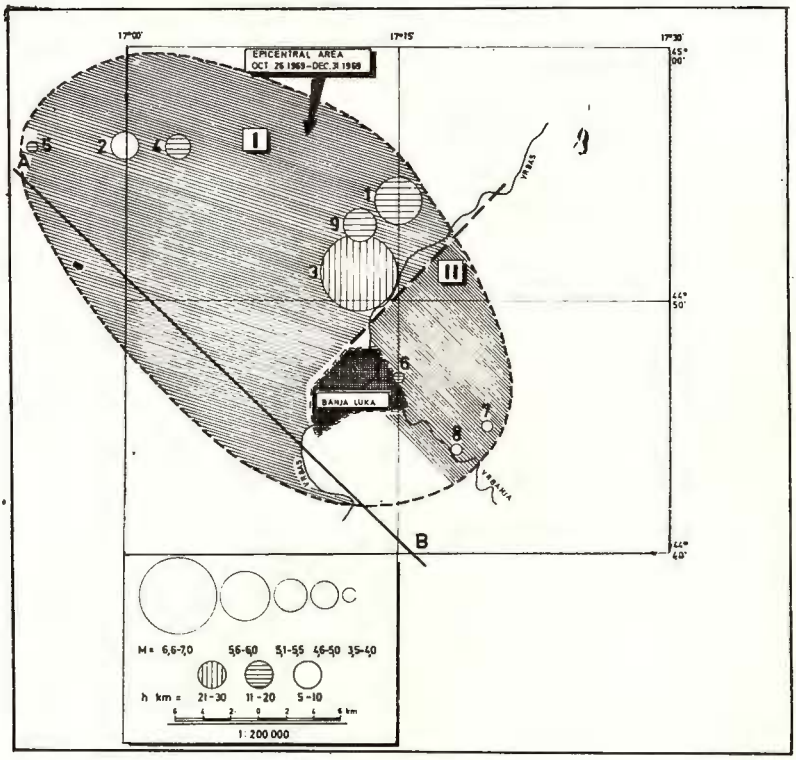

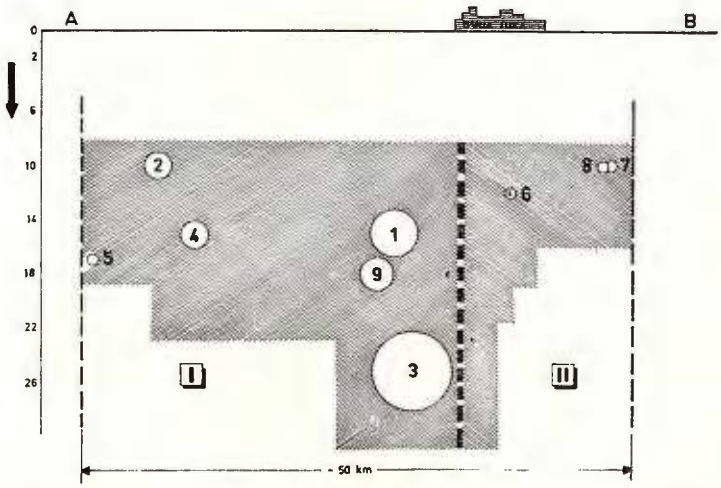

Fig. 7.— Map of epicentres of Banja Luka earthquakes 1969 ($M \geqslant 3.5$)

in 1931 in New Zealand and later, noticed somme manifestations and made theoretical analysis.

We would like to point out our observations made in our area. In order to investigate permanency of characteristics in Banja Luka focus area during a certain period we have taken into consideration a series of earthquakes which occured in 1935. In order to compare these we have simplified the case of the earthquake in 1969 with intention to observe the

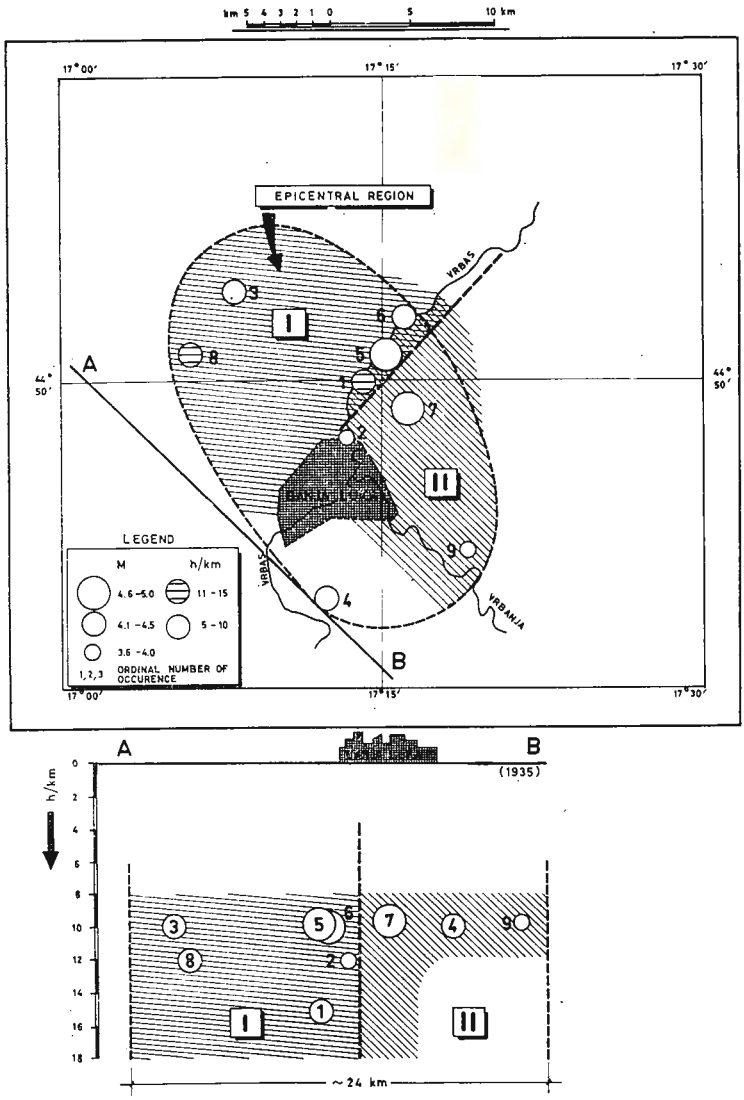

Fig. 8.— Map of epicentres of Banja Luka earthquakes 1935 ($M \geqslant 3.5$)

same period of 2 months taking in consideration the shocks with magnitude $M \geqslant 3.5$ as occured in 1935.

Such a simplified picture of the focus area of the earthquake in 1969 is presented in figure 7. There is no need for further explanations since it was previously done in figure 6. Therefore, we shall pay more attention to figure. It presents epicentres along the same cross-section A — B which was formerly explained. We shall underline here some similar or identical forms of epicentral region and foci area on cross-section. Observing simultaneously figures 6, 7 and 8 it can be seen that one vertical dislocation zone at the same place on Earth crust and its projection on the surface along the Vrbas river surrounded by the epicentres of earthquakes. It is obvious that there is a difference between the first and second part of focus area on the basis of the earthquakes but with smaller energy of the earthquake in 1935 in comparison to the earthquake in 1969 (Different maximum amplitudes is 1.9 of magnitude). The area of the focus of the earthquake in 1935 is smaller than the same area in 1969. The longitude of this area in 1935 is approx. 24 km and in 1969 approx. 50 km.

Unfortunately, due to the lack of data it was not possible to carry out graph of deformation release from part to part of focus area of the earthquakes in 1935 and 1969 which are completely analoguous.

CONCLUSIONS

a) Foci area of Banja Luka earthquake is characterized by relatively strong foreshock in relation to the main shock. The difference of their magnitudes is up to 1 —1.5 or the beginning of strongest shocks is in series, i.e. some large earthquake 2 or 3 with approximately same magnitudes or small difference 0.1 —0.6 (1935).

TABLE 1

Earthquake data of Banja Luka region

	H		h	M	I_0	Mo-Mf	Mo-Ma	Io-Ia	L km
20.V.1888	10^h 30^m	44° 47′—17° 13′	20	(5.6)	VII				
5.X.1935	14 02 51.4	44° 50′—17° 14′	15	4.1	V—VI				
11.X.1935	00 46 21.4	44° 51′—17° 15′	10	4.6	VII				24
21.X.1935	11 07 12.4	44° 49′—17° 16′	10	(4.7)	VII—VIII	0.6	0.6	15.8	
29.X.1935	22 06	44° 54′—17° 06′	n	(4.1)	VI			(days)	
10.XII.1935	11 04 51.5	44° 51′—17° 06′	12	4.1	V—VI				
26.X.1969	15 36 43.8	44° 54′—17° 15′	15	5.6	VII—VIII				
27.X.1969	08 10 56.2	44° 51′—17° 13′	25	(6.6)	IX	1.0	1.3	16.5	50
31.XII.1969	13 18 30.1	44° 53′—17° 13′	18	5.3	VI—VII			hours	

b) Foci area of Banja Luka earthquakes is distinguished by double processes of relasing of strain in one part due to stresses and in second part due to creep.

c) The configuration of epicentral region and foci area remained unchanged during this investigation. The longitude of the epicentral region is about 25—50 km and depth of *I* part of foci area is 10—25 km. We cannot exclude the possibility pf occurence of deeper foci in this area. The magnitude of the earthquakes was different, tending to increase. Due to that fact question concerning the maximum magnitude in this foci area is highly interesting.

d) Some important value of studied earthquakes in this paper are presented in the table.

REFERENCES

Bullen K.E. (1963) An introduction to the theory of seismology. University Press, Cambridge

Hadzievski D., Vasileva D., Ordev S. (1970) Instrumentalna seizmoloska istrazivanja aftersokova banjaluckih zemljotresa od 26 i 27.X.1969 god. u periodu od 29.X. 1969 do 17.X.1970. Institut za zemjotresno inzenerstvo i inzenerska seizmologija, *Rad. br. S*- 22/71, Skopje.

Psenikov K.V. (1965) Mehanizm vozniknovenia aftersokov i neuprugie svoistva zemnoi kori. AN SSSR, Izd. Nauka, Moskva.

Richter Ch. F. (1958) Elementary Seismology. Calif. Inst. Technol., Ed. W.H. Freeman & Co, San Francisco.

SEISMOLOGIC PREDICTION IN SOUTH—EASTERN ROMANIA USING THE STUDY OF YOUNG TERTIARY DEPOSITS

BY

VASILE LĂZĂRESCU, MATEI TRÎMBIȚAȘU[1]

INTRODUCTION

The seismic sensitivity of the region around the Vrancea epicentral area is a problem of great theoretical interest in seismotectonics and of high economic importance for town planning in Romania.

For this reason, beside the classical methods, already used for seismic prediction in our country, such as statistical study of earthquake frequency and magnitude (Constantinescu, Enescu, 1963, 1964; Radu, 1964), seismotectonical zoning [2,3], regional neotectonics using geomorphological criteria (Lăzărescu, 1969), geodetical establishing of recent vertical movements [4], we tried a purely geological approach of the problem.

WORKING METHODS AND RESULTS

For related geodynamical purposes [5,6] we compiled synthetic data on space and time distribution of the thickness and local average density of the pliocene formations from the carpathian fore-deep and from the intermountainous depression of Transylvania. The Pliocene is generally

[1] Institute of Oil, Gas and Geology. 6 Traian Vuia street, Bucharest, Romania.

[2] Constantinescu L., Cornea I., Lăzărescu V. Seismotectonic map of Earsten Carpathians. Communic. Symp. on seismotectonics of the UNDP/UNESCO Survey of the Seismicity of the Balkan region, Sofia, April 1972 (in press).

[3] Constantinescu L., Cornea I., Lăzărescu V. Seismotectonic map of Romania. Communic. 13rd Gen. Assem. Europ. Seism. Comm. Brașov (Romania), Aug.-Sept. 1972 (in press).

[4] Drăgoescu I. Map of recent vertical movements in Romania. 1972. Arch. Inst. Appl. Geophys., Bucharest.

[5] Lăzărescu V., Trîmbițaşu M., Manea A. Contributions to the paleo-geodynamical evolution of Carpathians during the Pliocene. 1971. Comm. Inst. Oil, Gas, Geol. Scient. Sess., Bucharest (in press).

[6] Lăzărescu V. Influence of isostasy on the pliocene evolution of deep fractures in front of Eastern Carpathians' Bend. Comm. 15th Gen. Ass. I.U.G.G. Moscow, Aug. 1971 (in press).

divided in Romania in the following stage sequence : Meotian, Pontian, Dacian and Levantine (classically also including the gravels of Cîndești, later proved as having a Villafranchian age, which is the first stage of Quaternary).

By means of maps with isopachs and density isolines, there were made maps with isolithobars (lines of equal weight in ton/sq. meter) for each stage of the Pliocene. Using the weight of the pliocene deposits developped outside and inside the Carpathians' Arc Bend, as well as data concerning the area then submitted to erosion, a certain information was obtained on the isostatical evolution of the whole region and on the passive component in the throw of deep fractures separating the mountains and the fore-deep.

The isolithobars' trend reflect a normal variation of the pliocene molasse thickness from high values (1000—7000 m) in the carpathian fore-deep to much smaller ones (200—500 m) in the platform between the Carpathians and the Balkans. At the same time, they reveal some distinct abnormal distorsions transversally directed to the general trend of the regional structures (fig. 1, 2). The amplitude of such distorsions is stronger to the fore-deep, and, little by little, waning out toward the inner zone of the epihercynian Moesian platform. It is reasonable to consider them as reflecting deep fractures or flexures which delineate blocks disclosing different tectonic behaviours.

A comparation of the isolithobars with the geological faults from Dobrogea, with the seismically detected deep faults from the Romanian Plain (Cornea, 1964; Cornea et al., 1965; Cornea, Enescu. 1968; Dicea et al. 1969), as well as with the seismic sensitive lines (Atanasiu, 1961), previously established by the above mentioned authors, easily leads to conclude on the following :

a) The Peceneaga-Camena fault was up to now considered of a purely cretaceous age, because the upper cretaceous sediments of the Babadag basin are overlapping it in some places without any subsequent dislocation. Consequently this fault and its NW-ern prolongation outside Dobrogea, could have been regarded as lines of little seismotectonic meaning, although they were proved by explosion seismology data to have a throw of about 5 km down to the base of the crust (Constantinescu, Cornea, 1972). The same tectonic history seemed to have had another deep fracture (Opresinești-Bordeiu Verde line), established by seismic survey in the basement of the Romanian Plain to the SW and close to the prolongation of the Peceneaga-Camena line. The change in thickness of the pontian and dacian beds proves that these two faults were submitted at least to a pliocene rejuvenation toward the carpathian fore-deep. Such a reactivation is conspicuous around the Focșani-Odobești depression which is a zone of strong pliocene subsidence.

It is not the same thing to be said about the prolongation of the Capidava-Ovidiu fault line. In Dobrogea, this line has an early cretaceous last tectonic activity, indicated by undisturbed aptian deposits which are overlapping in some zones the fracture line. No distorsion is to be

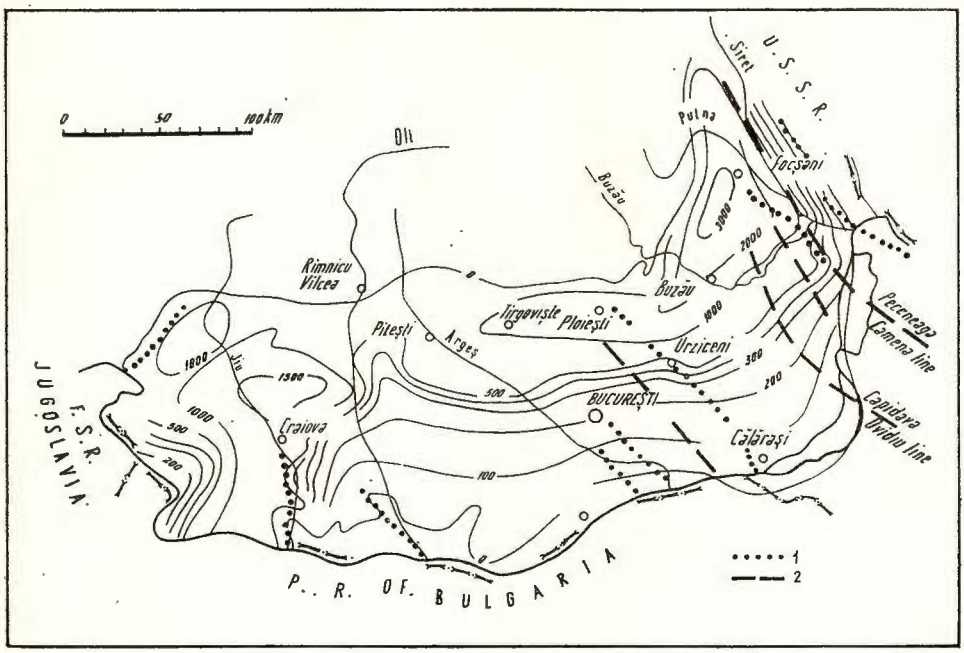

Fig. 1. — Map with isolithobars (lines of equal weight in ton/sq. meter) for Pontian deposits:
1, lineaments of higher seismic sensitivity; 2, deep-fault lines.

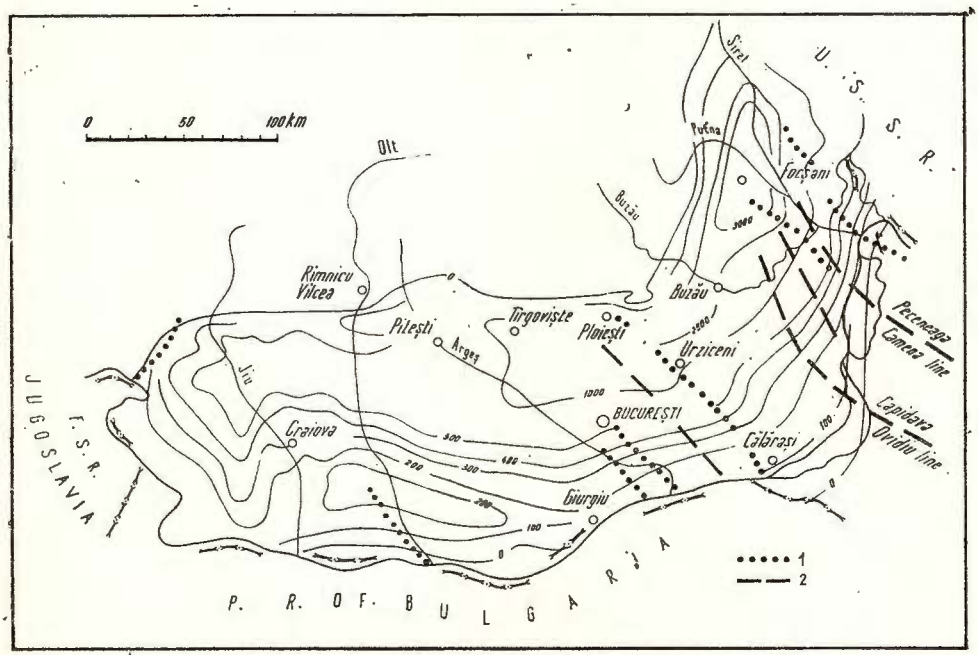

Fig. 2. — Map with isolithobars (lines of equal weight in ton/sq. meter) for Dacian deposits:
1, lineaments of higher seismic sensitivity; 2, deep-fault lines

observed along its prolongation under the Romanian Plain. It means that faults which remained welded in platform regions are able to be still active now in fore-orogenic zones of young and strong subsidence, whereas other ones remained inactive for a long time in zones of weak sinking.

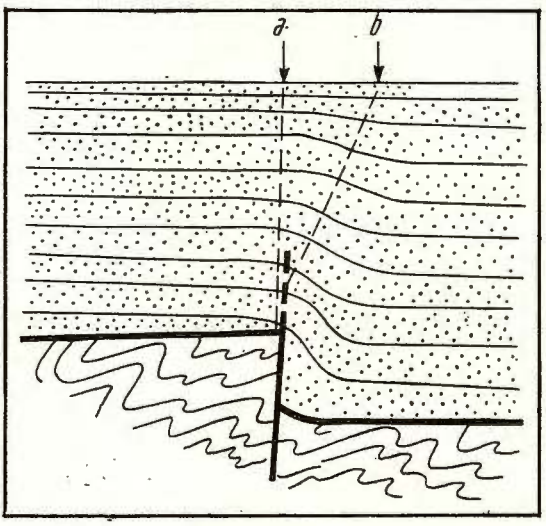

Fig. 3.—Vertical theoretical section of a deep fault passing upwards into a flexure. To be noticed the migration of disturbed beds over the sinking block of the fault which could explain the mutual positions of a seismically detected deep-fault line(a) and its corresponding line of higher seismical sensitivity (b).

b) Some other zones of tectonic warping, not related to already established faults, are also conspicuous in the map of isolithobars. Instead, they are parallel and close to certain lines of seismic sensitivity.

From this point of view, the most interesting zone is sited between Pogoanele and Urziceni (Romanian Plain) where a recent deep earthquake has been recorded. Here typical reverse movements, probably reflecting the rhodanian folding phase in the fore-deep, are proved during the pontian and dacian time. The vertical shift of these movements seems to have over 100 m amplitude inside the epicratonic flank of the fore-deep and is dying out toward the platform. It is important to emphasize the close fitting of isolithobars' distorsion with the seismic sensitive line and the fact that the next seismometrically detected fault (Fierbinți line) is also parallel but at a distance of 20 km. This difference could be explained by diagonal migration of a flexure to the surface, along which the seismic energy has been easier released, as shown by a vertical theoretical section (fig. 3).

CONCLUSIONS

From the above data it results that, beside the typical methods of seismic fore-casting and seismotectonic zoning, to trace and interpret maps with isopachs and isolithobars of the youngest bed-formation is useful too, as an auxilliary method, in prediction of future earthquakes and of zones of highest seismic sensitivity.

REFERENCES

A t a n a s i u I. (1961) Cutremurele de pămînt din România. Edit. Acad. R.P.R., Bucureşti.

C o n s t a n t i n e s c u L., E n e s c u D. (1963) The characteristic features of the mechanism of the carpathian earthquakes and their seismotectonical implications (in romanian). *Stud. Cerc. Geofiz.*, I, 1, Bucureşti.

— E n e s c u D. (1964) Energy-magnitude-intensity relations for the Carpathian earthquakes. Parameters of the seismic regime of the Vrancea region. *Rev. Roum. Géol. Géophys. Géogr., ser. Géophys.*, 8, Bucarest.

C o n s t a n t i n e s c u P., C o r n e a I. (1972) The results of the DSS measurements in the cooperating countries. 27. Romania. *Geofiz. Közl.*, Special edition, Budapest.

C o r n e a I. (1964) Contribuţii geofizice la studiul structurii geologice a Depresiunii Bîrladului. *Stud. Cerc. Geol. Geofiz. Geogr., ser. Geofiz.*, 2, 1, Bucureşti.

— et al. (1965) Contribuţii seismice la crearea unei imagini tectonice asupra marginii nordice a Platformei Moesice între Olt şi Buzău. *Stud. Cerc. Geol. Geofiz. Geogr., ser. Geofiz.*, 3, 1, Bucureşti.

— E n e s c u D. (1968) Sur la nature des ondes rencontrées au cours des travaux de prospection séismique en Roumanie et leur interprétation géologique. 23rd Int. Geol. Congr. Geological results of Applied Geophysics, Academia Prague.

D i c e a O., T o m e s c u L. II (1969) Tectonica zonei externe a avant-fosei carpatice din sectorul Motru-Buzău în lumina datelor prospecţiunii seismice. *Stud. Cerc. Geol. Geofiz. Geogr., ser. Geofiz.*, 7, 1, Bucureşti.

E n e s c u D., C o r n e a I., C o n s t a n t i n e s c u P., R ă d u l e s c u Fl., P ă t r u ţ Ş t. (1972) Structura scoarţei terestre şi a mantalei superioare în zona Curburii Carpaţilor. *Stud. Cerc. Geol. Geofiz. Geogr. ser. Geofiz.* 10, 1, Bucureşti.

L ă z ă r e s c u V. (1969) Indicaţiuni de mişcări neotectonice în regiunea dintre Valea Prahovei şi Valea Teleajenului. *Bul. Soc. St. Geol. din R.S.R.*, XI, Bucureşti.

R a d u C. (1964) Contribution à la détermination de la magnitude des tremblements profonds des Carpates. *Rev. Roum. Géol. Géophys. Géogr., ser. Géophys.*, 8, Bucarest.

SEISMICITY AND FOCAL VOLUME[1]

BY

RICHARD MAAZ, WOLFGANG ULLMANN[2]

Abstract

In the definition of seismicity as a field function with the dimension of energy density (or energy density flux), the distribution of the strain energy in the focal region represents the additive contribution of the single earthquake to seismicity in space. With respect to that, two simple models of the focal region and energy distribution are discussed, the ellipsoid and the elliptical cylinder. By central projection the projective seismicity is defined at the Earth's surface. The concerning additive contribution of the single quake is reduced to the corresponding spatial contribution by integration using the elliptical cylinder model. The dimensions of the focal region have been connected to seismological observations using the focal volume formula of B å t h and D u d a.

INTRODUCTION

In earlier papers of the authors the definition of seismicity as a continuous function in space and time was discussed. Seismicity with regard to space and time was defined as the local and momentary density flux of the accumulated strain energy. More precisely, the strain energy being released by all concerning earthquakes is taken into account. This seismicity definition requires to superpose the contributions of the single earthquakes in certain surroundings of the space-time point considered. Consequently, the knowledge of the contribution of the single earthquake is neccessary and sufficient to describe mathematically and physically the field and time function seismicity in the sense mentioned above, which seems to be most adequate to the study of tectonophysical processes of seismically active regions.

The following considerations are restricted to the variation of seismicity in space, that means that time dependence of the contributions is eliminated by taking the integral mean of the contribution function with respect to the time interval ϑ which is of interest. The amount of it, denoted

[1] Communication Nr. 275, Central Earth Physics Institute.

[2] Central Earth Physics Institute AdW der DDR, part Jena 69 Jena, Burgweg 11, GDR.

by $|\vartheta|$, must be large enough for getting a stationary quantity. Hence,

$$s\,[Z,\vartheta] = \frac{1}{|\vartheta|}\int_{\vartheta} s\,[Z,t]\,dt \tag{1}$$

represents the contribution of any fixed nearby earthquake to seismicity at point Z of time interval ϑ. For sake of simplicity the energy density flux $s\,[Z,t]$ at Z, t is separated with respect to the energy E of the quake, time t, and point Z,

$$s\,[Z,t] = E\,p\,(t)\,q\,(Z), \quad \int_{-\infty}^{\infty} p\,(t)\,dt = 1, \quad \int_{\text{earth}} q\,(Z)\,dv = 1. \tag{2}$$

Then we get

$$s\,[Z,\vartheta] = \frac{E}{|\vartheta|}\,P_\vartheta\,q\,(Z) \text{ with } P_\vartheta = \int_{\vartheta} p\,(t)\,dt \leqq 1. \tag{3}$$

Seismic events inside time interval ϑ at its beginning or end are sure to contribute with $P_\vartheta < 1$. On the other hand, events outside ϑ give also a certain contribution $P_\vartheta < 1$. In the best case their influence to $S\,[Z,\vartheta] = \Sigma\,s\,[Z,\vartheta]$ and the deficit of the first mentioned quakes is compensated. Then we have to regard exactly all quakes inside ϑ with $P_\vartheta = 1$. The same effect trivially results from the practical but physically irrelevant assumption of $p\,(t)$ being a DIRAC-function with its maximum at the focal time.

ENERGY DISTRIBUTION IN SPACE – ELLIPSOID MODEL

For the purpose to give a well defined mathematically and physically motivated representation of seismicity, the real but unknown energy distribution with a single earthquake has to be substituted by a simple suitable model. From the practical view-point of the numerical calculation and from geophysical reasons, too, it is reasonable to assume the deformation energy released in the single earthquake as concentrated inside the focal region ω,

$$s\,[Z,t] \geqq 0 \leftrightarrow Z \in \omega. \tag{4}$$

Consequently

$$q\,(Z) \geqq 0 \leftrightarrow Z \in \omega. \tag{5}$$

With respect to tectonics and focal mechanism it is recommendable to use an ellipsoid as a model for ω. Nevertheless, let us consider the mathematically possible special case of being ω a sphere ω_s with radius r and centre Q, the hypocentre of the quake.

The vector $\overrightarrow{QZ}$ fixed in Q may be represented by the co-ordinate triplet x_1, x_2, x_3 related to a Cartesian co-ordinate system in Q,

$$\overrightarrow{QZ} = (x_1, x_2, x_3), \quad \Sigma x_i^2 = x^2, \quad 0 \leqq x \leqq r. \tag{6}$$

The most convenient statement for $q(Z)$ certainly is

$$q(Z) = F(x_i) = f(x) \text{ with } f(x) = 0 \text{ for } x \geqq r. \tag{7}$$

This function must have its maximum at the hypocentre and decrease continuously when Z reaches the boundary of ω_s. In addition, we may require horizontal tangents at $x = 0$, r. Hence,

$$f(0) \geqq f(x) \geqq f(r) = 0, \qquad f'(0) = f'(r) = 0, \tag{8}$$

and the condition of normalization

$$\int_{\omega} q(Z)\, dv = 1. \tag{9}$$

Using a polynomial of the third degree we get after Maaz and Ullmann (1972)

$$f(x) = \frac{15}{4\pi r^3}\left[1 - 3\left(\frac{x}{r}\right)^2 + 2\left(\frac{x}{r}\right)^3\right] \text{ for } 0 \leqq x \leqq r. \tag{10}$$

More convenient may be the polynomial

$$f^*(x) = \frac{3 \times 5 \times 7}{2^5 \pi r^3}\left[1 - \left(\frac{x}{r}\right)^2\right]^2 \tag{11}$$

or

$$F^*(x_i) = \frac{3 \times 5 \times 7}{2^5 \pi r^3}\left[1 - \frac{x_1^2 + x_2^2 + x_3^2}{r^2}\right]^2 \tag{12}$$

also fitting the conditions mentioned above.

Now we consider an ellipsoid with the centre Q and r_1, r_2, r_3 as the lengths of the semiaxis ($r_1 \geqq r_2 \geqq r_3 > 0$), which may represent the focal region ω_e. The main axis may coincide with the x_1, x_2, x_3 — axis and the volumes may be equal, whence

$$r_1 r_2 r_3 = r^3. \tag{13}$$

By the linear equation system

$$u_i = \frac{r_i}{r}\, x_i \longleftrightarrow x_i = \frac{r}{r_i}\, u_i \tag{14}$$

the original sphere ω_s is deformed to the ellipsoid ω_e.

By the self-mapping system (14) the function $F^*(x_i)$ is transformed to

$$F_1^*(u_i) = \frac{3 \times 5 \times 7}{2^5 \pi r_1 r_2 r_3}\left[1 - \left(\frac{u_1}{r_1}\right)^2 - \left(\frac{u_2}{r_2}\right)^2 - \left(\frac{u_3}{r_3}\right)^2\right]^2 \tag{15}$$

for

$$(u_1/r)^2 + (tu_2/r)^2 + (u_3/r_3)^2 \leqq 1. \tag{16}$$

The conditions concerning the decrease of $F_1^*(u_i)$ are fulfilled again. The normalization condition (9) holds true for $F_1^*(u_i)$ because the amount of the volume element dv is not affected by the transition (14):

$$dv = dx_1\, dx_2\, dx_3 = du_1\, du_2\, du_3. \tag{17}$$

In practice, the main directions of the ellipsoid have to be determined by the focal mechanism, a problem being not solved in general and bringing additional computational expense.

PROJECTIVE SEISMICITY AND CYLINDER MODEL

If we can assume that the fault planes of the studied earthquakes are nearly vertical, a slightly different model of ω offers, which is more suitable for calculations and especially for the determination of the projective seismicity. Such a position of fault planes show most of the shallow-focus earthquakes, which are just of interest for the separate investigation of their horizontal and vertical distribution. In praxi there are two main reasons to neglect the focal depth of shallow quakes:

First, the depth values use to be relatively uncertain.

Second, the graphic representation of three dimensional seismicity is essentially more difficult than in case of less than three dimensions. The vertical variation of seismicity is eliminated by taking the integral mean of spatial seismicity along the vertical straight line ζ through the considered surface point Z' and the Earth centre. The contribution $s'\,[Z', \vartheta]$ of a single quake to the projective seismicity results from

$$s'\,[Z', \vartheta] = \frac{1}{|\varepsilon|}\int_{\varepsilon} s\,[Z, \vartheta^\circ]\, dv = \frac{3\,E\,P\vartheta}{R\,|\vartheta|}\int_{\zeta} q\,(Z)\, dz \tag{18}$$

where ε represents the infinitesimal projection cone around ζ R, the radius of the Earth, and z the depth of Z.

The announced new model consists in restricting the accumulated strain energy released by the concerned earthquake to a vertical elliptical cylinder ω_c with semiaxis a_1, a_2, altitude l, and volume $|\omega_c|$, outside of which $q\,(Z)$ vanishes and inside of which $q\,(Z)$ is separated with respect to horizontal and vertical variation. The special case $a_1 = a_2 = a$ leads under the conditions of normalization and continuous decrease of $q\,(Z)$ with increasing distance $\overline{QZ}$ including zero derivations $dq\,(Z)/d\,(\overline{QZ})$ at the centre Q and the boundary of the cylinder after M a a z and U l l m a n n (1972) to

$$q\,(Z) = f_1\,(x')\, f_2\,(y) \tag{19}$$

where

$$x' = \overline{Q'Z'}, \quad 0 \leqq x' \leqq a; \quad y^2 = \overline{QZ^2} - x'^2; \quad -1/2 \leqq y \leqq 1/2; \tag{20}$$

and

$$f_1\,(x') = \frac{3}{\pi a^2}\left[1 - \left(\frac{x'}{a}\right)^2\right]^2, \qquad f_2\,(y) = \frac{15}{8l}\left[1 - \left(\frac{2y}{l}\right)^2\right]^2. \tag{21}$$

Because of

$$\int_{\zeta} f_2\,(y)\, dy = 1, \tag{22}$$

(18), and (19) results

$$s_c'[Z', \vartheta] = \frac{3 E P_\vartheta}{R |\vartheta|} f_1(x'). \tag{23}$$

In the general case $a_1 \neq a_2$ a Cartesian co-ordinate system with origin Q' is introduced in the Earth's surface, whose x_1'—axis coincides with the fault direction that is identical with the greater main axis of the elliptic surface region ω_c', the vertical projection of ω_c. Then we get by considerations like that for the ellipsoid model

$$s_c'[Z', \vartheta] = \frac{3 E P_\vartheta}{R |\vartheta|} \frac{3}{\pi a_1 a_2} \left[1 - \left(\frac{x_1'}{a_1}\right)^2 - \left(\frac{x_2'}{a_2}\right)^2 \right]^2 \tag{24}$$

where l is not changed and

$$a_1 a_2 = a^2, \quad |\omega_c| = \pi a_1 a_2 l. \tag{25}$$

Naturally, also for the ellipsoid model the calculation of the projective seismicity is possible, at least numerically. For the spherical model the concerning contribution of the single quake to projective seismicity is derived,

$$s_s'[Z', \vartheta] = \frac{45 E P_\vartheta}{8 \pi R r^2 |\vartheta|} \left[-3 v' + 5 v'^3 + \frac{3}{2} (1 - v'^2)^2 \ln \frac{1 + v'}{1 - v'} \right] \tag{26}$$

where

$$v' = \left| \sqrt{1 - \left(\frac{x'}{r}\right)^2} \right| \text{ with } x' = \overline{Q'Z'} \tag{27}$$

which is more complicated than (23) for the cylinder model.

MODEL PARAMETER AND FOCAL VOLUME

The remaining question is how to determine the parameters r or (r_1, r_2, r_3) or (a_1, a_2, l). With the study of aftershock series of strong earthquakes of magnitude M, B å t h and D u d a (1964) stated statistically that the hypocentres of a complete series determine a volume V according to

$$\log V = -5.42 \pm 0.51 + (1.47 \pm 0.14) M, \qquad 5.3 \leqq M \leqq 8.7. \tag{28}$$

It is to suppose that a great deal of the energy of the main shock is concentrated in the focal volume. But the amount of energy of the main shock outside the focal volume may be comparable with the first energy part, because the main shock lies usually at the border of this region. On the other hand, the total energy of all fore- and aftershocks in ω is in general less than the main energy release and might be able to compensate the main shock energy part outside ω. Consequently we heuristically equalize the focal volume V after B å t h and D u d a with the volume $|\omega|$ of

the focal region ω. Then $|\omega_s| = V$ yields for the spherical and the elliptical model

$$\log r = \log \sqrt[3]{r_1 r_2 r_3} = -2.01 + 0.27 + (0.49 + 0.05)\ M. \tag{29}$$

To determine the parameters r_i, two seismological relations between them are necessary. As a first approximation $r_2 = \frac{1}{3} r_1$, $r_3 = \frac{2}{3} r_1$ may be suitable, wherefore

$$r_1 = \sqrt[3]{9/2}\ r \approx 1{,}65\, r, \quad r_2 = \frac{1}{2} r_1, \quad r_3 = \frac{2}{3} r_1 \tag{30}$$

From the seismological obvious conditions that the horizontal dimensions of ω_s and the cylindrical focal region ω_c are equal, i.e. from

$$r_1 = a_1, \quad r_2 = a_2, \tag{31}$$

and that the energy density in the hypocentre is dependent of the special model,

$$s_s\,[Q, \vartheta] = s_c[Q, \vartheta], \tag{32}$$

it follows

$$l = \frac{12}{7} r, \quad r^2 = r_1 r_2. \tag{33}$$

The volume of that cylinder is given by

$$|\widetilde{\omega_c}| = \frac{12}{7}\ r \pi r^2 \neq \frac{4}{3}\ \pi r^3. \tag{34}$$

If we accept the form of the ω_c by

$$l = \frac{12}{7} a, \quad a^2 = a_1 a_2. \tag{35}$$

and put

$$|\omega_c| = \frac{12\pi}{7}\ a^3 = V = \frac{4\pi}{3}\ r^3, \tag{36}$$

we get

$$a = \sqrt[3]{7/9}\ r \approx 0.92\, r. \tag{37}$$

A relation between a_1 and a_2 is required to determine all parameters. $a_2 = \frac{1}{3} a_1$ may be used. With (35) we get

$$a_1 = \sqrt{3}\ a, \quad a_2 = \frac{1}{3}\ a_1, \quad l = \frac{12}{7}\ a \tag{38}$$

as a rough estimation of the parameters.

It should be mentioned that there are other studies concerning the focal volume, e.g. K h a t t r i (1972), which possibly have to be taken into consideration at a later stage of the investigation. But also more detailed knowledge about the strain energy distribution in general are desirable.

REFERENCES

B å t h M., D u d a S. J. (1964), Earthquake Volume, Fault Plane Area, Seismic Energy, Strain Deformation, and Related Quantities. *Ann. Geofis.*, 17, Rome.

K h a t t r y K. N. (1971) On the Estimation of Volume of Strain in Earthquakes. *PAGEOPH*, 87, Richmond.

M a a z R., U l l m a n n W. (1972), Eine neue Darstellung der Seismizität unter Berücksichtigung des Herdvolumens. *Stud. Geophys. Geod.* 16, Prague.

U l l m a n n W., M a a z R., (1969). Prolegomena zur Seismizität, Teil I. *Veröff. Inst. Geodynamik Jena, Ser. A*, 13, Jena.

MIGRATION OF SEISMIC ACTIVITY

BY

DANA PROCHÁZKOVÁ[1]

From the point of view of longterm prediction it is necessary to determine when and in which place of the region under investigation strong earthquakes may be expected. The basic question if earthquakes occur incidentaly or whether their occurrence in space and time is determined by some laws is connected with this problem. The determination of space and time tendency in the occurrence of earthquakes has been the object of studies for a long time.

In Europe and Asia Minor a close investigation aiming at the determination of facultative space and time tendency was carried out. By migration of seismic activity is understood a shift of the foci of earthquakes with time in one direction in one region and in a certain period. Two kinds of migration of seismic activity were observed in the period from 1901 to 1969 :

1) migration of the depth of strong intermediate earthquakes with time, that is the migration in vertical plane;

2) migration of the epicentres of strong earthquakes with time in one direction, that is the migration in horizontal plane.

First some examples of the migration in vertical plane will be introduced. The data is based on K á r n í k 's European Catalogue for the period from 1901. The information on earthquakes deeper than normal earthquakes of a magnitude m smaller than 6.0 is incomplete over the whole considered time interval. Weak intermediate shocks of a magnitude m smaller than or equal to 5.0 were only located during the last decades. For this reason the migration of the foci in vertical direction is investigated only with strong earthquakes of a magnitude m greater than or equal to 6.0.

In region Vrancea, the epicentres of the intermediate earthquakes are in a small domain, in the bend of the Carpathians. The depths of foci are 100—200 km. The depths of the foci of strong earthquakes of magnitude $m \geqslant 6.0$ decreased with time from 1929 to 1947 (fig. 1).

[1] Geophysical Institute, Czechosl. Acad. Sci., Prague, Boční IIa, Praha 4 — Spořilov, Czechoslovakia.

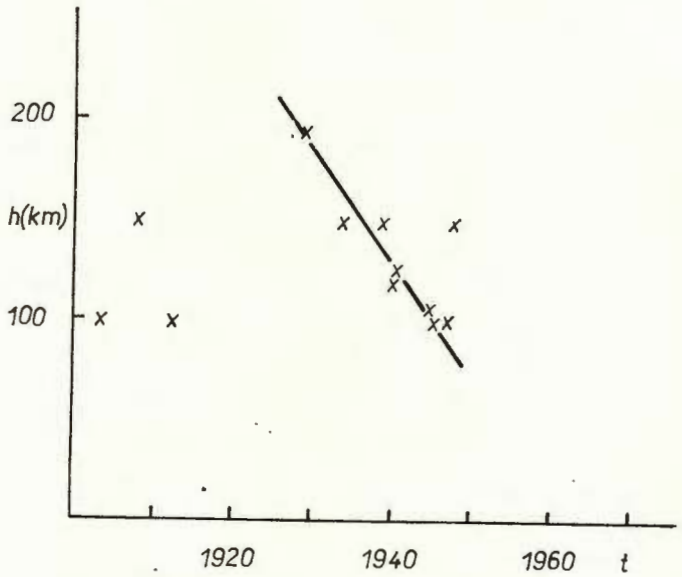

Fig. 1. — Region — Vrancea ; $h=h(t)$ for $m\geqslant 6.0$ and $h>n$.

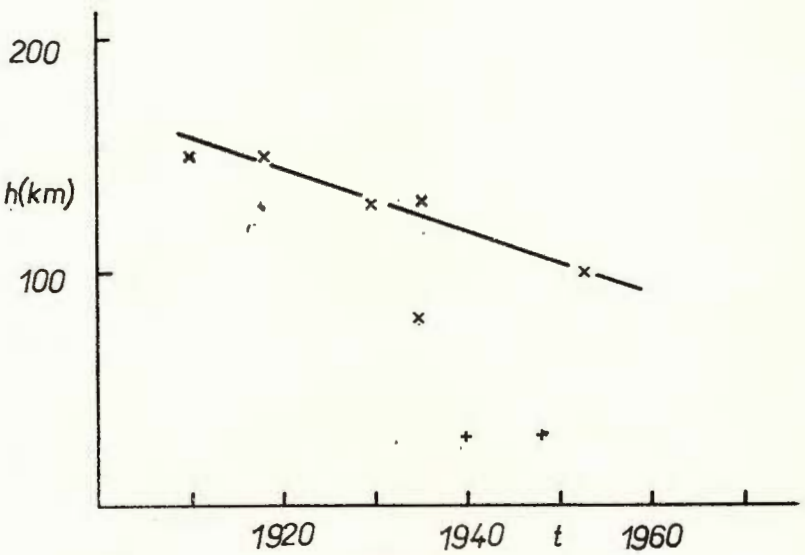

Fig. 2. — Region — Crete ; $h=h(t)$ for $m\geqslant 6.0$ and $h>n$.
+ denotes the occurrence of strong shallow earthquake of magnitude $M\geqslant 6.0$.

In the region of Crete the epicentres of the intermediate earthquakes are situated along two lines. The former is parallel to the northern coast and the latter parallel to the south coast of Crete. Along the first line the depth of the foci of intermediate shocks has been decresing with time since the year 1910 (fig. 2). Migration of depth with time was also observed by K á r n í k (1972).

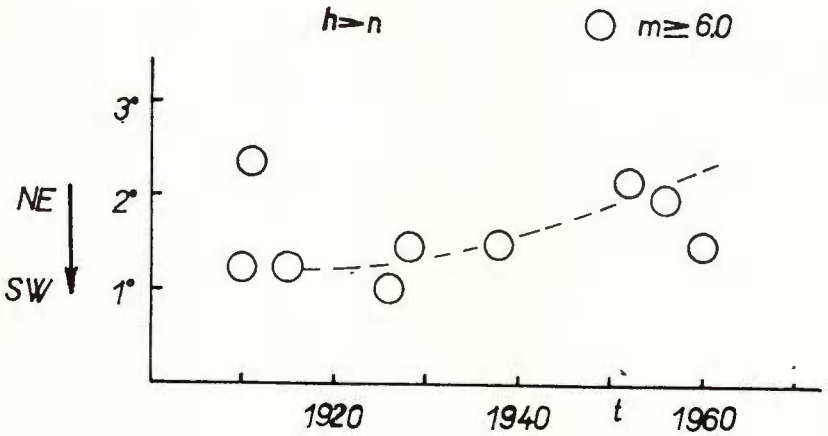

Fig. 3. — Region — Calabria ; time is given on the horizontal axis and the distance of epicentres measured from the south limit of the line on the vertical axis.

In both samples the decrease of the depths of the foci of strong intermediate earthquakes with time was observed during certain time intervals.

From the longterm decrease of the depth with time it is possible in some regions to determine short time intervals of a faster decrease of the depth with time (fig. 2). In some cases the occurrence of strong shallow earthquakes of magnitude $M \geqslant 6.0$ at the end of these time intervals was observed in the same region (fig. 2).

The observed decrease of the depth of intermediate shocks with time indicates that the source of earthquakes shifts from the depth to the surface. The occurrence of strong shallow earthquakes at the end of a sequence of intermediate shocks, the depth of which decreases with time, indicate that the cause of strong intermediate and strong shallow earthquakes is the same in one region.

Further we shall deal with the migration in horizontal plane. By the investigation of material in Europe and Asia Minor it was found that shallow earthquakes of a magnitude M smaller than 5.5 do not as a rule display any space and time tendency. For this reason the migration was studied for shallow shocks of a magnitude M greater than or equal to 5.5 and for intermediate shocks of a magnitude m greater than or equal to 6.0.

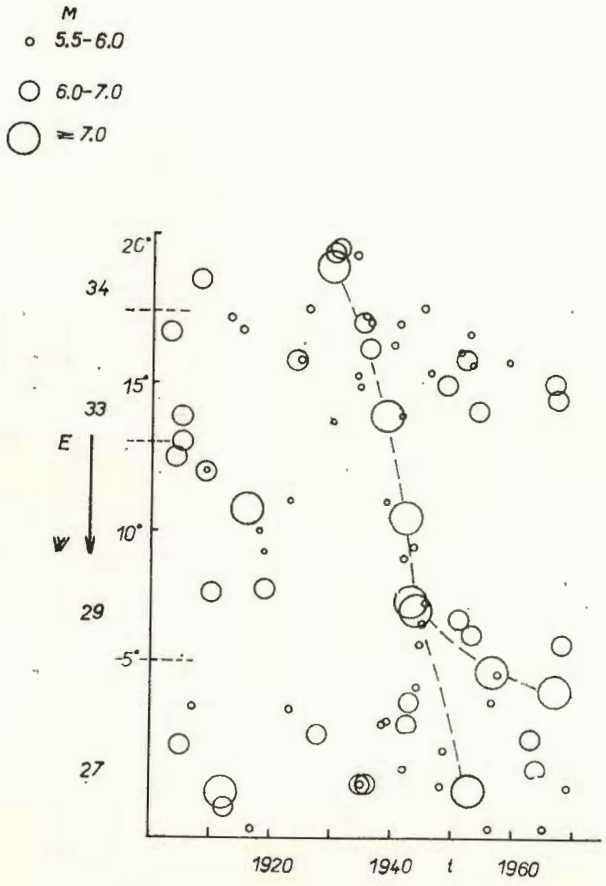

Fig. 5. — Region — North Anatolian zone; time is given on the horizontal axis and the distance of epicentres measured from the west limit of the line on the vertical axis.

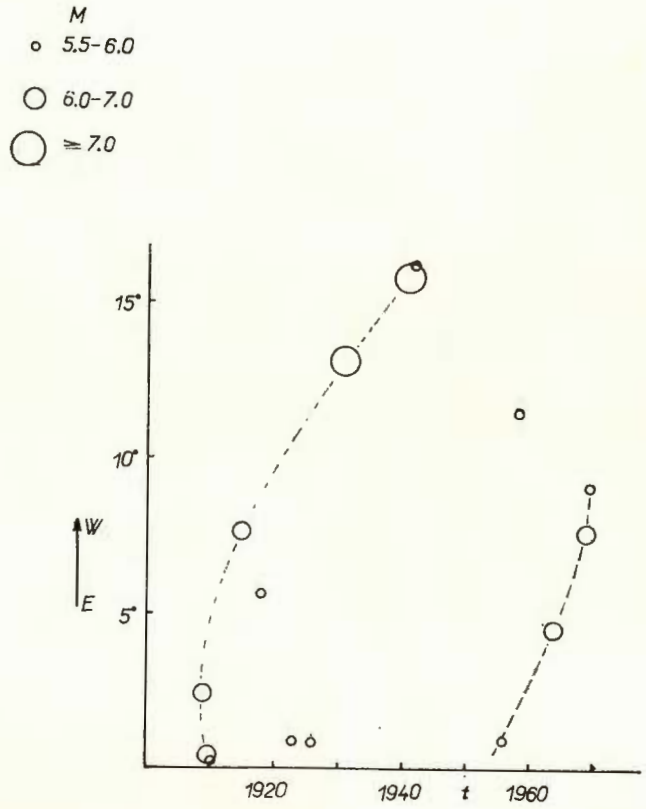

Fig. 4, — Region — Azores fault; time is given on the horizontal axis and the distance of epicentres measured from the east limit of the line on the vertical axis.

In some regions it is not possible to investigate the space and time tendency because of small member of large shocks (for example the region of the Alps and the Pyrenees etc.) or strong shocks were repeated in a small area (for example Western Yugoslavia) or it is difficult to determine seismotectonic lines along which the migration is studied (for example in

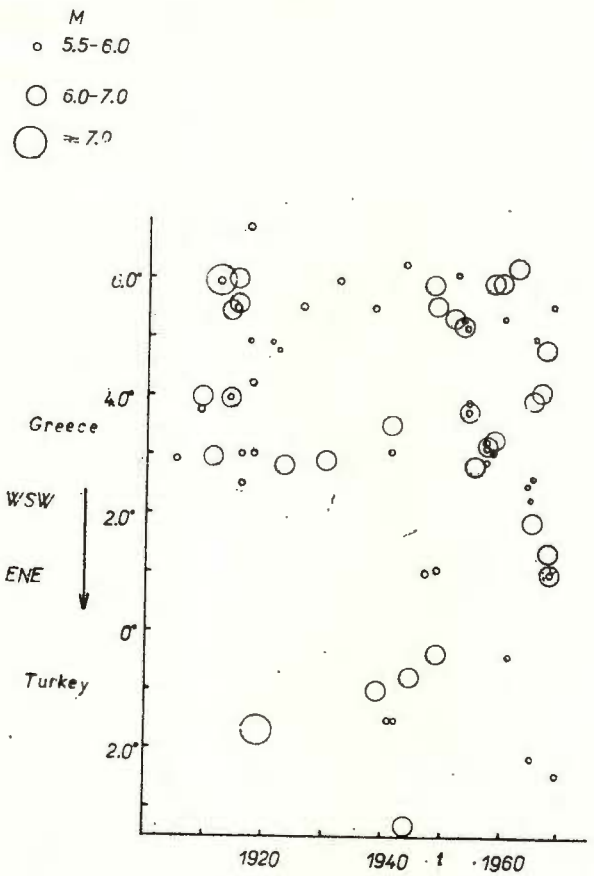

Fig. 6. — Region — Greece and Turkey; time is given on the horizontal axis and on the vertical axis the distance of epicentres measured from 25-th meridian on both sides.

Albania and Macedonia) or the migration is clear only in a certain time period (for example in Italy).

Finding or not finding the migration depends substantially on the delimitation of the region and on the choice of the seismotectonic line (the seismotectonic line is the line along which we study migration of foci of earthquakes). The magnitude of the region is also a very impor-

tant parameter. When we choose a small region we observe either oscillation of seismic activity or a disarranged distribution of foci. In regions in which there are clear fault zones or where there are young ranges of mountains the seismotectonic lines are selected parallelly to these elements.

In Calabria the seismotectonic line passes through volcanic islands from Sicily to South Italy. The foci of strong intermediate earthquakes shift from Sicily to South Italy since the year 1910 (fig. 3).

The next clear seismotectonic line passes along the Azores fault (R i t s e m a , 1969, 1970). The foci of strong shallow shocks shifted along this line from the east to the west in the period from 1910 to 1945. A further shift in the same direction has been observed since the year 1955 (fig. 4).

On the zone which extends along the North-Anatolian fault (R u n c o r n, 1962) the situation is more complicated (fig. 5). The simplest situation is in the central part where two shifts of foci from the east to the west are clear. On both ends three or four shifts from the east to the west may be determined according to subjective criteria. The shift of foci of strong earthquakes of a magnitude greater than or equal to 7.0 is clear. It is a question of subjective judgement whether we take shift this in the period from 1929 to 1953 as described by several seismologists or whether we take this shift in the period from 1929 to 1962. In both possible variants there are earthquakes with a magnitude greater than or equal to 7.0 that do not belong to any of both tendencies.

Very complicated is also the situation on the Balkan peninsula where several fault zones may intersect. The line passing from Greece to Turkey in the direction from west-south-west to east-north-east was determined by G a l a n o p o u l o s (1967 a,b) and M o u r a t o v (1971). On this line two different shifts may be investigated (fig. 6). First : In the period from 1912 to 1915 there were strong shallow earthquakes in Western Greece. Then there were two strong shocks in Eastern Greece and after 1940 there were strong earthquakes in western Turkey. The next shift from Western Greece to Eastern Greece can be observed in the period from 1948 to 1969. Both shifts can be regarded as a move of foci from the west to the east. The second trend of activity : the epicentres in Turkey shift from the east to the west. The same move may be observed in Eastern Greece — the foci from second degree to fourth degree. Both trends appear to be equally justified. In the first case it is the question of earthquakes from different zones of foci succeeding each other in a definite arrangement. In second case one zone of foci appears to shift slowly in one direction.

The earthquakes which display space-time tendency have probably the same cause. They originate owing to one stress system and the origin of strong shocks in one place affects the origin of strong shocks in another place.

REFERENCES

Galanopoulos A. G. (1967 a). The Seismotectonic Regime in Greece. *Ann. Geof.*, 20.
— (1967 b) The Large Conjugate Fault System and the Associated Earthquake Activity in Greece. *Ann. Géol. Hellén*, 18.
Kárník V. (1968). Seismicity of the European Area/1. Academia, Praha.
— (1972). A Note on the Morphology and Activity of Seismic Zones in the Aegean Region. *Nature*, London.
Mouratov M. V. (1971) Tectonic Structures of the Alpine Geosynklinal Area in the Eastern Europe and Asia Minor and the History of their Development. *Rep. 21 Sess. 1960*, Copenhagen.
Ritsema A. R. (1969) Seismo-Tectonic Implications of a Review of European Earthquake Mechanism. *Geol. Rundschau*, 59, Stuttgart.
— (1970) On the Origin of the Western Mediterranean Sea Basin . *Tectonophys.*, 10. Amsterdam.
Runcorn S. K. (1962) Continental Drift. Acad. Press, New York.

TIME DISTRIBUTION OF EARTHQUAKE OCCURRENCE IN THE EUROPEAN AREA[1]

BY

ZDEŇKA SCHENKOVÁ[2]

The prediction of earthquake is of course a hot topic at the present time, which is supported mainly by the economic interest in earthquake risk analysis. Earthquakes may be represented as a series of points occurring at irregular intervals along the time axis, each point being specified by parameters such as longitude, latitude, focal depth and magnitude. A sequence of this kind is a time series. Statistical prediction is in fact an extension of Fourier spectrum analysis of the time series. Therefore the aim of my short contribution is to investigate the first order properties of this time series and to find a statistical model which is consistent with the data and to examine the influence of magnitude classes (4.5, 4.9), (5.0, 6.4) or some threshold magnitudes which will be exceeded, on the time distribution of earthquake occurrence.

The original data of shallow-focus earthquakes with the focal depth $h < 60$ km are taken from K á r n í k's European catalogue 1901—1955 completed by additional information from 1956—1967. The one-year interval is applied as a most appropriate unit. Shorter intervals are not feasible because then the number of „empty" intervals increases. The investigated zones are: Jan Mayen, Iceland (Nos 1+2), the Azores-Tunis line (Nos 12 + 13 + 14 + 15 + 16), the Alps and the Apennines (Nos 18 + 19 + 20), Balkan region (Nos 21 + 22 + 23 + 24 + 25 + 26 + 27) the Crimea and Caucasus (Nos 28 + 32), Turkey (Nos 29 + 30 + 31 + + 33 + 34 + 35).

The earthquake occurrence may be considered as a stochastic point process. The probability structure of a point process is described by the distributions of the numbers of events in a particular interval. Because of the simplicity of the Poisson process and its success in describing many phenomena, it is the first process used to approximate earthquake in our

[1] A full version of the paper has been submitted for publication in *Pure and Applied Geophysics* under the name „Model of Earthquake Occurrence in the European Area".

[2] Geophysical Institute of the Czechoslovak Academy of Sciences, Prague 4-Spořilov Boční II, Czechoslovakia.

TABLE 1

The Poisson distribution P(λ)

Region	Magnitude class				
	$M \geqq 6.5$	$M \geqq 5.0$	$5.0 \leqq M \leqq 6.4$	$4.5 \leqq M \leqq 4.9$	$M \leqq 4.5$
1 + 2	P(0.7)	P(1.4)	P(1.4)	the hypothesis is rejected	the hypothesis is rejected
12 + 13 + 14 + 15 + 16		P(1.6)	P(1.5)	the hypothesis is rejected	the hypothesis is rejected
18 + 19 + 20		P(2.0)	P(1.9)	P(3.9)	the hypothesis is rejected
21 + 22 + 23 + 24 + 25 26 + 27		the hypothesis is rejected	the hypothesis is rejected	the hypothesis is rejected	the hypothesis is rejected
28 + 32		P(1.0)	P(1.0)	the hypothesis is rejected	the hypotehsis is rejected
29 + 30 + 31 + 33 + 34 + 35		the hypothesis is rejected	the hypothesis is rejected	the hypothesis is rejected	the hypothesis is rejected

TABLE 2

The negative binominal distribution NB (k; p)

Region	Magnitude class				
	$M \geqq 6.5$	$M \geqq 5.0$	$5.0 \leqq M \leqq 6.4$	$4.5 \leqq M \leqq 4.9$	$M \geqq 4.5$
1 + 2	NB(1.5; 0.70)	NB(1.9; 0.57)	NB(13; 0.9)	NB(0.4; 0.2)	NB(0.7; 0.19)
12 + 13 + 14 + 15 + 16		NB(1.8; 0.52)	NB(1.8; 0.55)	the hypothesis is rejected	the hypothesis is rejected
18 + 19 + 20		NB(1.8; 0.47)	NB(1.7; 0.47)	NB(3; 0.43)	NB(3; 0.33)
21 + 22 + 23 + 24 + 25 26 + 27		NB(4.5; 0.26)	NB(5; 0.29)	the calculated p and k are not included in the tables	the calculated p and k are not included in the tables
28 + 32		NB(0.8; 0.42)	NB(0.9; 0.46)	NB(0.9; 0.38)	NB(0.9; 0.27)
29+30+31+33+34+35		NB(2.2; 0.38)	NB(2.1; 0.38)	NB(1.2; 0.28)	NB(1.8; 0.21)

investigated areas. The Poisson distribution can be derived under assumptions reduced to a stationary process in which :
a) the number of events in time interval is independent of the number of events in any other nonoverlapping interval,
b) the probability of one event occuring in a small time interval dt is λdt, where λ is a constant in time,
c) the probability of more than one event occurring in the same interval of time is asymptotically negligible.
The probability distribution of a Poisson process

$$P(\lambda)_i = \frac{\exp(-\lambda)\,\lambda^i}{i!}, \quad \lambda > 0, \; i = 0,1,2,\ldots \quad ,$$

where $P(\lambda)_i$ is the probability that in an arbitrary interval of unit length i events will occur with intensity λ. The mean and variance of the number of events per unit time interval are both equal to the parameter λ.

For testing the actual distribution with Poisson distribution χ^2 test is used under the assumption that the theoretical frequencies $nP(\lambda)_i \geqq 2$, where n is the length of the observed period (tab. 1). The hypothesis about the simple Poisson process can be rejected at the 5% or 1% significance levels for shocks from the magnitude class (4.5, 4.9) and for shocks with magnitude exceeding threshold value 4.5 in all the investigated regions. There is a tendency for better fits when the low magnitude shocks are removed. When the magnitude threshold is raised, the likelihood of a possible interaction between successive earthquakes decreases and a large proportion of aftershocks will be filtered out. So the hypothesis about the Poisson distribution is not rejected at the 5% or 1% significance levels for shocks from the magnitude class (5.0, 6.4) and for earthquakes of $M \geqq 5$ in the zones of Jan Mayen and Iceland, in the zones of the Alps and the Apennines, the Crimea and Caucasus and for Balkan region with a sufficient number of observed shocks exceeding threshold magnitude 5.6. On the other hand for example the hypothesis is rejected at the same significance levels for shocks from the same magnitude class and for shocks with the same threshold magnitude in Balkan region. The rejection of the hypothesis can be explained by an occurence of the multiple shock sequences. Thirty to forty percent of shocks with the magnitude $M \geqq 6$ are main shocks in the multiple shock sequences and twenty five to thirty five percent of shocks with the magnitude $M \geqq 5$ are main shocks in the multiple shock sequences. The multiple shock sequence is a group in which there are more main shocks and the shocks that follow after each of these main shocks or after double shocks or triplet shocks approximately equal, have all the features of aftershocks.

The most important characteristic of the earthquake time series which the Poisson process has not taken into account is the tendency of earthquakes to come in groups. The assumption inherent in the Poisson series, however, is that the probability of an event remains constant, equal parameter λ, which in practice is not alway true. Any variation in

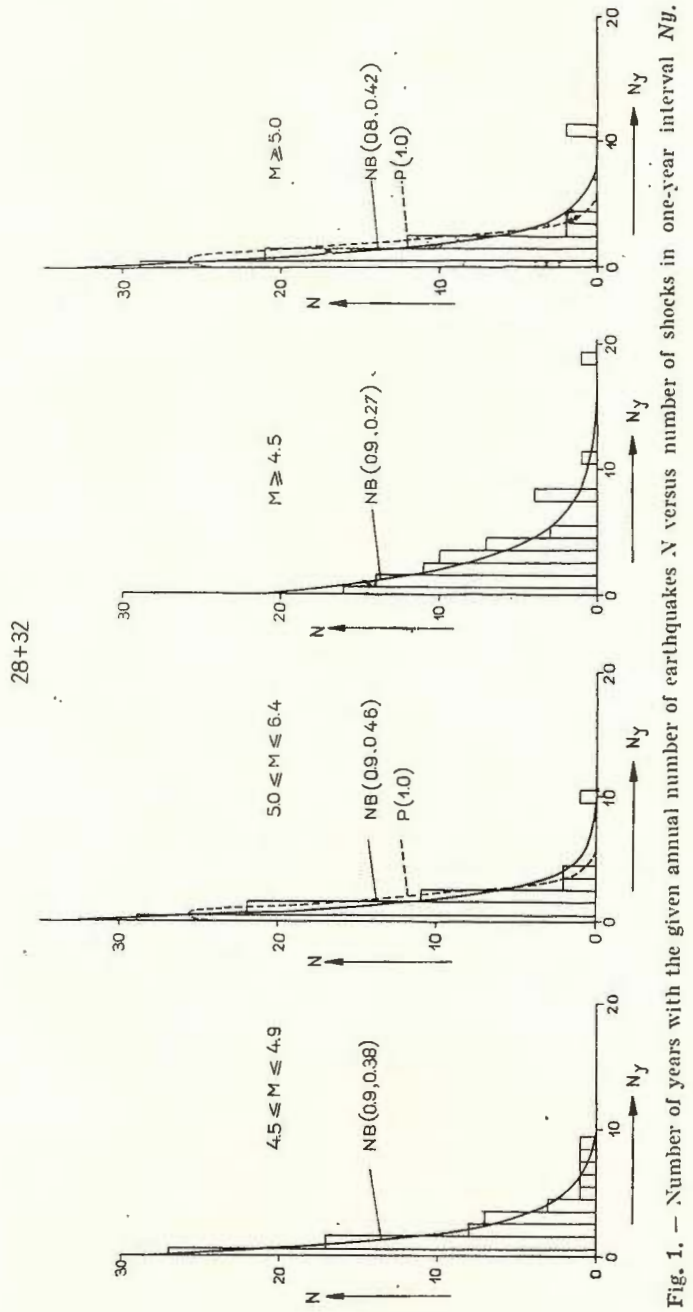

Fig. 1. — Number of years with the given annual number of earthquakes N versus number of shocks in one-year interval *Ny*.

the expectation of an event — in particular for one event to increase the probability of another — will increase the variance of the distribution relative to the mean and a negative bionomial distribution will invariably better describe the data. Writing the negative binomial distribution in the form $p^k (1-q)^{-k}$ the probability of i events is given by

$$NB(k,p)_i = \left(\frac{i+k-1}{k-1}\right) p^k q^i, \quad i = 0,1,2,\ldots$$

where k, p are parameters, $p + q = 1$. Thus as p is neccessarily less than unity, the variance is always greater than the mean. Having derived the negative bionomial distribution as a generalized Poisson process, it is evident that Poisson distribution is obtained as a limiting form of $p^k(1-q)^{-k}$ There are several methods of estimating the parameters p and k, one of them is the method of moments, which was used.

To test the observed distribution with the negative binomial distribution χ^2 test is used, too, under the same assumption about theoretical frequencies (tab. 2). The hypothesis about the negative binomial distribution is rejected at 5% or 1% significance levels only for shocks from the magnitude class (4.5, 4.9) and for shocks with threshold magnitude 4.5 in the zones of the Azores-Tunis line. The observed deviation from the negative binomial distribution is due to the incompleteness of our material, because the data are homogeneous from the magnitude $M = 5$. It is not possible to verify the hypothesis for shocks in Balkan region from the lowest magnitude class or with the lowest magnitude threshold value. The calculated parameters p and k are beyond the range of the tables of the negative binomial distribution, which are available.

For example the histogram for the frequency of earthquake occurrence in one-year interval is given for the zone of the Crimea and Caucasus in figure 1. In the cases when the hypotheses are not rejected the curves for the Poisson distribution whith parameter λ are drafted by dashed line and the curves for the negative binomial distribution with the parameters k, p are drafted by full line.

Though the solution of the problem of earthquake prediction must be based on a full understanding of the process in the focus we are so far limited in the development of ideas based on direct physical evidence or knowledge of the physical process leading to earthquake origin. Therefore various statistical models are being suggested and their properties are used for estimation of the probability of earthquake occurrence within a given area. According to the results of this paper it can be generally said that the process with the negative binomial entries as a model describing the occurrence of shallow earthquakes has more general validity than simple Poisson process in the diferent European areas. The occurrence of aftershocks can be interpreted into a theoretical model by this process to allow for the occurrence of more than one earthquakes in a time unit. Also the knowledge of the probability of events occurring within a short time interval enables to define a cluster more quantitatively.

DEEP SEISMOGENIC STRUCTURES OF THE EARTH'S CRUST AND UPPER MANTLE

BY

JU. K. SHCHUKIN[1]

INTRODUCTION

The paper deals with the use of the trends of anomalous attenuation of seismic waves (from macroseismic and instrumental data) as one of the possible criteria of locating the spatial position of seismogenic deep faults (dislocations) to study their relations and depth differentiation.

The main methodical procedures used in the work were previously described in co-operation wich the Bulgarian geophysicist Dobrev in a few publications on the example of the seismic areas of Bulgaria (Dobrev, Shchukin, 1967; Shchukin, Dobrev, 1970; Shchukin, Dobrev, 1972).

The maps and other constructions were made on the basis of the published macroseimic evidence (Atanasiu, 1961; Grigorova, Grigorov, 1964; Grigorova, Rijikova, 1966; Drumia et al., 1964; Evseyev, 1969; Rustanovich, 1967; Sagalova, 1964) as well as using the instrumental data of the earthquakes of the Carpathian-Balkan, Crimea-Caucasus and Kopet-Dagh seismic regions (Grigorova, Grigorov, 1964; Grigorova, Rijikova, 1966; Petrescu, Radu, 1962; Radu, 1963; Rustanovich, 1967; Sagalova, 1964).

GENERAL CONSIDERATIONS

While making the maps and other constructions we made the following assumptions:

a) The Earth is anisotropic, i.e. the rocks in the focus area are inhomogeneous in their physical and mechanical properties. The present inhomogeneities will differently but necessarily affect attenuation of seismic waves and surficial effects of earthquakes and, hence, the shape

[1] VNII Geofizica (All Union Research Institute of Geophysical Exploration), Chernishevsky 22, Moscow, USSR.

of isoseismal lines of earthquakes with deviations of the observed forms from the theoretical ones, computed for a point or linear focus of elastic waves in a space (Riznichenko, ed., 1960).

b) Thr focus is linear. The seismic energy is released in the zone most closely located to the deep fault (the zone of the disturbance of the Earth continuity) with which the focus is associated. The energy released by the focus is redistributed in the upper part of the Earth's crust depending upon the main trends of the regional tectonic structures and accompanying faults. It is believed that only the first isoseismal lines of the macroseismic field bear information about the focus whereas the marginal ones provide less information, characterizing regional structures, engineering geology, topography, etc.

c) Mechanism of the focus. It is assumed that accumulation of the potential energy in the zone of a linear (elongated) focus occurs simultaneously at several points located at relatively close depths. In general, regarding the focus of a tectonic earthquake as a rupture of the Earth continuity with the sides sliding along the displacer plane (Kostrov 1970), we assume that the release and redistribution of the stresses as well as radiation of the energy in the focus occur along the entire plane of the rupture. Orientation of the focus radiation is an indication of not only crustal (tectonic) earthquakes but also deep (mantle) earthquakes. The latters are also marked by persistence of trends of anomalous attenuation and by asymetry of the focus radiation (Soboleva, 1968). Our graphics confirm it.

ANALYSIS OF MACROSEISMIC DATA.

While analysing the macroseismic field we paid attention to the dominating elements of the pattern (morphology) of the isoseismal lines and to the main alignments drawn along the axes of anomalous tremors. This method is generally used in interpretation of the anomalies of gravity, magnetic and other geophysical fields. From the shape, size, area and intensity of the anomalies one can judge of the elements of the geological objects which cause these anomalies.

This approach agrees with the known views of a number of Soviet and foreign investigators (Ananyin, 1964; Galanopoulos, 1959; Raghimov, 1964; Shebalin, 1968; Woollard, 1972) on the fact that the analysis of the distortion of the macroseismic field (considering the focal seismicity) may be applied for studying the structure of the Earth's crust and upper mantle.

In cas of tectonic (crustal) earthquakes it is hard to explain the fact that within one and the same focal zone the release of seismic energy occurs in non-oriented directions. In this case seismologically interesting is a total effect of anomalous tremors rather than their individual directions. Similar to physical fields, the former may be expressed in terms of the density of lines of anomalous tremors per a unit of a certain selected area (Shchukin, Dobrev 1970). This definition of the density of

anomalies axes of a macroseismic field (in the simplest case it is a long axis of an ellipse of maximum isoseismal lines), patricularly when calculation is made for a long period of time (in our case about 80 years), may more precisely delineate the most probable location of extending focal zones, seismogenic faults (dislocations) and joints of their intersection in a horizontal projection to the surface of the Earth.

The data obtained enable one to determine the length of seismogenic structures and size of extended focal zones. Using also vertical sections

Fig. 1. — Map of density of deep seismogenic dislocations of the Carpathian-Balkan region. Contour lines show density of seismogenic dislocations of tectonic (crustal) earthquakes expressed in terms of conventional units $n \cdot km^{-2}$ (the area of the square summarizing template is 625 km^2 and the time of observation for the earthquakes is 80 years). The question marks stand for the lack of data from the adjacent territories.

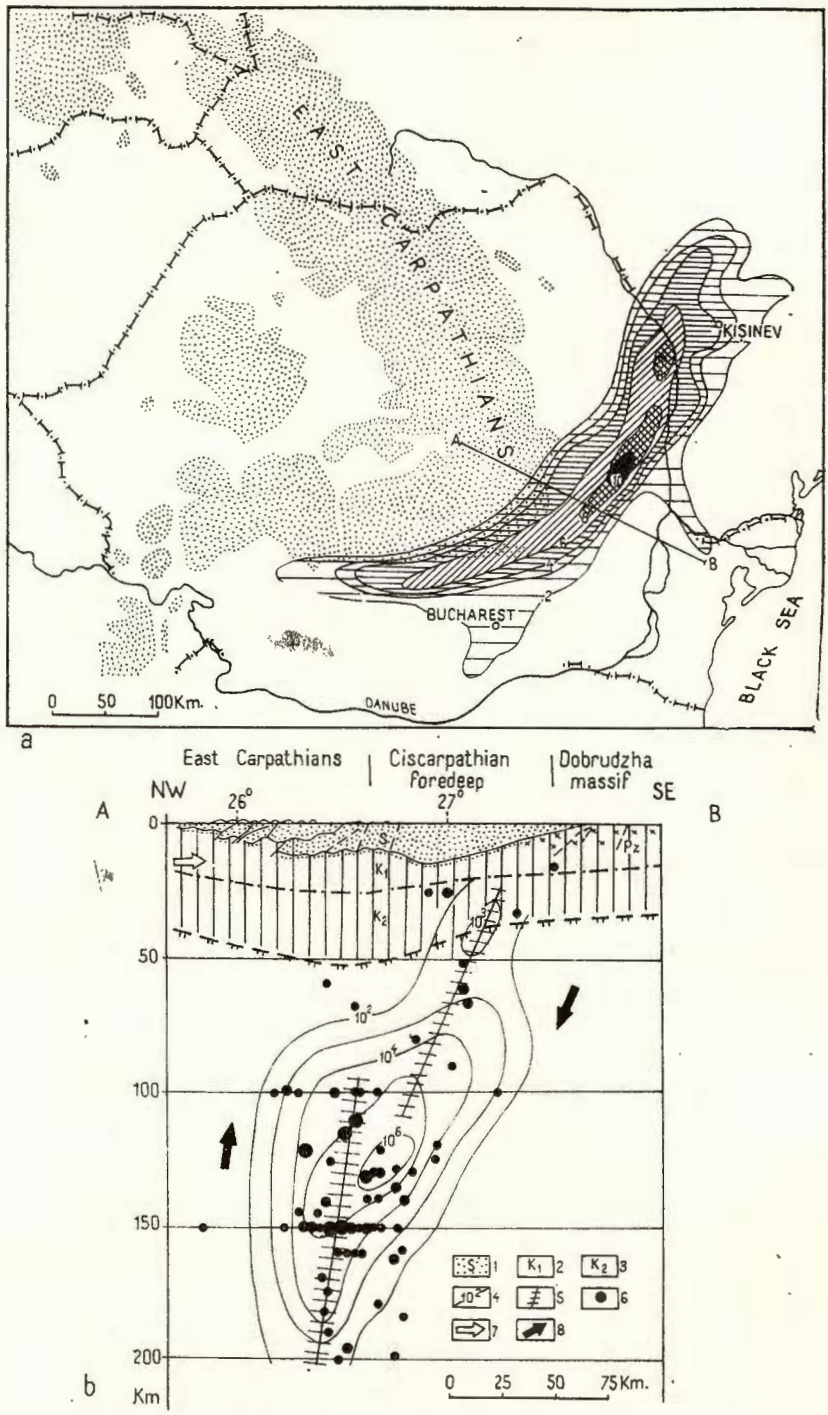

Fig. 2. — Deep foci of the earthquakes in the area of the East Carpathians :

a, map of density of seismogenic dislocations of deep (mantle) earthquakes; b, deep seismogeologic section. 1, sediments (S); 2, „granite" layer (K_1) of the consolidated crust; 3, „basalt" layer (K_2); 4, contour lines of specific seismic energy in $10^n \cdot 10^{-12}$ erg/cm^3 s; 5, supposed position of deep fault zones; 6, hypocenters of strong earthquakes with a magnitude $M \geqslant 4\ 1/2$; 7, prevailing orientation of tangential stresses; 8, principal trends of possible displacements of major lithosphere blocks.

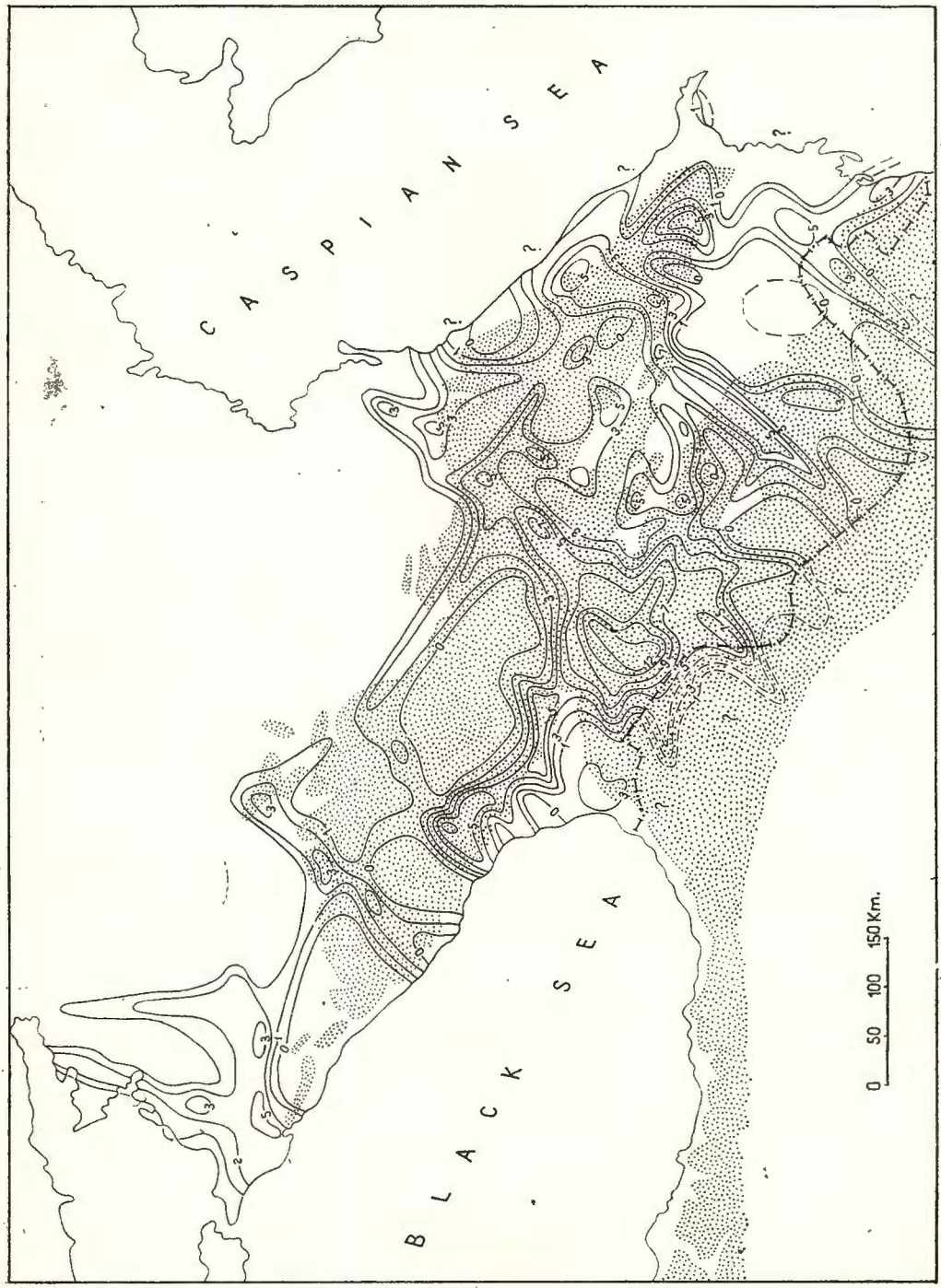

Fig. 3. — Map of density of deep seismogenic dislocations of the Caucasus.
Dots show outlines of mountanous structures with absolute elevations of 500 m and more above sea level.

of the latters one can learn about the real sizes of a hypocentral area as applied to the problems of seismic zoning, seismogeologic constructions and evaluation of a most probable earthquake in a given area.

RESULTS

On the basis of the above mentioned methods of analysis of macroseismic data a map of density of deep seismogenic dislocations has been constructed for the first time for an extensive belt of the Alpine folded struc-

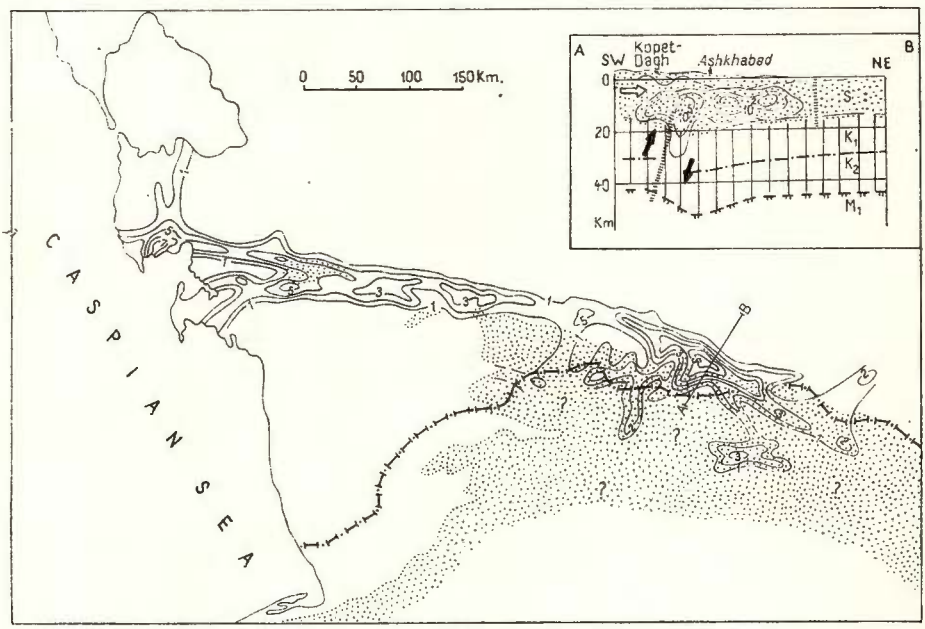

Fig. 4. — Map of density of deep seismogenic dislocations of Turkmenia (Great Balkhan and Kopet-Dagh.)

The insert map shows a deep seismogeologic section of the focal zone of the Ashkhabad earthquake of 1948 and of aftershocks. The legend in the same as in figure 2.

tures of the south USSR and Carpathian-Balkan region. The fact that guarantees the positive results of the calculations and constructions made is sufficiently good (though irregular) knowledge of the regions and availability of macroseismic and instrumental seismogeologic data for a long period of time, as well as proper geological and geophysical knowledge that enabled verification of the results obtained.

The supplemented map (fig. 1—4) shows two parameters characterizing the stressed condition of the Earth's crust and some zones of the upper ,mantle which are :

a) density of seismogenic dislocations, a quantitative parameter, in conventional units $n.km^2$ (i.e. a number of dislocation lines cutting

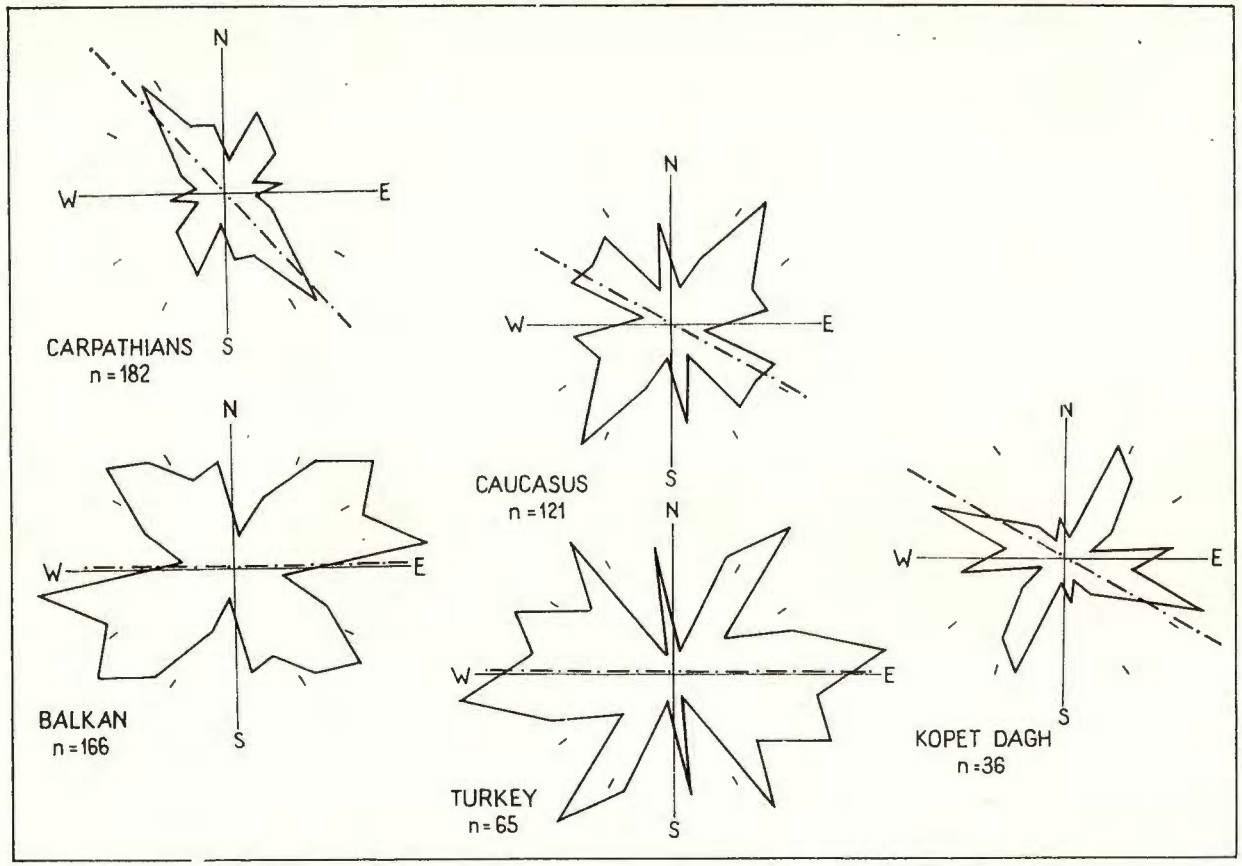

Fig. 5. — Diagramm of trends of characteristic classes of deep seismogenic dislocations.
Dotted lines show trends of the Alpine folded structures, figures indicate the number of measurements.

a unit area), *b*) orientation of zones of high density of seismogenic dislocations.

According to the genetic belonging the located zones may be divided into the following :

the zones exactly coinciding with the geological faults extending to the surface ;

the zones confidently comparable with the position of hidden faults proved from geological and geophysical data ;

the zones having no distinct relation with structures but conciding with anomalies of physical fields, which reflect other inhomogeneities of the earth than faults.

Diagrammes of the strikes of typical classes of deep seismogenic dislocations are shown in figure 5. Nearly in all the investigated regions the most typical were northeastern and northwestern strikes of the seismogenic structures and in the Kopet-Dagh, Caucasus and Turkey regions also southnorthern ones. The latitudinal trends are easily recognized in the Kopet-Dagh, Turkey, Carpathians and probably in the Balkan area. There is a definite relationship that one of the prevailing trends coincides with the strike of the major tectonic structures or folded mountains (particularly for the case of the Caucasus, Turkey and Carpathians) and the orther, trend — transverse or diagonal — complicates the linear folded structures.

In the plan of the deep structure the main trends of the high density of the seismogenic dislocations shown on the maps (fig. 1—4) are aligned along the outlines of the major crustal blocks separated by the regional faults. The age of these faults involved into seismic processes varies from Pre-Riphean (the southwest Russian platform) and Hercynian (the Skyphian, Mizian, and Turanian (plates) to Alpine (the Carpathian-Balkan region, the Caucasus, the Kopet-Dagh).

From geological and geophysical data it is known that the depth of the origin of these faults is variable ranging from a few kilometers to several hundred kilometers (for instance, the East Carpathians). In this connection the delineated zones of the anomalous densities of the seismogenic dislocations appear to be confined to different levels. It is very well recognized in the Romanian East Carpathians where the total Earth's crust and even theupper part of the mantle appear to be seismically active. Differentiation of the network of the seismogenic faults in depth is very interesting both for studying the extent of the present-day tectonic activity of individual horizons of the Earth's crust and for determining the thickness of the seismic layer in calculations of the most probable carthquake that could occur in a given zone. It is clear that the trends of the seismogenic structures got separated from the released zones located generally along the contacts of the blocks having a different surface and deep geological structure.

Not detailed geological and geophysical analysis of the delineated seismogenic structures is given here.

SOME CONCLUSIONS.

The anomalies of the macroseismic field bear substantial information of the properties and morphology of the focus and the overlying earth. The analysis of the macroseismic data made on the basis of the instumental seismological observations and geological and geophysical constructions (see the deep seismoenergetic sections of individual focal zones) enables one to solve a direct problem of seismology related with studying deep crustal conditions, earthquake mechanism and the transfer of tremors from the focus to the surface via the geological structures.

The supplemented map of the density of deep seismogenic dislocations contains information of an important element of the earth — zones of anomalous attenuation of seismic oscillations which are in most cases identified with the present-day „living" seismogenic faults and also of the differences of the absorbing properties of the Earth. If we scan this map in time bearing in mind different levels and energy of the individual zones, we can get a reliable picture of the spatial distribution and orientation of developing seismogenic structures. It is evident that the constructions reported in this paper may be used for practical purposes.

REFERENCES

Ananyin I. V. (1964) The seismic effect of near earthquakes in the East Caucasus. *Proc. Inst. Phys. Earth.* USSR Acad. Sci, 33, Moscow.

Atanasiu J. (1961) Cutremurele de pământ din România. Ed. Acad. R.P.R., București.

Dobrev T. B., Shchukin Ju. K. (1967) Investigation of the Earth's crust and nature of seismicity of the Carpathian-Balkan province. *Internal. Geol. Rev.*, 9, 12. Washington.

Drumia A. V., Ustinova T. I., Shchukin Ju. K. (1964) Problems of the tectonics and seismology of Moldavia, iss. II, Karta Moldoveniaske, Kishinev.

Evseyev S. V. (1969) Intensity of the earthquakes of the Ukraine. *In*: Seismicity of the Ukraine, Naukova Dumka, Kiev.

Galanopoulos A. G. E(1959) Macroseismic evidence for the fault plane. *Ann. Geofis.*, XII, 2., Roma.

Gorshkov G. P., Shebalin N. V., Shenkareva G. A., Shchuk in Ju. K. (1969). The energy characteristics of the deep zones of seismic activity. *Geotectonics*, 6., Moscow.

Grigorova E., Grigorov B. M. (1964) Epicenters and seismic lines in Bulgaria. Publ. Acad. Sci., Sophia.

— Rijikova S. (1966) Earthquakes in Bulgaria during 1961—1964. Publ. Acad. Sci., Sophia.

Kittel C h. (1965) Solid state physics, Nauka, Moscow.

Kostrov B. V. (1970) The theory of the foci of tectonic earthquakes. *Izv. Acad. Sci. Ser. Phys. Earth*, 4, Moscow.

Petrescu G., Radu C. (1962) Seismicity of the territory of Rumania for the period of 1901—1960. *Izv. Mold. Acad. Sci.*, 4.

Radu C. (1963) Determinarea magnitudinii cutremurelor normale din R.P.R. *Stud. Cercet. Geol. Geogr. Geofiz., Ser. Geofiz.*, 1, București.

Raghimov Sh. S. (1964) Study of crustal faults from macroseismic data. *Izv. Acad. Sci. Ser. Geofiz.*, 7, Moscow

Riznichenko Ju. V. (Editor) (1960) Methods of detailed study of seismicity. Publ. Acad. Sci. USSR, Moscow.

Rustanovich D. N. (1967) Seismicity of the territory of Turkmenia and the Ashkhabad earthquake of 1948. Nauka, Moscow.

Sagalova E. A. (1964) Earthquakes of Bukovina. *In*: Catalog of Carpathian earthquakes, 7—8 (10—11), Naukova Dumka, Kiev.

Soboleva O. V. (1968) The effect of asymmetry of radiation from the focus on distribution of displacements around the epicentre of a deep earthquake. *Izv. Acad. Sci. Ser. Earth Phys.* 10, Moscow.

Shebalin N. V. (1968) Methods of using engineering seismology data or seismic zoning *In*: Seismic zoning of the USSR. Nauka, Moscow.

Shchukin Ju. K., Dobrev T. B. (1970) Detection of deep seismically active faults from macroseismic data. *Izv. USSR Acad. Sci., Ser. Earth Phys.* 3, Moscow.

— Dobrev T. B. (1972) Characteristics of the seismogenous faults in the Earth's crust. Methods and results of the investigations of the Earth's crust and upper mantle. *Upper Mantle*, 8, Nauka, Moscow.

Woollard J. P. (1972) Earthquakes as indicators of the tectonic activity of North America. *In*: The Earth's crust and upper mantle, Russian Edition, Mir. Moscow.

Redactor: MARGARETA PELTZ
Tehnoredactori și corectori: ELEONORA SPÂNOCHE, LIVIA DIACONU
Ilustrația: V. NITU

Dat la cules: sept. 1974. Bun de tipar: dec. 1974 Tiraj: 900 ex. Hîrtie scris IA. Format 70 × 100/49 g. Coli de tipar: 22¼. Pentru biblioteci indicele de clasificare 55(058)

Tiparul executat la Intreprinderea poligrafică „Informația", str. Brezoianu nr. 23–25, București-România

c. 371